Scottish Natural Heritage
Commissioned Report No. 947

Analysis of the possible displacement of bird and marine mammal species related to the installation and operation of marine energy conversion systems

Scottish Natural Heritage
Dualchas Nàdair na h-Alba
All of nature for all of Scotland
Nàdar air fad airson Alba air fad

marinescotland

The Scottish Government
Riaghaltas na h-Alba

COMMISSIONED REPORT

Commissioned Report No. 947

Analysis of the possible displacement of bird and marine mammal species related to the installation and operation of marine energy conversion systems

For further information on this report please contact:

George Lees
Scottish Natural Heritage
Battleby
Redgorton
PERTH
PH1 3EW
Telephone: 01738 444177
E-mail: george.lees@snh.gov.uk

This report should be quoted as:

Long, C. 2017. Analysis of the possible displacement of bird and marine mammal species related to the installation and operation of marine energy conversion systems. *Scottish Natural Heritage Commissioned Report No. 947.*

COMMISSIONED REPORT

Summary

Analysis of the possible displacement of bird and marine mammal species related to the installation and operation of marine energy conversion systems

Commissioned Report No. 947
Project No: 014685
Contractor: EMEC
Year of publication: 2017

Keywords

Environmental monitoring; wildlife displacement; marine renewable energy; device impact; vantage point observations.

Background

Under the European Environmental Impact Assessment and Habitats Directives, there is a regulatory need to determine whether the deployment and operation of marine energy conversion systems (MECS) is likely to have any significant effect on the environment or affect the integrity of European Protected Sites (e.g. designated Natura 2000 sites). An important part of this is to identify whether MECS have any impact on the abundance or distribution of wildlife species in the vicinity of such devices. Using information collected at its grid-connected tidal and wave test sites, the European Marine Energy Centre (EMEC) in Orkney has led in-depth analyses of land-based wildlife observation data with respect to the operational status of different devices. With the aim of addressing this key concern for the industry, this project looks at the possible displacement of marine birds and marine mammals from the sea areas that they habitually use around EMEC's two grid-connected test sites (Fall of Warness and Billia Croo).

This data analysis project has brought in expertise from the Centre for Research into Ecological and Environmental Modelling (CREEM) in the application of the statistical package MRSea to quantify any spatially-explicit change attributable to MECS testing. This report describes the survey techniques used to gather the test site observations, explains the statistical methodology subsequently applied to analyse the resulting dataset, and sets out the results of the analyses with respect to the potential displacement of key wildlife species that can be associated with the various testing phases for marine energy converters. Data limitations and assumptions which underpin the analysis are highlighted and reference is made to the potential use of the dataset for future analyses. Further recommendations are made regarding the continuation of land-based observation programmes run at EMEC and, if continued, how the data collection methodologies could be amended to improve dataset quality.

Main findings

- The purpose of the EMEC Wildlife Data Analysis Project was to assess the extent of any displacement of key wildlife species arising from the installation and operation of marine energy converter systems (MECS).

- Nearly 18,000 hours of land based observations data, collected since 2005, were utilised for the project, drawn from EMEC's Wildlife Observations Programme. These data were collected, primarily, to aid in site characterisation of EMEC's two MECS test sites, at Fall of Warness (tidal energy) and Billia Croo (wave energy), rather than to inform an impact assessment study. Accordingly, though the datasets are extensive, the survey design was not optimal in terms of discerning change related to development activity, for example lacking a control site. This was addressed, in part, by comparing species data collected under four differing levels of site activity / impact. Comprehensive analyses were conducted on data for ten species/groups of species selected from each of the two test sites.

- Alongside the data collected during the Wildlife Observations Programme, this data analysis project utilises device operational data collected from developers testing at EMEC. These data are commercially sensitive and, therefore, are not available for public dissemination. An anonymization process was implemented to ensure commercial confidentiality was maintained throughout the project, which meant that it was necessary to apply site-wide impact levels. The result of this constraint is that inferences regarding the effect of device presence/operation at a device- or developer-specific level cannot be drawn from the analyses.

- Using the statistical modelling R package 'MRSea', developed by the Centre for Research into Ecological and Environmental Modelling (CREEM) at the University of St Andrews, it was possible to produce models that have the ability to estimate the distribution and abundance of species. These models also allow the effect of device presence and operation to be investigated by considering if there is any evidence of spatially-explicit changes in species density.

- Statistical significance was attributed to some of the predicted density changes. However, for some species, the natural variation evident under baseline conditions made it difficult to distinguish changes associated with the changing site operational level within the wider range of natural variation. An attempt was made to model natural variation for each species by including temporal and environmental terms within the model; however, no attempt was made to include wider variables that may in some instances affect the population e.g. harbour seal decline in Orkney.

- Fitted models for each of the species tend to include terms to account for seasonality and interannual variation in abundance. Environmental influences on species density were also taken into consideration, including environmental terms such as precipitation, cloud cover and wind strength.

- Power analyses were conducted on some of the final fitted models in order to understand their capability to detect certain scenarios of species changes, particularly whether the model result reflects the true situation or indicates that the model is unable to detect such a change.

- Effects directly associated with the presence, operation, or related infrastructure of MECS, are inferred only where there are spatially-explicit differences in density that can be associated with grid cells containing test berths.

- Many of the outputs produced from the fitted models, particularly at the Fall of Warness test site, suggest that the greatest change in density occurs when device-associated infrastructure (including anchoring systems, foundations and mooring systems) is installed onsite. This change in density is not limited to test berths but tends to stretch beyond, to the rest of the survey grid. For most species in the Fall of Warness survey area, the extent of this change is reduced with the installation of devices and when they are operating. This would suggest that it may not be the physical presence of the device or its infrastructure that is causing this change in density, but rather the increased vessel movements that are associated with installation activities. Vessel movements are expected to reduce when devices become operational. Although vessel movement data were collected throughout the observations programme run at both sites, these data tended to be anecdotal, rather than systematic, and not of sufficient quality to be included in the analyses. Further research regarding this particular potential impact pathway, possibly using the Automatic Identification System (AIS) data collected at both sites, may prove valuable.

- While it is tempting to interpret the reduction in the scale of change with increasing site impact level as evidence of habituation, the overall operational status of the site has continually altered, rather than progressing steadily to a more developed state, making such an inference debatable.

- Almost all the species surveyed at the Billia Croo test site show similar densities for all site impact levels and there appears to be no correlation between changes in densities and the location of test berths. Due to the size of the Billia Croo site, the density estimates produced from the fitted models tend to have a greater uncertainty surrounding them, compared to the Fall of Warness models.

- Power analyses were conducted on the fitted models in order to determine whether a modelling result that shows no change in species density actually reflects a true situation or is the result of the model being unable to detect such a change. Varying results have been gained from the power analyses conducted on the Fall of Warness models, with models able to detect a 50% decline in density for certain species (even when survey effort is halved) and others unable to do so. Where models have shown to have good power in detecting change, there has tended to be variation across the site. It is possible that this is associated with areas of high density estimates for some species or areas of low uncertainty. It has not proved possible to conduct power analyses on the fitted Billia Croo models due to low species densities there, resulting in the vast majority of data points being zeros, once survey effort is included. This led to the fitted data used in the power analysis simulation having means that were too small to allow generation from an overdispersed Poisson distribution.

- Although, within the project's limitations, it was only feasible to investigate ten species or groups of species from each of the sites, the method applied during the analyses should, data permitting, allow for further species observed at the sites to be investigated at a later date. It is worth noting, however, that the low densities recorded at the sites for certain species may curtail the scope for any further analyses involving these species.

For further information on this project contact:
George Lees, Scottish Natural Heritage, Battleby, Redgorton, Perth, PH1 3EW.
Tel: 01738 444177 or george.lees@snh.gov.uk
For further information on the SNH Research & Technical Support Programme contact:
Knowledge & Information Unit, Scottish Natural Heritage, Great Glen House, Inverness, IV3 8NW.
Tel: 01463 725000 or research@snh.gov.uk

Table of Contents **Page**

Table of Figures **Page**

Abbreviations

AIS	Automatic Identification System
acf	autocorrelation function
ANOVA	Analysis of variance
CI	Confidence intervals
CLT	Central Limit Theorem
CREEM	Centre for Research into Ecological and Environmental Modelling
CReSS	Complex Region Spatial Smoother
CV	Coefficient of Variation
df	Degrees of freedom
EMEC	European Marine Energy Centre
GAM	Generalised Additive Model
GEE	Generalised Estimating Equation
GLM	Generalised Linear Model
HIE	Highlands and Islands Enterprise
MAG	EMEC Monitoring Advisory Group
MECS	Marine Energy Conversion Systems
MPA	Marine Protected Area
MRSea	Marine renewables strategic environmental assessment software package
PEMP	Project Environmental Monitoring Plan
QBIC	Quasi Bayesian Information Criterion
QGIS	Quantum Geographic Information System
SALSA	Spatially Adaptive Local Smoothing Algorithm
SIL-0	Site impact level 0 – Baseline conditions when no device-associated infrastructure or devices are onsite
SIL-1	Site impact level 1 – When device-associated infrastructure is onsite but no devices are installed onsite
SIL-2	Site impact level 2 – When device/s are installed onsite but not operational
SIL-3	Site impact level 3 – When device/s are installed onsite and operational
SMRU	Sea Mammal Research Unit
SNH	Scottish Natural Heritage
SQL	Structured Query Language

Acknowledgements

The European Marine Energy Centre (EMEC) wishes to thank the many contributors to this project, including the Steering Group, comprising members from Scottish Natural Heritage, Marine Scotland and Scottish Government. Particular mention should go to George Lees, Karen Hall, Jared Wilson and Ian Davies and the additional support provided through the EMEC Monitoring Advisory Group.

Particular thanks is given to Lindesay Scott-Hayward and Monique Mackenzie from the Centre for Research into Ecological and Environmental Modelling (CREEM, University of St Andrews), for their great contribution to the project in terms of the modelling methodology and results interpretation.

Further, special thanks is given to the wildlife observers without whose long-running and committed service to the observations programme, such a large and useful dataset would not have been compiled.

And finally, many thanks to former EMEC staff, who made substantial contributions to the project at various stages, in particular, Jennifer Norris, David Cowan and Christina Bristow.

This project was funded by Scottish Natural Heritage, Marine Scotland and EMEC.

1. INTRODUCTION

Understanding the environmental impacts that may arise from the siting and operation of marine renewable energy developments is crucial to the success of the wave and tidal energy industry. Understanding any constraints on its development is essential to assisting the industry's progress towards commercialisation. Recently, extensive research and effort has gone into furthering our understanding of potential issues and consequences of deploying such infrastructure in our oceans. However, several questions remain unanswered regarding the potential environmental impacts associated with such developments.

The key unknowns will, to some extent, vary depending upon location but some of the issues will be common to the tidal and/or the wave energy sectors as a whole, regardless of where the deployment is located. The following list outlines the key unknowns that apply to the industry currently, but it is important to realise that these are not the only potential risk areas and that the uncertainties extend beyond environmental matters:

- Collision – potential for physical interaction between marine wildlife and underwater moving parts of devices. This is a particular concern in relation to marine mammals and diving birds. An accurate potential rate of collision cannot be determined until further research has been undertaken into the extent of avoidance behaviour that may be employed by different species.
- Displacement – potential for the loss of habitat due to disturbance or barrier effects. This may be in the form of redistribution from an area or complete avoidance of an area.
- Noise emissions – potential for harmful effects on wildlife (particularly marine mammals and some fish species) from noise emitted underwater during the installation and operation of devices. It is important to understand whether the level or type of noise produced is likely to have any deleterious effects. The likely issues that arise if noise emissions are found to be of concern are displacement (hearing disruption) and/or physical harm (hearing impairment).

To begin to answer these questions, it is essential that data are gathered from the first devices deployed and operational in the sea so that early assessment can commence as to whether or not there are any harmful effects and, if so, the extent of such effects.

In addition to the key environmental issues, other matters such as navigational safety and the potential effects on leisure and commercial uses of the marine environment remain as areas of unknown impact. In terms of navigational safety, it is crucial that devices are safely marked and that the sea space is utilised in a safe manner. Safety is regarded as paramount; the main issues include marking devices in strong tides, under-keel clearance and safe co-operative use of the seas. Managing marine renewable activities in relation to other sea users is essential but the extent of the effects on leisure and commercial industries is still not fully understood. Inevitably, there will be overlap in the use of sea space between marine renewable deployments and established and future leisure and commercial activities, and consideration requires to be given to the potential commercial impact of limiting access to areas of the sea and/or making sea space navigationally difficult for commercial activities. For example, further research needs to be undertaken to understand whether such deployments affect the composition of commercial fisheries' landings by creating a 'stepping stone' habitat. It is crucial that developers establish and maintain ongoing liaison with a range of interested parties, including other sea users, to be able to safely and effectively manage activities in the interests of all sea users.

There is a regulatory need, under the Habitats Directive, to demonstrate that the installation and operation of Marine Energy Conversion Systems (MECS) has no significant effect on

site integrity, with respect to designated or proposed European sites, or Favourable Conservation Status, with respect to European Protected Species (EPS). An important part of this may be to determine whether the deployment of MECS is likely to have any significant impact on the abundance or distribution of marine wildlife in the vicinity of such devices[1]. This analytical study examines evidence for changes in the absolute abundance and distribution of key bird and marine mammal species at the European Marine Energy Centre (EMEC) in Orkney in a bid to help address some of the unknowns regarding the potential environmental effects of MECS. It is considered that the potential displacement of key wildlife species from their normal range of habitats is a critical factor which needs to be addressed in order for the marine renewable energy industry to progress (Langton *et al*., 2011).

It is recognised that assessing marine species' usage of particular near-shore areas is an extremely challenging task due to limited sample sizes, temporal/spatial variation in abundance and distribution, and calculating detection functions, in addition to the complexities of analysing vantage point data. Through a programme funded by Marine Scotland, Scottish Natural Heritage (SNH) and Highlands and Islands Enterprise (HIE), EMEC has collected shore-based wildlife observation data at its grid-connected tidal and wave energy test sites. In an effort to resolve industry-wide concerns regarding the potential environmental effects of MECS, SNH, Marine Scotland and EMEC have led in-depth analyses of these vantage point surface wildlife observation data. Included in the analyses is an assessment of the interannual and seasonal variations in abundance and distribution for seabird and marine mammal species at the Fall of Warness and Billia Croo, EMEC's tidal and wave energy test sites respectively. With particular regard to the operational status of devices being tested at the sites, the Wildlife Data Analysis Project aimed to produce prediction models which hindcast the likely effect that different site-wide operational statuses would potentially have on the abundance and distribution of species that commonly frequent the sites. The models were based on data collected at the Fall of Warness over ten years and at Billia Croo over six years. These long-running observation data were analysed in conjunction with device operational data (from real-sea testing at EMEC) which sets this study apart from those previously conducted on these datasets. It is important to note that, for each site, a site-wide operational status value has been used; this is the maximum device operational status occurring within the site at any one time and, therefore, neither berth-specific nor device-specific inferences can be made.

Through experience, EMEC has recognised the benefits of using consistent monitoring methodologies and equipment to monitor different devices under test, using the best available methods. The main beneficiaries of the project are: i) developers testing their devices at EMEC; ii) parties charged with advising on the likely environmental effects of such technologies; iii) decision makers determining applications for the construction and operation of MECS; and iv) parties involved in policy development and strategic planning of wave and tidal industries.

In summary, the Wildlife Data Analysis Project provides an insight into the potential displacement and/or redistribution of wildlife within a wave and tidal test site that can be associated with small scale MECS activity there, and appropriate data analysis methodologies. Further, the study considers whether there is a need for ongoing monitoring and, if so, recommends potential improvements to the data collection methodology.

[1] Although understanding abundance and distributional changes is important, consideration of population level impacts is likely to be crucial to assessing the significance of an impact.

1.1 Background to the European Marine Energy Centre

Established in 2003, Orkney-based EMEC is the first and only centre of its kind in the world to provide developers of both tidal and wave energy converters with purpose-built, grid-connected open-sea testing facilities. With 14 full-scale test berths, there have been more grid-connected marine energy converters deployed at EMEC than at any other site in the world, with developers attracted from around the globe. These developers use the facilities to prove what is achievable in some of the harshest marine environments, while in close proximity to sheltered waters and harbours.

EMEC's grid-connected tidal energy test site is situated just west of the island of Eday, lying in a narrow channel between the Westray Firth and Stronsay Firth (known as the Fall of Warness). The tidal passage was chosen for its high velocity marine currents which reach almost 4m/sec (7.8 knots) at spring tides. As tides flow from the North Atlantic Ocean to the North Sea, they quicken as they are funnelled through Orkney's northern islands. The EMEC site covers an area of approximately 9km^2 and offers seven test berths at depths ranging from 12m to 50m.

The EMEC grid-connected wave energy test site was constructed in 2003 and is ideally placed on the western edge of Orkney Mainland, at Billia Croo outside Stromness. Subjected to the powerful forces of the North Atlantic Ocean, it is an area with one of the highest wave energy potentials in Europe with an average significant wave height of 2-3m, but reaching extremes of up to 17m (the highest wave recorded by EMEC so far). The site covers an area of approximately 9km^2 and consists of five cabled test berths in up to 70m water depth (four at 50m, one deeper), located approximately 2km offshore and 0.5km apart. In addition to this, two near-shore berths are situated closer to the substation for shallow water projects.

EMEC is also host to scale test sites for both tidal and wave energy devices, which offer developers the opportunity to test their devices in real-sea test sites in the less challenging conditions of Shapinsay Sound and Scapa Flow respectively. These sites provide a more flexible sea space helping close the gap from tank testing, and acting as a stepping stone towards larger-scale projects.

The proximity of the EMEC test sites within the Orkney Islands is shown in Figure 1.1.1 below.

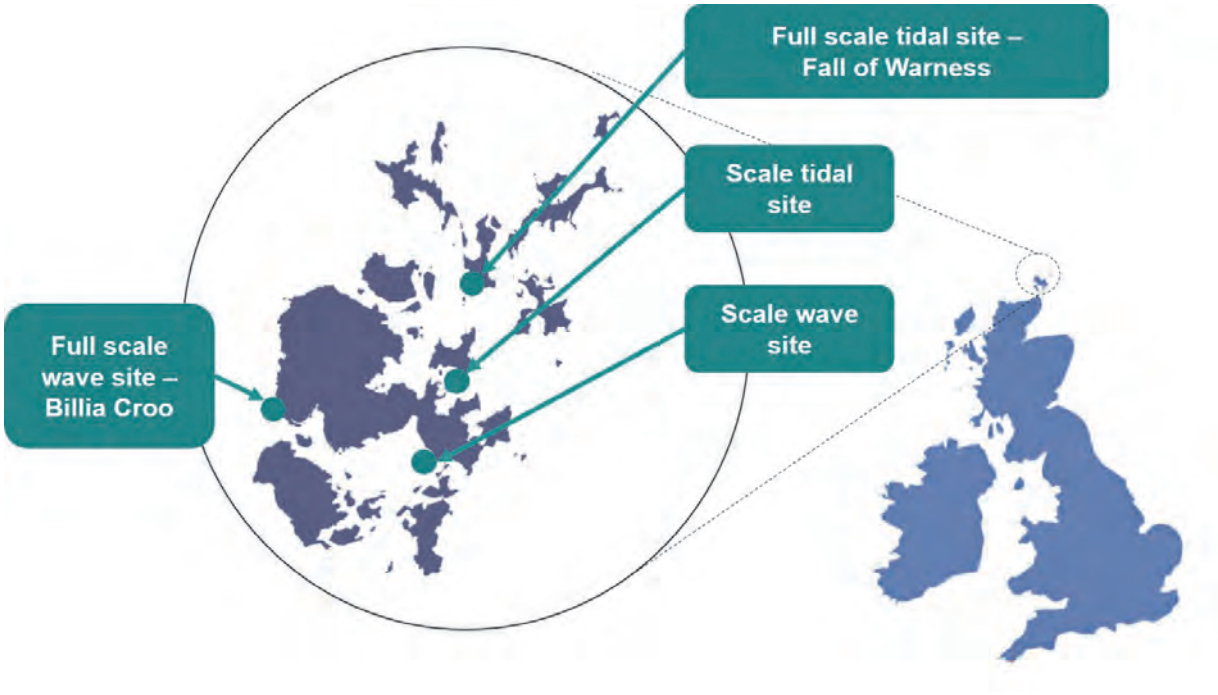

Figure 1.1.1. European Marine Energy Centre's test sites situated within the Orkney Islands

The Wildlife Observations Programme run at EMEC sits within a suite of environmental monitoring projects carried out at the test sites. The outputs of these projects are provided to EMEC developers to enable their inclusion in their Project Environmental Monitoring Plans (PEMPs), through which developers identify any environmental risks associated with their devices and propose suitable mitigation and monitoring methodologies that will be employed to address such risks. EMEC has managed the Wildlife Observations Programme since its outset and maintains a close working relationship with the wildlife observers whom it subcontracts to collect the data. Through this involvement with the day-to-day running of the programme, EMEC has gained a thorough understanding of the detailed workings of the data collection methods and practicalities of undertaking wildlife observations in the often challenging conditions of its sites. EMEC has also been closely involved with several studies conducted on the data since the programme's inception. This wealth of working knowledge and history of the data collection programme placed EMEC in a good position to perform a meaningful, comprehensive and tailored analysis of the datasets through the Wildlife Data Analysis Project.

1.2 Project scope

The aim of this project was to carry out a comprehensive analysis of all the data gathered at the EMEC full-scale test sites. For Billia Croo wave energy test site, data collection covered the period from March 2009 to March 2015, whereas observations at the Fall of Warness tidal energy test site were conducted for a longer period of time from July 2005 to March 2015.

The preliminary phase of the project was to select the appropriate supplier to provide the special input and training to enable the EMEC staff to conduct the necessary data preparation, statistical analysis and interpretation techniques. In liaison with the EMEC Monitoring Advisory Group (MAG), the Centre for Research into Ecological and Environmental Modelling (CREEM) at the University of St Andrews was identified as the most appropriate subcontractor to provide expertise and training support to EMEC.

The project scope established the following key research questions:

- *Is there a relationship between changes in abundance and distribution of key species with the presence or operation of test devices on site?*
- *How effectively can the models detect changes in species abundance and distribution due to an event such the installation of device-associated infrastructure or the installation/operation of devices?*
- *Are any effects detected that can be associated with the emplacement of marine renewable devices or related infrastructure, or their subsequent operation?*
- *Are any such effects significant when considered against other factors that influence wider populations?*

The scope of the project included implementing a data cleansing methodology for the entirety of each dataset. Annex 1 outlines the methodology employed and any assumptions that had to be applied during the extensive data cleansing exercise.

The data analysis phase was guided by advice provided by CREEM in line with the project scope. Initially, exploratory data analysis was conducted to enable an understanding of the behavioural patterns, both temporal and spatial, associated with each species. This initial analysis allowed more robust conclusions to be drawn from the outputs of the secondary analysis, particularly for any seasonal patterns and environmental influences on species abundance and distribution at each site. The second part of the analysis considered periods of device operation.

The two key relationships investigated were as follows:

- The effects of turbine presence on species abundance and distribution. Relationships between species abundance and variations in the status of turbine installation on site were considered (e.g. the effect of turbine associated infrastructure installation (moorings and foundations) was also considered).
- The effects of turbine operation on species abundance and distribution. The analysis considered relationships between abundance and turbine operation.

Statistical techniques, based on the MRSea package (Mackenzie *et al.*, 2013, Scott-Hayward *et al.*, 2013a) developed by CREEM and commissioned by Marine Scotland, were used to quantify any spatially-explicit change attributable to MECS testing on key seabird and marine mammal species at test site scale. The modelling procedure employed spatially-adaptive smoothing methods (e.g. CReSS/SALSA (Walker *et al.*, 2011, Mackenzie *et al.*, 2013)) which also took into account residual auto-correlation (via Generalised Estimating Equations (Hardin & Hilbe, 2002)). Environmental and grid-specific covariates were included in the modelling process to enable the most accurate predictions to be gained. The impact analysis considered impact type associated with the various development phases of a MECS' lifespan. For each phase, any differences in animal numbers or distribution were identified, with a particular focus on any redistribution within the test sites (in terms of changes in distribution between grid cells). Although redistribution might occur naturally over time for many species, the spatially-explicit attribute of the modelling assists in interpretation of observed change (Scott-Hayward *et al.*, 2014a).

The uncertainty inherent in the parameters estimated in such models was reflected in the geo-referenced confidence intervals (CIs) returned for each fitted surface and any differences across the surfaces. Outputs of this process were geo-referenced predictions accompanied by 95% CIs to reflect their uncertainty.

2. DATA COLLECTION METHODOLOGY

The Wildlife Data Analysis Project undertook analyses of the land-based wildlife observation data collected through the EMEC Wildlife Observations Programme. The analysis project ran in parallel with the observations programme using observations recorded to the end of March 2015. The observations programme continued beyond this date with funding ending in September 2015, although EMEC maintained the programme until December 2015 when it was discontinued for the foreseeable future. The potential for continuation and further funding of the observation programme partly depends upon the outcomes of the analysis project.

Observations at the Fall of Warness commenced in July 2005 and, over the 11-year duration of the programme, were funded through Marine Scotland, SNH and HIE. During this period, approximately 2300 shore-based surveys (typically each of four hours' duration) were conducted at the site.

The Billia Croo observations ran for a six-year period, from March 2009. The available funding allowed 1450 shore-based surveys (each of four hours' duration) to be implemented here.

As the project was established to ascertain whether there is evidence for displacement of wildlife that could be caused by the presence and/or operation of MECS devices, device operational data have been sought from the developers present at both of EMEC's grid-connected test sites. EMEC's unique position within the industry has facilitated the process of obtaining these crucial data. However, understandably, the operational data supplied by developers for use in this project are highly commercially sensitive and therefore site-wide operational statuses have been applied throughout the analyses. Using a site-wide operational status has led to no berth or device-specific inferences being drawn from the outputs of the analyses.

2.1 Survey methodology

Due to the differing nature of the two grid-connected test sites, the survey methodology applied varies between the sites. The following sections provide an overview of the survey methodology employed at each site. In-depth observation protocols for Fall of Warness and Billia Croo are available in Annex 2 and Annex 3, respectively.

2.1.1 Fall of Warness

The observation methodology employed at the Fall of Warness tidal energy test site was initially developed by local environmental consultants Aurora Environmental Ltd, who were commissioned by HIE in 2005. The methodology was developed with input from SMRU Ltd who also provided initial training for the wildlife observers. The robust survey methodology facilitated the recording of presence, distribution and behaviour data relating to seabirds and marine mammals present at the Fall of Warness. As the methodology was not documented in the initial years, EMEC and SMRU Ltd, in 2010, produced documentation to accurately record the methodology employed at the site[2].

Although the observation methodology remained largely unchanged throughout the duration of the programme, slight amendments were implemented over the years. The observation survey area was expanded to the north in August 2005 to accommodate the addition of new test berths outwith the original survey area. A formal watch rota, implemented in April 2011,

[2] The methodology, Fall of Warness Observation Methodology, is available to download from the Marine Scotland Interactive website, see http://www.gov.scot/Topics/marine/science/MSInteractive/Themes/EMEC-Wildlife

was relaxed in May 2011 due to the inherent inflexibility in the rota creating difficulties in securing a high watch attainment rate. Four observers carried out the surveys, two of whom were present consistently since observations commenced at the site in 2005. Over the programme's duration, additional observers were recruited to assist the original observers in achieving a high watch attainment rate. When any new observer commenced observations, they underwent a period of training with an original trained observer and parallel/dual watches were conducted to maintain comparable and consistent methods of data collection at the site. All the observers at the site had appropriate experience and training to undertake the observations.

The survey area viewed from the Fall of Warness vantage point, Ward Hill, was subdivided into a grid system for recording purposes. The matrix of 35 grid cells ranged in area between 0.304km^2 and 0.979km^2. The observers superimposed the grid on the survey area using geographical reference points to delineate the edges of grid cells or as markers within a grid cell. As Ward Hill is positioned 50m above sea level, the whole of the tidal test site was observable. The survey area visible from Ward Hill stretched beyond the test site (shown in blue in Figure 2.1.1), extending to Muckle Green Holm and Little Green Holm to the west and close to Seal Skerry in the north. Figure 2.1.2 shows the survey area relative to the island of Eday and the small uninhabited islands nearby.

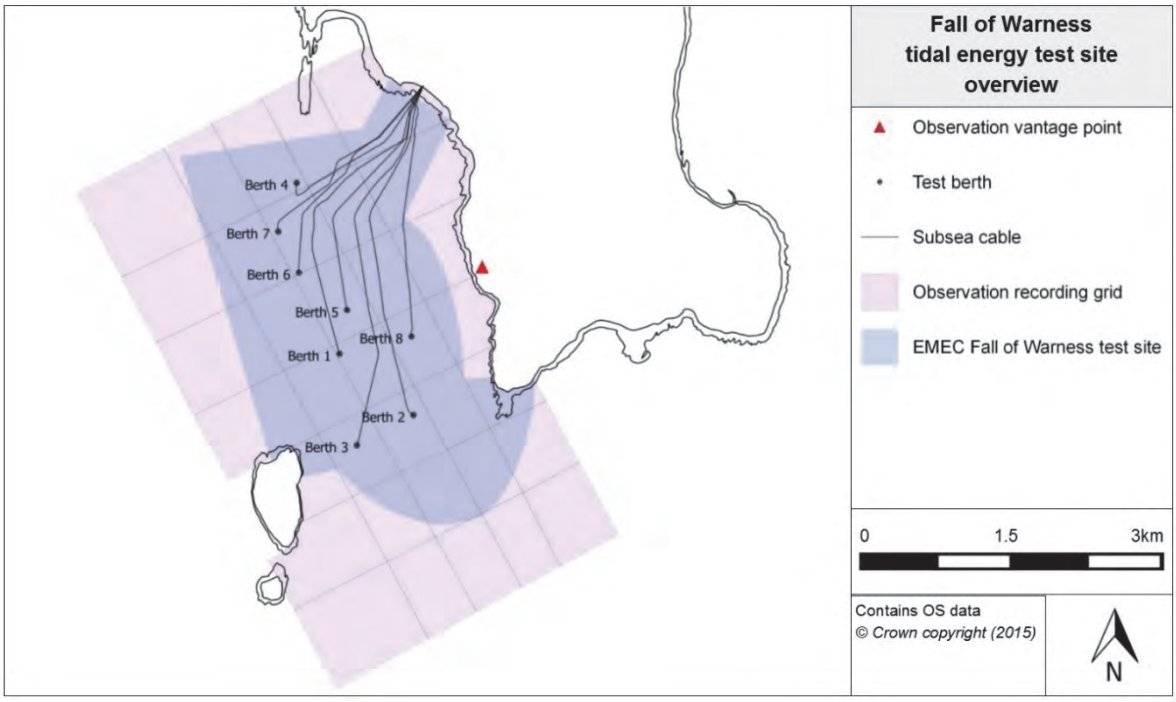

Figure 2.1.1. Survey grid and observation vantage point relative to the EMEC tidal energy test berths at Fall of Warness

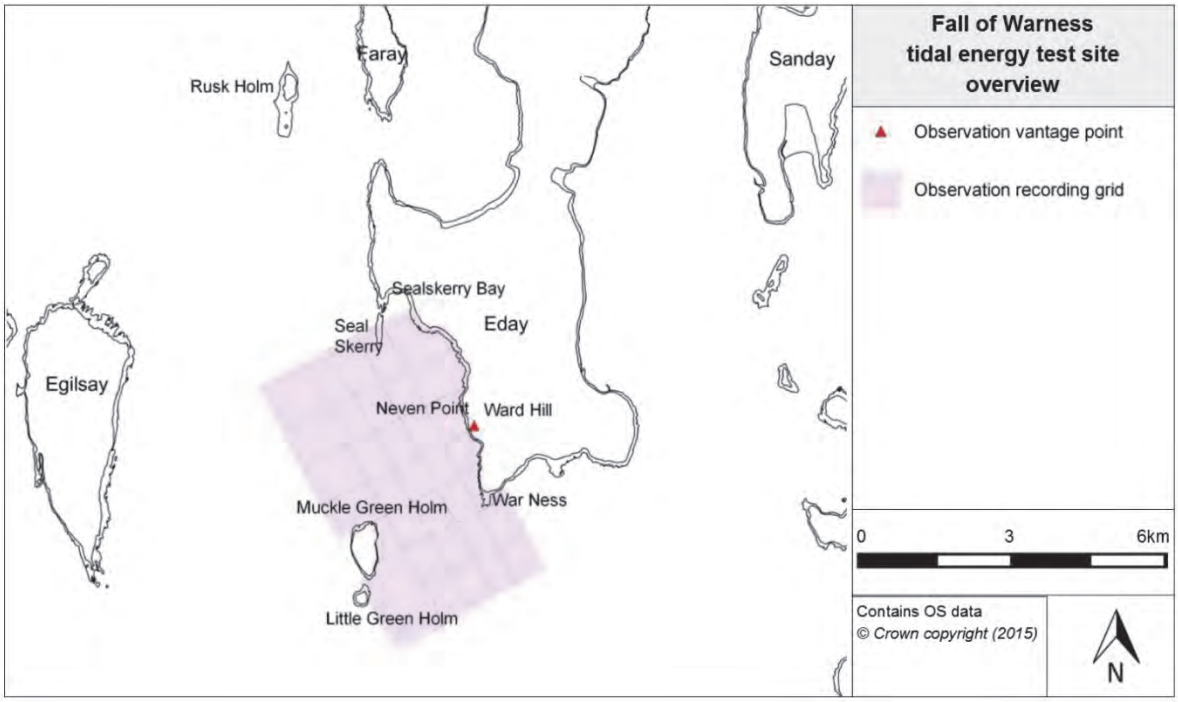

Figure 2.1.2. Observation survey area at Fall of Warness relative to the island of Eday

In order to analyse the sightings in a spatial context, the grid-based reference system had to be documented. Waggitt *et al*. (2014) developed a method for determining the coordinates of the centroid for each of the grid cells. Using these results as guidance alongside the original methodology set out for the programme (and in consultation with the observers), it was possible to map out the grid reference system in QGIS. Figure 2.1.3. presents this grid system with reference to the observers' vantage point and tidal energy testing berths.

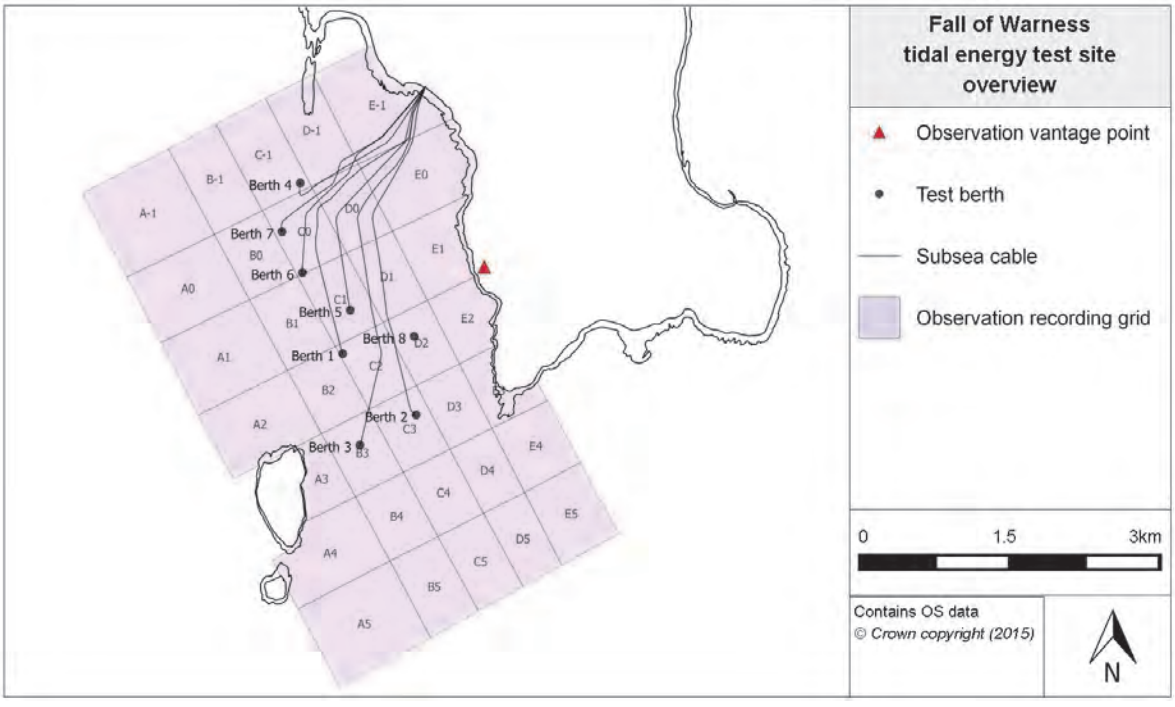

Figure 2.1.3. Fall of Warness observation grid relative to test berths

2.1.1.1 Observations

Wildlife sightings were recorded to species level using a telescope or binoculars and their positions within the predefined grid were recorded to provide locational information. The fully trained observers stationed on Ward Hill, Eday, carried out observations through regular scanning of the test site using a telescope (Opticron GS 815, set at 20x magnification) or a pair of standard binoculars. The telescope could be increased in magnification to 60x to aid species identification. Each scanning period lasted an hour with four sets of scans carried out on each watch. As the vantage point was positioned at an elevation of approximately 50m, this offered good visibility of the whole test site area.

The distance that the survey area extended away from the observer approximated to the sighting limit of the equipment, beyond which accurate identification of small cetaceans was not possible. The observers experienced difficulties in accurately identifying seals to species level at the perimeters of the survey area. Although bird observations were significantly reduced in the outer areas of the observation grid, accurate identification of bird species in these grid cells was constrained by the limits of the equipment due to the distance from the observation vantage point[3]. This has resulted in several bird categories which are not recorded to species level but, instead, are at family level.

2.1.1.2 Survey Effort

Data were collected for 20 hours per week, split over five four-hour watch periods (based on five working days per week). A watch typically lasted for a four-hour period and there was generally only one watch per day. Watches were carried out throughout the year during daylight hours, covering the period from 04:00hrs to 20:00hrs during summertime, and 09:00hrs to 15:00hrs in winter. On some occasions, two watches were performed on the same day in order to maintain a high attainment of watches in periods of bad weather. On rare occasions, watches were abandoned part-way through due to deterioration in weather conditions. A watch rota was designed annually in advance, to ensure relatively uniform coverage across diurnal and tidal cycles. This rota was adhered to as far as possible; however, attainment of watches in good environmental conditions was a priority.

As described above, the observers carried out regular scans of the survey area. It took approximately one hour to complete a single set of scans. This timing was designed to maximise the probability of sighting wildlife whilst minimising observer fatigue. A rest period was taken between each set of scans in order to further reduce observer fatigue, making it possible to complete four sets of scans per four-hour watch period.

Although the methodology set out the way in which the site should be surveyed, each observer adopted their own observation pattern. The observers at the Fall of Warness had observer-specific surveying patterns with the result that the observation grid was surveyed to varying extents and in a different order by each of the observers. Notably, the spatial extent of the observation patterns varied between observers, with some grid cells not being observed at all by certain observers (refer to Appendix 1 for further discussion regarding observer-specific surveying patterns). It was important for each observer-specific observation pattern to be recorded to account for the differing levels of observer effort applied to each grid cell during surveying. Information was obtained from each observer regarding the general pattern followed when carrying out observations (observer-specific patterns are provided in Appendix 1). The observer-specific observation patterns alongside grid cell area were taken into account in the analyses by applying an ‘areatime’ variable as a proxy for observer effort. Using an ‘areatime’ variable during the analyses has resulted in

[3] As discussed in more detail in Section 2.4, a limiting factor of these analyses was the lack of application of detection function/s. It is highly recommended that no further analyses are conducted on these data until detection function/s have been established for the site.

observations in grid cells where there was reduced observer effort (e.g. grid cells with larger area) to be weighted higher during the analyses compared to observations made in other grid cells that are observed more regularly (e.g. grid cells with smaller area).

2.1.1.3 Data Recording

The methodology used by the observers to collect the data is outlined in the Fall of Warness Observation Methodology (attached in Annex 2). Few variations in the collection method used at the site occurred over the programme's duration, the greatest changes happening in the first couple of years as the observers adapted the protocol in line with their experiences.

For marine mammals and other species (e.g. basking shark and European otter), observations were only recorded if the individual or group was sighted in or on the surface of the sea. Details of any hauled out species were not recorded in a consistent manner and, therefore, any such recordings were excluded from the analyses. Birds were recorded as sightings if they were on the water or hovering directly above the surface (limited to within a few metres of the water surface). Any birds flying higher than this, or birds that were clearly transiting through the survey area, were not recorded. Diving birds were recorded if they were seen penetrating the water surface or returning to the surface subsequent to the dive. Details recorded included: species, grid cell, number of individuals in the group (single species), and any distinct behavioural details (e.g. whether the individual/group was feeding, diving, swimming, stationary). Information regarding the number of different species in a group was not recorded and other species within the group were instead recorded as separate species sightings. It is worth noting that the observers often had difficulty discriminating between grey and harbour seals, great cormorants and European shags, gull species, auk species and different cetaceans.

The details of any sightings made were recorded on paper field forms by the observer, to be later transcribed into a Microsoft Excel spreadsheet template. In addition to sighting data, the observer also recorded information relating to survey effort (e.g. date, watch start time, watch end time) and details of any vessels observed in the survey area during the watch. Environmental conditions were also recorded at the end of each watch (approximately every hour); key parameters recorded include sea state, tidal conditions, wind strength, visibility, glare extent and precipitation. A completed spreadsheet was submitted to EMEC each month.

At the recording stage, quality control for the Fall of Warness data was limited as no filtering controls were set for the Excel template. Once EMEC received the data, quality control was in the form of scanning the data to identify anomalies. If mistakes and misnomers were found at this stage, a query was sent to the observer to check if an error had occurred at the inputting stage or if the misnomer was real. Annex 1 provides an in-depth look at the data acquisition and database integration process once the data was received by EMEC.

2.1.2 Billia Croo

EMEC and SMRU Ltd developed a robust survey method for use at the Billia Croo wave energy test site to facilitate recording the presence, distribution and behaviour of marine mammals and seabirds. In addition to documenting the methodology, SMRU Ltd provided initial training for the wildlife observers who remained constant throughout the duration of the programme.

As the survey area viewed from the Billia Croo vantage point, Black Craig, lacks natural features, a grid-based recording system, similar to that employed at other EMEC sites, was deemed unsuitable for use at this particular site. Instead, the survey area was defined as a hemispherical shape extending offshore from the observation vantage point (as can be seen

in Figure 2.1.4). From Black Craig, positioned 110m above sea level, the majority of the wave test site was observable, with limited views towards the inshore berths[4]. The survey area visible from Black Craig stretched beyond the test site (shown in blue in Figure 2.1.4), extending to approximately 5km from the shore. Figure 2.1.5 provides an overview of the survey area relative to locations along Mainland Orkney.

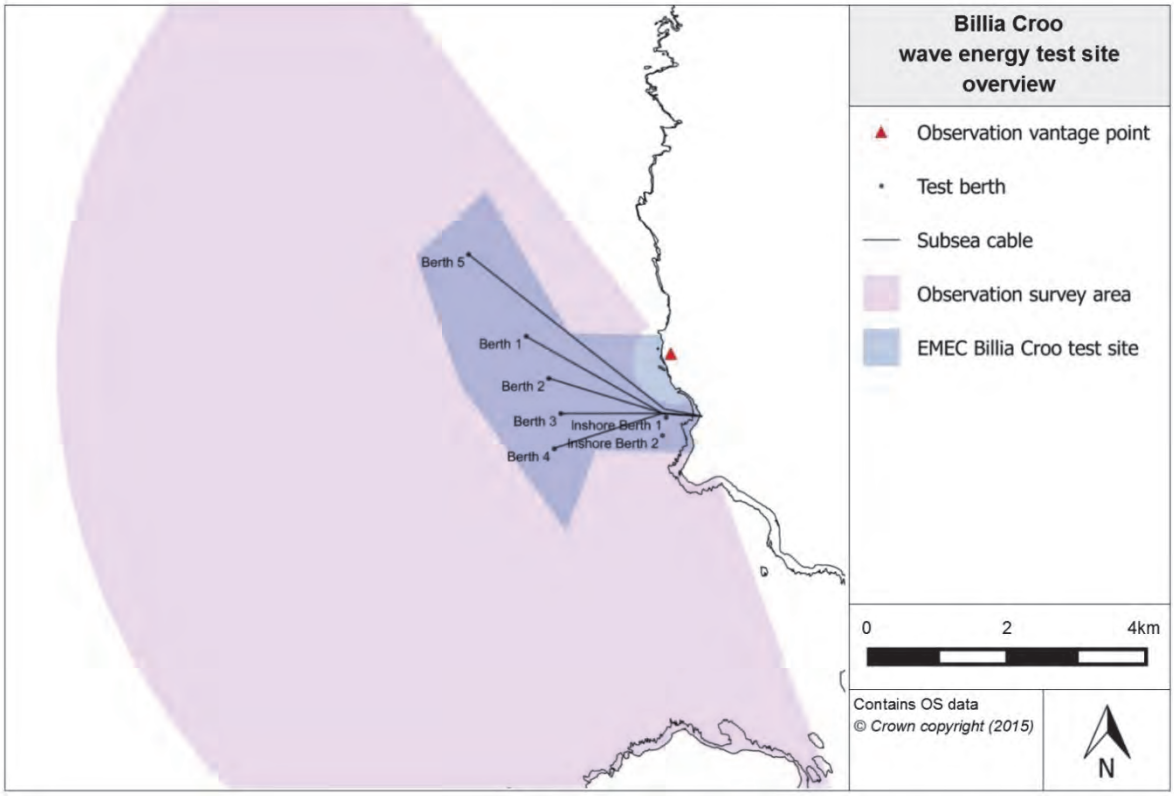

Figure 2.1.4. Wildlife observation survey area relative to leased area for EMEC wave test site

[4] Although according to the Billia Croo observation methodology, the view of the closer inshore berths is limited, observations have been recorded in this region of the survey area.

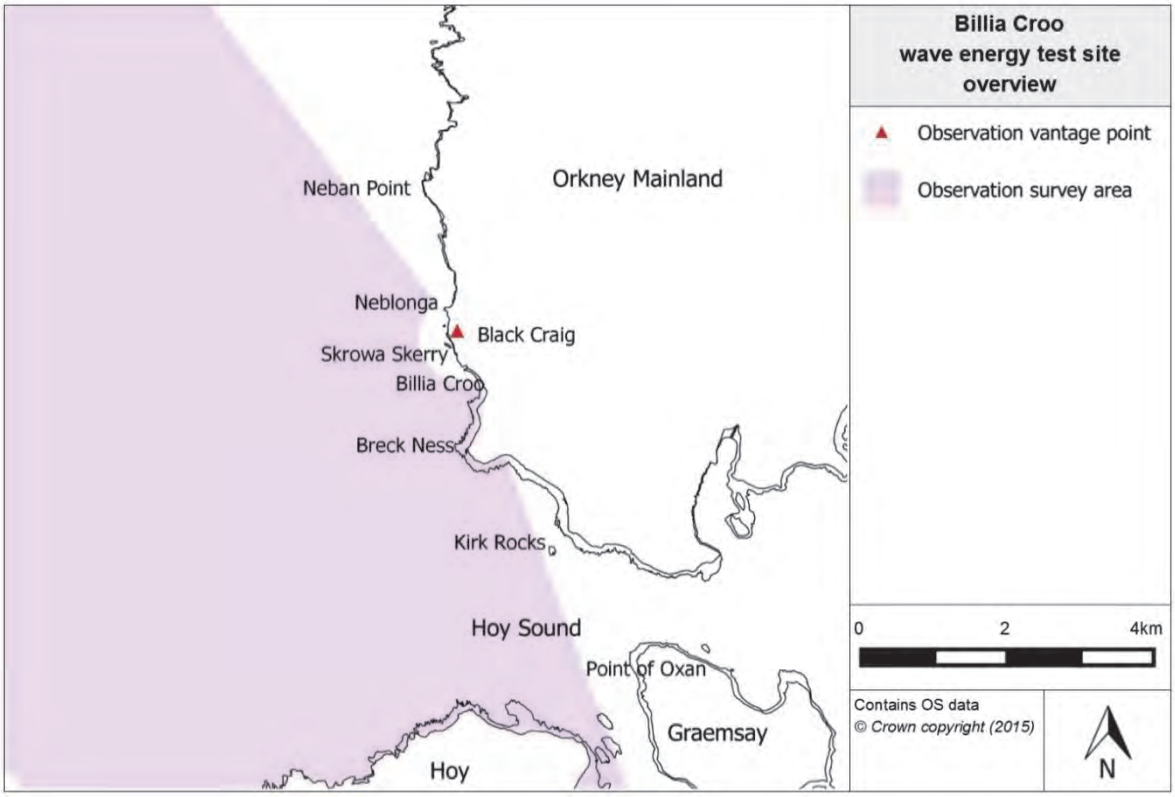

Figure 2.1.5. Observation survey area at Billia Croo relative to Mainland Orkney

Wildlife sightings were recorded to species level using high powered binoculars ('Big Eyes') and horizontal and declination angles from the viewing tripod were recorded to provide locational information. These angles could later be converted into geographical coordinates, for use in the analyses. Following the establishment of the methodology and subsequent training of the wildlife observers, a boat-based calibration was undertaken to validate the angle measurements (refer to SMRU Ltd, 2010, for further information regarding the methodology employed during this exercise).

2.1.2.1 Observations

Fully trained observers carried out the observations from an ex-coastguard lookout station situated on a cliff-top, approximately 110m above sea level, overlooking the site. Observations were made using a pair of 25x power binoculars (25x100 Monk Leviathan Binoculars), known as 'Big Eyes', as seen in Figure 2.1.6. The 'Big Eyes' were mounted on a tripod with horizontal and declination angle boards. The location of sightings was quantified by recording the horizontal and declination angles displayed on the binoculars' angle board and inclinometer to allow estimates of the geographical locations (spatial coordinates) of wildlife sightings to be made. The horizontal and declination angles were checked each day and realigned if necessary using pre-defined reference points. The angles were corrected using equations for the relationship between the measured and actual angles (obtained during a boat-based calibration exercise), following which the corrected angles had standard trigonometry applied to obtain a geographical location. This methodology is outlined in a report produced by SMRU Ltd (2010).

As mentioned, the survey area extended to about 5km from the vantage point (this approximated to the equipment's sighting limit for accurate identification of small cetaceans from a cliff-top at the elevation of the vantage point). The observers rarely observed seal or bird species at the perimeters of the survey area. The sighting equipment used at Billia Croo

was more powerful than that used at Fall of Warness. However, where observations were constrained by sighting equipment limitations and species-level identification was not possible, the observers opted to record species to family-level. As previously mentioned for the Fall of Warness, detection functions were not used in the analyses but the application of detection functions would be highly recommended for any further analyses of the data (refer to Section 2.4 for further discussion).

Figure 2.1.6. 25x100 Monk Leviathan Binoculars used at Billia Croo (Credit: Orkney Photographic)

Figure 2.1.7 below shows the observation area with respect to the EMEC test berths and the observation equipment used. The observation area was surveyed in a consistent manner from left to right at a series of distances from land, ensuring that the whole study area was covered. The area was divided into three sub-areas (Near, Mid, and Far), as seen in Figure 2.1.8; the Near sweep (Sweep 1) extends to 800m, the Mid sweep (Sweep 2) is 800-1500m and the Far sweep (Sweep 3) is 1500m and beyond.

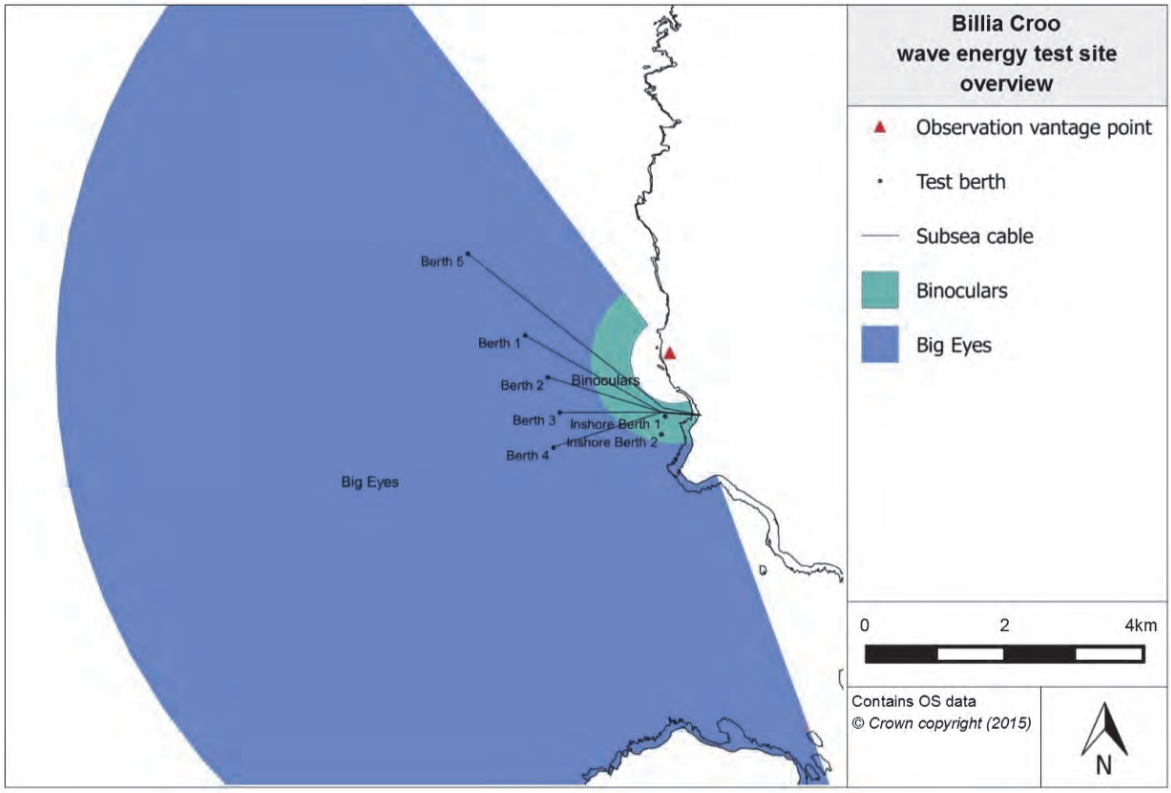

Figure 2.1.7. Observation survey area with relative viewing extents for sighting equipment at EMEC's wave test site, Billia Croo

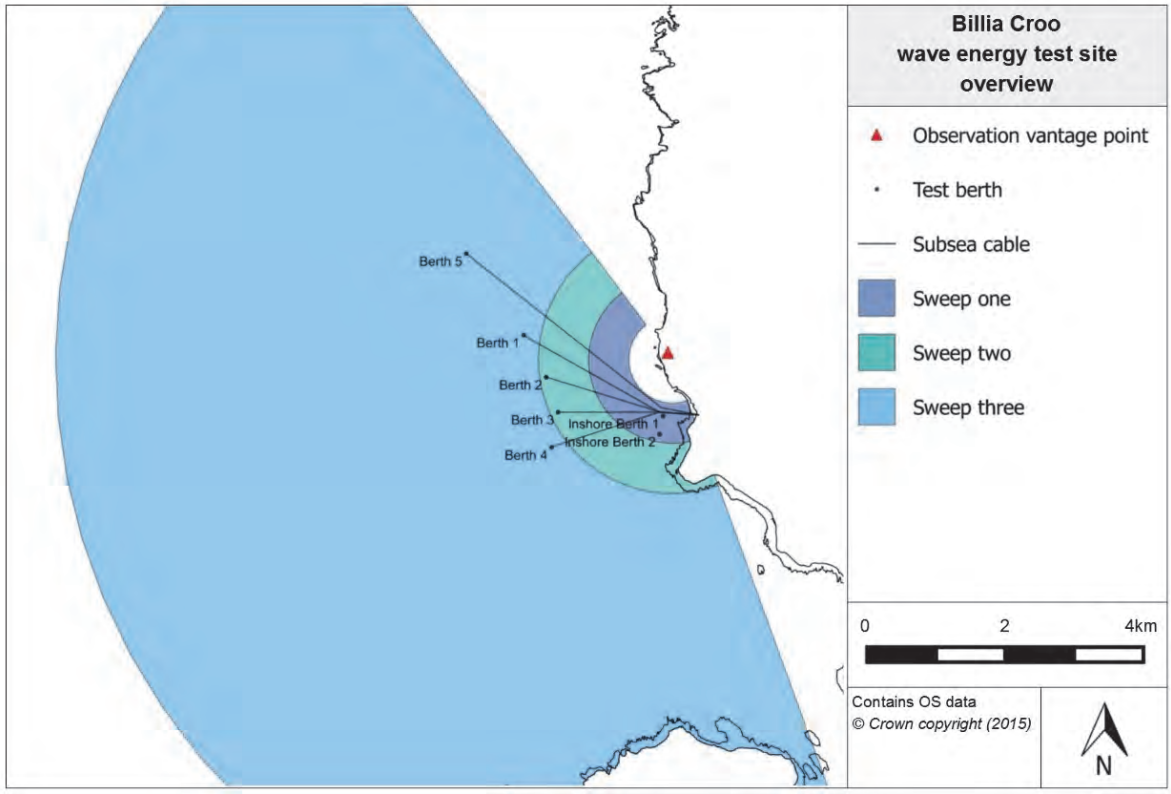

Figure 2.1.8. Observation survey area with sweep locations and observation vantage point relative to EMEC wave energy test berths at Billia Croo

To aid the analyses, a radial grid was created (Figure 2.1.9 and Figure 2.1.10). For the purposes of the analyses, each sighting was appointed a grid cell number corresponding to the geographical coordinates obtained. It should be noted that the size of the grid cells increases outwards to account for the margin of error built into the system when the observers record the horizontal/declination angle (to the nearest degree).

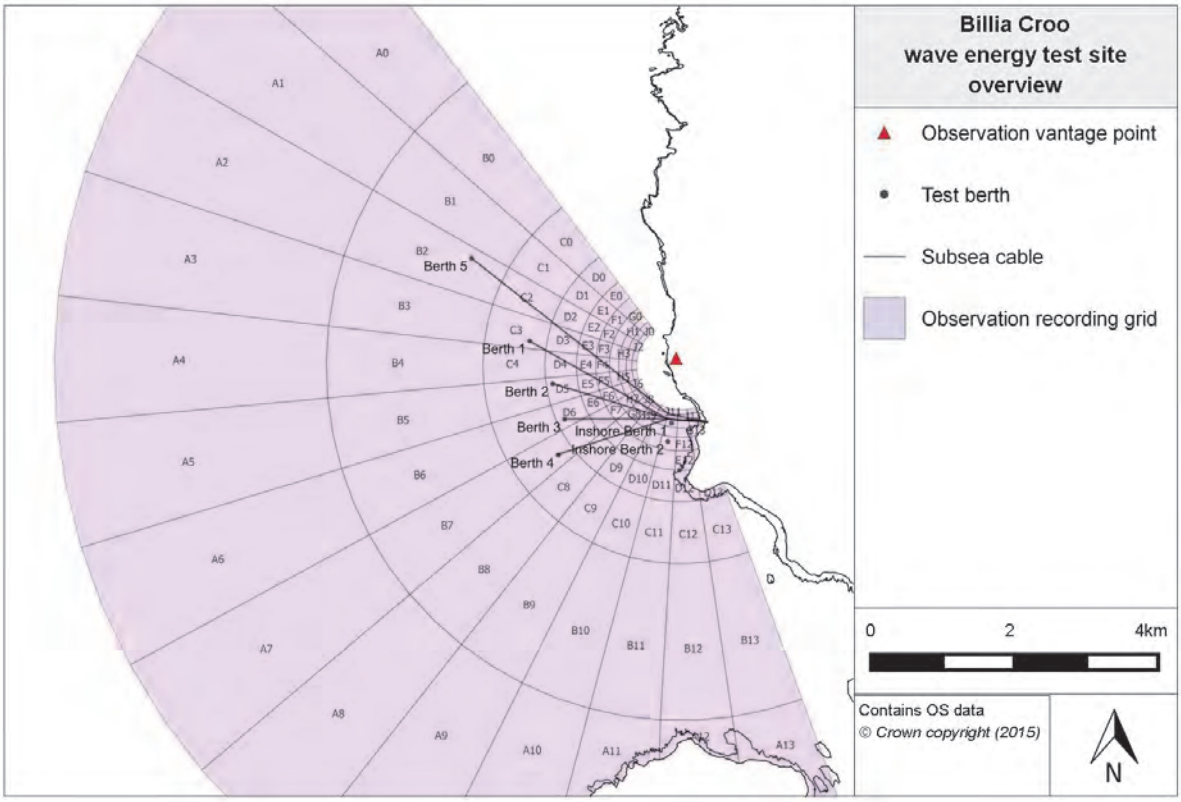

Figure 2.1.9. Billia Croo radial observation grid relative to test berths

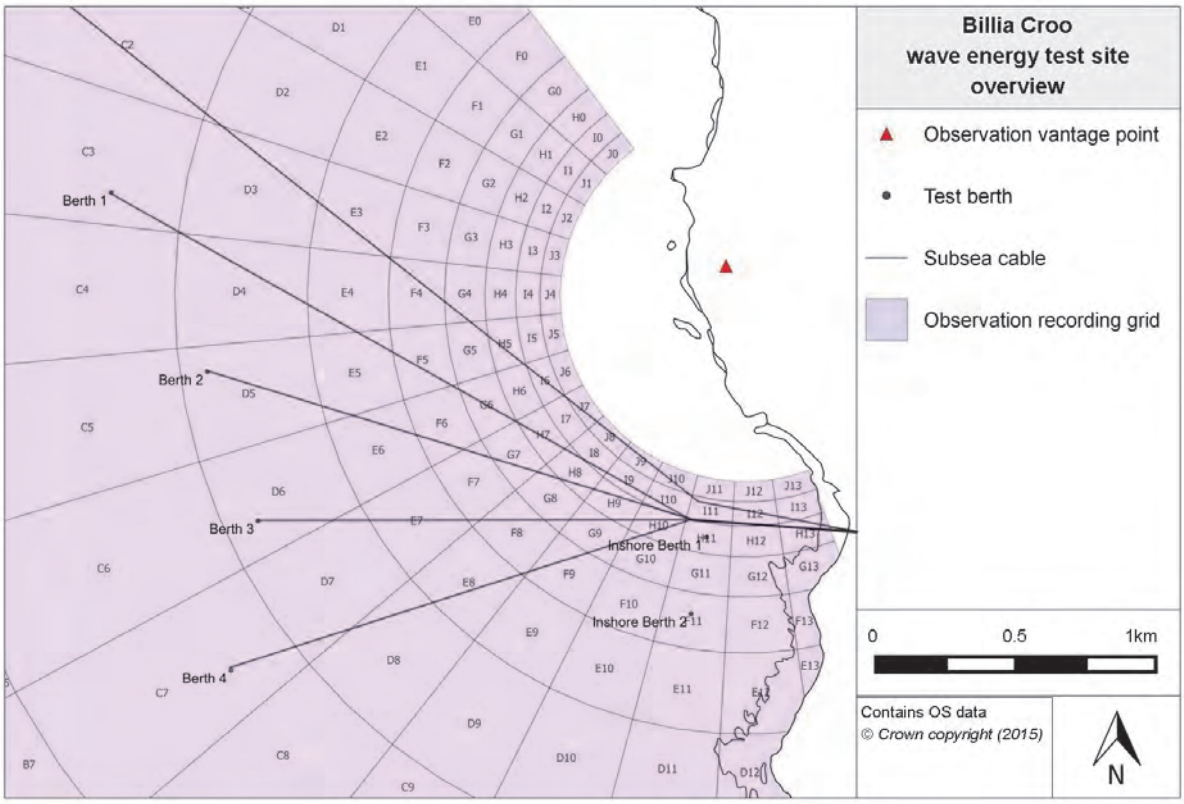

Figure 2.1.10. Inner region of Billia Croo radial observation grid relative to test berths

Further, although the observation methodology (updated version available in Annex 3) indicates that the survey area at Billia Croo should be limited to 5km from the vantage point, some sightings recorded by the observers were located beyond 5km. All sightings were included in the analyses provided that they occurred within the grid which stretched to 8.5km from the vantage point.

2.1.2.2 Survey Effort

Data were collected at Billia Croo for 20 hours per week, split over five four-hour watch periods (based on five working days per week). A watch typically lasted for a four-hour period and there was generally only one watch per day. Watches were carried out throughout the year during daylight hours, covering the period from 04:00hrs to 20:00hrs during summertime, and 09:00hrs to 15:00hrs in winter. It was sometimes necessary, for two watches to be performed on the same day in order to maintain a high attainment of watches in periods of bad weather. On rare occasions, a watch was abandoned part-way through due to deterioration in weather conditions. A watch rota was designed annually in advance, to ensure relatively uniform coverage across diurnal and tidal cycles. This rota was adhered to as far as possible; however, attainment of watches in good environmental conditions was a priority.

The observation area was subdivided into separate zones denoting the area covered during each sweep (Figure 2.1.8). The observers carried out regular scans of the survey area. It took approximately 40 minutes to complete a single sweep of the survey area, although this varied by observer and sweep. Although sweeps varied in duration, in general, between three and six sweeps were conducted during a four-hour period. This timing was designed to maximise the probability of sighting wildlife whilst minimising observer fatigue. A rest period of 10 minutes was taken between scans in order to further reduce observer fatigue. At the start and end of each sweep, the environmental conditions were recorded in a format similar to that used for the Fall of Warness.

The two observers carrying out observations at Black Craig were constant throughout the duration of the programme at Billia Croo. Both observers were sufficiently qualified and experienced in carrying out observation work and underwent site-specific training provided by SMRU Ltd in 2009. To ensure the methodology was applied consistently by the two observers, dual watches were conducted periodically throughout the first year of observations.

Variations in observation patterns employed by the observers were similar to those experienced at the Fall of Warness; the survey area varied between the two observers with one surveying further north and the other surveying further south. Although the extent of each sweep was outlined in the methodology, the extents of the sweeps also varied slightly between the observers, with one observer delineating Sweep Two as stretching further out. As a radial grid was superimposed on the site (Figure 2.1.9 and Figure 2.1.10), a proxy for observer effort could be gained from calculating the observer-specific sweep area. The extent of the two observers' sweeps varied; further information regarding this is provided in Appendix 1. The observer-specific sweep area was combined with sweep duration to calculate an 'areatime' variable for each sweep conducted at the site for each observer which was subsequently used as a proxy for observer effort throughout the analyses. Appendix 1 provides a discussion on how observer effort has been accounted for during the analyses.

2.1.2.3 Data Recording

The methodology used by the observers to collect the data is outlined in the Billia Croo Observation Methodology (updated version available in Annex 3). There were few variations in the collection method used at the site throughout the programme's duration, the greatest changes occurring in the first couple of years.

Similar to the Fall of Warness data recording method, marine mammals' and other species' (e.g. basking shark and European otter) observations were only recorded if the individual or group was sighted in or on the surface of the sea and details of any hauled out species were not recorded. Again, birds were only recorded as sightings if they were on the water or hovering directly above the surface (limited to within a few metres of the water surface). Any birds flying higher than this, or birds that were clearly transiting through the survey area, were not recorded. Seabirds involved in feeding activities such as diving were also recorded. Details recorded included: species, number of different species in the group, horizontal and declination angle (spatial information), number of individuals in the group (per species), and any distinct behavioural details (e.g. whether the individual/group is feeding, diving, swimming, stationary). The observers often had problems discriminating certain species; if this was the case, the observers opted to record the sighting to family-level, often providing a note of clarification. If this was not possible, the observers recorded an additional species category which captured undefined sightings.

The details of any sightings made were recorded on paper field forms by the observer, to be later transcribed into a Microsoft Access database, designed by SMRU Ltd when creating the observation methodology. In addition to sighting data, the observer also recorded information relating to survey effort (e.g. date, sweep start time, sweep end time), environmental conditions (tide state, meteorological conditions), and details of any vessels observed in the survey area during the watch. An updated database was submitted to EMEC each month. Although the observers submitted a database for each month throughout the year, the database was not a monthly dataset but an aggregated database which added information to the data for each previous month of that observation year cumulatively.

At the recording stage, quality control for the Billia Croo data was slightly superior to that pertaining to the tidal test site with the Access database using some internal data structures to cross-reference the data tables in the form of 'lookup tables'. This generated a more consistent data source than the simpler systems in use at the Fall of Warness site. Once EMEC received the data, quality control was limited to scanning the data to identify anomalies. If mistakes and misnomers were found at this stage, a query was sent to the observer to check if an error had occurred at the inputting stage or if the misnomer was real. Further information on the data acquisition and integration process are supplied in Annex 1.

2.2 Data cleansing

The Wildlife Observations Programme datasets held by EMEC (and made available to the public through Marine Scotland Interactive[5]) had minimal quality control and data cleansing applied prior to storage. It was recognised at the outset of the project that, during the various analyses previously undertaken on the datasets, subsets of the data existed in a cleansed format. It was therefore necessary to conduct a review of the data cleansing routines applied previously to determine whether any such routines would be appropriate to apply to the dataset in its entirety. Subsequently, it was concluded that none of the data cleansing routines applied previously were deemed suitable for application across the entirety of each dataset. Instead, it was necessary to implement new data cleansing methodologies.

To aid data cleansing, organisation and future data analyses, the data collected by the observers were transposed from Microsoft Excel spreadsheets and Microsoft Access databases to a 'master database'. Aggregating the wildlife data into a single database schema allowed analyses to be conducted on the entire dataset for each site which was vital to the success of the Wildlife Data Analysis Project, and also provided the opportunity to extract and cross-reference information from other datasets of relevance to the wildlife data collected from the EMEC test sites. In order to allow assimilation between the different datasets, EMEC developed an SQL 'master database' containing all data collected at its sites (e.g. meteorological information, AIS, tidal, wave and acoustic data) alongside the data collected through the Wildlife Observations Programme. To achieve this integration with the EMEC master database, all the monthly Excel spreadsheets from the Fall of Warness and yearly cumulative Access databases from Billia Croo required aggregation. This involved a large amount of data cleansing and rationalisation of inputs to ensure that the dataset was in a single coherent structure and that appropriate outputs could be achieved.

Annex 1 provides an in-depth report on the data handling methodology used by the observers; how the data were integrated within the EMEC SQL database; the data cleansing process employed; and any subsequent assumptions applied to the data. The initial section of Annex 1 comprises an overview of the data received by EMEC from the wildlife observers, providing a description of each of the elements in the raw data. Annex 1 then summarises how the data were integrated into the EMEC SQL master database and describes the mapping used for each of the data elements. Before the wildlife data could be input into the master database, a certain level of rationalisation and data cleansing had to be performed. However, the majority of the data cleansing occurred after the integration process, which allowed all-encompassing procedures to be performed. This process is described for each of the elements contained within the main schemas of the 'WildlifeObservations' SQL database.

Any subsequent analysis of the data within the SQL database must take into account any assumptions applied to the data during the data cleansing process. An overview of the

[5] http://www.gov.scot/Topics/marine/science/MSInteractive/Themes/EMEC-Wildlife

assumptions made is provided in Annex 1, together with a comprehensive list of the key outputs from the process.

2.3 Device operational data

EMEC occupies a unique position within the wave and tidal energy industries. Although it has links with a range of different wave and tidal energy device developers, as well as academic institutions and regulatory bodies, the nature of EMEC's business means that it is, and must remain, independent. This enables EMEC to play an independent and objective role in the monitoring of potential device effects or impacts on the receiving environment, which is particularly important for the developing marine energy industries, where such effects/impacts are as yet unknown. EMEC is also in a position to present information that may be commercially sensitive in an anonymous context, thus increasing the likelihood of developers being willing to share their device-specific data in a collective yet anonymised fashion.

The cooperation of developers who were testing their devices at EMEC's sites was essential and, in recognition that commercial confidentiality had to be respected, EMEC received and anonymised the operational data. Details of all site activities, including device installation activity/operational status, scientific surveys/deployments and any other pre-installation or maintenance activities, over the period for which the data were being analysed, were required. This included historical data dating back to when developers were first active on the site, for example, covering preliminary scientific surveys and device or foundation installation.

As the project was established to ascertain whether there was evidence for any displacement effect on wildlife that could be attributable to the presence and/or operation of MECS devices, the wildlife observations data were analysed with respect to device operational data obtained from the developers present at each of EMEC's grid-connected test sites. As there are multiple devices being tested at both of EMEC's test sites, the sites are not in a single development phase at any one time. The wildlife observations data were analysed with respect to the overall status of each test site, taking account of the various operational statuses pertaining to the different devices. The latter information is sought from developers through the licensing authority, Marine Scotland.

A method of anonymising the data during the analysis and for subsequent analytical outputs was applied, by assigning the highest operational status occurring at the time of the sighting, across the whole site. Each site had a site impact level assigned to it for each wildlife observation. The site-wide impact level corresponded to the maximum level of potential device impact occurring at that time, regardless of the number of different potential device impact levels recorded. Table 2.3.1 below summarises the various site-wide operational statuses (site impact levels). As can be seen in Table 2.3.1, operational status was categorised as: no infrastructure and device offsite (baseline conditions) (SIL-0); infrastructure only (this includes foundations and moorings) (SIL-1); device onsite (SIL-2); and device onsite and operational (SIL-3). Also provided was information on any scientific deployments at the site, the location, date/time, instrumentation and any associated buoyage.

Table 2.3.1. Site operational statuses

Site-wide Impact Level	Site Impact Level Shorthand	Operational Status Description
0	SIL-0	No devices onsite and no infrastructure installed (baseline conditions)
1	SIL-1	Infrastructure (foundations/moorings) installed
2	SIL-2	Device/s onsite but not operational
3	SIL-3	Device/s onsite and operational

This method of anonymising the data resulted in the maximum site operational status not including information on: the number of devices of that status, which devices were operating at that status level, the location of any device (i.e. berth position), or device type. Although the theoretical impact level was assigned across the whole site, it is useful to know for the predictions that the grid cells which contain test berths tend to be towards the centre of the study region (grid cells with reference letters B-D).

The outputs of the analyses were limited by the extent of anonymity required as only a site-wide status was used and no defined effects could be associated with a single berth; due to the coarse scale of the grid used, particularly at the Fall of Warness, making any further inferences could prove erroneous. The fact that predictions were only able to be calculated at a site-wide impact level meant that, in some cases, a change in species density or abundance may appear to be location-specific (and therefore able to be associated with a single testing berth). However, it is important to note that, due to the site-wide nature of the operational data used in the analysis, this inference (or any inference at berth-specific level) cannot be drawn from the data.

For the project's duration, all developers[6] who occupied a berth at either of the EMEC full-scale test sites, Fall of Warness or Billia Croo, were included in the project.

2.4 Detection functions

It was recognised that, in order to generate accurate figures of species abundance and distribution across the site, a suitable detection function should be applied. This would allow the observed counts to be corrected for imperfect detection using distance sampling methods (Buckland *et al*., 2001). Although distance from the observer would tend to be the dominant factor taken into account in detection functions (as the further the wildlife were from the observer, the less likely they were to be seen), due to the complex nature of the high energy environment in which the test sites are situated, it was also important to consider environmental variables. For instance, detectability may also be affected by sea surface roughness and glare, with increased roughness and surface glare reducing the likelihood of detection from the shore.

Unfortunately, for vantage point data such as those gathered in the course of this wildlife data analysis project, the estimation of a detection function was confounded by the complexity of the distribution of animals (uniformity from a cliff top vantage point being assumed but not realistic). At the outset of the project, it was planned to use data acquired through boat-based surveys carried out by the RESPONSE project (Waggitt *et al*., 2014), other on- and off-site projects (e.g. Hebridean Marine Energy Futures) and potentially further

[6] Information regarding developers that have been testing at EMEC throughout the duration of the Wildlife Observations Programme can be accessed via http://www.emec.org.uk/about-us/our-tidal-clients/ and http://www.emec.org.uk/about-us/wave-clients/.

calibration surveys completed during the duration of the project (i.e. East Scotland Strategic Survey for Scottish Government). However, it was found that these surveys/projects did not obtain sufficient sample sizes to assist in detection function estimation for the sites. Due to this issue and limited project timescale and funding, it proved not to be feasible to develop such detection functions.

Therefore, for this project, the observed counts were not corrected for imperfect detection with distance from the vantage point, and instead assume a constant detection function during the study period and across the site. All estimates are relative rather than absolute.

2.5 Effort inclusion

As the wildlife observations only recorded species sightings (presence only data), there was a requirement to include the search effort used to gather the data. For example, if the study area was surveyed once per hour but a sighting was only noted in one grid cell, it was assumed that no animals were sighted in the remaining grid cells during that hour.

For the Fall of Warness, this procedure was carried out by creating a full grid of data for each watch period (lasting one hour). A grid of 35 empty cells for each hour of surveying was thus generated. As the observers surveyed the sites to varying extents (refer to Section 2.1.1.2 and 2.1.2.2), it was necessary to apply the observer-specific observation patterns when creating the grid. This resulted in the range of cells for a sighting being different between the different observers. As there were no actual observation data in the gridded data (just environmental covariate information), the relevant sighting information was then merged. As could be expected, a significant number of the grid cells had no sightings recorded during a watch; these were applied a SpeciesCode 'XX' and Number '0'[7].

For the Billia Croo data, effort was included by calculating the number of grid cells in each sweep using the superimposed grid outlined in Figure 2.1.9 and Figure 2.1.10. To be able to create the gridded data for each of the sweeps, it had to be assumed that the observers placed all their effort on looking only at the area defined within that sweep and not surveying areas outside of the sweep boundaries. This assumption led to many observations that fall outwith the sweep (specified by the observer as being conducted) being removed from the analysis. Similar to the Fall of Warness, a significant number of the grid cells were found to have no sightings recorded during each sweep and therefore these were applied a SpeciesCode 'XX' and Number '0'.

[7] 'SpeciesCode' is a code used to identify each species (this includes codes for sightings where the species is inconclusive and instead the family, etc. is recorded). 'Number' is the number of individuals within the group of that species.

3. STATISTICAL ANALYSIS METHODOLOGY

3.1 Species selection

Ten species or groups of species, selected on the basis of abundance at the sites and most likely to be potentially sensitive to MECS (Furness *et al*., 2012), underwent modelling for each of the survey sites. Table 3.1.1 and Table 3.1.2 below outline those species/groups selected for analysis at Fall of Warness and Billia Croo, respectively.

Table 3.1.1. Species present at the Fall of Warness tidal test site selected for analysis

Fall of Warness Selected Species	
Species/Group Name	Species
Black guillemot	Black guillemot
Common guillemot	Common guillemot
Razorbill	Razorbill
Divers	Great northern diver, red-throated diver
Shags and cormorants	Unidentified *Phalacrocorax*, European shag, great cormorant
Auks	Black guillemot, common guillemot, little auk, Atlantic puffin, razorbill, unidentified auk species
Ducks and geese	Eider duck, long-tailed duck, red-breasted merganser, common goldeneye, black scoter, common scoter, goosander
Seals	Unidentified seal species, harbour seal, grey seal
Harbour seal	Harbour seal
Cetaceans	Harbour porpoise, minke whale, Risso's dolphin, killer whale, unidentified cetacean species, white-beaked dolphin, white-sided dolphin, common dolphin

Table 3.1.2. Species present at the Billia Croo wave test site selected for analysis

Billia Croo Selected Species	
Species/Group Name	Species
Common guillemot	Common guillemot
Black guillemot	Black guillemot
Atlantic puffin	Atlantic puffin
Northern gannet	Northern gannet
Auks	Unidentified auk species, common guillemot, black guillemot, Atlantic puffin, razorbill
Divers	Red-throated divers, great northern diver
Gulls	Herring gull, great black-backed gull, mew gull, unidentified gull species, black-legged kittiwake, Sabine's gull, Iceland gull, lesser black-backed gull, glaucous gull
Seals	Unidentified seal species, grey seal, harbour seal
Harbour porpoise	Harbour porpoise
Cetaceans	Unidentified cetacean species, harbour porpoise, minke whale, Risso's dolphin, white-sided dolphin, killer whale, short-beaked common dolphin, long-finned pilot whale, pilot whale, white-beaked dolphin, common dolphin, humpback whale, bottlenose dolphin, sperm whale

3.2 Exploratory data analysis

Initially, exploratory data analysis was carried out on each species' data in order to identify any clearly erroneous data and to provide summary characteristics for that species. Histograms showing the distribution of animal numbers were assessed so that any outlying values could be identified and checked. Plots were also made to show the relationships between each covariate and the response. This also allowed for identification of outliers and the assessment of the likely strength of the covariate-response relationships.

To specify an appropriate model for these data, it was important to consider how the species abundance/distribution varied with respect to other covariates. This provided an understanding of whether or not any of the environmental covariates (available through the Wildlife Observations Programme) made good predictors of species density, particularly with changing device operational status. The covariates that were available are listed in Table 3.2.1.

Table 3.2.1. Covariates available during model specification

Covariate	Available at site (Fall of Warness/ Billia Croo/ Both)	Continuous/Factor
Year	Both	Continuous
Month	Both	Cyclical
Spatial surface	Both	Continuous
Depth	Fall of Warness	Continuous
Distance to land	Both	Continuous
Tide state	Both	Factor
Wind strength	Both	Factor
Sea state	Both	Factor
Cloud cover	Both	Factor
Weather	Billia Croo	Factor
Swell height	Billia Croo	Factor
Wind direction	Both	Factor
Precipitation	Fall of Warness	Factor
Site-wide impact level	Both	Factor

3.3 Model specification

The response data were animal counts and there were large numbers of zeros, therefore the response data were likely to be more variable than assumed under some model types (e.g. overdispersed). This variability had to be allowed under the selected model and so the response data were modelled using a quasipoisson distribution, with a log link function[8].

One of the assumptions of the modelling process was that the model residuals are independent; however, given that the observations were close together in space and/or time, they would likely be more similar (i.e. correlated) than observations that were spatially or temporally distant. If covariates were available to model this correlation, then the residuals should be independent. However, if the covariates were unavailable, then residuals would be correlated and the assumption violated. The violation of this assumption, if positive correlation was present, would lead to standard errors that were too small, and hence p-values that were too small. This would mean covariates that might otherwise be removed

[8] The link function restricts the model from returning negative animal counts.

from the model during p-value based selection would be falsely retained. If this were the impact covariate, an effect of device presence/operation could be falsely concluded when there was not one present.

To deal with the potential presence of correlated residuals, the GAMs were run in a GEE framework which explicitly permits correlation and returns standard errors that have been adjusted appropriately. The GEE was constructed with an independent working correlation matrix and robust standard errors were used for uncertainty estimation (see Section 3.6.1). In this case, residuals pertaining to data from the same day of survey (Billia Croo) or from the same grid zone-fortnight (Fall of Warness) were permitted to be correlated, while independence was assumed between blocks. The robust standard errors were standard errors that have been adjusted for the autocorrelation in the 'block' residuals. These were robust to misspecification of the correlation structure and were based on the observed correlation in the Pearsons residuals within blocks. The blocking structure and its necessity for each site described above was determined using ACF plots of Pearsons residuals and a runs test (Mendenhall & Reinmuth, 1982) was used to assess the presence of correlation in the residuals.

The observation methods used at both sites, though different, resulted in uneven surveying effort between observers and across the survey grid. It was crucial to include this varying effort in the modelling process so that, for example, some areas are not considered high density just because more effort was expended searching those areas. To account for this, the surveying effort was explicitly included in the model by using an offset term. This meant that the response was modelled as counts per unit area, rather than just counts. In the case of the Fall of Warness, the observer-specific patterns allowed the number of times viewed in an hour to be calculated for each grid cell which, combined with grid cell area, could be used as a proxy for effort, known as 'areatime'. For Billia Croo, due to the different observation methodology employed here, survey effort was accounted for by calculating the duration of each sweep and the number of grid cells within a sweep. This, alongside grid cell area, was used to create an 'areatime' variable that was again used as a proxy for observer effort.

Smooth terms were fitted using B-splines (degree = 2) for one-dimensional (1D) covariates and a CReSS smooth (Complex Region Spatial Smoother) (Scott-Hayward *et al*., 2014b) for two-dimensional (2D) spatial coordinates (e.g. x position and y position). The Spatially Adaptive Local Smoothing Algorithm (SALSA) and SALSA2D (Walker *et al*., 2011; Scott-Hayward *et al*., 2013b) were used to select the number and location of knots for the two types of smooth term. These methods allowed for spatially-adaptive smooth terms, rather than uniform smoothness, permitting some parts of the smooth to be more undulating than others. The CReSS method for the spatial component allowed the accommodation of potentially patchy numbers of animals across the survey areas.

An interaction term between the two-dimensional spatial smooth and the site-wide impact level was also considered. This allowed the spatial distribution of animals to vary between impact levels and provided an opportunity to identify spatially-explicit changes, should they be present. Furthermore, the covariate of Month was considered as a cyclic spline to accurately represent the annual cycle and to avoid artificial breaks between years. Therefore, any unnaturally sharp changes in numbers occurring between December and January were prevented.

If, for some species, the final model did not include the interaction term, a site characterisation for that species was provided instead.

3.4 Model selection

An overview of the model selection process is provided in Figure 3.4.1. In this two-stage process, the one-dimensional (1D) predictor covariates (i.e. depth, month, etc.) were considered first to produce a best-fit model. Thereafter, the spatial component with the interaction term was added to the model. At each stage, covariate selection was undertaken using backwards GEE-based p-value selection, whilst the flexibility of each of the smooth terms (1D and 2D) was undertaken using a quasi-likelihood based information criterion, with penalty log(n) for each additional parameter (QBIC)[9]. Covariates were retained in the model if the GEE-based p-value was <0.05.

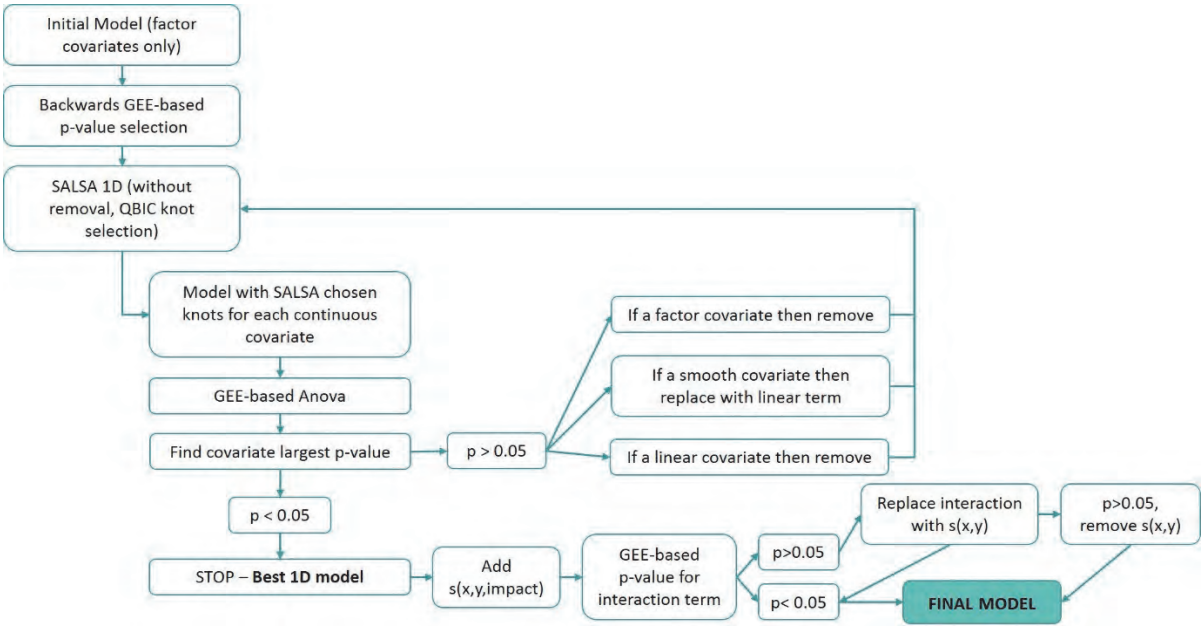

Figure 3.4.1. Model selection process

The following table (Table 3.4.1) provides the starting parameters for SALSA 1D and 2D. Additionally for SALSA2D, ten ranges for the CReSS basic function were permitted.

Table 3.4.1. Starting parameters for SALSA 1D and SALSA 2D process

Starting parameters	SALSA 1D (df)	SALSA 2D (df)
Start knots	1 (3)	4 (4)
Min knots	1 (3)	4 (4)
Max knots	5 (7)	10 (10)
Degree	2	-

Models were fitted using R 3.2.0 (R Core Team, 2015) and packages MRSea (Scott-Hayward *et al*., 2013a) and geepack (Højsgaard *et al*., 2006).

3.5 Model assessment/diagnostics

Assessment of the model included checking of assumptions and model fit. Diagnostic outputs are not presented in this report but were used to assess any modelling issues during analyses. Partial residual plots on the scale of the link function (log(animal counts)) were

[9] When using the independent working correlation matrix, the QICb (an information criterion for GEEs, Pan, 2001) is equivalent to the QBIC.

used to assess the strength and shape of the relationship of each covariate with species abundance. If the confidence intervals (CIs) were small, then this indicated a relatively precise relationship (Figure 3.5.1), whereas wide CIs for a smooth term might suggest that a linear term was more appropriate (Figure 3.5.1).

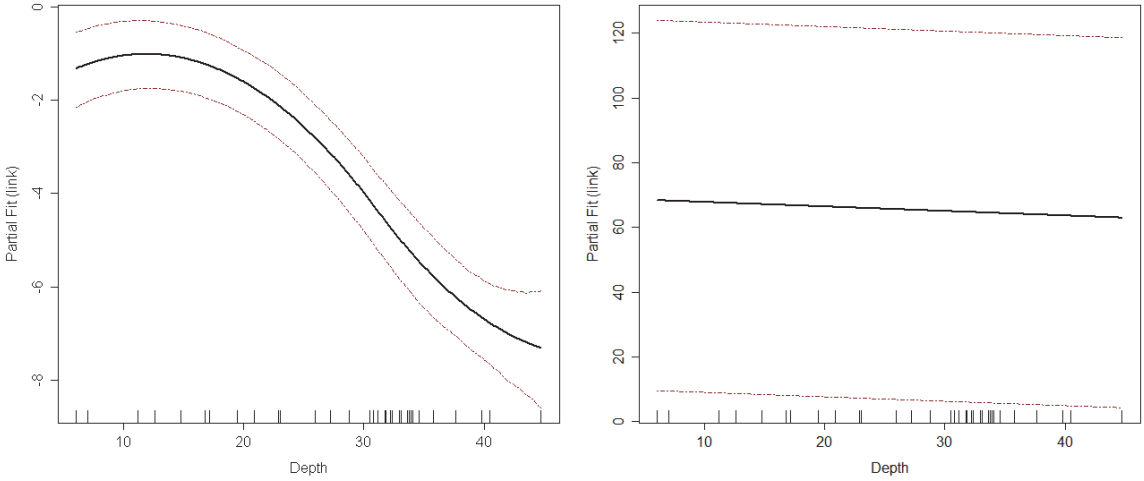

Figure 3.5.1. Example of partial fit plots with varying confidence intervals (left: narrow confidence intervals, right: wide confidence intervals). Modelled relationship represented by black line whereas red lines represent the associated GEE-based confidence intervals

The mean-variance relationship ($\lambda = \mu = Var(\mu)$) was assessed using plots of fitted values vs scaled Pearsons residuals. If the relationship was modelled appropriately, then there should not be any pattern observed in the output plot. If extra dispersion in the model was ignored, then this could have led to inappropriate CIs and *p*-values.

It was difficult to assess overall model fit due to the large dispersion present in the data, which renders diagnostics such as observed vs fitted values and R^2 ineffective.

3.6 Prediction and inference

Once the most suitable model was selected, predicted density estimates could be created. Predictions were made for each year (if retained during model selection) on the same grid as used for data collection, thereby producing prediction surfaces. Predictions were made for each site impact level, for one month[10]. It should be noted that, although predictions were made for each year, a mean of all years is presented in this report. Data regarding each year's predictions are available on the Marine Scotland Information portal.

To be able to produce the prediction surfaces, it was necessary to set the environmental and temporal covariates in the fitted model to fixed conditions. The environmental covariates excluded from this were those that were grid-specific (e.g. depth, distance to land). If not otherwise stated, all the predictions discussed in the results have been made when environmental and temporal covariates were set at conditions when the greatest number of sightings was made for that species/group. It should be noted that these conditions may not necessarily be the optimum ones for surveying that species/group of species. Hence, the prevailing conditions at each of the sites will have a bearing. Appendix 5 provides an overview of the fixed conditions selected for the environmental and temporal covariates for each species/group.

[10] As the month with the greatest abundance varied between species, the month chosen for predictions varied for each species.

Once such conditions were selected, prediction surfaces providing abundance estimates and the predicted spatial distribution of each of the species/groups across the survey region could be formed. The predicted density changes across the site for each site impact level and between site impact levels were qualified.

In addition to providing predictions for these conditions for each species, prediction surfaces have been produced for the most common surveying conditions in both January and July. These are provided on The Marine Scotland Information portal. These surfaces should give an indication of the difference in predicted abundance and distribution between winter (January) and summer (July). An area for further research would be to produce prediction surfaces for the breeding and wintering periods for each of the species analysed. This may help identify any relationships that may be associated with site impact level that are only present at certain stages of a species life history.

3.6.1 Uncertainty estimation

It was crucial to understand whether any change in abundance or distribution was real or if it was 'noise' within the system and, if real, whether any of these changes could be classified as significant. Uncertainty was estimated by a parametric bootstrap, with 1000 realisations, using a multivariate normal with parameters, on the estimated model coefficients and their associated GEE-based standard errors. This process resulted in 1000 relative density estimates for each grid cell (given a set of covariates and point in time). The central 95% of these values were used to define the upper and lower 95 percentile confidence limits. The Coefficient of Variation (CV) is the ratio of the standard deviation to mean and was calculated for ease of presentation (one figure as opposed to two for upper and lower CIs). This provided a measure of relative variability in the animal densities and could be compared across species and sites. The smaller the CV, the more reliable the estimate (i.e. lower variability within the prediction). The downside of using CV as a measure of uncertainty was that, when the mean approached zero, the CV tended to infinity, so it was sensitive to small changes in the mean. This meant that, if an estimate for a grid cell was very close to zero, the CV could be very large, even though the uncertainty was quite small (narrow percentile interval). For the Fall of Warness, all CV values were presented; however, large values should be checked against the predicted density plot to assess if it has been affected by a very small density estimate. For Billia Croo, where the overall species densities were generally much smaller, the grid cells highly affected by a small mean density (<0.0001) have been greyed out to prevent misrepresentation of uncertainty.

3.6.2 Spatially-explicit change

It was essential to identify spatially-explicit changes across the site. To demonstrate any such changes, the difference between model predictions for each site impact level was calculated for each bootstrap iteration and a median density difference was plotted for each grid cell within the prediction grid. Model predictions for each site impact level and the transitions between them (site impact levels: 1-0, 2-0, 3-0, 2-1, 3-1, and 3-2 (refer to Section 2.3)) were calculated for each bootstrap iteration. This provided a median predicted density difference between site impact levels for each cell within the prediction grid. Their associated 95% CIs were calculated using the percentile method which allowed the significance of the difference to be determined. If the CIs contained the value zero, then it was considered that there was no significant difference between impact levels, at the 95% level of confidence. However, if the intervals did not contain a zero and the lower confidence limit was above zero, then the difference was determined as significantly positive (increase in abundance from site impact level 0 to 1), and, if the upper confidence limit was below zero, the difference was determined as significantly negative (decrease in abundance from site impact level 0 to 1). If a displacement reaction occurred with device presence, these projections were expected to show negative density differences, particularly towards the

centre of the site (where the test berths are located). It should be noted that, if there was a real impact, then the impact location should be identifiable from the differences observed in species distribution.

When drawing conclusions, it is important to remember that, when generating the models, the highest site impact level was assumed across the whole site regardless of other site impact levels occurring. Therefore, when a maximum site impact level was being simulated across the whole site, any potential effects caused at lower site impact levels may be masked in the model predictions. Additionally, it is important to note that the significance of the increase/decrease in abundance was relative to the density of the species observed at the site (across the ten-year observation period for the Fall of Warness, and six-year period for Billia Croo), and did not apply at population or sub-population level.

3.6.3 Density changes with distance from impact

Density difference projections were also used to understand how species' density changes with distance from a potential impact location (i.e. a grid cell containing a test berth). The spatially-explicit differences calculated above were collapsed down into one dimension to examine the change in animal density with distance from a potential impact location between each of the various site impact levels (e.g. the six site impact level comparisons). Again, bootstrap-based 95% CIs were used to show uncertainty in predictions. If a decrease in density was predicted with device presence with a reasonable level of certainty placed on the prediction, this plot would show a median density difference line below zero, with narrow CIs on either side of the median line which does not cross the y-axis at 0. Similarly, if an increase in density was predicted with device presence (with a reasonable level of certainty), the median density difference line would be above zero with narrow CIs on either side. Neither the median line nor the CIs would cross the y-axis at 0. If changes in predicted density could be associated with a change in site impact level, it is expected that with increasing distance away from the potential impact location, the density difference would reduce (i.e. the level of effect reduces with increasing distance away from source).

Any conclusions drawn from these analyses have some caveats that need to be taken into consideration. In the plots created, the centre point of the grid cell containing the test berth was taken as distance 0m. This is the reason why none of the density difference predictions start at 0m. This therefore assumed that the location of the potential impact (test berth) was at the centre of the grid cell, whereas, as can be seen in Figure 2.1.3, Figure 2.1.9 and Figure 2.1.10, this is not the case. During the making of these plots, it was also assumed that there was only one impact location within the grid cell whereas, at the Fall of Warness, one grid cell actually contains two test berths. In addition, these analyses did not take into account that there are other potential impact sources within close proximity to the test berth (e.g. other grid cells containing test berths). It may be possible to pick up the effect of other test berths in the plot for another test berth. As a site-wide impact level was used, it cannot be assumed that the test berth presented was actually at that device operational level.

A single grid cell was selected for each species/group of species to provide an indication of the relationship being observed. It should be noted that, for presentation purposes, the grid cell containing a test berth which most clearly showed a relationship in terms of density difference with changing site impact level, was selected. If inferences are to be made from these analyses, plots from all the grid cells containing one or more test berths should be studied. Plots for each species/group of species containing all the grid cells (that contain test berths) have been included in the Marine Scotland Information portal. Additionally, for specific conclusions to be drawn, then only grid cells operating at a known operational status should be analysed rather than using a site-wide impact level.

3.7 Power analysis

The power analysis methodology and the results obtained during the power analysis are available in Section 5. Three power analysis scenarios have been tested on the fitted bird and marine mammal data from the Fall of Warness to understand the power behind the models. The three scenarios tested were: a site-wide decline in abundance of 50%; a redistribution in abundance defined as a 50% decline in grid cells with test berths and an increase in grid cells without test berths; and, finally, a 50% side-wide decrease in abundance, with an additional 50% reduction in survey effort. The first stage of the power analysis (simulated data generation) was attempted for the Billia Croo data. However, this was not successful due to the inclusion of the survey effort data, resulting in the vast majority of the data being zeros with the effect that the means of the fitted data were too small to allow simulated data generation from an overdispersed Poisson distribution. Future alternative methods for conducting the Billia Croo power analysis have been suggested in Section 5.

3.8 Summary of data issues and analytical assumptions

This section provides a summary of the various data issues that arose during the analyses. Some of these issues were rectified during the data cleansing whereas others required more substantial solutions e.g. the inclusion of effort data. Throughout the data analyses, assumptions were made in order to resolve some of the data issues and in response to the limited analytical methodologies available. All assumptions made during the analyses are detailed in Appendix 3, alongside the associated data issue.

Annex 1 presents an overview of the data cleansing process and the assumptions applied during this process.

The main issues and consequent assumptions are outlined below:

- As mentioned previously, part of the planned scope of this project was to construct an appropriate detection function using survey data that had previously been collected at the site employing an alternative survey methodology. However, it was found that the data available from previous surveys could not feasibly be utilised to construct a detection function. In these circumstances and due to funding and time limitations, the option to conduct a separate survey specifically for the purpose of creating a detection function did not exist and, therefore, no detection function was applied to the data. The lack of a detection function means that a key assumption made during this analysis is that the detectability of species across each of the sites was the same, regardless of distance from the vantage point or the environmental conditions in which surveying was conducted.
- No method was implemented to account for repeat counting. Due to the observation methodologies employed at the sites (repeat scanning), the potential for systematic repeat counting was an inherent issue that could not be resolved. At the project outset, it was hoped that a novel methodology could be developed to estimate accurately the extent of double counting during a watch. However, apart from the use of Generalised Estimating Equations (GEE models) to account for temporal auto-correlation (as outlined by Robbins, 2012), it did not prove possible to develop a method to eliminate double counting. It has therefore been assumed that each sighting made by the observers is unique and has not been recorded at the site previously.
- No correction of the data for availability was implemented, as model predictions outputted by spatially adaptive models assume that all animals present at the surface had been sighted and identified correctly. However, many marine species (particularly marine mammals) spend the majority of their time underwater and are therefore,

typically, rarely seen at the surface. This is usually accounted for when estimating genuine abundances. However, as neither detection functions nor instantaneous availabilities were taken into consideration during this analysis, only relative abundances could be obtained from the analyses.

It is worth noting, as an aside, that it may be possible in the future to insert an availability correction by simply inflating the fitted surfaces by the appropriate availability correction for each species. Currently, there is a lack of reliable published data on availability estimates and their uncertainty, but for many marine mammals these can be very low figures. As an example, Harrison *et al*. (2006) estimated the probability of grey seals being available to be seen at the surface, while at sea, as 10%. This figure highlights the issue of surface presence and underestimation in terms of abundance that is inherent within the current analysis.

4. RESULTS

As outlined in the project scope, this section presents the results of the statistical analyses of the survey data from EMEC's Wildlife Observations Programme. The analysis outputs predominantly consist of spatial surfaces with an estimated abundance of marine species, with associated confidence intervals, for both the Fall of Warness and Billia Croo test sites. Ten species/groups of species were investigated for each site (as previously outlined in Table 3.1.1 and Table 3.1.2). Importantly, the data were analysed with respect to MECS testing activity at each site by using various site-wide operational statuses (site impact levels) (as described in Table 2.3.1). Only the key outputs from the analysis are presented within this report and adjusted to accommodate each species' modelling output. As such, many of the detailed deliverables for this report (including graphics and associated datasets) are provided in a supplementary project folder available through the Marine Scotland Information portal: http://marine.gov.scot/.

4.1 Exploratory Data Analysis

The results from the exploratory data analysis are not provided within this report and, instead, basic summary statistics regarding the number of observations and mean group size are included. A plot showing the raw observation data in relation to the survey grid cells is provided in the Marine Scotland Information portal. In addition, the same plot broken down into each site impact level can also be found in the Marine Scotland Information portal, to allow an understanding of the raw data used in the modelling process.

Before starting the modelling process, it was important to establish how many records there were at each site impact level for each of the sites, and how these were split across the survey periods. It was noted that the analysis was likely to be confounded with year for both sites, since site impact level 0 (baseline conditions) was restricted to the first couple of the survey years at both sites. Table 4.1.1 and Table 4.1.2 below provide an indication of the number of records relative to the site impact level and year for the Fall of Warness and Billia Croo, respectively. It is worth remembering that the data have effort included at this stage and, therefore, the number of records is different to the number of species observations.

Table 4.1.1. Number of records at the Fall of Warness relative to site impact level and survey year (see table 2.3.1 for definition of site impact levels)

Site impact level	Year										
	2005	2006	2007	2008	2009	2010	2011	2012	2013	2014	2015
SIL-0	10475	13025	0	0	0	0	0	0	0	0	0
SIL-1	0	10775	23175	20715	22200	9535	665	0	12890	0	0
SIL-2	0	0	0	2525	655	5950	920	13210	12115	8585	3965
SIL-3	0	0	0	100	3480	13140	24055	16400	4780	20750	1345

Table 4.1.2. Number of records at Billia Croo relative to site impact level and survey year (see table 2.3.1 for definition of site impact levels)

Site impact level	Year						
	2009	2010	2011	2012	2013	2014	2015
SIL-0	21244	0	0	0	0	0	0
SIL-1	8745	0	15952	0	0	0	0
SIL-2	731	16569	25787	23586	11964	13245	9621
SIL-3	8377	35554	9104	25822	36659	35520	0

In addition, for each site, a summary has been provided of the number of records at each site impact level and the associated percentage relative to the total number of records for the site (Table 4.1.3 and Table 4.1.4).

Table 4.1.3. Summary of records for the Fall of Warness relative to site impact levels (see table 2.3.1 for definition of site impact levels)

Site impact level	Number of records	Percentage of records (%)
SIL-0	23500	9.2
SIL-1	99955	39.1
SIL-2	47925	18.8
SIL-3	84050	32.9

Table 4.1.4. Summary of records for Billia Croo relative to site impact levels (see table 2.3.1 for definition of site impact levels)

Site impact level	Number of records	Percentage of records (%)
SIL-0	21244	7.1
SIL-1	24697	8.3
SIL-2	101503	34.0
SIL-3	151036	50.6

From the above tables, it is clear that there are far fewer observations at baseline conditions (SIL-0) compared to the other site impact levels. In addition, the percentage of records for Billia Croo at SIL-1, when device-associated infrastructure is installed onsite, is much lower compared to the percentage of records available for SIL-2 and SIL-3. It is likely that this uneven distribution of records between pre-impact and post-impact data may reduce the power of the fitted models to be able to detect species changes.

Table 4.1.5 summarises the issues raised during the exploratory analysis of covariates. It was concluded that some of the data would benefit from some further rationalisation being applied to combat the effect of such issues affecting the robustness of the analyses.

Table 4.1.5. Issues identified during exploratory data analysis and subsequent solutions

Test site	Environmental covariate	Issue	Action
Fall of Warness	Cloud cover	Observer preference for even oktas of cloud cover, with the exception of 7 oktas	Combine cloud cover variables into five cloud cover categories: 0, 2 (1, 2 oktas), 4 (3, 4 oktas), 6 (5, 6 oktas), 7, 8
	Wind strength	Very few recordings of wind strengths 5 and 6 (as expected)	Combine all wind strengths of 4 and above into a 4+ category
	Sea state	Very few recordings over sea state 4 (as expected)	Combine all sea states of 4 and above into a 4+ category

	Wind direction and wind strength	A wind direction is provided when there is no wind and, likewise, no direction is provided when there is a wind strength of 1	N/A
	Precipitation and cloud cover	Precipitation conditions are recorded as showers when there is no cloud	N/A
	Wind strength	Very few recordings of wind strengths 5 and above	Combine all wind strengths of 5 and above into a 5+ category
	Swell height	Swell heights of 20m and 21m. If this was correct, the observer should not have been out in these conditions	Combine all swell heights of 6m and greater to a 6m+ category
Billia Croo	Sea state	Very few recordings over sea state 4	Combine all sea states of 4 and above into a 4+ category
	Wind direction	One observer records wind direction only rarely and many recordings have been null. Too many wind direction categories	Remove wind direction from Billia Croo analyses
	Distance to land and x.pos (spatial component)	Distance to land is highly correlated with x.pos (as expected)	Distance to land will not be included in the analyses – any effect will be carried forward by x.pos

4.2 Presentation of results of analyses

The following is an explanation of how the graphical summaries for the abundance estimates and predictive model are presented for each species and species groups that have undergone analyses.

4.2.1 Species overview

For each species/group of species at each site, a discussion of the typical behaviour observed for this species, including any breeding and migrating information, is given in the report together with a brief summary of any trends in species abundance and distribution observed at the site and any notable local population trends documented.

4.2.2 Data Summary

A table of basic summary statistics including the number of observations and mean group size is presented.

4.2.3 Model overview

An overview of the final fitted model has been produced for each species. A summary table of the GEE-based p-values for all the models fitted during the analyses is provided in Appendix 4. In addition, a discussion of any key relationships fitted by the model, with regards to the environmental and temporal terms, is included. Partial fit plots for all terms included in the final fitted models are available in the Marine Scotland Information portal.

4.2.4 Density predictions and uncertainty estimation

Density prediction surfaces for each modelled species/group have been produced and are presented for covariate values where the most sightings were recorded for each species/group. Appendix 5 provides a summary of these values. In addition to the prediction surface, the corresponding CV values for each predicted grid cell are also presented for all of the prediction surfaces.

When interpreting the resultant prediction surfaces, it is important to note that, due to the size of the Billia Croo surface, the latter has been split into outer and inner areas. The three outermost bands within the Billia Croo survey grid, grid rows A-C, are described as the outer area/bands whereas the remaining bands, grid rows D-J, are denoted as the inner area/bands.

4.2.5 Relative abundance estimates

In addition to providing the prediction surfaces, relative abundance estimates have been created for each month throughout the observations programme's duration. These have been combined to provide seasonal estimates (alongside their associated confidence intervals) for each survey year. It is worth noting that these values are relative abundances as only surface visible observations[11] have been recorded during the observations programme.

This information is presented in a table for each species/group of species. In Appendix 7, plots of the changing seasonal relative abundance estimate across years for each site impact level are provided.

It should be noted that the winter abundance prediction includes data from December of the preceding year, where available.

4.2.6 Spatially-explicit change

Using the prediction surfaces for each site impact level, it has been possible to calculate the estimated change in density and distribution of densities between the site impact levels for each study species/group. Surfaces displaying the estimated change in density between the various site impact levels are presented, as well as positive ('+') and negative ('-') symbols to indicate where the difference has been deemed statistically significant[12]. When interpreting whether these results show any evidence of spatially-explicit change, it is important to remember that, when generating the models' outputs, the highest device operational status from across the site was assumed when establishing the site impact level and, therefore, any effects associated with lower device operational statuses were not considered.

4.2.7 Density changes with distance from impact

These plots provide an indication of the distances within which any density changes, that are associated with the location of test berths, begin to subside. In addition to the plotting of the estimated density difference, the confidence intervals (CIs) help to identify areas where there

[11] This is referring to the fact that bird and marine mammal recordings are only made when at the sea surface. Therefore, in terms of marine mammals who spend the majority of their time below the sea surface, the actual number of mammals will not be able to be recorded accurately, and hence this is only a relative abundance estimate. For birds, recordings are made when they interact with the sea surface (or within 3m of the sea surface); therefore, if the observers see a diving bird interacting with the sea surface, this will be recorded. However, if a diving bird is below the water surface for the entirety of time that the observer is recording that area, this individual will not be recorded.

[12] Calculated using the 95% confidence intervals from 1000 bootstrap iterations.

are large uncertainties surrounding the predictions. It is worth noting that any inferences drawn from these analyses should be caveated as indicated in Section 3.6.3.

4.2.8 Diagnostics

Mean-variance relationships and plots of observed versus fitted values are included in the Marine Scotland Information portal.

4.3 Fall of Warness marine birds

4.3.1 Black guillemot (Cepphus grylle)

4.3.1.1 Species overview

The black guillemot, *Cepphus grylle*, is an exclusively marine species that tends to be located near cliffs and rocky shores. The bird forages on mostly benthic organisms with the majority of its prey comprising benthic fish (e.g. sandeels, *Ammodytes* spp.) and invertebrates, including crustaceans. Typical foraging behaviour consists of pursuit diving; this type of diving involves the guillemot propelling itself through the water using its wings (BirdLife International, 2015). In April 2013, SNH conducted surveys of the black guillemot population at Papa Westray (an island and Marine Protected Area (MPA) located approximately 20km from the Fall of Warness). Results showed a 38% increase in numbers over a previous count conducted in 1999 by Seabird 2000 (Swann, 2013).

4.3.1.2 Data summary

Black guillemots are observed regularly at the Fall of Warness. Table 4.3.1 below provides a summary of raw survey data from the site including information on the number of observations and mean group size. These summary statistics have also been broken down for each site impact level in order to provide an understanding of the data used to create the black guillemot model.

Table 4.3.1. Summary of black guillemot raw data

	Total	Site Impact Level 0	Site Impact Level 1	Site Impact Level 2	Site Impact Level 3
Number of observations	23687	2098	10059	3588	7942
Minimum (group size)	1	1	1	1	1
Maximum (group size)	151	97	100	129	151
Mean (group size)	5.79	6.16	5.31	6.03	6.20
(s.d.)	(8.44)	(9.13)	(7.04)	(9.38)	(9.36)

4.3.1.3 Model overview

Once the model selection process was completed, the GEE-based p-values for each of the terms that remained in the final fitted model were recorded. The model identified 11 terms that were highly significant for the black guillemot (Table 4.3.2).

Table 4.3.2. GEE-based p-values for the terms in the final black guillemot model for the Fall of Warness

Model term	ρ-value
Tide state	<0.0001
Site impact	<0.0001
Wind direction	<0.0001
Precipitation	<0.0001
Wind strength	<0.0001
Cloud cover	<0.0001
Sea state	<0.0001
Month	<0.0001
Depth	<0.0001
Spatial surface	<0.0001
Spatial surface / site impact	<0.0001

As mentioned previously, the relevant partial fit plots have been provided in the Marine Scotland Information portal for all terms included the model. The fitted model estimated similar levels of abundance at ebb and flood tide and a dramatic decrease in abundance during slack tide. Similarly, a relationship exists between wind direction and black guillemot numbers with lowest abundances present when the wind is in a southerly or south-westerly direction. The relationship between black guillemot abundance and precipitation suggests that fewer birds are anticipated during constant rain, heavy rain or showers[13]. Greater abundances are expected when there is no precipitation or just light showers, mist or drizzle[14]. In terms of wind strength, black guillemot density is expected to decrease as wind strength increases. A greater abundance of black guillemots is estimated with greater cloud cover[15]. Within the fitted model, sea state has a statistically significant relationship with abundance; it is predicted that abundance will decrease with increasing sea state[16]. This relationship is strong and can be observed in Figure 4.3.1. Similarly, a statistically significant relationship is observed between abundance and depth. However, there is no clear relationship between depth and black guillemot abundance for depths up to 24m whereas, at depths greater than 24m, there is a clear reduction in abundance estimated.

[13] Note that these categories include times when the observers recorded sleet, hail and snow showers.
[14] There is a possibility that the reduced estimated abundances during heavy precipitation conditions are due to reduced detectability rather than being associated with the weather conditions.
[15] Similarly, this may be due to greater detectability due to reduced glare or less contrast in brightness levels across the viewing area.
[16] Again, this modelled relationship may be due to changing detectability with sea state rather than an observed relationship between black guillemot numbers and sea state levels.

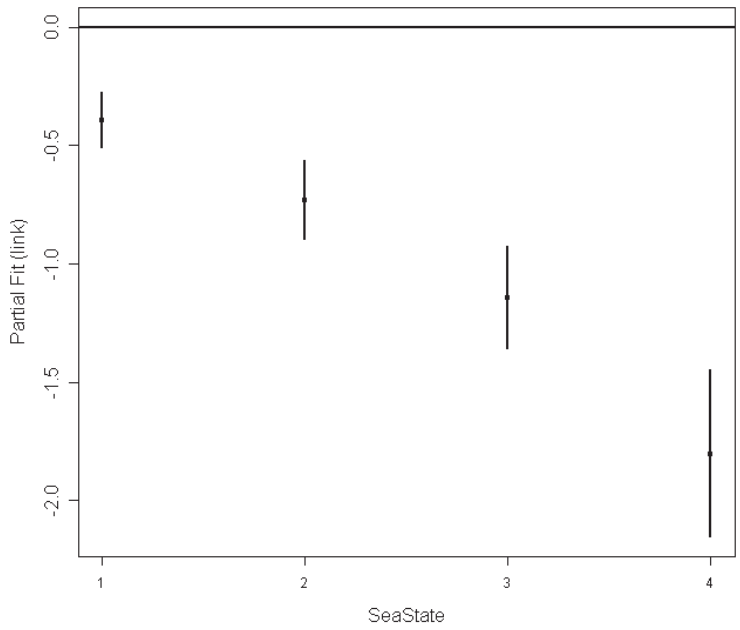

Figure 4.3.1. Estimated partial relationship of black guillemot density (on the scale of the log link) with sea state at the Fall of Warness. The points are the parameters for the estimated change in log density from the baseline (seastate = 0) and the vertical lines represent 95% confidence intervals about the parameter estimates.

It was necessary that 'month' was put into the model as a cyclic spline to take account of the changes in month between years; therefore, it was only possible to fit 'month' as a smooth term but fitting it as a factor covariate may have proved useful[17]. The fitted spatial surface was relatively smooth, with eight knots fitted. The relationship between the interaction term (site impact/spatial surface) and the response term (species abundance) was also found to be statistically significant. 'Year' was removed during the first SALSA 1D loop as it was found not to be statistically significant and therefore redundant in the model.

Various diagnostic tests were undertaken on the black guillemot model to understand how well the model fitted and whether it was appropriate for the data. It was found that there is a general underestimation of variance by the model for higher fitted values, which is common for data that display this degree of overdispersion.

4.3.1.4 Density predictions and uncertainty estimation

As the model contains a spatial surface, it was possible to plot estimated density for different site impact levels across the survey region. To enable this, predictions were made for certain conditions. The optimum conditions[18] contributing to greater predicted black guillemot abundance were chosen for each term and are provided in Appendix 5. The estimated density for each site impact level is provided in Figure 4.3.2. The associated CV value for each prediction grid cell is shown in Figure 4.3.3. These provide a measure of

[17] This is due to the relationship between month and black guillemot numbers being plotted to reduce at a constant rate through the year. However, the confidence intervals are wide on the predictions, suggesting that there is no clear relationship.

[18] It should be noted that these conditions may be those where greatest abundances have been estimated; however, some of these predictions may reflect optimum viewing conditions rather than actually being associated with black guillemot numbers. This project has not taken account of any detection functions when producing density estimates.

uncertainty in the estimated densities, with the smaller CV values indicating a more precise estimate (lower variability).

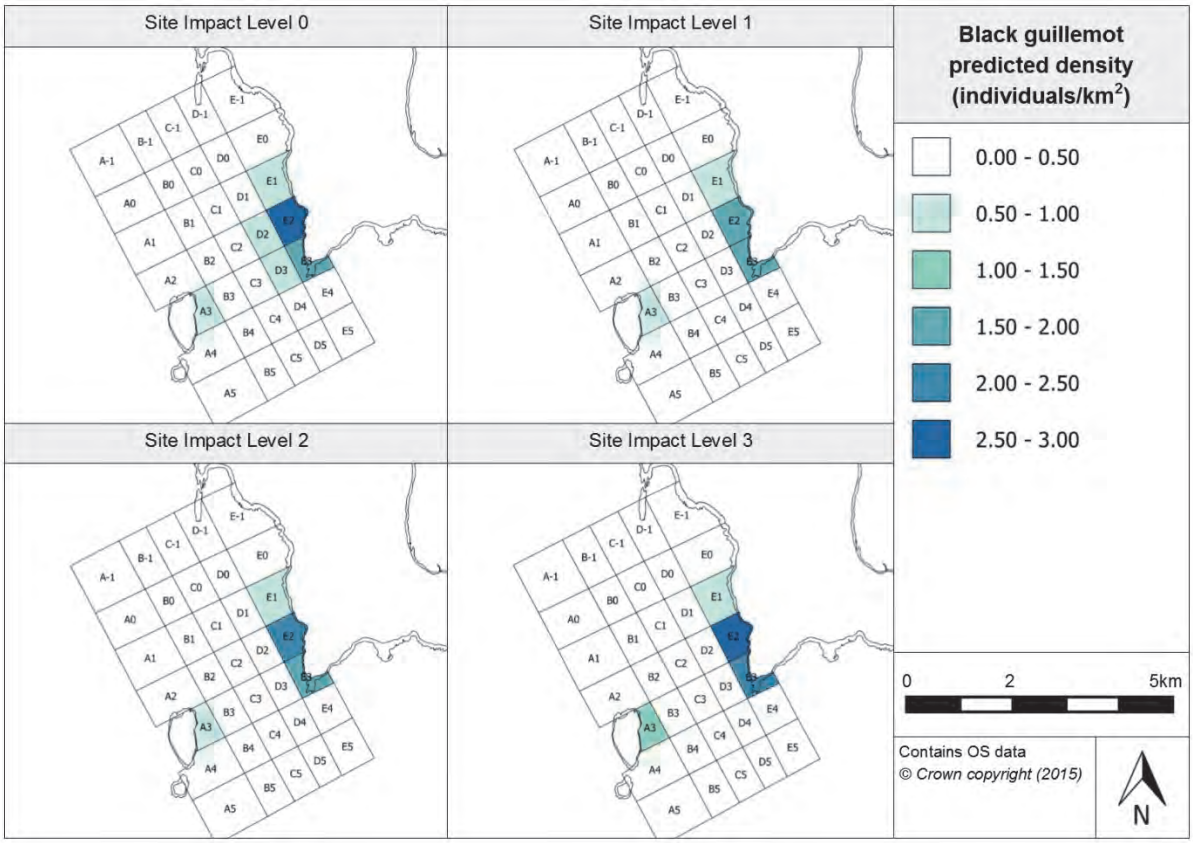

Figure 4.3.2. Estimated black guillemot density at each site impact level

Baseline conditions (site impact level 0 (SIL-0)) show that there is a higher estimated density of black guillemots in the cell closest to the observer (E2), with estimated density levels dropping away smoothly from this grid cell. There is also a peak in density towards Muckle Green Holm, suggesting that black guillemot density is higher closer to land.

In terms of how the estimated density changes between the site impact levels, it appears that densities in grid cell E2 are smaller - compared to baseline conditions - when infrastructure is onsite (i.e. site impact level 1 (SIL-1)). In addition, the number of grid cells where this peak in estimated density is evident is lower when compared to baseline conditions. However, a similar density to baseline conditions is observed near Muckle Green Holm when infrastructure is onsite. For the expected density when one or more devices are onsite (but not operational) (i.e. site impact level 2 (SIL-2)), it appears that the density in grid cells E2 and E3 increases to levels near comparable with baseline conditions; however, a smooth drop in density away from these cells, similar to that seen during baseline conditions, is not observed. Again, similar levels of density are estimated in the grid cells close to Muckle Green Holm (e.g. cell A3). The estimated density when devices are present and operational shows similar heightened levels of abundance compared to times when devices are present but not operational. The greatest densities are expected during this site impact level and again are present in cells E2 and E3.

Consistently, it appears that black guillemot density is estimated to be greater in grid cells E2 and E3. These grid cells are adjacent to cliffs on the island of Eday (see Appendix 6) which is a habitat type that black guillemots are known to frequent.

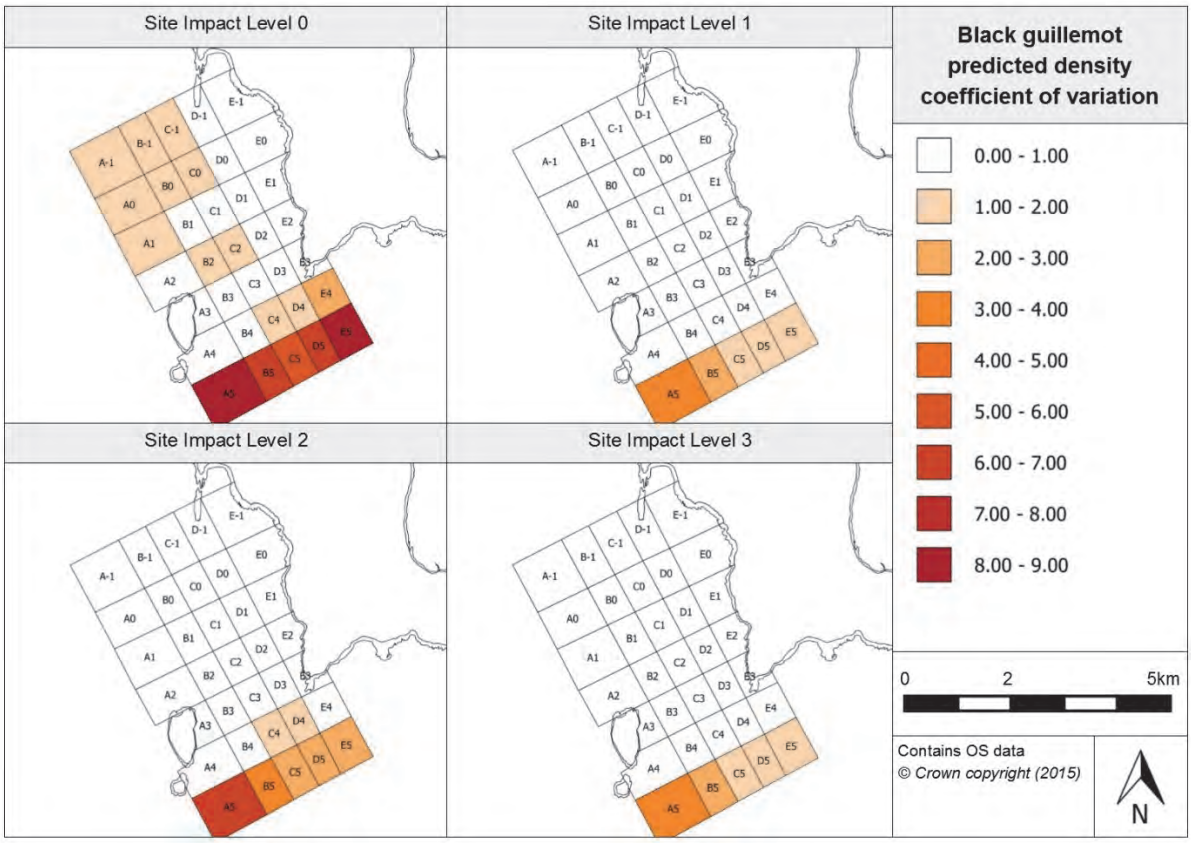

Figure 4.3.3. Associated coefficient of variation values for the density predictions for black guillemot

Figure 4.3.3 provides the associated CV values for each of the prediction surfaces. It is clear that, for each surface, there is high uncertainty about the predictions in grid cells A5-E5. This is likely to be due to there being fewer observations in these grid cells which may result from two of the observers not including this row (A5-E5) in their observer-specific observation patterns (i.e. two observers do not survey in this row) or could be due to very small density estimates in this area of the grid (see Figure 4.3.2). Several other grid cells have higher variability surrounding their predictions at baseline conditions (SIL-0); this would suggest higher uncertainty in this prediction surface. It is worth noting that the grid cells with the higher CV values are the areas of lowest density predictions which may influence the CV score.

4.3.1.5 Relative abundance estimation

Using the produced model, it is possible to estimate the abundance of black guillemots in each survey month. Applying the same environmental covariates as previously described, estimated seasonal abundance values for each survey year have been produced; these are provided in Table 4.3.3.

Table 4.3.3. Relative abundance for black guillemot during each season (associated confidence intervals are provided in brackets)

Year	Season			
	Winter (Dec†, Jan, Feb)	Spring (Mar, Apr, May)	Summer (Jun, Jul, Aug)	Autumn (Sep, Oct, Nov)
2005	-	-	35.51 (25.68, 49.86)	24.14 (17.32, 34.53)
2006	44.84 (13.4, 72.18)	43.33 (34.21, 55.38)	29.45 (23.11, 37.59)	20.6 (16.34, 25.89)
2007	49.32 (14.29, 83.3)	47.65 (35.88, 63.59)	32.39 (24.38, 43.25)	24.87 (20.07, 30.9)
2008	59.58 (17.46, 97.7)	57.57 (44.89, 74.7)	39.13 (30.4, 50.69)	24.14 (17.32, 34.53)
2009	54.08 (15.13, 95.68)	52.25 (37.9, 73.19)	33.75 (23.11, 49.86)	20.02 (15.4, 25.89)
2010	44.84 (13.4, 72.18)	43.33 (34.21, 55.38)	31.28 (24.38, 38.08)	22.01 (16.34, 29.77)
2011	49.32 (14.29, 83.3)	47.65 (35.88, 63.59)	39.13 (30.4, 50.69)	26.59 (20.07, 34.75)
2012	59.58 (17.46, 97.7)	56.02 (37.9, 74.7)	35.51 (25.68, 49.86)	24.14 (17.32, 34.53)
2013	54.08 (15.13, 95.68)	46.69 (34.21, 73.19)	29.45 (23.11, 37.59)	20.02 (15.4, 25.89)
2014	44.84 (13.4, 72.18)	47.65 (35.88, 63.59)	32.39 (24.38, 43.25)	22.01 (16.34, 29.77)
2015	53.57 (14.29, 85.35)	57.57 (44.89, 74.7)	-	-

†December data are from the preceding year, where available.

The expected abundance values across site impact levels are provided in Appendix 7, taking into consideration the site impact status for each month. It shows that there tends to be a seasonal peak in winter to spring, with fewer birds during the late autumn months.

It is worth noting that prediction surfaces (with associated CV values) have also been produced for typical surveying conditions in January and July, to provide an indication of any distributional changes that may occur between winter and summer. These plots can be accessed in the Marine Scotland Information portal. Upon initial examination, there are no distributional changes observed between the two months, but greater numbers are recorded during July. This seasonal peak has already been identified in Table 4.3.3 above.

4.3.1.6 Spatially-explicit change

Given the focus of this project on any spatially-explicit changes in abundance or distribution of marine species occurring across the site due to a change in device operational status, the difference between model predictions for each site impact level has been investigated. The significance of the difference has also been calculated using their associated 95% CIs. For the black guillemot, first impressions would suggest a dramatic increase in guillemot density associated with the installation of infrastructure onsite in the northern and south-eastern parts of the site (Figure 4.3.4). A significant decrease in density is estimated in five cells positioned in the centre of the site close to land. The most significant decline in black guillemot density is seen in grid cell E2, with a decrease of 1.19 individuals/km^2 anticipated.

When the change in density between baseline conditions and devices being installed onsite is investigated further, there appears to be a significant decrease in density in cells located towards the centre of the site. Cell E2 again shows a substantial increase in density expected but, due to the large CIs, the change in density is found to be not significant. Many of the grid cells towards the perimeter of the survey area show a significant increase in black guillemot density with devices being installed onsite.

The change in black guillemot density in association with operational devices, in comparison to baseline conditions, is very similar to the difference between baseline conditions and devices being present (but not operational). The marked density decrease in grid cell E2 is

not as evident and remains not significant. More grid cells around the perimeter of the survey area show a significant increase from baseline conditions.

When considering the change in density between site impact levels 1 and 2, it appears that no great change in density is estimated when devices are installed as compared to infrastructure only being present (Figure 4.3.4). There is a significant reduction in density expected in cells located in the northern centre of the site (in the vicinity of cells B0 and C0) as well as a couple of cells towards the southern end of the site (cells C4 and D4). On the contrary, a significant increase in density is expected in cells inland of Seal Skerry and grid cell E2, positioned directly below the observation vantage point. Unlike the density difference between baseline conditions and infrastructure being installed, cell E2 experiences a marked increase in density of 0.62 individuals/km^2 when one or more devices are installed.

It appears that a comparison of species density between that expected when infrastructure only is present and when device/s are installed onsite and become operational, demonstrates a decrease in the northern half of the centre of the site and a decrease in the south-eastern corner of the site. Both areas exhibit similarities to the comparison of densities between site impact levels 1 and 2. In contrast, there is a significant increase in density in areas close to land near Seal Skerry, the observation vantage point and Muckle Green Holm. The most significant estimated increase in black guillemot density is observed in grid cell E2, with an increase of 1.12 individuals/km^2.

Investigation of the difference in density between devices being present onsite and devices becoming operational suggests that there is little change in density across the site (Figure 4.3.4). There is a density increase estimated across the middle of the site between Muckle Green Holm and the observation vantage point; however, due to the large CIs associated with these density estimations, these changes have been found to be not significant. Nevertheless, a significant increase in density is estimated in eight cells located in the north-eastern part of the site. Similar to the difference between site impact levels 1 and 3, there is a decline in density in the south-eastern corner; however, this is not significant.

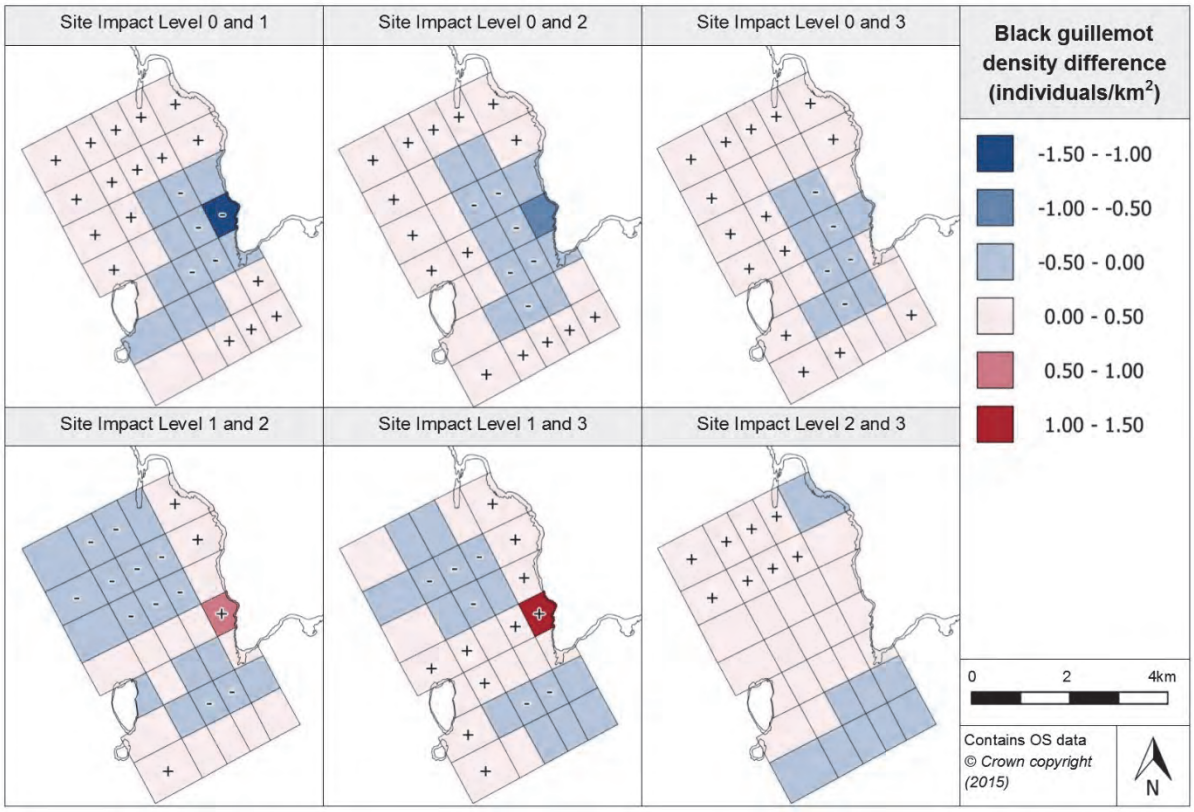

Figure 4.3.4. Estimated density difference between various site impact levels for black guillemot at the Fall of Warness. A plus symbol (+) marks cells where a significant increase in density is modelled whereas a minus symbol (-) marks cells where a significant decrease in density is modelled.

4.3.1.7 Density changes with distance from potential impact location

The density difference projections have been used to understand how the species density changes with distance from an impact location. Figure 4.3.5 illustrates how density between impact levels change with increasing distance from a grid cell containing a test berth.

Firstly, inspecting the plot for the density change between SIL-0 (baseline conditions) and SIL-1 (when infrastructure is installed), there is a clear decrease estimated in birds up to 0.4km from the grid cell, albeit less than 1 individual/km^2. Beyond 0.4km, the predicted change in density upper CI is close to zero, suggesting that the change in density could be negligible. In terms of the change in density between SIL-0 and SIL-2 (when devices are installed but not operational), up to 0.4km from the grid cell there is a decrease in density, as the upper CI is below zero; however, beyond 0.4km, the CIs widen. As the upper CI is above zero beyond 0.4km, limited inferences can be drawn regarding density change beyond this distance. The estimated density changes between SIL-0 and SIL-3 (when devices become operational) are very similar to changes observed between SIL-0 and SIL-2. For the density difference between SIL-1 and SIL-2, there appears to be very little change with increasing distance from the grid cell, except that the confidence behind the expected changes decreases (i.e. the CIs increase in width) between 0.4km and 1.1km. The increased width of the CIs between 0.4km and 1.1km is observed across all the SIL difference graphs; this suggests that either the model is affected by anomalous raw observations located between these distances or there is an increased number of varying observations between these distances. In terms of the density change for SIL-1 and SIL-3, there appears to be an increase in density at 600m from the grid cell; otherwise, the density is estimated to be constant with increasing distance from the grid cell. Lastly, the density difference between

SIL-2 and SIL-3 appears to be minimal with increasing distance from the grid cell (Figure 4.3.5).

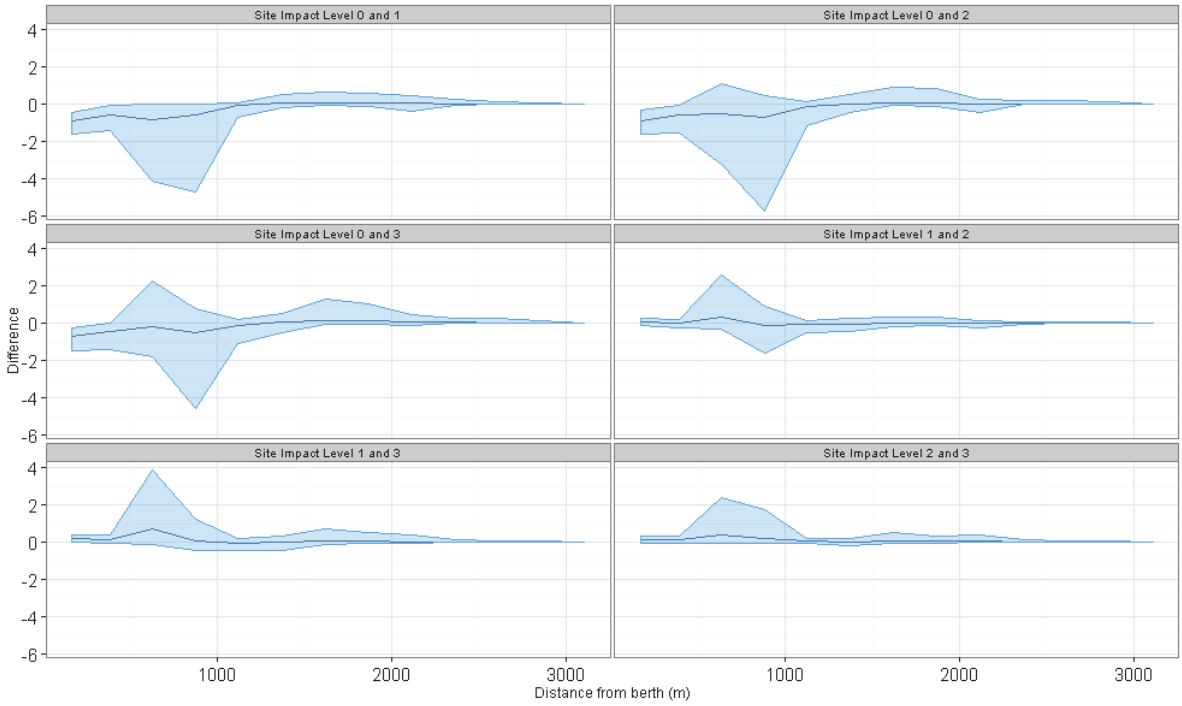

Figure 4.3.5. Density change between site impact levels with increasing distance from a potential impact location, with associated confidence intervals, for black guillemot at the Fall of Warness

4.3.1.8 Discussion

The model developed for black guillemots at the Fall of Warness tidal energy test site is fitted with 11 highly significant terms, more than for any other species. This implies that the presence of black guillemots is controlled by a greater number of environmental factors, as well as temporal and spatial terms, which need to be considered when elucidating the impact of MECS. Under the most favourable conditions for black guillemots, the model predicts that they are most abundant in close proximity to the cliffs of Eday between War Ness and Neven Point (grid cells E1 to E3) and also near to the cliffs on the eastern side of Muckle Green Holm (grid cell A3). This distribution pattern is evident at all four site impact levels.

Generally, the prediction estimates have a high precision for all grid cells, except where there are lower density estimates (Figure 4.3.2) or where there is reduced survey effort. The model shows a change in black guillemot numbers with changes in site impact level. The greatest change in density from baseline conditions (SIL-0) is expected with the emplacement of infrastructure (SIL-1), with a decrease in density in the middle of the survey grid and an increase towards the north-western and south-eastern corners. Although there is a reduction in density estimated in the areas of highest black guillemot occurrence, this is expected to return to baseline conditions as devices are installed (SIL-2) and become operational (SIL-3).

When considering the effect of installing infrastructure at a test berth, the model anticipates a further decrease in density from the already low values in the centre of the survey area. The model shows that this reduction is limited to approximately 0.4km away from the impact location and the reduction becomes less when the device is operational. This may reflect the reduction in site disturbance by vessels when devices reach the operational stage.

4.3.2 Common guillemot (Uria aalge)

4.3.2.1 Species overview

The common guillemot, *Uria aalge,* is one of the most abundant species around the UK with approximately 10-11% of the world population present (Mitchell *et al*., 2004). This exclusively marine species tends to be located on rocky cliffs and offshore islands. The species predominantly breeds on steep sea cliffs although they have also been observed nesting on some low-lying islands (SNH, 2012). Foraging tends to be limited to daylight hours with behaviour displaying pursuit diving (BirdLife International, 2015). In terms of prey species, schooling pelagic species tend to be the most common food source although benthic species can also be important to the species' diet. Similar to the black guillemot, the main prey taxa are sandeels (*Ammodytes* spp.) as well as clupeids and small gadoids.

4.3.2.2 Data summary

A summary of the raw survey data collected during the observations programme is available in Table 4.3.4. It provides information regarding the number of observations as well as the number of individuals sighted together. These summary statistics have also been broken down by site impact level to provide an understanding of the data used to make the common guillemot model.

Table 4.3.4. Summary of common guillemot raw data

	Total	Site Impact Level 0	Site Impact Level 1	Site Impact Level 2	Site Impact Level 3
Number of observations	6014	1055	2136	796	2027
Minimum (group size)	1	1	1	1	1
Maximum (group size)	900[†]	900	500	600	540
Mean (group size)	11.570	32.347	5.593	6.412	9.079

[†] Note that, on 18/05/2006 within the same hour, three grid cells were recorded with 2500, 1500 and 1500 individuals. It was concluded that these were anomalous as, according to the comments associated with these observations, it appears that the observations were recorded across many grid cells and included razorbills. As analysis had begun by the time these anomalies were found, it was decided that the most appropriate action would be to reduce the number of individuals recorded to 900, 600 and 600 respectively, in line with the greater numbers sighted later in 2006, and not to spread them across many grid cells.

4.3.2.3 Model overview

GEE-based p-values could be defined for the remaining terms once the model selection process had been completed and the final model fitted. The model identified 11 terms that were significant for the common guillemot (Table 4.3.5).

Table 4.3.5. GEE-based p-values for the terms in the final common guillemot model for the Fall of Warness

Model term	ρ-value
Tide state	<0.0001
Site impact	<0.0001
Precipitation	<0.0001
Wind strength	<0.0001
Cloud cover	0.000988
Sea state	<0.0001
Depth	<0.0001
Month	<0.0001
Year	<0.0001
Spatial surface	0.0195
Spatial surface / site impact	<0.0001

The final model contains tide state as greater abundances have been expected during an ebb tide compared to a flood tide, with lowest abundances observed during slack water. Surprisingly, greatest abundances of common guillemot are modelled to occur during heavy precipitation but lowest abundances are anticipated during showery conditions. Middling abundances are likely to occur during light precipitation or no precipitation. Similar abundances are expected at wind strengths 1, 2 and 4 (Beaufort scale) with lowest abundances seen at wind strength 3. The modelled abundances do not tend to vary much with increasing cloud cover; however, at 8 oktas (completely overcast) there tends to be an increase in abundance. Similar abundances are estimated to occur at sea states 1, 2 and 3 (Beaufort scale) with lower abundances estimated at sea state 4. In terms of common guillemot relationship with depth, the model anticipates there to be increasing individuals recorded with increasing depth.

Common guillemot levels appear to have a strong relationship to ‘month’, with greatest number of birds estimated during May and June. Figure 4.3.6 provides the partial plot produced from the fitted model showing the clear seasonal relationship in common guillemot numbers.

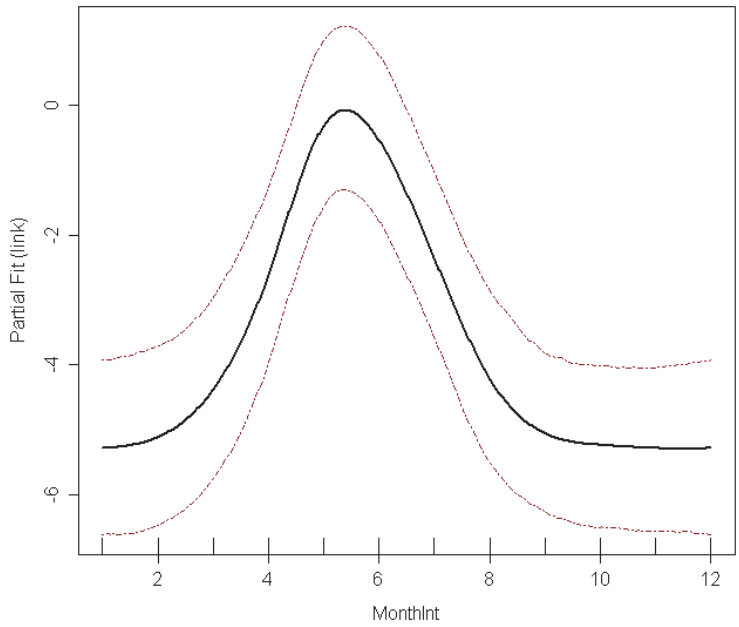

Figure 4.3.6. Estimated partial relationship of month against log(density) for common guillemot at the Fall of Warness. The red lines represent 95% confidence intervals about the estimated relationship and the tick marks show where the data lie in the covariate range.

'Year' was also retained in the model as common guillemot numbers have been found to vary significantly with survey year. Figure 4.3.7 shows a slight dip in numbers during 2007 and a greater drop in numbers between 2010 and 2012, with a recovery during 2013.

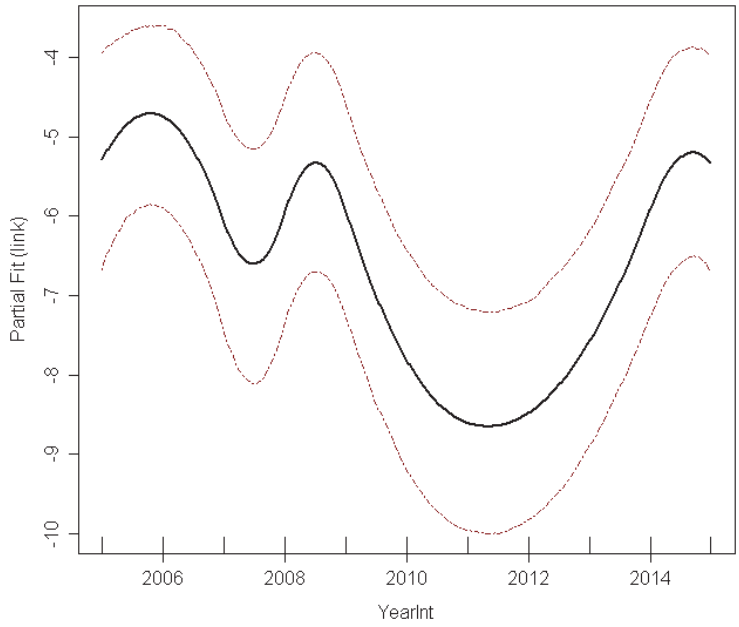

Figure 4.3.7. Estimated partial relationship of year against log(density) for common guillemot at the Fall of Warness. The red lines represent 95% confidence intervals about the estimated relationship and the tick marks show where the data lie in the covariate range.

Only a limited number of knots (three knots) were fitted for the spatial surface. The relationship between the interaction term (site impact/spatial surface) and the response term (species abundance) was found to be statistically significant.

Various diagnostic tests were undertaken on the common guillemot model to understand how well the model fitted and whether it was appropriate for the data. Due to the over dispersed nature of the species data, only limited conclusions can be drawn from performing diagnostics. Initially, the mean-variance relationship was investigated; similar to the black guillemot, there is a general underestimation of the variance by the model which is common for data with this level of over dispersion.

4.3.2.4 Density predictions and uncertainty estimation

As the model contains a spatial surface, it was possible to plot density estimates for different site impact levels across the survey region. As before, predictions had to be made for certain conditions and the optimum conditions for common guillemot sightings were chosen for each term; these are given in Appendix 5. Figure 4.3.8 provides the predicted density for each site impact level. The associated CV value for each prediction grid cell was calculated (Figure 4.3.9). As previously mentioned, CV values provide a measure of the relative variability in the densities, with the smaller values indicating a more precise estimate (lower variability).

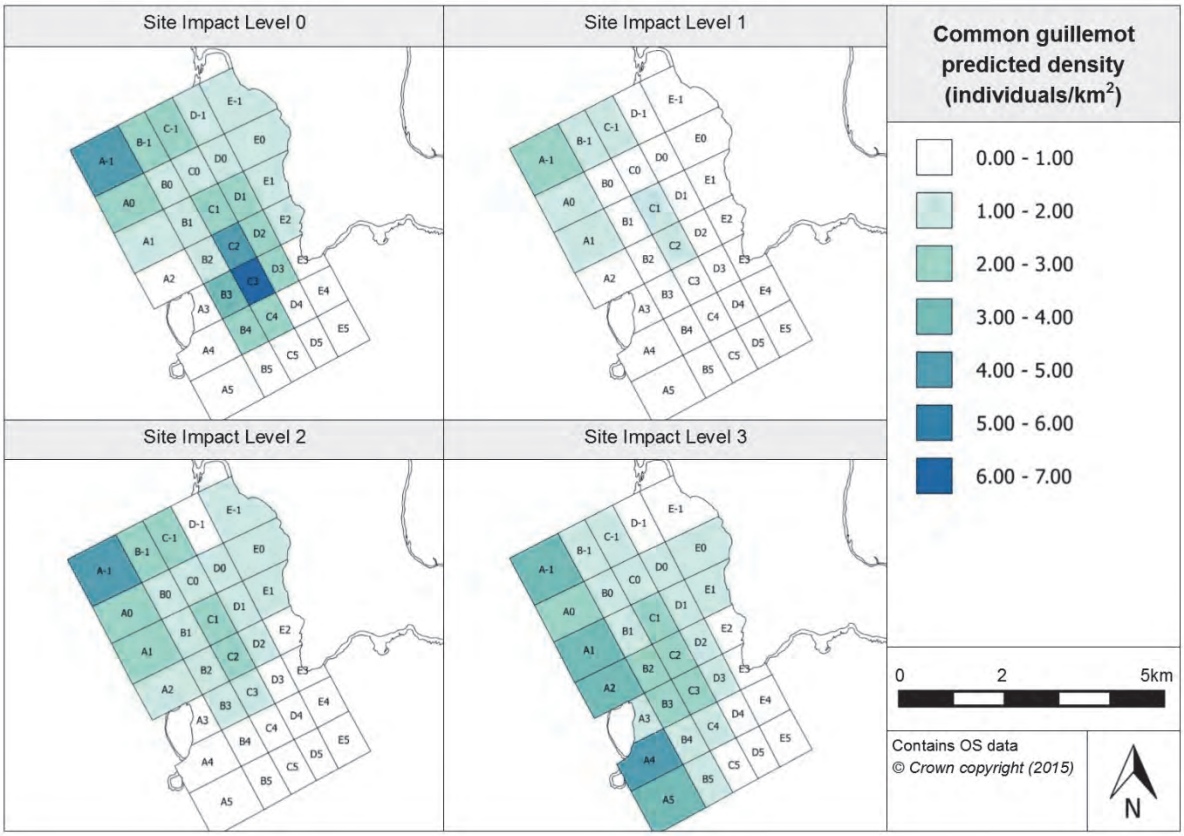

Figure 4.3.8. Estimated common guillemot density at each site impact level

From initial observations, it appears that, at baseline conditions (SIL-0), common guillemot density is greatest around grid cell C3 in the middle of the survey site with another aggregation of greater density values in grid cell A-1. In both cases, the density levels drop away smoothly from these grid cells. The greatest density estimated across all site impact levels occurs during baseline conditions in grid cell C3.

When considering the density surface at SIL-1 (when infrastructure is onsite), lower density values are expected across the site. There is a similar cluster of greater density values towards the north-west corner of the site (around grid cell A-1 again) but not to the same extent as previously observed at SIL-0. The aggregation of greater abundances around grid cell C3 that was present during baseline conditions is not present when infrastructure is installed.

For the estimated density when one or more devices are onsite (but not operational) (i.e. SIL-2), density values appear to rise from the levels expected when infrastructure is present. The same peak in abundance around grid cell A-1 is observed, with greater density values expected across the northern half of the site. When the prediction surface for device presence and operation is considered (SIL-3), there appears to be a shift from the northern half of the site towards the western side of the site (especially in the grid cells in row A). In grid cell A4, particularly great abundances were estimated; this cell is located south of Muckle Green Holm.

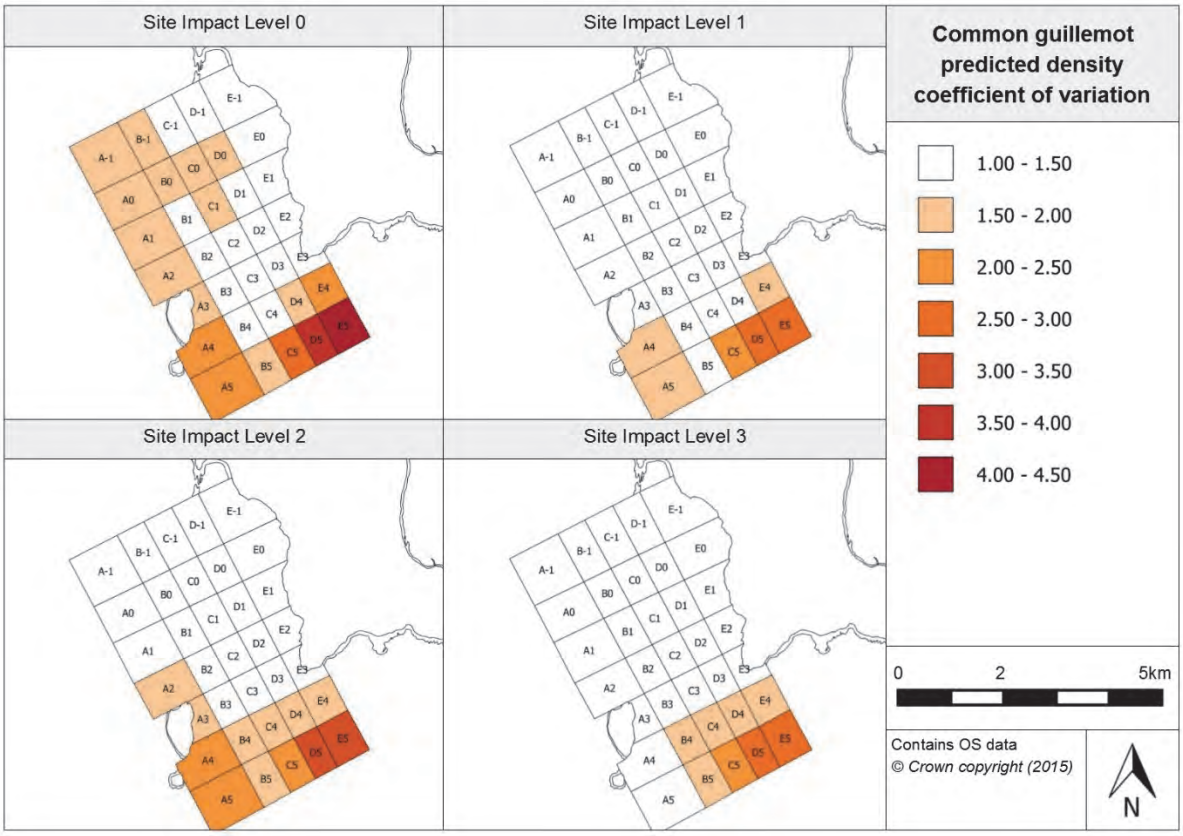

Figure 4.3.9. Associated coefficient of variation values for the density predictions for common guillemot

Figure 4.3.9 provides the associated CV values for each of the prediction surfaces. From these plots, it appears that there is higher uncertainty in the prediction surface towards the south-east corner of the site. This may result from lower density predictions in this corner or from the observer-specific observation patterns (as previously discussed). At baseline conditions, the grid cells contained in row A appear to have higher CV values suggesting that there is greater uncertainty in the predictions for grid cell A-1. Interestingly, under these same conditions, little variability appears in the predictions for grid cell C3 where a particularly large abundance was estimated.

4.3.2.5 Relative abundance estimation

Using the produced model, predicted abundance values for common guillemots for each survey month were created, applying the same environmental covariates as previously, and seasonal predictions are provided in Table 4.3.6. As already mentioned, these values are relative abundances as only surface visible observations were recorded during the observations programme.

Table 4.3.6. Relative abundance for common guillemot during each season (associated confidence intervals are provided in brackets)

Year	Season			
	Winter (Dec, Jan, Feb)	Spring (Mar, Apr, May)	Summer (Jun, Jul, Aug)	Autumn (Sep, Oct, Nov)
2005	-	-	182.55 (5.89, 1081.5)	4.43 (1.77, 9.68)
2006	2.84 (0.72, 6.38)	163.4 (4.25, 811.25)	139.26 (5.5, 645.76)	4.09 (1.80, 11.75)
2007	2.75 (0.72, 11.34)	74.08 (1.81, 367.87)	63.13 (2.06, 310.86)	1.81 (0.93, 4.12)
2008	2.07 (0.94, 4.96)	107.39 (2.57, 530.3)	91.52 (2.62, 453.61)	2.26 (0.93, 6.19)
2009	2.22 (0.98, 5.08)	111.91 (2.84, 567.09)	94.24 (1.47, 456.85)	1.04 (0.57, 2.07)
2010	0.42 (0.07, 1.59)	7.64 (0.17, 40.52)	7.23 (0.38, 30.21)	0.27 (0.12, 0.6)
2011	0.16 (0.06, 0.48)	5.84 (0.15, 27.27)	6.44 (0.22, 25.58)	0.16 (0.08, 0.33)
2012	0.17 (0.08, 0.36)	8.72 (0.22, 50.43)	7.45 (0.20, 39.07)	0.18 (0.07, 0.54)
2013	0.35 (0.07, 1.11)	9.79 (0.46, 46.19)	8.19 (0.27, 33.72)	0.2 (0.10, 0.43)
2014	0.76 (0.10, 2.30)	86.21 (2.19, 422.35)	73.47 (2.55, 334.11)	1.78 (0.81, 3.91)
2015	3.00 (0.86, 8.83)	200.17 (4.95, 1161.35)	-	-

There is a clear variation in common guillemot abundance by 'year' (as previously outlined in Figure 4.3.7); the estimated abundances show dramatic reductions between 2010 and 2013.

These expected abundance values are split into each of the site impact levels and shown in Appendix 7 alongside their associated CIs. A seasonal peak tends to emerge in spring, with numbers lower during winter.

As mentioned for black guillemots, prediction surfaces for common guillemots have been produced for typical surveying conditions in January and July. The surfaces and associated CV values are provided in the Marine Scotland Information portal. Distribution across the prediction surfaces appears to be similar but there is a dramatic difference in the density levels estimated between the two seasons, with July densities 50 times greater than those recorded in January.

4.3.2.6 Spatially-explicit change

To understand any spatially-explicit changes in abundance or distribution of common guillemot that occur across the site in connection with a change in device operational status, the difference between model predictions for each site impact level has been investigated. The significance of the difference has also been calculated using their associated 95% CIs. As 'year' was in the final model, the prediction surfaces for the least and most variable years have been provided (2011 and 2006, respectively).

For common guillemots, there appears to be a reduction in density associated with the installation of infrastructure onsite, with significant declines around grid cell C3 and near land between the observation vantage point and the bay at Seal Skerry (Figure 4.3.10).

Significant declines are also observed in the most northern part of the site out towards grid cell A-1. The most significant declines in estimated density were observed in grid cell C3, with a decrease of 0.44 individuals/km^2 in 2011 and 20.00 individuals/km^2 in 2006.

When the change in density between baseline conditions and devices being installed onsite is investigated further, a significant decline in density in grid cell C3 remains, together with three grid cells to the south of C3, but no other grid cells display a significant decline. When the change in density between SIL-0 and SIL-3 (when devices are present and operational) is considered, C3 continues to show a significant reduction in density. However, in grid cells A1-A5, a significant density increase is expected, with dramatic increases in abundance in grid cells A4 and A5 particularly, located south-east of Muckle Green Holm. The greatest increase in abundance recorded between two site impact levels is in grid cell A4 during these conditions (between SIL-0 and SIL-3), with an increase of 0.27 individuals/km^2 in 2011 and 13.54 individuals/km^2 in 2006.

When considering the change in density between infrastructure being present and device/s being installed (Figure 4.3.11), there is a density increase across the north of the site with a significant increase observed around grid cell C1 and towards the observation vantage point. There is also a marked increase in density in grid cell A-1; however, this is not found to be significant. Although not deemed to be significant, there is a density reduction estimated in the south of the site which may suggest that, with the presence of devices, common guillemots move north.

It appears that the difference in density between the presence of infrastructure and device/s being installed onsite and becoming operational causes an increase in density across the whole survey site. This increase is found to be significant around Muckle Green Holm with the extent of the decrease reducing closer to the middle of the survey site. This may suggest that, with the presence and operation of devices, there is an attraction towards land; however, if this was the case, a reduction in density in the middle of the site would be expected and this is not observed (Figure 4.3.10).

When investigating the difference in density between devices being present onsite (SIL-2) and becoming operational (SIL-3), a reduction in density appears in the north of the site with an increase in density in the south (Figure 4.3.10). However, the change is only found to be significant in the south of the site, particularly in grid cells A4 and A5. This change suggests that, with the operation of devices, there is redistribution of common guillemots within the site from the north to the south. However, the reduction in the north is not deemed be at a significant level. It should be noted that this potential redistribution is in a direction contrary to what was suggested for the installation of devices onsite.

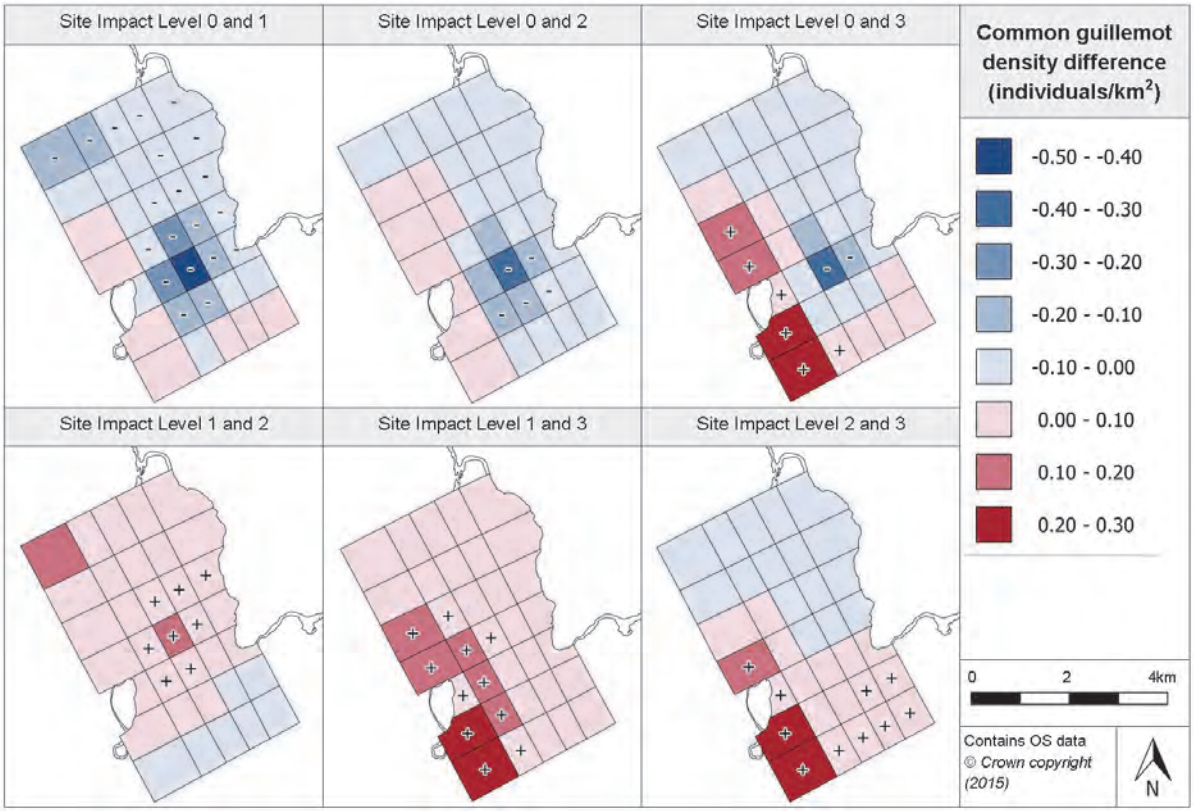

Figure 4.3.10. Estimated density difference between various site impact levels for common guillemot during 2011 (year with least variation)

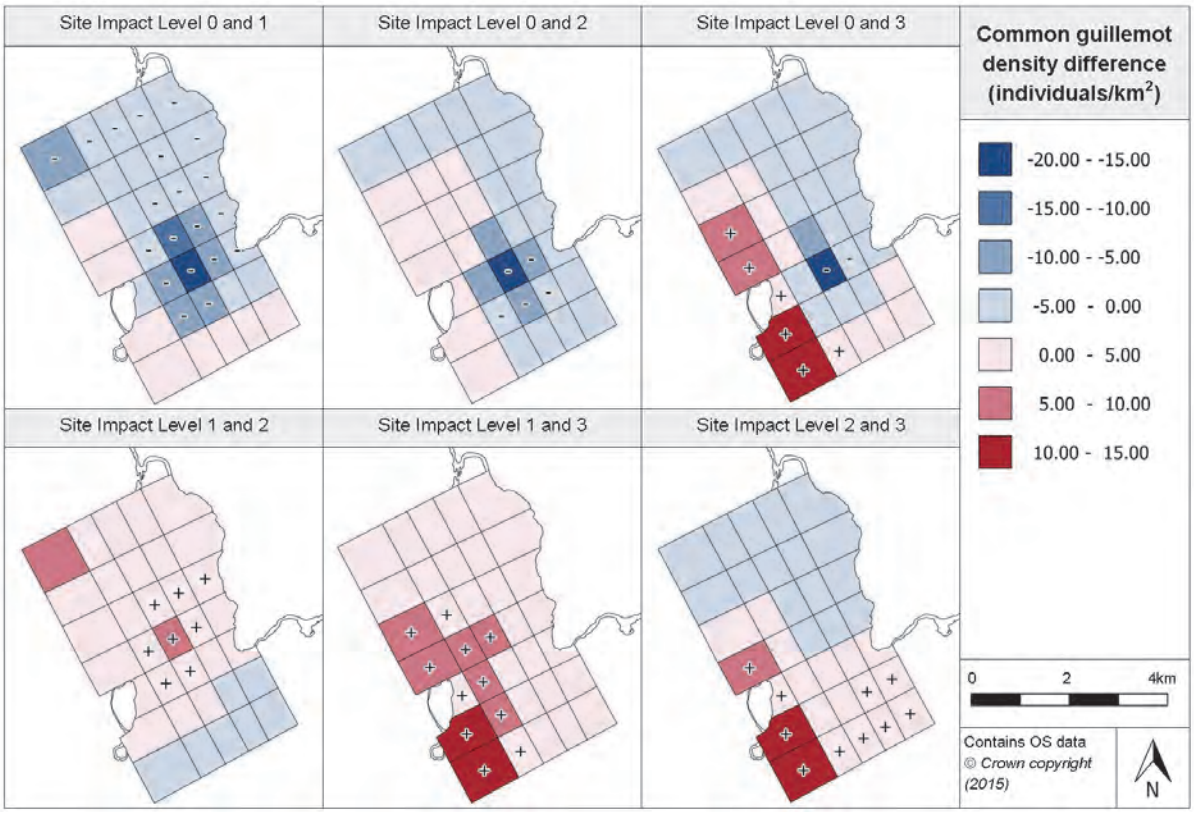

Figure 4.3.11. Estimated density difference between various site impact levels for common guillemot during 2006 (year with most variation)

4.3.2.7 Density changes with distance from potential impact location

The density difference projections have been used to understand how the species density changes with distance from an impact location. Figure 4.3.12 shows how the difference in density between impact levels changes with increasing distance from a grid cell containing a test berth. Firstly, the plot for density change between SIL-0 (baseline conditions) and SIL-1 (when infrastructure is installed), indicates that the reduction in abundance directly at the grid cell containing the test berth slowly recovers to pre-installation (baseline conditions) levels at approximately 1.3km from the grid cell. A similar relationship is estimated for density difference between baseline conditions and device/s being installed; however, common guillemot numbers appear to recover to baseline conditions early, at around 800m from the test berth grid cell. In terms of the density difference between baseline conditions and device/s being installed and operational, there remains a definite reduction in numbers directly at the affected grid cell but numbers seem to recover at a distance of around 400m.

When considering the density difference between SIL-1 and SIL-2 (when devices are installed but not operational), a very slight increase in abundance is expected at the grid cell when the device is present as compared to only infrastructure being present. Either no change or a very slight increase in density remains with increasing distance from the grid cell. Again device presence and operation produces a slight increase in density levels from that seen when only infrastructure is installed. This increase in density slowly declines with growing distance away from the grid cell, to the density levels expected when only infrastructure is installed. There appears to no great change between SIL-2 and SIL-3 (when devices become operational), with the density change not altering with increasing distance from the grid cell.

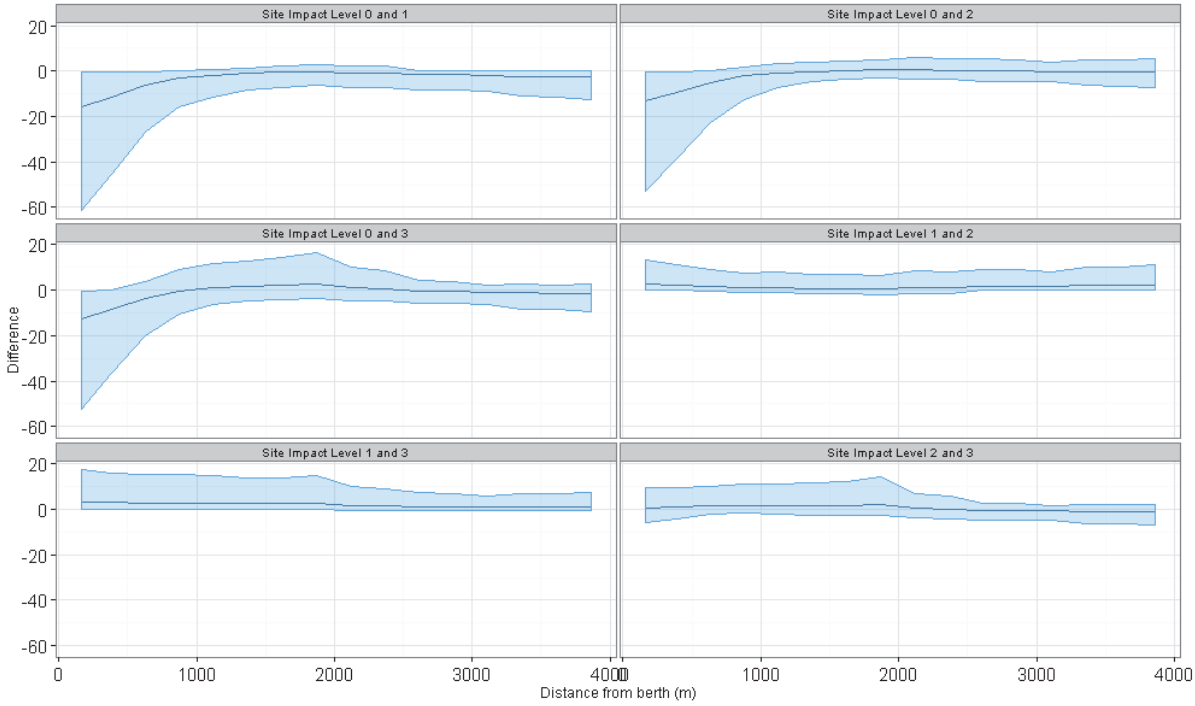

Figure 4.3.12. Density change between site impact levels with increasing distance from a potential impact location for common guillemots, with associated confidence intervals, at the Fall of Warness

4.3.2.8 Discussion

The model developed for common guillemots at the Fall of Warness includes nine highly significant and two significant environmental and temporal terms as well as spatial terms. This implies that the presence of common guillemots is controlled by a large number of environmental and temporal factors, which should be considered when interpreting the impact of MECS. Common guillemot density is strongly seasonal, with July densities 50 times greater than those recorded in January. Under the most favourable conditions for common guillemots, the model shows that they are most abundant in the centre of the survey area and in deeper water areas in the west. Estimated abundances reduce gradually with increasing site impact levels (see below), with more precision in the results where densities are lower.

The model shows a change in prediccted common guillemot numbers with changes in site impact level. The biggest change in density from baseline conditions is estimated to occur with the deployment of infrastructure (SIL-1), with a decrease in density in the centre of the survey area and an increase towards the western edge. The density reduction is in the areas of highest common guillemot occurrence, but numbers recover towards baseline conditions as devices are installed (SIL-2) and become operational (SIL-3), with density increasing along the western edge of the survey area.

When considering the effect of installing device-associated infrastructure at a test berth, the model shows a large decrease in estimated density, but this reduction is limited to approximately 1.3km from the impact location and becomes slightly less when the device is operational. However, there are very wide CIs surrounding these predictions, pointing to a low level of confidence in these results.

4.3.3 Razorbill (Alca torda)

4.3.3.1 Species overview

Razorbills, *Alca torda*, are found in coastal areas with rocky outcrops and sea cliffs. They typically nest on cliff ledges or in cracks in the cliff although they are also known to be associated with boulder-fields and scree (Mitchell *et al*., 2004). The species' foraging behaviour is pursuit diving using their wings to propel themselves through the water. Razorbills have the ability to dive to great depths but are typically observed carrying out shorter surface dives (Piatt & Nettleship, 1985). The diet of razorbills is similar to common guillemot, generally consisting of mid-water schooling fish. Particular prey species include krill (*Meganyctiphanes norvegica*), sprat (*Sprattus sprattus*), sandeel (*Ammondytes* spp.) and capelin (*Mallotus villosus*) (BirdLife International, 2015). Razorbills tend to be associated with colonies of other seabirds such as common guillemots and black-legged kittiwakes (*Rissa tridactyla*).

4.3.3.2 Data summary

Razorbills are rarely observed at the Fall of Warness with less than 500 observations made throughout the ten-year duration of the observations programme. A summary of the raw survey data collected during the programme is available in Table 4.3.7. The table provides information regarding the number of observations as well as the typical group sizes. In addition, these summary statistics have also been presented for each site impact level to provide an understanding of the data used in the modelling process.

Table 4.3.7. Summary of razorbill raw data

	Total	Site Impact Level 0	Site Impact Level 1	Site Impact Level 2	Site Impact Level 3
Number of observations	448	126	158	37	127
Minimum (group size)	1	1	1	1	1
Maximum (group size)	200	56	200	5	11
Mean (group size)	2.66	2.75	3.22	1.89	2.10
(s.d.)	(9.95)	(5.11)	(16.08)	(1.13)	(1.36)

As can be seen in Table 4.3.7, there appears to be an anomaly in the raw observation data, with a group size of 200 being recorded. This observation was made in 2007 and there were other observations in 2006 and 2007 where group sizes of greater than 20 individuals were recorded. Lavers and Jones (2007) recorded mean group sizes for razorbills at 4.3 individuals, with the maximum group size recorded during that study's duration of 15 individuals. It should be noted that this identified anomaly was included in the analysis.

4.3.3.3 Model overview

Once the model selection process had been completed, GEE-based p-values were defined for the terms in the final fitted model. The model identified nine terms that were highly significant for the razorbill (Table 4.3.8).

Table 4.3.8. GEE-based p-values for the terms in the final razorbill model for the Fall of Warness

Model term	ρ-value
Site impact	0.008954
Wind direction	<0.0001
Cloud cover	0.021657
Sea state	<0.0001
Year	0.00087
Month	<0.0001
Depth	<0.0001
Spatial surface	<0.0001
Spatial surface / site impact	<0.0001

Wind direction has remained in the final model as razorbill abundance appears to vary depending on the wind direction; it is greatest when there is no clear wind direction (i.e. when there is no wind) or when the wind direction is variable. Abundance tends to reduce when the wind comes from the north (including north-east and north-west) and seems to increase with increasing cloud cover, with greatest abundances expected when cloud cover is recorded as 7 or 8 oktas. In terms of sea state, greatest razorbill abundances are observed when the sea is calm (0 on the Beaufort scale), with density decreasing at higher sea states. Over the period of the observations programme at the Fall of Warness, razorbill abundance appears to have reduced, as 'year' has been included in the model as a declining linear term. Due to large CIs of the partial fit plot for 'month', it is difficult to interpret the relationship between abundance and 'month'; however, an increase in razorbill abundance seems to be anticipated around April with a decrease in October. Similar to 'month', depth has been plotted with large CIs, thus making it hard to interpret the relationship between species abundance and depth. The spatial surface for razorbill is not particularly complex as only three knots have been fitted.

Diagnostic tests were undertaken on the razorbill model to assess the model fit and the suitability of the model. The outputs from these tests are available in the Marine Scotland Information portal. However, due to the over dispersed nature of the species data and because there were very few observations of razorbills, these species data are particularly zero-inflated, meaning that only very limited conclusions can be drawn from the diagnostics. Cut points are used to group the data when plotting the mean-variance relationship; due to the low abundance of razorbills, all of the razorbill data have been plotted under two cut points.

4.3.3.4 Density predictions and uncertainty estimation

The razorbill model contains a spatial surface and, therefore, it is possible to produce prediction surfaces for different site impact levels across the survey region. These prediction surfaces (Figure 4.3.13) estimate the varying levels of razorbill density during June under certain environmental conditions (as outlined in Appendix 5). The associated CV value for each prediction grid cell was calculated (Figure 4.3.14). Due to anomalies in the data, it was necessary to reduce the number of iterations in the bootstrap; 868 iterations were implemented rather than the 1000 carried out for most other species/groups.

At baseline conditions (SIL-0), there is a peak in the estimated razorbill density in the south-western corner of the observation grid, in grid cells A5, B5, C5 and D5. Grid cell B5, positioned towards the centre of the southern end of the test site, has razorbill density predictions of greater than 1.80 individuals/km^2. The remaining grid cells in the prediction surface have density predictions of below 0.20 individuals/km^2. When considering the prediction surfaces at site impact levels SIL-1, SIL-2 and SIL-3 (when infrastructure is installed, devices are installed and devices are operational, respectively), the estimated density is not expected to be greater than 0.20 individuals/km^2. It is likely that there is greater variation across the prediction surfaces; however, the peaks in density seen at SIL-0 are likely to be masking any smaller variations across the prediction surface for SIL-1, SIL-2 and SIL-3.

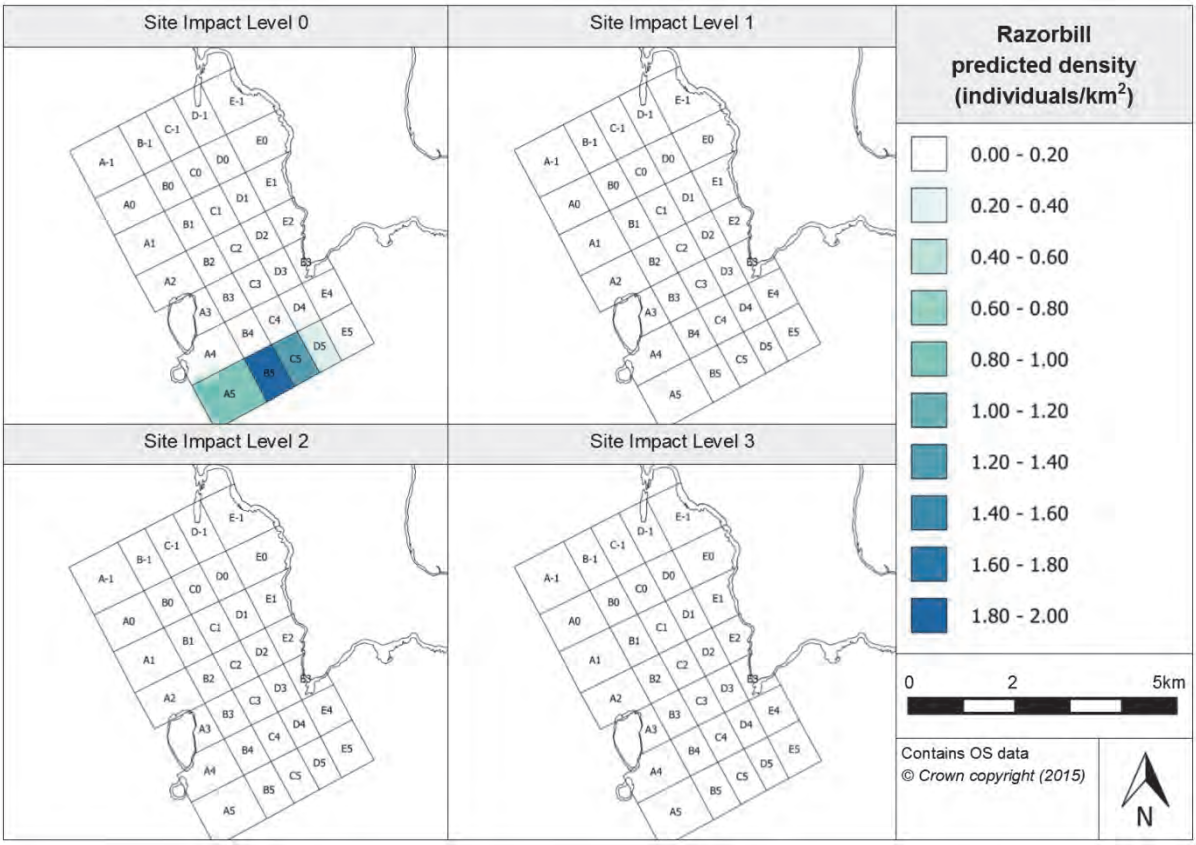

Figure 4.3.13. Estimated razorbill density at each site impact level

Figure 4.3.14, provides the associated CV values for each of the prediction surfaces. From these plots, it is clear that there is considerable uncertainty behind the predictions across the majority of the various prediction surfaces. Some CV values are unavailable (marked in grey in Figure 4.3.14). This is likely to be due to very low density predictions in these grid cells, leading to unrealistic CV values. Where available, the CV values are above 1 in every grid cell across the prediction surfaces. In terms of the CV values for the SIL-0 prediction surface, there appears to be less uncertainty in the predictions in the northern half of the grid in comparison to the southern half. In contrast, the CV values for the SIL-1 prediction surface are quite different, with higher CV values around the perimeter of the site, including the northern cells. The grid cells in the centre of the grid (around C2 and C3) appear to have lower CV values (between 1.00-2.00), suggesting that the prediction estimate is more precise than elsewhere in the grid. The majority of the southern half of the SIL-2 CV values are unavailable; this is likely to be due to very low density estimates. The remaining grid cells within the prediction surface for SIL-2 have CV values of greater than 2.00, suggesting high uncertainty in the predictions. For the SIL-3 prediction surfaces, it appears that the grid cells neighbouring the Eday shoreline have CV values of between 2.00 and 3.00, whereas grid cells in the southern and south-western corner of the site either do not have CV values available or they are greater than 3.00. This would suggest that there is very high uncertainty in this area of the prediction surface, which is probably due to very low density predictions.

In general, due to the very low density estimates across the razorbill prediction surfaces, and a very localised area of high prediction estimates under SIL-1 conditions, very high CV values have been obtained or are unable to be calculated, which suggests that there is great uncertainty behind these predictions.

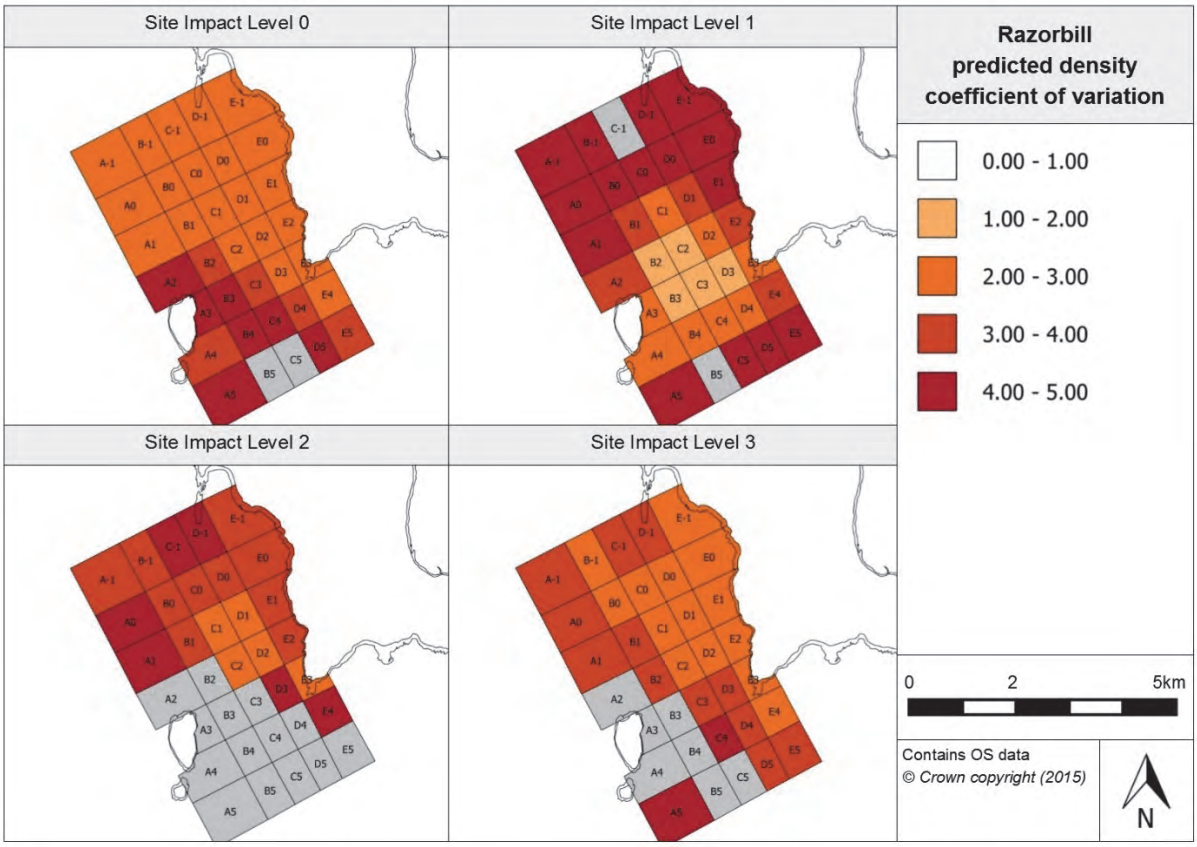

Figure 4.3.14. Associated coefficient of variation values for the density predictions for razorbill

4.3.3.5 Relative abundance estimation

Using the final fitted razorbill model, relative abundance values for each survey month can be produced. These were created using the same environmental covariates as previously. The monthly abundances have been combined to produce seasonal predictions in Table 4.3.9.

Table 4.3.9. Relative abundance for razorbill during each season (associated confidence intervals are provided in brackets)

Year	Season			
	Winter (Dec, Jan, Feb)	Spring (Mar, Apr, May)	Summer (Jun, Jul, Aug)	Autumn (Sep, Oct, Nov)
2005	-	-	1.50 (0.24, 106.90)	0.06 (0.01, 2.38)
2006	0.07 (0.05, 0.78)	1.62 (0.86, 8.27)	0.68 (0.43, 8.49)	0.03 (0.01, 0.38)
2007	0.08 (0.07, 0.66)	1.53 (1.30, 10.09)	0.64 (0.61, 5.82)	0.03 (0.02, 0.14)
2008	0.04 (0.02, 0.21)	0.48 (0.31, 1.68)	0.20 (0.11, 1.85)	0.31 (0.04, 9.48)
2009	0.40 (0.05, 13.29)	5.20 (0.52, 194.91)	2.07 (0.33, 116.57)	0.00 (0.00, 0.05)
2010	0.01 (0.01, 0.07)	0.17 (0.10, 0.83)	0.07 (0.04, 0.93)	0.00 (0.00, 0.04)
2011	0.06 (0.06, 0.56)	1.25 (0.90, 7.23)	0.50 (0.48, 2.62)	0.02 (0.01, 0.11)
2012	0.07 (0.07, 0.26)	22.35 (3.06, 2143.70)	18.92 (2.44, 1105.39)	0.80 (0.07, 33.41)
2013	0.70 (0.09, 31.60)	1.08 (0.16, 126.23)	0.09 (0.09, 0.71)	0.00 (0.00, 0.03)
2014	0.03 (0.03, 0.19)	0.48 (0.37, 2.59)	0.20 (0.15, 1.95)	0.01 (0.00, 0.08)
2015	0.00 (0.00, 0.12)	0.00 (0.00, 0.00)	-	-

Table 4.3.9 above shows the extremely wide interannual variability with particularly high razorbill numbers in spring and summer 2012 (this is likely to be the year that the anomaly occurred). Razorbills are obviously a seasonal species with low numbers in winter and autumn in all years. In addition to the estimated relative abundance values provided in Table 4.3.9, relative abundance values are split into each of the site impact levels and provided in Appendix 7 alongside their associated CIs.

Prediction surfaces for razorbills have also been produced for typical surveying conditions in January and July; the surfaces and associated CV values are provided in the Marine Scotland Information portal.

4.3.3.6 Spatially-explicit change

As the focus of this project is to identify any evidence of spatially-explicit change in species abundance or distribution arising from a shift in device operational status, the difference between model predictions for each site impact level has been investigated. The significance of the difference has also been calculated, using their associated 95% CIs. As 'year' was included in the final model, the prediction surfaces for the least (Figure 4.3.15) and most (Figure 4.3.16) variable years have been provided (2010 and 2007, respectively).

Razorbill densities at each site impact level are illustrated in Figure 4.3.13. In terms of the razorbill simulations, decreases in density are expected across the majority of the prediction grid when infrastructure is installed compared to baseline conditions, with a reduction of 0.20 individuals/km^2 across most of the site, with the exception of the south-western corner of the site. In this area, decreases in density range between 0.20 and 1.00 individuals/km^2 during 2010 (and 2.00-12.00 individuals/km^2 in 2007), with the exception of grid cell B5, where the largest decrease in density is estimated to occur (1.06 individuals/km^2 in 2010 and 12.76 individuals/km^2 in 2007). The decrease in density in the southern part of the grid and in the cells neighbouring Eday, has been deemed significant. Between SIL-0 and SIL-1, grid cells A2-A3, B2-B3 and C2-C3 have estimated increases in density of up to 0.03 individuals/km^2 in 2010 and 0.04 individuals/km^2 in 2007 (in grid cell C3). These grid cells are located in close proximity to Muckle Green Holm, suggesting that razorbills' density is influenced by proximity to this island rather than the possible locations where infrastructure will be installed.

Between SIL-0 and SIL-2, when devices are installed, the majority of the site is expected to experience a decrease in density, with most of the site having a decrease of below 0.20 individuals/km^2 during 2010 and 2.00 individuals/km^2 during 2007. Again, the south-western corner of the site shows a greater decrease in density of 0.20-1.20 individuals/km^2 and 2.00-14.00 individuals/km^2 in 2007. The density decreases in the northern and southern cells within the prediction surface have been deemed significant. Two grid cells, D2 and E2, have increases in density estimated during 2010, Cell E2 has a slight increase of 0.002 individuals/km^2 in this year whereas, in 2007, it is estimated that the increase in density would be 0.013 individuals/km^2. In terms of the estimated density difference between SIL-0 and SIL-3, when devices become operational, the expected density differences are very similar to those estimated between SIL-0 and SIL-2 (devices installed but not operating). An increase in density is only expected to occur in grid cell E2. Across the remaining grid cells, the distribution and extent of the decrease in density is expected to be very similar to that seen between SIL-0 and SIL-2, with similar grid cells having the negative change in density deemed significant.

When considering the change in density between SIL-1 (infrastructure installed) and SIL-2 (devices installed but not operating), then there is an increase in density expected in eight grid cells clustered around cells E1 and E2. The increase in density is not expected to be greater than 0.007 individuals/km^2 during 2010 and 0.066 individuals/km^2 in 2007, and in

only three cells is this change deemed significant. In the southern row of grid cells, A5-E5, there is an expected increase in density, with the greatest increase across the row during 2010 being 0.005 individuals/km^2 and, during 2007, being 0.076 individuals/km^2. Across the remaining grid cells, decreases in density are anticipated, with devices being installed compared to infrastructure deployment. The decreases are not expected to be greater than 0.004 individuals/km^2 during 2010 and 0.046 individuals/km^2 in 2007, with reductions around Muckle Green Holm deemed significant. The prediction surface between SIL-1 and SIL-3 is very similar to the estimated density differences between SIL-1 and SIL-2. Increases in density are expected in a similar area, around grid cells E1 and E2. Across the rest of the prediction grid, decreases in density of up to 0.004 individuals/km^2 during 2010 are expected and 0.051 individuals/km^2 during 2007, with the reduction in cells around Muckle Green Holm and towards the centre of the site being deemed significant.

It is predicted that, when devices become operational (between SIL-2 and SIL-3), a decrease in density would be evident across the entire site but this is not expected to be greater than 0.006 individuals/km^2 during 2010 or 0.076 individuals/km^2 during 2007. None of the grid cells have their decrease in density deemed significant.

As a general observation, across the six density difference surfaces, there is no clear relationship between the location of the test berths (that tend to be in the centre of the site) and the estimated density changes at the various site impact levels. However, due to the anomaly that exists in the razorbill data, there is a substantial razorbill density in the south-western corner of the site which is potentially masking other, much more minor, density changes that are occurring across that site with changing site impact levels.

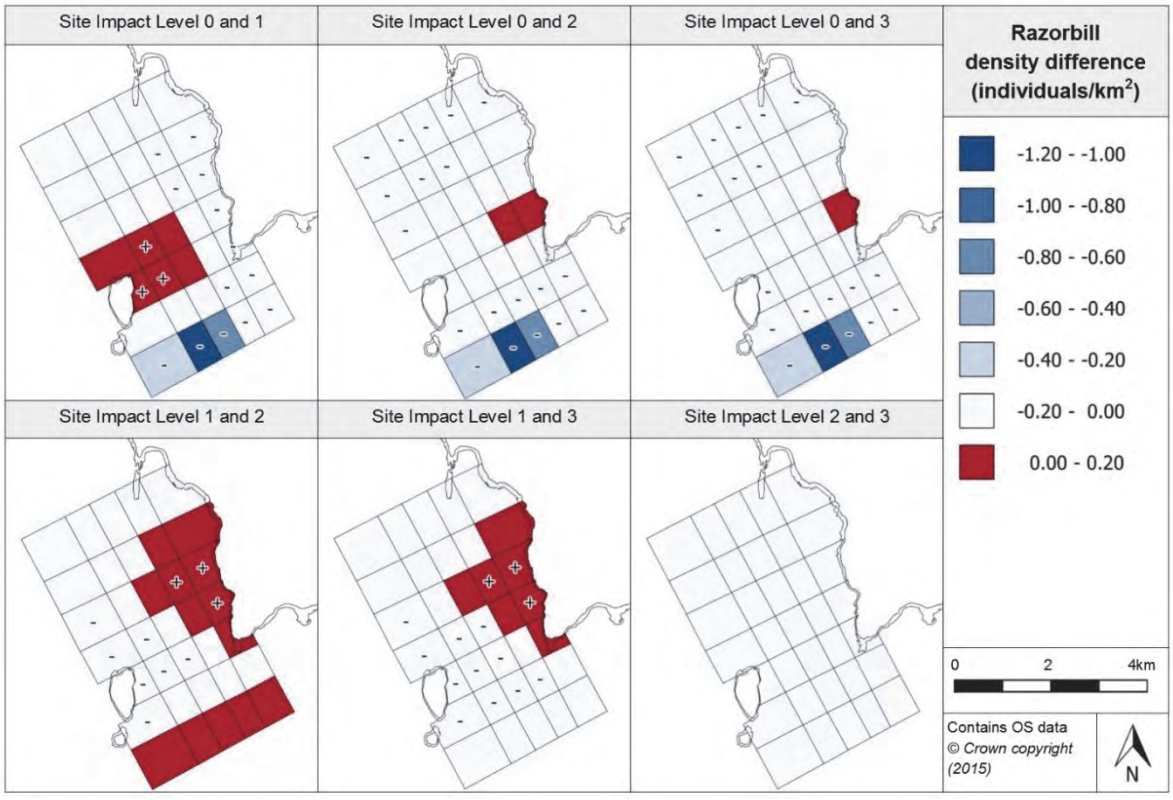

Figure 4.3.15. Estimated density difference between various site impact levels for razorbill during 2010 (year with least variation)

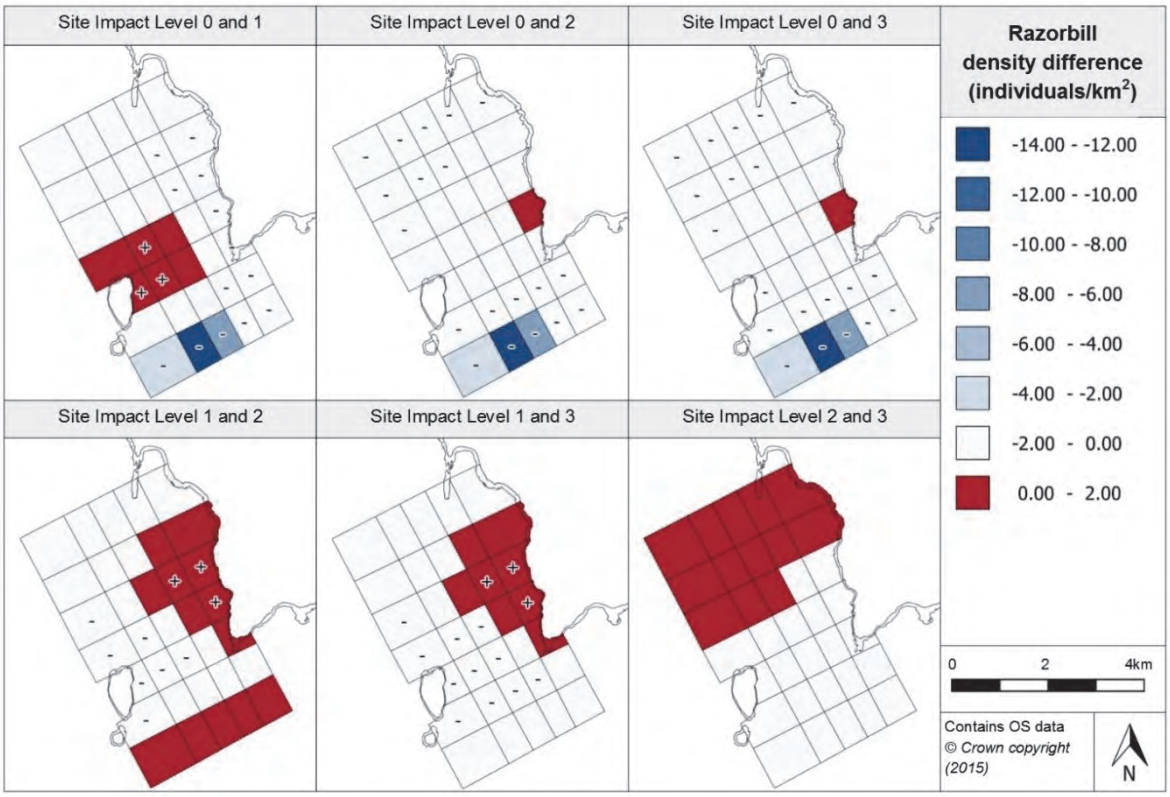

Figure 4.3.16. Estimated density difference between various site impact levels for razorbill during 2007 (year with most variation)

4.3.3.7 Density change with distance from potential impact location

The density difference projections have been used to gain an understanding of how the species density changes with distance from an impact location. Figure 4.3.17 provides an illustration of the density differences that occur across the site between the various site impact levels with increasing distance from a grid cell containing a test berth. As already discussed, there is a high density expected in the south-western corner of the test site during SIL-0 conditions. As a result, Figure 4.3.17 has been skewed by this density prediction, with a large decrease in density estimated at approximately 2.8km away from the test berth location, between SIL-0 and SIL-1, SIL-0 and SIL-2, and SIL-0 and SIL-3. In terms of the density changes between SIL-1 and SIL-2, SIL-1 and SIL-3, and SIL-2 and SIL-3, Figure 4.3.17 provides very little indication of smaller density changes that could be occurring with increasing distance from the test berth location.

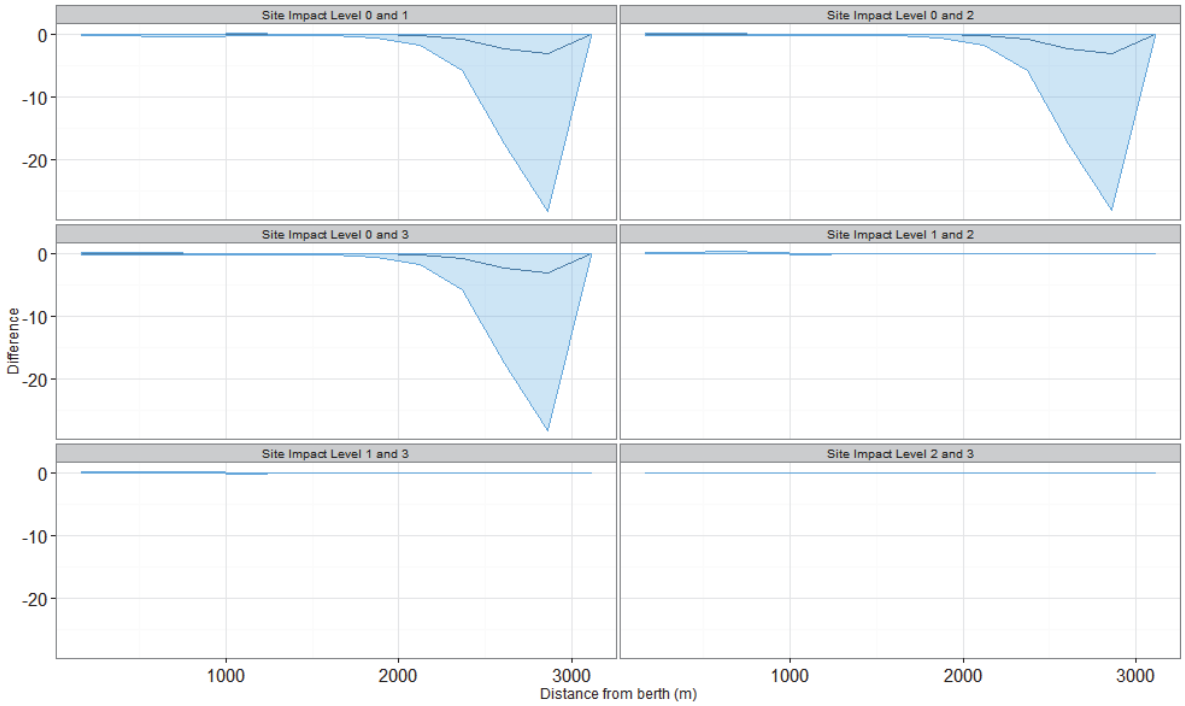

Figure 4.3.17. Density change between site impact levels with increasing distance from a potential impact location for razorbill, with associated confidence intervals, at the Fall of Warness

4.3.3.8 Discussion

The model developed for razorbills at the Fall of Warness shows six highly significant and three significant environmental, temporal and spatial terms. This implies that the presence of razorbills is controlled by a large number of factors, which should be considered when elucidating the impact of MECS. Across the prediction surfaces densities are very low across the survey sites for all site impact levels; as a result, there are particularly high CV values indicating very high uncertainty in these results, possibly due to there being very few sightings of razorbills recorded during the observations programme. Due to an anomaly in the razorbill raw observation data, it was necessary to carry out fewer bootstrap iterations for this species model. The anomaly has resulted in a very high density prediction during SIL-0 conditions in the south-western corner of the site; which means that many of the more minor density changes occurring across the site are masked. This is illustrative of a case where an alternative modelling methodology may be more appropriate, due to the very low density predictions across the site. Therefore, further analyses of the data for this species should take account of these limitations.

4.3.4 Divers

4.3.4.1 Species overview

The diver species recorded at the Fall of Warness site over the period of the observations programme are limited to the great northern diver (*Gavia immer*) and red-throated diver (*Gavia stellata*).

The great northern diver, known as the common loon in North America, is one of the larger members of the diver family. The species exhibits strong migratory patterns, utilising deep freshwater lakes for breeding then wintering either singularly or in pairs in marine habitats (Carboneras *et al*., 2014a). Occupying both freshwater and marine habitats, the species has

both freshwater and saltwater diets. Typical marine prey encompass cod (*Gadus morhua*), haddock (*Melanogrammus aeglefinus*), herring (*Clupea harengus*), sea trout (*Salmo trutta trutta*), etc. as well as crustaceans and molluscs (BirdLife International, 2015). Typical foraging behaviour is pursuit diving with the species known to dive to depths of 60m. Nesting tends to take place on offshore islands where there is limited predation. The nest is typically built very close to the water's edge and appears as a hollowed-out mound of dirt and/or vegetation.

In contrast, the red-throated diver is the smallest of the diver species that frequent the UK. Flock size during migration tends to vary from single individuals to loose groups or even large flocks (up to 1,200 individuals); such numbers have also been observed on marine feeding grounds. Similar to the great northern diver, the species' breeding sites tend to be located on freshwater lakes or amongst wet peatland habitat (Carboneras *et al*., 2014b), with the species' breeding area extending to Scotland (BirdLife International, 2015). The species preys on fish as well as crustaceans and molluscs. Red-throated divers tend to use a seizing action when diving for prey rather than the spearing action typically seen in seabirds. They carry out much shorter dives than the great northern diver, typically only diving to 2-9m depth during pursuit dives propelling themselves through the water using their feet. They usually dive from the water's surface using a jumping action rather than during flight.

4.3.4.2 Data summary

Divers are observed fairly regularly at the Fall of Warness and tend to occur solitarily.

Table 4.3.10 below provides a summary of raw survey data from the site including information on the number of observations and the mean group size. These summary statistics are also broken down for each site impact level in order to provide an understanding of the data used when creating the diver model.

Table 4.3.10. Summary of divers raw data

	Total	Site Impact Level 0	Site Impact Level 1	Site Impact Level 2	Site Impact Level 3
Number of observations	4243	423	2137	653	1030
Minimum (group size)	1	1	1	1	1
Maximum (group size)	11	8	11	6	7
Mean (group size)	1.51	1.50	1.58	1.36	1.46
(s.d)	(1.00)	(0.98)	(1.11)	(0.77)	(0.87)

4.3.4.3 Model overview

Once the model selection process was completed, the GEE-based p-values for each of the terms that remained in the final fitted model were produced. Within the final diver model, ten terms were identified as significant (seven of which were highly significant) (Table 4.3.11).

Table 4.3.11. GEE-based p-values for the terms in the final diver model for the Fall of Warness

Model term	ρ-value
Tide state	0.000254
Site impact	0.00549
Wind strength	0.000231
Cloud cover	<0.0001

Sea state	<0.0001
Depth	<0.0001
Year	<0.0001
Month	<0.0001
Spatial surface	<0.0001
Spatial surface / site impact	<0.0001

Tidal state is included in the final fitted model for divers, as the model has estimated very similar abundances of divers during flood and ebb tide with a marked increase in the number of divers during slack water. Diver abundance is anticipated to reduce with increasing wind strength. However, the confidence levels around these predictions are wide. A reduction in diver numbers is also expected with partial cloud cover but, during clear skies or full cloud cover, greater numbers are recorded. Sea state has remained in the diver model as diver abundance seems to reduce with increasing sea state, therefore suggesting that greater diver numbers are likely to be observed during calmer conditions. As seen with the razorbill model, the CIs surrounding the 'month' term in the diver model are large, making it difficult to draw any conclusions about seasonal diver abundance. However, a decline in diver numbers has been anticipated in July with greater densities expected in winter time during November/December. Again, the CIs surrounding the 'depth' term are large, creating problems for identifying any particular relationship, but it does appear that abundance has been estimated to decrease with increasing depth. The model suggests that, over the period of the observations programme, diver numbers have reduced as a declining linear relationship with 'year' has been predicted, as seen in Figure 4.3.18. Only two knots have been fitted for the spatial surface suggesting that the final fitted spatial surface is not particularly complex.

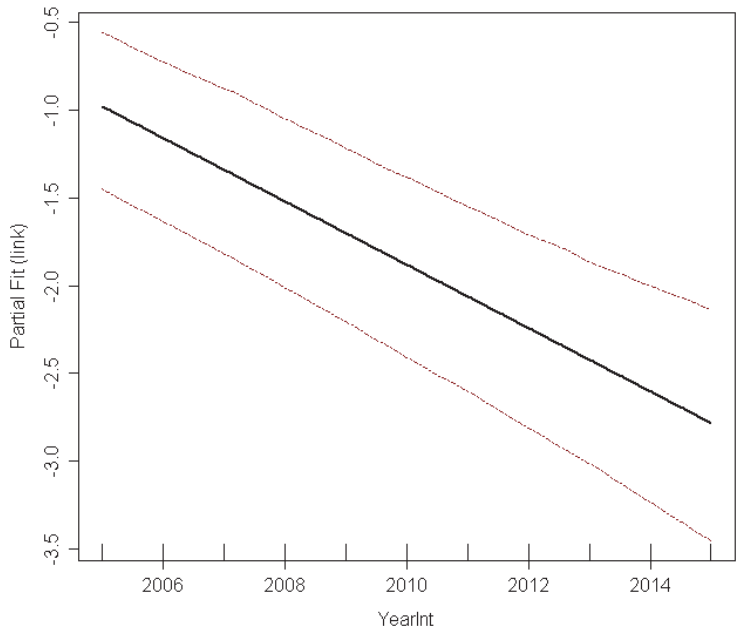

Figure 4.3.18. Estimated partial relationship of year against log(density) for divers at the Fall of Warness. The red lines represent 95% confidence intervals about the estimated relationship and the tick marks show where the data lie in the covariate range.

Various diagnostic tests were undertaken on the diver model in order to assess how well the model accounted for uncertainty and whether it was appropriate for the data. Due to the

over dispersed nature of the species data, only limited conclusions can be drawn from performing diagnostics. Initially, the mean-variance relationship was investigated; this is generally well captured by the model although there may be a slight overestimation of uncertainty for low fitting values. All diagnostic plots are also available in the Marine Scotland Information portal.

4.3.4.4 Density predictions and uncertainty estimation

As the spatial surface was included in the final fitted model, it was possible to plot the density for different site impact levels across the survey region. Predictions were made for optimum diver surveying conditions, see Appendix 5. The estimated density for each site impact level is provided in Figure 4.3.19 with the associated CV values for each prediction surface shown in Figure 4.3.20. CV values provide a measure of the relative variability in the densities, with smaller values indicating a more precise estimate (lower variability).

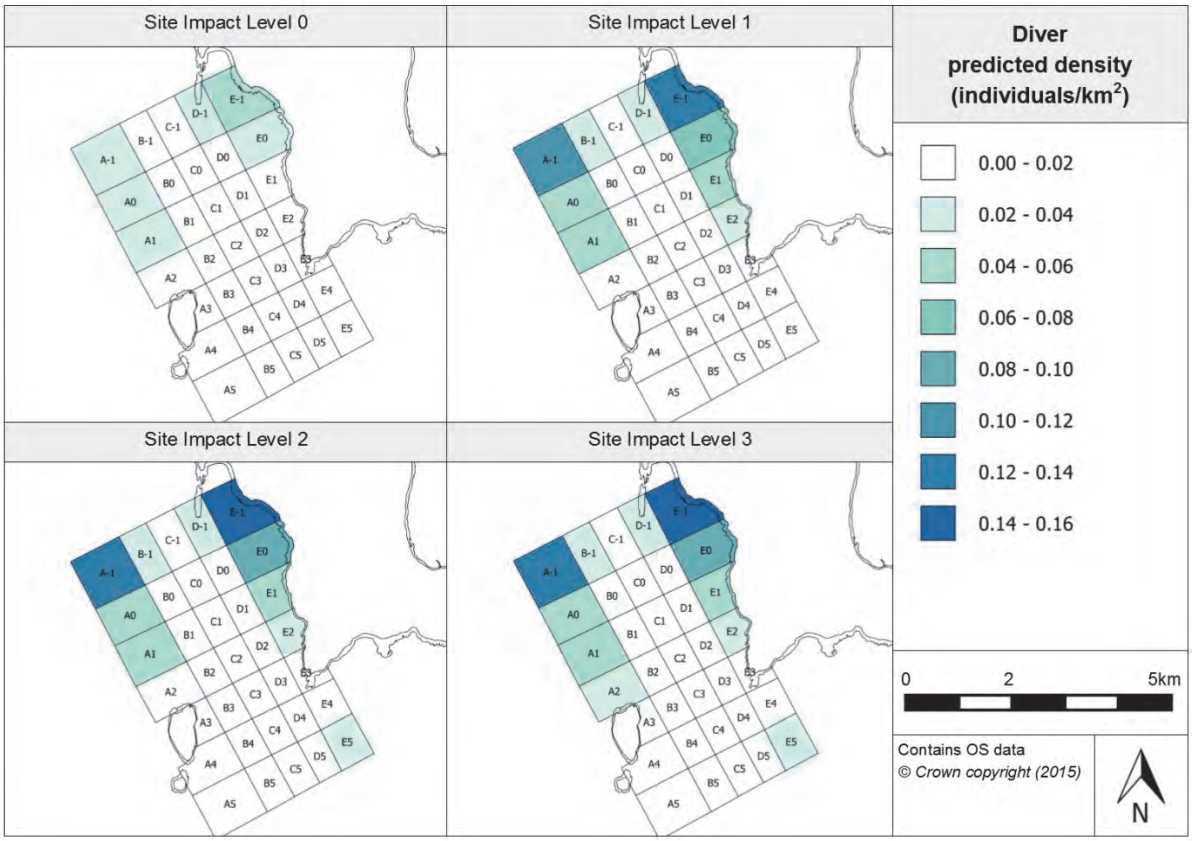

Figure 4.3.19. Estimated diver density at each site impact level

Figure 4.3.19 shows that, at baseline conditions (SIL-0), a greater density of divers in the bay near Seal Skerry (cell E-1) and in the north-west corner of the site (cell A-1) has been estimated. However, the variation in density values across the site at baseline conditions is minimal. In terms of how density changes between the site impact levels, it appears that variation in density values across the site increases with increasing site impact level, with SIL-1 (when infrastructure is installed onsite) having much greater levels of abundance in grid cells E-1 and A-1 modelled. From both these grid cells where a peak in density is anticipated, there is a smooth reduction in the estimated density values towards the centre of the site, where the majority of the test berths are located.

For the expected density when one or more devices are onsite (but not operational) (i.e. SIL-2), a further increase in diver density is modelled in grid cells E-1 and A-1, reaching a peak across all conditions in grid cell E-1 (Figure 4.3.19). When devices become operational (SIL-3), the predicted density surfaces appear to remain very similar in terms of abundance and distribution when compared to conditions when device/s were only present but not operational. This may suggest that device operation has minimal effect on diver numbers and distribution.

A further point worth noting is that, during baseline conditions and when only infrastructure was onsite, the estimated density in the south of the site was negligible in comparison to the north whereas, at SIL-2 and SIL-3, grid cell E5 is estimated to have a slight peak in density, compared to its surrounding grid cells.

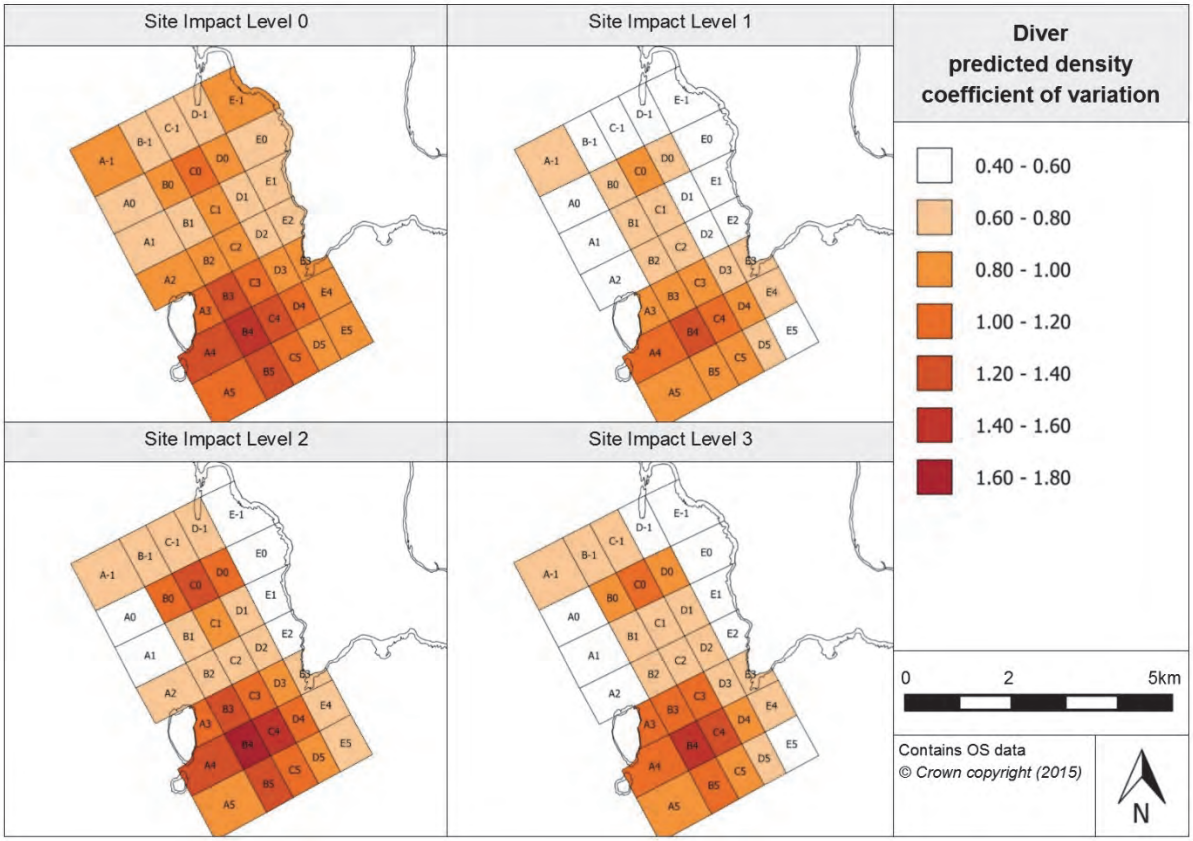

Figure 4.3.20. Associated coefficient of variation values for the density predictions for divers

Figure 4.3.20 provides the associated CV values for each of the prediction surfaces. From these plots, it emerges that there is high uncertainty in the prediction surface around grid cell B4 at the southern end of the survey site. This is likely due to there being fewer observations in this area, which has already been translated into a low estimated abundance in the south of the survey site. Higher CV values also exist around grid cell C0, suggesting high variability in the prediction surface at this point in the site. However, it appears that there is a more precise estimate around the predictions for grid cells A-1 and E-1 at site impact levels 1, 2 and 3, where greater diver abundances are anticipated.

4.3.4.5 Relative abundance estimation

Using the produced model, estimated abundance values for divers for each survey month can be created applying the same optimum environmental conditions as used previously. The seasonal predictions have been provided in Table 4.3.12. As mentioned already, these

values are relative abundances as only surface visible observations have been recorded during the observations programme. The estimated abundances have also been provided across site impact levels (see Appendix 7) with their associated CIs to highlight the degree of precision underlying each estimated abundance.

Table 4.3.12. Relative abundance for divers during each season (associated confidence intervals are provided in brackets)

Year	Season			
	Winter (Dec, Jan, Feb)	Spring (Mar, Apr, May)	Summer (Jun, Jul, Aug)	Autumn (Sep, Oct, Nov)
2005	-	-	0.56 (0.31, 0.9)	2.61 (1.23, 4.30)
2006	3.89 (2.33, 6.16)	3.58 (1.61, 6.33)	1.08 (0.62, 1.64)	5.34 (2.60, 9.54)
2007	4.48 (2.71, 7.20)	3.87 (1.72, 6.90)	1.16 (0.64, 1.93)	5.40 (2.49, 8.69)
2008	2.70 (1.14, 6.18)	1.60 (0.71, 2.85)	0.48 (0.27, 0.77)	1.19 (0.48, 2.23)
2009	0.82 (0.42, 1.54)	0.65 (0.26, 1.33)	0.25 (0.10, 0.51)	1.58 (0.81, 2.38)
2010	1.10 (0.68, 1.74)	0.89 (0.42, 1.46)	0.29 (0.18, 0.47)	1.44 (0.72, 2.24)
2011	1.74 (0.97, 2.88)	1.82 (0.85, 3.12)	0.54 (0.31, 0.86)	2.53 (1.21, 4.06)
2012	1.27 (0.57, 2.74)	0.68 (0.15, 1.27)	0.12 (0.06, 0.22)	0.56 (0.22, 1.06)
2013	0.54 (0.29, 0.97)	0.74 (0.40, 1.31)	0.27 (0.16, 0.42)	1.27 (0.63, 2.01)
2014	1.02 (0.66, 1.44)	1.02 (0.48, 1.72)	0.31 (0.18, 0.47)	1.44 (0.73, 2.21)
2015	1.71 (0.96, 3.18)	1.76 (0.73, 3.50)	-	-

In addition to the above, two further prediction surfaces have been created for January and July. In making these surfaces, the typical surveying conditions for each month have been used. The surfaces and associated CV values have been provided in the Marine Scotland Information portal. The distribution across the prediction surfaces appears similar except for the difference in the density level between the two seasons. Greater densities are expected in January in comparison to July.

4.3.4.6 Spatially-explicit change

To understand any spatially-explicit changes in abundance or distribution of divers that occur across the site due to a change in device operational status, the differences between model predictions for each site impact level have been investigated (Figure 4.3.21 and Figure 4.3.22). As 'year' was in the final model, the prediction surfaces for the least and most variable years have been provided (2012 and 2006, respectively).

In terms of the change in density from baseline conditions with the installation of infrastructure, a redistribution within the site is anticipated; abundances reduce significantly in the centre of the site (particularly in the south) and a significant increase in divers is estimated in the grid cells neighbouring Eday, as well as in the far west of the survey site. This redistribution away from the centre grid cells is in line with the location of test berths and may suggest that, with the installation of infrastructure, divers move away from the infrastructure and towards the perimeter of the site.

When considering the change in estimated density between baseline conditions and devices being installed (but not operational), abundance and distribution looks similar to that observed for the difference between SIL-0 and SIL-1. The extent of the decrease in density in the centre is estimated to reduce, with the change in fewer grid cells being determined as significant. However, it is between these conditions (SIL-0 to SIL-1) when the largest decrease in density is estimated, with the density in grid cell C0 reducing by 0.0021

individuals/km^2 in 2012 and by 0.011 individuals/km^2 in 2006. In addition, it appears that the density changes anticipated at the site's perimeter have grown in magnitude. It is also between SIL-0 and SIL-1 when the greatest increase in density is estimated, with an increase of 0.040 individuals/km^2 in 2012 and 0.22 individuals/km^2 in 2006 in grid cell E-1 (adjacent to the bay at Seal Skerry).

For the density difference between SIL-0 and SIL-3 (when devices are installed and operational), the extent of the reduction in density for the grid cells in the centre of the site is less than the differences between SIL-0 and SIL-1 and between SIL-0 and SIL-2, and fewer cells show a significant decline. However, there are six more grid cells where a positive change in density is expected for 2012 and seven cells for 2006. For the density difference between SIL-0 and SIL-3, the increase in density in all the grid cells in row E is deemed to be significant and similarly for the grid cell north of Muckle Green Holm. This may indicate that the impact of infrastructure or device presence reduces when devices become operational, or that greater numbers are attracted to the perimeters of the site due to the operation of devices.

Between SIL-1 and SIL-2 (when devices are installed but not in operation), there are no significant changes experienced. There is a slight decline in grid cells in the northern centre of the site but otherwise, very little change or only a slight positive change is expected. This would seem to indicate that the addition of devices onsite has very little impact on diver numbers.

Similarly, between SIL-1 and SIL-3 (when devices become operational), either no change or a slight positive change occurs. The slight positive change in grid cells E3 and E4 has been deemed significant. Again, this would suggest the presence and operation of devices causes very little change in terms of diver numbers compared to only infrastructure being onsite.

When considering the change between SIL-2 and SIL-3, there appears to be only slight changes, with a reduction in abundance estimated in the north-east and north-west corners of the site; however, these changes are not deemed to be significant. Across the rest of the site, the change is expected to be negligible or slightly positive.

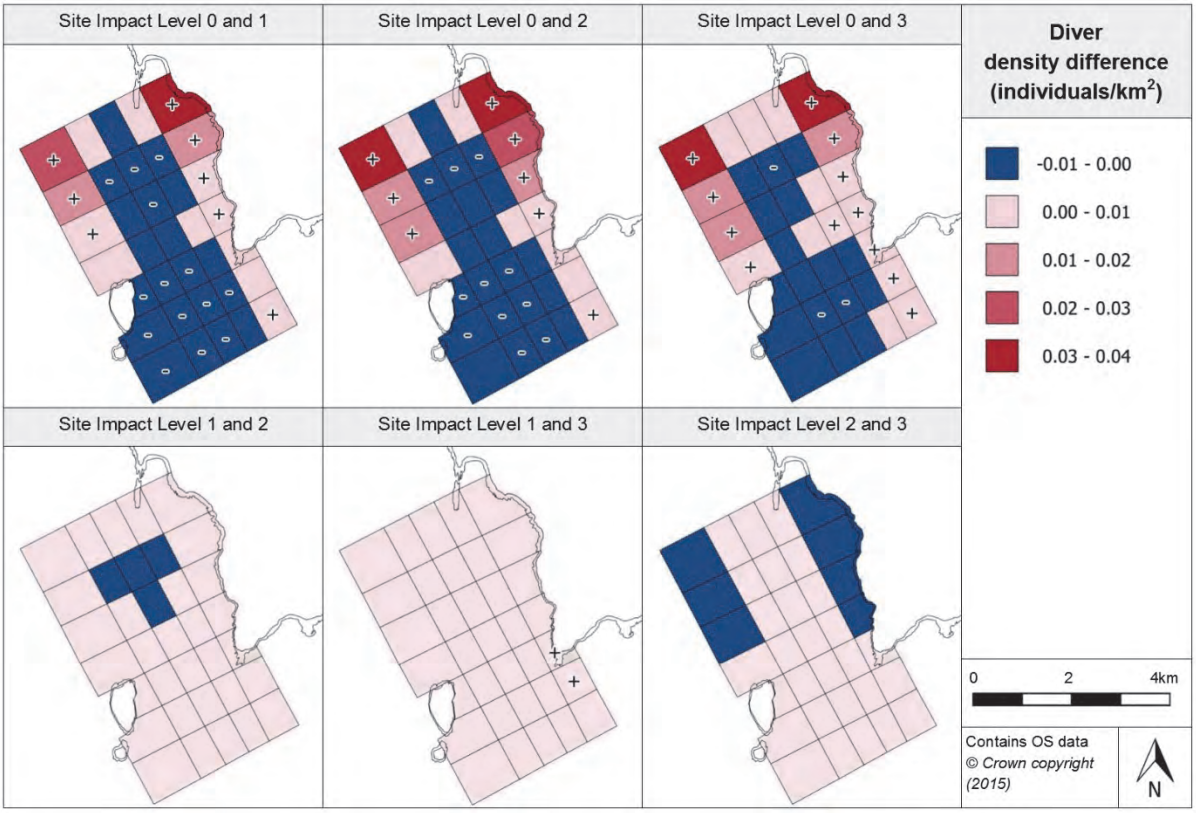

Figure 4.3.21. Estimated density difference between various site impact levels for divers during 2012 (year with least variation)

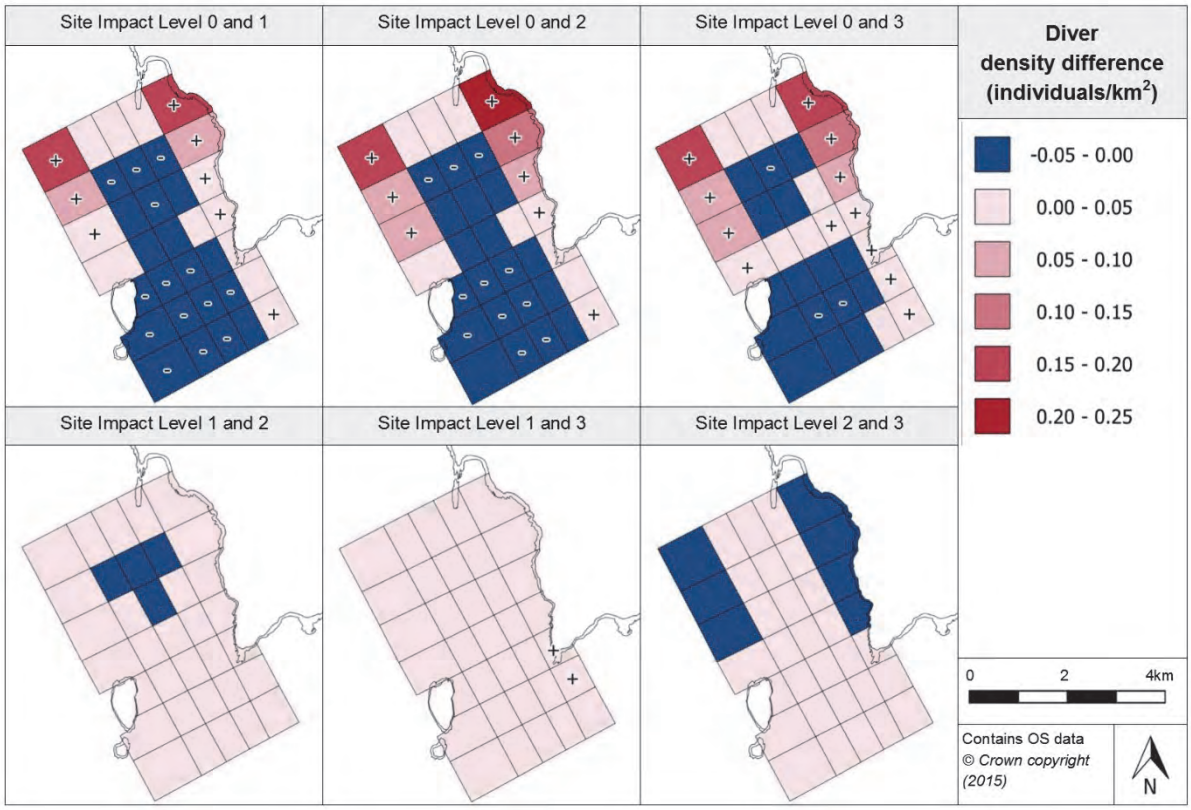

Figure 4.3.22. Estimated density difference between various site impact levels for divers during 2006 (year with most variation)

4.3.4.7 Density change with distance from potential impact location

The density difference projections have been used to understand how species density changes with distance from an impact location. Figure 4.3.23 shows how the difference in density between impact levels changes with increasing distance from a grid cell containing a test berth.

When inspecting the plots for diver density change between baseline conditions and site impact levels 1, 2 and 3, the density difference projections in terms of distance away from the grid cell all look remarkably similar. There is a reduction in abundance in the grid cells close to the test berth's location which slowly recovers to baseline conditions at approximately 500m distance. There is then an increase in density from baseline between approximately 1.1km and 1.7km (from the grid cell containing the test berth). From 1.7km, densities appear to return back to baseline conditions; however, there then appears to be a gradual increase in density beyond 4.1km.

When considering the change in density between SIL-1 (when infrastructure is installed) and SIL-2 and SIL-3, similar patterns in density changes with increasing distance from the grid cell are observed. There is very little change anticipated with increasing distance from the grid cell and no explicit increase or decrease in density as the CIs lie on either side of the zero line. There appears to no great change between SIL-2 and SIL-3 with the change in density not altering with increasing distance from the grid cell.

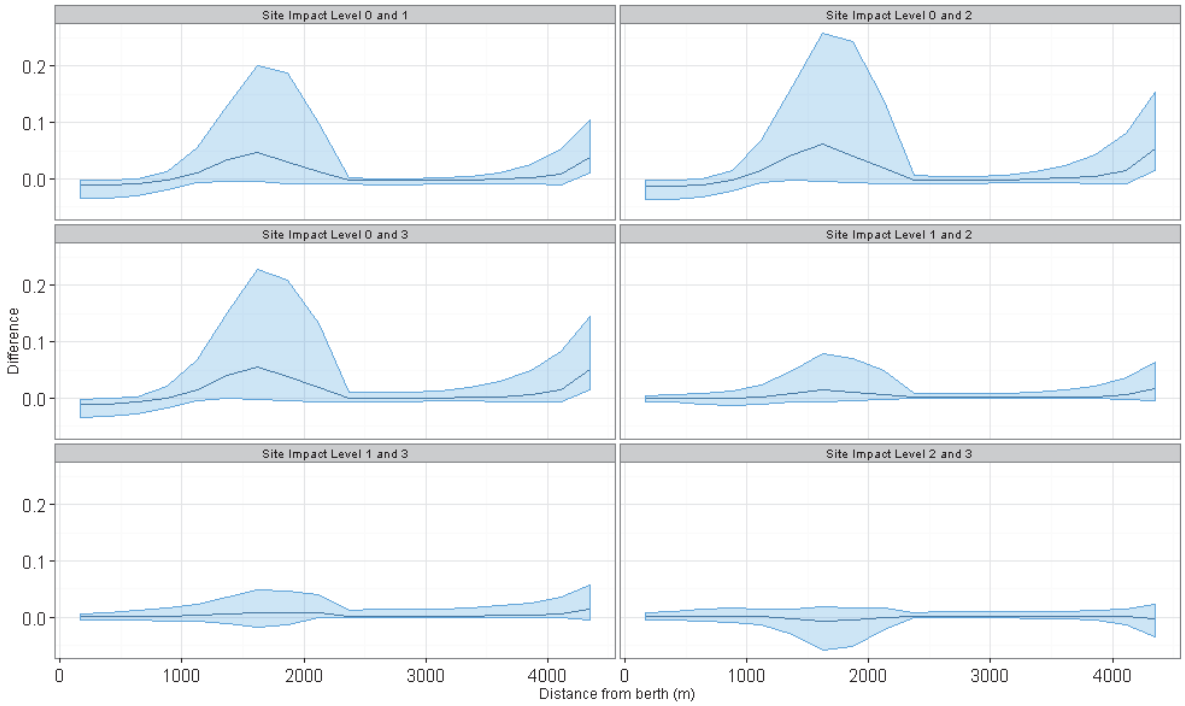

Figure 4.3.23. Density change between site impact levels with increasing distance from a potential impact location, with associated confidence intervals, for divers at the Fall of Warness

4.3.4.8 Discussion

The model developed for divers (great northern diver and red-throated diver) at the Fall of Warness has been fitted with seven highly significant and three significant environmental, temporal and spatial terms. This implies that the presence of divers is controlled by a large number of factors, which should be considered when explicating the impact of MECS. Diver abundance is strongly seasonal, with greater abundance in winter and spring compared to summer and autumn. Under the most favourable conditions for divers, the model shows that they are expected to be most abundant in close proximity to the coast of Eday (grid cells E-1 to E2) and also in cells along the north-western edge of the survey area. These cells have very low uncertainty. This distribution pattern was evident at all four site impact levels, with the lowest densities estimated under baseline conditions.

The model estimates a change in diver numbers with a change in site impact level. The biggest change in density from baseline conditions (SIL-0) occurs with the deployment of infrastructure (SIL-1), with a large decrease in density identified in the middle of the survey grid, which is also the general location of all the test berths at the Fall of Warness. Between SIL-0 and SIL-1, there is also an increase in diver density in grid cells along the eastern and north-western edges of the survey area, where densities tend to be greatest. The extent of change lessens slightly with the progression through site impact levels (SIL-1, SIL-2 and finally, SIL-3).

The increase in numbers along the edges of the survey area is also evident in the plots of density change away from the impact location, which all appear to indicate small decreases in estimated density at the potential impact location (single test berth) and a large increase in density at a distance of approximately 1.6km.

4.3.5 Shags and cormorants

4.3.5.1 Species overview

European shags and great cormorants have been grouped together for the analysis as there are many observations at the Fall of Warness where the observers have not been able to distinguish between the two species and so *Phalacrocorax* spp. has been recorded.

The European shag, *Phalacrocorax aristotelis*, is a coastal species which tends not to stray far from land. It shows a preference for coastal habitats that have rocky coasts and islands and are near to deep water (Orta *et al*., 2014a). It has a wide ranging diet but typically preys on benthic-dwelling species with the most common prey species being sandeels (*Ammodytes marinus).* Foraging habitat is predominantly sandy and rocky seabeds (BirdLife International, 2015). The species is known for its deep dives to the benthos, and can reach at least 45m depth.

The great cormorant, *Phalacrocorax carbo*, has a habitat differing slightly from the European shag, as the species can be found in more inland habitats as well as on the coast. When on the coast, the species is typically found in more sheltered areas e.g. estuaries, saltpans, coastal lagoons (Orta *et al*., 2014b). However, the species also requires to access rocky shores and cliffs (like those found around Orkney) for nesting. Marine prey for the species includes benthic-dwelling fish, but cormorants have also been observed preying on shoaling fish in deeper waters (BirdLife International, 2015). Although the great cormorant can dive to great depths similarly to the European shag, the species tends to forage in shallower waters, frequently bringing its prey to the surface.

4.3.5.2 Data summary

European shags and great cormorants were two of the most common species recorded at the Fall of Warness. Table 4.3.13 below provides a summary of the raw survey data in terms of the number of observations as well as the mean group size. This information has been broken down for each site impact level to provide an overview of the raw data used during the modelling process.

Table 4.3.13. Summary of shags and cormorants raw data

	Total	Site Impact Level 0	Site Impact Level 1	Site Impact Level 2	Site Impact Level 3
Number of observations	42677	2417	17704	8245	14311
Minimum (group size)	1	1	1	1	1
Maximum (group size)	1300	185	500	302	1300
Mean (group size) (s.d)	5.28 (17.73)	3.98 (9.80)	6.25 (18.95)	4.80 (14.74)	4.56 (18.72)

4.3.5.3 Model overview

GEE-based p-values were produced for each of the terms that remained in the final fitted model. Ten terms were found to be significant and therefore were kept in the final shag and cormorant model (Table 4.3.14).

Table 4.3.14. GEE-based p-values for the terms in the final shag and cormorant model for the Fall of Warness

Model term	ρ-value
Tide state	<0.0001
Site impact	<0.0001
Precipitation	0.002921
Wind direction	<0.0001
Cloud cover	<0.0001
Depth	<0.0001
Year	0.021075
Month	<0.0001
Spatial surface	<0.0001
Spatial surface / site impact	<0.0001

Tidal state has been kept in the final shag and cormorant model as the model has estimated that, during ebb tide, much greater abundance of shags and cormorants is likely, whereas lower abundances are expected during flood tide and slack water. In terms of precipitation, more birds are estimated when there is no rain, light rain or showers (as compared to heavy and constant precipitation). It is anticipated that shag and cormorant abundance increases with cloud cover, as seen in Figure 4.3.24.

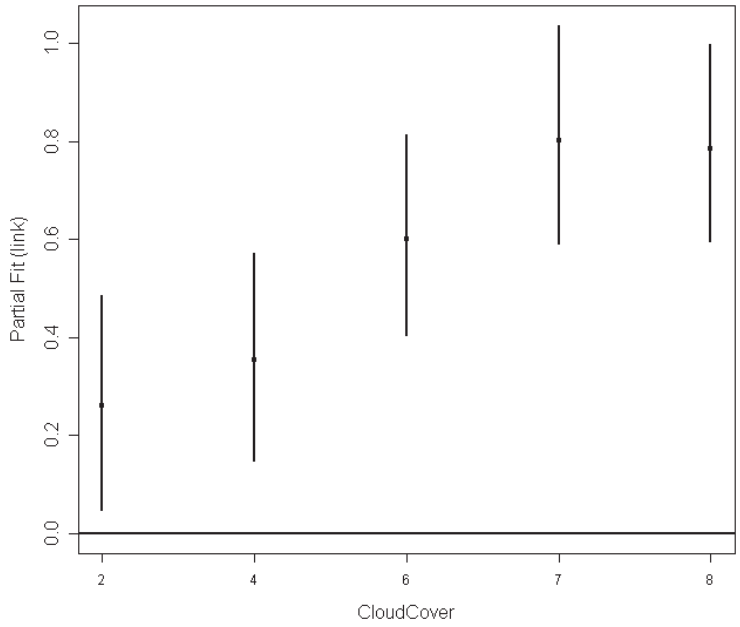

Figure 4.3.24. Estimated partial relationship of shag and cormorant density (on the scale of the log link) with cloud cover at the Fall of Warness. The points are the parameters for the estimated change in log density from the baseline (cloudcover = 0) and the vertical lines represent 95% confidence intervals about the parameter estimates.

There are wide CIs surrounding the depth predictions; however, abundance is expected to reduce with increasing depth. In terms of the seasonal distribution of shags and cormorants, again there are wide CIs surrounding the predictions but the model has estimated there to be a peak during winter, December/January, and lower abundances are expected during

June/July. In addition, the partial plot for 'year' suggests that shag and cormorant abundance has reduced gradually over the period of the observations programme.

Various diagnostic tests were undertaken on the shag and cormorant model to assess how well it accounted for uncertainty and whether it was appropriate for the data. The mean-variance relationship is generally well captured by the model although there may be some underestimation of uncertainty on high fitting values. The observed versus fitted values plot, which compares the raw data simulations with the shag and cormorant model is also available on the Marine Scotland Information portal. It appears that the relationship (observed versus fitted values) for the model is similar to the relationship observed for the simulated data.

4.3.5.4 Density predictions and uncertainty estimation

Due to the spatial surface being included in the final shag and cormorant model, the estimated density for different site impact levels across the survey region was plotted. Predictions were made for March at optimum shag and cormorant surveying conditions which are provided in Appendix 5. The predicted density for each site impact level is provided in Figure 4.3.25 with the associated CV values for each prediction surface given in Figure 4.3.26.

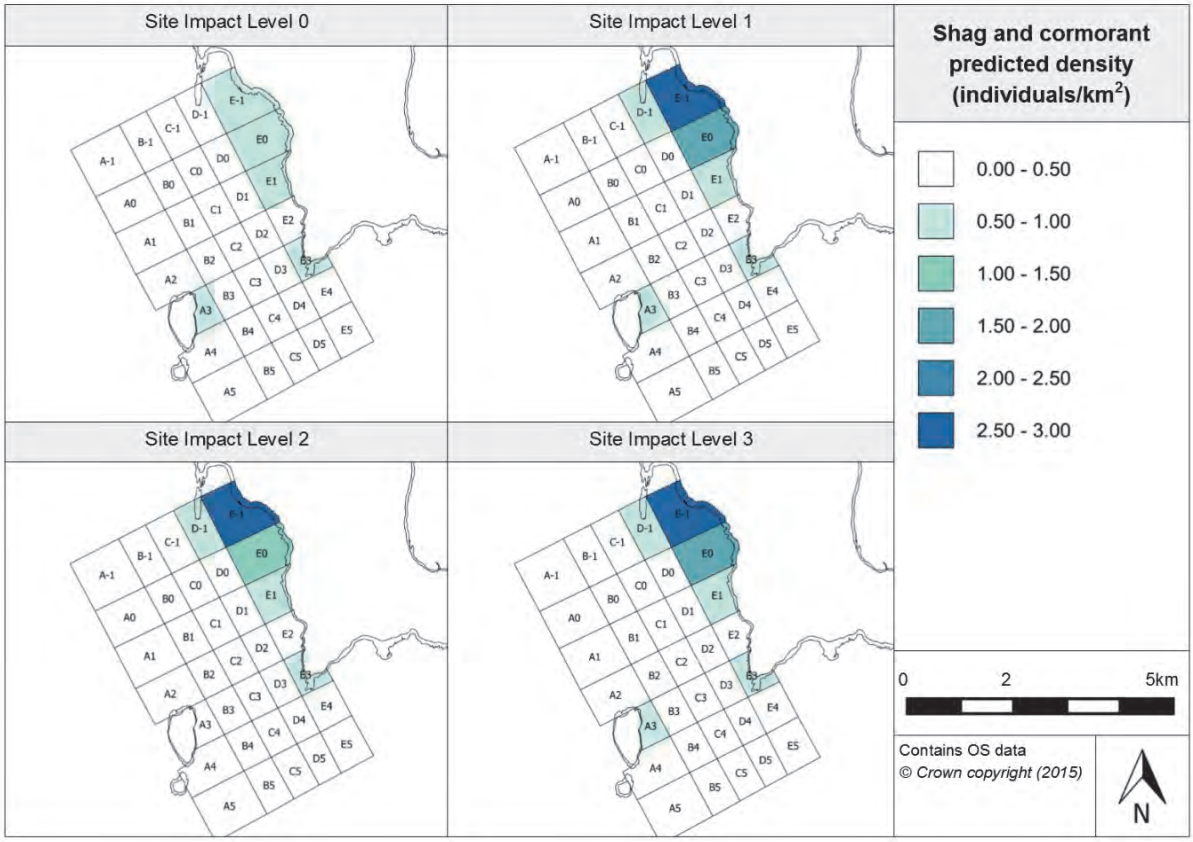

Figure 4.3.25. Estimated shag and cormorant density at each site impact level

From Figure 4.3.25, it is clear that a higher density of shags and cormorants is estimated to occur close to shore with grid cells adjacent to land showing the greatest abundances. At baseline conditions (SIL-0), a peak in density is expected in grid cells E-1 to E1 and E3. Grid cell E2 (directly below the observer) is predicted to have a lower density in comparison to the other grid cells close to shore in grid cell row E, though the reason for this is not clear.

Greater densities are also observed across the Fall at grid cell A3 which is adjacent to Muckle Green Holm.

This peak in density close to land heightens when infrastructure is onsite (SIL-1), with greatest densities expected in grid cell E-1. Adjacent to E-1, grid cell D-1, which includes the southern end of Seal Skerry, has been modelled to increase in density from baseline conditions. A lower density in grid cell E2 continues to be predicted in comparison to the other cells in grid row E which are adjacent to land. Shag and cormorant density at SIL-2 (when devices are present on site but not operational) is anticipated to be similar to SIL-1, except that there is a slight decrease in density in grid cell E0. The peak previously estimated in grid cell A3 (adjacent to Muckle Green Holm) is not present when devices are present but not operational (SIL-2).

When devices become operational (SIL-3), shag and cormorant density is expected to be very similar to conditions when only infrastructure is installed. Again, greatest density is expected in grid cell E-1 and a gap exists at grid cell E2, with the typical peak in density close to land (Figure 4.3.25).

Consistently, it appears that, the model estimated that at the Fall of Warness, shags and cormorants do not stray far from land with greater densities being limited to grid cells adjacent to land. This finding is consistent with typical behaviour recorded elsewhere for both species.

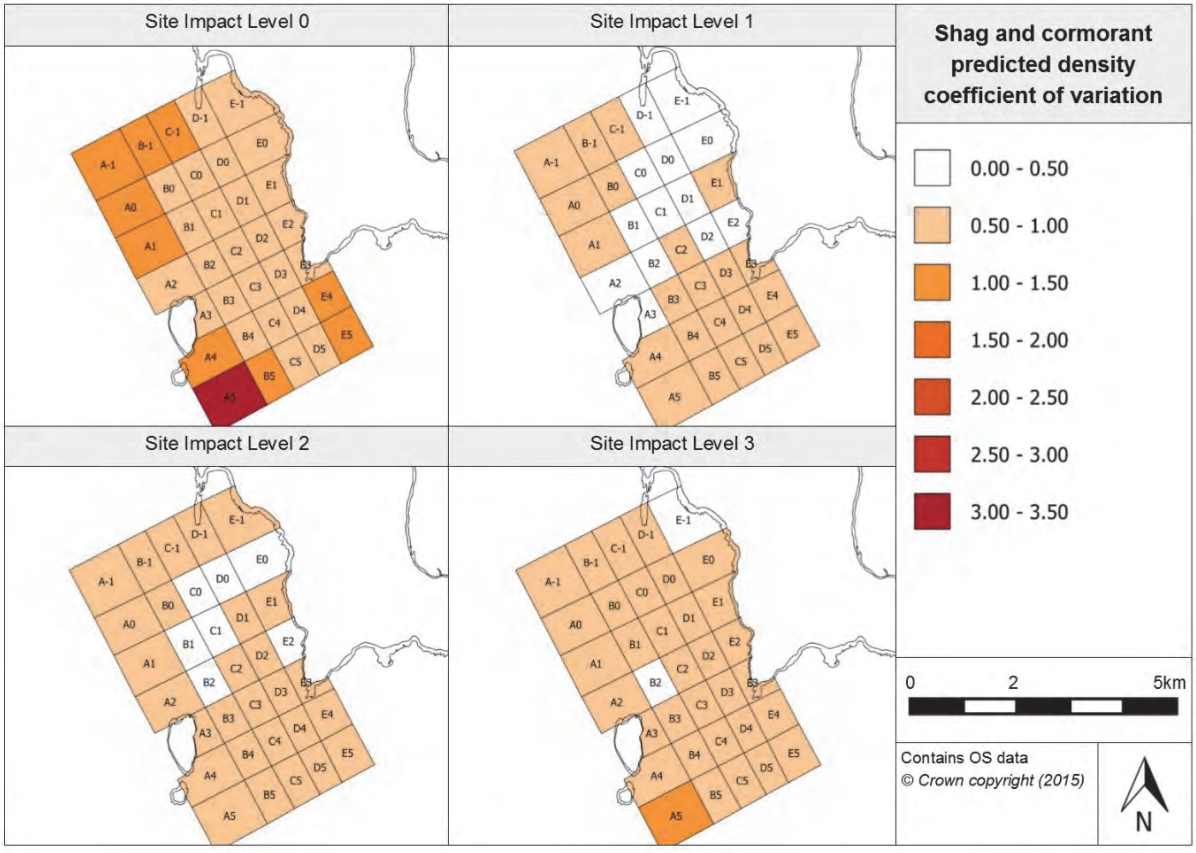

Figure 4.3.26. Associated coefficient of variation values for the density predictions for shags and cormorants

The associated CV values for each of the prediction surfaces is provided in Figure 4.3.26. It is clear that, for the prediction surface at SIL-0 (baseline conditions), there is high

uncertainty in the results (due to high CV values) in the north-western, south-western and eastern corners of the survey area. This is most likely due to low density predictions in these areas which may reflect the natural distribution of shags and cormorants. For the prediction surfaces for site impact levels 1, 2 and 3, there are generally fairly low CV values which indicate low uncertainty in the estimated densities for these surfaces. The higher CV values obtained for the SIL-0 prediction surface in comparison to the other prediction surfaces may also indicate fewer observations of shags and cormorants during baseline conditions and, therefore, less evidence from which to make predictions.

4.3.5.5 Relative abundance estimation

By using the shag and cormorant model, it was possible to produce relative abundance values for each survey month. These have been combined to create seasonal abundance predictions over the survey duration using the same environmental covariates as previously (Table 4.3.15). This information has been split across site impact levels to produce a visual representation of the changing relative abundance values across the survey years (Appendix 7).

Table 4.3.15. Relative abundance for shags and cormorants during each season (associated confidence intervals are provided in brackets)

Year	Season			
	Winter (Dec, Jan, Feb)	Spring (Mar, Apr, May)	Summer (Jun, Jul, Aug)	Autumn (Sep, Oct, Nov)
2005	-	-	5.86 (3.35, 11.69)	32.42 (13.17, 61.56)
2006	75.94 (40.29, 142.14)	30.24 (14.90, 52.86)	16.81 (10.41, 29)	87.92 (43.21, 148.86)
2007	89.2 (43.97, 144.43)	31.89 (15.83, 55.77)	17.73 (10.84, 31.21)	102.51 (44.47, 180.96)
2008	84.69 (31.68, 157.59)	24.55 (11.61, 45.05)	13.65 (7.98, 25.35)	47.91 (18.64, 96.60)
2009	51.69 (23.73, 96.72)	18.33 (8.13, 36.23)	13.59 (5.69, 29.18)	96.24 (45.47, 160.20)
2010	116.39 (63.99, 198.14)	43.84 (22.77, 73.68)	22.14 (14.06, 35.70)	118.23 (56.69, 199.96)
2011	80.8 (26.88, 166.68)	19.17 (9.45, 33.23)	11.25 (7.09, 19.51)	62.25 (29.32, 106.68)
2012	61.16 (28.87, 95.96)	18.93 (5.53, 36.00)	7.22 (3.92, 15.12)	39.96 (15.45, 81.02)
2013	48.24 (22.59, 97.72)	25.03 (15.12, 38.84)	17.22 (10.41, 30.45)	95.3 (44.25, 175.74)
2014	80.42 (34.13, 145.47)	21.02 (11.11, 34.87)	11.68 (7.61, 19.91)	64.68 (31.39, 108.57)
2015	78.93 (41.28, 134.17)	30.95 (14.69, 56.31)	-	-

In Table 4.3.15 a well-defined seasonal peak in abundance appears during autumn and winter months, with the lowest number of shags and cormorants observed during summer months. In addition, the table shows that shag and cormorant numbers have varied quite dramatically over the years, particularly during the winter months.

Prediction surfaces for shags and cormorants have also been produced for typical surveying conditions in January and July. The surfaces and associated CV values are provided in the Marine Scotland Information portal.

4.3.5.6 Spatially-explicit change

Given the focus of this project on any spatially-explicit changes in species abundance or distribution arising in response to a change in device operational status, the difference between model predictions for each site impact level has been investigated. The significance of the difference has also been calculated using their associated 95% CIs. As

'year' was included in the final model, the prediction surfaces for the least (Figure 4.3.27) and most (Figure 4.3.28) variable years have been provided (2011 and 2010, respectively).

For the shag and cormorant simulations, there is an increase in density in the majority of the survey area except for six grid cells just south of the centre of the site, with the installation of infrastructure as compared to baseline conditions. This change is deemed to be significant in the north and north-eastern corner of the survey area. The greatest increase in density between two conditions is expected to occur between SIL-0 (baseline conditions) and SIL-1 (when infrastructure is installed) with grid cell E-1 exhibiting an increase of 1.40 individuals/km^2 in density in 2011 and 2.80 individuals/km^2 in 2010 (Figure 4.3.27 and Figure 4.3.28, respectively). It is also worth noting that the increase in density in grid cell E5 (south-eastern corner of the site) has also been deemed significant.

When considering the change in density between SIL-0 and SIL-2 (presence of devices), a similar distribution of positive and negative changes in density to that estimated between SIL-0 and SIL-1 (infrastructure present) is apparent, with the exception that more grid cells, stretching from E1 to A5 (in south-western corner of the site), are deemed to have a decrease in density with the presence of devices, and in four of these cells the decrease is deemed to be significant. Similar to the change between SIL-0 and SIL-1, grid cells in the north and north-eastern corner of the site, as well as E5, have been deemed to have a significant increase.

The change in shag and cormorant density between SIL-0 and SIL-3 (presence and operation of devices) appears to be similar to that observed between SIL-0 and SIL-1 and between SIL-0 and SIL-2. An increase in density is expected in the majority of grid cells with the presence and operation of devices. This is deemed to be significant in 14 grid cells. The area where a decrease in density is anticipated is smaller than between SIL-0 and SIL-2, and only two grid cells (B4, C4) are deemed to show a significant decrease in shag and cormorant density.

When investigating the density difference between SIL-1 and SIL-2 (devices installed but not operational), a decrease in density is estimated in the majority of grid cells. A total of 11 grid cells are deemed to have a significant decrease in density between infrastructure being on site and devices being on site. The largest decrease in shag and cormorant density between two site impact levels is estimated in grid cell A3 where, between only infrastructure being onsite and devices becoming installed, there is a decrease of 0.19 individuals/km^2 in 2011 and 0.38 individuals/km^2 in 2010 (Figure 4.3.27 and Figure 4.3.28 respectively). A positive change in density is expected in the north-western and south-eastern corners of the site.

When comparing shag and cormorant density difference between SIL-1 (infrastructure onsite) and SIL-3 (devices present and operational), a decrease in density is estimated in all but three grid cells. The three grid cells where an increase in density is seen are positioned in close proximity to observation vantage point. Although the majority of grid cells show a decrease in density, only in two grid cells (both in the south-western corner of the site) is this deemed to be significant.

Finally, when investigating the change in shag and cormorant density between SIL-2 and SIL-3 (devices becoming operational), there appears to be an increase in density estimated in the central area of the site stretching from the coastline north of the vantage point across the Fall of Warness to Muckle Green Holm towards the south-western corner of the site. Eight grid cells show a significant increase in density, all of which are towards the western side of the site. The northern part of the site (from Seal Skerry to the north-western corner) shows a decrease in density although the decrease is not deemed to be significant in any of the grid cells. A decrease in density is also expected in the south-eastern corner of the site.

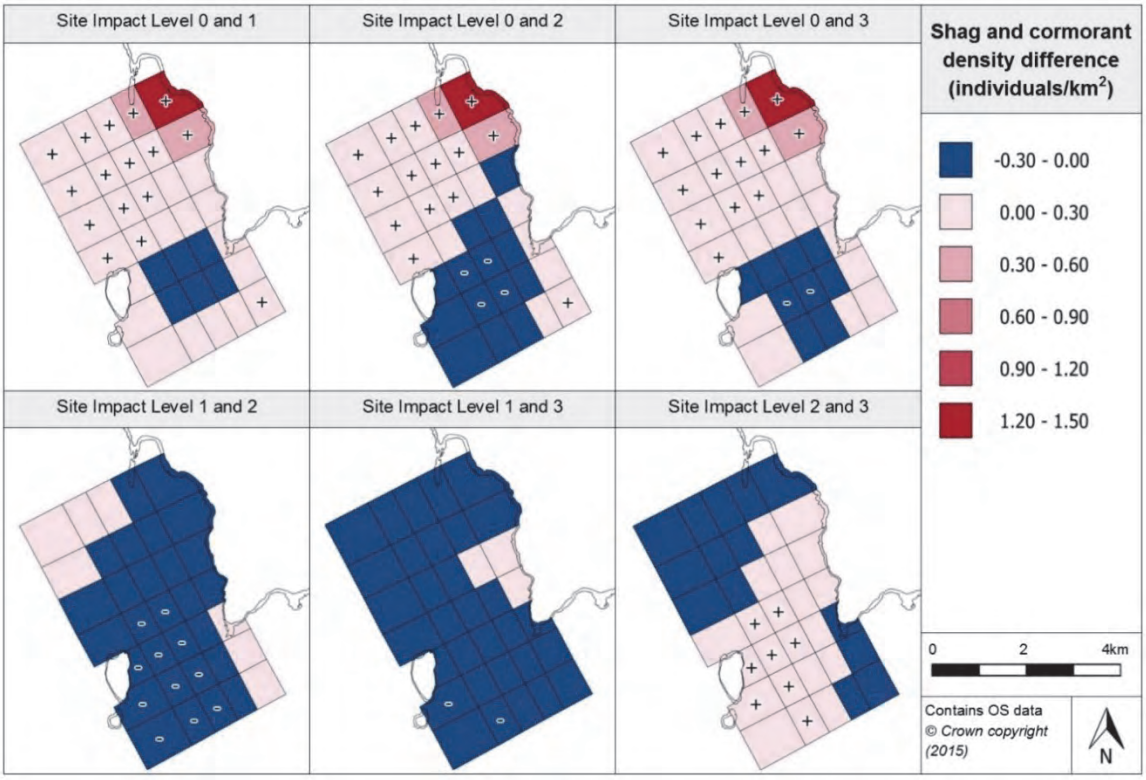

Figure 4.3.27. Estimated density difference between various site impact levels for shags and cormorants during 2011 (year with least variation)

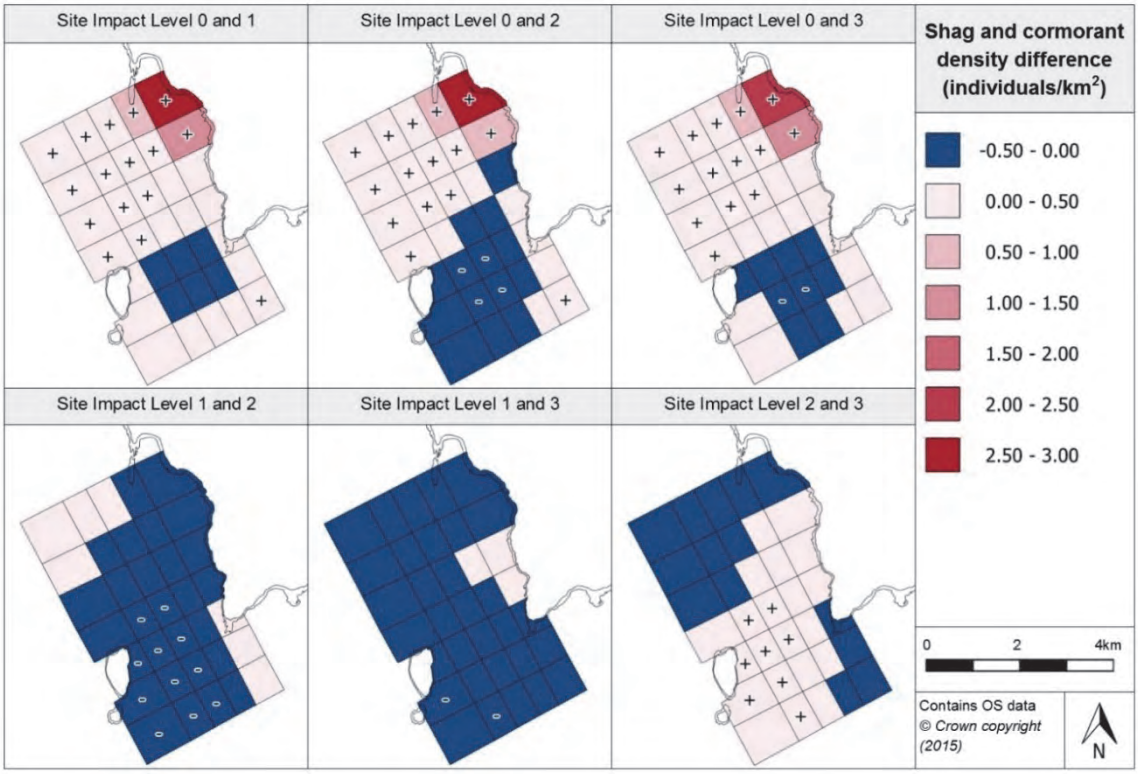

Figure 4.3.28. Estimated density difference between various site impact levels for shags and cormorants during 2010 (year with most variation)

4.3.5.7 Density change with increasing distance from potential impact location

The above density difference projections have been used to investigate how shag and cormorant density changes with increasing distance from the impact location. Figure 4.3.29 illustrates how the difference in density between impact level changes with increasing distance from a potential impact location (a grid cell containing a test berth).

From initial inspection of the plots for the density difference between baseline conditions (SIL-0) and site impact levels 1, 2 and 3, the pattern emerging with increasing distance away from the grid cell appears similar. From the potential impact location to just beyond 2km, there seems to be a positive change in density. This suggests that the presence of the impact (whether related to infrastructure, device presence or device operation) may produce an increase in density as far as 2km from the impact location. Beyond 2km, there is a less certainty, due to widening CIs, over whether the density change would be positive or negative

When considering how the density difference between SIL-1 (infrastructure installed) and SIL-2 (devices installed but not operational) changes with distance from a potential impact location, it appears that up to 1.5km away from the grid cell containing the test berth there is no clear change in density. However, beyond 1.5km from the grid cell there is a distinct decrease in density which continues up to 3km from the grid cell. Beyond 3km, there is no distinct relationship to show whether the change in density would be positive or negative.

Due to wide CIs, there seems to be no clear density difference between SIL-1 and SIL-3 (devices becoming operational) with increasing distance from a grid cell containing a test berth.

When shag and cormorant density differences between SIL-2 and SIL-3 are investigated in terms of increasing distance from a potential impact location, a slight decrease is estimated when devices become operational which is evident up to 1km from the grid cell. Beyond 1–1km from the potential impact location, there is no clear increase nor decrease evident whereas, beyond 1.8km, there is an increase in density which may be associated with device operation. It should be noted that, beyond 3km, the CIs surrounding the density difference projections widen, raising a question about whether the change would definitely be positive.

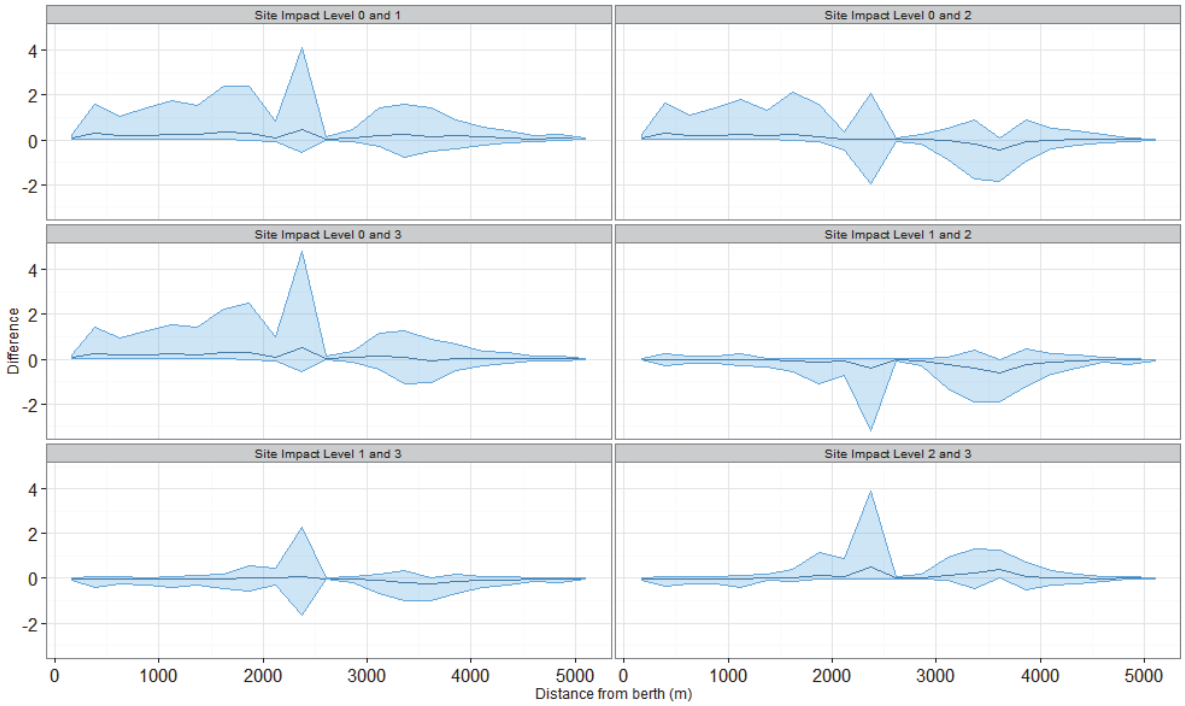

Figure 4.3.29. Density change for different site impact levels with increasing distance from a potential impact location, with associated confidence intervals, for shags and cormorants at the Fall of Warness

4.3.5.8 Discussion

The European shag and the great cormorant are two of the most common species recorded at the Fall of Warness, with over 40,000 observations over 11 years. The model developed for them includes ten significant terms. This implies that the presence of shags and cormorants is controlled by a great number of environmental factors, which need to be considered when elucidating the impact of MECS. Fewer shags and cormorants are expected during flood and slack tides, under clear skies and during summer months. Predicted abundance shows large interannual variations, with numbers sometimes halving or doubling between years.

Under the most favourable conditions for shags and cormorants, the model shows that they were most abundant in close proximity to the coast of Eday (grid cells E-1 to E3) and also off the eastern coast of Muckle Green Holm (grid cell A3) for all site impact levels. The estimated densities in these grid cells tend to increase with increasing site impact levels. Due to the large number of observations, there tends to be a higher degree of precision in these shag and cormorant predictions.

Changes in site impact levels show a shift in numbers of shags and cormorants from the south to the north within the central zone between Eday and Muckle Green Holm as compared with baseline conditions. This change is primarily from baseline conditions to conditions when device-associated infrastructure is installed (SIL-1) as changes in density associated with SIL-1 to SIL-2 (when devices are installed) are reversed with the change from SIL-2 to SIL-3 (when devices become operational). These differences in density are seen in the predictions for both the years with most variability and with least variability. Analysis of predicted density changes away from a potential impact location shows negligible change with distance.

4.3.6 Auks

4.3.6.1 Species overview

For this analysis, a group has been created named *Auks* which includes all the species from the auk family that have been observed at the Fall of Warness over the duration of the observations programme. The group includes the following species as well as unidentified auk species:

- black guillemot (*Cepphus grylle*)
- common guillemot (*Uria aalge*)
- little auk (*Alle alle*)
- Atlantic puffin (*Fratercula arctica*)
- razorbill (*Alca torda*)

Information regarding the distribution and behaviour of black guillemots, common guillemots and razorbills has been outlined in Sections 4.3.1, 4.3.2 and 4.3.3 above, respectively.

The Atlantic puffin spends the majority of the autumn and winter dispersed widely across the open ocean and tends to return to the coast during the breeding season (typically late spring). The birds tend to aggregate into small colonies on high clifftops during the breeding season. Nesting sites are typically grassy maritime slopes, sea cliffs and rocky shores which allow individuals to form burrows (Nettleship *et al*., 2014). The puffin's foraging behaviour is similar to the other auks using pursuit diving. This mimics flying through water as the bird only semi-extends its wings, using them as paddles and its feet as a rudder. The Atlantic puffin typically preys on small fish in the top 30m of the water column with the most commonly consumed species being sandeel (*Ammodytes marinus*), herring (*Clupea harengus*), sprat (*Sprattus sprattus*) and capelin (*Mallotus villosus*) (BirdLife International, 2015). Puffins are able to catch several small fish in a single dive, holding them in their beaks all at once and swallowing underwater.

The smallest of the auk species at the Fall of Warness, the little auk, spends the summer months in the high Arctic, breeding in large colonies on cliffs (Nettleship & Garcia, 2015). During winter, the species migrate south into the North Atlantic and stormy conditions may push them into the North Sea. Therefore, little auks are not observed at the site very often. Similar to the other auk species at the site, they tend to feed on small fish, crustaceans (particularly copepods), small invertebrates (e.g. amphipods and euphausiids) and fish larvae (BirdLife International, 2015).

4.3.6.2 Data summary

As already discussed, auk species as a whole are observed frequently at the Fall of Warness. Table 4.3.16 below provides a summary of raw survey data from the site including information on the number of observations and the mean group size. These summary statistics have also been broken down for each site impact level, to provide an understanding of the data used to create the auk model.

Table 4.3.16. Summary of auks raw data

	Total	Site Impact Level 0	Site Impact Level 1	Site Impact Level 2	Site Impact Level 3
Number of observations	29921	3381	12397	4367	9776
Minimum (group size)	1	1	1	1	1
Maximum (estimated group size)	900	900	500	600	540
Mean (group size) (s.d)	7.41 (22.86)	14.19 (55.25)	5.79 (11.13)	6.46 (15.30)	7.54 (16.20)

4.3.6.3 Model overview

GEE-based p-values were produced for each of the terms that remained in the final fitted model. Ten terms were found to be significant and therefore kept in the final auk model (Table 4.3.17).

Table 4.3.17. GEE-based p-values for the terms in the final auks model for Fall of Warness

Model term	ρ-value
Tide state	<0.0001
Site impact	<0.0001
Precipitation	<0.0001
Wind strength	<0.0001
Cloud cover	<0.0001
Sea state	<0.0001
Month	<0.0001
Year	<0.0001
Spatial surface	<0.0001
Spatial surface / site impact	<0.0001

All the terms that remained in the final model were found to be highly significant (ρ-value<0.001). Tidal state has remained in the final model; it appears that the model predicts auk abundance to not be particularly affected by whether it is an ebb or flood tide but, instead, predicts a marked decrease in abundance during slack tide. In terms of precipitation, as expected greater abundances are estimated during light or no precipitation. Lowest abundances are expected during constant precipitation and showers. When precipitation has been recorded as heavy, the abundances recorded vary greatly, resulting in wide CIs. Wind strength has remained in the final model; however, the relationship between wind strength and auk abundance is not particularly clear except that greatest auk abundance is expected when there is no wind or low wind strengths. In terms of cloud cover, auk abundance is estimated to increase with increasing cloud cover although, due to wide CIs, this relationship is not always true. Similar auk abundances are observed at sea states 0, 1, 2 and 3 (Beaufort scale); however, it is expected that abundance reduces dramatically at sea state 4 and above.

Auk abundance seems to have a strong seasonal relationship as shown in the partial plot, Figure 4.3.30, produced from the fitted model. There is a clear peak in abundance during spring and summer months with greatest abundances being in May. The model predicts there to be few auks in autumn, with November expected to have the least number of observations.

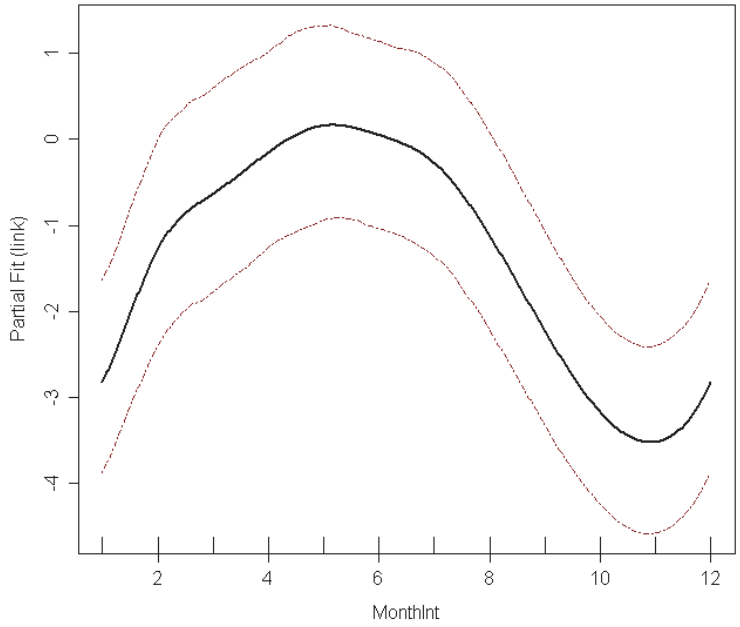

Figure 4.3.30. Estimated partial relationship of month against log(density) for auk at the Fall of Warness. The red lines represent 95% confidence intervals about the estimated relationship and the tick marks show where the data lie in the covariate range.

'Year' has also been kept in the model as auk numbers have varied over the years. The fitted model has peaks in abundance during 2006, 2008 and 2014. There is a linear relationship between depth and auk abundance, with a slight decrease in abundance with increasing depth.

A spatial surface was included in the final model; however, only a couple of knot locations were appointed. In addition, the relationship between the interaction term (site impact/spatial surface) and the response term (species abundance) was found to be statistically highly significant.

As with the other species models, diagnostic tests were carried out on the auk model. These were undertaken to understand the model's fit and whether it was appropriate for the data. It appears that the model has captured the mean variance relationship well, however there is a clear underestimation by the model on higher fitted values. A plot of the observed versus fitted values the model in comparison to the raw data simulations has also been provided. This again indicates that the model has captured the data well. All diagnostic plots are available in the Marine Scotland Information portal.

4.3.6.4 Density predictions and uncertainty estimation

As the final model contained a spatial surface, it was posbble to predict the auk densities for each grid cell across the survey area. As previously, predictions had to be made under certain conditions and therefore the optimum conditions for auk sightings were chosen for each term, as provided in Appendix 5. The estimated density for each site impact level is provided in Figure 4.3.31 and the predictions' associated CV values are provided in Figure 4.3.32. CV values are being used to provide a measure of the relative variability in the densities, with larger values indicating higher uncertainty in the prediction estimate.

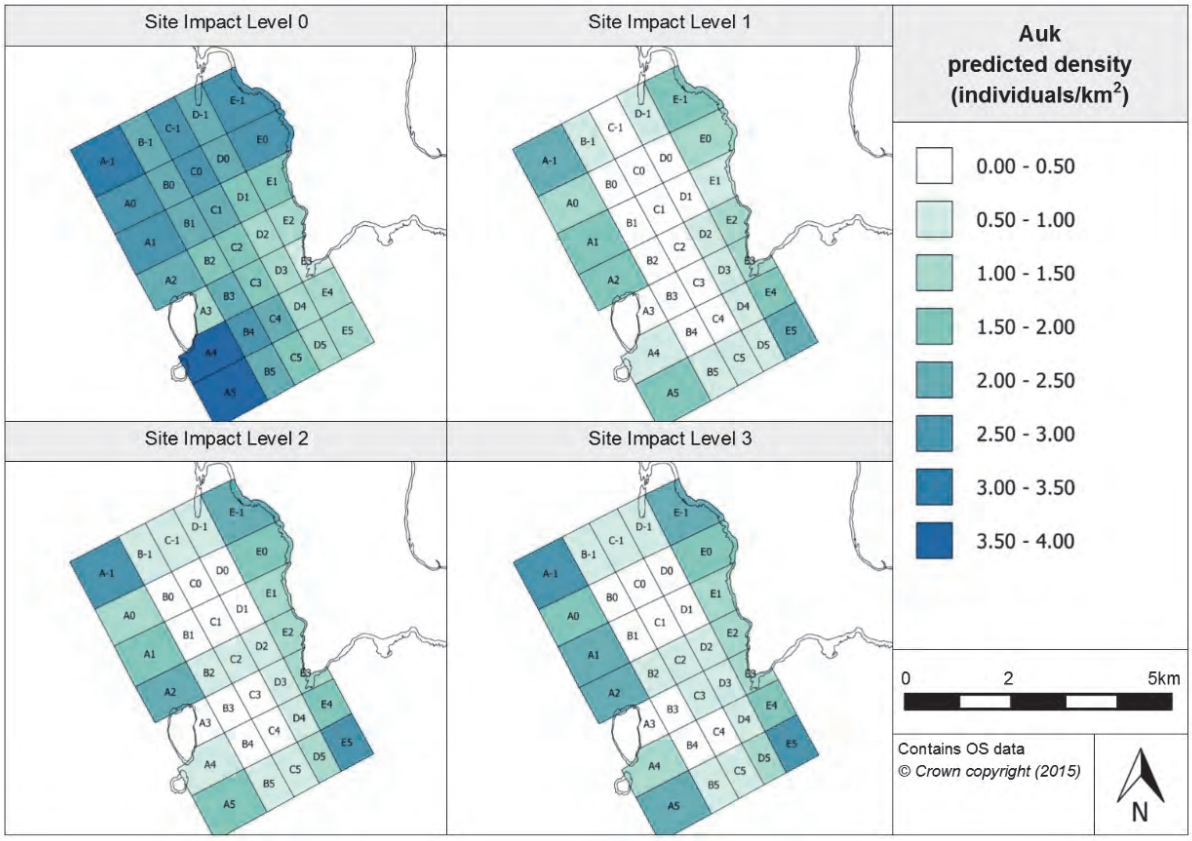

Figure 4.3.31. Estimated auk density at each site impact level

At baseline conditions (SIL-0), there is generally a high density of auks estimated across the survey area, particularly in comparison to the other site impact levels. This may suggest that auk numbers have decreased as infrastructure and devices have been installed but this change requires further investigation to understand whether it is significant and spatially-explicit in any way. There are particular peaks in density estimated in the northern region of site but the cells with the highest densities are in the south-western corner (south of Muckle Green Holm) (grid cells A4 and A5).

The pattern of densities across the prediction surface is similar across site impact levels 1, 2 and 3. Density predictions at SIL-1 (when only infrastructure is installed) are generally lower than those expected when devices are present or operational. Across the three site impact levels, the grid cell rows A and E have the highest densities across the prediction surfaces with particularly peaks expected in grid cells A-1 and E5. Grid cell A3 (adjacent to Muckle Green Holm) consistently shows lower density predictions than the other cells in grid cell row A. This may suggest that auk species avoid this area due to tidal patterns or proximity to land. However, the peak in density estimated in grid row E would suggest an attraction to land.

The reduction in density in the centre of the site at SIL-1, SIL-2 and SIL-3 in comparison to baseline conditions (SIL-0) may suggest a movement away from test berth locations (generally positioned in the central row of the site) with the introduction of infrastructure, devices and the operation of devices. Whether this indication is true will be further investigated when considering the evidence for spatially-explicit change.

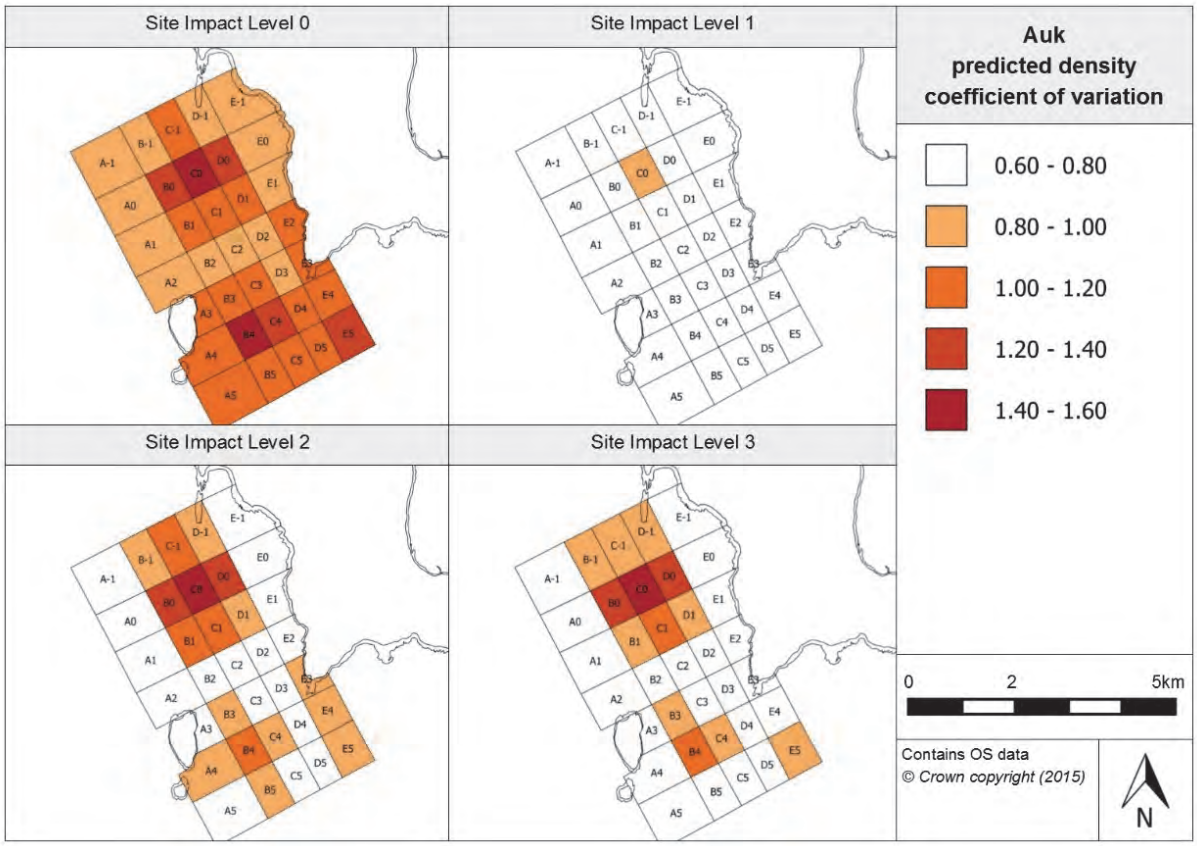

Figure 4.3.32. Associated coefficient of variation values for the density predictions for auks

Although Figure 4.3.31 has shown higher estimated densities during baseline conditions, when the associated CV values for these predictions are considered it is clear that there is high uncertainty surrounding the predictions, see Figure 4.3.32. This may be due to fewer observations when the site impact level is 0 and therefore less evidence upon which to base predictions.

For the SIL-1 prediction surface (when infrastructure is installed), there appears to be fairly low CV values across the prediction surface suggesting that these density predictions are more precise estimates. It seems that, for the SIL-2 (devices installed) and SIL-3 (devices operational) prediction surfaces, there are high CV values in the centre of the site. These areas are in line with where the lowest densities are expected at these impact levels. It is likely that these high CV values arise from the low density predictions in these grid cells at SIL-2 and SIL-3. Consistently, across the site impact levels, grid cell C0 has the highest CV values.

4.3.6.5 Relative abundance estimation

Using the produced final model, it was possible to estimate auk abundance for each survey month by applying values to the environmental covariates remaining in the model. As previously, the optimum environmental covariate values for auk sightings were used to produce seasonal abundance predictions which are outlined in Table 4.3.18. It is worth noting that these values are relative abundances as the observations programme was limited to surface visible observations.

Table 4.3.18. Relative abundance for auks during each season (associated confidence intervals are provided in brackets)

Year	Season			
	Winter (Dec, Jan, Feb)	Spring (Mar, Apr, May)	Summer (Jun, Jul, Aug)	Autumn (Sep, Oct, Nov)
2005	-	-	87.04 (24.95, 214.10)	7.31 (2.20, 22.27)
2006	18.22 (1.47, 65.27)	131.22 (55.00, 265.42)	109.01 (35.78, 232.38)	9.40 (3.44, 23.13)
2007	19.94 (6.37, 59.05)	124.81 (55.14, 236.43)	103.69 (34.49, 210.92)	9.14 (3.52, 22.32)
2008	23.77 (7.20, 72.08)	155.97 (72.23, 285.23)	129.57 (45.51, 245.87)	21.45 (6.33, 67.66)
2009	44.78 (12.72, 150.48)	286.28 (115.26, 640.53)	215.57 (32.51, 585.52)	7.80 (2.90, 18.74)
2010	13.31 (4.25, 36.63)	81.49 (37.71, 149.74)	73.16 (27.99, 125.48)	6.59 (2.47, 15.87)
2011	12.91 (4.33, 37.38)	81.51 (37.18, 148.69)	76.02 (26.45, 143.61)	6.39 (2.45, 15.59)
2012	14.43 (4.90, 43.01)	135.01 (42.96, 425.12)	153.08 (41.03, 376.11)	12.86 (3.73, 41.40)
2013	33.63 (7.59, 123.46)	115.28 (60.29, 230.34)	72.35 (24.04, 136.52)	6.08 (2.13, 15.78)
2014	18.45 (4.36, 61.98)	144.64 (66.26, 275.20)	120.16 (40.54, 232.33)	10.10 (3.65, 24.86)
2015	21.37 (4.43, 91.40)	139.61 (45.12, 398.77)	-	-

Auks' close relationship with season, as already highlighted in Figure 4.3.30, is exemplified again in Table 4.3.18, with the estimated abundance values during spring and summer being particularly high. In addition, there is a clear peak in abundance in survey year 2009. These abundance values have been split into each of the site impact levels and are provided in Appendix 7. The associated CIs by each density prediction is also provided. The 2009 peak in abundance is clear under SIL-0 (as baseline conditions were the site operational conditions during this period) as well as an additional smaller peak in abundance in 2012.

As with the other species, the model has been used to produce prediction surfaces for auks for typical surveying conditions in January and July. Both surfaces and their associated CV values are provided in the Marine Scotland Information portal. Although the distribution across the prediction surface between the two seasons appears to be very similar, there is a dramatic difference in the estimated densities between the seasons, with the July densities expected to be over 30 times greater than those found in January.

4.3.6.6 Spatially-explicit change

To identify any evidence for spatially-explicit changes in auk abundance and distribution that can be associated with site operational status, the difference between model predictions for each site impact level has been investigated. To understand the significance of the difference, the predictions' associated 95% CIs have also been calculated. As the final model for auks contained 'year', the prediction surfaces for the least and most variable years have been produced (2011 and 2014, respectively). These are presented in Figure 4.3.33 and Figure 4.3.34 for 2011 and 2014, respectively.

Between baseline conditions (SIL-0) and infrastructure being installed (SIL-1), it appears that there is a general decrease in density across the majority of the site except for the south-eastern corner. In all but four of the grid cells where a reduction in density is estimated, the change has been deemed significant. The largest reduction in density is seen in grid cell A4 where a reduction of 2.33 individuals/km^2 in 2011 and 4.08 individuals/km^2 in 2014 was observed between baseline conditions and infrastructure being installed.

A similar distribution of density changes are expected between SIL-0 and SIL-2 (devices present onsite but not operational), with the exception that fewer grid cells are deemed to

show a significant reduction in density. There appears to be a cluster of grid cells exhibiting a reduction in density when devices are installed onsite in the centre of the survey area. Curiously, test berths tend to be located in the centre of the site which may suggest that, with the installation of devices, a reduction in auk density is expected in the areas in close proximity to the device/s. Although from the prediction surface it may suggest that there is a redistribution occurring within the site (due to the significant reduction observed in the central area and an area of increase in density in the south-eastern corner); it is unlikely that this simply represents redistribution within the site as the level of density reduction is substantially greater than the extent of the density increase estimated in the south-eastern corner of the site.

Again, a similar distribution of density changes are estimated between baseline conditions and SIL-3 (when devices are onsite and operational). Fewer grid cells are deemed to show a significant reduction in auk density but the cluster of cells where the reduction is significant remains in grid cell rows B and C. Incidentally, although a reduction in auk numbers is expected across the majority of the site, the largest increase in auk density between two site impact levels is exhibited in grid cell E5. In 2011, the density increased by 0.99 individuals/km^2 and, in 2014, the density increased by 1.70 individuals/km^2 in this grid cell.

When the change in auk density between SIL-1 and SIL-2 is investigated, a slight increase is seen across the whole site except for grid cell B4 (where a slight decrease in observed). However, despite the widespread increase in auk density across the site, in no grid cell is this increase deemed to be significant.

The increase in auk density continues when SIL-1 and SIL-3 are compared; between these two site impact levels, the increase has been deemed significant in 18 grid cells. The distribution of the significant increases seems fairly random, with the majority of the cells in southern half of the site, as well as a cluster in the bay near the EMEC substation. The fact that there are no areas where a reduction in auk density is estimated this suggests that there is an influx of auks to the site rather than redistribution within the site. Between SIL-2 and SIL-3 (devices becoming operational), a site-wide increase in auk density is again expected, although this is deemed to be significant in only two grid cells (C5 and D4).

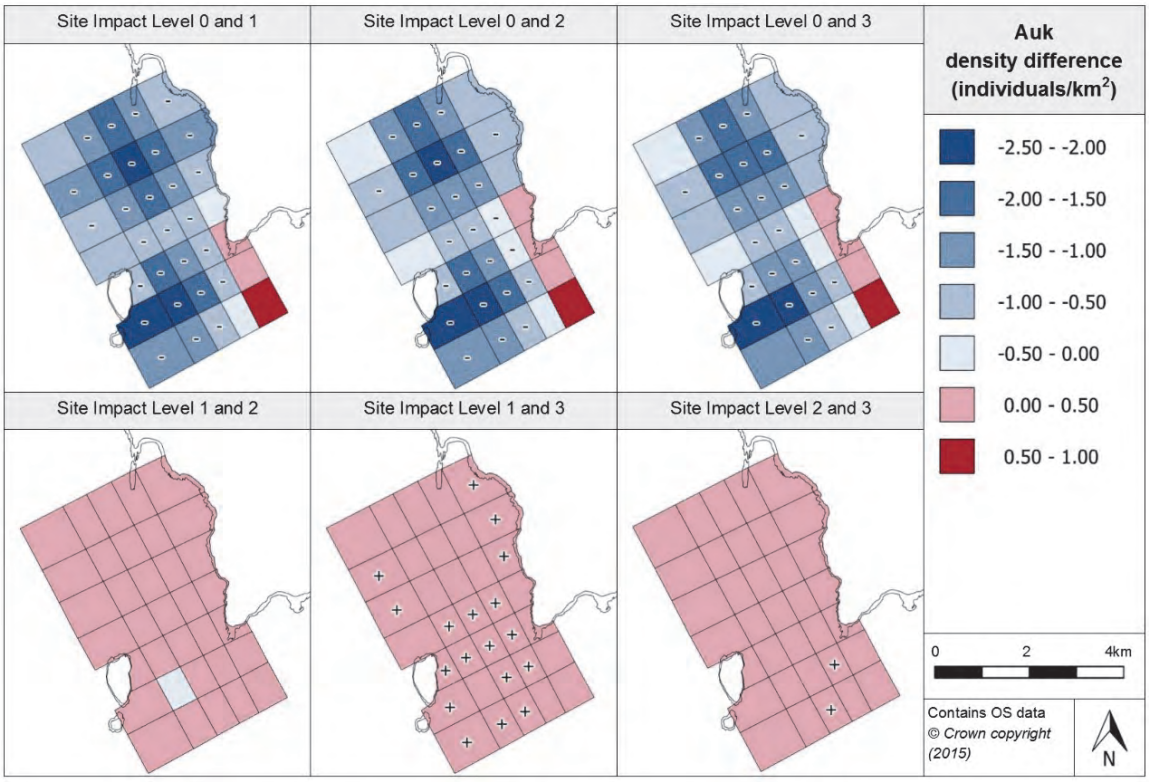

Figure 4.3.33. Estimated density difference between various site impact levels for auks during 2011 (year with least variation)

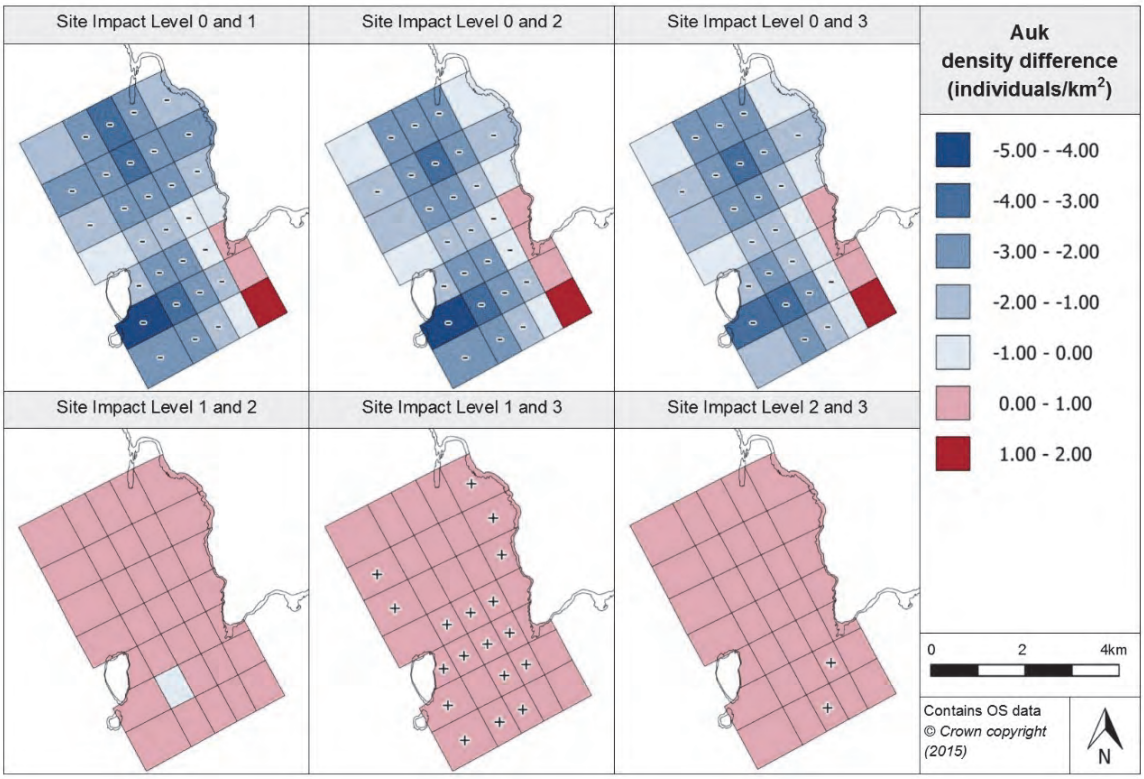

Figure 4.3.34. Estimated density difference between various site impact levels for auks during 2014 (year with most variation)

4.3.6.7 Density change with distance from potential impact location

By using the spatially-explicit change projections, it has been possible to map out the density difference between various site impact levels relative to increasing distance from a grid cell containing a test berth. The prediction density change with distance is provided for one grid cell containing a test berth, Figure 4.3.35, but further plots for each grid cell containing test berths can be found in the Marine Scotland Information portal.

Figure 4.3.35 below shows a decrease in auk density with the installation of infrastructure onsite when compared to baseline conditions. The decrease is maintained up to 4km from the potential impact location. The decrease is deemed to be significant (highest CI is below baseline conditions (0)) up to 1.5km from the test berth. Beyond 1.5km, the upper CI is sometimes above baseline conditions and therefore the decrease cannot be determined as significant at this distance from the impact location. The same pattern in density change with increasing distance from an impact location is apparent when comparing baseline conditions to SIL-2 and SIL-3, also see Figure 4.3.35.

When the changes in auk density between SIL-1 and SIL-2, SIL-1 and SIL-3, and SIL-2 and SIL-3 are considered, there appears negligible changes in density with increasing distance from a potential impact location.

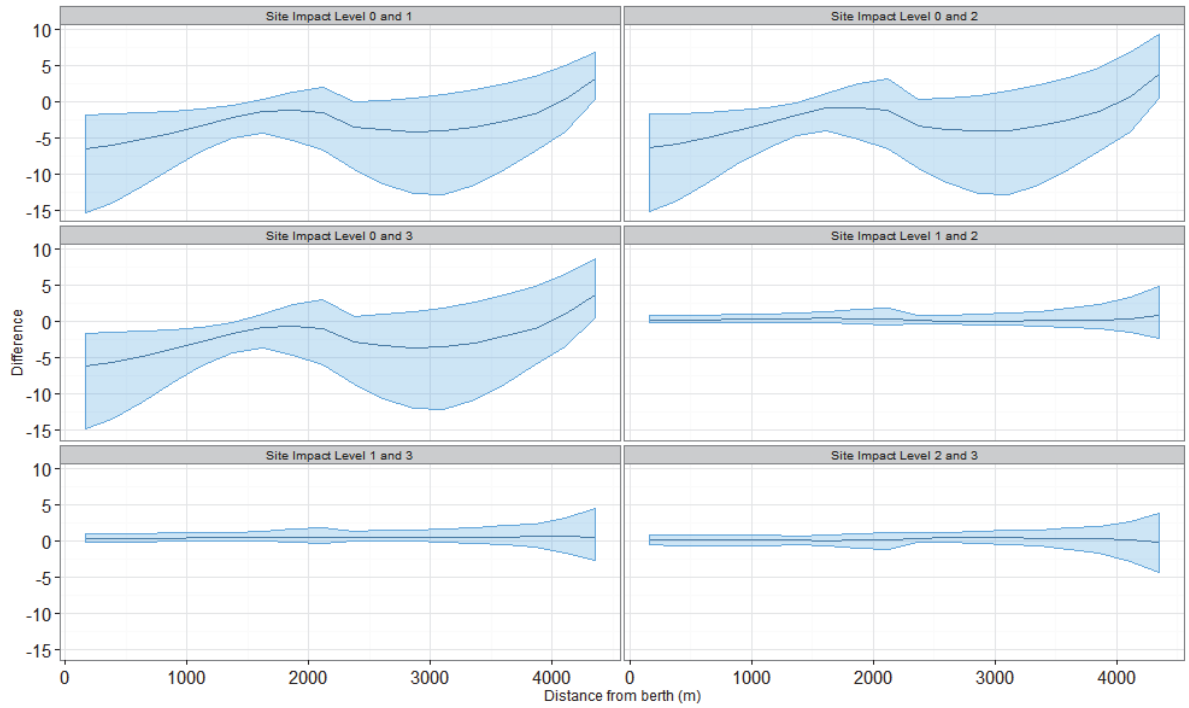

Figure 4.3.35. Density change between site impact levels with increasing distance from a potential impact location, with associated confidence intervals, for auks at the Fall of Warness

Interestingly, when the density difference between baseline conditions and site impact levels 1, 2 and 3 with increasing distance from a test berth location is considered for all the potential impact locations at the Fall of Warness, a decrease in density is immediately observed and tends to be maintained for up to 3km from every potential impact location. When the CIs are considered, the upper CIs tend to be below the baseline conditions to around 800m from the impact location. This would imply that there is a definite decrease in auk density at the test berth, a reduction which is maintained to at least 800m from the berth.

This evidence for a change in species density is the strongest indicator of change amongst the species studied at the Fall of Warness.

4.3.6.8 Discussion

Members of the auk family have been grouped into a family group to allow some of the less frequently recorded species in the family to be analysed. The family group includes the species black guillemots, common guillemots, little auks, Atlantic puffin and razorbills, and are commonly seen at the Fall of Warness (nearly 30,000 observations). However, as black guillemots have more than four times the number of observations than the next most common auk species at the site (common guillemots), it is likely that the observed patterns from the fitted auk model will most likely be associated with black guillemots rather than general auk patterns. The model fitted for the auk family includes ten highly significant terms. This implies that the presence of members of the auk family is controlled by a great number of environmental, temporal and spatial factors. It is important that these factors are considered when attempting to understand the potential impact of MECS.

The estimated abundances exhibit very large interannual and intra-annual changes. The model shows a large reduction in auk density from baseline conditions when infrastructure is installed, particularly within the central zone of the survey area (grid bands B, C and D). Numbers only recover slightly when devices are installed and become operational. Due to the great number of auk observations, there is generally high precision in the predictions. As the reduction in numbers is focused in the central grid cells of the site where the test berths are positioned (rows B-D), modelling the impact with distance from a potential location shows a drop of approximately 6 individuals/km^2 at the site, which decreases with increasing distance but does not return to baseline conditions until approximately 1.5km away. This modelled change in density is the strongest indicator of change associated withinfrastructure installation amongst the species/groups studied at the Fall of Warness. The fact that this change does not increase but, in fact, reduces when devices are installed or become operational, may suggest that it is vessel movements associated with the installation activities, rather than stationary objects, that impact on auk densities.

4.3.7 Ducks and geese

4.3.7.1 Species overview

To be able to analyse the data collected for duck and geese species, all species from the Anatidae family observed at the Fall of Warness over the period of the observations programme have been amalgamated[19]. The group includes the following species:

- common eider (*Somateria mollissima*)
- long-tailed duck (*Clangula hyemalis*)
- red-breasted merganser (*Mergus serrator*)
- common goldeneye (*Bucephala clangula*)
- goosander (*Mergus merganser*)

The common eider is the most common duck species at the Fall of Warness and is rarely found away from the coastal environment. The highly gregarious common eider is known to breed on offshore islands and along low-lying rocky shores (BirdLife International, 2015). Its primary food source is benthic molluscs, although they have been known to take crustaceans, echinoderm, other marine invertebrates and fish (Carboneras *et al*., 2014c). The species tends to nest in colonies with breeding commencing in early April.

[19] Due to small sample sizes for individual species.

The long-tailed duck is a small sea duck and is not commonly sighted at the Fall of Warness. The species only winters in UK waters, tending to migrate in large flocks at night. The wintering period tends to be between early October and mid-March (Carboneras and Kirwan, 2014a). Typical prey include benthic molluscs including mussels, cockles and clams, as well as crustaceans and small fish (BirdLife International, 2015).

Typically spotted around the coastline, the red-breasted merganser is part of the sawbill family. It is known to both winter and breed in Scotland, with the gregarious species tending to flock on the coast from late summer, reaching a peak in numbers during late autumn/early winter (Carboneras and Kirwan, 2014b). Typical prey species include small shoaling fish species (particularly salmon and trout) and sometimes plant material and aquatic invertebrates (BirdLife International, 2015).

The common goldeneye is very rarely sighted at the Fall of Warness and is typically restricted to shallow waters (less than 10m deep) (BirdLife International, 2015). Orkney tends to be used for wintering, with birds arriving between August and December and returning to their breeding sites in February and March. Primary food sources include aquatic invertebrates e.g. molluscs, worms, crustaceans and aquatic insects (Carboneras *et al*., 2014d).

As goosanders are a largely freshwater species, they are only rarely spotted at the Fall of Warness. When in a marine environment, the species tends to be located in sheltered areas and typically stays in shallow waters (less than 10m deep). Prey species are predominately fish species (in particular salmon and trout) but can also include aquatic invertebrates (Carboneras and Kirwan, 2014c).

4.3.7.2 Data summary

Duck and geese species are regularly sighted at the Fall of Warness, with the common eider being the most observed species. Table 4.3.19, provides a summary of the raw survey data from the site with respect to duck and geese species, including information on the number of observations and mean group size. This information is broken down for each site impact level, to provide an overview of the data used in the subsequent predictions.

Table 4.3.19. Summary of ducks raw data

	Total	Site Impact Level 0	Site Impact Level 1	Site Impact Level 2	Site Impact Level 3
Number of observations	11928	551	5862	2099	3416
Minimum (group size)	1	1	1	1	1
Maximum (group size)	225	183	225	120	210
Mean (group size) (s.d)	8.82 (17.27)	18.47 (33.39)	9.32 (18.70)	6.36 (8.37)	7.91 (14.08)

4.3.7.3 Model overview

GEE-based p-values have been created for each of the terms that have remained in the final model, once the model selection process was completed. Nine terms have remained in the model; these were all deemed to be significant in terms of predicting duck and geese abundance at the site and are outlined in Table 4.3.20.

Table 4.3.20. GEE-based p-values for the terms in the final ducks and geese model for the Fall of Warness

Model term	ρ-value
Tide state	<0.0001
Wind strength	<0.0001
Cloud cover	0.000464
Depth	<0.0001
Year	0.004104
Month	<0.0001
Site impact	0.000309
Spatial surface	<0.0001
Spatial surface / site impact	<0.0001

Tidal state has remained as a term in the final fitted model. It appears that the model has estimated similar abundances during flood and slack tide, and lower densities during ebb tide. In addition to tidal state, wind strength has also remained in the model, and the modelled relationship between wind strength (measured on the Beaufort scale) and duck and geese density can be viewed in Figure 4.3.36. With increasing wind strength, there seems to be a reduction in duck and geese abundances, with the lowest abundances expected when the wind strength is 4 or above on the Beaufort scale.

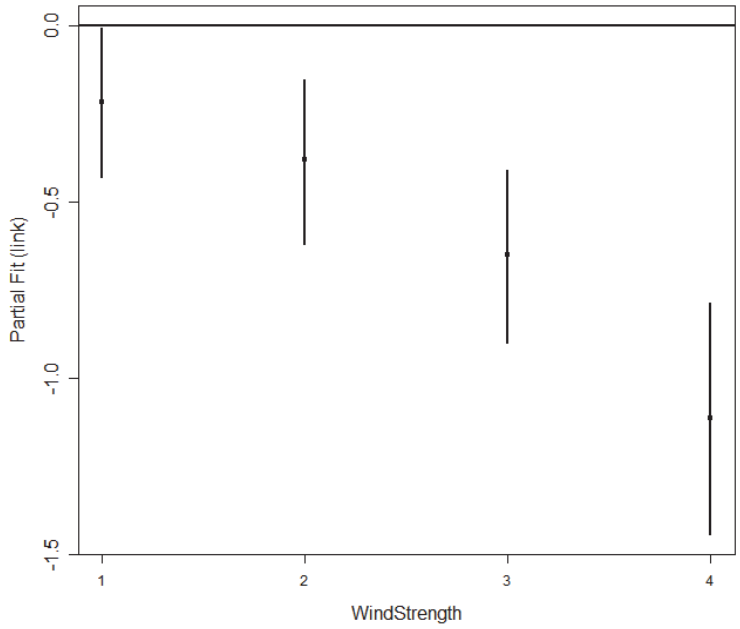

Figure 4.3.36. Estimated partial relationship of duck and geese density (on the scale of the log link) with wind strength at the Fall of Warness. The points are the parameters for the estimated change in log density from the baseline (wind strength = 0) and the vertical lines represent 95% confidence intervals about the parameter estimates.

Although cloud cover has remained in the final model, there is no clear relationship with duck and geese density as similar abundances are estimated for cloud cover states 2-8 oktas, with the exception that the lowest abundances are expected when there is no cloud cover.

A significant relationship exists between duck and geese density and depth, as depth remains in the final model. From a produced partial plot, it appears that the model has predicted the number of duck and geese to reduce with increasing depth, as expected from the known coastal behaviour of these species. 'Year' has a very clear relationship with duck and geese abundance in the fitted model, as a sustained reduction in density over the duration of the survey programme is estimated. Further work may be advisable to understand whether this decline in abundance is a population-wide problem, or if limited to a site-specific occurrence. Similarly, 'month' remained in the final model, as there appears to be seasonality in the peaks and troughs of duck and geese abundance. A clear trough in abundance values emerges during summer months, with July expected to have the lowest abundance. Peaks in abundance are anticipated during November and March, with greater abundances maintained throughout winter.

A spatial surface was able to be fitted to the model, but only a limited number of knots (three knots) were used in fitting. Also included in the model, as found to be statistically significant, was the interaction term (site impact/spatial surface).

Similarly to the other species' models, diagnostic tests were undertaken to form an idea of how well the model fits. The outputs from these tests are available on the Marine Scotland Information portal. From these tests, it appears that the model is well fitted to the data. Although there are fluctuations in the model, these accurately reflect the natural fluctuations in the data. At high fitting values, the model underestimates the variance present within the data, however this is expected in data that as over dispersed in nature as that seen in the species data.

4.3.7.4 Density predictions and uncertainty estimation

As already mentioned, because the model contains a spatial surface, the densities can be plotted for each of the grid cells within the survey region, allowing any distributional changes in abundance to be investigated. As before, predictions have had to be made for certain conditions and optimum conditions for sighting ducks and geese at the Fall of Warness were chosen (provided in Appendix 5). The estimated densities across the survey area are provided in Figure 4.3.37 alongside their associated CV values, (Figure 4.3.38) which give an insight into the level of the uncertainty that underpins these predictions.

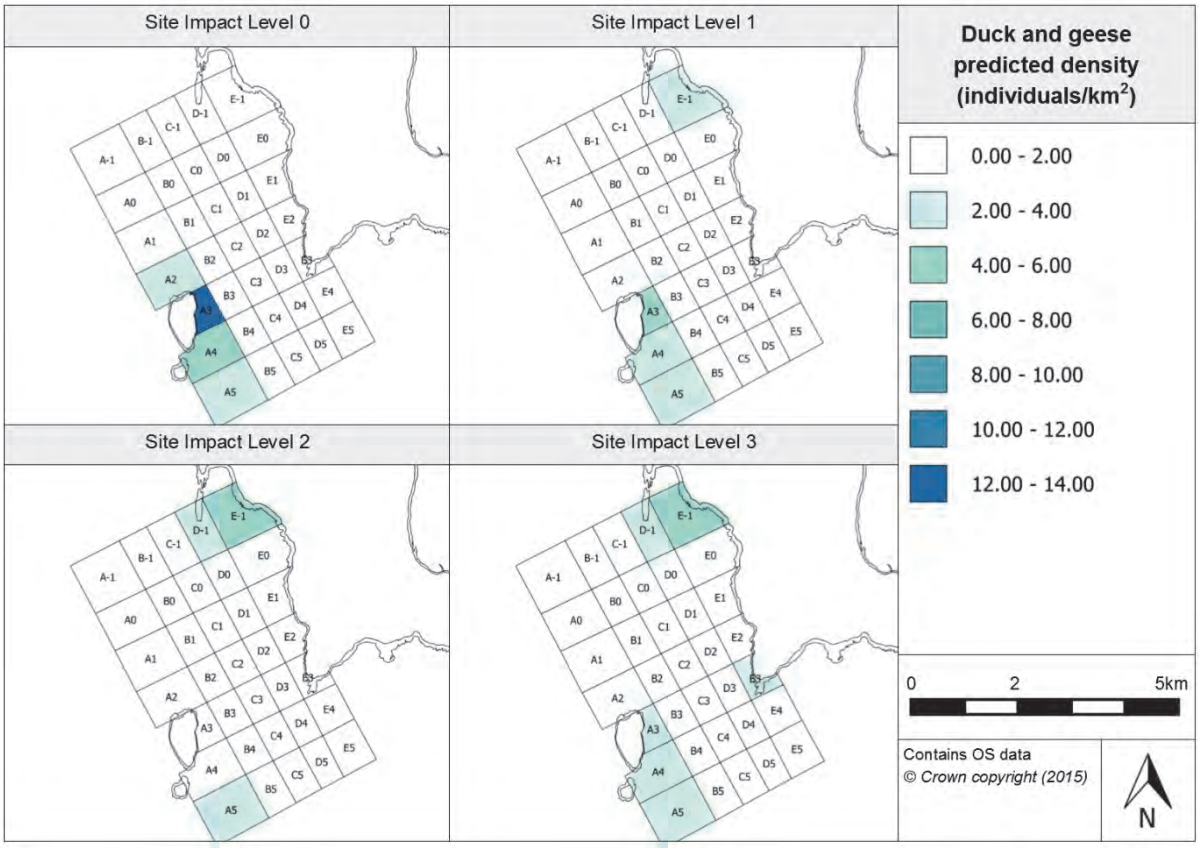

Figure 4.3.37. Estimated duck and geese density at each site impact level

From initial observations, there are clear patterns in duck and geese predicted distributions across the survey area and dramatic changes in density between different areas of the site. At baseline conditions (SIL-0), there is a distinct cluster of grid cells where greater abundances of duck and geese are estimated. The area of high density is focused around Muckle Green Holm and to the south. The highest density is present in grid cell A3 (adjacent to Muckle Green Holm) during baseline conditions.

Estimated density levels during SIL-1 (when only infrastructure is installed) show a cluster of greater densities around Muckle Green Holm (although this is not to the same extent as during baseline conditions) and another peak in density towards the bay at Seal Skerry (grid cell E-1). This peak in density towards Seal Skerry increases when devices are installed; however, the model no longer expects there to be a peak in density around Muckle Green Holm and instead only a slight increase in density is expected in the south-western corner of the site (grid cell A5).

At SIL-3 (when devices are installed and operational), there is a cluster grid cells around Muckle Green Holm and to the south-western corner of the site where the estimated density has increased from that anticipated when devices were present but not operational (SIL-2). The peak in abundance towards Seal Skerry is maintained from SIL-2 conditions. In addition, there is a peak in abundance in grid cell E3, which is adjacent to the peninsula south of the observation vantage point (War Ness).

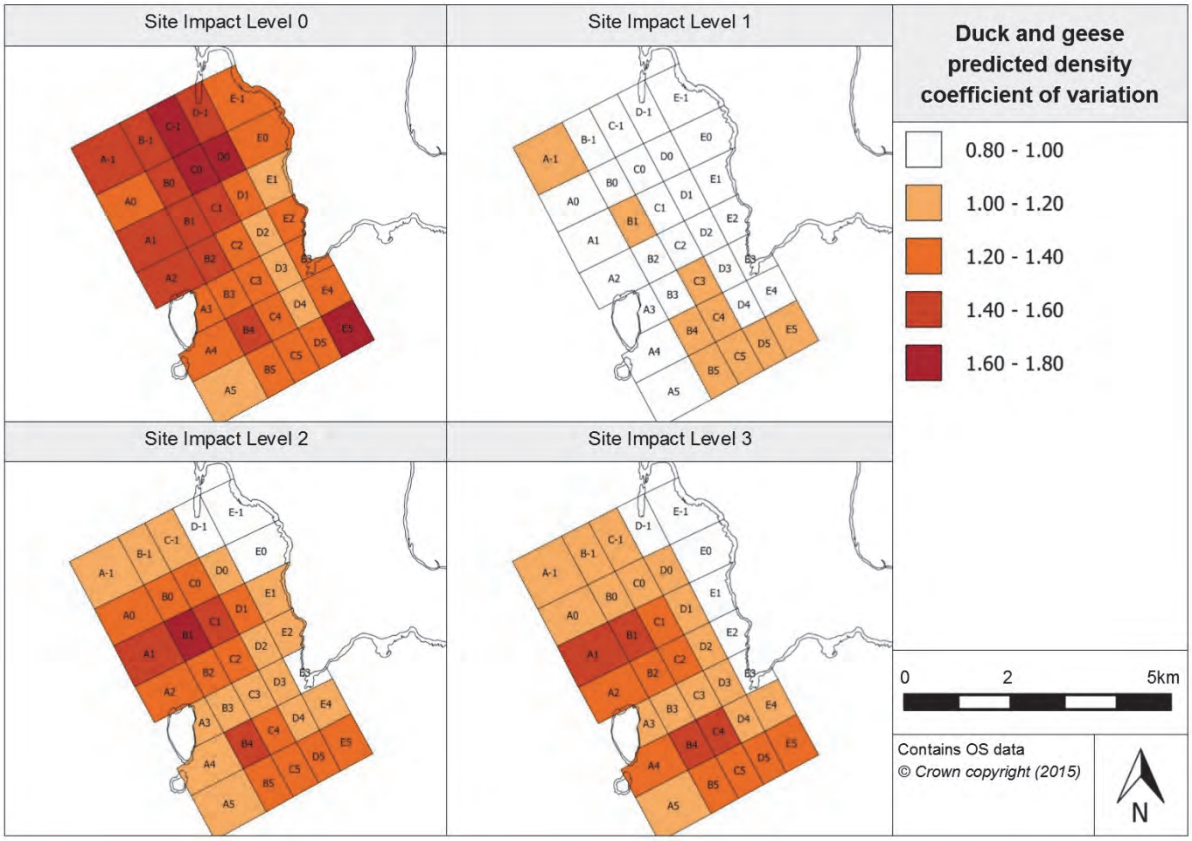

Figure 4.3.38. Associated coefficient of variation values for the density predictions for ducks and geese

When considering the predictions associated CV values, it is clear that the predictions made for baseline conditions are the least reliable, see Figure 4.3.38. During these conditions, the areas with highest CV values are positioned just south of Seal Skerry and in grid cell E5, in the south-eastern corner of the site. It is likely that these high CV values are due to low density predictions of duck and geese species in these areas which is predictable due to the high flow rates and turbulence present in these particular parts of the site.

SIL-1 (when only infrastructure is installed) shows the highest CV values, implying that these predictions benefit from the lowest uncertainty. The pattern of CV values seen at SIL-2 and SIL-3 are very similar, with low values present for the grid cells adjacent to Seal Skerry and the coastline to the east and south of it (cell D-1 and cells E-1 to E3). Additionally, there appears to be a peak in CV values around grid cell B1 and high values at cells B4 and C4.

4.3.7.5 Relative abundance estimations

By using the final model, it is possible to produce estimated abundances for each survey month. By applying the optimum environmental covariates values for observing duck and geese species, as outlined previously, seasonal abundance predictions for ducks and geese could be created, as shown in Table 4.3.21.

Table 4.3.21. Relative abundance for ducks and geese during each season (associated confidence intervals are provided in brackets)

Year	Season			
	Winter (Dec, Jan, Feb)	Spring (Mar, Apr, May)	Summer (Jun, Jul, Aug)	Autumn (Sep, Oct, Nov)
2005	-	-	2.08 (1.29, 3.80)	17.77 (1.98, 62.23)
2006	56.56 (36.00, 109.18)	94.16 (8.35, 252.33)	3.06 (2.00, 4.76)	19.06 (3.08, 53.71)
2007	33.86 (20.20, 68.64)	56.37 (4.73, 157.61)	1.83 (1.10, 3.11)	19.46 (1.70, 63.51)
2008	39.52 (24.73, 75.76)	65.79 (6.00, 178.85)	2.14 (1.34, 3.38)	14.13 (1.58, 52.30)
2009	28.36 (15.81, 56.94)	47.22 (3.59, 132.87)	1.82 (0.90, 3.13)	20.75 (2.56, 62.28)
2010	41.66 (27.26, 71.26)	69.35 (6.40, 166.94)	1.76 (0.93, 3.40)	12.42 (1.46, 36.56)
2011	24.94 (16.39, 44.00)	41.51 (3.81, 100.83)	1.70 (1.11, 2.60)	14.50 (1.81, 44.66)
2012	29.11 (18.87, 50.14)	47.99 (2.57, 116.55)	1.22 (0.67, 2.48)	10.41 (1.07, 42.95)
2013	20.89 (10.22, 46.46)	43.28 (4.83, 106.21)	1.79 (1.15, 2.87)	15.29 (1.81, 50.34)
2014	30.68 (18.35, 54.14)	33.01 (2.99, 76.09)	1.07 (0.71, 1.70)	9.15 (1.12, 27.89)
2015	20.46 (11.66, 40.72)	38.52 (3.40, 93.64)	-	-

The greatest estimated abundances are apparent during winter and spring, and there is evidence of a dramatic dip in abundance during summer. In 2006, the relative abundances are particularly large, for reasons which are unclear; however, as mentioned previously, a slow decline in abundance values is seen over the duration of the observations programme.

The estimated relative abundance of ducks and geese throughout the survey programme, but divided across the appropriate site impact levels for each prediction, are provided in Appendix 7. It is worth noting here that the associated CIs have been included to show the variability behind the relative abundance estimates. This plot shows the clear peaks observed in spring of each year and how the extent of the peak has reduced over the programme's duration.

As provided for the other species, prediction surfaces for ducks and geese have been produced under typical surveying conditions for January and July. The surfaces and their associated CV values are available in the Marine Scotland Information portal. Density predictions for January tend to be ten times greater than those modelled for July.

4.3.7.6 Spatially-explicit change

To consider whether there is any evidence of spatially-explicit change in either abundance or distribution in ducks and geese which can be associated with the presence or operation of devices, or their related infrastructure, the difference between model predictions for each site impact level had to be investigated. The density differences between site impact levels for ducks and geese have been calculated for the least and most variable years (2011 (Figure 4.3.39) and 2009 (Figure 4.3.40), respectively). It is worth noting that the significance of any changes has also been calculated using their associated 95% CIs.

When considering the distribution of changes between site impact levels, there appears to be a redistribution within the site between baseline conditions (SIL-0) and either SIL-1, SIL-2 or SIL-3. There is an increase in density predicted along the northern and eastern perimeter of the site as well as in its south-eastern corner. All the grid cells along the site's northern perimeter and in the north-eastern corner have been found to show a significant increase in density. The remainder of the site exhibited a decrease in density; around Muckle Green

Holm and to the north, stretching into the centre of the site the decrease in density has been deemed significant.

When considering the change in density between SIL-0 and SIL-1 in particular, there are seven grid cells marked as having a significant increase in duck and geese density and nine grid cells marked as having a significant decrease in density. Grid cells E-1 and A3 display the greatest changes (positive and negative, respectively) under these conditions.

As already mentioned, between SIL-0 and SIL-2 (devices installed), the distribution of changes is very similar to that seen between SIL-0 and SIL-1 except that five additional grid cells have been marked as showing a significant decrease in density. This suggests that the effect on duck and geese density with the presence of devices is more pronounced than when only infrastructure is installed. The largest estimated decrease between two impact levels is experienced between SIL-0 and SIL-2. At grid cell A3, there is a density decrease of 8.73 individuals/km^2 during 2011 and 20.62 individuals/km^2 during 2009. In addition, under the same conditions, the largest increase in density is predicted. During 2011, there is an increase of 3.53 individuals/km^2 in density estimated and, similarly, in 2009 an increase in density of 8.68 individuals/km^2.

When the density difference between baseline conditions and SIL-3 (devices installed and operational) is examined in more detail, it is apparent that there are more grid cells marked with an increase in density and fewer (8 grid cells) where the decrease in in density is marked as significant. This suggests that, although there remains an apparent redistribution within the site, the extent of the decrease seen in the centre of the site and around Muckle Green Holm is not to the same extent (when compared to that observed between SIL-0 and SIL-1 and between SIL-0 and SIL-2).

Between SIL-1 and SIL-2, a similar distribution of density changes exist, with a positive change around the northern and eastern perimeter of the site and a negative change in the remainder of the site. Only one grid cell is deemed to have an increase in density which is significant, whereas 15 grid cells have significant decreases in density estimated. This highlights the reduction in duck and geese numbers observed near to Muckle Green Holm (and towards the centre of the site) with the presence of devices.

When the change in density between SIL-1 and SIL-3 is investigated, there is an increase in density observed in the northern half of the site and an increase also seen along its eastern perimeter. Only one grid cell was deemed to show a significant change in density; this was grid cell E-1, where an increase in density was estimated.

When considering the change in density between SIL-2 and SIL-3, there is an increase in density expected across the site, with the exception of grid cell E-1. The increase is deemed to be significant in two grid cells adjacent to Muckle Green Holm (A3 and A4) and in six grid cells positioned in centre of the site.

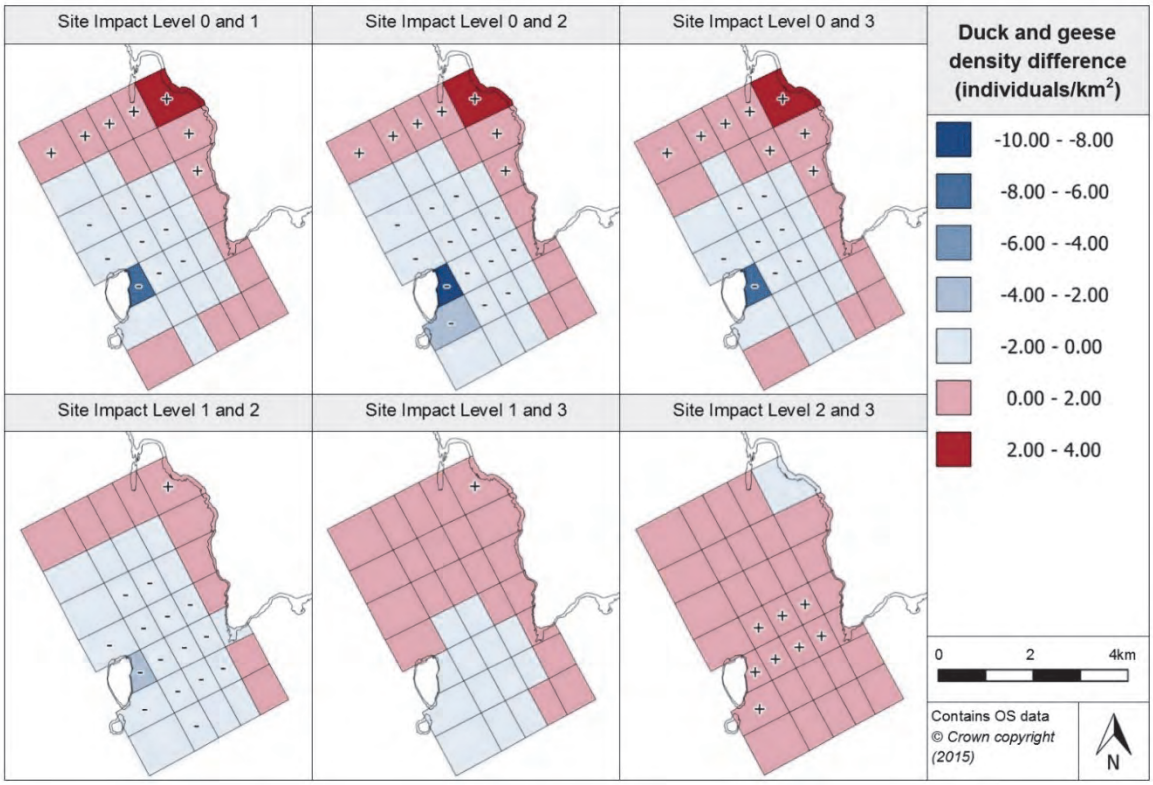

Figure 4.3.39. Estimated density difference between various site impact levels for ducks and geese during 2011 (year with least variation)

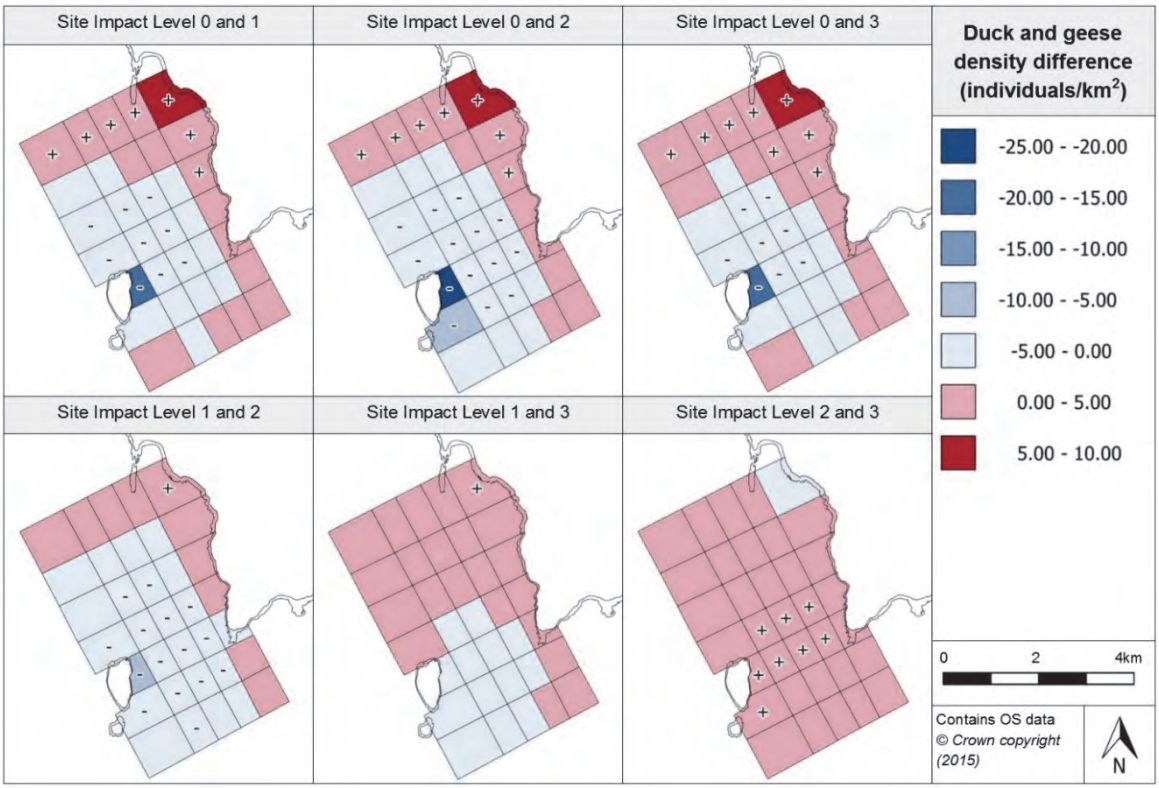

Figure 4.3.40. Estimated density difference between various site impact levels for ducks and geese during 2009 (year with most variation)

4.3.7.7 Density change with distance from potential impact location

Using the density difference projections, it has been possible to map out how the density change alters with increasing distance from the test berths (potential impact locations). The estimated density change from one test berth has been provided in Figure 4.3.41.

Between SIL-0 and SIL-1, there is a drop in density in the zone up to 900m from the impact location; however, this change is unlikely to be significant as the upper CIs are approximately zero. Beyond 900m, there is then a negligible increase or no change in density.

When considering the change in density between SIL-0 and SIL-2 and between SIL-0 and SIL-3, a very similar pattern is observed. There is a decrease in density with devices being present or operational for the first kilometre. Beyond 1km, the introduction of devices or the operation of devices appears to have a negligible effect on duck and geese density.

This same decrease is evident when looking at the density change between SIL-1 and SIL-2, and between SIL-1 and SIL-3. However, the estimated decrease appears to occur over the first 1.5km from the impact location. Again, there seems to be very little change in density beyond 1.5km. Both of these results emphasise that it appears as if the presence of devices may cause a reduction in duck and geese numbers and the effect may extend to 1.5km from the test berth. From examining the change in density between SIL-2 and SIL-3, there is potential for a slight increase in density with increasing distance from the test berth. As before, beyond 1.5km there appears to be little change in density. This final result suggests that a negative change in density relates to the presence of the device/infrastructure and the operation of the device may in fact serve to lessen this negative effect.

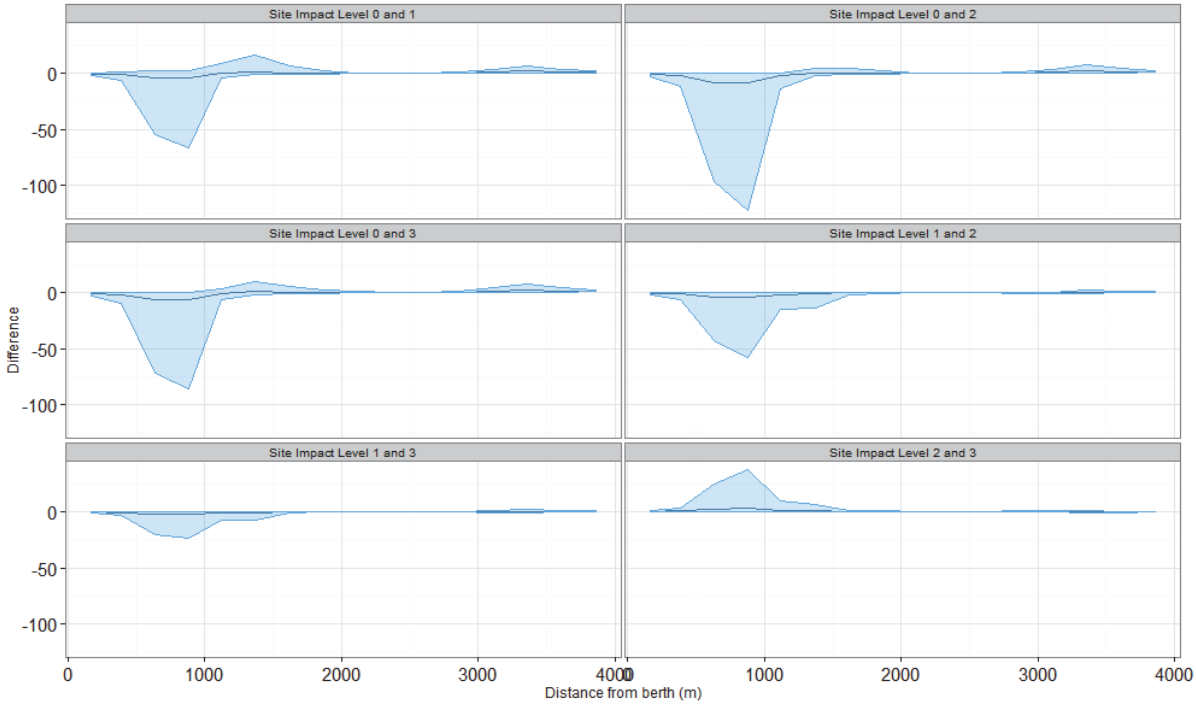

Figure 4.3.41. Density change between site impact levels with increasing distance from a potential impact location, with associated confidence intervals, for ducks and geese at the Fall of Warness

4.3.7.8 Discussion

Duck and geese species are regularly sighted at the Fall of Warness, with the common eider being the most observed species. The model developed for their distribution incorporates nine significant terms. This implies that the presence of ducks and geese is controlled by a great number of environmental, temporal and spatial factors, which need to be included in any analysis when elucidating the impact of MECS. There is strong seasonal variability, with particularly few ducks and geese seen in the summer, between May and September.

The distribution of higher density grid cells is similar for all site impact levels with greater densities with increasing proximity of the grid cells to the coastline. The higher CV values for baseline conditions (suggesting higher uncertainty in the predictions) probably reflect the far fewer observations at this site impact level. As with many other species/groups, the biggest change in Anatidae density is estimated to occur with the installation of infrastructure when a reduction in density is seen. This involves a reduction in density over most of the survey area but with density increases along the eastern and northern edges. These changes are repeated with the installation of devices. However, when the devices become operational, there is an increase in duck and geese numbers across virtually the entire survey area. These results are in line with the results gained when the density changes was plotted against increasing distance from a potential impact location. This may imply that the placement of infrastructure or devices (or the vessel movements associated with the installation activities) may cause a reduction in duck and geese density. The effect of this reduction may decrease a devices become operational.

4.4 Fall of Warness marine mammals

4.4.1 Seals

4.4.1.1 Species overview

In the UK, two species of seal are typically found and both have been recorded at the Fall of Warness site. They are the harbour seal (otherwise known as the common seal (*Phoca vitulina*)) and the grey seal (*Halichoerus grypus*). As the observers at the Fall of Warness sometimes experience difficulty in identifying seals to species level, due to the distance between the seal and the observation vantage point, some sightings are recorded as 'unclassified seals'. However, it is believed the majority of these sightings are grey seals.

Scotland is home to around 79% of the UK's population of harbour seals whilst the UK as a whole holds around 30% of Europe's harbour seals, this proportion declining from approximately 40% in 2002 (SCOS, 2011). They are found widespread around the west coast of Scotland and throughout the Hebrides and Northern Isles, with more limited distributions restricted to concentrations along Scotland's east coast. Major declines have been documented around Scotland since 2000 with the overall population in Orkney decreasing by more than 10% per year since 2006 (Duck & Morris, 2014). However, within this overall decline, there is some variation at a subregional level, with harbour seal numbers remaining level in the Eday and Calf of Eday SMRU subregion between 2006 and 2010 but more than halving in 2013 (Duck & Morris, 2014). In contrast, the Muckle and Little Green Holms SMRU subregion shows a reduction by three quarters in the harbour seal population between 2006 and 2009 but recovering substantially by 2013 (Duck & Morris, 2014).

Telemetry studies focusing on seals within the Pentland Firth and Orkney Waters (PFOW) area have followed harbour seals' tracks through the Fall of Warness site (SMRU Ltd, 2011). The test site is approximately 15km from Sanday Special Area of Conservation (SAC) which has the largest colony of breeding harbour seals in Orkney. In addition, the test site is within the 50km typical maximum foraging range for this species (SCOS, 2012). Harbour seals in UK waters show some degree of fidelity to their breeding sites year round and so remain in

relative proximity to these sites outwith the breeding season (SMRU Ltd, 2011). They are expected to be observed year round at the test site but their annual moulting season occurs between July to September when they are more likely to be seen out of the water at haul-out sites. The harbour seal pupping season is between June and July, and they tend to pup in intertidal areas such as sandbanks and rocks (SMRU, 2013). Harbour seal pups are fairly precocious as they are able to swim with their mothers just hours from birth and are born with their adult waterproof coats.

Around 38% of the world's grey seal population breed in the UK, with 88% of these breeding in colonies in Scotland, the majority in the Hebrides and Orkney. While grey seal pup numbers have increased steadily since the 1960s, current evidence suggests that this growth may have levelled off, particularly in Orkney (SCOS, 2011). Although the overall numbers measured around Orkney in August may have remained constant, there has been greater interannual variation within the SMRU subregions. Duck and Morris (2014) recorded a fall of around 50% in the Eday and Calf of Eday subregion between the 2007/2008 surveys and those in conducted in 2010 and 2013, and very variable population counts year on year in the Muckle and Little Green Holms SMRU subregion.

Grey seals are present at the site during both breeding (late September to early October) and moulting periods. Female grey seals moult in January to March (following the breeding season) whereas males generally moult later, March to May. Tagging studies have shown that individuals transit through the Fall of Warness and it is likely that they are also using this area when foraging (SMRU Ltd, 2011). The nearby Faray and Holm of Faray SAC has grey seals as one of its qualifying features as a great number of individuals congregate here (Duck & Morris, 2011). Muckle Green Holm and Little Green Holm in the west of the site are also designated as an SSSI (Site of Special Scientific Interest) for their grey seal population. Similar to the harbour seals, grey seals are expected to occur in the Fall of Warness year round. Their annual moulting season is between December and March when they are more likely to be spotted on the shoreline at haul-out sites. During pupping season, grey seals tend to congregate on remote beaches and islands above the high water mark (SMRU, 2013). Pupping season is typically between September and December and females can remain ashore for three weeks whilst their pup is suckling.

Much greater numbers of grey seals are expected to use the Fall of Warness haul-out sites in comparison to harbour seals (Robbins, 2011). When surveying, Duck and Morris (2011) recorded counts of harbour seals during moults at haul-out sites surrounding the Fall of Warness and there were notably fewer of these than the number of grey seals recorded.

The Fall of Warness site lies within the Orkney and North Coast Seal Management Area and in a Seal Conservation Area for harbour seals. In 2014, 194 seal haul-out sites were designated through The Protection of Seal (Designation of Haul-Out Sites)(Scotland) Order 2014; three of these designated sites are within the Fall of Warness (Marine Scotland, 2014). Included within the designated haul-out sites is the entire island of Seal Skerry and the rocky outcrops immediately to the north of Seal Skerry and the area east of Seal Skerry Bay on the coast of Eday. This site has been designated due to its year-round use by harbour seals (Scottish Government, 2014). Additionally, the entire islands of Muckle Green Holm and Little Green Holm have both been designated due to their use by grey seal breeding colonies and the importance of the sites particularly during their pupping season.

4.4.1.2 Data summary

Both harbour and grey seals are regular visitors to the Fall of Warness. Sometimes the observers at the Fall of Warness site were unable to distinguish between the grey and harbour seal species and the observations are recorded as 'unidentified seal' i.e. unclassified seal. The following section provides a discussion of the outputs and predictions

from a model based on a combined dataset of grey seal and harbour seal as well as the unclassified seal observations. Table 4.4.1 provides a summary of the raw survey data from the site including information on the number of observations and the mean group size. This information is also presented for each site impact level, to provide an understanding of the data used in the analysis.

Table 4.4.1. Summary of seals raw data

	Total	Site Impact Level 0	Site Impact Level 1	Site Impact Level 2	Site Impact Level 3
Number of observations	9511	1294	4104	1468	2645
Minimum (group size)	1	1	1	1	1
Maximum (group size)	100	100	63	70	50
Mean (group size)	1.77	2.15	1.80	1.64	1.59
(s.d)	(2.73)	(4.62)	(2.40)	(2.65)	(1.86)

4.4.1.3 Model overview

For all the remaining terms in the final fitted seal model, GEE-based p-values have been produced. The final model contained ten terms, three of which were found to be significant and seven highly significant (see Table 4.4.2 for terms' associated p-values).

Table 4.4.2. GEE-based p-values for the terms in the final seal model for the Fall of Warness

Model term	ρ-value
Precipitation	0.002936
Wind strength	<0.0001
Cloud cover	<0.0001
Sea state	0.004321
Depth	<0.0001
Year	<0.0001
Month	<0.0001
Site impact	0.026765
Spatial surface	<0.0001
Spatial surface / site impact	<0.0001

Precipitation has been included as a term in the final model. The model has estimated greatest abundances when there is no precipitation and lowest abundances when the precipitation is classed as heavy. Wind strength has also been included in the model, where species density has been modelled as reducing with increasing wind strength (measured using the Beaufort scale). Figure 4.4.1 below displays this clear relationship.

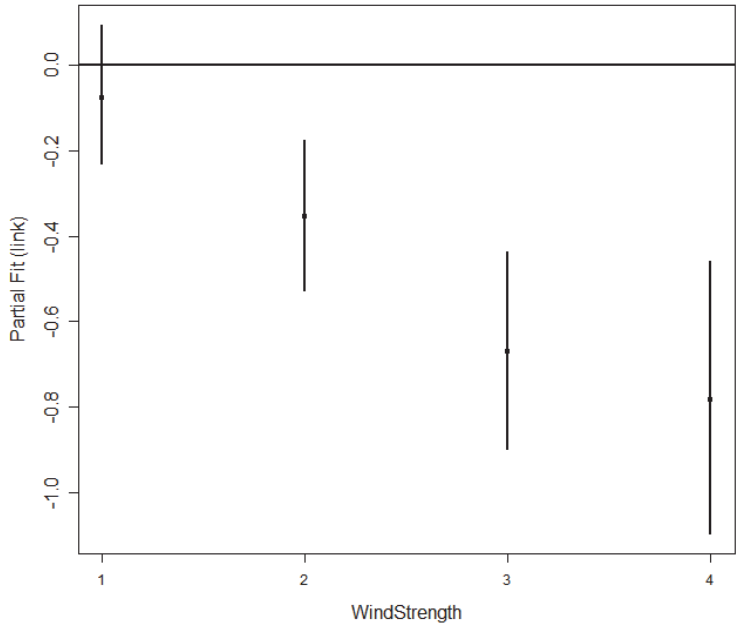

Figure 4.4.1. Estimated partial relationship of seal density (on the scale of the log link) with wind strength at the Fall of Warness. The points are the parameters for the estimated change in log density from the baseline (wind strength = 0) and the vertical lines represent 95% confidence intervals about the parameter estimates.

Cloud cover has been retained in the final model. It appears that the model has estimated the greatest seal abundances to occur when cloud cover is between 6 and 7 oktas and lowest abundances when cloud cover is 0 oktas (clear skies)[20]. Although sea state has been included as a term in the final seal model, due to wide CIs there is no clear relationship between seal density and sea state except that there may be a decrease in seal density at sea states 3 and 4 (Beaufort scale). Depth has been included in the final model. The model has estimated that, as depth increases, there is a steady reduction in seal abundance.

Over the duration of the observations programme, there appears to have been a reduction in seal abundance which has been modelled to be reducing at a steady rate from the programme's inception in 2005. As would be expected, due to seals having well-defined breeding and moulting seasons, 'month' has been included in the model. However, as the model encompasses both harbour and grey seals (who have differing moulting and breeding seasons), the peaks and troughs in estimated seal abundance may not be in line with expected peaks and troughs. The model predicts there to be a peak in seal abundance between late September and early November. This peak aligns with the grey seal breeding season (which tends to be between late September and early October (Robbins, 2011)). There are two troughs in seal numbers, between early December and early January and between early March and late April. These two troughs may be associated with the moulting season as the grey seal moulting period falls between January and March and males moult later during March-May (Robbins, 2011). It is worth mentioning that Robbins (2011) noted that harbour seals occur year round in the Fall of Warness with an increase in average encounter rate between May and October, even though this overlaps with their moulting period when fewer animals might be expected to be in the water.

[20] As fewer seals are estimated when there is no cloud cover, this would suggest that fewer seal observations were made under these conditions. There are several reasons why this may be the case. These include, but are not limited to, more seals may be hauled out and therefore less observable at the sea surface, and seals may be harder to sight due to increased glare affecting the survey area.

A spatial surface was able to be fitted to the model and four knots were used during the fitting. Also included in the model, as found to be statistically significant, was the interaction term (site impact/spatial surface).

Diagnostic tests have been run on the fitted model, the outputs of which are available on the Marine Scotland Information portal. Although the mean variance relationship would suggest that the model fits the data well, when investigating further, the log mean variance relationship would suggest that the model underestimates the variance in the data.

4.4.1.4 Density predictions and uncertainty estimation

Due to the spatial surface being included in the model, it was possible to plot the estimated density for different site impact levels across the survey region. Seal density predictions have been made for optimum environmental conditions for seal observations, these are outlined in Appendix 5. The density predictions for each site impact level and their associated CV values (for measuring the reliability of the estimate) have been provided in Figure 4.4.2 and Figure 4.4.3, respectively.

The seal density predictions at baseline conditions (SIL-0) show a clear aggregation of high density values around Muckle Green Holm (one of the seal haul-out sites). In grid cell A3, adjacent to the eastern coastline of Muckle Green Holm, is the greatest estimated abundance across all impact levels. There is also a slight peak in density in grid cell E3, adjacent to the peninsula south of the observation vantage point.

At SIL-1, when infrastructure is on site, a peak in density near to Muckle Green Holm remains which stretches to the most south-western corner of the survey site. A further peak in density is observed in the bay at Seal Skerry. This is another known haul-out site for seals within the Fall of Warness.

During SIL-2 conditions (when devices are onsite but not operational), the peak in seal density at Muckle Green Holm and to the south continues to exist. The peak previously seen in the bay at Seal Skerry also continues to be apparent and the slight peak in grid cell E3 has reappeared. The distribution of the density peaks appears to be very similar during SIL-3 conditions (when devices are onsite and operational); however, the number of individuals/km^2 appears to have increased, in particular in grid cell A2 to the north of Muckle Green Holm.

It is unclear whether the heightened density at grid cell E3 is due to close proximity to a haul-out site, as seen in the other areas of high density, as this is not a designated haul-out site like those at Seal Skerry, Muckle Green Holm and Little Green Holm.

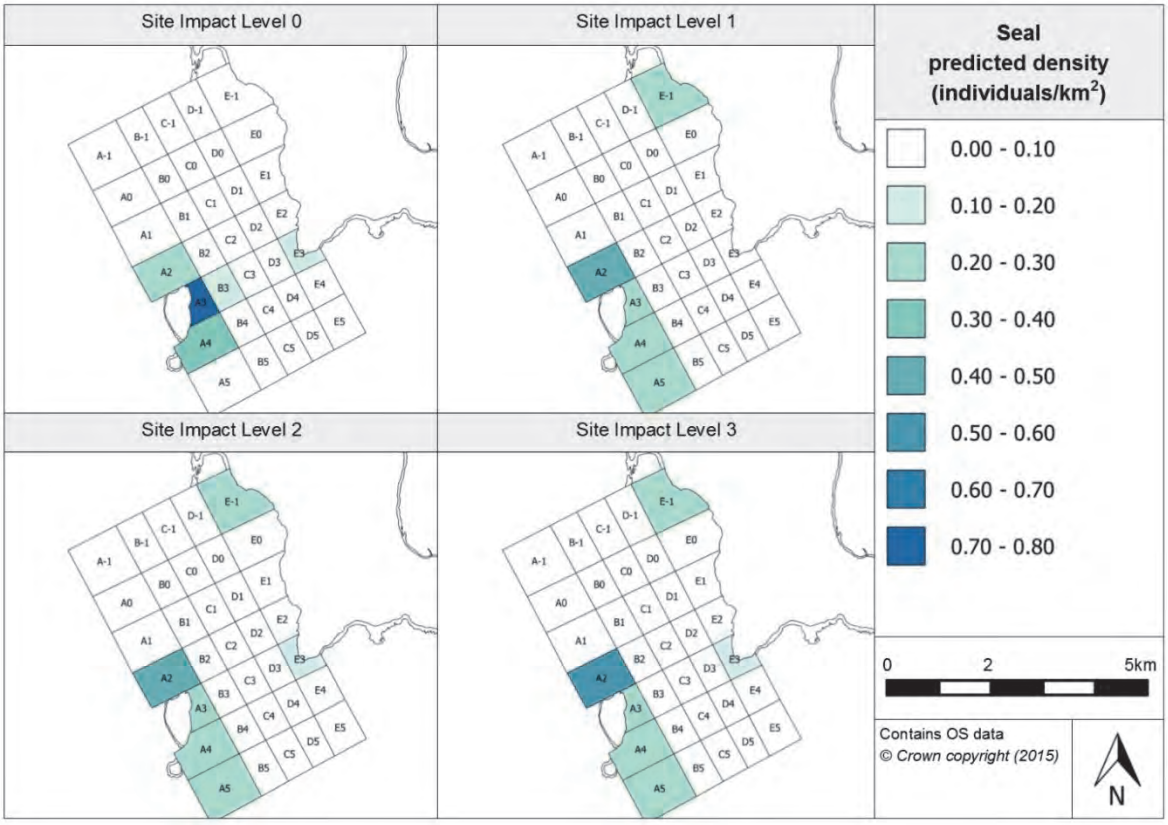

Figure 4.4.2. Estimated seal density at each site impact level

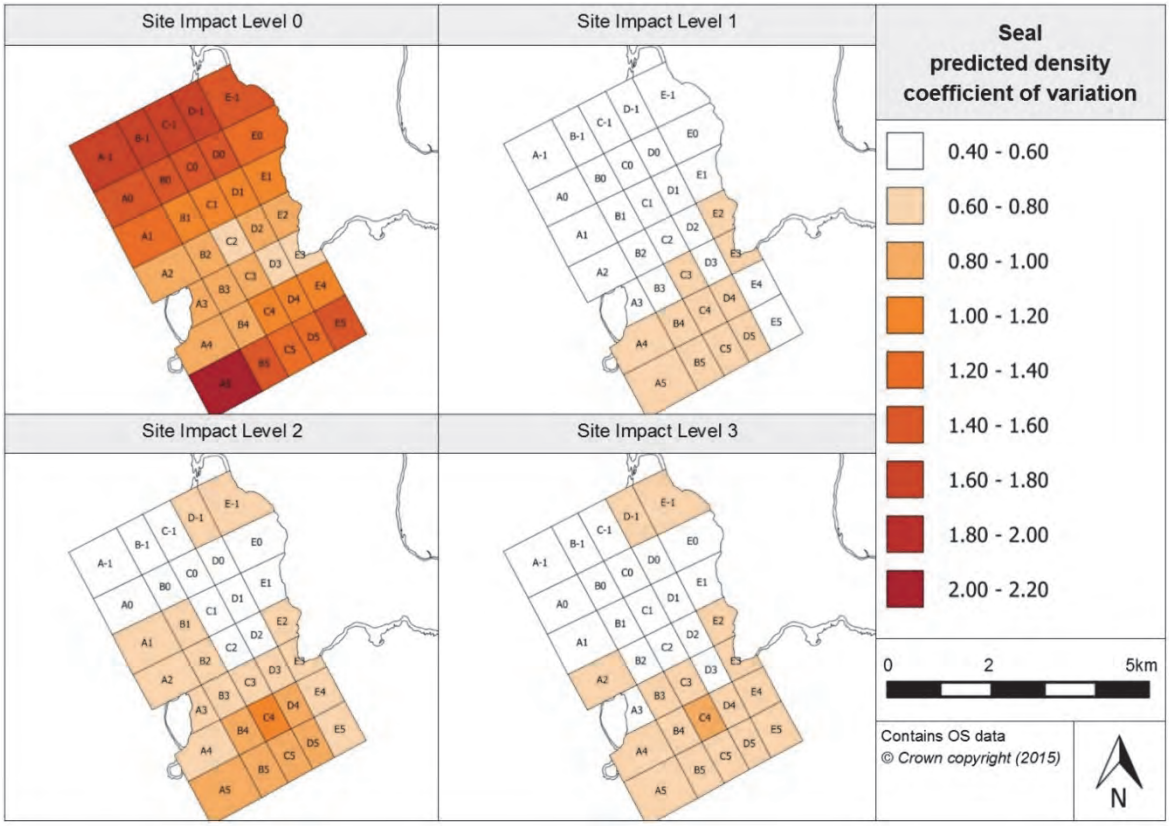

Figure 4.4.3. Associated coefficient of variation values for the density predictions for seals

When considering the prediction surfaces' associated CV values, it is clear that there is higher uncertainty in the prediction surface for SIL-0 compared with the other site impact levels, particularly in the south-western corner and on the northern edge of the site. This is likely due to there being lower density estimates at this impact level.

At SIL-1, there is generally more precision in the predictions, with slightly higher uncertainty with regard to the predictions around the southern half of the site.

Higher uncertainty exists with respect to the predictions for SIL-2 when compared to SIL-1, with higher CV values experienced around grid cell C4. In addition, the CV values at Seal Skerry are minimally raised, suggesting that there is greater uncertainty behind the predictions for this area as compared to a SIL-1. When considering the CV values for the prediction surface at SIL-3, these are fairly low, suggesting overall high precision in the prediction surface, with a slight increase in uncertainty in grid cell C4 and its surrounding cells.

4.4.1.5 Relative abundance estimations

By using the final seal model, it was possible to produce abundance predictions for each of the survey months. The same environmental conditions were used in making the predictions. The monthly predictions have been combined to provide seasonal predictions, as seen in Table 4.4.3. It should be emphasised that these are relative abundances as only surface visible observations were recorded.

Table 4.4.3. Relative abundance for seals during each season (associated confidence intervals are provided in brackets)

Year	Season			
	Winter (Dec, Jan, Feb)	Spring (Mar, Apr, May)	Summer (Jun, Jul, Aug)	Autumn (Sep, Oct, Nov)
2005	-	-	5.23 (3.41, 8.41)	11.94 (4.29, 26.38)
2006	2.13 (1.25, 3.85)	1.92 (1.15, 2.94)	3.41 (2.43, 4.94)	7.79 (2.85, 13.85)
2007	1.79 (1.14, 3.06)	1.77 (1.09, 2.62)	3.14 (2.14, 4.65)	7.24 (2.82, 13.51)
2008	1.44 (0.79, 2.36)	1.32 (0.79, 2.01)	2.35 (1.58, 3.58)	5.65 (1.90, 12.82)
2009	1.36 (0.78, 2.70)	1.37 (0.76, 2.29)	2.36 (1.48, 3.47)	5.13 (2.07, 9.25)
2010	1.26 (0.81, 2.30)	1.28 (0.75, 2.02)	2.28 (1.61, 3.25)	5.21 (2.07, 9.61)
2011	1.36 (0.84, 2.48)	1.41 (0.86, 2.11)	2.54 (1.81, 3.61)	5.81 (2.32, 10.45)
2012	1.36 (0.87, 2.36)	1.38 (0.82, 2.42)	2.54 (1.55, 4.62)	5.79 (1.88, 13.15)
2013	1.36 (0.77, 2.73)	1.30 (0.76, 2.35)	2.24 (1.65, 3.24)	5.12 (2.05, 9.55)
2014	1.00 (0.57, 1.62)	0.92 (0.57, 1.38)	1.64 (1.19, 2.33)	3.74 (1.51, 6.78)
2015	1.08 (0.60, 2.15)	1.17 (0.67, 1.85)	-	-

Greatest estimated abundances occur during autumn, with lowest abundances occurring in either winter or spring. As already discussed, it is expected that the increase in abundance seen during autumn is associated with the grey seal breeding season.

Table 4.4.3 demonstrates how the seasonal abundance predictions have reduced over the observations programme's duration, with the lowest predictions during 2014 and highest predictions in the first survey year, 2005.

The above abundance predictions have been divided into each of the site impact levels and are provided in Appendix 7. Their associated CIs have also been provided to give an

indication of the reliability of the estimate. The seasonal peak in abundance during autumn can be observed in each year.

Prediction surfaces for seals have also been provided for typical surveying conditions in January and July. The surfaces and associated CV values are available in the Marine Scotland Information portal. The distribution across the prediction surfaces is very similar. Predictions during July tend to be two and half times greater than those for January, which is in line with the relationship previously observed between seal density and season.

4.4.1.6 Spatially-explicit change

In order to understand the extent of any spatially-explicit changes in either seal abundance or distribution that have arisen due to the site's operational status, it is necessary to investigate the difference in the prediction surfaces for each of the site impact levels. The density difference for each of the prediction surfaces has been produced alongside an indication of whether the change is significant. The significance of the change has been calculated using the predictions' associated 95% CIs. As the model contains the term 'year', the estimated spatially-explicit change for both the least and most variable years (2014 and 2006, respectively) have been provided, see Figure 4.4.4 and Figure 4.4.5.

When comparing the change in density between SIL-0 (baseline conditions) and SIL-1 (infrastructure installed), there appears to be a redistribution of seals across the site, with an increase in density in the site's northern half (including grid cell A2) and decrease in density in the site's southern half. The increase observed in the northern half is deemed to be statistically significant in 14 grid cells and the decrease, seen in the south, is deemed to be significant in 11 grid cells. It is worth highlighting the extent of the reduction observed in grid cell A3, which is nearly four times greater a reduction than observed anywhere else within the site. The south-north redistribution, however, is not seen in grid cell A5 (south-western corner of the site), where a significant increase in density is estimated with the introduction of infrastructure.

This same south - north redistribution is observed between baseline conditions and devices being installed onsite (i.e. from SIL-0 to SIL-2). However, in the north, more grid cells (15) exhibit a statistically significant increase in density and fewer grid cells in the south (8) show a significant decrease in density. Under these conditions (installation of devices), although a large density increase is estimated in grid cell A2, the change is not calculated as statistically significant. The decrease in density seen in grid cell A3 remains the largest decrease across the site and a significantly greater decrease than that observed anywhere else within the site. There remains an increase in density estimated in the south-western corner of the site; however, between baseline conditions and the installation of devices, this change is not deemed to be significant.

Again, a similar south-north redistribution is observed between SIL-0 and SIL-3 (devices present and operational). A total of 16 grid cells have their density difference recorded as significantly positive and in only 9 grid cells is the change in density recorded as significantly negative. Grid cell A3 continues to exhibit a much greater decrease in density than anywhere else in the site. There is no obvious correlation between those grid cells where test berths are located and the estimated change in density of seals between baseline conditions and those expected when devices are installed and operating (in both 2006 and 2014, the years of most and least variability, respectively). Three of the cells show increases and four show decreases, only some of which changes are deemed significant. This suggests that though seal distribution may be affected by initial installation of infrastructure, it is not influenced by subsequent installation and operation of devices.

When considering the density difference between SIL-1 (infrastructure on site) and SIL-2 (devices present), there is a reduction in density estimated on both the northern and southern perimeter of the site. An increase in density is experienced in the middle of the site and towards the shores of Eday. In the grid cell directly below the observation vantage point, E2, and the grid cells surrounding it, the increase in density is deemed to be significant.

Between SIL-1 and SIL-3 (devices installed and operational), there appears to be a reduction in density on the northern perimeter of the site and in the south-western corner of the site. However, in none of the grid cells where a decrease in density is identified is the decrease deemed to be significant. An increase in density is again estimated in the centre of the survey area and towards the Eday shoreline. This increase is deemed to be significant in two grid cells, C2 and D2. Grid cells in the south-eastern corner of the site now appear to experience an increase in density rather than a decrease, but this change in density is not expected to be significant.

When comparing the prediction surface for SIL-2 and SIL-3 (devices becoming operational), there appears to be an increase in density expected on the northern, western and southern edges of the site, including around Muckle Green Holm. This positive change in density, however, has not been distinguished as significant. There has been a decrease in density in the centre of the survey area and towards the Eday shoreline. This decrease is not deemed to be significant in any of the grid cells.

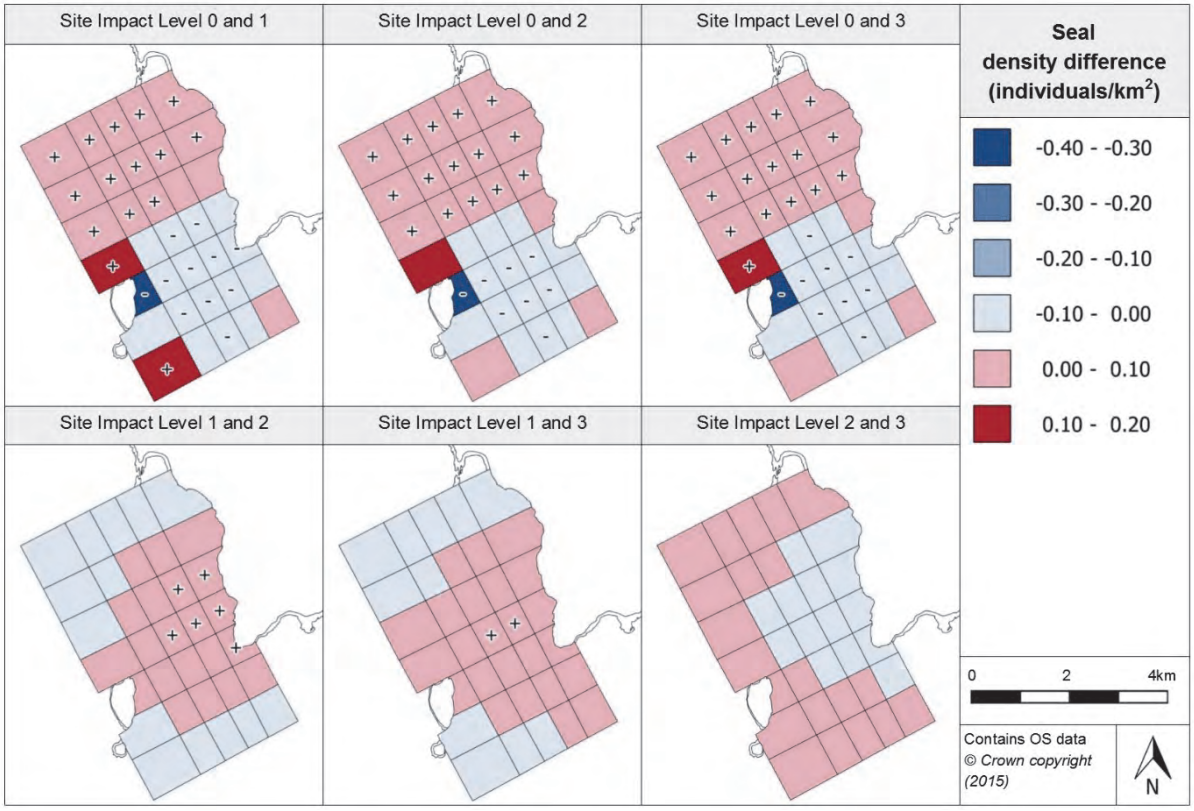

Figure 4.4.4. Estimated density difference between various site impact levels for seals during 2014 (year with least variation)

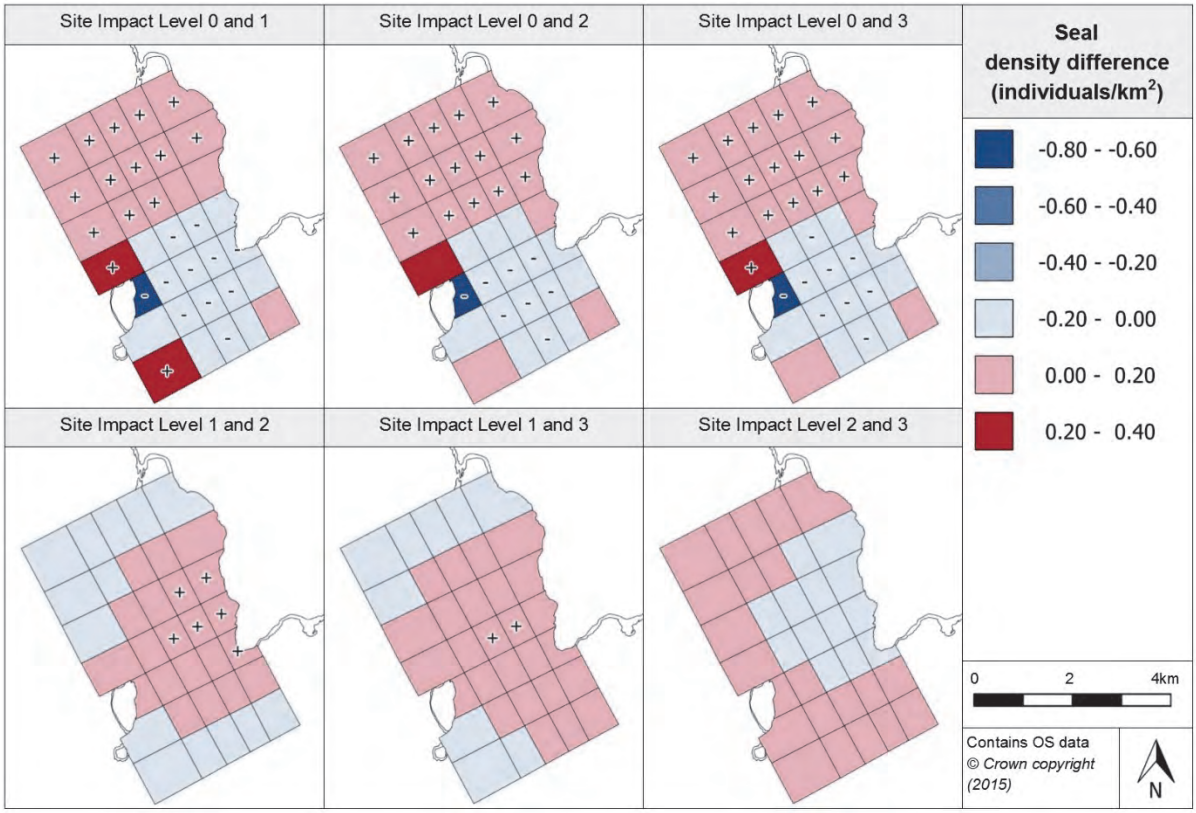

Figure 4.4.5. Estimated density difference between various site impact levels for seals during 2006 (year with most variation)

4.4.1.7 Density change with distance from potential impact location

Using the density difference projections, it has been possible to plot out how the species density changes with increasing distance from a potential impact location. The changes for various site impact levels are shown in Figure 4.4.6. When inspecting the plots between baseline conditions and site impact levels 1, 2 and 3, it appears that there is a decrease in density estimated up to 600m from the impact location. The density then slowly rises to around baseline conditions at 1km from the impact location. Beyond 1km, there appears to be very little change in density from baseline levels.

When considering the change in density between SIL-1 and SIL-2, between SIL-1 and SIL-3, and between SIL-2 and SIL-3, increasing distance from a potential impact location appears to have very little effect on density. This suggests that the biggest changes in seal density are expected to occur between baseline conditions and the other site impact levels, and such changes tend to happen within the first 600m. However, because this relationship is not seen at all the test berths (plots provided in the Marine Scotland Information portal), the effect being demonstrated here may only be a coincidence of the chosen test berths' proximity to a grid cell where large changes in seal density are estimated.

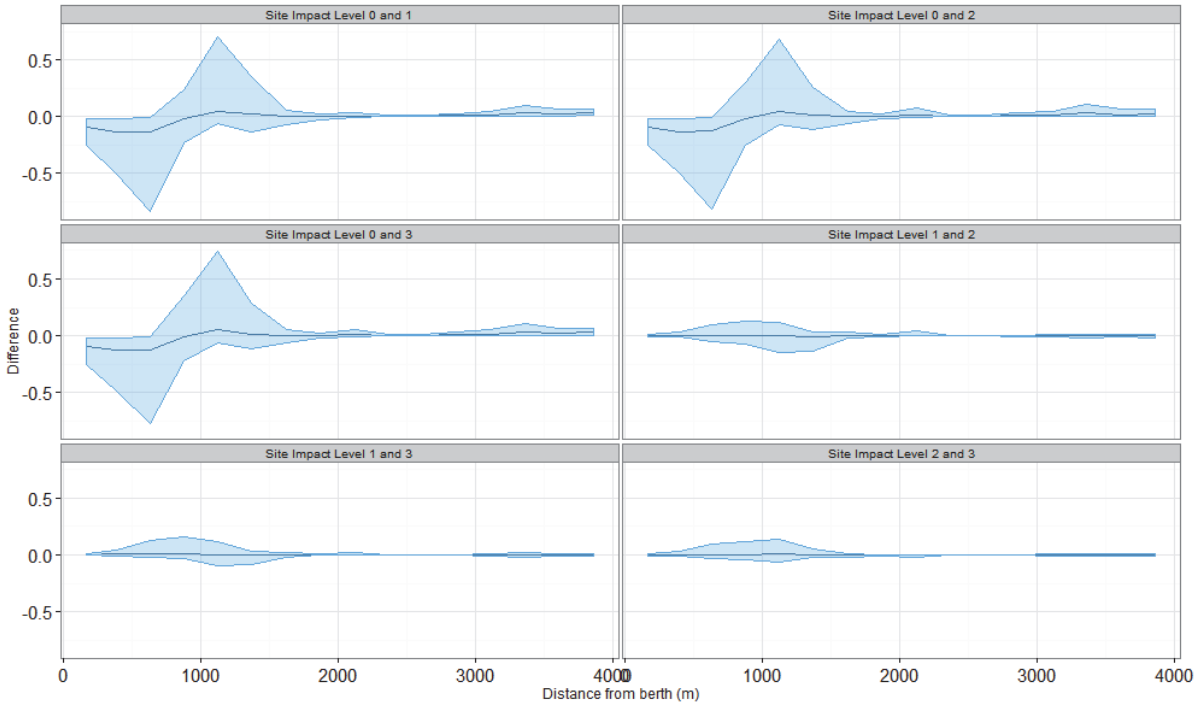

Figure 4.4.6. Density change between site impact levels with increasing distance from a potential impact location, with associated confidence intervals, for seals at the Fall of Warness

4.4.1.8 Discussion

The model developed for all seals observed (both grey and harbour) indicates that their distribution includes ten significant terms. This implies that the presence of seals is influenced by a great number of environmental, temporal and spatial factors, which need to be considered when analysing the impact of MECS. The analysis of all seals at the Fall of Warness shows a clear peak in density around Muckle Green Holm, a known seal haul-out site, at all site impact levels. There is also a slight peak in estimated density in grid cell E3, adjacent to the War Ness headland south of the observation vantage point, and grid cell E-1 by Seal Skerry.

Changes in seal density are apparent with each change in site conditions. At the same time as infrastructure is installed, there is a decrease in seal density between War Ness and Muckle Green Holm, and a corresponding increase in density to the north and the south. The change in most of the grid cells is statistically significant. These increases and decreases are repeated with the change in site impact level following the installation of devices. However, with the change in site impact level from devices being installed to actually operating, there is a switch back in seal numbers, so the grid cells between War Ness and Muckle Green Holm show an increase in seal density whilst those grid cells to the north and south show a decrease. However, this reversal is insufficient to overcome the large shift in numbers that coincided with the change from baseline conditions to those when device-associated infrastructure was installed (SIL-0 to SIL-1). Although the areas of these changes in species density are consistent between the different site impact levels, they bear no resemblance to the layout of the test berths.

The greatest change in seal distribution from baseline conditions is anticipated to occur with the installation of infrastructure, but the extent of this change is reduced with the installation of devices and their operation. This suggests that perhaps it is the movement of vessels that is influencing seal abundances rather than devices in the water. For both 2006 and 2014,

the years of most and least variability respectively, there is no obvious correlation between those grid cells where test berths are located and the estimated change in density of seals between baseline conditions and the conditions occurring when devices are installed and operating (SIL-0 to SIL-3). Of the cells that contain test berths, when the site impact level is changed from baseline conditions to SIL-3, three of the cells have increases in density expected, whereas four cells have decreases in density anticipated. This would suggest there is no clear relationship between seal density and test berth location (when devices become operational). In addition, only some of the changes in the cells have been deemed statistically significant. Therefore, it appears that changes in seal distribution are not influenced by the installation and operation of devices.

Examination of the impact of a device at a location, and at distances away from it, suggests that there is a decrease in density expected immediately adjacent to the potential impact location (single test berth); however, beyond 1km there is no apparent effect.

4.4.2 Harbour seal (Phoca vitulina)

4.4.2.1 Species overview

This section provides an analysis focused solely on harbour seals. Information regarding the distribution and behaviour of harbour seals has been outlined in Section 4.4.1 above. Harbour seals have been selected for particular attention due to their well-documented decline, particularly in the Orkney archipelago.

4.4.2.2 Data summary

Table 4.4.4, provides a summary of the raw survey data for harbour seals collected over the duration of the observations programme. It should be noted that many seal observations at the Fall of Warness are unclassified in terms of species. This analysis is solely based upon observations where the species is recorded as 'harbour seal' and, therefore, does not include the portion of unclassified seal observations that were likely harbour seals. These summary statistics have been presented for each of the site impact levels and include information on the number of harbour seal observations and typical group sizes.

Table 4.4.4. Summary of harbour seals raw data

	Total	Site Impact Level 0	Site Impact Level 1	Site Impact Level 2	Site Impact Level 3
Number of observations	973	272	573	42	86
Minimum (group size)	1	1	1	1	1
Maximum (group size)	23	10	23	5	5
Mean (group size)	1.49	1.47	1.56	1.24	1.23
(s.d)	(1.40)	(1.21)	(1.58)	(0.73)	(0.66)

4.4.2.3 Model overview

Once the final model had been selected, it was possible to derive GEE-based p-values for each of the remaining terms in the model. The model included seven terms which were deemed to be highly significant (p-value < 0.001) and two terms that were significant (p-value < 0.05). Table 4.4.5 provides an overview of each of the remaining terms in the final model and their associated p-values.

Table 4.4.5. GEE-based p-values for the terms in the final harbour seal model for the Fall of Warness

Model term	ρ-value
Wind direction	<0.0001
Precipitation	0.000369
Sea state	<0.0001
Year	<0.0001
Depth	<0.0001
Month	<0.0001
Site impact	0.032374
Spatial surface	<0.0001
Spatial surface / site impact	<0.0001

The selected model contained the wind direction as a term; however, there are no clear patterns in the relationship between wind direction and harbour seal density. Greatest abundances are estimated when there is no clear wind direction (this tends to be recorded when there is no wind and therefore this increase in density is likely to be associated with wind strength rather than wind direction) and lowest abundances are expected when the wind direction is recorded between west and north-west. In terms of precipitation, the model has estimated that greatest densities are likely when there is either no precipitation or showers and lowest densities are expected to occur when there is heavy precipitation. Although sea state has been included in the final model, the model has estimated that harbour seal densities remain very similar at various levels of sea state (measured on the Beaufort scale) with the exception that, at sea state 4, there is a clear reduction in harbour seal density.

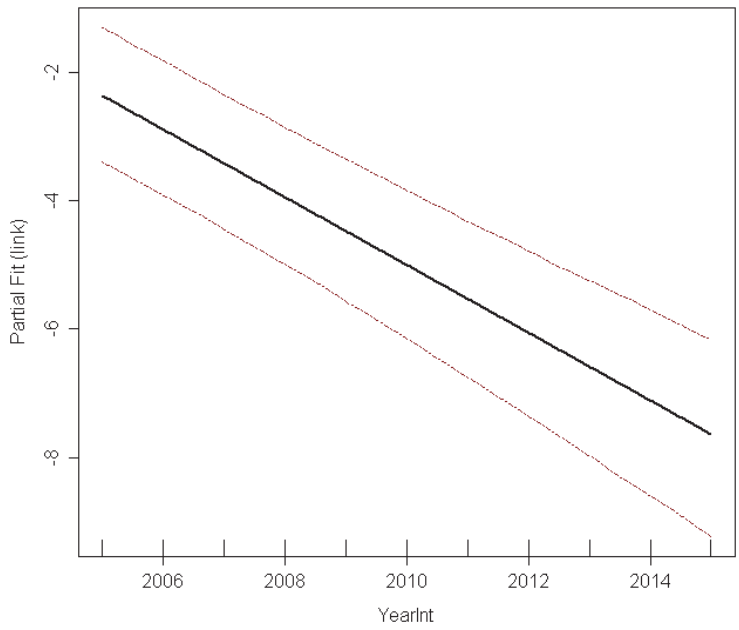

Figure 4.4.7. Estimated partial relationship of year against log(density) for harbour seal at the Fall of Warness. The red lines represent 95% confidence intervals about the estimated relationship and the tick marks show where the data lie in the covariate range.

The model has also estimated that, over the duration of the observations programme, there has been a decline in harbour seal densities. As seen in Figure 4.4.7, this decline has been modelled to occur at a constant rate. In terms of the predicted relationship between harbour seal density and depth, it is expected that harbour seal observations will reduce with increasing depth. When considering harbour seals' relationship with 'month', it appears that the species shows an increase in density from April to September. This finding is in line with Robbins (2011), who noted that harbour seals occur year round in the Fall of Warness with an increase in average encounter rate between May and October, even though, due to the moult, a proportion of the local population may be expected to be onshore, rather than in the water, during some of this time.

The final model also included a spatial surface (fitted using four knots) allowing spatial prediction surfaces to be created. The interaction term (site impact/spatial surface) was found to be highly significant and therefore was kept in the final model.

Like the other species models, various diagnostic tests have been undertaken on the harbour seal model to assess how well it accounted for uncertainty and whether it was appropriate for the data. The outputs from these tests are provided on the Marine Scotland Information portal. When the mean-variance relationship was investigated it was found that the model captured variance that exists in the data for lower fitted values well but for higher fitted values the model struggles to predict the variance accurately. In terms of the observed versus fitted values, it appears that the model captures the relationship accurately.

4.4.2.4 Density predictions and uncertainty estimation

As already mentioned, as the model contains a spatial surface, prediction surfaces have been produced which provide estimated densities across the survey area. Prediction surfaces for each site impact level are available (see Figure 4.4.8) as well as surfaces with each predictions' associated CV values (provided in Figure 4.4.9). CV values provide a measure of the relative variability in the predictions, with the smaller values indicating a more reliable estimate. In order to produce the prediction surfaces, the environmental conditions had to be specified and, therefore, the environment conditions within which the most harbour seal observations occurred were selected. This is discussed in more detail in Appendix 5.

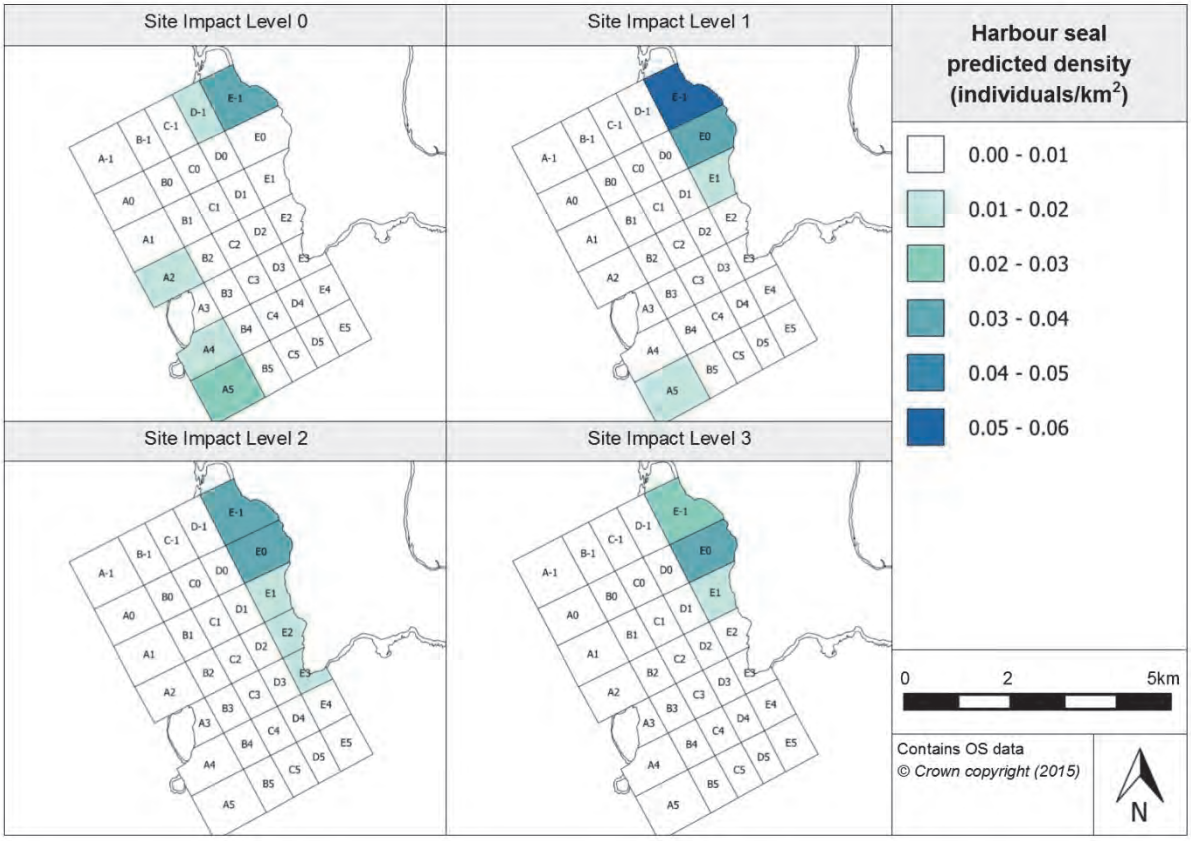

Figure 4.4.8. Estimated harbour seal density at each site impact level

The prediction surface for SIL-0 (baseline conditions) shows a peak in density in the grid cells to the north and south of Muckle Green Holm (although not in the grid cell adjacent to the offshore island) and another, more intense, peak in density in Seal Skerry and Seal Skerry Bay. This peak is abundance near to Seal Skerry is expected, since the rocky outcrop is a known haul-out site for harbour seals (and a designated haul-out site for the species).

At SIL-1 (when infrastructure is installed onsite), there is a very slight peak in abundance in the south-western corner of the survey site, in grid cell A5. There is a prominent cluster of high densities at Seal Skerry and Seal Skerry Bay. Grid cell E-1 is the grid cell where the highest density is expected to occur across all the site impact levels.

When considering the prediction surface for SIL-2 (when devices are installed but not operational), grid cells adjacent to the shoreline of Eday show greater abundance than the other grid cells. There are particularly heightened densities in grid cells E-1 and E0. This same peak in density in grid cells E-1 and E0 remains in the prediction surface for SIL-3 (devices onsite and operational). However, the same increase in density in grid cells E2 and E3 no longer appears.

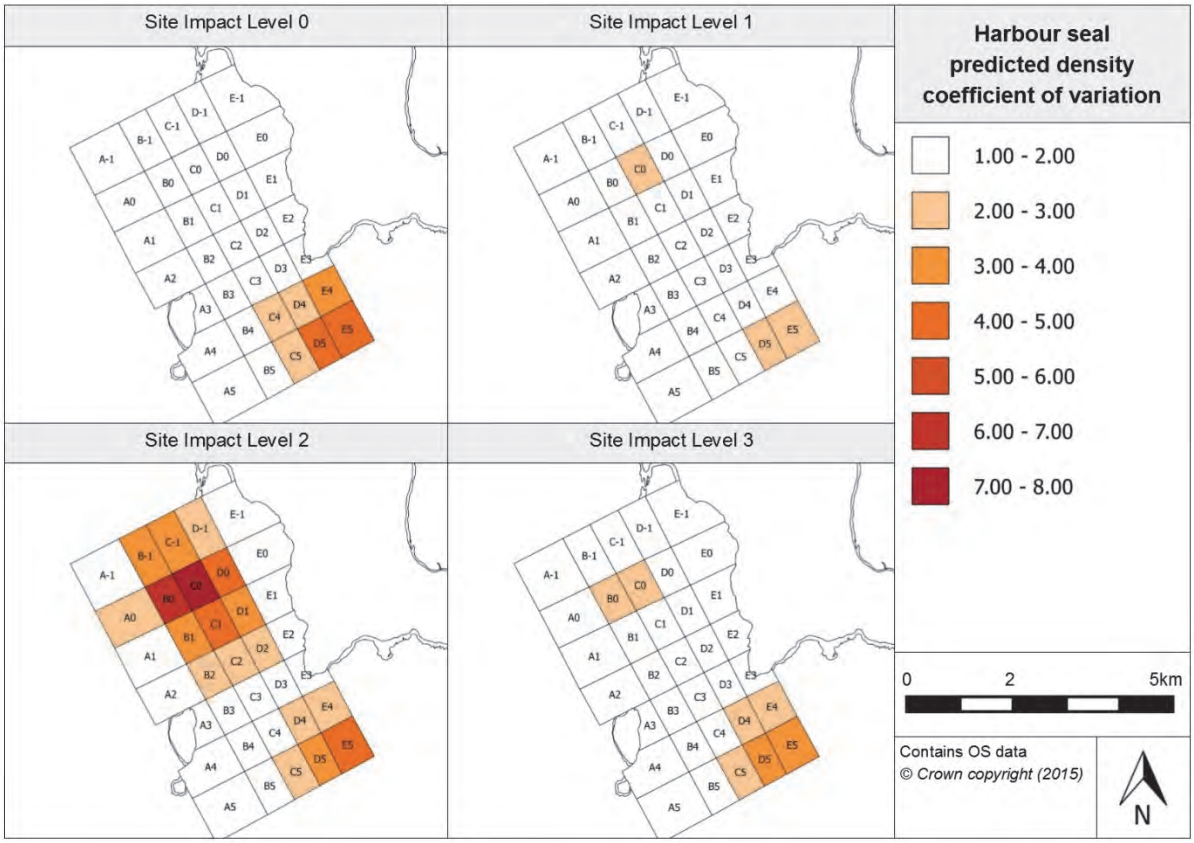

Figure 4.4.9. Associated coefficient of variation values for the density predictions for harbour seals

When looking at the CV values for SIL-0, there is a cluster of high CV values in the south-eastern corner of the site, suggesting that there is little evidence upon which to base predictions in this region of the survey area and/or low density predictions in this area of the grid. There are lower CV values in the other areas of the site including those where high densities were predicted. When comparing the CV values for the SIL-1 prediction surface, there is a slight increase in CV in the south-eastern corner of the site and at grid cell C0.

The CV values for SIL-2 prediction surface show that there continues to be high variability in the predictions in the south-eastern corner of the site. The grid cells surrounding cell C0 show a cluster of particularly high CV values. This suggests that there is high uncertainty behind the predictions made for this area of the site; this probably arises from low density predictions in this area of the site under SIL-2 conditions.

The CV surface for SIL-3 predictions is similar to that observed for SIL-1. There is a cluster of grid cells in the south-eastern corner of the site which have higher CV values recorded and grid cells around B0 and C0 have particularly high CV values, relating to the higher harbour seal densities estimated in this area of the survey grid.

Importantly, for each of the prediction surfaces at each site impact level, there appears to be fairly low uncertainty in the areas where a high density of harbour seals is expected.

4.4.2.5 Relative abundance estimations

Using the produced model, predictions could be made regarding the abundance of harbour seals for each of the survey months. This was only made possible by applying certain values for the environmental covariates. The same environmental covariates as used

previously have been applied to produce seasonal relative abundance predictions, see Table 4.4.6.

Table 4.4.6. Relative abundance for harbour seals during each season (associated confidence intervals are provided in brackets)

Year	Season			
	Winter (Dec, Jan, Feb)	Spring (Mar, Apr, May)	Summer (Jun, Jul, Aug)	Autumn (Sep, Oct, Nov)
2005	-	-	0.57 (0.27, 1.19)	0.24 (0.09, 0.61)
2006	0.55 (0.06, 1.37)	1.56 (0.50, 4.34)	3.26 (1.84, 6.06)	1.37 (0.48, 2.88)
2007	0.39 (0.12, 1.60)	0.47 (0.15, 1.41)	0.98 (0.53, 2.06)	0.37 (0.13, 1.06)
2008	0.12 (0.04, 0.42)	0.17 (0.05, 0.46)	0.35 (0.16, 0.67)	0.21 (0.06, 0.77)
2009	0.10 (0.04, 0.29)	0.18 (0.05, 0.56)	0.37 (0.19, 0.89)	0.16 (0.06, 0.37)
2010	0.08 (0.05, 0.16)	0.16 (0.05, 0.42)	0.32 (0.17, 0.61)	0.13 (0.05, 0.33)
2011	0.05 (0.02, 0.14)	0.09 (0.02, 0.32)	0.15 (0.07, 0.29)	0.06 (0.02, 0.17)
2012	0.02 (0.01, 0.07)	0.04 (0.01, 0.19)	0.10 (0.03, 0.29)	0.04 (0.01, 0.18)
2013	0.01 (0.00, 0.07)	0.02 (0.00, 0.09)	0.04 (0.01, 0.13)	0.02 (0.00, 0.07)
2014	0.02 (0.00, 0.07)	0.05 (0.01, 0.18)	0.11 (0.05, 0.27)	0.05 (0.02, 0.15)
2015	0.01 (0.00, 0.07)	0.00 (0.00, 0.00)	-	-

From the estimated seasonal abundances, it is clear that there is a peak in abundance observed in summer; consistently greater abundance is expected between June and August when compared to the other seasons. Greatest abundances were observed in 2006 and, by contrast, there was a well-defined dip in observations in 2013. Obviously, there were very few observations during 2015 upon which to base predictions, and therefore abundances have been estimated as very low.

Appendix 7 provides the estimated abundance values split into each of the site impact levels. Additionally, the predictions' associated CIs have also been provided. It is very clear from the figure that greatest abundances occurred in 2006 when the operational status of the site was SIL-1 (infrastructure installed).

Prediction surfaces for harbour seals have also been produced for typical surveying conditions in January and July. The surfaces and associated CV values are available in the Marine Scotland Information portal. The distribution across the prediction surfaces appears to be very similar but great differences in the density levels are observed between the two seasons, with July densities ten times greater than those recorded in January.

4.4.2.6 Spatially-explicit change

Figure 4.4.10 and Figure 4.4.11, illustrate spatially-explicit changes in the predictions of harbour seal abundance or distribution between each of the site impact levels. This is calculated by finding the density difference between model prediction surfaces for each of the site impact levels. The significance of the difference can be calculated using their associated 95% CIs. As 'year' was included in the final model, the spatially-explicit change surfaces were calculated for the least and most variable years (2013 and 2006, respectively).

The expected density difference between SIL-0 (baseline conditions) and SIL-1 (infrastructure onsite) appears to show a decrease in density across the majority of the site, with 17 grid cells displaying a significant decline. In the grid cells directly adjacent to the

island of Eday and in the south-eastern corner of the site, an increase in density is observed with the exception of grid cells E2 and E3 where there is a slight decrease in density. A significant increase in density appears in grid cells E0 and E1. Across all the conditions, it is between SIL-0 and SIL-1 where the largest increase in density, in these cells, is predicted. In 2013, an increase of 0.00251 individuals/km^2 is predicted and, in 2006, an increase of 0.177 individuals/km^2.

When considering the change in density between SIL-0 and SIL-2 (devices onsite but not operational), there is less of a decrease across the site than between SIL-0 and SIL-1 (infrastructure only installed) and only 11 grid cells are deemed to show a significant decrease in density. The increase in density in the south-eastern corner of the survey site has become more prominent, and now grid cells E4, E5 and D5 are deemed to show a significant increase in density. The grid cells along the shoreline of Eday continue to show an increase in density, with the exception of grid cell E-1. A significantly positive change remains in grid cells E0 and E1. The fact that there is a decrease in one area of the site and an increase in another suggests that there may be redistribution within the site related to the introduction of devices. If this is correct, this is a west to east redistribution, with a reduction in harbour seal densities in the grid cells further from the island of Eday and an increase in density in the grid cells close to Eday's shores.

In terms of the density difference between SIL-0 and SIL-3 (devices installed and operational), the reduction in density seen on the western side of the site appears to deepen. There are 19 grid cells where a significant decrease in density is expected with device presence onsite and operational when compared to baseline conditions. Fewer grid cells have an increase in density estimated, but grid cells E0 and E1 continue to be deemed to have a significant increase in density. There is no obvious correlation between those grid cells where test berths are located and the change in density of harbour seals in 2013 between baseline conditions and those predicted to occur when devices are installed and operating. Although all these grid cells show a reduction in density of less than 0.001 individuals/km^2, only some of these reductions are deemed significant.

When looking at the density changes between SIL-1 and SIL-2, there is a density increase in the grid cells in the centre of the site and towards its south-eastern corner. None of these grid cells are deemed to show a significant increase. In the grid cells along the site's western and northern edges, it is estimated that there will be a slight decrease in density although none of these grid cells show a significant decrease. Grid cell E-1 exhibits a greater decrease than the other grid cells but this is still not deemed to be significant.

Between SIL-1 and SIL-3, the majority of the grid cells show a slight decrease in density. There appears to be a cluster of grid cells in the site's south-western corner which have been deemed to have a significant decrease in density. Between the installation of infrastructure and devices becoming operational, the largest decrease expected across the site occurs in grid cell E-1, where there is an anticipated decrease of 0.00187 individuals/km^2 in 2013 and 0.129 individuals/km^2 in 2006. The grid cells in the northern centre of the site and those cells directly below the observation vantage point show a slight increase in density; however, this change is not deemed to be significant.

Between SIL-2 and SIL-3 (devices becoming operational), it appears that the majority of the site has an estimated decrease in abundance. Four grid cells show a significant decrease in density, three towards the site's southern end and one adjacent to the peninsula to the south of the observation vantage point. In the northern centre of the site and towards the Eday shoreline, there appears to be a slight increase in abundance with the exception of grid cell E-1 where a decrease in abundance is still evident.

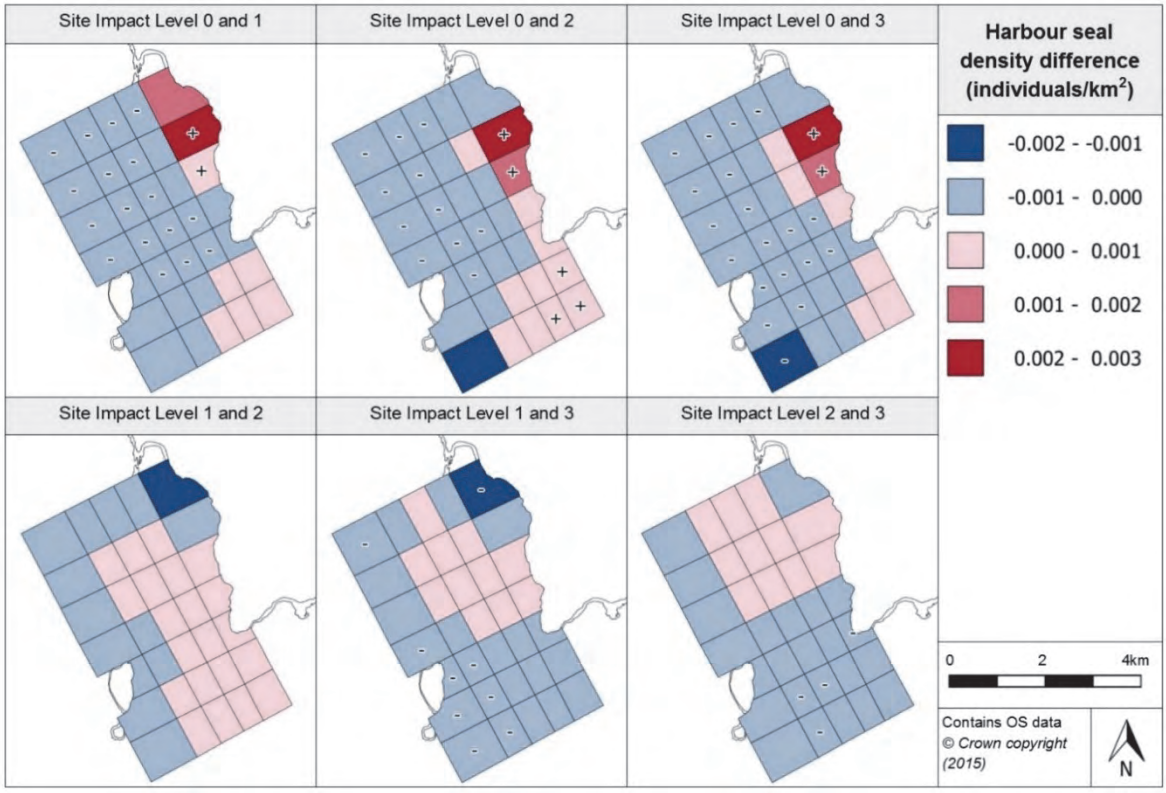

Figure 4.4.10. Estimated density difference between various site impact levels for harbour seals during 2013 (year with least variation)

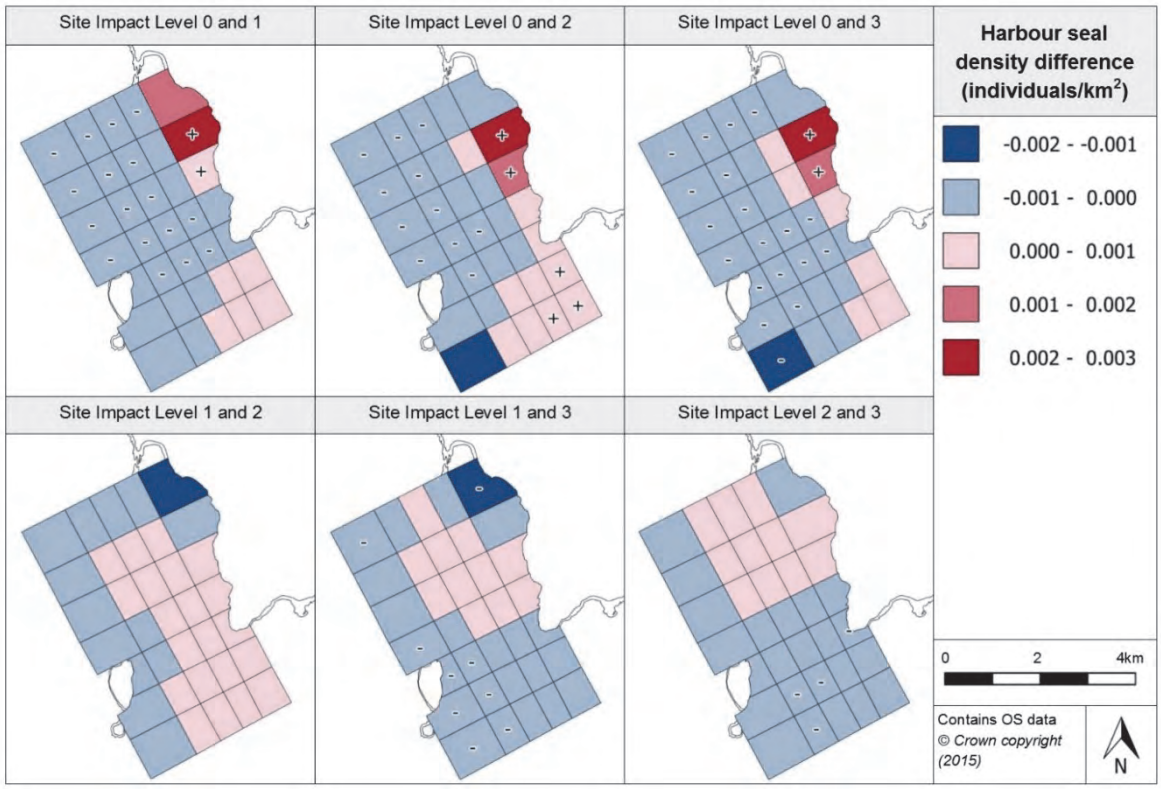

Figure 4.4.11. Estimated density difference between various site impact levels for harbour seals during 2006 (year with most variation)

4.4.2.7 Density change with distance from potential impact location

The spatially-explicit change projections have been used to demonstrate how the estimated density difference between site impact levels changes with increasing distance from a potential impact location. Figure 4.4.12 shows how the difference in densities change with increasing distance from one test berth at the Fall of Warness.

When inspecting the plots for the density change between baseline conditions and site impact levels 1, 2 and 3, it appears that there is a consistent decrease in density expected up to 0.9km from the impact location. Between 0.9km and 1.4km, a negative change in density from baseline conditions is expected to continue but the widening CIs mean that this is not necessarily always true and that a positive change could also occur. Beyond 1.4km, the density levels at this distance from the impact locations are likely to be higher than baseline conditions. However, due to the CIs including negative values, this may not necessarily always be true.

When considering the change in density between SIL-1 and SIL-2 and between SIL-1 and SIL-3, there appears to be little change from predictions when only infrastructure is installed.

When considering the density difference between SIL-2 and SIL-3 with increasing distance from a potential impact location, it appears that there is very little difference between the density predictions for the two impact levels and minimal difference with increasing distance.

The plots of density change (Figure 4.4.12) show very little variation with distance away from the impact location suggesting that seal abundance is not influenced by the location of a test berth.

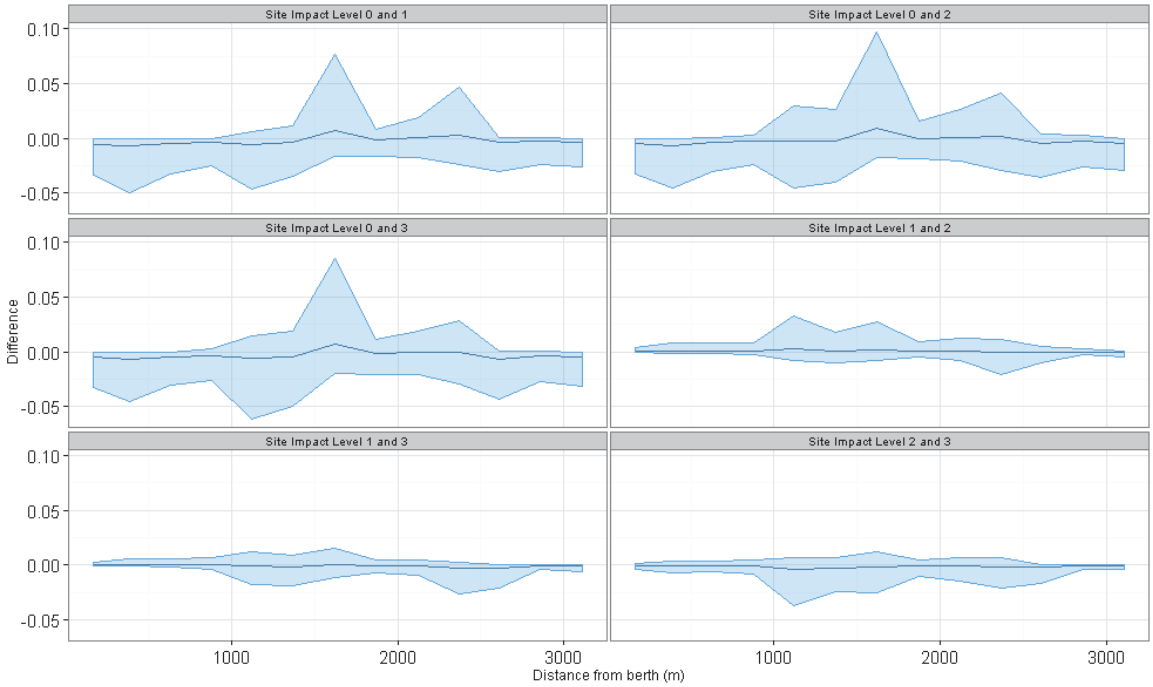

Figure 4.4.12. Density change between site impact levels with increasing distance from a potential impact location, with associated confidence intervals, for harbour seals at the Fall of Warness

4.4.2.8 Discussion

The harbour seal model incorporates nine significant terms. This implies that the presence of harbour seals is controlled by a large number of environmental, temporal and spatial factors, which need to be considered when assessing the impact of MECS. The model predicts a steady decline in densities over the duration of the survey. It also shows that harbour seals exhibit a similar distribution to the wider seal group, except that they tend to be concentrated along the coastline of Eday and only occasionally near Muckle Green Holm. Harbour seal abundance tends to increase adjacent to Eday and decline at Muckle Green Holm, with the progression through site impact levels. There is generally good precision in these predictions, except in areas of lowest density which are usually the furthest from the coastline.

The grid cells where test berths are located are areas of low abundance and all show small but statistically significant reductions in density with the installation of infrastructure. However, these cells variously show increases and decreases in estimated density with progression through the site impact levels but none of these changes are statistically significant. The plots of density change indicate very little variation with distance away from the impact location, suggesting that seal abundance is not influenced by the location of a test berth.

4.4.3 Cetaceans

4.4.3.1 Species overview

All species of cetacean are listed in Annex II of CITES, Annex II of the Bern Convention, and Annex IV of the EC Habitats Directive as species of European Community interest and in need of strict protection. Those species listed in Annex IV are termed European Protected Species (EPS). The harbour porpoise (*Phocoena phocoena*) is also covered by the terms of ASCOBANS (Agreement on the Conservation of Small Cetaceans of the Baltic and North Seas).

The most frequently occurring cetacean species observed in Orkney waters are: harbour porpoise, killer whale (*Orcinus orca*), minke whale (*Balaenoptera acutorostrata*), Risso's dolphin (*Grampus griseus)*, white-beaked dolphin (*Lagenorhynchus albirostris*) and bottlenose dolphin (*Tursiops truncatus*) (Evans *et al*., 2011). Cetacean species which are much rarer in Orkney waters are: Atlantic white-sided dolphin (*Lagenorhynchus acutus*), short-beaked common dolphin (*Delphinus delphis*), sperm whale (*Physeter macrocephalus*) and long-finned pilot whale (*Globicephala melas*) (Evans *et al*., 2011). All of the above species have been sighted at the Fall of Warness over the duration of the observations programme. In addition to the above species, a humpback whale (*Megaptera novaeangliae*) has been observed once by the observers as well as observations not specified to species level e.g. pilot whale (*Globicephala* spp) and common dolphin (*Delphinus* spp).

The following provides a brief description of the cetacean species regularly sighted at the Fall of Warness. However, further information on the other species that have been sighted can be found in Evans *et al*. (2011) and Reid *et al*. (2003).

The harbour porpoise is the only porpoise species seen in Scotland, 90% of the global population being found in UK waters. Orkney's waters are clearly important for the species with concentrations found in Scapa Flow and the Stronsay Firth (Evans *et al*., 2011). Although the species is present in UK waters throughout the year, peak numbers are recorded in summer months, with Evans *et al*. (2011) suggesting that, in northern Scotland, greatest numbers are observed between July and September (particularly in August). In terms of diet, porpoises mostly consume small fish (typically juvenile herring, cod and whiting as well as sandeel and flatfish), with evidence showing the majority of the diet is

made up of whiting and sandeel (Santos *et al*., 2004). Evans *et al*. (2008) suggest that breeding occurs between April and August, with June being the most popular month.

The killer whale is relatively common in Orkney waters and the Pentland Firth. The most common areas for sighting the species are Dunnet Head and Duncansby Head (Evans *et al*., 2011). Although the species is found year round in UK waters, the majority of sightings occur between May and July (Bolt *et al*., 2009). Foote *et al*. (2009; 2010) suggest that sightings off Orkney comprise a population of around 30 individuals which are known to follow the Icelandic summer-spawning herring. However, typical group sizes (known as pods) are between one and ten individuals. The breeding season for killer whales tends to occur between October and March (but particularly during the autumn months) (Boran *et al*., 2008). Killer whales spend more time offshore during the winter months due to the mackerel and herring fisheries (Evans *et al*., 2003; 2011; Luque *et al*., 2006), whereas during summer months, the whales tend to spend more time in coastal waters, feeding on harbour seals, harbour porpoises, otters and common eiders (Evans *et al*., 2003; Bolt *et al*., 2009).

Evidence has shown that minke whale numbers have been increasing since the 1980s in the north and west of Scotland (Hammond, 2008; Anderwald *et al*., 2008). Minke whales have a wide distribution in northern Scotland, occurring both offshore and around the coastline. Particular locations around Orkney include western Hoy, the western mainland of Orkney, around the coastline of Copinsay, and around the island of Stroma (Evans *et al*., 2011). Minke whales tend to be spotted off Orkney only between January and October, the greatest number of observations usually occurring between June and August (Anderwald & Evans, 2007). It has been suggested that the species perform a general migration to more offshore waters which may be associated with their breeding schedule; however, little is known regarding their breeding or typical breeding locations (Anderwald *et al*., 2008). Feeding tends to occur in areas of upwelling or strong currents during the summer whereas during winter, minke whales have been associated with flocks of northern gannets, kittiwakes and *Larus* gulls. Prey species typically include sandeel, sprat, herring and mackerel (Pierce *et al*., 2004).

The major population of Risso's dolphins in the UK occurs around the Hebrides; however, the species is also regularly observed in the Northern Isles. The dolphins tend to be recorded year round, with greatest numbers being observed between May and September (particularly June-August) (Evans *et al*., 2011). The Orkney region is believed to be used for feeding and possibly for breeding. Calves are usually born between early spring and summer and have been sighted within groups around Orkney (Evans *et al*., 2008). Their diet is expected to comprise mainly cephalopods (e.g. octopus and small squid) (Santos *et al*., 1994); however, they have also been recorded taking fish (Evans *et al*., 2011).

The white-beaked dolphin's distribution is focused around the central and northern North Sea, extending towards the north and north-west of Scotland (Reid *et al*., 2003). The species are found both offshore and in coastal waters but particular concentrations have been recorded at Strathy Bay, Thurso Bay and Duncansby Head (Evans *et al*., 2011). In northern Scotland, the species has been sighted in nearly every month of the year, but particularly large numbers of cetaceans tend to be seen between June and October. It is believed that the Orkney region is used for both feeding and breeding (Evans *et al*., 2011). Typical prey species include haddock, whiting, cod, mackerel, etc. but squid, octopus and crustaceans have been recorded too (Canning *et al*., 2008).

The bottlenose dolphin has been recorded all around the coast of northern Scotland; however, the species tends to occur in concentrations and many of the individuals observed down the eastern side of the UK stem from the large population which inhabits the Moray Firth (Thompson *et al*., 2009). The greatest number of sightings in Orkney tends to occur around May and June but there is a general increase in group size observed between May

and September (Evans *et al*., 2011). No clearly defined breeding season has been identified but the number of births tends to peak between May and October (Pesante *et al*., 2008). The bottlenose dolphin's prey tend to comprise both benthic and mid-water fish (e.g. flounder, cod, salmon and herring) but they have also been recorded consuming marine invertebrates (such as cephalopods and shellfish)(Santos *et al*., 2001; Wilson, 2008).

4.4.3.2 Data summary

Cetaceans are rarely spotted at the Fall of Warness but the following table, Table 4.4.7, provides a summary of the raw survey data. This information has been split into each of the site impact levels and includes data on the number of observations and typical group sizes.

Table 4.4.7. Summary of cetaceans raw data

	Total	Site Impact Level 0	Site Impact Level 1	Site Impact Level 2	Site Impact Level 3
Number of observations	403	70	222	24	87
Minimum (group size)	1	1	1	1	1
Maximum (group size)	55	7	55	8	30
Mean (group size) (s.d)	2.72 (3.40)	2.74 (1.89)	2.59 (3.81)	2.71 (2.27)	3.02 (3.51)

4.4.3.3 Model overview

Once the modelling was complete, it was possible to produce GEE-based p-values for each of the remaining terms in the model. The final model contained eight terms, four of which were highly significant. Table 4.4.8 below provides an overview of the remaining terms and their associated p-values.

Table 4.4.8. GEE-based p-values for the terms in the final cetacean model for the Fall of Warness

Model term	ρ-value
Wind strength	<0.0001
Cloud cover	0.001714
Sea state	0.000857
Month	<0.0001
Depth	0.011231
Site impact	<0.0001
Spatial surface	<0.0001
Spatial surface / site impact	0.05791

Wind strength is included within the final cetacean model. It is estimated that, with increasing wind strength, the density of cetaceans decreases. Figure 4.4.13 shows how the lowest cetacean densities are expected at wind strength 4 and above (measured on the Beaufort scale). The final model includes cloud cover as a term; however, the predicted relationship between cetacean density and cloud cover has no clear pattern. Highest densities of cetaceans are expected when there is full cloud cover (8 oktas) and nearly full cloud cover (6-7 oktas). Similarly, sea state has been included in the final model, but it is difficult to determine any patterns in the relationship between cetacean density and sea

state. It appears that lowest densities are expected when the sea state (measured on the Beaufort scale) is between 1 and 3 and highest densities are seen at sea state 0 and 4.

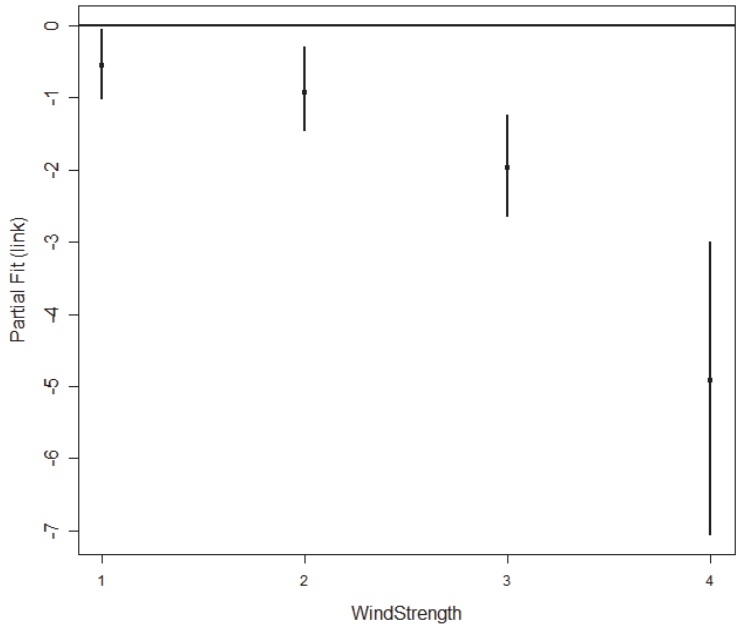

Figure 4.4.13. Estimated partial relationship of cetacean density (on the scale of the log link) with wind strength at the Fall of Warness. The points are the parameters for the estimated change in log density from the baseline (wind strength = 0) and the vertical lines represent 95% confidence intervals about the parameter estimates.

'Month' has been included in the final model; the model has estimated that the greatest cetacean abundances occur between June and September and lowest abundances between November and February. As expected, for the depth term, the model has estimated that, with increasing depth, there is an increase in cetacean abundance.

The final model included a spatial surface with four knots fitted. The relationship between the interaction term (site impact/spatial surface) and the response term (species abundance) was found to be statistically significant and, therefore, the interaction term was included in the final model.

Various diagnostic tests were undertaken on the cetacean model in order to assess how well the model accounted for uncertainty and whether it was appropriate for the data. Firstly, the mean-variance relationship was investigated; this appears to be well captured by the model. As expected due to the very few numbers of cetaceans observed, the model would be limited to producing low density predictions. All diagnostic plots are also available in the Marine Scotland Information portal.

4.4.3.4 Density predictions and uncertainty estimation

As a spatial surface remained in the fitted model, it was possible to produce density prediction surfaces. To do this, values for the environmental covariates had to be set; as with the other species, it was decided that conditions where the optimum number of observations were made would be the most appropriate (provided in Appendix 5). Prediction surfaces have been created for each of the site impact levels and the associated CV value for each prediction has also been plotted for the prediction surfaces, see Figure 4.4.14 and Figure 4.4.15 respectively.

The SIL-0 prediction surface (baseline conditions) estimates higher densities in the northern half of the site, particularly in grid cells D1 and D2. Around these two grid cells, density reduces steadily with distance. Additionally, high densities are also observed in grid cells A-1-A1 in the north-western corner of the site. Cell E-1, situated near to Seal Skerry, also has a density higher than the majority of grid cells.

The prediction surface for SIL-1 (infrastructure installed) estimates there to be higher densities in the most northern grid cells. The greatest densities across all four prediction surfaces occur between grid cells A-1 and E-1, with grid cell C-1 showing the highest density. Across the rest of the prediction surface, there are no areas marked as having density predictions greater than 0.015 individuals/km^2.

For the SIL-2 (devices installed but not operational) prediction surface, it appears that there are no grid cells across the surface where the density is estimated to be higher than 0.015 individuals/km^2. Similarly, the SIL-3 prediction surface (devices installed and operational) estimates that all the grid cells have a density of lower the 0.015 individuals/km^2 with the exception of grid cell C-1.

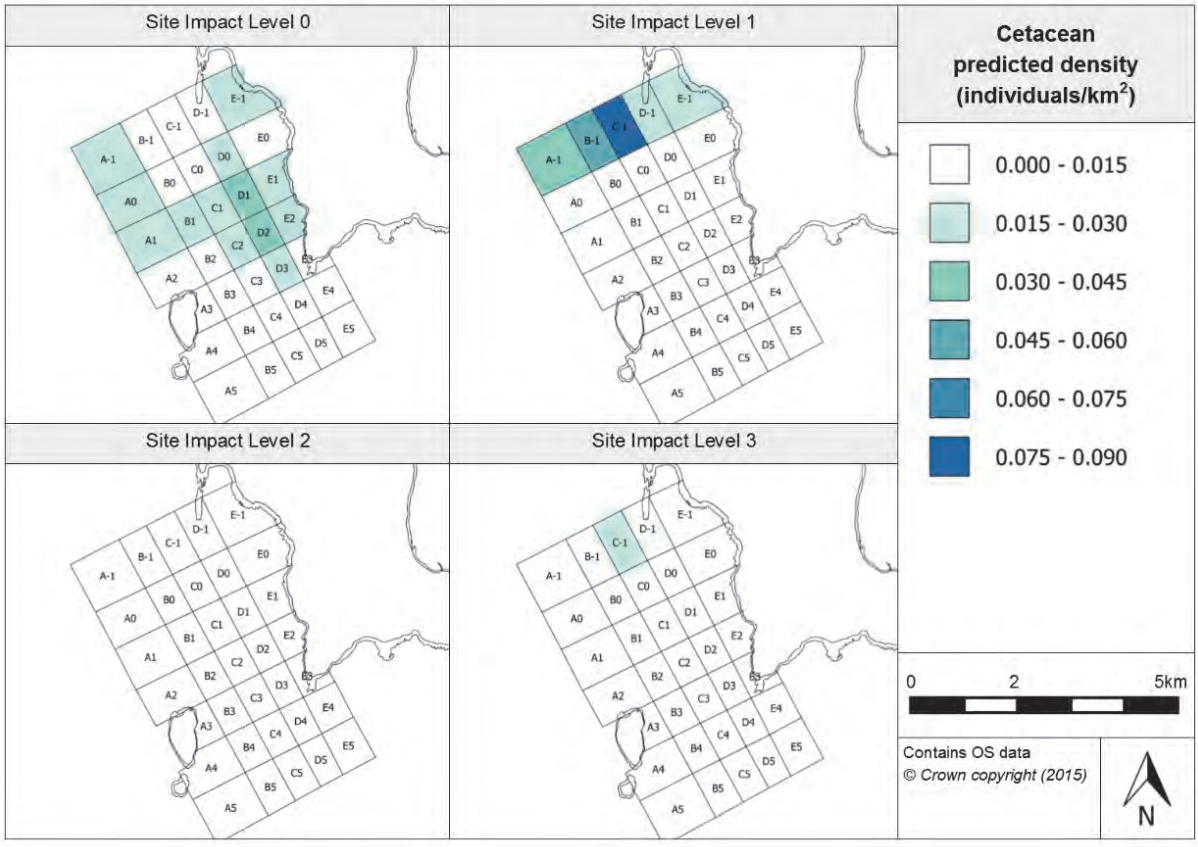

Figure 4.4.14. Estimated cetacean density at each site impact level

In terms of the surfaces with CV values, it appears that there is greatest precision in the predictions under SIL-0 conditions, with all CV values lower than 4 (Figure 4.4.15). This would suggest that there are a reasonable number of observations at this site impact level. The CV values for SIL-1 again indicate fairly low uncertainty in the results, with only grid cell C-1 showing a CV value greater than 4. Notably, it is at this site impact level and in this grid cell, that the greatest density of cetaceans is estimated. This result suggests that there may be a sighting of a pod of cetaceans large enough to elevate this predicted density, and the consequential higher CV value is a result of a large disparity in raw observations.

The CV values for the SIL-2 prediction surface show higher uncertainty in the predictions for grid cells C-1-C0 and B0-B1. The high CV values may be due to minimal observations in these four grid cells at this site impact level. In the south-eastern corner of the survey grid, there are five grid cells where high to very high CV values are found, particularly in grid cell E5. This will be due to few or no raw observations in these grid cells when the site was deemed to be operating under these conditions, resulting in a very low predicted density estimate.

Similarly, the CV values for SIL-3 show the same very high CV values in the south-eastern corner of the site. This is likely due to low density predictions in this corner of the site when the operational status was classed at SIL-3.

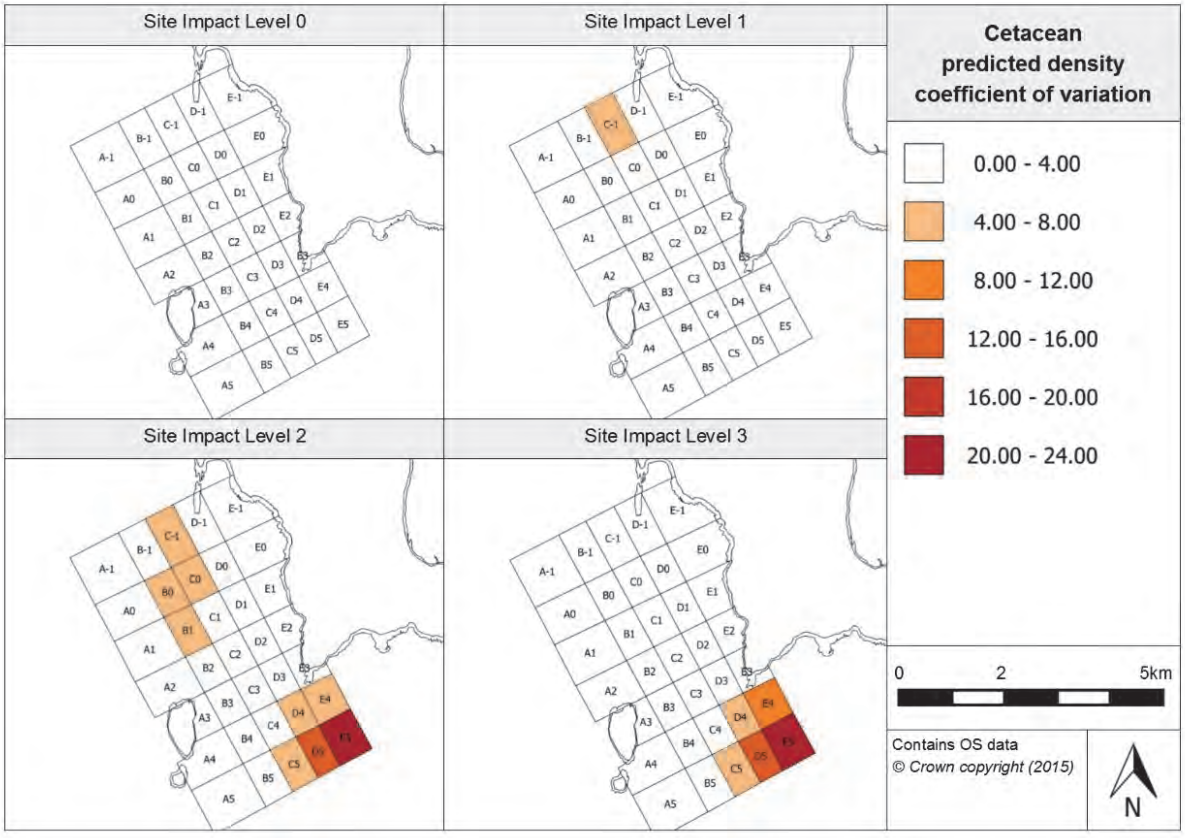

Figure 4.4.15. Associated coefficient of variation values for the density predictions for cetaceans

4.4.3.5 Relative abundance estimations

Using the fitted cetacean model, abundance predictions were able to be produced for each survey month. To be able to produce such predictions, the environmental covariates again had to be set at certain values, the same ones as previously used. By combining the survey month predictions, it was possible to produce seasonal abundance estimates; these can be seen in Table 4.4.9. It is worth noting that these abundance estimates are only relative abundance as only surface visible observations have been recorded.

Table 4.4.9. Relative abundance for cetaceans during each season (associated confidence intervals are provided in brackets)

Year	Season			
	Winter (Dec, Jan, Feb)	Spring (Mar, Apr, May)	Summer (Jun, Jul, Aug)	Autumn (Sep, Oct, Nov)
2005	-	-	1.62 (0.65, 3.70)	0.87 (0.24, 2.53)
2006	0.20 (0.10, 0.57)	0.41 (0.14, 1.78)	1.13 (0.34, 4.32)	0.54 (0.06, 2.87)
2007	0.06 (0.04, 0.14)	0.12 (0.05, 0.40)	0.33 (0.14, 1.00)	0.26 (0.11, 0.68)
2008	0.11 (0.07, 0.22)	0.24 (0.09, 0.60)	0.65 (0.28, 1.29)	0.87 (0.24, 2.53)
2009	0.28 (0.16, 0.58)	0.59 (0.23, 1.44)	1.42 (0.65, 4.32)	0.61 (0.15, 2.87)
2010	0.20 (0.10, 0.57)	0.41 (0.14, 1.78)	0.50 (0.24, 2.53)	0.18 (0.06, 0.68)
2011	0.06 (0.04, 0.14)	0.12 (0.05, 0.40)	0.65 (0.28, 1.29)	0.35 (0.11, 0.88)
2012	0.11 (0.07, 0.22)	0.40 (0.09, 1.44)	1.62 (0.65, 3.70)	0.87 (0.24, 2.53)
2013	0.28 (0.16, 0.58)	0.45 (0.20, 1.78)	1.13 (0.34, 4.32)	0.61 (0.15, 2.87)
2014	0.20 (0.10, 0.57)	0.12 (0.05, 0.40)	0.33 (0.14, 1.00)	0.18 (0.06, 0.68)
2015	0.08 (0.04, 0.22)	0.24 (0.09, 0.60)	-	-

From Table 4.4.9, it is estimated that the highest abundances always occur during the summer months and lowest abundances tend to be during winter months. However, there appears to be large interannual variation. For instance, in 2007 and 2011, there are clearly lower abundances estimated than for other years, e.g. 2005, 2009 and 2012 where much greater abundances tend to be expected. It is therefore surprising that 'year' as a term is not included in the final fitted model, although this may be due to the peaks and troughs not necessarily always being year-long and therefore not evident in every season. In addition to the above, Appendix 7 provides relative abundance estimates across the years for each of the site impact levels. To illustrate the extent of uncertainty behind some of the predictions, the associated upper and lower CIs for the predictions have also been provided.

Similar to the other species modelled at the Fall of Warness, prediction surfaces for cetaceans have also been produced for typical surveying conditions in January and July. Both the surfaces and their associated CV values are available in the Marine Scotland Information portal. The distribution of the peaks and troughs in density across the prediction surfaces looks very similar between January and July; however, July's density estimates appear to be about 15 times greater than those for January.

4.4.3.6 Spatially-explicit change

To understand whether there is any evidence for spatially-explicit change, the density difference between model prediction surfaces for each site impact level is calculated. Figure 4.4.16 provides the density difference surface for cetaceans. The significance of any differences has been calculated using their associated 95% CIs.

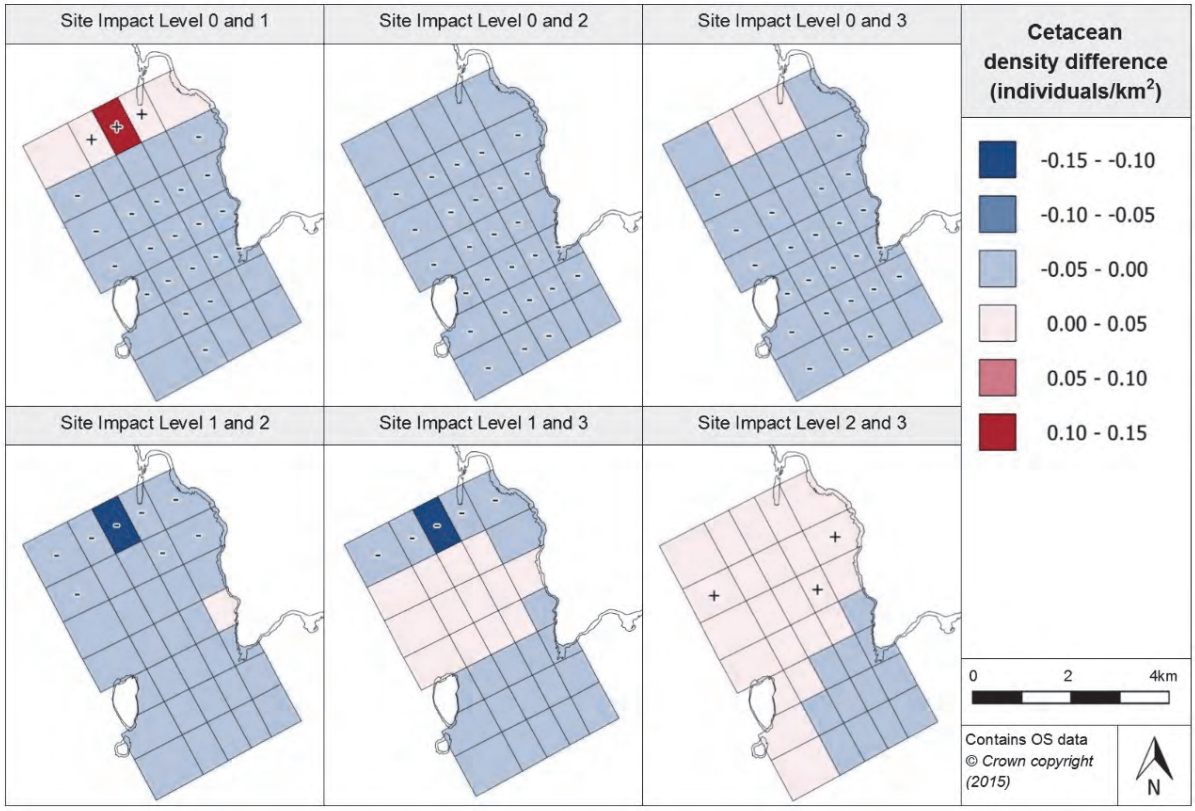

Figure 4.4.16. Estimated density difference between various site impact levels for cetaceans

When considering the change in density between SI0 (baseline conditions) and SIL-1 (when infrastructure is installed), it appears that a decrease in density is evident across the majority of the site with a total of 20 grid cells marked as showing a significant decrease in density. In terms of the distribution of these significant decreases, it appears that they are situated across the centre rows of the site as well as most of the cells adjacent to Eday. The grid cells in the most northern row A-1–E-1 show an increase in density, with three cells marked as the change being significant. Grid cell C-1 is marked as having the largest increase in density across all the differences in site impact levels, with an increase of 0.69 individuals/km^2 anticipated.

Between SIL-0 and SIL-2 (when devices are installed but not operational), it is estimated that there will be a decrease in density in every grid cell across the survey grid. The majority of the grid cells are also marked as having a significant density decrease, with a total of 27 grid cells out of 35 showing a significant decrease in density. None of the cells in the most northern row of the survey grid, nor those in the south-eastern corner, are expected to have a significant decline in density.

The extent of the decline in density seen between SIL-0 and SIL-2 is not apparent between SIL-0 and SIL-3 (when devices become operational), as three grid cells in the most northern row of the survey grid show a slight increase in density, although none of the changes in these cells is deemed significant. In terms of the rest of the survey grid, all the other grid cells are anticipated to have a negative change in density, with 24 marked as experiencing a significant decline in density. These surfaces suggest that, with the presence and operation of devices, it is expected that cetacean density across the site will reduce, except for the extreme north of the site where there may be a slight increase in density.

When considering the change in density between SIL-1 and SIL-2 (when devices are installed but not operational), it has been estimated again that a reduction in density will be observed in all grid cells, with the exception of grid cell E2 where a slight increase in density is estimated. However, fewer grid cells (only eight) are marked as having a significant reduction in density. Interestingly, all the grid cells that are marked as having a significant reduction are within the two northernmost rows of the survey grid, with grid cell C-1 showing a striking reduction in comparison to the surrounding grid cells.

Between SIL-1 and SIL-3 (when devices become operational), cells situated in the north of the centre of the site are expected to see a slight increase in density, with a total of 13 grid cells showing this increase. All other grid cells are expected to have a slight reduction in density with the exception of grid cell C-1 where again a marked decrease is indicated. Again, the most northern row of grid cells is marked as having a significant decrease in density. The southern area of the site is estimated to have a slight decrease in density but none of the changes in these cells has been deemed significant.

When looking at the density difference between SIL-2 and SIL-3, it appears that there is a slight increase in density in the majority of the grid cells, except in the south-eastern quarter of the site where 12 grid cells are marked as having a slight decrease in density. However, in none of the cells where a decrease in density is expected is the change marked as significant. When considering the area estimated to have an increase in density, only three grid cells are marked as showing a significant change. The pattern of change within the site suggests that there is a redistribution within the site from the south-eastern corner to the north; however, due to the large range of the cetaceans within this site, redistribution is unlikely.

4.4.3.7 Density change with distance from potential impact location

Using the spatially-explicit change projections, it has been possible to produce plots showing how the change (between site impact levels) varies with increasing distance from a grid cell containing a test berth (a potential impact location). These plots have been created for each grid cell containing a test berth but only two are presented here, Figure 4.4.17 and Figure 4.4.18; the other plots can be found in the Marine Scotland Information portal.

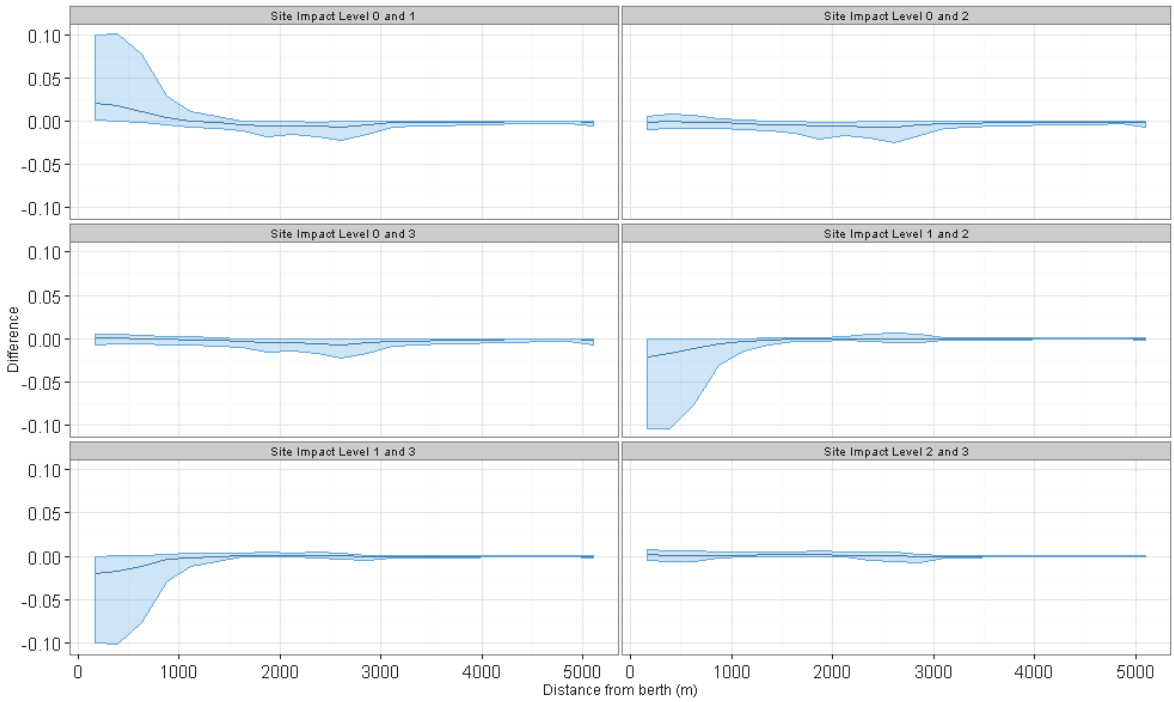

Figure 4.4.17. Density change between site impact levels with increasing distance from a potential impact location, with associated confidence intervals, for cetaceans at the Fall of Warness

When inspecting the plot for the difference between SIL-0 and SIL-1, it is clear that, at the test berth location, there is a large increase in density with the introduction of infrastructure which slowly reduces in extent with increasing distance from the test berth location. The increase in density is evident up to 1km away from the potential impact location although the lower CI is negative from beyond 500m. When the density change with the introduction of devices onsite is considered, it appears that there is little change in density from baseline conditions directly at the grid cell (containing the test berth) and there is no change with increasing distance from the potential impact location. This is the same when looking at the density change between SIL-0 and SIL-3. There is very little change at the potential impact location from baseline conditions, and the change stays minimal with increasing distance from the impact location.

However, when the change in density between SIL-1 and SIL-2 is investigated, there is a clear reduction in density levels directly at the grid cell with the presence of devices as compared to only infrastructure being onsite; this slowly recovers to SIL-1 density levels at approximately 1.5km from the grid cell. Beyond 1.5km, there is very little change in the density levels. Similarly, when investigating density difference between SIL-1 and SIL-3, there is again a distinct reduction in density which recovers to SIL-1 levels at about 1.5km from the potential impact location. Again, there is very little change in density levels beyond 1.5km. Between devices being onsite and them becoming operational, it appears that there is little density change at the potential impact location or with increasing distance from the grid cell.

Figure 4.4.17 would suggest that there are large changes in density with changes in device operational status which are more profound with proximity to the potential impact location. This is the only grid cell where a corresponding large change in density is seen with proximity to the impact location and all the other grid cells plots show peaks or troughs in density at random distances from the potential impact location, as seen in Figure 4.4.18.

This would suggest that either the impact is associated with only the type of device being tested at the test berth located in the grid cell shown in Figure 4.4.17, or it is just a coincidence that the test berth occurs where a peak in density exists within the prediction surface; the latter is more likely to be the correct assumption. Similarly, the larger density changes (increases and decreases) at approximately 2.2km from a different potential impact location, as displayed in Figure 4.4.18, probably also reflect a single anomalous observation (e.g. an unusually large pod of cetaceans) as all these large changes are expected at SIL-1. Examining the changes in density over the wider SIL-0 to SIL-3 change in site impact level, i.e. the difference between baseline conditions and when devices are installed and operational, shows very little difference in cetacean density (Figure 4.4.18).

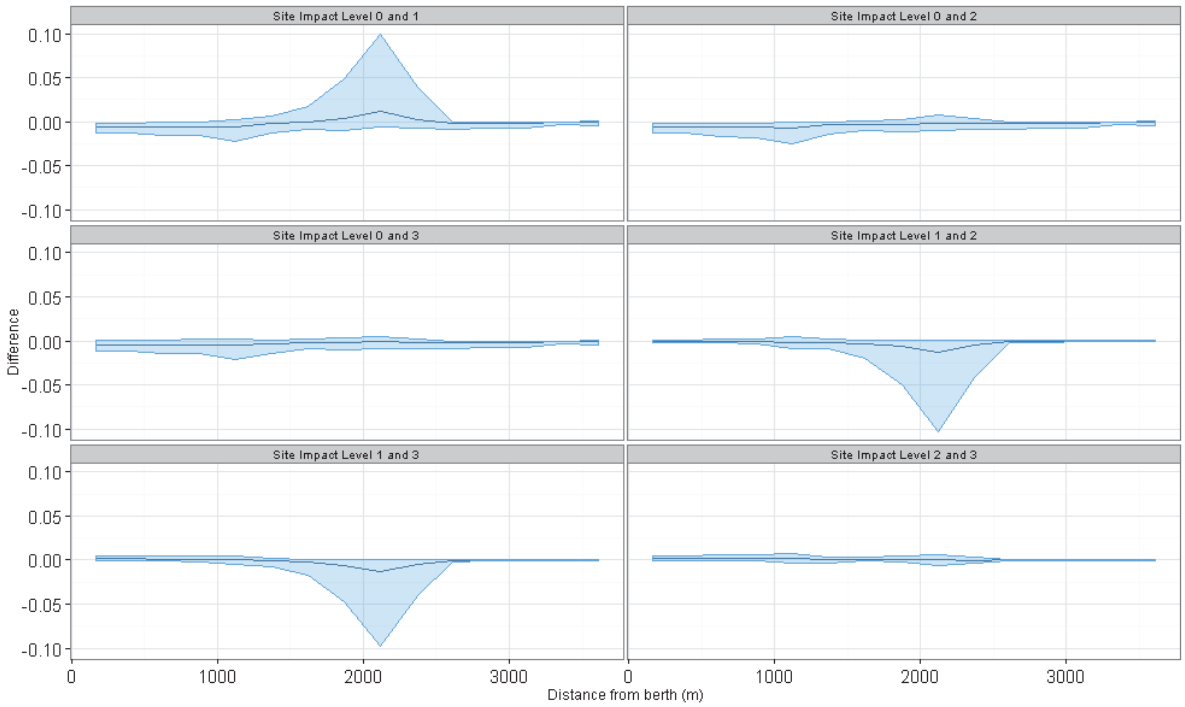

Figure 4.4.18. Density change between site impact levels with increasing distance from another potential impact location, with associated confidence intervals, for cetaceans at the Fall of Warness

Examining the assessment of density changes with increasing distance from a potential impact site, as given in Figure 4.4.17 and for an alternative potential impact site (Figure 4.4.18), suggests that, when devices are installed and operational (SIL-3), there is very little difference in cetacean behaviour from that under baseline conditions (SIL-0).

4.4.3.8 Discussion

Observation numbers of cetaceans are lower than for other species/groups analysed and, therefore, CVs are very large (implying higher uncertainty). The model includes only four terms as highly significant. Higher densities are restricted to the northern half of the survey grid and there is little consistency in location between different site impact levels. Assessing the changes in density at and away from impact locations is inherently flawed, due to the effect of single anomalous observations greatly influencing analyses and producing wide CIs. In other words, modelling the distribution of marine mammals is difficult as the observations will include occasional large groups (pods) transiting through the site which can create anomalous local high densities.

4.5 Billia Croo marine birds

4.5.1 Common guillemot (Uria aalge)

4.5.1.1 Species overview

Similar to the Fall of Warness, the common guillemot (*Uria aalge*) is a frequent visitor to Billia Croo. This species, together with the black guillemot and Atlantic puffin, have been modelled separately in addition to a model including all of the auk family species that have been sighted at the site. This section discusses the fitted common guillemot model. Information regarding the general distribution and behaviour of common guillemots is outlined in Section 4.3.2.1 above.

4.5.1.2 Data summary

Common guillemots are one of the most common species from the auk family found at Billia Croo. Table 4.5.1 below provides a summary of the raw survey data from the site including the number of observations and typical number of birds seen together. This information has also been split into each site impact level, in order to provide an understanding of the extent of data used when developing the common guillemot model.

Table 4.5.1. Summary of common guillemot raw data for Billia Croo

	Total	Site Impact Level 0	Site Impact Level 1	Site Impact Level 2	Site Impact Level 3
Number of observations	9644	1229	600	2547	5268
Minimum (group size)	1	1	1	1	1
Maximum (group size)	338	91	134	338	200
Mean (group size)	2.62	3.30	3.52	2.22	2.55
(s.d)	(7.15)	(5.38)	(9.12)	(8.02)	(6.79)

4.5.1.3 Model overview

Once the model selection process was completed, the GEE-based p-values for each of the terms that remained in the fitted model were recorded (Table 4.5.2).

Table 4.5.2. GEE-based p-values for the terms in the final common guillemot model for Billia Croo

Model term	ρ-value
Distance to land	<0.0001
Month	<0.0001
Site impact	0.10703
Spatial surface	<0.0001
Spatial surface / site impact	<0.0001

One of the remaining terms in the fitted model is distance to land, as it was found that this was highly significant when predicting common guillemot numbers. The model has estimated that common guillemot numbers decrease at a constant rate with increasing distance from land[21]. This estimated partial relationship is shown in Figure 4.5.1. 'Month' is also one of the remaining terms in the fitted model and is deemed to be statistically highly significant. As can be seen from Figure 4.5.2, the predicted relationship between common

[21] This may reflect, at least in part, the drop-off in detection rate with increasing distance.

guillemot density and month is complex. There is a clear peak in abundance expected during the month of June and a sudden drop to a trough in estimated abundance in August. Between October and January, it appears that the model predicts a fairly constant common guillemot density.

In the final fitted model, a spatial surface was able to be fitted using four degrees of freedom. An interaction term (site impact/spatial surface) was also fitted and found to be statistically highly significant.

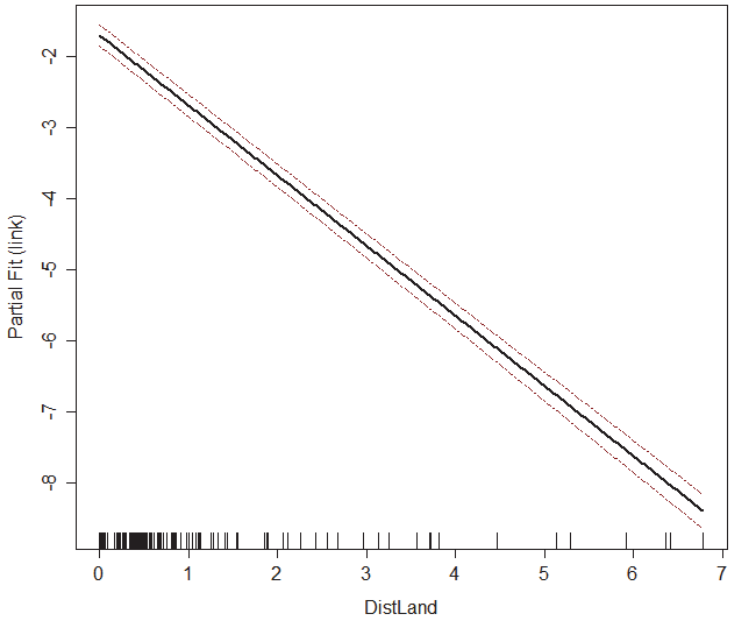

Figure 4.5.1. Estimated partial relationship of distance to land against log(density) for common guillemot at Billia Croo. The red lines represent 95% confidence intervals about the estimated relationship and the tick marks show where the data lie in the covariate range.

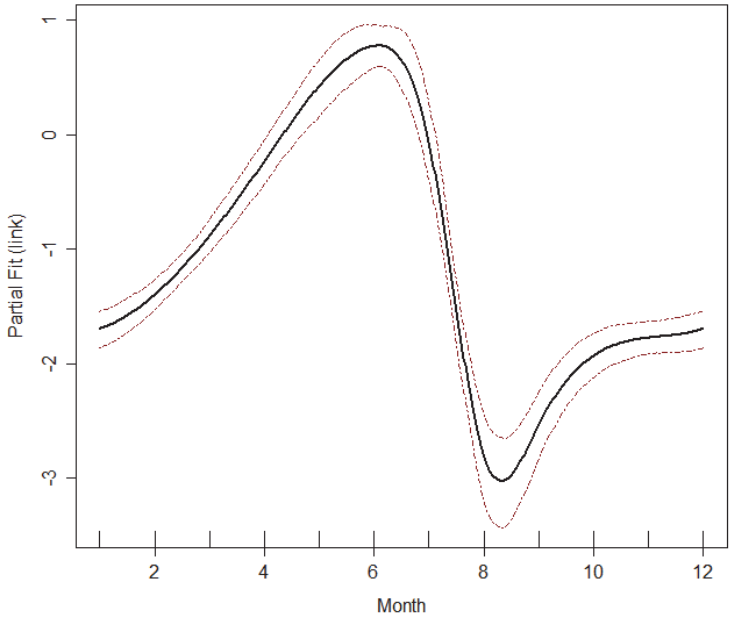

Figure 4.5.2. Estimated partial relationship of month against log(density) for common guillemot at Billia Croo. The red lines represent 95% confidence intervals about the estimated relationship and the tick marks show where the data lie in the covariate range.

4.5.1.4 Density predictions and uncertainty estimate

Due to the final model including a spatial surface, it was possible to predict common guillemot density across the survey grid. To facilitate the creation of this prediction surface, it was necessary to set certain environmental conditions. It was decided that optimum conditions for common guillemots should be selected for each term, these are discussed further in Appendix 5. The prediction surface for each site impact level under these conditions has been produced and is available in Figure 4.5.3 and Figure 4.5.4. For each of the predictions, the associated CV value is also provided (Figure 4.5.5 and Figure 4.5.6), which represents the level of uncertainty about each prediction.

Reference should be made to Figure 2.1.9 and Figure 2.1.10 for the grid cell labelling system.

From Figure 4.5.3, it is clear that there are higher densities in the inner area of the observation grid. In the two outer grid cell bands (A and B), there is not expected to be common guillemot densities greater than 0.30 individuals/km^2 in any grid cell at all site impact levels. The only exception is when the operational status of the site is SIL-3 (devices installed and operational); in this case, grid cell A13 has a estimated common guillemot density greater than 0.30 individuals/km^2.

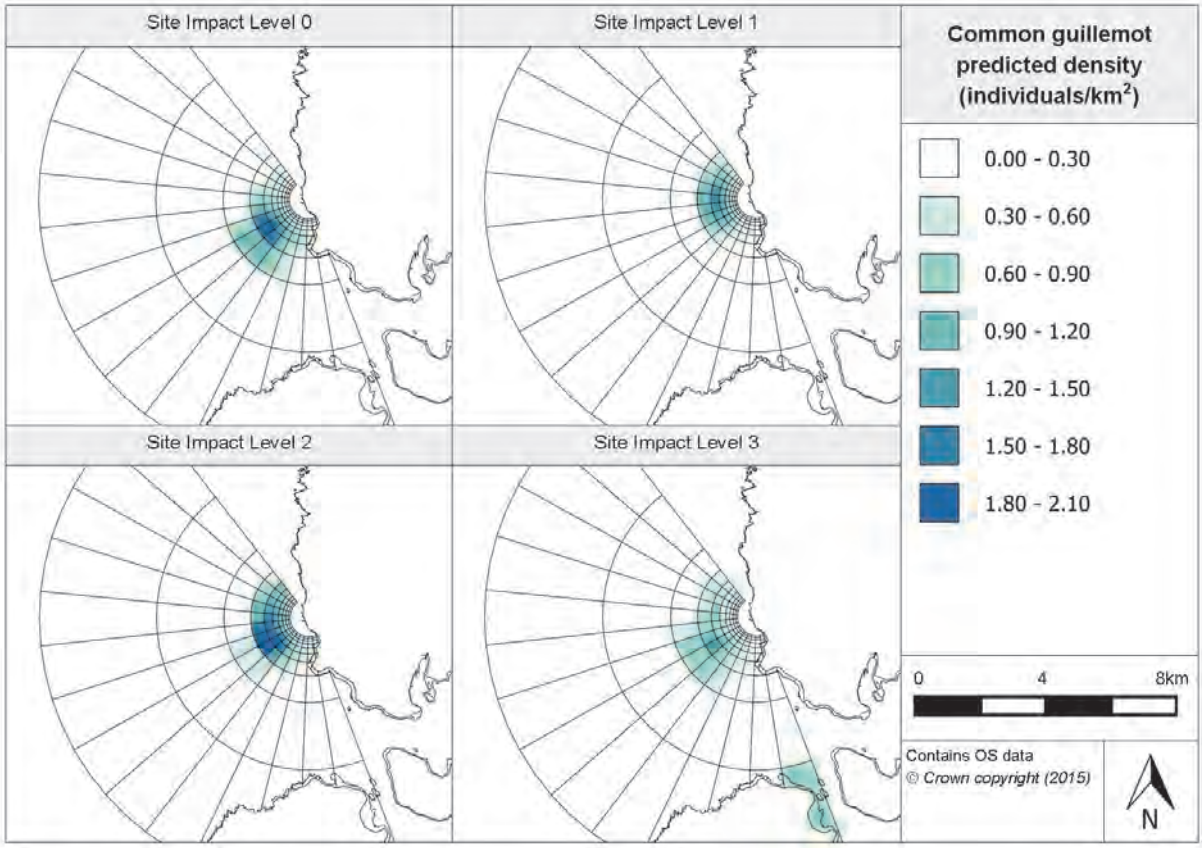

Figure 4.5.3. Prediction surfaces for common guillemot density at Billia Croo for each site impact level

During baseline conditions (SIL-0), there appears to be a peak in density in grid cells D6-D8 and E7, see Figure 4.5.4. The adjoining cells show higher densities suggesting that the peak in density estimated in these cells slowly subsides with increasing distance from these particular grid cells. The majority of grid cells in the inner bands of the observation grid are showing estimated densities greater than 0.30 individuals/km^2. The most inner band of grid cells J0-J13 (closest to the observation vantage point) has lower density predictions than the majority of the grid cells in the inner area, with no grid cells in this band having density predictions greater than 0.30 individuals/km^2.

At SIL-1 (infrastrucure installed), the common guillemot densities are low (compared to the rest of the prediction surface) for the outermost grid bands (A-C), with no grid cell having a estimated density greater than 0.30 individuals/km^2 (Figure 4.5.3). From Figure 4.5.4, there appears to be an area of higher density predictions in the northern half of the inner observation grid. Highest densities at SIL-1 are expected in grid cell E4, with densities in adjoining cells slowly reducing with increasing distance from the peak. Again, the innermost band of grid cells (grid band J) is not expected to have densities greater than 0.30 individuals/km^2.

When the operational status of the site is SIL-2 (devices installed but not operational), the estimated density in grid bands A, B and the majority of C is between 0.00 and 0.30 individuals/km^2. As can be seen in Figure 4.5.3, grid cells C6-C8 exhibit an estimated density of 0.30-0.60 individuals/km^2. In terms of the inner grid cells, there is a clear peak in density in grid cells D6-D7 and E6-D7, although, to a lesser extent, grid cells D5, E4-E5, E8 and F7 are all predicted to have greater common guillemot abundance in comparison to the surrounding cells (Figure 4.5.4). There is a clear gradual reduction in abundances away

from this peak area, except on the south-western side of grid cells D6-D7 where there is a pronounced drop in estimated density from above 1.80 individuals/km^2 to abundances lower than 0.60 individuals/km^2.

At SIL-3 (devices installed and operational), in the outer grid bands, the only cells showing estimated abudances greater than 0.30 individuals/km^2 are grid cells C5-C9 where densities below 0.90 individuals/km^2 are expected (Figure 4.5.3). In the inner grid bands, there appears to be, in general, lower densities predicted when compared to the other site impact levels. There is a slight rise in estimated density in grid cell D7, and then lower densities in the surrounding grid cells. The innermost grid bands, H0-H13, I0-I13 and J0-J13, all have estimated densities below 0.30 individuals/km^2 (Figure 4.5.4).

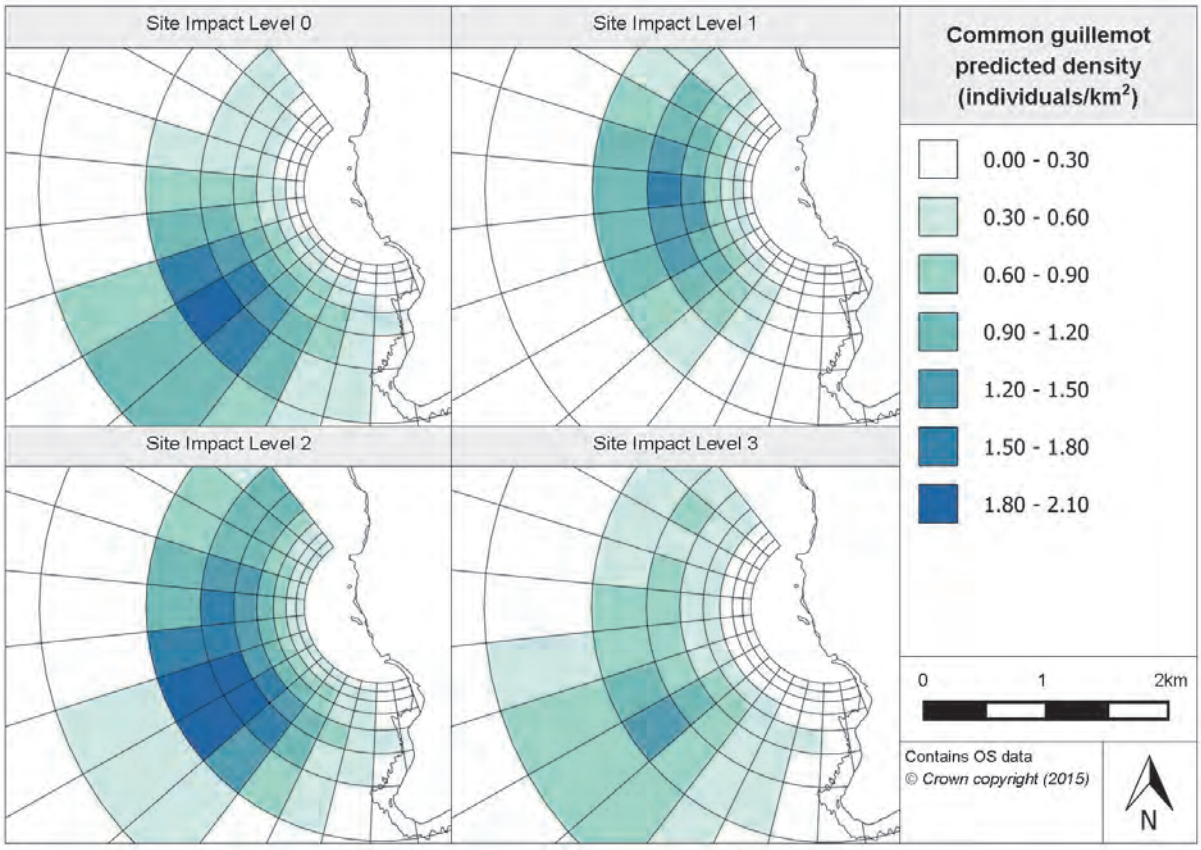

Figure 4.5.4. Inner prediction surfaces for common guillemot density at Billia Croo for each site impact level

From Figure 4.5.5, it becomes clear that many of the CV values in the outer grid bands are unavailable as a result of very low density predictions in these grid cells, leading to unrealistic CV values. For the SIL-0 prediction surface, the CV values for all of the outer grid band A are unavailable, with the exception of cell A13 which has a CV value of 3.00-4.00. The CV values for the northern half of grid band B are also unavailable. The other half of grid band B appears to have CV values between 1.00 and 3.00, which suggests that there is high uncertainty in the predictions from these grid cells. Grid band C has five grid cells where the CV value is between 1.00 and 2.00 suggesting high uncertainty but, other than these cells, the rest of grid band C and the inner grid bands D-J have a CV value below 1.00 suggesting that the density estimates are fairly precise for these grid cells (Figure 4.5.6).

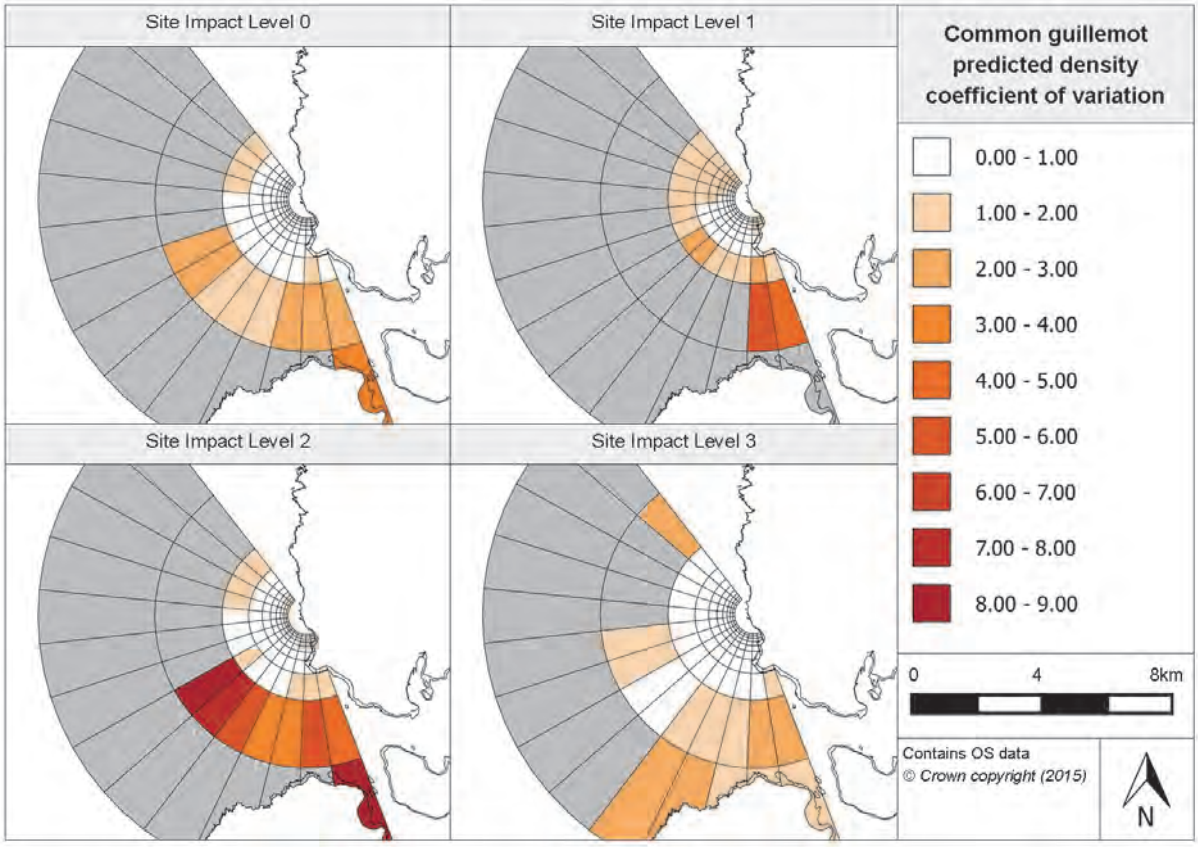

Figure 4.5.5. Associated coefficient of variation values for common guillemot density prediction surfaces at Billia Croo. Grey cells represent predictions where CV values are unavailable.

The CV values for the SIL-1 prediction surfaces show that CV values are unavailable for grid band A and the majority of B, which is likely to be due to very low density predictions, as above. As seen in Figure 4.5.5, grid cells B12 and B13 have CV values between 4.00 and 6.00, suggesting high uncertainty in the predictions made for these grid cells. The CV values for grid band C vary between 1.00 and 3.00, again suggesting high uncertainty in these predictions. When looking at Figure 4.5.5, grid cells in the northern part of the inner grid bands and the easternmost grid cells have higher CV values than the rest of the inner band grid cells (Figure 4.5.6). This would imply that these predicted values for the central inner grid cells are more precise.

For the SIL-2 prediction surfaces, the majority of grid bands A and B have their CV values unavailable, see Figure 4.5.5. Those parts of these bands that have CV values, exhibit very high ones of between 3.00 and 9.00 which would imply high uncertainty in these areas of the prediction surfaces. There are eight cells in grid band C with CV values between 1.00 and 2.00 and other cells have values below 1.00. As seen in Figure 4.5.6, the inner grids generally have CV values below 1.00 except for grid bands J and I, where the majority of grid cells have CV values between 1.00 and 2.00.

At SIL-3, fewer grid cells are deemed to have their CV values unavailable; this may be due to more observations at this site impact level (Table 4.5.1) upon which to base the models. In general, there are higher CV values in the cells in the south, with CV values ranging between 1.00 and 3.00 (Figure 4.5.5). In addition to these cells, grid cells B0 and B5-6 also have CV values in the range 1.00-3.00. The CV values for the inner grid bands appear to be

mostly below 1.00, as seen in Figure 4.5.6. This suggests there is high precision in these predictions.

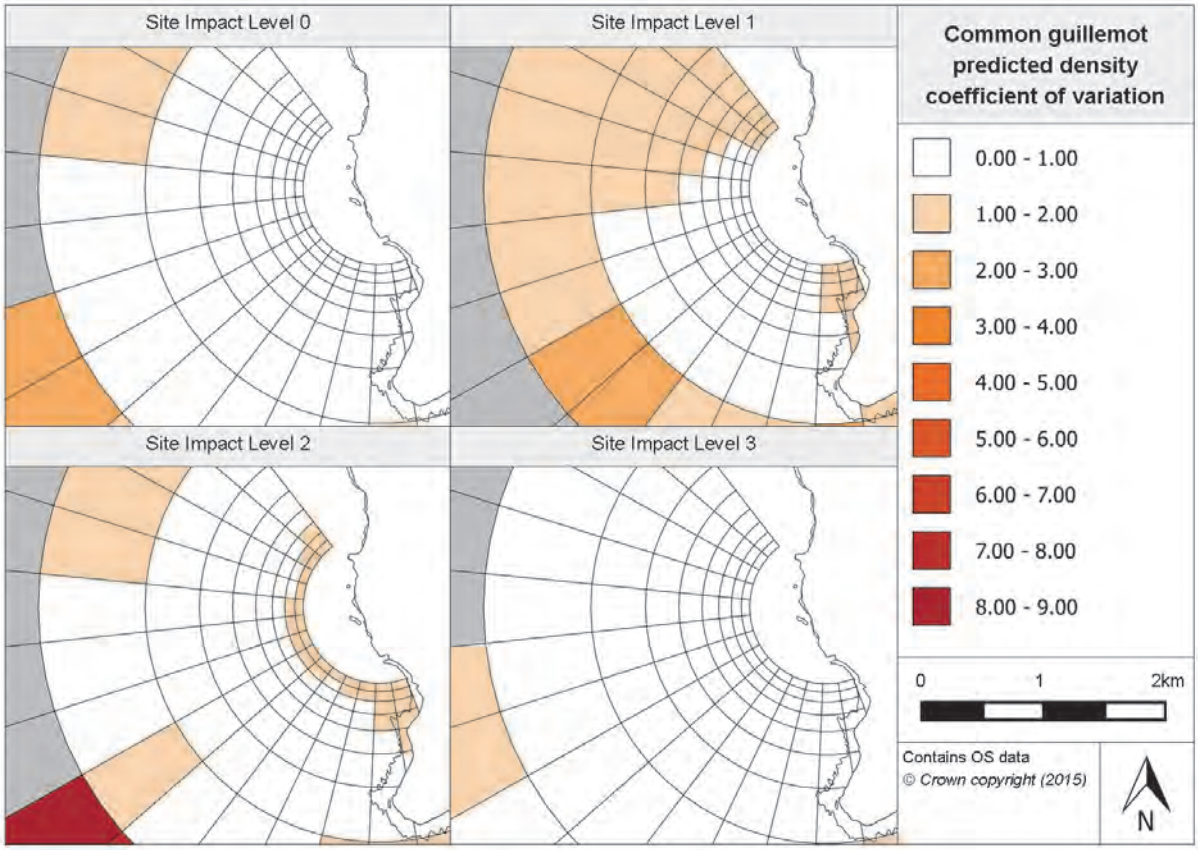

Figure 4.5.6. Associated coefficient of variation values for common guillemot inner density prediction surfaces at Billia Croo

4.5.1.5 Relative abundance estimations

By using the fitted common guillemot model, it was possible to produce relative abundance estimates for each survey month. In producing such predictions, it was necessary to set values for the environmental parameters which, as before, were chosen as optimum conditions where the most number of common guillemots had been sighted at Billia Croo. Seasonal predictions were then produced by combining the survey months; these, alongside their associated CIs, are provided in Table 4.5.3. It is worth emphasising that these abundance estimates are only relative abundances as only surface visible observations have been recorded.

Table 4.5.3. Relative abundance for common guillemots during each season (associated confidence intervals are provided in brackets) at Billia Croo

Year	Season			
	Winter (Dec, Jan, Feb)	Spring (Mar, Apr, May)	Summer (Jun, Jul, Aug)	Autumn (Sep, Oct, Nov)
2009	-	73.77 (22.30, 169.65)	97.25 (3.72, 256.29)	9.03 (3.83, 21.51)
2010	13.96 (7.26, 30.63)	109.11 (33.22, 330.23)	144.10 (5.33, 522.31)	9.54 (6.26, 15.53)
2011	12.48 (8.14, 20.37)	68.40 (19.21, 169.65)	97.42 (4.39, 256.29)	9.83 (4.68, 18.63)
2012	13.96 (7.26, 30.63)	67.81 (17.63, 213.65)	106.86 (5.33, 322.83)	14.53 (6.44, 23.58)
2013	18.46 (11.35, 26.61)	60.63 (19.21, 144.69)	80.08 (3.68, 203.08)	9.83 (4.68, 18.63)
2014	15.19 (9.18, 26.94)	68.62 (22.30, 213.65)	89.56 (3.72, 322.83)	11.32 (3.83, 23.58)
2015	22.46 (16.12, 36.41)	109.11 (33.22, 330.23)	-	-

Table 4.5.3 does not show any clear peaks in the abundance lasting an entire year. However, there do seem to be considerably greater abundances expected in the spring and summer of 2010 when compared with other years. The autumn of 2012 also seems to have greater estimated abundances than during that season in other years. Additionally, in the winter of 2015, greater common guillemot abundances are predicted when compared to previous years.

This information has been presented in Appendix 7 split across site impact levels. To illustrate the extent of uncertainty behind some of the predictions, the associated upper and lower CIs for the predictions have also been provided in Appendix 7. Due to the disparity in abundance predictions between seasons, the only clear peaks in abundance are expected during the summer. The high abundance prediction in the summer of 2010 is particularly noticeable.

As conducted for the Fall of Warness species, prediction surfaces for common guillemots have also been produced under typical surveying conditions for January and July. Both the surfaces and their associated CV values are available in the Marine Scotland Information portal. The prediction surfaces' peaks and troughs in density look very similar between January and July; however, July's density estimates are approximately eight times greater than those for January.

4.5.1.6 Spatially-explicit change

In understanding the extent of any spatially-explicit changes in common guillemot numbers across the site with differing site impact levels, it was necessary to calculate the density differences between each site impact level's prediction surface. The 95% CIs were used when investigating the significance of any changes (note that grid cells where a significant change is found are marked with a corresponding '+' or '-'). 'Year' was not included as a term in the final fitted model for common guillemots; therefore, the variability in predictions across years does not exist, resulting in an average year being presented below, see Figure 4.5.7 and Figure 4.5.8.

When looking at the spatially-explicit change between SIL-0 (baseline conditions) and SIL-1 (when device-associated infrastructure is installed), there is a reduction in density in grid bands A and B and the southern half of grid band C. Of these outer bands, generally the cells in the southern half show a significant decrease in density, with grid cell C7 showing a particular decrease of 1.03 individuals/km^2 which gradually reduces in strength across the surrounding cells. In terms of the inner band cells, it appears that the southern half of the grid cells show a negative change whilst the northern half show a positive change in density.

As with grid cell C7, cells D7 and D8 show a much greater decrease than the other negative changes. In terms of the northern increase in density, there appears to be a cluster of more notable increases around grid cell E3. This pattern of change would suggest that there is a redistribution of common guillemots from the southern and outer part of the site to the inner northern part of the site with the introduction of device-related infrastructure.

In terms of the change in density between SIL-0 and SIL-2 (when devices are in place but not operational), there is a similar redistribution evident within the site, again with a movement from the south to the north, but this time to a lesser extent. Fewer grid cells where a decrease is predicted are marked as having a significant reduction (only five grid cells). In the outer bands, the positive change in density is present in the northern half, although none of changes within these grid cells are deemed as significant. As seen in Figure 4.5.8, the northern half of the inner grid bands exhibit a much more extensive increase in density compared to that modelled between SIL-0 and SIL-1, with many deemed as significant. The positive change is also seen in the southern half of the four innermost grid bands, although these have not been deemed as significant.

When investigating the change in density between SIL-0 and SIL-3 (when devices are present and operational), it is clear that there is an increase in density across the majority of the grid. In terms of the outer bands, all of grid band A is expected to have a significant increase in density. Grid band B shows a positive change across its entire length, with the change being deemed significant in the northern half of the grid band. Within grid band C, there is a positive change in density expected in the northern half of the grid band with some of the increases in density in the grid cells deemed significant. In contrast, in the south half of the grid band, there is a negative change in density anticipated, with two cells having their estimated decrease in density deemed significant. In terms of the density change predictions for the inner grid cells, the majority of the grid cells show a negative change in density, with a notable decrease around grid cells D7-D8 and E7-E8. In most of the cells where a negative change is predicted, the change has been deemed to be significant. In the very northern grid cells of the inner bands, the estimated density change has been deemed positive and in some cells significant. There appears to be no correlation between significant changes in density for SIL-0 - SIL-3 and the location of test berths, as some berths are located in grid cells that show a positive change and others in grid cells showing a negative change.

In terms of the estimated density change between SIL-1 and SIL-2 (when devices are installed), there is an increase in density expected across the surface, with only six grid cells altogether showing a density decrease. In the outer bands, it appears the cells located on the south-western side of the site are deemed to show a significant change. When considering the inner band (Figure 4.5.8), it is clear that, in the southern half of the bands, more grid cells are deemed to show a significant increase in density. There are 11 grid cells which show a notably greater density increase, but grid cell D7 shows the greatest increase across all site impact levels, with approximately 1.28 individuals/km^2.

Between SIL-1 and SIL-3 prediction surfaces (when devices are installed and operating), a density increase is expected in the majority of the grid cells. As seen in Figure 4.5.7, a positive change in density is expected in all the grid cells in the outer three grid bands. The change in all but four of the grid cells in these bands is deemed to be significant. A heightened density increase is anticipated in C6-C8 and A13 as compared to the other grid cells. Although many of the cells in the inner bands are expected to show an increase in common guillemot estimated density with devices becoming operational (when compared to just device-associated infrastructure being onsite), a group of cells (in the northern region of the inner bands) are expected to exhibit a negative change in density. Sixteen of these grid cells have been predicted to show a significant negative change, with a decrease greater

than 0.50 individuals/km^2 noted in 11 grid cells. There may be some evidence of redistribution across the observation grid.

When considering the estimated density difference between devices being onsite and becoming operational, there appears to be a redistribution across the observation grid, with common guillemots moving away from the inner grid cells to the outer ones, further away from the observation vantage point (Figure 4.5.7). The majority of grid cells in the outer two grid bands are expected to show a significant increase in density, whereas for grid band C, although a density increase is modelled in all its grid cells, only one change in density is deemed to be significant. As can be seen in Figure 4.5.8, a decrease in density is expected in almost all the grid cells within the inner bands. A significant decrease in density is expected in many of these cells which appear to be grouped just north of the central cells within the inner bands. In three of the grid cells, the density decrease is anticipated to be greater than 1.00 individual/km^2.

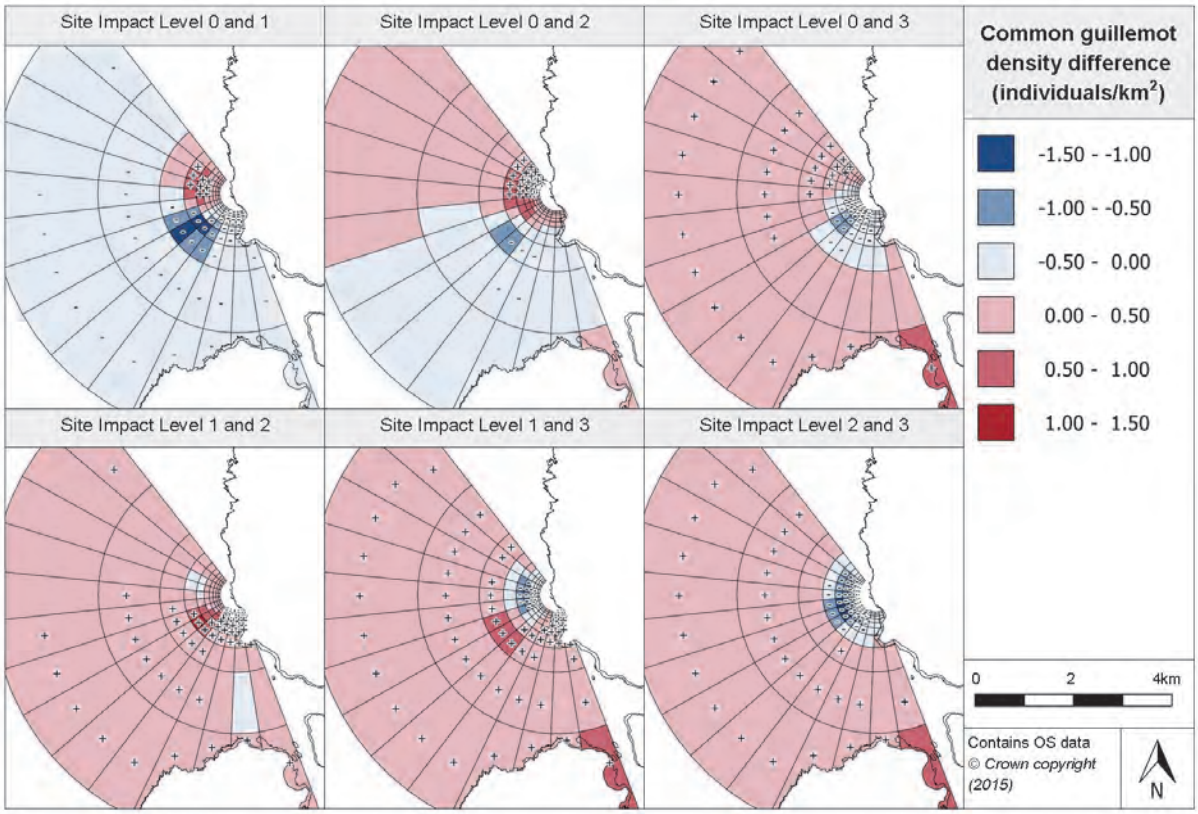

Figure 4.5.7. Density differences between common guillemot site impact level prediction surfaces at Billia Croo

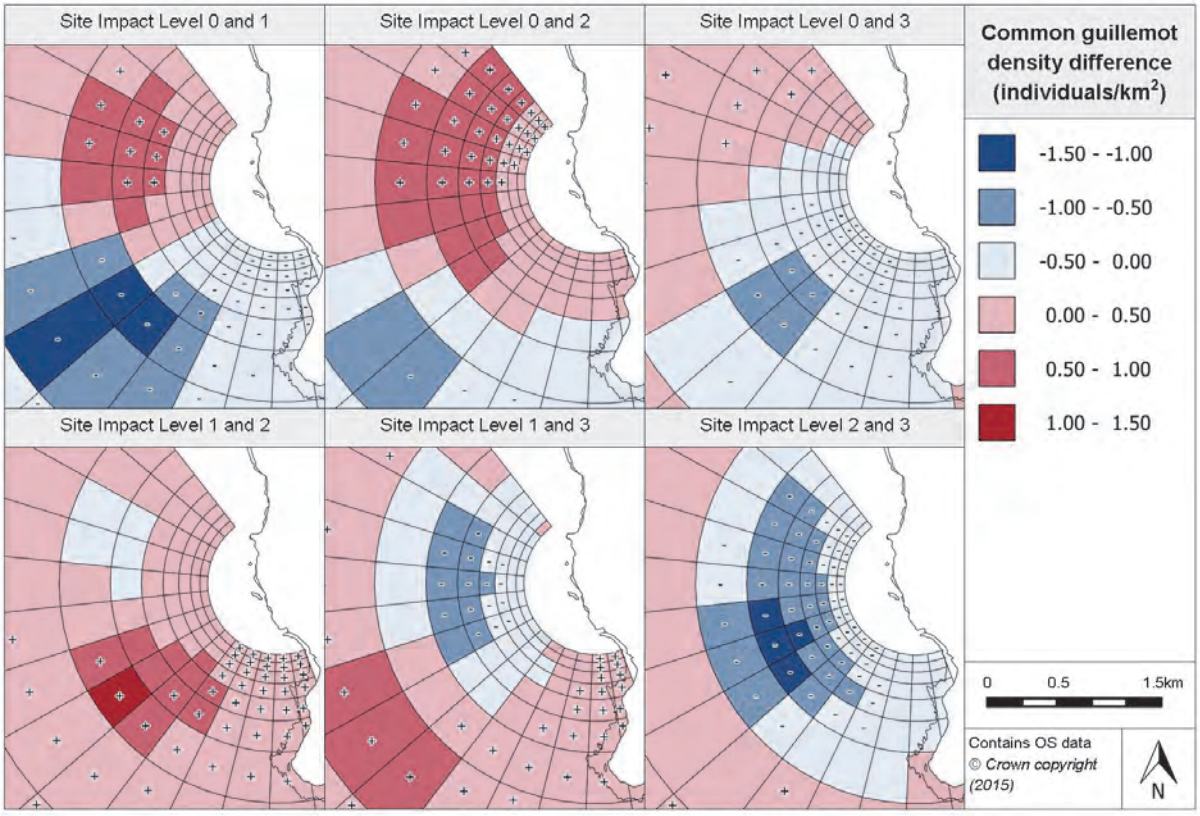

Figure 4.5.8. Density differences between common guillemot site impact level inner prediction surfaces at Billia Croo

4.5.1.7 Density change with distance from potential impact location

Similar to the Fall of Warness species, plots have been created using the spatially-explicit change predictions to depict how the density difference between site impact levels changes with increasing distance from a potential impact location. The following figure, Figure 4.5.9, presents the changes in estimated density difference for common guillemots for a single test berth at Billia Croo.

Between SIL-0 and SIL-1, there is a reduction in estimated density in the immediate vicinity of the test berth; as the 95% CIs are below zero, it is expected that the decrease in density seen in the first 500m from the potential impact location is significant. Beyond 500m, the upper CI is above zero, suggesting that there may be negligible change in density. Beyond 1.2km, the density difference approximates to baseline conditions, thus suggesting little change beyond this distance in terms of common guillemot density with the installation of device-associated infrastructure.

Due to the wide CIs between SIL-0 and SIL-2, it is not possible to determine any particular positive density change as the lower CI is below zero, suggesting the change in density is not significant. Beyond 2.5km away from the test berth, there appears to be very little modelled change in density from baseline conditions.

There is a decrease in density estimated between SIL-0 and SIL-3, which is expected to be evident until approximately 1.6km away from the test berth. The reduction in estimated density gradually reduces, reaching baseline conditions at 1.6km. As the upper CI is above zero, it is unlikely that the decrease in density is significant.

Between SIL-1 and SIL-2, there is an increase in estimated density directly at the test berth's location. The heightened density prediction slowly reduces with increasing distance to reach SIL-1 levels. The lower confidence level is above zero until about 800m from the test berth, the latter suggesting a significant difference up to this distance.

Between SIL-1 and SIL-3, there is an increase in abundance at the immediate location of the test berth. This heightened density quickly reduces, reaching SIL-1 levels at approximately 800m from the potential impact location. Between 800m and 1.5km, there is a slight reduction in density. The upper and lower CIs lie on either side of zero. At 1.5km from the test berth, the common guillemot estimated density is expected to be maintained at SIL-1 levels.

There is a distinct reduction in density between SIL-2 and SIL-3. This reduction decreases very gradually with increasing distance from the potential impact location until about 2km away where it is in line with SIL-2 estimated density levels. As the upper CI, is slightly above or around zero for the first 2km, it is unlikely that a decrease in density will always be experienced. Beyond 2km, the density difference varies very little.

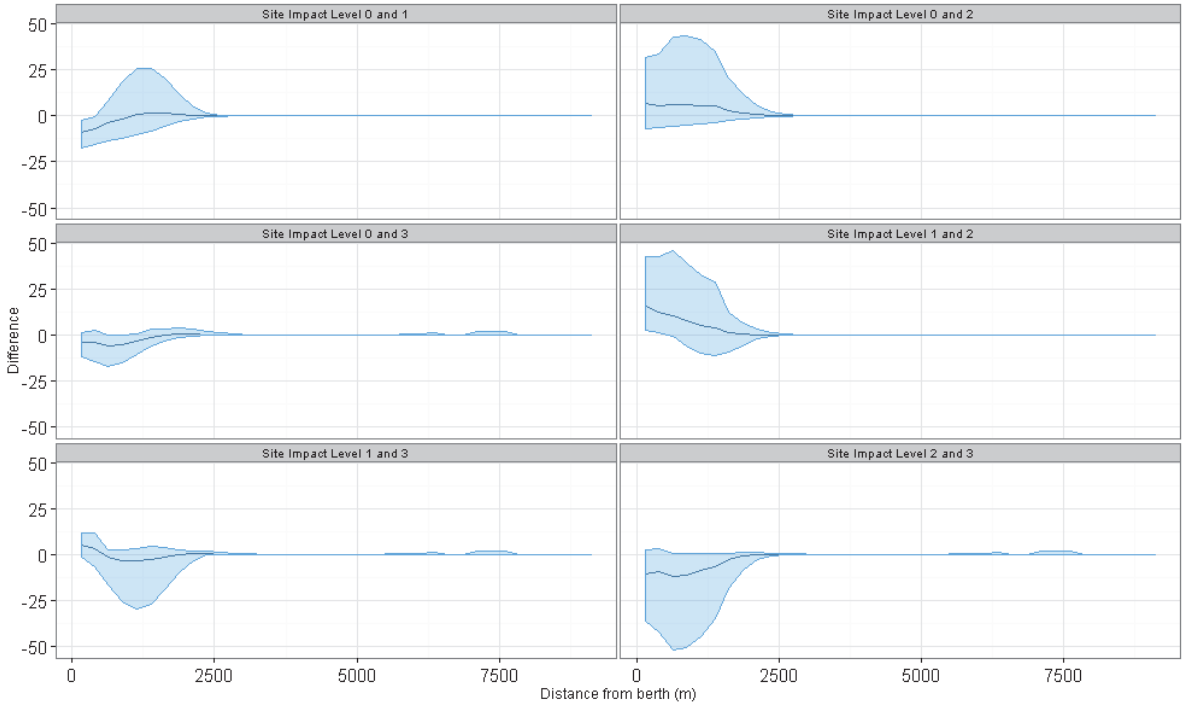

Figure 4.5.9. Density change between site impact levels with increasing distance from a potential impact location, with associated confidence intervals, for common guillemots at Billia Croo

4.5.1.8 Discussion

Common guillemots are one of the most common species from the auk family found at Billia Croo. The model developed for them includes four significant terms. This implies that their presence is not controlled by as many environmental factors as was identified at the Fall of Warness: however, factors such as distance from land and month are important controls on common guillemot distribution. The density predictions are similar for all site impact levels with the highest densities generally 1-2km west to south-west of the Black Craig cliffs[22]. The

[22] This peak in density in this area of the grid may be attributable to the distance and direction that the observers were best able to see and identify common guillemots.

predictions for this area have high to very high precision. Elsewhere, CV values are high or not available, indicating high uncertainty which reflects the few raw observations made in these areas of the survey grid. Grid cells within the area of highest densities show both increases and decreases in density in response to changes in site impact levels, with most showing a slight decrease in density between baseline conditions (SIL-0) and devices operating (SIL-3).

The location of the grid cells where significant changes in density are expected between baseline conditions and device operational conditions, appears to not be correlated with the location of test berths. In addition, as the grid cells that contain test berths are predicted to experience increases and decreases in density between these conditions, there is no clear conclusion that can be drawn regarding the effect of operational devices on common guillemot density. Modelled density changes with increasing distance from a potential impact location exhibit a decrease at the impact site with respect to the baseline, but return to baseline conditions within 2km.

4.5.2 Black guillemot (Cepphus grylle)

4.5.2.1 Species overview

As with common guillemots, the black guillemot (*Cepphus grylle)* is a frequent visitor to Billia Croo. As mentioned previously, although black guillemots have been modelled separately (as discussed in this section) the species is also included in the modelling of a wider group comprising all auk species that have been observed at Billia Croo. Information regarding the general distribution and behaviour of black guillemots is outlined in Section 4.3.1.1 above.

4.5.2.2 Data summary

Black guillemots are observed less often at Billia Croo in comparison to common guillemots. A summary of the raw data is provided in Table 4.5.4. This includes information on the number of observations and typical group size across each of the site impact levels. It is worth noting the fewer number of observations at site impact levels 0 and 1 in comparison to site impact levels 2 and 3.

Table 4.5.4. Summary of black guillemot raw data for Billia Croo

	Total	Site Impact Level 0	Site Impact Level 1	Site Impact Level 2	Site Impact Level 3
Number of observations	5098	356	304	1540	2898
Minimum (group size)	1	1	1	1	1
Maximum (group size)	42	13	10	42	23
Mean (group size)	1.54	1.78	1.48	1.48	1.55
(s.d)	(1.40)	(1.58)	(1.15)	(1.43)	(1.39)

4.5.2.3 Model overview

GEE-based p-values could be obtained for each of the terms that remained in the final fitted model. The model identified six terms that were highly significant when predicting black guillemot density across the survey area at Billia Croo (Table 4.5.5).

Table 4.5.5. GEE-based p-values for the terms in the final black guillemot model for Billia Croo

Model term	ρ-value
Distance to land	<0.0001
Cloud cover	<0.0001
Month	<0.0001
Site impact	<0.0001
Spatial surface	<0.0001
Spatial surface / site impact	<0.0001

Distance to land remains as a smooth term in the final black guillemot model for Billia Croo. The model predicts fewer observations of black guillemot with increasing distance from land[23]. This prediction fits with the information already known on black guillemot behaviour. Cloud cover also remains in the final fitted model as it was found that this was highly significant when predicting black guillemot numbers. The model has estimated that fewer black guillemots are observed when there is more cloud cover, with total cloud cover (8 oktas) having the lowest density. As seen in Figure 4.5.10, the fitted model has estimated that black guillemot numbers vary dramatically throughout the year. There is a clear peak in estimated density during March with numbers slowly declining to a low during the autumnal months (September-December). There is a rapid rise in density during the winter months (December-February) to a peak in March.

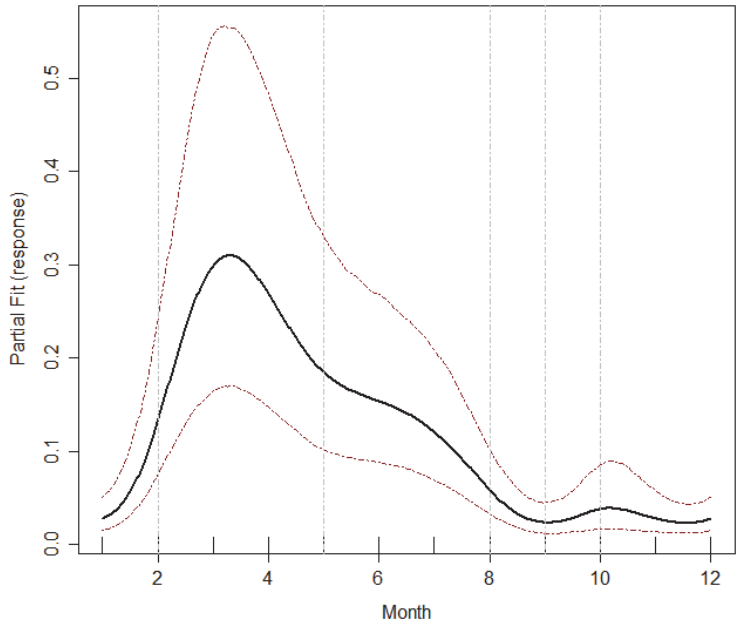

Figure 4.5.10. Estimated partial relationship of month against log(density) for black guillemot at Billia Croo. The red lines represent 95% confidence intervals about the estimated relationship and the tick marks show where the data lie in the covariate range.

A spatial surface was able to be fitted for the final model using four knots. Additionally, an interaction term (site impact/spatial surface) was also fitted and found to be statistically highly significant.

[23] As with the common guillemots, this may, or partly, reflect the drop off in detection rate with increasing distance.

4.5.2.4 Density predictions and uncertainty estimate

As the final fitted model included a spatial surface, it was possible to produce prediction surfaces for the black guillemot density predictions, allowing the latter to vary across the observation grid. To be able to make these predictions, it was necessary to set the environmental covariates to certain conditions. As with the Fall of Warness species, it was decided that the most appropriate conditions would be when the greatest number of black guillemot observations were made. These conditions are provided in Appendix 5. Due to anomalies in the data, it was necessary to reduce the number of iterations in the bootstrap; 853 iterations were implemented rather than the 1000 carried out for most other species/groups. A prediction surface for each site impact level is given in Figure 4.5.11, together with a detailed view of the inner grid cells in Figure 4.5.12. As there are differing levels of uncertainty surrounding each prediction, the associated CV value is provided for each prediction in Figure 4.5.13 and Figure 4.5.14.

Reference should be made to Figure 2.1.9 and Figure 2.1.10 for the grid cell labelling system.

Similar to the common guillemot predictions, there is a clear disparity in the black guillemot density predictions across the prediction surfaces for all site impact levels, as there are much higher density predictions in the inner grid cells as compared to the outer grid cells.

In terms of the density predictions for SIL-0 (baseline conditions), across the entire prediction surface only very low black guillemot densities are expected. As can be seen in Figure 4.5.11, density predictions in the outer grid bands are less than 0.10 individuals/km^2, whereas some grid cells in the inner grid bands have greater densities anticipated, up to 0.20 individuals/km^2. There is no clear group of heightened densities within the inner bands (Figure 4.5.12). For the density predictions at SIL-1, when device-associated infrastructure is installed, the outer grid bands again appear to have only very low densities expected. None of the grid cells in the outer bands have an estimated density greater than 0.10 individuals/km^2. In terms of the inner grid bands (see Figure 4.5.12), similar grid cells to SIL-0 are highlighted as having density greater than 0.10 individuals/km^2, except for three grid cells (D9-D11) marked as having estimated densities of 0.20-0.30 individuals/km^2.

The density predictions relating to when devices are onsite but not operational (SIL-2) again show that the highest densities are in the inner grid bands with very low density predictions in the outer grid bands. In the outer bands, none of the grid cells have estimated densities greater than 0.10 individuals/km^2 (Figure 4.5.11), whereas, as can be seen in Figure 4.5.12, such higher densities are expected in the inner grid bands, with grid cell D11 having a estimated density of 0.50 individuals/km^2. Around this grid cell, there is also clustering of higher densities. There is also a cluster of estimated densities above 0.10 individuals/km^2 just north of the central grid cells within the inner band.

In terms of SIL-3, when devices are onsite and operational, much lower black guillemot densities tend to be expected in the outer grid bands as compared to the inner grid bands. In the outer bands, all but one of the grid cells has an estimated density below 0.10 individuals/km^2 (Figure 4.5.11). Grid cell C4 has a density of 0.10-0.20 individuals/km^2. In terms of the inner bands, as seen in Figure 4.5.12, there is a cluster of grid cells in the centre with densities between 0.10 and 0.20 individuals/km^2. To the southern end of the inner grid bands, once again there is a cluster of the higher estimated density around grid cell D11 which has a density of 0.59 individuals/km^2, with adjoining grid cells also having heightened densities which slowly reduce with increasing distance from grid cell D11.

These prediction surfaces imply that much higher densities of black guillemots are likely be observed closer to land.

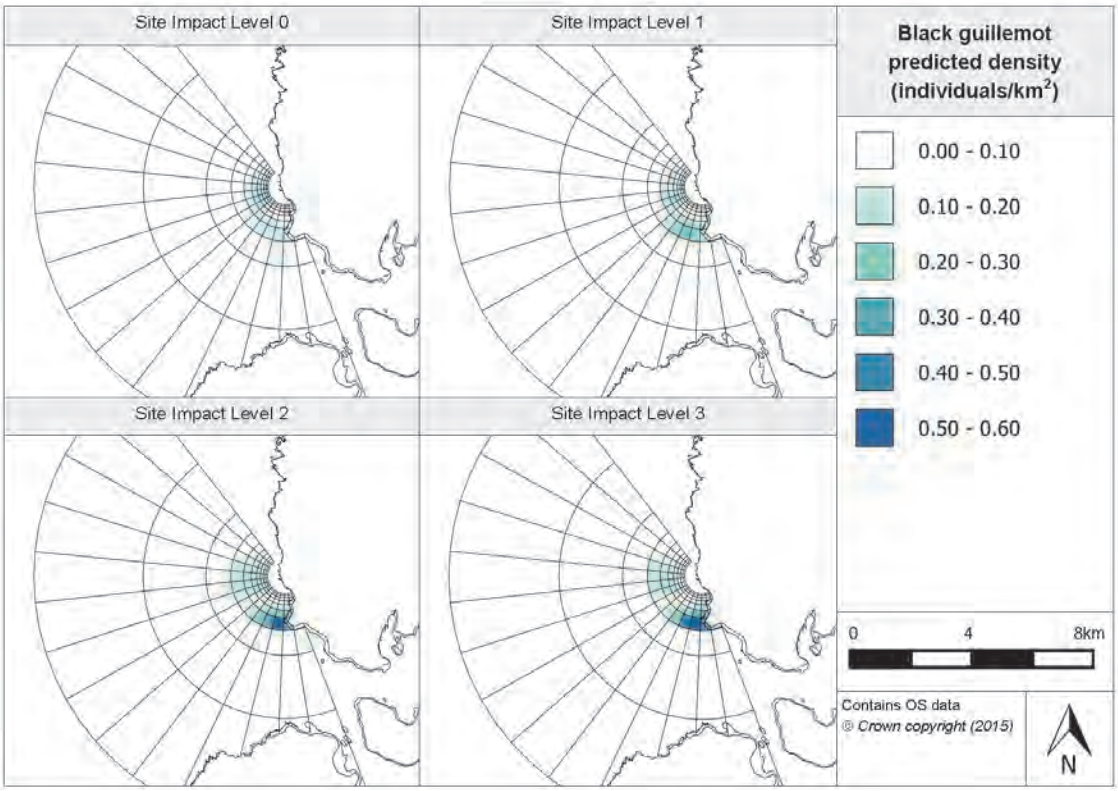

Figure 4.5.11. Prediction surfaces for black guillemot density at Billia Croo for each site impact level

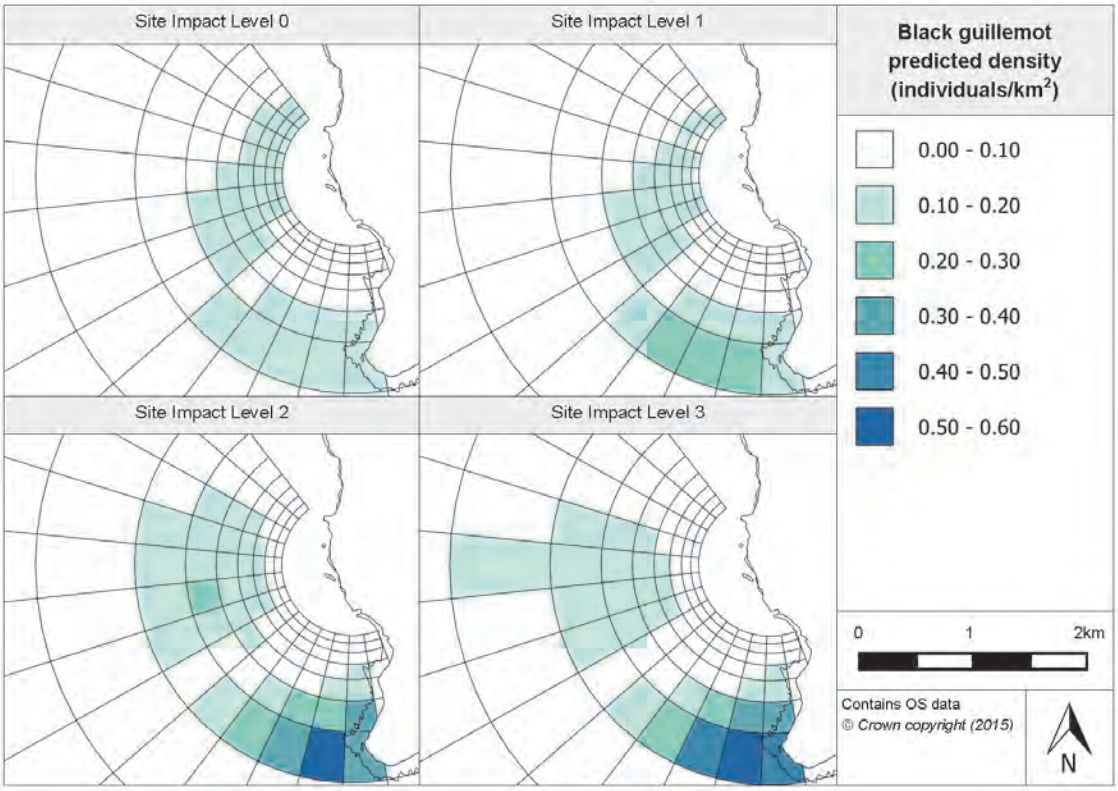

Figure 4.5.12. Inner prediction surfaces for black guillemot density at Billia Croo for each site impact level

In terms of the uncertainty behind these predictions, the associated CV values have been created for each of the density predictions. For the SIL-0 prediction surface, no CV values are available for the majority of the outer grid cells which is likely due to very low density estimates leading to unrealistic CV values. Grid cells A10-A11 have CV values of between 1.50 and 2.50, which suggests that there is high uncertainty in these predictions. CV values have also been calculated for the southern half of grid band C; these are in the range 0.00-2.00 suggesting the precision in the predictions in this area varies greatly. As can be seen in Figure 4.5.14, CV values across the inner grid area also vary substantially. Some of them are unavailable which is likely to be due to the reason given above but there are also grid cells with 0.00-0.50 CV values which would suggest greater precision in the predictions.

In terms of the CV values for the SIL-1 prediction surface, again many of the outer grid cells have unavailable CV values and, where available, the CV values tend to be high suggesting high uncertainty in the predictions. The exception to this is grid cells C7-C11 where CV values of 0.50-1.00 suggest fairly low uncertainty in the predictions. In terms of the inner grid bands (Figure 4.5.14), there are high CV values or CV values are unavailable in grid cells D0-D5 and E0-E4 but, with the exception of these grid cells, the inner grid CV values vary between 0.00 and 1.00, suggesting confidence in the predictions.

The CV values for the SIL-2 predictions are very similar to those described for SIL-1, except that, within the inner grid cells, all grid cells have CV values of 0.00-1.00 suggesting low uncertainty in predictions in this area of the prediction surface. These low CV values are also apparent in the majority of grid band C.

For the SIL-3 prediction surface, many grid cells in the outer grid bands have CV values unavailable, most likely due to low density predictions leading to unrealistic CV values which are therefore incalculable. However, grid cells A10 and B4 have CV values between 0.50 and 1.00 which suggests high precision in the predictions, and the majority of grid band C has CV values ranging between 0.00 and 0.50, except for C12 and C13 which have values of 0.50-1.00. These results suggest a generally lower uncertainty in the predictions for SIL-3 which may be due to a greater number of raw observations when compared to the other site impact levels. As seen in Figure 4.5.13 and Figure 4.5.14, the CV values for the inner grid bands are all between 0.00 and 0.50, suggesting the predictions relating to this area of the site are very precise for the SIL-3 inner prediction surface.

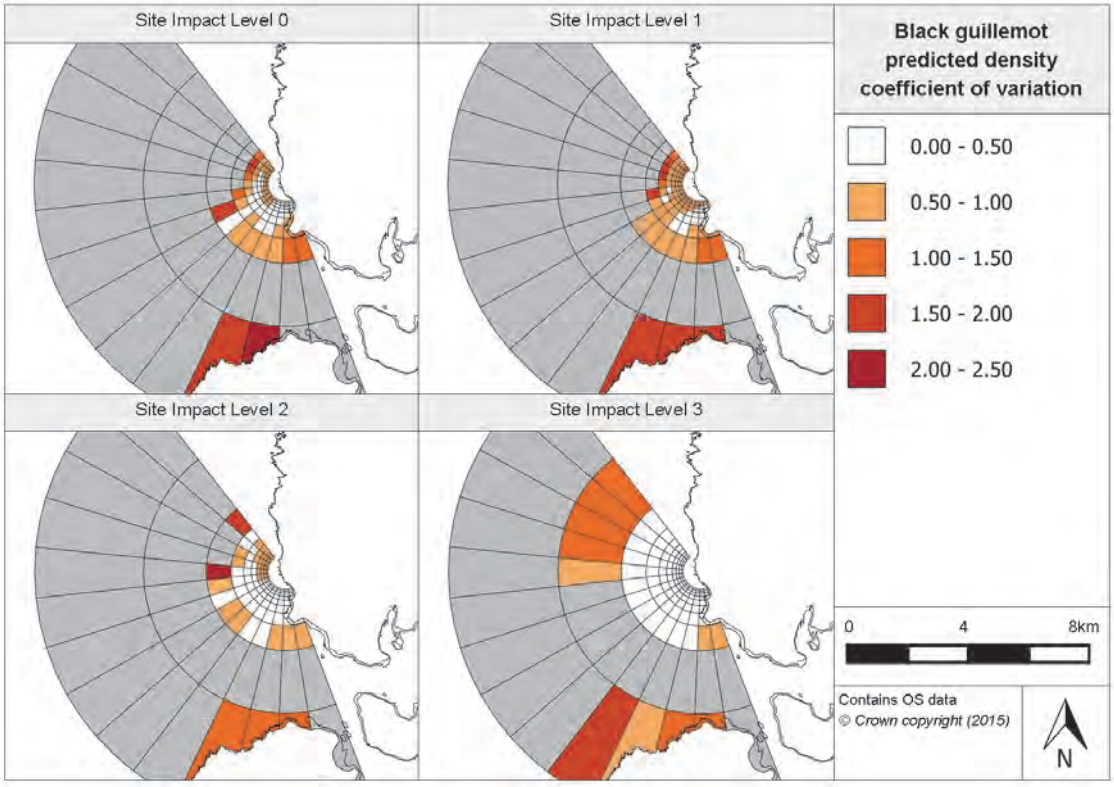

Figure 4.5.13. Associated coefficient of variation values for black guillemot density prediction surfaces at Billia Croo

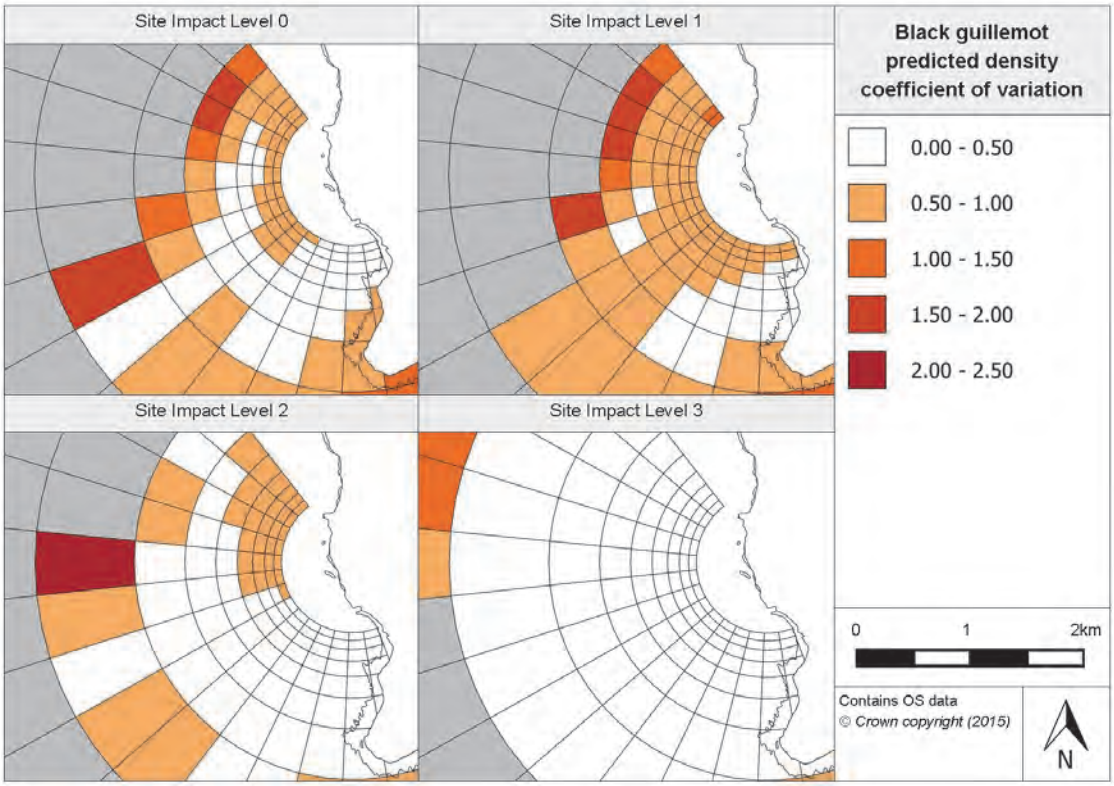

Figure 4.5.14. Associated coefficient of variation values for black guillemot inner density prediction surfaces at Billia Croo

4.5.2.5 Relative abundance estimations

Using the fitted black guillemot model, relative[24] abundance estimates were produced for each survey month. As before, the environmental terms were set to certain conditions (refer to Appendix 5). By combining survey month predictions, it was possible to produce seasonal abundance predictions; these are provided in Table 4.5.6 alongside their associated CIs.

Table 4.5.6. Relative abundance for black guillemots during each season (associated confidence intervals are provided in brackets)

Year	Season			
	Winter (Dec, Jan, Feb)	Spring (Mar, Apr, May)	Summer (Jun, Jul, Aug)	Autumn (Sep, Oct, Nov)
2009	-	28.53 (16.80, 44.79)	14.00 (5.36, 25.19)	7.95 (2.12, 34.09)
2010	8.11 (2.82, 24.78)	36.58 (22.07, 58.38)	17.85 (7.42, 34.82)	9.63 (2.81, 39.89)
2011	9.80 (3.76, 23.67)	33.90 (16.80, 48.73)	13.92 (5.24, 25.19)	7.67 (2.05, 31.94)
2012	8.11 (2.82, 24.78)	29.55 (16.55, 51.69)	16.28 (7.42, 28.27)	9.84 (2.81, 43.99)
2013	9.88 (3.85, 23.67)	35.69 (23.57, 48.73)	17.41 (7.26, 26.72)	7.67 (2.05, 31.94)
2014	7.83 (2.75, 21.32)	29.15 (16.55, 45.12)	14.42 (5.36, 28.27)	8.59 (2.12, 34.09)
2015	10.04 (3.85, 27.35)	36.58 (22.07, 58.38)	-	-

As can be seen in Table 4.5.6, there are no particular years where a peak in abundance is visible. There is a slight increase in abundance during the spring and summer of 2010 and 2013. In general, it appears that greater abundances of black guillemots are expected during spring months which tend to decrease by half for summer and further during autumn and winter.

The relative abundance predictions have also been presented in Appendix 7. These have been split across site impact levels to illustrate any relationships between site operational status and estimated abundance. The peaks in the abundance during spring can be observed at each site impact level.

In addition to the prediction surfaces presented in Figure 4.5.11, prediction surfaces for black guillemots have also been created under typical surveying conditions in January and July. The surfaces are provided in the Marine Scotland Information portal together with their associated CV values. The prediction surfaces' peaks and troughs in density appear to be very similar between the two months' surfaces; however, July's density estimates are approximately three times greater than those for January.

4.5.2.6 Spatially-explicit change

The difference in density between each site impact level's prediction surface has been calculated in order to understand if there is any evidence of spatially-explicit change in black guillemot numbers across the site with differing site-wide operational status. To analyse the significance of any changes, it was necessary to calculate the 95% CIs for each prediction. Similar to common guillemots, 'year' was not included as a term in the final fitted model for black guillemots; therefore, variability in predictions across years does not exist, resulting in a single year being presented in Figure 4.5.15 and Figure 4.5.16. It should be noted that the grid cells where a significant change was found are marked with a corresponding '+' or '-'.

[24] It should be noted that these are relative abundance predictions as only surface visible observations have been recorded.

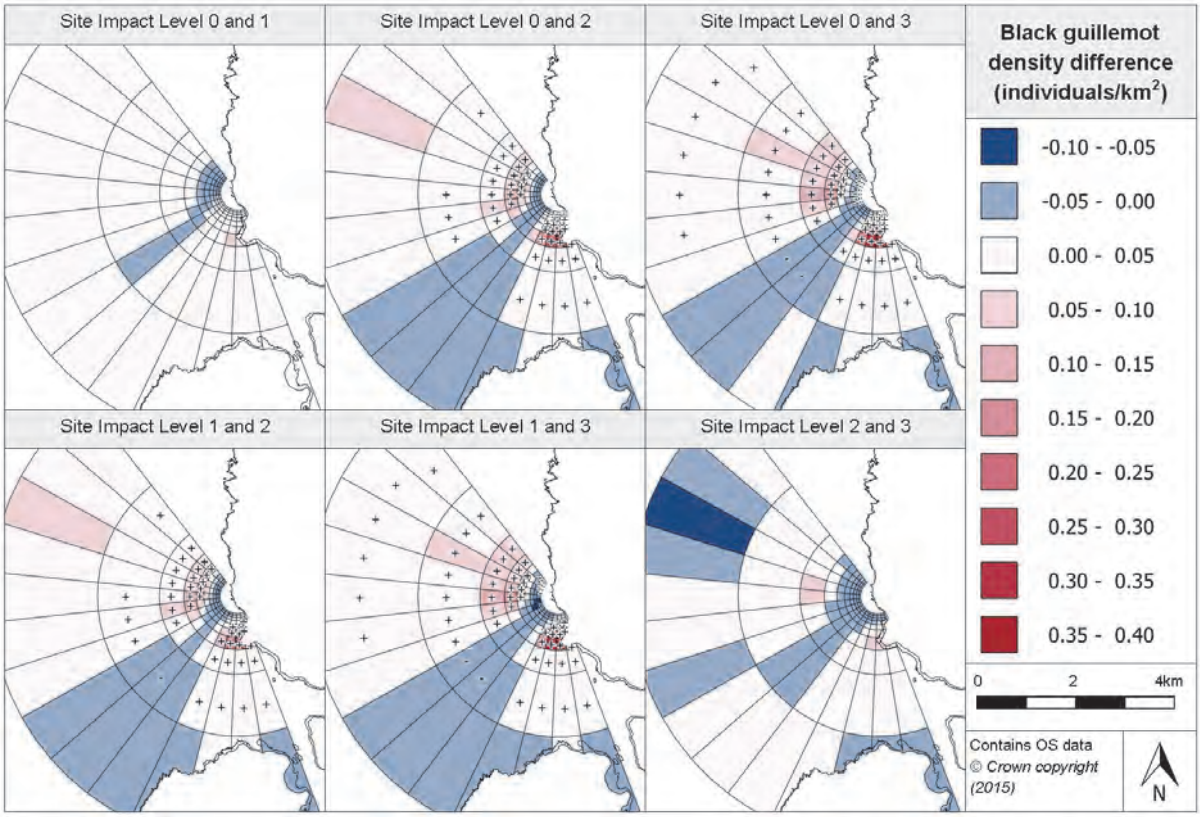

Figure 4.5.15. Density differences between black guillemot site impact level prediction surfaces at Billia Croo

As can be seen in Figure 4.5.15, there is very little estimated density difference between SIL-0 (baseline conditions) and SIL-1 (when device-associated infrastructure is installed). In the outer grid bands, the majority of the grid cells show a slight increase in estimated density; however, none of these are found to be significant. Grid cells B7 and C6-C7 are the only cells within the outer grid bands that appear to have a density decrease modelled. In terms of the inner grid bands, an area to the north of the inner bands shows a density decrease between 0.00 and 0.05 individuals/km^2. The remainder of the inner grid bands show a slight increase in density with the introduction of the infrastructure when compared to baseline conditions. Grid cell D11 sees a larger density increase as compared to the surrounding grid cells (0.10-0.15 individuals/km^2).

When considering the change in density between SIL-0 and SIL-2 (when devices are in place but not operational), there is an increase in density expected in the northern cells within the outer grid bands, see Figure 4.5.15. Grid cells C0-C6 have all been deemed to have significantly positive change in density as well as grid cells B0 and B4-B6. There is a decrease in density expected in cells in the south-west of the observation grid; however, none of these changes are significant. Grid cells B10-B13 and C10-C13 are all marked as having a significant increase in density although this increase is only slight (0.00-0.05 individuals/km^2). In terms of the inner grid cells (Figure 4.5.16), there appears to be an increase in density in the northernmost grid cells extending to the middle of the observation grid around grid band D, and another increase in density in the south and south-east of the inner grid cells. Many of the grid cells where a density increase is expected have been marked as showing a significant change, whereas none of the grid cells within the inner grid cells that show a density decrease have been marked as significant. The grid cells showing a negative change in density are in the northern half of grid bands G-J in addition to grid cells D7-D8, E7-E8 and F6-F8 (Figure 4.5.16).

In terms of the change in density between SIL-0 and SIL-3 (when devices are present and operational), there is a marked density increase in the grid cells in the northern half of the outer grid bands. The change in the majority of these northern grid cells has been deemed significantly positive (Figure 4.5.15). There is also an area to the south-east where an increase in density is expected and most of these cells have been marked as significant. Similar to the pattern seen between SIL-0 and SIL-2, there continues to be a line of grid cells in the south-west with a decrease in density (A7-A8, B7-B9, C7-C8). This south-west line showing a negative density change is also present within the inner grid bands and extends to the northern half of grid bands G-J (as observed between SIL-0 and SIL-2). However, this reduction in density is expected to be greater in some cells, with a reduction of up to 0.10 individuals/km^2 in some cells. As for the density change between SIL-0 and SIL-3, there are areas to the north and south-east within the inner grid cells where an increase in density is expected, see Figure 4.5.16. The change is significant in the majority of these, with a much greater increase in density estimated in grid cells D11-D13 and E12-E13 and grid cell D11 having a increase of 0.40 individuals/km^2.

Similar to the change in density between SIL-0 and SIL-2 and SIL-0 and SIL-3, there are areas to the north and south-east where an increase in density is expected and a section towards the south-west of the observation grid where a decrease in density is expected (Figure 4.5.15). The density increase is deemed significant in fewer grid cells in the outer grid bands. None of the inner grid cells where a density decrease is anticipated are marked as significant, as shown in Figure 4.5.16. An increase in density is again expected in the north and south-east of the inner grid bands, some of which have the change marked as significant. All the grid cells where a test berth is located show a positive change in density for SIL-0 to SIL-3 but not all these grid cells are deemed as statistically significant.

A similar pattern in density differences is observed between SIL-1 and SIL-3, with an increase in density in the north and south-east and a decrease towards the south-west and within the northern part of the inner grid bands. The number of cells in the outer grid band estimated to have a density decrease increases, with more cells in the far south being marked as negative, as seen in Figure 4.5.15. The cells where a density reduction is expected are not marked as significant. Nearly all the cells in the north of the outer grid bands are marked as having a significant increase in density as well as cells B10-B13 and C10-C13. The distribution of density differences within the inner grid cells is very similar to that modelled between SIL-0 and SIL-3 (Figure 4.5.16), with significant decreases estimated in the north-eastern corner of grid bands G-J. Significant increases in density are again predicted in the north-western and south-eastern corners of the inner grid bands.

When considering the change in density between SIL-2 and SIL-3, the majority of the grid cells are expected to see an increase in density except in a few locations. In the outer grid band A, there is an area of density decrease in the north, far south and one grid cell in the south-west (Figure 4.5.15). A density decrease is expected in the south-west region which exhibited similar decreases between the other site impact levels, SIL-2 and SIL-3. None of the cells in the outer grid bands are deemed to have significant changes. Within the inner grid bands, the majority of the grid cells are expected to have an increase in density, see Figure 4.5.16. All of grid bands H-J are expected to experience a reduction in density, together with the majority of grid bands E, F and G. Again, none of the cells within the inner grid bands are marked as having significant changes in density.

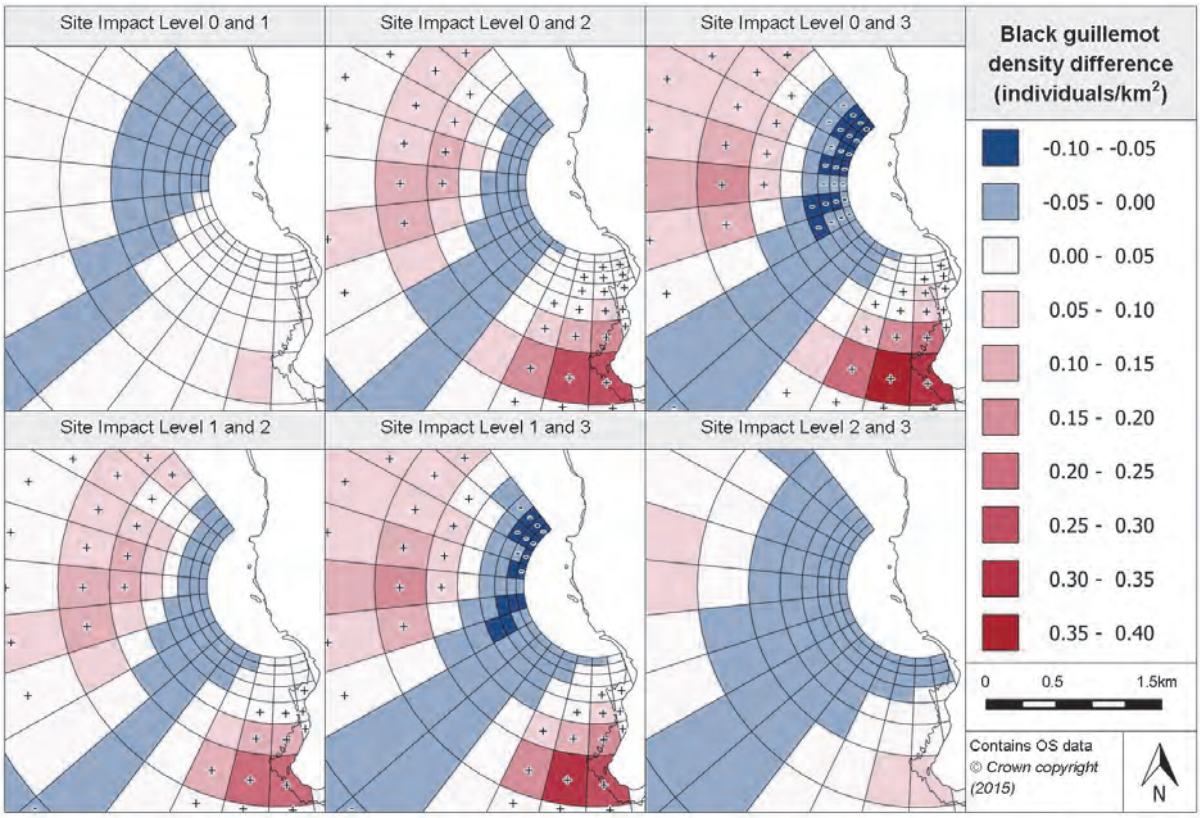

Figure 4.5.16. Density differences between black guillemot site impact level inner prediction surfaces at Billia Croo

4.5.2.7 Density change with distance from potential impact location

Due to large variability in the predictions for this species, it was not possible to produce a figure showing how the density difference between the predictions for each site impact level varies with increasing distance from a potential impact location.

4.5.2.8 Discussion

Black guillemots are a common species from the auk family found at Billia Croo. The model developed for them incorporates five significant terms. Key factors such as distance from land and month appear to be important controls on their distribution. The prediction surface for each site impact level using the environmental conditions when the greatest number of black guillemot observations are made, shows similar results to the common guillemot predictions in that there is a clear disparity in distribution with much higher density predictions in the inner grid cells, within 2km of the observation vantage point, as compared to the outer grid cells. All site impact levels exhibit a similar distribution within the inner grid with one cluster located 1-2km west of the cliffs at Black Craig, and the other extending approximately 1km westwards from Breck Ness. There is a general increase in density for the cluster offshore of Breck Ness with increasing site impact level, whereas the cluster west of Black Craig appears to move slightly westwards (~500m) with increasing site impact level (SIL-1, SIL-2 and SIL-3).

All the grid cells where test berths are located show a positive change in density from baseline conditions to the conditions pertaining when devices are installed and operational, but not all of the results in these grid cells are deemed to be statistically significant.

4.5.3 Atlantic puffin (Fratercula arctica)

4.5.3.1 Species overview

Atlantic puffins (*Fratercula arctica*) are regularly sighted at Billia Croo, and have been modelled separately as well as within a wider model for the auk family. The following section discusses the results from the modelling. Atlantic puffins' distribution and behaviour are summarised in Section 4.3.6.1 above.

4.5.3.2 Data summary

Atlantic puffins tend to be a seasonal species and therefore are only seen periodically throughout the year at Billia Croo. Table 4.5.7 below provides a summary of the raw data. This includes information on the number of observations and typical group size across each of the site impact levels. It is worth highlighting the greater number of observations made at site impact level 3 when compared to the other site impact levels. This is likely to affect the confidence in the predictions made at SIL-3.

Table 4.5.7. Summary of Atlantic puffin raw data

	Total	Site Impact Level 0	Site Impact Level 1	Site Impact Level 2	Site Impact Level 3
Number of observations	1891	182	139	350	1220
Minimum (group size)	1	1	1	1	1
Maximum (group size)	27	21	27	27	24
Mean (group size)	1.72	1.52	2.18	1.91	1.65
(s.d)	(1.87)	(1.62)	(3.50)	(2.28)	(1.46)

4.5.3.3 Model overview

Six terms remained in the final fitted model for Atlantic puffins. The GEE-based p-values could be obtained for each of these terms, five of which were deemed to be highly significant when predicting Atlantic puffin density across the survey area at Billia Croo (Table 4.5.8).

Table 4.5.8. GEE-based p-values for the terms in the final Atlantic puffin model for Billia Croo

Model term	ρ-value
Distance to land	<0.0001
Month	<0.0001
Year	<0.0001
Site impact	0.000209
Spatial surface	<0.0001
Spatial surface / site impact	<0.0001

The final fitted model for Atlantic puffins at Billia Croo includes the smooth term 'distance to land'. The model has estimated that Atlantic puffin density decreases with increasing distance from land. As already mentioned, Atlantic puffin is a seasonal species which tends to peak in abundance in Orkney between May and July. Figure 4.5.17 below clearly shows how the model has captured this seasonality, with heightened densities expected between April and August.

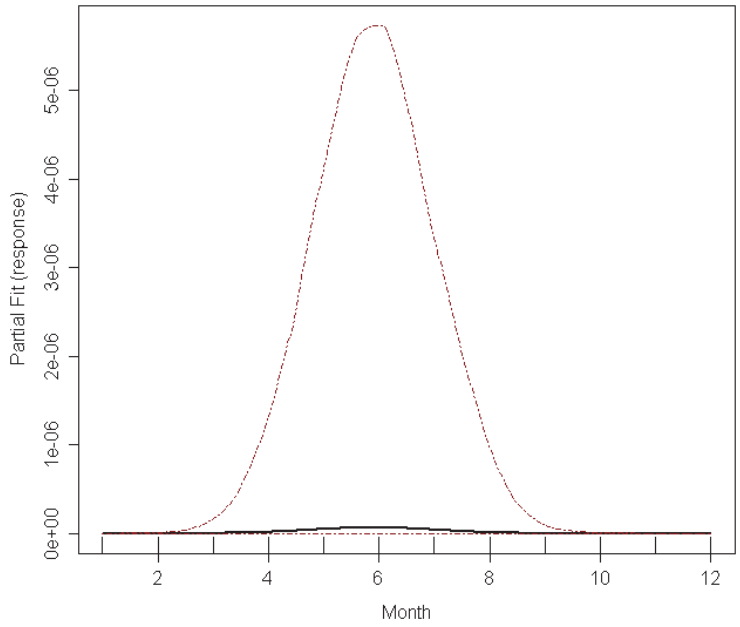

Figure 4.5.17. Estimated partial relationship of month against log(density) for Atlantic puffin at Billia Croo. The red lines represent 95% confidence intervals about the estimated relationship and the tick marks show where the data lie in the covariate range.

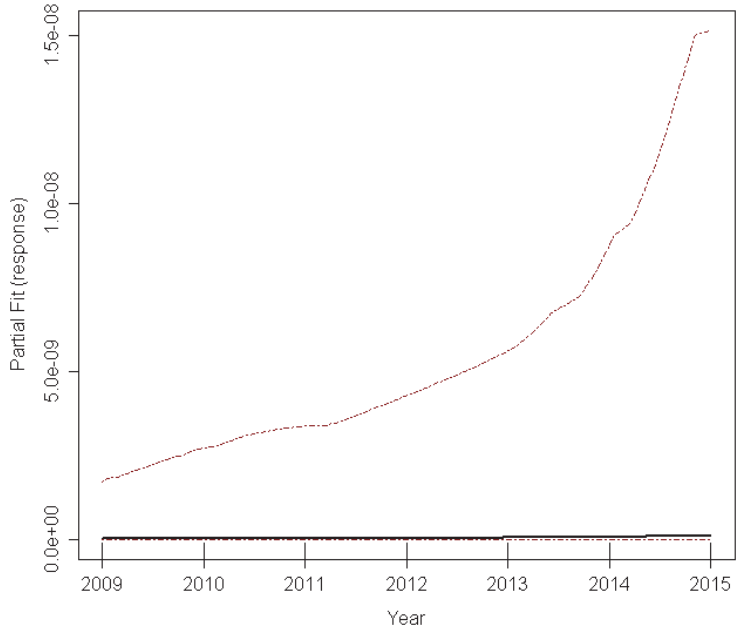

Figure 4.5.18. Estimated partial relationship of year against log(density) for Atlantic puffin at Billia Croo. The red lines represent 95% confidence intervals about the estimated relationship and the tick marks show where the data lie in the covariate range.

'Year' has also been included in the final fitted model, and the modelled relationship between puffin density and year is shown in Figure 4.5.18. The model has estimated that Atlantic puffin density has increased as the observations programme has proceeded, with the

greatest abundances predicted for 2015. The model expects the rate to increase exponentially over the course of the programme.

In addition to the above terms, a spatial surface was also able to be fitted for the final model. Four knots were used when fitting the model. An interaction term (site impact/spatial surface) was also fitted and found to be statistically highly significant.

4.5.3.4 Density predictions and uncertainty estimate

The final fitted Atlantic puffin model contained a spatial surface, allowing prediction surfaces across the observation grid to be created. The environmental covariates contained within the model were fixed at certain levels as discussed in Appendix 5. As with the black guillemot model, due to anomalies in the Atlantic puffin data, it was necessary to reduce the number of iterations in the bootstrap; 875 iterations were implemented rather than the 1000 carried out for most other species/groups. Figure 4.5.19 provides the prediction surfaces for each site impact level and Figure 4.5.20 gives an insight into the prediction surfaces at the inner grid cells. As expected, there are differing levels of uncertainty underpinning each prediction. Therefore, the associated CV values for the entirety of the prediction surfaces are provided in Figure 4.5.21 and Figure 4.5.22.

Reference should be made to Figure 2.1.9 and Figure 2.1.10 for the grid cell labelling system.

Overall, it is clear from Figure 4.5.19 that there is very low Atlantic puffin density estimated in the outer grid cells as compared to the inner grid cells across each site impact level.

At SIL-0, the density in grid bands A-C is 0.00-0.05 individuals/km^2 (Figure 4.5.19), whereas within the inner grid bands, generally higher densities are estimated. As seen in Figure 4.5.20, there is a cluster of higher densities in the northern region of the observation grid particularly around grid cells G2-G5, with the highest density within these grid cells expected at grid cell G3 - 0.35 individuals/km^2.

A similar distribution of densities is estimated at SIL-1 to that for SIL-0, as shown in Figure 4.5.19. Again, the density in the outer grid cells is not expected to be greater than 0.05 individuals/km^2. Within the inner grid cells (Figure 4.5.20), higher densities are estimated in the northern half of the grid bands. There is a particular peak in density in grid cells G3-G5 which slowly subsides with increasing distances from these cells.

For SIL-2, the Atlantic puffin estimated density distribution is slightly different. In grid bands A and B, Atlantic puffin density is anticipated to be less than 0.05 individuals/km^2. However, as can be seen in Figure 4.5.19, in grid band C the density is expected to range between 0.00 and 0.15 individuals/km^2 across the cells. Within the inner grid cells (Figure 4.5.20), the cluster of grid cells where there are higher densities expected is not as defined as that modelled for SIL-0 and SIL-1. The three south-easternmost grid cells in each inner grid band have a estimated density not exceeding 0.05 individuals/km^2. In addition to these cells, the density for the innermost grid band (J) again does not exceed 0.05 individuals/km^2. For the other cells within the inner grid cells, the estimated density varies greatly, with the majority of density predictions between 0.05-0.15 individuals/km^2. Grid cell E0 has a particularly high density with 0.30 individuals/km^2 expected.

At a glance, it appears that the lowest densities are estimated at SIL-3. From Figure 4.5.19, it is clear that Atlantic puffin density within the outer grid bands is not expected to be higher than 0.05 individuals/km^2, with the exception of grid cells C0, C4 and C5 which have expected densities of 0.05-0.10 individuals/km^2. Within the inner grid cells, see Figure 4.5.20, the density is expected to be less than 0.15 individuals/km^2 across all the grid cells.

The estimated density is less than 0.05 individuals/km^2 within either of the two innermost grid bands or for the majority of the inner grid cells in the south (with the exception of D9-D10 and E9-E10). There is a cluster of densities between 0.05-0.15 individuals/km^2 in a similar position as the cluster described under SIL-0.

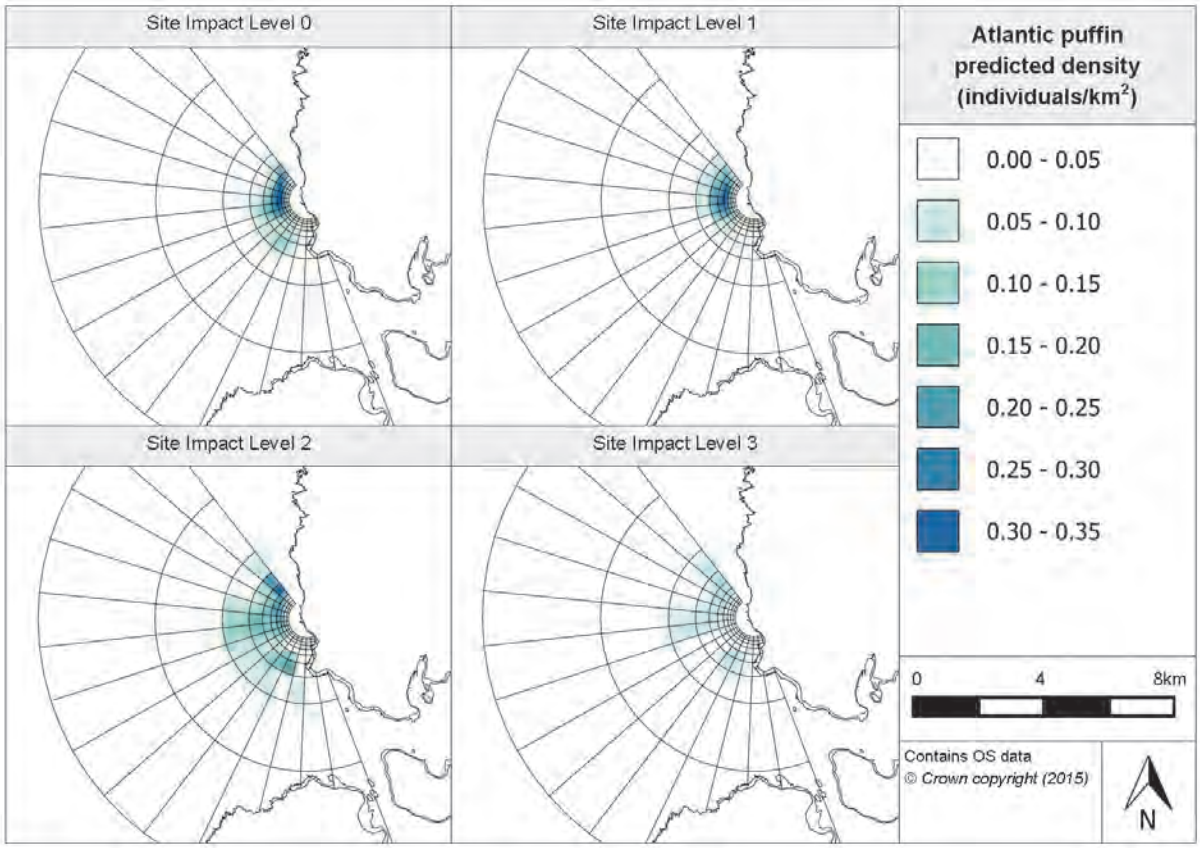

Figure 4.5.19. Prediction surfaces for Atlantic puffin density at Billia Croo for each site impact level

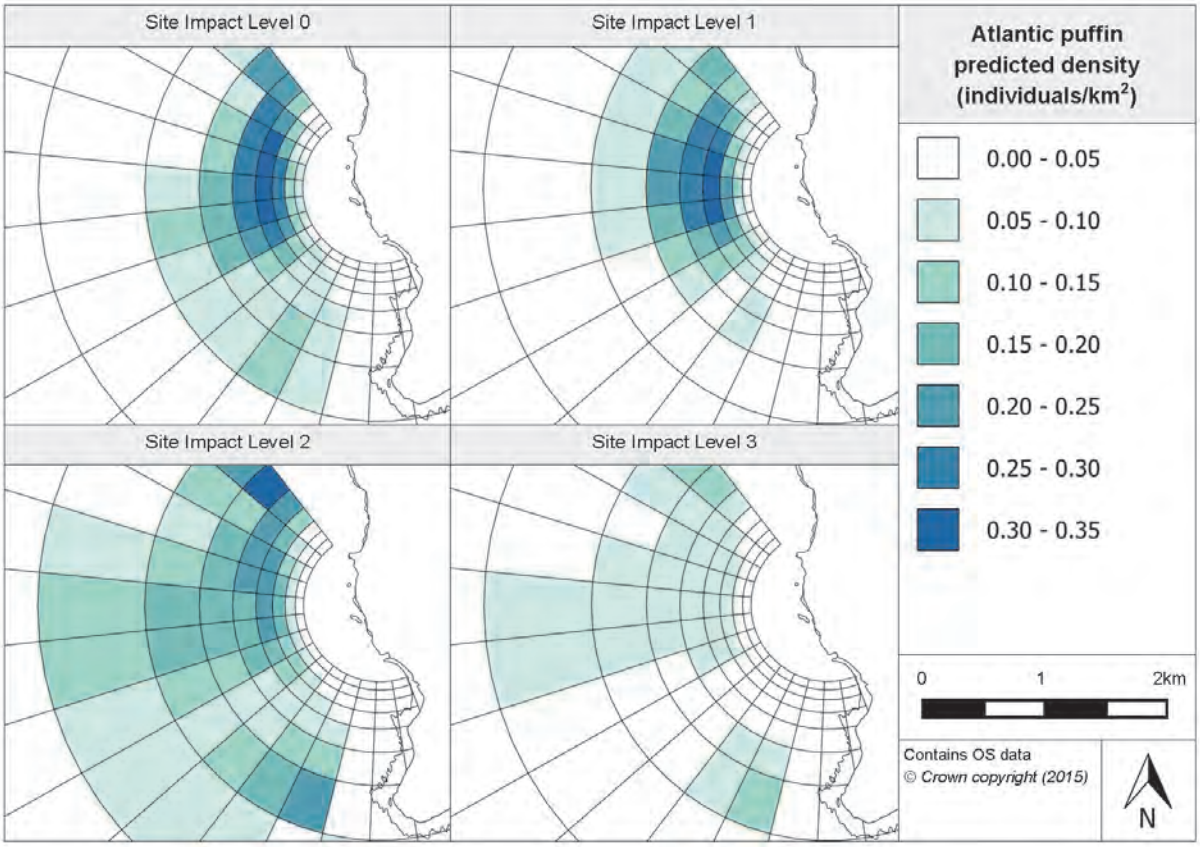

Figure 4.5.20. Inner prediction surfaces for Atlantic puffin density at Billia Croo for each site impact level

In Figure 4.5.19 and Figure 4.5.22, the associated CV values are provided for each of the density predictions.

The CV values for SIL-0 suggest that the estimated density in the majority of the cells in the outer grid bands A and B is too low to provide feasible CV values. B6 and B7 are the only two grid cells with CV values, both of which are very high, suggesting very high uncertainty in these density predictions. As seen in Figure 4.5.21, the majority of grid band C has CV values between 1.50 and 3.00, which suggest high variability in the predictions, whereas the majority of the inner grid bands (Figure 4.5.22) have CV values between 0.00 and 1.50 which suggest high-medium precision in the density predictions for these grid cells. It should be noted that, in the last two grid cells in each of the inner grid bands, CV values are unavailable; this suggests there is a lack of raw data in these grid cells, resulting in very low density predictions leading to incalculable CV values.

For SIL-1, the CV values suggest even higher uncertainty in the density predictions. The CV values are not available for all of the density predictions in grid bands A and B, see Figure 4.5.21. In grid band C, the southern cells have CV values of greater than 7.50 whereas, in the northern cells, the CV values are between 1.50 and 6.00 (suggesting more precision in these predictions compared to the southern cells). As can be seen in Figure 4.5.22, the majority of cells in the inner grid bands have CV values below 1.50, suggesting low uncertainty in these results. Again, the south-westernmost grid cells in the inner grid bands do not have CV values available.

For SIL-2, CV values are available for more grid cells (see Figure 4.5.21). Whilst the majority of grid band A continues to have CV values unavailable, the southern half of grid

band B has CV values between 0.00 and 4.50 suggesting that, in some of these cells, there is fairly high precision with respect to the density predictions. In addition, the southern half of the grid band has CV values below 1.50 suggesting low uncertainty in the density predictions in this area of the observation grid. In terms of the inner grid cells (Figure 4.5.22), nearly all of them have CV values below 1.50, again suggesting low uncertainty with respect to the density predictions. It is worth noting that, in the last two grid cells of each the inner grid bands (the most south-easterly cells), the CV values remain unavailable which continues to suggest a lack of Atlantic puffin raw observations in these grid cells.

For the final site impact level, SIL-3, even fewer grid cells have unavailable CV values. This suggests that there were more raw observations at this site impact level and therefore more evidence upon which to base predictions. As can be seen in Figure 4.5.21, the greatest abundance of unavailable CV values is in the northernmost grid cells. In the southern region of the outer grid bands, apart from a few grid cells where the CV values are unavailable, the CV values range between 0.00 and 3.00. For the inner grid bands (Figure 4.5.22), all of the grid cells have CV values between 0.00 and 1.50 suggesting high precision in the density predictions. In the last two grid cells of the inner grid bands (again the south-easternmost cells), the CV values remain unavailable, as observed for the other site impact levels.

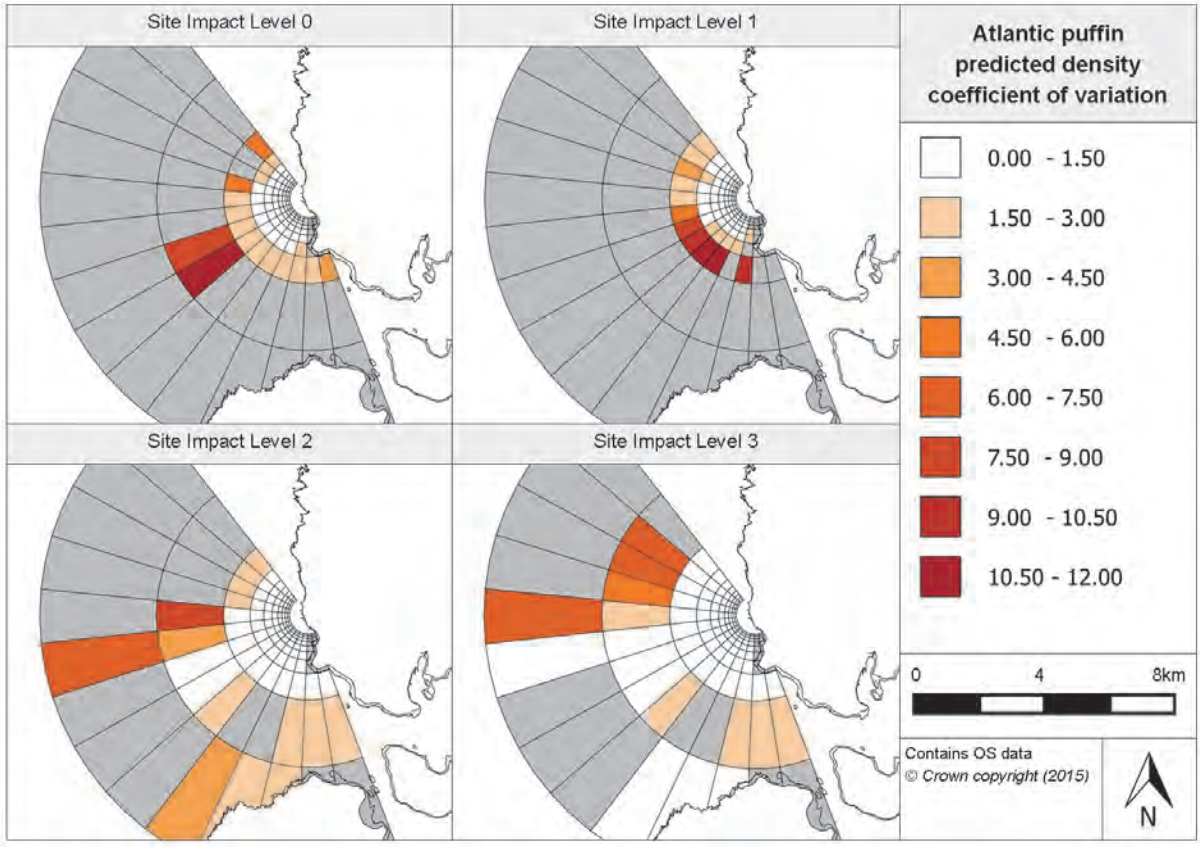

Figure 4.5.21. Associated coefficient of variation values for Atlantic puffin density prediction surfaces at Billia Croo

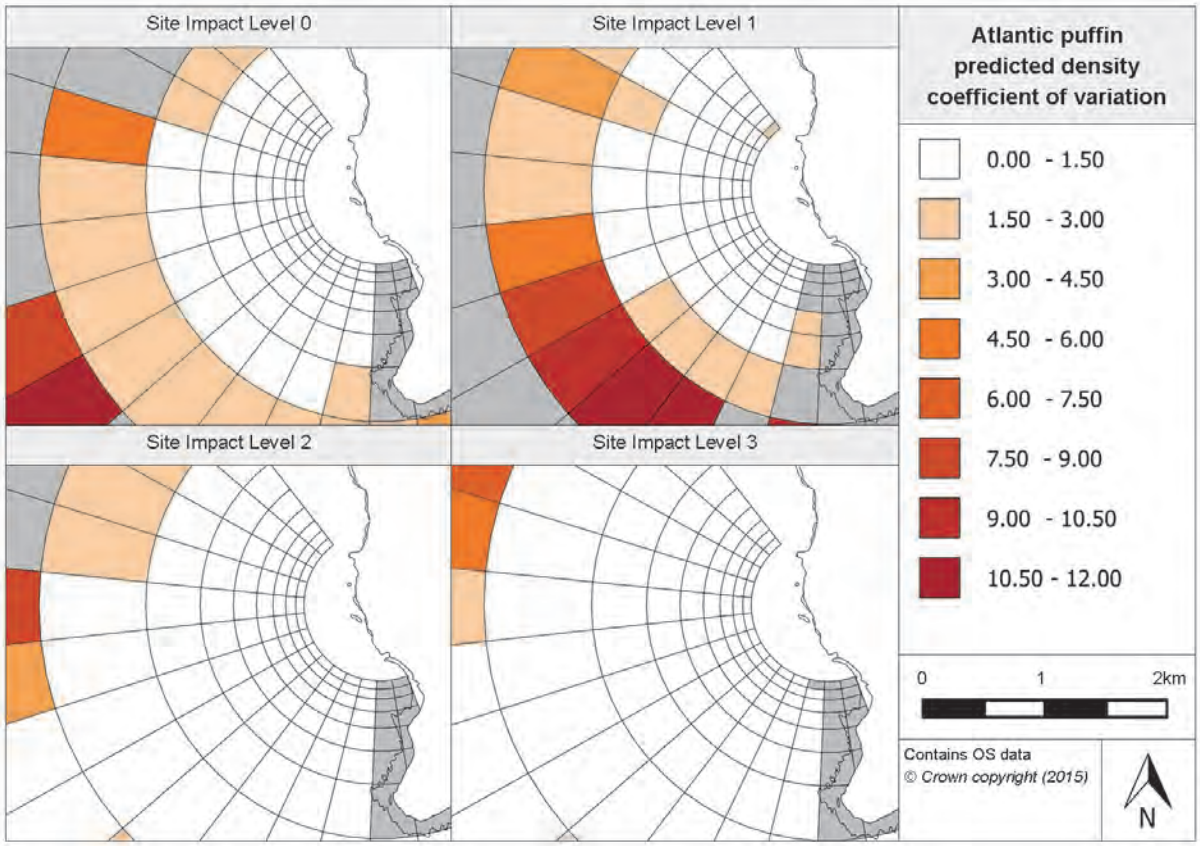

Figure 4.5.22. Associated coefficient of variation values for Atlantic puffin inner density prediction surfaces at Billia Croo

4.5.3.5 Relative abundance estimations

Relative abundance estimates have been able to be produced using the fitted Atlantic puffin model. Such estimates have been generated for each survey month by setting the environmental covariates to certain values (these are outlined in Appendix 5). By combining the survey month estimates, it was possible to produce seasonal predictions. These, alongside their associated CIs, are provided in Table 4.5.9. It should be noted that these are relative estimates as only surface visible observations have been used in the formation of these models.

Table 4.5.9. Relative abundance for Atlantic puffins during each season (associated confidence intervals are provided in brackets)

Year	Season			
	Winter (Dec, Jan, Feb)	Spring (Mar, Apr, May)	Summer (Jun, Jul, Aug)	Autumn (Sep, Oct, Nov)
2009	-	6.74 (0.29, 19.25)	11.55 (1.13, 26.21)	0.08 (0.00, 1.11)
2010	0.02 (0.00, 0.49)	10.20 (0.44, 38.25)	17.86 (2.91, 52.56)	0.16 (0.00, 1.26)
2011	0.01 (0.00, 0.16)	12.17 (0.26, 69.24)	25.31 (2.53, 95.32)	0.23 (0.00, 2.03)
2012	0.02 (0.00, 0.83)	13.18 (0.54, 72.33)	25.31 (4.65, 92.60)	0.26 (0.00, 2.22)
2013	0.02 (0.00, 0.29)	9.60 (0.45, 25.12)	16.82 (2.81, 34.09)	0.38 (0.00, 3.32)
2014	0.07 (0.00, 1.10)	26.60 (1.12, 157.45)	46.15 (6.84, 205.78)	0.43 (0.00, 4.54)
2015	0.10 (0.00, 1.83)	52.99 (2.37, 220.11)	-	-

As expected, Atlantic puffin show high seasonal peaks in abundances, with much greater abundances exected in spring and summer compared to autumn and winter. As can be seen in Table 4.5.9, the greatest abundances are expected during the summer, with sometimes twice the abundance as that modelled for spring. The annual predictions identify the greatest abundances during 2014 and the years with the lowest abundances are anticipated to be 2009 and 2013.

Further to the above table, the relative abundance predictions are given for each site impact level in Appendix 7, which should highlight any relationships between site operational status and relative abundance predictions. The seasonal peaks in abundance during spring and summer of each year are depicted clearly in Appendix 7.

As already mentioned, the prediction surfaces presented in Figure 4.5.19 are for the optimum environmental conditions for Atlantic puffin observations at Billia Croo (i.e. conditions in which the most number of observations were made). In addition to these surfaces, Atlantic puffin prediction surfaces for typical surveying conditions in January and July have been provided in the Marine Scotland Information portal. Inevitably, these surfaces show the species' high seasonality, with density predictions multiple times larger (over 1000) in July as compared to January. It is unlikely that there have been many, if any, sightings of puffins in January at Billia Croo upon which to base the predictions.

4.5.3.6 Spatially-explicit change

The difference in density predictions for each site impact level could be calculated to understand the extent of any spatially-explicitly changes in species abundance or distribution. The significance of any Atlantic puffin density variations with the changing of site-wide operational status has also been investigated using the 95% CIs for each of the predictions. Unlike the common guillemot and black guillemot models, 'year' is included in the final fitted Atlantic puffin model. This has resulted in the density difference for the least and most variable years being presented (2010 and 2014, respectively); the density difference surface for 2010 is presented in Figure 4.5.23 and for 2014 can be found in Appendix 8, and their respective inner surfaces are provided in Figure 4.5.24 and Appendix 8, respectively.

From Figure 4.5.23, it appears that, between SIL-0 (baseline conditions) and SIL-1 (when device-associated infrastructure is installed), there is predominately a reduction in Atlantic puffin density in the outer grid cells, with the exception of grid cells C0-C3 where a slight increase in density, 0.03 individuals/km^2, is estimated. None of the density changes within the outer grid cells have been deemed significant. Within the inner grid cells, see Figure 4.5.24, there is a cluster where an increase in density is anticipated with the introduction of device-associated infrastructure as compared to baseline conditions. This cluster of positive density changes is around grid cells E2-E4 where an increase of 0.03-0.06 individuals/km^2 is expected. Otherwise, a reduction in density is anticipated in all the other inner grid cells, mostly between 0.00 and 0.03 individuals/km^2. A reduction of between 0.03 and 0.06 individuals/km^2 has been modelled in grid cells F0, G0-G1 and H2. Similar to the outer grid cells, none of the density changes in the inner grid cells are expected to be significant.

Between site impact levels SIL-0 and SIL-2 (when devices are in place but not operational), a positive change in Atlantic puffin density is estimated in most of the cells. From Figure 4.5.23, it is clear that, in the outer grid cells, nearly all of the cells see an increase in density of between 0.00 and 0.03 individuals/km^2. Grid cells C0 and C4-C6 are expected to exhibit a greater increase in Atlantic puffin density, with a change up to 0.06 individuals/km^2 expected. Note that the changes in the cells in the northern half of grid bands B and C are deemed to be significant as well as in cells A4-A5 and C9-C12. However, there is a reduction in density of up to 0.03 individuals/km^2 in grid cells A7-A10. For the inner grid cells

(Figure 4.5.24), there is a cluster of grid cells positioned around G2-G6 and H2-H6 where a reduction in density of up to 0.06 individuals/km^2 is expected. Most of the rest of the inner grid cells are expected to have an increase in density from baseline conditions with the introduction of devices. The largest increases are estimated in grid cells D0 and D10 where an increase of up to 0.09 individuals/km^2 is modelled. Within the inner grid cells, only four grid cells have had their change is density deemed as significant; these are located in grid cells D1-D3 and D11.

Similar to the difference between SIL-0 and SIL-2, the density difference between SIL-0 and SIL-3 (when devices are present and operational) in the outer grid bands is predominantly positive (Figure 4.5.23). There are only five grid cells in the three outermost grid bands where a reduction in density is anticipated, and this is not expected to be greater than 0.03 individuals/km^2. In the northern half of all three grid bands, the increase in density has been deemed significant in nearly all the grid cells. As can be seen in Figure 4.5.24, in the inner grid bands only eight grid cells have an estimated increase in density when operational devices are in place as compared to baseline conditions. The rest of the grid cells in the inner grid bands are estimated to have a reduction in density which appears to be at its greatest around grid cells G2-G6 and H3-H5 (with decreases in density of up to 0.12 individuals/km^2). The extent of the density decrease appears to reduce with increasing distance from these grid cells. In addition, the cells located in this cluster of density reductions have also had the changes in density deemed as significant There appears to be no correlation between changes in density for SIL-0 to SIL-3 and the location of test berths, as some berths are located in grid cells that show a positive change and others in grid cells showing a negative change, not all of which are significant.

When considering the change in density predictions between SIL-1 and SIL-2, the majority of grid cells have an increase in density estimated with the installation of devices compared to when just infrastructure was installed. From Figure 4.5.23, it is clear that a positive change in density is expected for all of the grid cells in the outer grid bands, with all but four grid cells having their increase in density deemed as significant. Within the outer grid cells, the largest increases in density are anticipated to be in grid band C, particularly in C5 where an increase of up to 0.09 individuals/km^2 is estimated. Within the inner grid bands, again the majority of grid cells are showing a positive change in density (Figure 4.5.24). There is a cluster of grid cells where a reduction in density is expected. These cells are located around grid cells F3-F5 and G3-G5; however, none of the reductions seen within these cells have been deemed significant. Grid cell E11 appears to have the largest increase in density across all grid cells, with an increase of up to 0.12 individuals/km^2 estimated. The last four grid cells within each of the inner grid bands (i.e. the south-easternmost grid cells) have all been marked as significantly positive change. In addition to these grid cells, six additional cells in grid band D have been marked as significantly positive.

Between site impact levels SIL-1 and SIL-3 (devices installed and operating), most of the grid cells are expected to have an increase in density. As can be seen in Figure 4.5.23, all of the cells in the outer grid bands are anticipated to have a positve change in density and, in all but two grid cells, this change in density has been deemed signficant. This increase in density has been predicted to be no more than 0.03 indivduals/km^2, with the exception of grid cell C0 where the increase has been estimated to be 0.03-0.06 individuals/km^2. From Figure 4.5.24, there is a clear cluster of grid cells in the inner grid bands where a reduction in density is anticipated. This cluster appears to be centred around grid cells F2-F5 and G3-G5. Most of the cells within this large cluster have had their negative change in density deemed to be significant. Otherwise, the south-easternmost cells of the inner grid bands have been modelled to experience a positive change in density, with seven grid cells having their increase in density deemed signficant.

When comparing the density difference between SIL-2 and SIL-3, it appears that a reduction in density is expected in the majority of grid cells. Looking at the outer grid cells in particular, Figure 4.5.23, it appears that, except from cell B0, all of the grid cells where a density increase is expected to lie between grid cells A5 and A11. None of the changes in these cells have been deemed significant. In all of the other grid cells, the change in density has been estimated to be negative. The only cells in the outer grid bands with a density difference deemed significant are located between cells C5 and C10. In terms of the inner grid bands (Figure 4.5.24), all of the grid cells are expected to have a reduction in density. In addition, density decreases within these grid bands are deemed significant. The level of density decrease varies across the grid cells from 0.00 to 0.09 individuals/km^2.

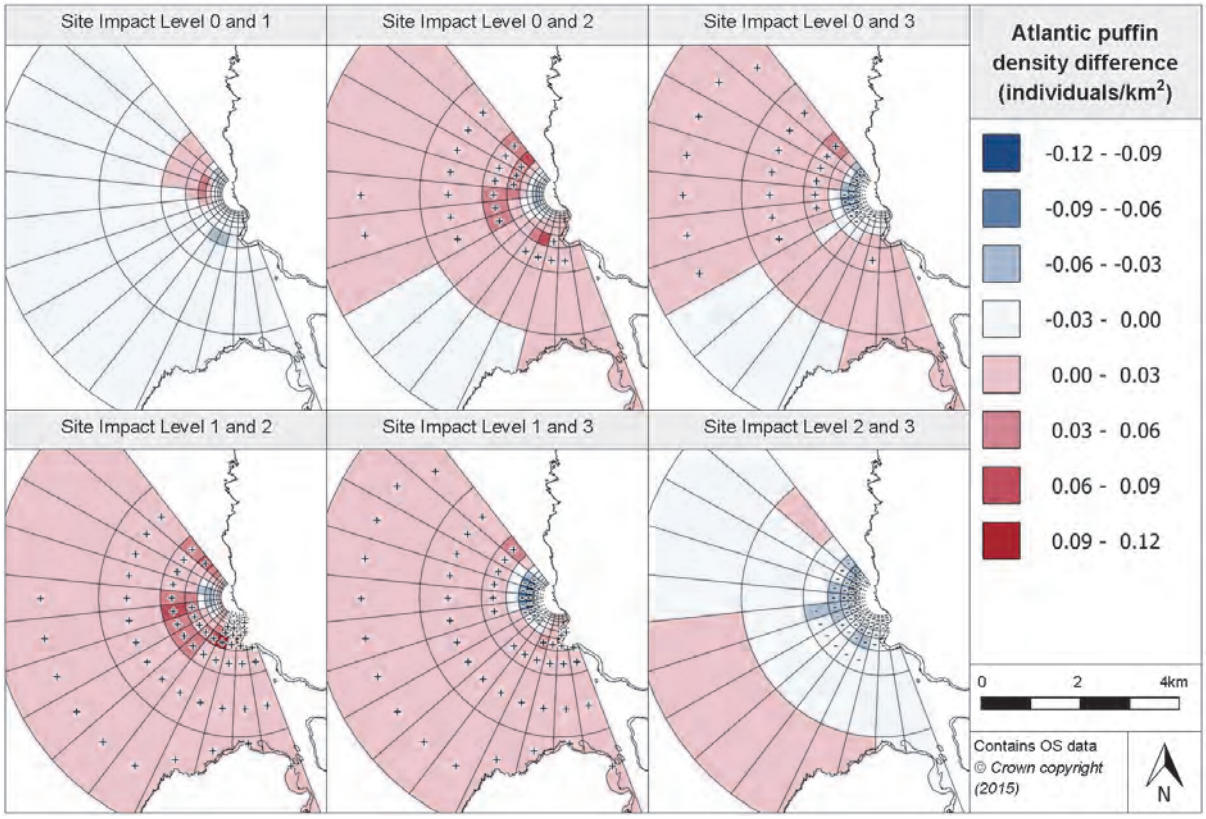

Figure 4.5.23. Estimated density difference between various site impact levels for Atlantic puffin during 2010 (year with least variation) at Billia Croo

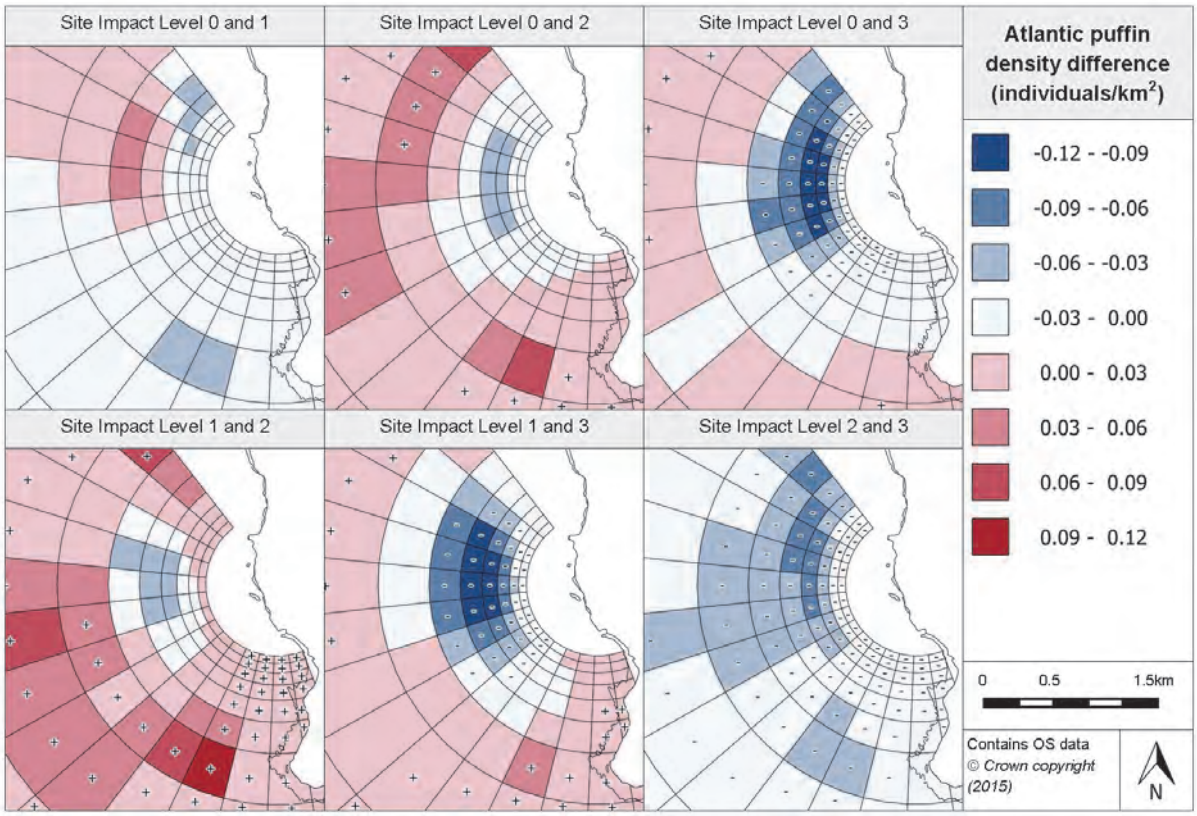

Figure 4.5.24. Density differences between Atlantic puffin site impact level inner prediction surfaces during 2010 (least variable year) at Billia Croo

4.5.3.7 Density change with distance from potential impact location

Using the spatially-explicit change predictions, it has been possible to show how the density differences between site impact levels changes with increasing distance from a potential impact location. Figure 4.5.25 demonstrates the changes in Atlantic puffin density difference with increasing distance from a single test berth at Billia Croo.

Between baseline conditions and SIL-1 and SIL-2, there is no clear trend in density difference visible. The upper and lower CIs are on either side of zero, therefore suggesting that there is no particular change in density. Between SIL-0 and SIL-3, at 1.2km to 2.3km, the upper confidence limit appears to be around zero, suggesting that the decrease in density estimated at this distance is likely to be significant. Otherwise, between SIL-0 and SIL-3 there is no clear trend in density difference.

When considering the density difference between SIL-1 and SIL-2, there appears to be a slight density increase within the first 300m. The lower CI then reduces to below zero suggesting that there is no clear density difference beyond 300m. Beyond 2.3km, density does not alter greatly from SIL-1 conditions.

The changing density difference between SIL-1 and SIL-3, and SIL-2 and SIL-3, is very similar. There is a gradual reduction in density with increasing distance from the impact location. The density difference is at its greatest at approximately 1.2-1.5km between SIL-1 and SIL-3 and 0.8-1.3km between SIL-2 and SIL-3. The extent of the difference then slowly subsides, returning to SIL-1 and SIL-2 conditions (respectively) at approximately 2.4km from the test berth. It is worth noting that, when the reduction in density between SIL-1 and SIL-3 is present, the upper confidence limit is above zero up to 1.3km away from the test berth. This would suggest that a reduction in density may not occur, whereas beyond this to 2.4km,

the upper confidence limit is around zero, suggesting a change that may be significant. Between SIL-2 and SIL-3, the reduction in density seen up to 2.4km away from the test berth is likely to be significant as the upper CI appears to be around zero.

It should be noted that, although there is a decrease in Atlantic puffin density is estimated to be in close proximity to this grid cell (containing a test berth), this same relationship is not apparent in the other grid cells that contain test berths (see figures in the Marine Scotland Information portal portal).

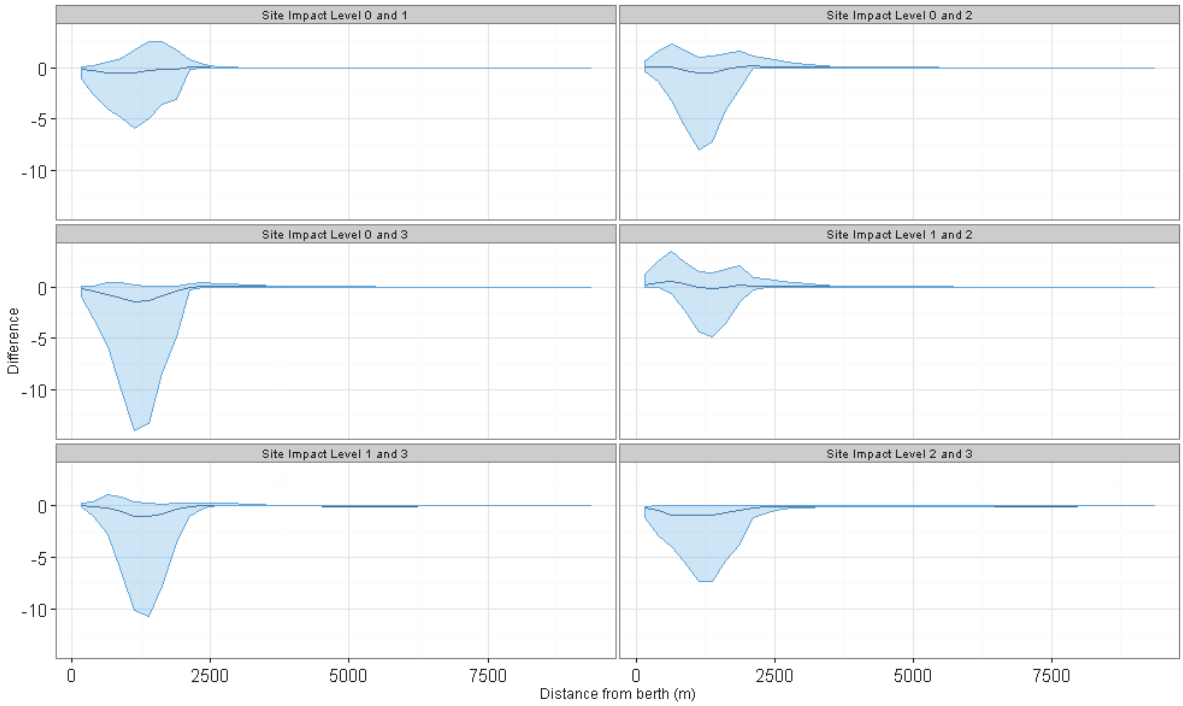

Figure 4.5.25. Density change between site impact levels with increasing distance from a potential impact location, with associated confidence intervals, for Atlantic puffin at Billia Croo

4.5.3.8 Discussion

Atlantic puffins tend to be a seasonal species and, therefore, are seen only periodically during the year at Billia Croo. The model developed for them has been fitted with five highly significant terms. Key factors such as distance from land and month appear to be important controls on their distribution. The higher densities are located predominantly within the inner grid cells west of the cliffs of Black Craig, with a smaller cluster west of Breck Ness. The grid cells within these clusters show varying increases and decreases in density, with the progression through site impact levels, but with an apparent overall reduction in density. As this general decrease in density is not estimated at every grid cell containing a test berth, there is no apparent correlation between the change in Atlantic puffin density with site impact level varying from SIL-0 to SIL-3 and the location of test berths. This is underlined by the fact that some berths are located in grid cells that have a positive change modelled and others in grid cells predicting a negative change, not all of which changes are deemed significant.

4.5.4 Northern gannet (Morus bassanus)

4.5.4.1 Species overview

The largest member of the gannet family and the largest seabird in the North Atlantic, the northern gannet is frequently spotted in small groups at Billia Croo. Northern gannets are known for forming large colonies on offshore islands and high cliffs (BirdLife International, 2015). There are two gannetries located ~60km west of Orkney on Sule Skerry and Sule Stack, and one of Orkney's Northern Isles, Westray, also has a colony (Murray *et al*., 2015). Typical diving behaviour for the species is plunge-diving, with northern gannets tending to dive from greater heights than other species observed at Billia Croo. Dives to depths of over 20m have been recorded and the birds are known to stay submerged for over 30 seconds. Their main prey are shoaling pelagic fish including species like herring (*Clupea harengus*), mackerel (*Scomber scombrus*), sprat (*Spattus sprattus*) and sandeel (*Ammodytes*). This highly seasonal species tends to breed between March and April and migrates south to the Mediterranean during winter (Carbonera *et al*., 2014e).

4.5.4.2 Data summary

Northern gannets are observed regularly at Billia Croo. The following table, Table 4.5.10, gives an overview of the raw data used in fitting the Northern gannet model. The data summary provides information for each site impact level including typical group sizes. It is worth highlighting the greater number of observations made at site impact level 3 when compared to the other site impact levels. This is likely to affect the confidence in the predictions made at site impact level 3.

Table 4.5.10. Summary of northern gannet raw data

	Total	Site Impact Level 0	Site Impact Level 1	Site Impact Level 2	Site Impact Level 3
Number of observations	5644	254	787	1415	3188
Minimum (group size)	1	1	1	1	1
Maximum (group size)	250	50	60	250	250
Mean (group size)	3.89	4.65	3.85	2.76	4.35
(s.d)	(9.81)	(7.60)	(7.33)	(8.87)	(10.81)

4.5.4.3 Model overview

GEE-based p-values were produced for each of the remaining terms in the final fitted model. Five terms were found to be highly significant and one term was significant at Billia Croo. A summary of these terms, and their associated p-values, are provided in Table 4.5.11.

Table 4.5.11. GEE-based p-values for the terms in the final northern gannet model for Billia Croo

Model term	ρ-value
Sea state	<0.0001
Year	0.0204
Month	<0.0001
Site impact	<0.0001
Spatial surface	<0.0001
Spatial surface / site impact	<0.0001

Sea state is one of the remaining terms in the model and is deemed to be highly significant when predicting northern gannet numbers at Billia Croo. The model predicts there to be a lower density of gannets when the sea state is 0 (calm) whereas, between sea state 1 and 4 (and above), there appears to be very little change in estimated density. Survey year has also been included in the final fitted model, and although only said to be significant (rather than highly significant) to the model, the model clearly predicts northern gannet numbers to reduce throughout the survey's duration. Peak abundances were expected to be obtained in 2009 with numbers slowly reducing until 2015, when fewest gannet numbers are anticipated to be recorded. As seen in Figure 4.5.26, the rate of reduction is estimated to be slightly higher in the early years of the survey.

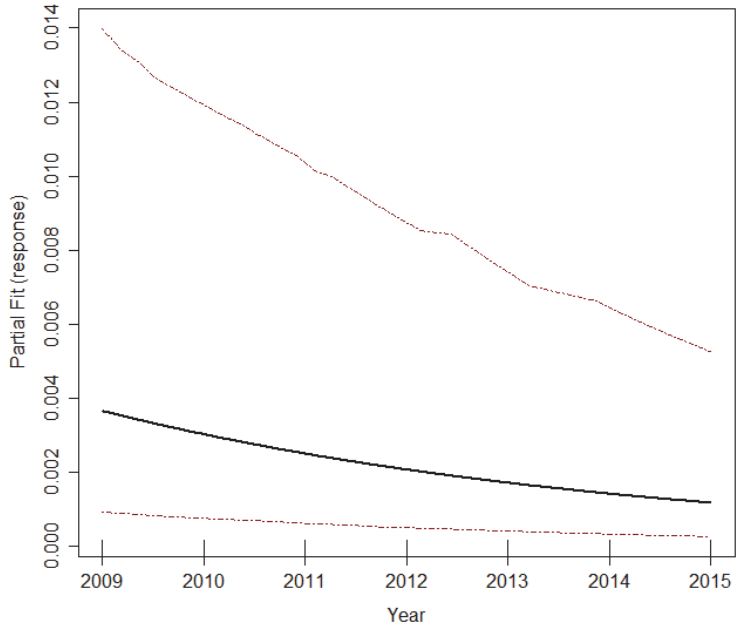

Figure 4.5.26. Estimated partial relationship of year against log(density) for northern gannet at Billia Croo. The red lines represent 95% confidence intervals about the estimated relationship and the tick marks show where the data lie in the covariate range.

Survey month has also been included in the final model and is deemed to be highly significant. It is estimated that highest northern gannet numbers will be observed between August and October and far fewer during their wintering season, between December and March.

A spatial surface was able to be fitted to the model and four knots were used during the fitting. Also included in the model, due to being statistically significant, was the interaction term (site impact/spatial surface).

4.5.4.4 Density predictions and uncertainty estimate

As the final northern gannet model contains a spatial surface, it has been possible to plot the modelled density surfaces for each site impact level. To be able to create the prediction surface, it is necessary to set conditions at specified levels. It was decided that the conditions in which the most northern gannet observations were made should be used, this is discussed further in Appendix 5. Using the prediction surfaces, density plots for each site impact level have been produced and are provided in Figure 4.5.27. Also provided is a plot showing only the inner grid bands, Figure 4.5.28. In addition to these plots, the associated

CV values provide an indication of the variability in the predictions, see Figure 4.5.29 and Figure 4.5.30.

Reference should be made to Figure 2.1.9 and Figure 2.1.10 for the grid cell labelling system.

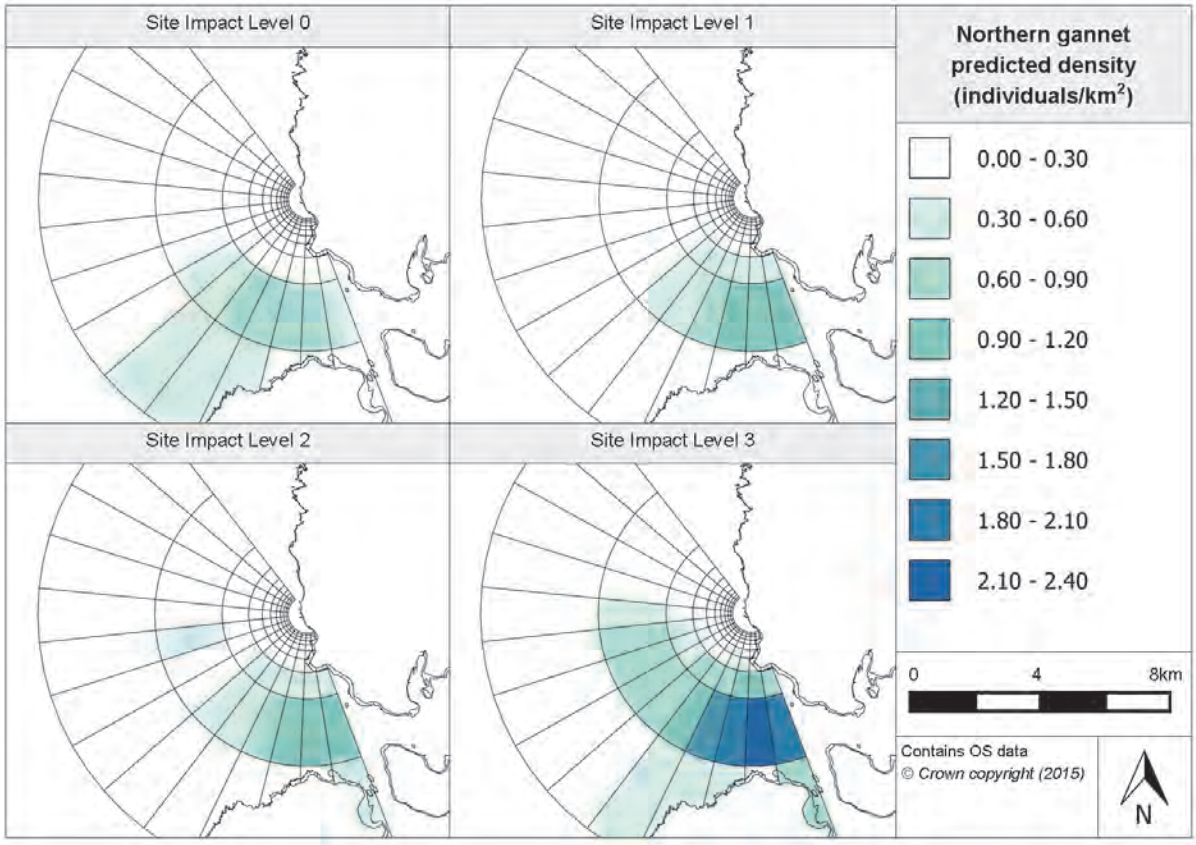

Figure 4.5.27. Prediction surfaces for northern gannet density at Billia Croo

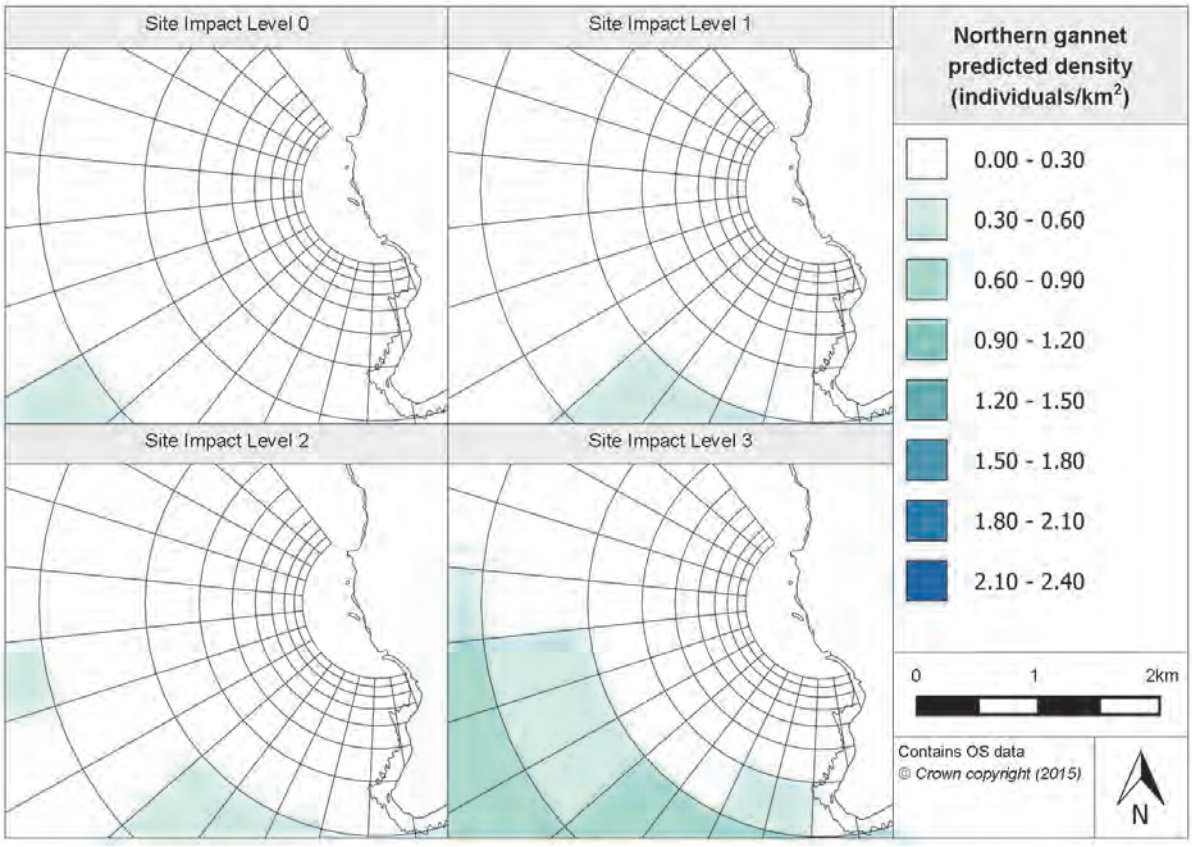

Figure 4.5.28. Inner prediction surfaces for northern gannet density at Billia Croo

At baseline conditions, it appears that there is a slight peak in density in the southern area of the survey grid, near to the island of Hoy. The peak exists in three grid cells (A8-A10) within the outermost band, one adjacent to Hoy (see Figure 4.5.27), and also in band B from grid cells B7 to B13, with the highest values (0.6-0.9 individuals/km^2) in cells B9-B12. Grid cells further landward (Figure 4.5.28), close to the observer, and those in the north of the observation area, show no signs of a peak in density. At SIL-1, there again appears to be a peak in density to the south of the observation vantage point in grid band B, as can be seen in Figure 4.5.27. The peak is most prominent in the grid cells that are at the entrance to Hoy Sound (grid cells B8-B13 and C8-C13), with highest densities estimated in three grid cells (B11-B13). When investigating Figure 4.5.28, it is clear that the low density predictions at SIL-0 are maintained at SIL-1.

The prediction surface under SIL-2 conditions appears to be very similar to that gained for SIL-1. As seen in Figure 4.5.27, greatest abundances continue to be observed in the grid cells at the entrance to Hoy Sound (B11-B13). Additionally, there is a slight peak in abundance in grid cell B5 that has not been present under baseline conditions nor at SIL-1. There is also higher density estimated for grid cell A13, adjacent to the north-eastern side of Hoy. Similar to the other site impact levels, there are no clear peaks in density within the inner grid cells (Figure 4.5.28).

For the prediction surface produced for SIL-3, the area where a heightened density can be observed is greater in size, and stretches further north and landward including grid cells D10 and D11 (Figure 4.5.27 and Figure 4.5.28). Peaks in density cover a slightly wider area than for SIL-2 and, under SIL-3 conditions, the highest densities across all the prediction surfaces are expected, with the greatest peak in grid cell B12 where 2.10-2.40 individuals/km^2 are estimated (and slightly lower densities in grid cells B10, B11 and B13 (1.50-2.10 individuals/km^2)).

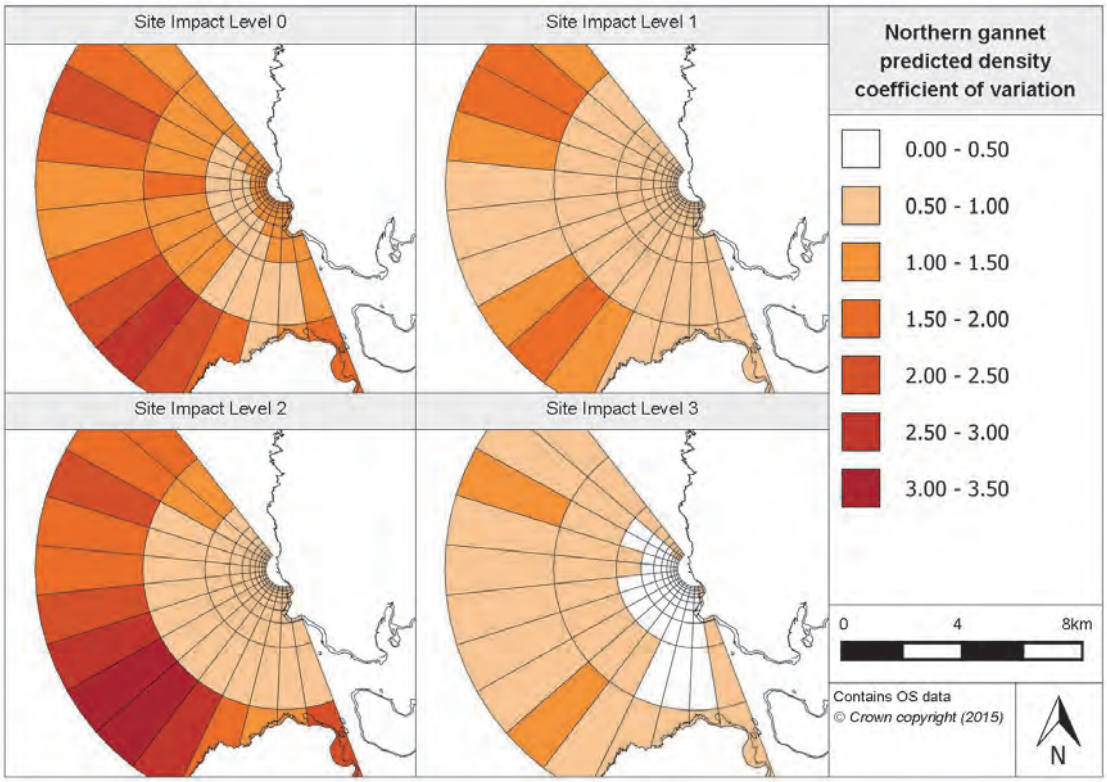

Figure 4.5.29. Associated coefficient of variation values for northern gannet density prediction surfaces at Billia Croo

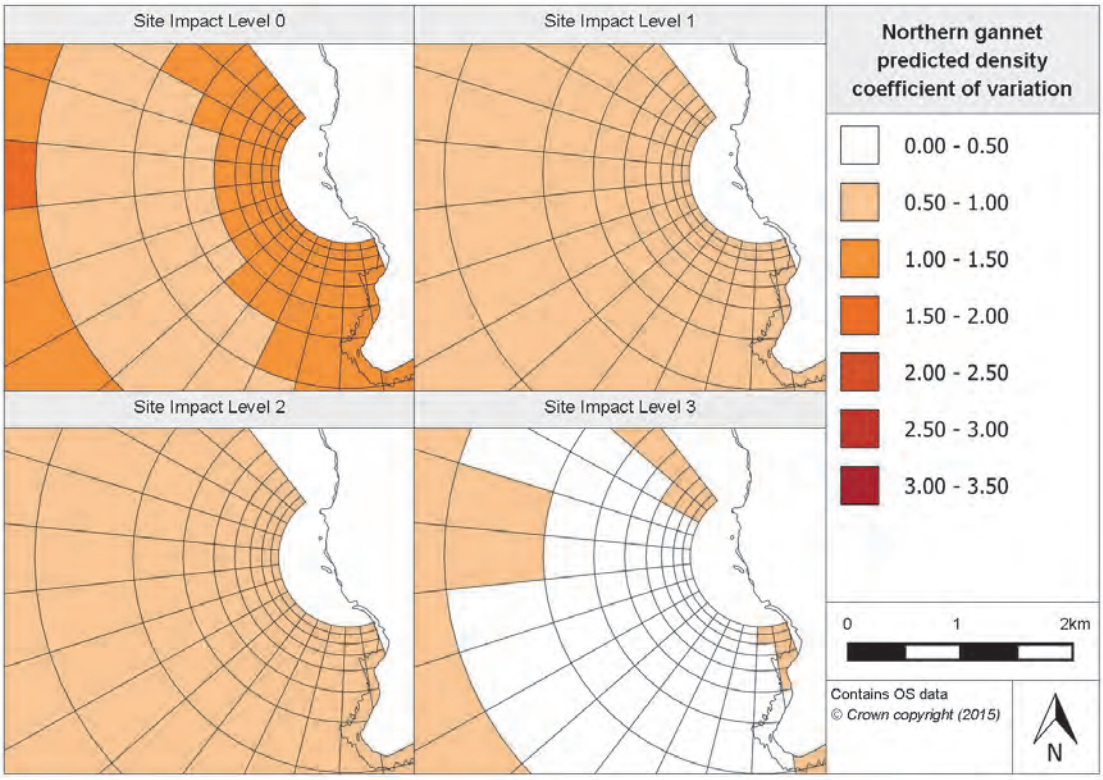

Figure 4.5.30. Associated coefficient of variation values for northern gannet inner density prediction surfaces at Billia Croo

At SIL-0, there appears to be fairly high CV values across most of the prediction surface, with highest values observed in the outer band of grid cells (A8 and A2) (Figure 4.5.29). These high CV values are probably due to low density predictions. Lowest CV values under these conditions are present in grid cells B9-B12 and in the majority of grid band C. Grid cells B9-B12 are where the highest densities at baseline conditions are expected and therefore this suggests that there is high precision behind this peak in density. In addition, as illustrated in Figure 4.5.30, the inner grid cells have CV values between 0.50 and 1.50; this suggests that there is reasonable precision in the inner grid cells of the prediction surface.

For the CV prediction surface at SIL-1, there seems to be lower CV values in general across the site. The highest CV values under these conditions are estimated to be in the far north of the observation area (A0-A3) and in grid cells to the north-west of Hoy (A7-A9) (Figure 4.5.29). As shown in Figure 4.5.30, the inner grid cells have CV values between 0.50 and 1.00.

At SIL-2, high CV values are observed in the outer band of grid cells (Figure 4.5.29), whereas across the rest of the site (with the exception of cells B0 and B1) and including the inner grid bands (Figure 4.5.30), there appears to be much lower CV values (between 0.50 and 1.00). This suggests that there is low uncertainty in the predictions made for the majority of the site. The high values in the outer band of grid cells may suggest that there are very few sightings of northern gannets in these cells or there is high variation in the numbers observed; therefore, there is large variability surrounding the predictions. Grid cells A7 and A8 have the highest CV values across all four site impact levels.

The CV values at SIL-3 suggest that there is little variability behind the prediction surface. There is particularly high precision in the results (low CV values) in the inner grid bands (close to the observation vantage point), as shown in Figure 4.5.30. Only two grid cells exhibit CV values greater than 1.00 and both of these cells are located in the outermost grid band, as can be seen in Figure 4.5.29. The grid cells where the highest densities are expected are also cells where low CV values exist suggesting that these predictions are realistic.

4.5.4.5 Relative abundance estimations

The fitted northern gannet model can be used to produce relative abundance values for each of the survey months. By combining these values, relative seasonal abundance predictions can be created. Table 4.5.12, below, provides these predictions for the survey's duration using the same environment covariates as previously specified.

Table 4.5.12. Relative abundance for northern gannet during each season (associated confidence intervals are provided in brackets)

Year	Season			
	Winter (Dec, Jan, Feb)	Spring (Mar, Apr, May)	Summer (Jun, Jul, Aug)	Autumn (Sep, Oct, Nov)
2009	-	14.40 (2.96, 38.17)	46.53 (13.41, 129.69)	85.41 (38.94, 178.33)
2010	3.26 (0.94, 7.86)	18.56 (3.72, 50.39)	50.27 (16.16, 138.55)	124.35 (59.26, 276.44)
2011	5.43 (1.89, 11.44)	17.74 (5.46, 48.76)	26.58 (8.58, 81.12)	43.94 (17.30, 121.85)
2012	2.22 (0.63, 5.44)	10.74 (2.05, 26.47)	33.40 (9.51, 93.04)	56.65 (23.94, 128.09)
2013	2.44 (1.25, 5.25)	17.92 (3.77, 42.38)	48.52 (17.70, 117.38)	29.96 (10.29, 93.38)
2014	1.14 (0.31, 3.52)	7.13 (0.97, 19.82)	19.83 (5.89, 56.58)	34.22 (14.78, 85.33)
2015	1.47 (0.44, 3.80)	7.13 (1.39, 19.46)	-	-

From the above table, the model clearly shows seasonality in the northern gannet estimated abundance. The greatest abundances are expected in summer and autumn with a definite low in abundance during winter reflecting the migratory nature of this species. In general, greatest abundances are estimated in autumn with sometimes double those expected for summer. However, in 2013, there appears to be a drop in abundance during autumn. There is potential for a further study to investigate whether this drop in northern gannet numbers modelled in autumn 2013 was experienced regionally, nationally or neither, and what may be the cause. The abundance predictions have also been divided across all impact levels and are provided in Appendix 7.

The northern gannet prediction surfaces have been produced for typical surveying conditions in January and July. The surfaces and associated CV values are provided in the Marine Scotland Information portal. The prediction surfaces are very similar between January and July except that the density predictions are approximately tenfold higher in July as compared to January, reflecting that northern gannets are migratory.

4.5.4.6 Spatially-explicit change

To understand the extent of any spatially-explicit changes in northern gannet density across the site with varying site impact levels, the difference between model predictions for each site impact level has been calculated. The significance of any changes has been investigated by using the 95% CIs for the predictions. As 'year' was in the final northern gannet model, it was necessary to produce plots for both the least and most variable years (2014 and 2010, respectively). The surface for the least variable year is presented in Figure 4.5.31 and the plots for the most variable year are available in Appendix 8. In addition, two further plots have also been produced, one for each year, showing the inner grid cells in more detail; see Figure 4.5.32 and Appendix 8, respectively.

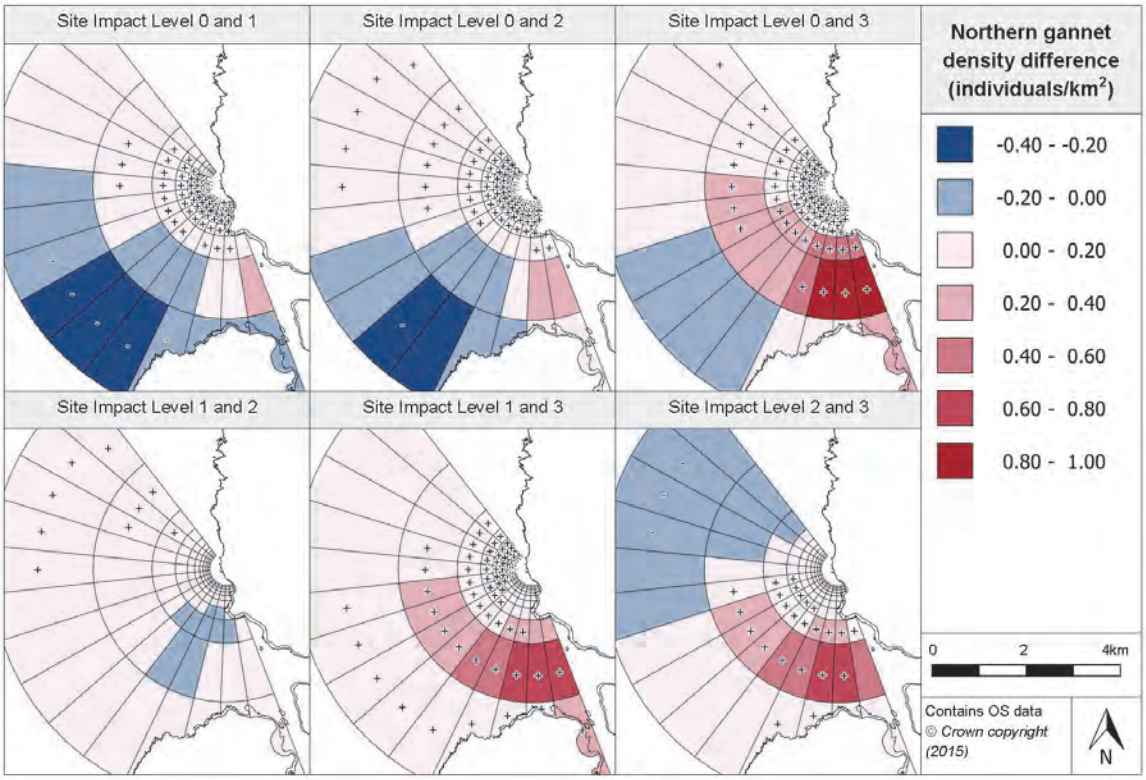

Figure 4.5.31. Estimated density difference between various site impact levels for northern gannet during 2014 (year with least variation) at Billia Croo

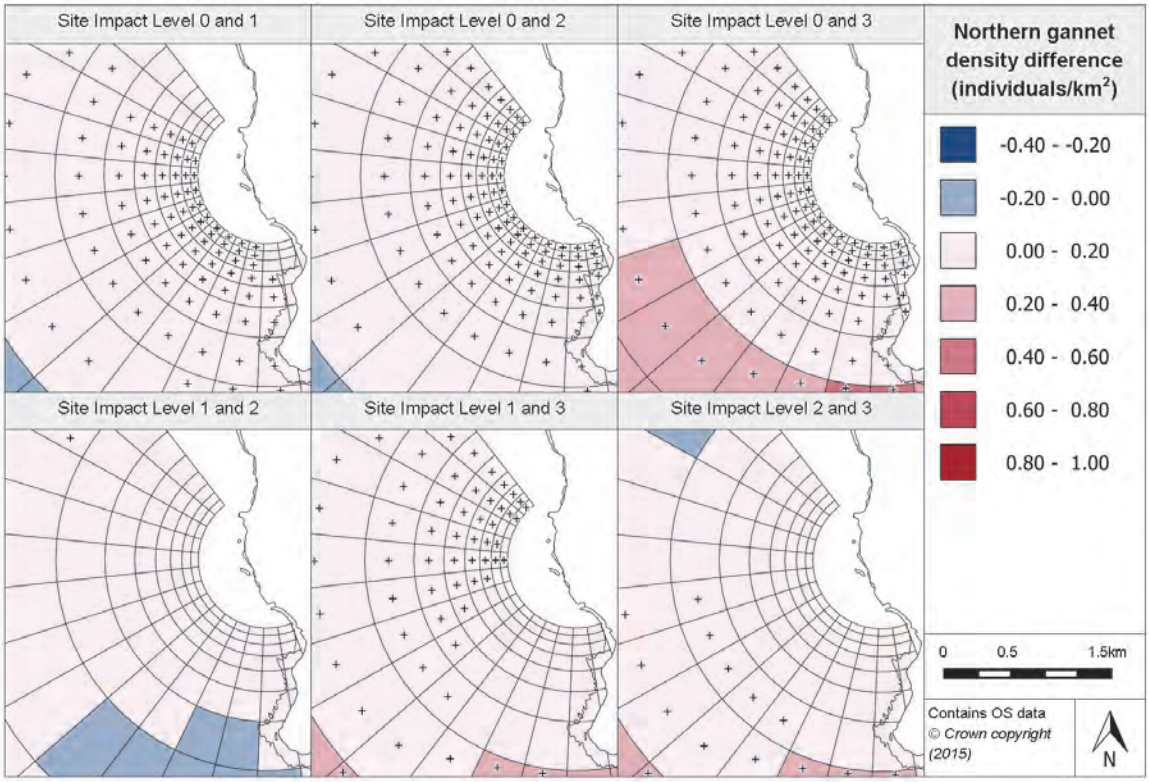

Figure 4.5.32. Density differences between northern gannet site impact level inner prediction surfaces during 2014 (least variable year) at Billia Croo

Between baseline conditions (SIL-0) and infrastructure being onsite (SIL-1), there appears to be a general increase in density in the grid cells in the inner grid bands of the survey area (Figure 4.5.32). There is a decrease from baseline conditions in the southern part of the grid, most noticeably in the outer band (Figure 4.5.31). Five grid cells show a significant decline in density, all positioned between grid cells A6 and A10. In grid cell A9, there is a decrease of 0.332 individuals/km^2. As noticeable in Figure 4.5.32, the majority of the grid cells within the inner grid bands have predicted increases in density and most of the grid changes are deemed significant.

Between SIL-0 and SIL-2 (when devices are in place but not operational), the majority of grid cells show an increase in density, with the majority being deemed significant. As seen in Figure 4.5.32, all the grid cells in the inner grid bands have an increase in density estimated and all are marked as significant. Ten grid cells (all in the outer grid bands, see Figure 4.5.31) show a decrease in density with the introduction of devices onsite; however, only grid cell A8 exhibits a significant decline in northern gannet numbers.

As devices become operational, the number of grid cells where a decrease in density is anticipated reduces to four (cells A6-A9) and none of these declines are deemed to be significant (see outer grid cells in Figure 4.5.31). As previously, the majority of the site has a density increase modelled and even more of the grid cells have their increase marked as significant. Again, all of the cells in the inner grid bands have significant increases in density anticipated (Figure 4.5.32). The largest density increase between two site impact levels occurs with the introduction of operational devices from baseline conditions. There is an estimated increase of 0.885 individuals/km^2 in grid cell B12 above baseline conditions. The largest increases in density are expected to be in the grid cells at the mouth of Hoy Sound and adjacent cells. All the grid cells that are the location of a test berth show a significant change in density for SIL-0 to SIL-3; however, as the majority of grid cells across the

observation area show a statistically significant change, there is probably no correlation between test berths and modelled density changes.

Between baseline conditions and SIL-1, SIL-2 or SIL-3, there is no clear relationship between any spatially-explicit change and the positioning of test berths. For instance, there are no peaks or troughs in density that can be associated with berth position. However, all the grid cells containing berths show a significant increase in density with the introduction of infrastructure or devices or their operation when compared to baseline conditions.

When considering the change in density between SIL-1 and SIL-2 (devices being installed), the majority of grid cells show a slight increase in density. As can be seen in Figure 4.5.31, only six grid cells are documented as having a density decrease; these are cells B9-B10 and C9-C13. Although most of the grid cells show a slight increase in density, only nine exhibit a significant increase, all of which are located in the outer grid bands. Only one grid cell containing a berth is found to have a significant density increase between these two site impact levels. Within the inner grid bands (Figure 4.5.32), with the exception of cells D10 and D11, all the grid cells demonstrate an increase of between 0.00 and 0.20 individuals/km^2.

Between SIL-1 and SIL-3 (devices installed and operating), all grid cells show an increase in density. There is a cluster of particularly large increases in the grid cells at the mouth of Hoy Sound, see Figure 4.5.31. The extent of the increase slowly reduces to only a very slight increase in the inner band of the survey grid (Figure 4.5.32). Some of the grid cells show a significant density increase with the introduction of operational devices as compared to just infrastructure being present onsite. These tend to be located in the northern half of the grid within the inner grid bands, and in the southern half of the grid for the outer grid bands.

When looking at spatially-explicit change between SIL-2 and SIL-3 (devices becoming operational), there is a density decrease estimated in the northern area of the site over parts of grid bands A, B and C (Figure 4.5.31). However, only the decrease in three grid cells is deemed to be significant. There continues to be a peak in density increase in the grid cells at the entrance to Hoy Sound. Between these two impact levels, there is a large reduction in the number of the grid cells showing a significant increase in density. In addition, from Figure 4.5.32, it is clear that, within the inner grid bands, only a slight density increase is modelled (0.00-0.20 individuals/km^2) and this increase is only deemed significant in grid cells D5-D9. This reduction in the number of grid cells marked as significant may suggest that the increases expected are only slight or that there is large variability behind the predictions. Three grid cells that contain test berths are exhibiting a significant increase in density; the other grid cells containing berths show either a slight increase or decrease which is not deemed to be significant.

4.5.4.7 Density change with distance from potential impact location

Using the density difference projections, it has been possible to plot out how the species density changes with increasing distance from a potential impact location (a single test berth). The changes for various site impact levels are shown in Figure 4.5.33.

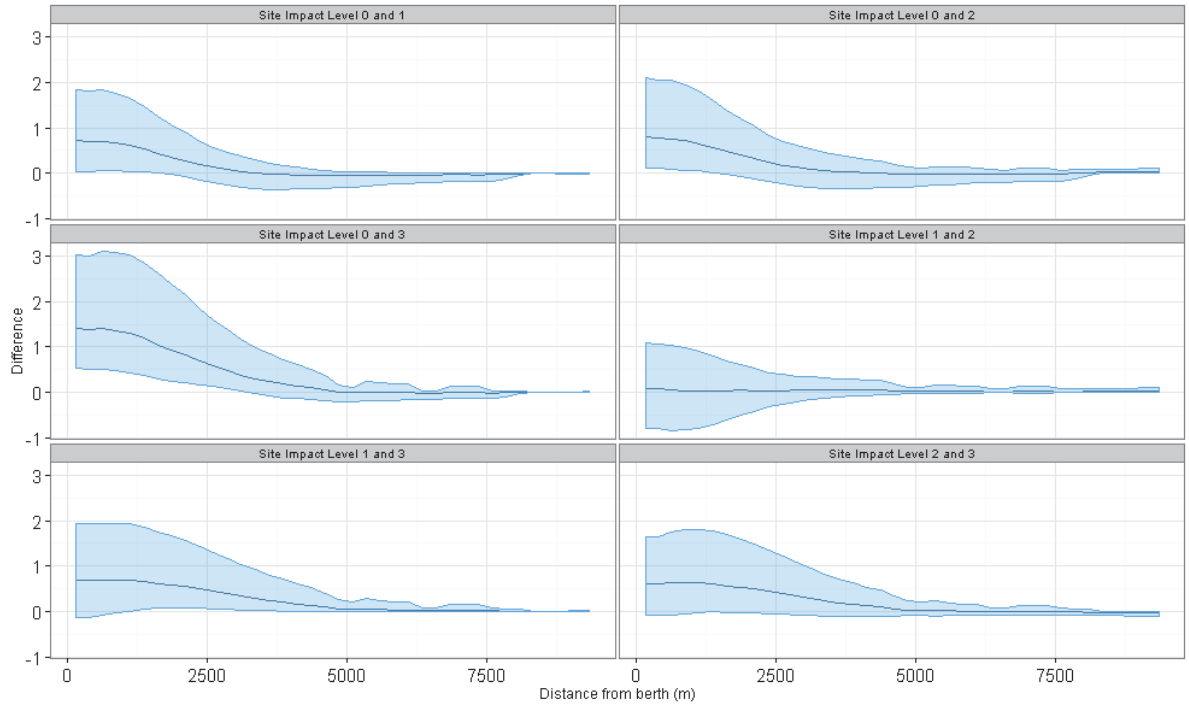

Figure 4.5.33. Density change between site impact levels with increasing distance from a potential impact location, with associated confidence intervals, for northern gannet at Billia Croo

Between baseline conditions and SIL-1, SIL-2 and SIL-3, there is a clear increase in density directly at the impact location which tends to extend to at least 1.8km away from the potential impact location. Between SIL-0 and SIL-1, it appears that the increase is sustained up to 1.8km away from the test berth before the lower CI is below zero. Beyond, the density difference does not vary much from pre-impact (baseline) conditions. The density difference between SIL-0 and SIL-2 remains positive until approximately 1.7km from where the lower CIs is below zero. Between SIL-0 and SIL-3, the increase in density estimated at the potential impact's immediate location is much greater. The increase gradually reduces in extent, with the lower CI dropping below zero at approximately 3km. Beyond 3km, the lower CI is around or below zero which suggests the increase is unlikely to be significant beyond this point. Between SIL-1 and SIL-2, there is very little density difference suggesting the northern gannet density predictions at SIL-2 are very similar to those anticipated at SIL-1.

Between SIL-1 and SIL-3, there is a large increase in density estimated at the test site which continues to about 3km in distance away. However, the lower CI is below zero for the initial 1.7km which may mean that an increase in density was not experienced in the initial distance.

Again, an increase in density is estimated between SIL-2 and SIL-3. This increase extends up to 4.9km away from the potential impact's location. The increase reaches its peak at about 800m from the test berth and then gradually reduces with distance, returning to SIL-2 levels at 4.9km away. However, as the lower confidence limit appears to vary around zero, this may not always represent an increase in density.

4.5.4.8 Discussion

The northern gannet is frequently spotted in small groups at Billia Croo. The model developed for them includes five highly significant terms. The key factors include distance from land and month; these are important controls on their distribution. There were only a

few observations undertaken during baseline conditions which means that, in areas of low density, there is high uncertainty. A high degree of precision in the predictions occurs at site impact level 3 (devices installed and operational) when most observations were made. All site impact levels show a similar distribution, with the greatest estimated densities occurring at the entrance to Hoy Sound. There is generally an increase in density with increasing site impact level over most of the survey area, with many grid cell increases being considered significant; however, there appears to be no direct correlation, in terms of test berth location, as test berth sites are not located in the area of highest northern gannet density.

4.5.5 Auks

4.5.5.1 Species overview

In addition to the separate analysis for common guillemots, black guillemots and Atlantic puffins, all species within the auk family occurring at Billia Croo have been collated into a group; the group created has been named *Auks*. The group includes the following species as well as unidentified auk species:

- black guillemot (*Cepphus grylle*)
- common guillemot (*Uria aalge*)
- Atlantic puffin (*Fratercula arctica*)
- razorbill (*Alca torda*)

Information regarding the general distribution and behaviour of black guillemots, common guillemots, razorbills and Atlantic puffin is outlined in Sections 4.3.1.1, 4.3.2.1, 4.3.3.1 and 4.3.6.1 above, respectively.

4.5.5.2 Data summary

The auk family are the most common family of birds present at Billia Croo. The following table, Table 4.5.13, provides an overview of the raw data used in fitting the auk model. The data summary provides information for each site impact level including typical group sizes. Note that more than half the observations are for SIL-3. This is likely to affect the confidence in the predictions made for this level.

Table 4.5.13. Summary of auk raw data

	Total	Site Impact Level 0	Site Impact Level 1	Site Impact Level 2	Site Impact Level 3
Number of observations	19257	2236	1250	5329	10442
Minimum (group size)	1	1	1	1	1
Maximum (group size)	372	350	134	372	228
Mean (group size)	2.60	4.75	3.15	2.07	2.35
(s.d)	(7.75)	(14.55)	(7.73)	(6.93)	(5.70)

4.5.5.3 Model overview

The final fitted auk model contains six terms, five of which are deemed statistically highly significant and one statistically significant (Year). Table 4.5.14 below provides a summary of the GEE-based p-values for each of the remaining terms.

Table 4.5.14. GEE-based p-values for the terms in the final auks model for Billia Croo

Model term	ρ-value
Distance to land	<0.0001
Month	<0.0001
Year	0.000176
Site impact	<0.0001
Spatial surface	<0.0001
Spatial surface / site impact	<0.0001

Distance to land as a term has been kept in the final model. The model predicts that auk density will decrease exponentially with increasing distance from land. 'Month' has also been kept in the final model as it has been found to be highly significant when predicting auk numbers at Billia Croo. As seen in Figure 4.5.34, there appears to be a peak in auk density between April and July, with greatest numbers estimated during June. During autumn, it is estimated that there will continue to be fewer auks recorded.

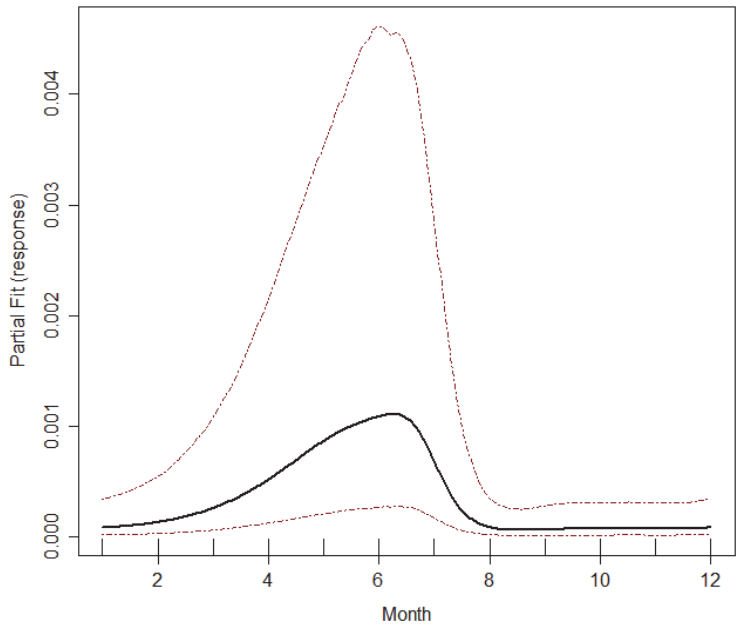

Figure 4.5.34. Estimated partial relationship of month against log(density) for auk at Billia Croo. The red lines represent 95% confidence intervals about the estimated relationship and the tick marks show where the data lie in the covariate range.

Survey year is also included in the final auk model. Figure 4.5.35 provides an indication of how the model has estimated the rise and fall of auk numbers over the survey's duration. The model predicts that auk density has risen during 2009 and 2010 then, in 2011, auks experienced a fall in numbers, recovering in 2012. Between 2013 and 2015, numbers have risen exponentially. An interesting further study could examine what factors may have caused the sudden decrease in auk numbers in 2011 and whether the rapid increase in density during 2014 is expected to plateau.

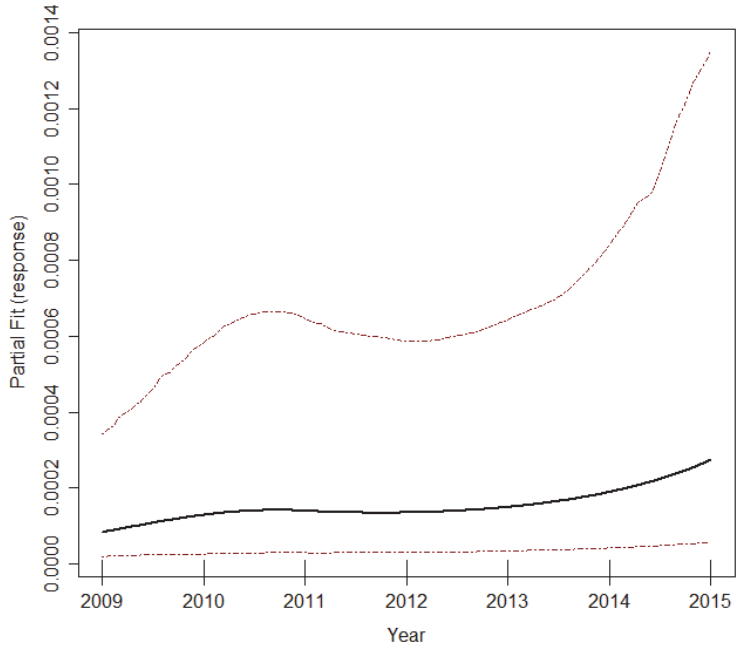

Figure 4.5.35. Estimated partial relationship of year against log(density) for auk at Billia Croo. The red lines represent 95% confidence intervals about the estimated relationship and the tick marks show where the data lie in the covariate range.

The final auk model for Billia Croo had a spatial surface fitted; four knots were used in the fitting. The interaction term (site impact/spatial surface) was also in the model, as it was found to be statistically significant.

4.5.5.4 Density predictions and uncertainty estimate

The final fitted auk model contains a spatial surface which allows density prediction surfaces to be created. These have been generated for each site impact level and are provided in Figure 4.5.36, with a more detailed view of the inner grid cells in Figure 4.5.37. To be able to do this, it was necessary to fix the environmental covariates at specified levels; as with the other species, these were chosen to be those when the greatest number of auk observations were made (see Appendix 5 for further information). For each of the prediction surfaces, it was also necessary to provide the associated CV values, see Figure 4.5.38 and Figure 4.5.39.

Reference should be made to Figure 2.1.9 and Figure 2.1.10 for the grid cell labelling system.

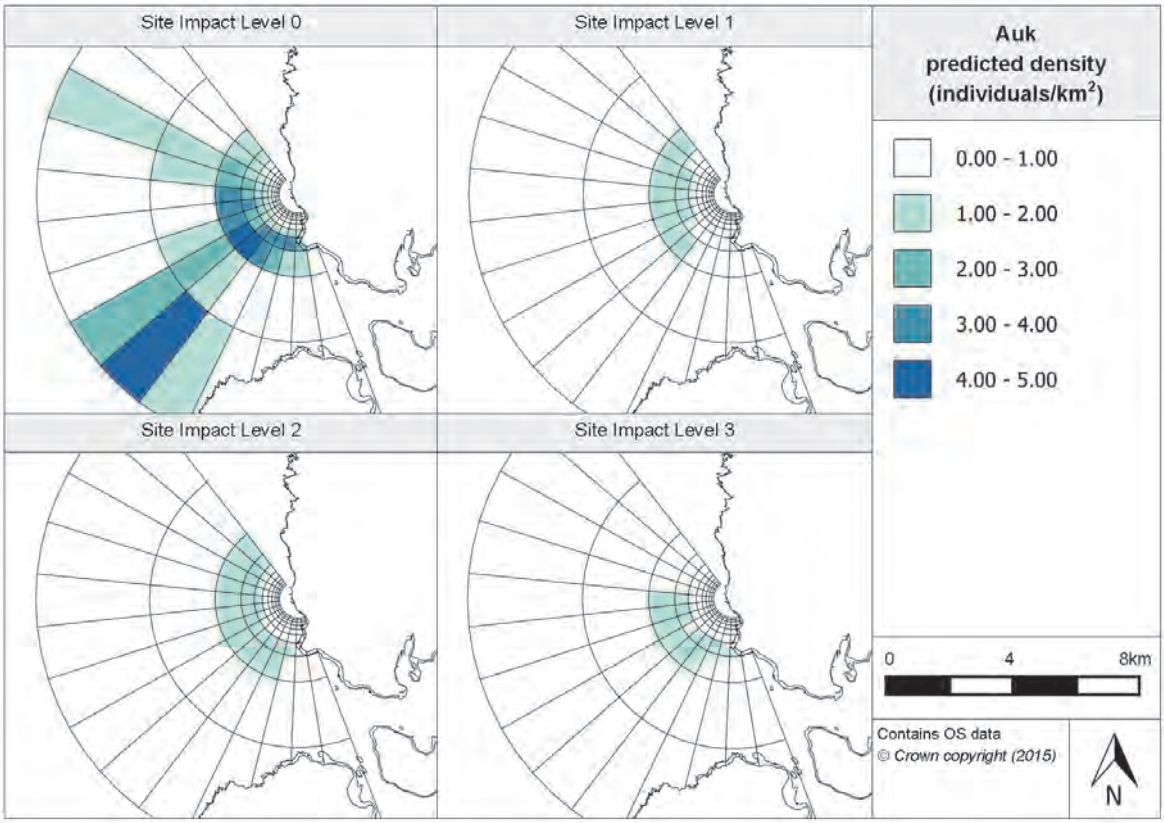

Figure 4.5.36. Prediction surfaces for auk density at Billia Croo

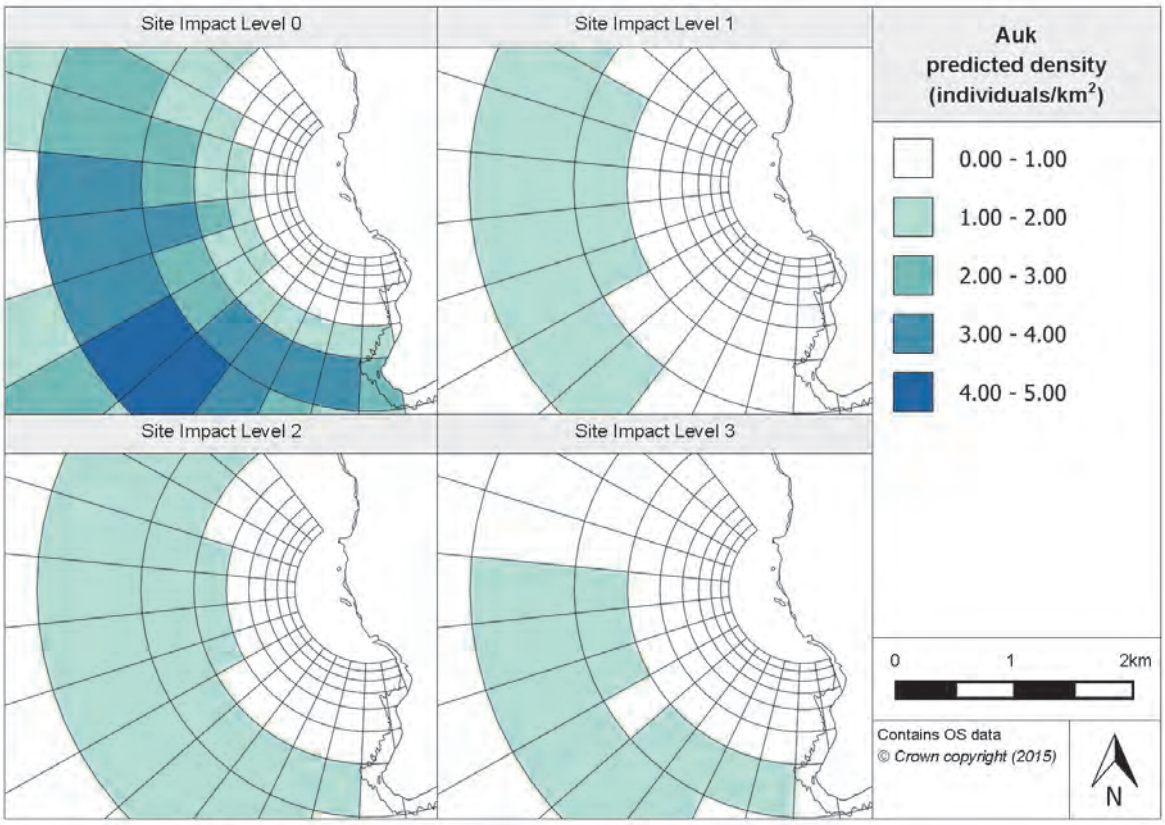

Figure 4.5.37. Inner prediction surfaces for auk density at Billia Croo

From Figure 4.5.36 above, it is clear that the highest auk densities exist at SIL-0. Higher densities are expected through grid bands A-E, with the majority of grid bands C-E having estimated densities above 1.00 individual/km^2 (see Figure 4.5.37). There is a distinct peak in estimated density values between cells C7 and C8 which gradually declines to levels that are just slightly raised in the adjacent grid cells. There are some grid cells in grid bands A and B where higher densities are also estimated, the highest of these being located to the north-west of Hoy (cells A7-A9). It should be noted that, in the four innermost grid bands (Figure 4.5.37), the density is not expected to be greater than 1.00 individual/km^2.

At SIL-1, the model predicts density values to remain below 1.00 individual/km^2 for the majority of the site. The only grid cells that have a density above 1.00 individual/km^2 are C0-C8 in the outer grid bands (Figure 4.5.36) and D2-D6 in the in inner grid bands (Figure 4.5.37). The prediction surface for SIL-2 is very similar to that estimated for SIL-1. A heightened density is expected in grid bands C and D and grid cells E3-E7, although this is limited to between 1.00 and 2.00 individuals/km^2. At SIL-3, even fewer grid cells have an estimated density of greater than 1.00 individual/km^2. Again, the highest densities at this impact level are expected in grid bands C and D.

Figure 4.5.38 and Figure 4.5.39 below provide the associated CV values for each of the prediction surfaces, some of which are very high and perhaps should be considered as unavailable. At SIL-0, the highest CV values are recorded between cells A0 and A6. Only a single grid cell within this area has a modelled density above 1.00 individual/km^2; in general, this suggests that there is high precision in the estimates where higher densities are expected. At SIL-1, high CV values are again estimated for the northern end of grid band A. Particularly high CV values occur for grid cells A1-A3. As the density prediction surface for SIL-1 estimates that higher densities occur within grid bands C and D, the CV surface suggests that there is low variability and fairly low uncertainty surrounding these predictions.

Similar to that modelled for SIL-1, the CV surface for SIL-2 shows high CV values in the most north-westerly area of the survey grid, with highest values estimated in grid cells A1-A3; all other cells have CV values less than 2. At SIL-3, only four grid cells show a CV value greater than 2. This suggests that there is fairly high precision in the model for this impact level, which is likely due to the great number of raw observations at this impact level and, therefore, more evidence upon which to base a model. In general, the same area of the survey grid is exhibiting higher CV values for all four impact levels. This suggests that there is high uncertainty in the prediction estimates for this region of the grid which is probably due to few auk observations occurring in this area. Note that the majority of the grid cells have CV values below 2 (Figure 4.5.38), with all the grid cells in the inner area having CV values below 2 (Figure 4.5.39).

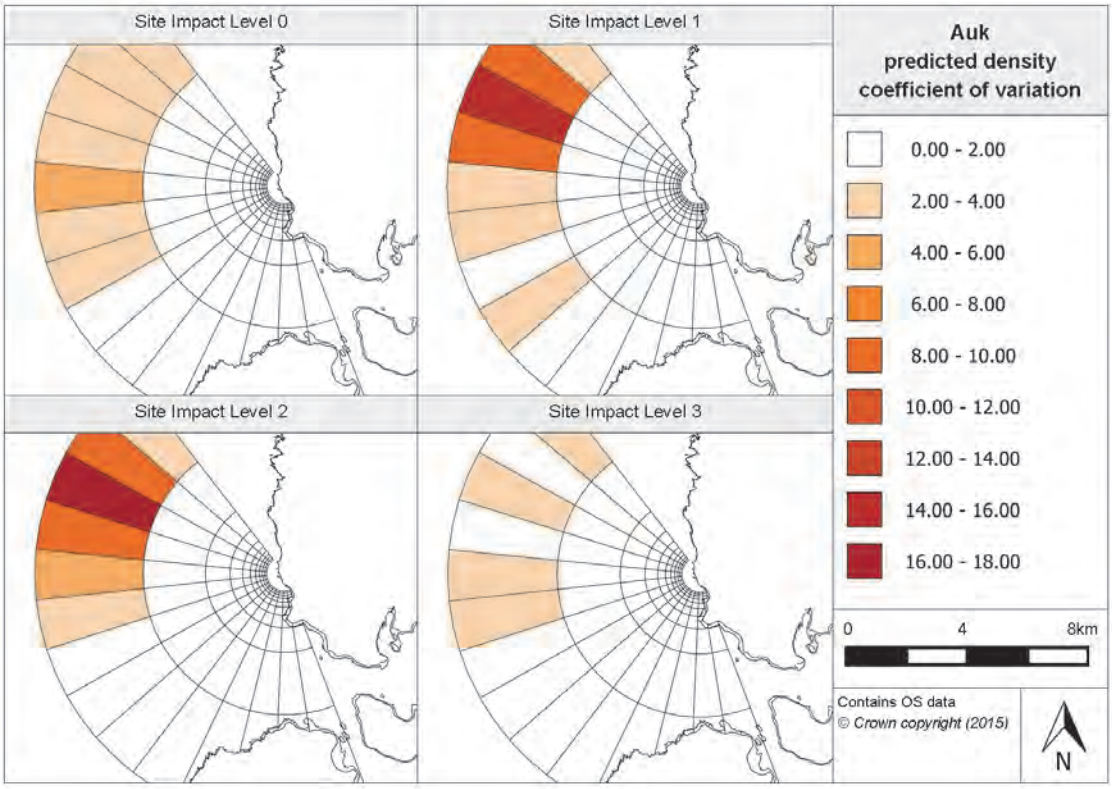

Figure 4.5.38. Associated coefficient of variation values for auk density prediction surfaces at Billia Croo

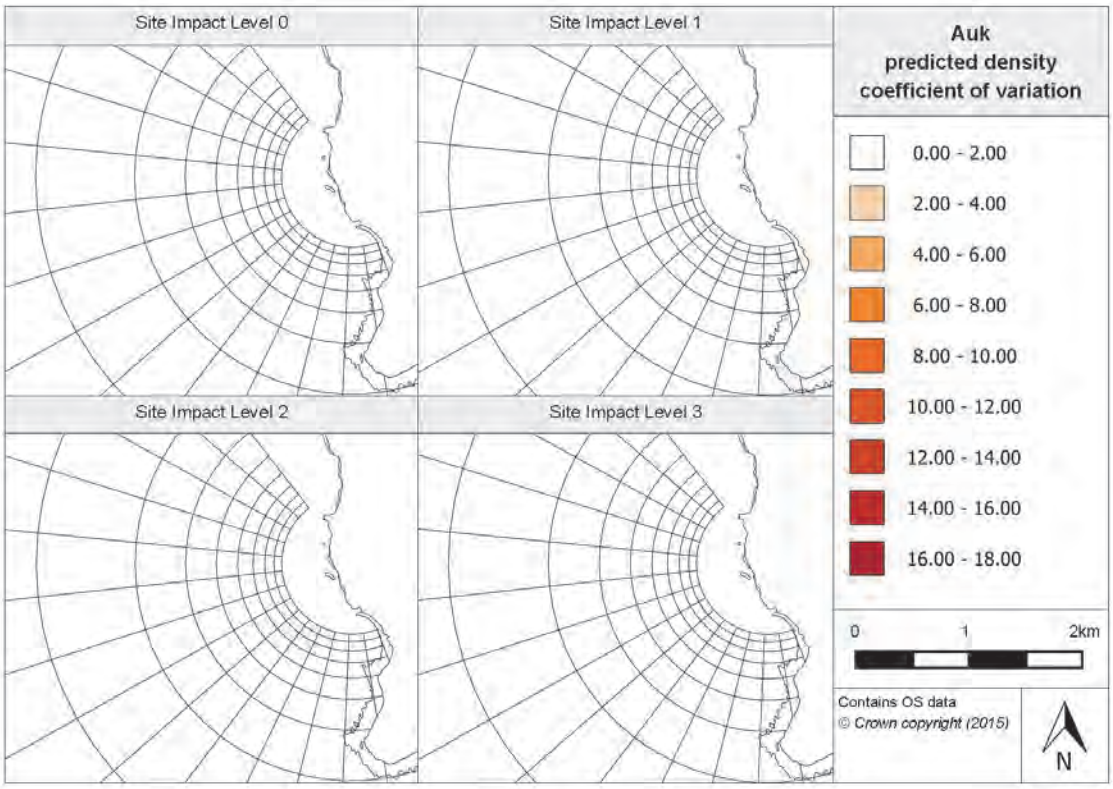

Figure 4.5.39. Associated coefficient of variation values for auk inner density prediction surfaces at Billia Croo

4.5.5.5 Relative abundance estimations

Using the fitted auk model, it is possible to produce relative abundance values for each of the months during the observation programme's duration. These values have been combined to produce seasonal abundance predictions which are provided in Table 4.5.15 alongside their associated 95% CIs.

Table 4.5.15. Relative abundance for auks during each season (associated confidence intervals are provided in brackets) for Billia Croo

Year	Season			
	Winter (Dec, Jan, Feb)	Spring (Mar, Apr, May)	Summer (Jun, Jul, Aug)	Autumn (Sep, Oct, Nov)
2009	-	162.25 (56.17, 403.93)	177.64 (5.83, 465.61)	7.66 (4.86, 12.35)
2010	14.99 (5.49, 35.00)	120.48 (45.16, 268.48)	135.87 (12.98, 337.98)	12.26 (7.98, 19.10)
2011	15.96 (8.73, 30.10)	186.45 (34.10, 888.88)	307.52 (21.81, 1046.85)	35.26 (15.30, 84.96)
2012	17.60 (9.25, 36.94)	96.32 (32.58, 226.76)	122.65 (13.06, 295.58)	16.33 (11.37, 21.57)
2013	21.16 (14.11, 30.07)	96.50 (38.94, 185.93)	108.81 (11.59, 229.17)	37.76 (17.40, 85.14)
2014	63.01 (24.38, 175.00)	171.90 (87.63, 336.48)	152.16 (14.05, 418.90)	19.30 (10.69, 30.09)
2015	42.37 (21.29, 79.29)	256.09 (97.48, 574.87)	-	-

The relative abundance figures provided in Table 4.5.15 suggest that there are much greater auk numbers during the spring and summer months as compared to autumn and winter, reflecting the migratory nature of some species. With the exception of only 2014, the summer months have the greatest abundance. Autumn or winter have equally lower abundances when compared to the other two seasons. In terms of year to year variability, it appears that 2011 was a particularly good year for auks, with a least double the abundance expected in summer as compared to the majority other years. The relative abundance estimates have also been plotted against time for each site impact level (see Appendix 7). The spring and summer peaks are evident in this plot as well as the particularly high peak in summer 2011 (under SIL-0).

In addition, the auk prediction density surfaces have also been created for typical surveying conditions in January and July. These and their associated CV surfaces are provided in the Marine Scotland Information portal. The prediction surfaces for these months appear to be very similar, except that density predictions in July are approximately eight times greater than those for January. Similar to the northern gannet prediction surfaces, these suggest that auks are likely to be observed much more frequently during summer months when compared to winter months.

4.5.5.6 Spatially-explicit change

Using the auk density prediction surfaces, it is possible to understand the extent of spatially-explicit change that exists in auk density across the various site-wide operational statuses. This is produced by calculating the difference in the model's density prediction surfaces. Using the 95% CIs for the predictions, it is possible to understand the significance of any changes. Similar to the northern gannet and Atlantic puffin, 'year' was included in the final fitted auk model. It was therefore necessary to produce plots for both the least and most variable years (2014 and 2010, respectively). The surfaces for the least variable year are presented within this section, see Figure 4.5.40, and the more detailed plot of the inner grid cells in Figure 4.5.41, whereas the surfaces for the most variable year are given in Appendix 8.

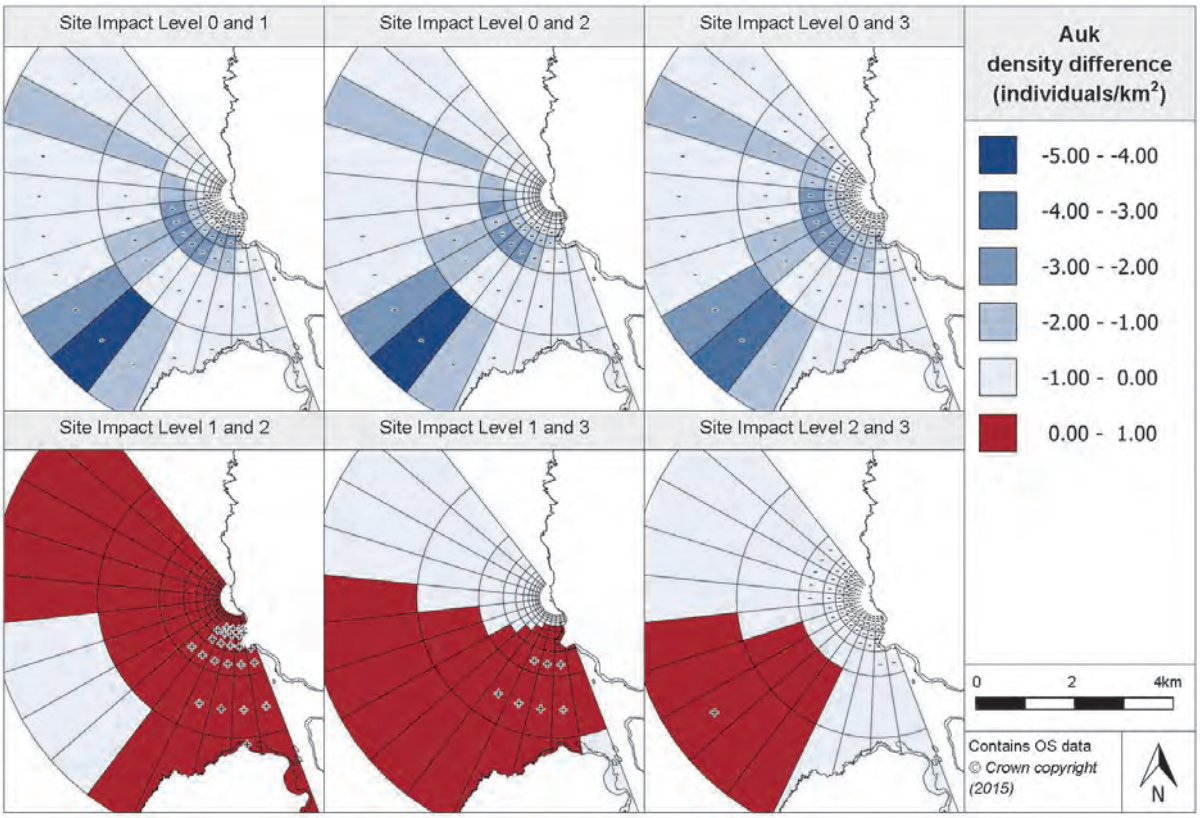

Figure 4.5.40. Estimated density difference between various site impact levels for auks during 2010 (year with least variation) at Billia Croo

The spatially-explicit change surfaces for the difference between baseline conditions and SIL-1, SIL-2 and SIL-3 are all very similar, with density differences determined as negative in all grid cells. There are also areas of greater decreases in density around grid cells A8 and C5-C9, see Figure 4.5.40. The density difference between density surfaces SIL-0 and SIL-1 indicates decreases of less than 3.00 individuals/km^2, except for grid cell A8 where a reduction of 4.05 individuals/km^2 is expected. In addition, the majority of grid cells have been marked as showing significant decreases in density (Figure 4.5.40). For the inner grid bands (Figure 4.5.41), all of the southern grid cells have been marked as significant, with density decreases ranging between 0.00 and 2.00 individuals/km^2, except for grid cells D9-D11 where a reduction of 2.00-3.00 individuals/km^2 is estimated. Between SIL-0 and SIL-2, there are fewer grid cells marked as showing a significant decrease in density, and these are predominantly in the south-west of the survey area. Within the inner grid bands, the density reduction is limited to between 0.00 and 2.00 individuals/km^2. The number of grid cells where the reduction in density between SIL-0 and SIL-3 has been deemed as significant increases markedly when compared with between SIL-0 and SIL-2. All the grid cells in the outer grid bands (except A13), show a significant decrease between SIL-0 and SIL-1. For the inner grid cells (Figure 4.5.41), the decrease in density when devices are onsite and operational, as compared to baseline conditions, is expected to be between 0.00 and 2.00 individuals/km^2, with this decrease marked as significant. All the grid cells that have a test berth located within them sare modelled to experience a significant reduction in density between SIL-0 to SIL-3; however, as the vast majority of grid cells across the observation area show a statistically significant reduction, there is probably no correlation between test berths and estimated density changes for auks.

When considering the density difference between SIL-1 and SIL-2, it appears that all the grid cells are expected to experience an increase in density with devices coming onsite, except

for four grid cells (A5-A8) where a reduction in density is estimated; however, this reduction is not expected to be significant (Figure 4.5.40). This increase in density is marked as significant for cells close to Breck Ness and the mouth of Hoy Sound (Figure 4.5.40).

In terms of the density difference between SIL-1 and SIL-3, there is a clear north-south divide, with the southern majority of grid cells marked as showing an increase in density (Figure 4.5.40). However, only seven grid cells have been marked as showing a significant change in density, these being located at the mouth of Hoy Sound (B9-B12 and C10-C13).

The majority of grid cells are showing a modelled decrease in density of up to 1.00 individual/km^2 with the operation of devices as compared to devices being onsite but not operating (change from SIL-2 to SIL-3). From Figure 4.5.40, there is a clear cluster of grid cells in the south-west of the area, covering grid cells A5-A9 and B6-B9, where an increase in density of up to 1.00 individual/km^2 is expected. Only the increase in density at grid cell A7 has been marked as significant. Of the cells showing a decrease in density, all of the inner cells (apart from grid cells D7-D9) and grid cells C0-C4 and C12-C13 have the decrease in density marked as significant (Figure 4.5.41).

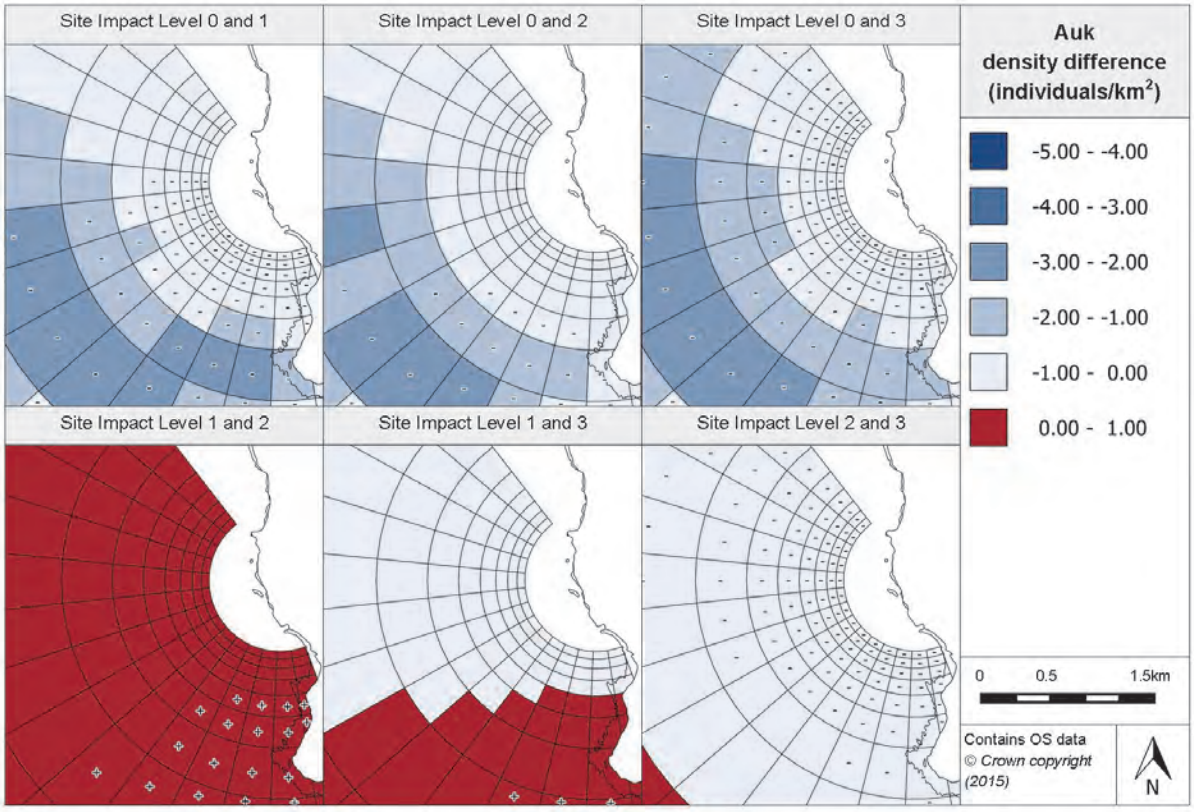

Figure 4.5.41. Density differences between auk site impact level inner prediction surfaces during 2010 (least variable year) at Billia Croo

4.5.5.7 Density change with distance from potential impact location

The following figure, Figure 4.5.42, illustrates how the density difference projections between site impact levels change with increasing distance from a potential impact location (a single test berth).

The effect of increasing distance on the estimated density difference between site impact levels is very similar between baseline conditions and SIL-1, SIL-2 and SIL-3. For all three scenarios, there is a distinctly lower density estimated at the immediate location of the

potential impact for SIL-1, SIL-2 and SIL-3 as compared to baseline conditions. With increasing distance away from the potential impact location, the disparity in density predictions between SIL-1, SIL-2 and SIL-3 and baseline reduces, SIL-1, SIL-2 and SIL-3 returning to baseline condition levels at around 2.6km away from the test berth. Beyond 2.6km, the difference in density predictions between SIL-0 and SIL-1, SIL-2 and SIL-3 varies little. When considering the upper and lower CIs, the upper confidence limit is above zero between SIL-0 and SIL-2 which suggests that the decrease in density estimated between these impact levels is unlikely to be significant whereas, between SIL-0 and SIL-3, the upper CI is clearly below zero, suggesting that the density difference modelled between SIL-0 and SIL-3 is significant. Between the SIL-0 and SIL-1, the upper CI waivers around zero therefore suggesting that a decrease in density will not necessarily always be estimated.

Between SIL-1 and SIL-2, the CIs are on either side of zero, which suggests the slight increase in density modelled initially is highly unlikely to be significant. Beyond 2km, there is very little difference between SIL-1 and SIL-2.

The estimated density differences between SIL-1 and SIL-3 and between SIL-2 and SIL-3 both have very similar trends. There is a slight decrease in density at the test berth when devices are operational, decreasing with increasing distance from the berth and reaching SIL-1 and SIL-2 levels at approximately 2km away. The upper CI between SIL-1 and SIL-3 is slightly above zero which suggests it is unlikely to be significant whereas, between SIL-2 and SIL-3, the upper confidence level is at or below zero which implies that the decrease estimated between these two impact levels may be significant.

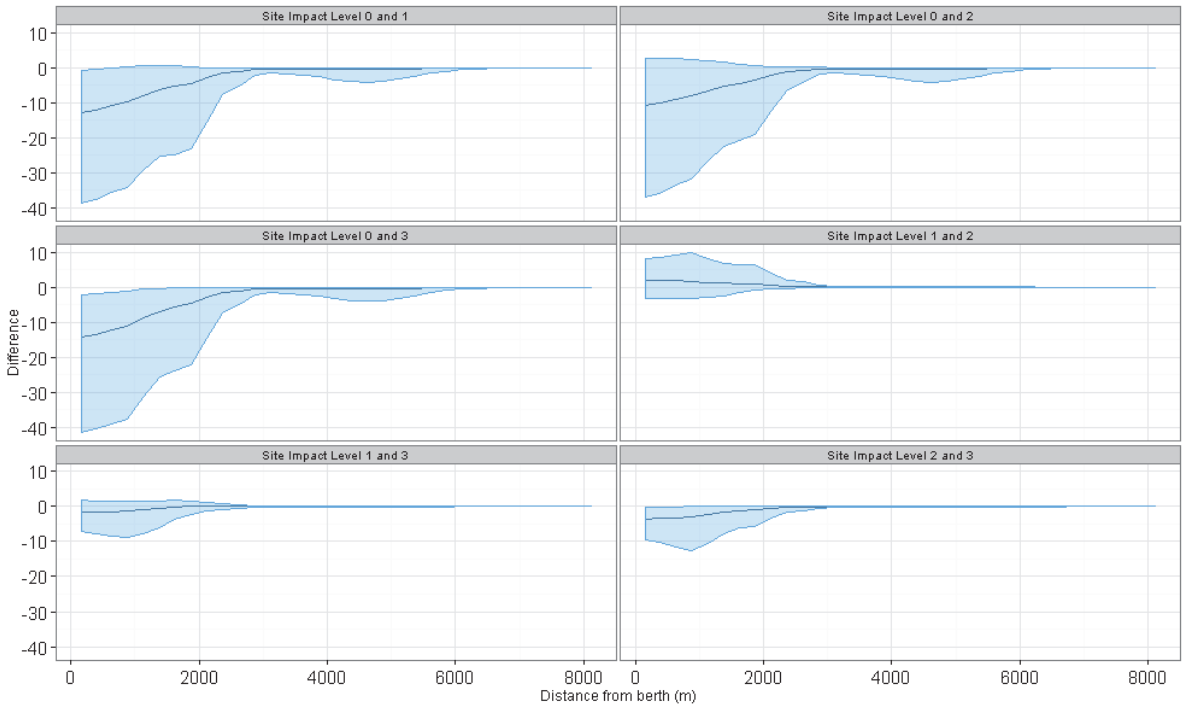

Figure 4.5.42. Density change between site impact levels with increasing distance from a potential impact location, with associated confidence intervals, for auks at Billia Croo

4.5.5.8 Discussion

The model for the auk group of species contains six terms, five of which are deemed statistically highly significant. These include distance from land and month. The model also indicates an increase in auk numbers with year. Higher densities are generally estimated to occur west of Billia Croo. These higher densities are apparent under baseline conditions

(SIL-0), with a reduction in density over the entire survey area with the installation of infrastructure (SIL-1). Densities reduce further over most of the area with increasing site impact levels (SIL-2 and SIL-3).

All the grid cells that contain a test berth show a significant reduction in density with increasing site impact level; however, as the vast majority of grid cells across the observation area show a statistically significant reduction, there is unlikely to be any correlation between test berths and estimated density changes for auks.

Analysing the density change at a potential impact location and how this varies with increasing distance, appears to indicate a reduction at the impact location under SIL-1, SIL-2 or SIL-3 conditions but a return to baseline conditions at approximately 2.6km distance. The reduction in density between baseline conditions and SIL-3, is the only reduction that can be deemed significant. The biggest reduction in density at an impact site is coincident with the installation of infrastructure, and only modest increases and decreases correspond with the change in impact level to SIL-2 (devices installed) and SIL-3 (devices becoming operational), respectively.

4.5.6 Divers

4.5.6.1 Species overview

As with the Fall of Warness, only two diver species have been observed at Billia Croo during the observation programme's duration. The diver species recorded at the site are the great northern diver (*Gavia immer*) and red-throated diver (*Gavia stellata*). Both species are infrequent visitors to the site but have been seen in nearly equal numbers and, therefore, no one species is more common than the other. Section 4.3.4.1 provides information regarding the general distribution and behaviour of these birds.

4.5.6.2 Data summary

A summary of the raw data collected for the two diver species at Billia Croo is presented in Table 4.5.16. Included in the table is information regarding the maximum, minimum and mean group size. This information has also been split across site impact levels. As with other species analysed, more than half the observations occurred when devices were operational.

Table 4.5.16. Summary of diver raw data

	Total	Site Impact Level 0	Site Impact Level 1	Site Impact Level 2	Site Impact Level 3
Number of observations	159	10	4	45	100
Minimum (group size)	1	1	1	1	1
Maximum (group size)	4	4	2	2	4
Mean (group size)	1.28	1.70	1.50	1.09	1.32
(s.d)	(0.62)	(0.95)	(0.58)	(0.29)	(0.66)

4.5.6.3 Model overview

Six terms were included in the final fitted diver model. GEE-based p-values were able to be obtained for each of these terms in the model. Five terms were found to be statistically highly significant (p-value<0.0001) and one as statistically significant (site impact). Table 4.5.17 below provides a summary of the GEE-based p-values for each of the remaining terms.

Table 4.5.17. GEE-based p-values for the terms in the final divers model for Billia Croo

Model term	ρ-value
Distance to land	<0.0001
Month	<0.0001
Year	<0.0001
Site impact	0.00014
Spatial surface	<0.0001
Spatial surface / site impact	<0.0001

Within the final fitted model is the term 'distance to land'. The final model has estimated that diver density is higher closer to land and reduces with increasing distance from land. 'Month' has also been included in the model; this is in line with the seasonality already known for the species in the north of Scotland. In addition, 'year' has been included in the model. Figure 4.5.43 below shows the modelled relationship between diver density and survey year. It is clear that diver density has been estimated to increase exponentially over the observations programme.

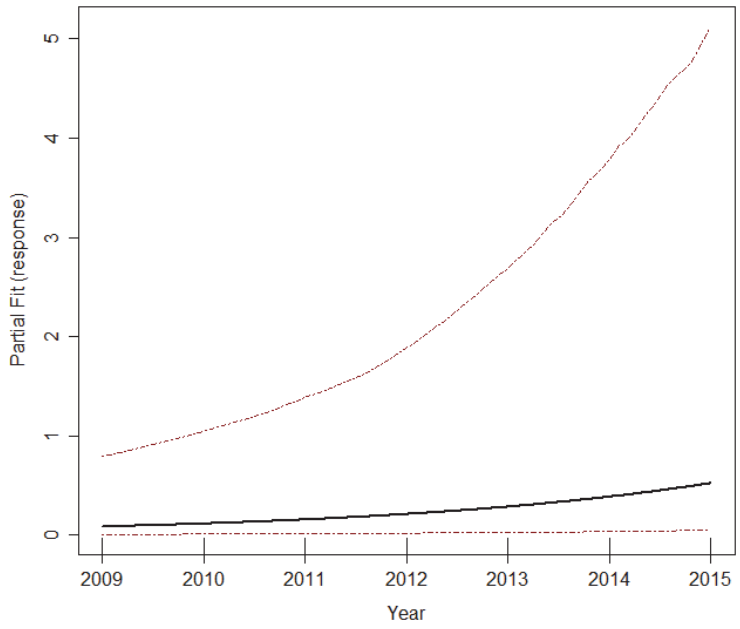

Figure 4.5.43. Estimated partial relationship of year against log(density) for divers at Billia Croo. The red lines represent 95% confidence intervals about the estimated relationship and the tick marks show where the data lie in the covariate range.

Also included in the fitted diver model is a spatial surface which allows predictions to be made across the observation grid at Billia Croo. Four knots were used in fitting the spatial surface. An interaction term (site impact/spatial surface) has also been included in the model, and found to be statistically highly significant when predicting diver density across the site (Table 4.5.17).

4.5.6.4 Density predictions and uncertainty estimate

As with the other species discussed in this section, the fitted diver model contains a spatial surface which allows density prediction surfaces to be created. To do this, it was necessary to set the environment covariates that are contained within the models at certain conditions,

as outlined in Appendix 5. As with the black guillemot and Atlantic puffin models, as there are anomalies in the diver data, it was necessary to reduce the number of iterations in the bootstrap; 845 iterations were implemented rather than the 1000 carried out for most other species/groups. Prediction surfaces have been created for each site impact level, see Figure 4.5.44. To provide a more detailed view of the inner grid cells, Figure 4.5.45 focuses on the inner grid bands. To understand the uncertainty behind these predictions, the predictions' associated CV values are provided in Figure 4.5.46 and Figure 4.5.47.

Reference should be made to Figure 2.1.9 and Figure 2.1.10 for the grid cell labelling system.

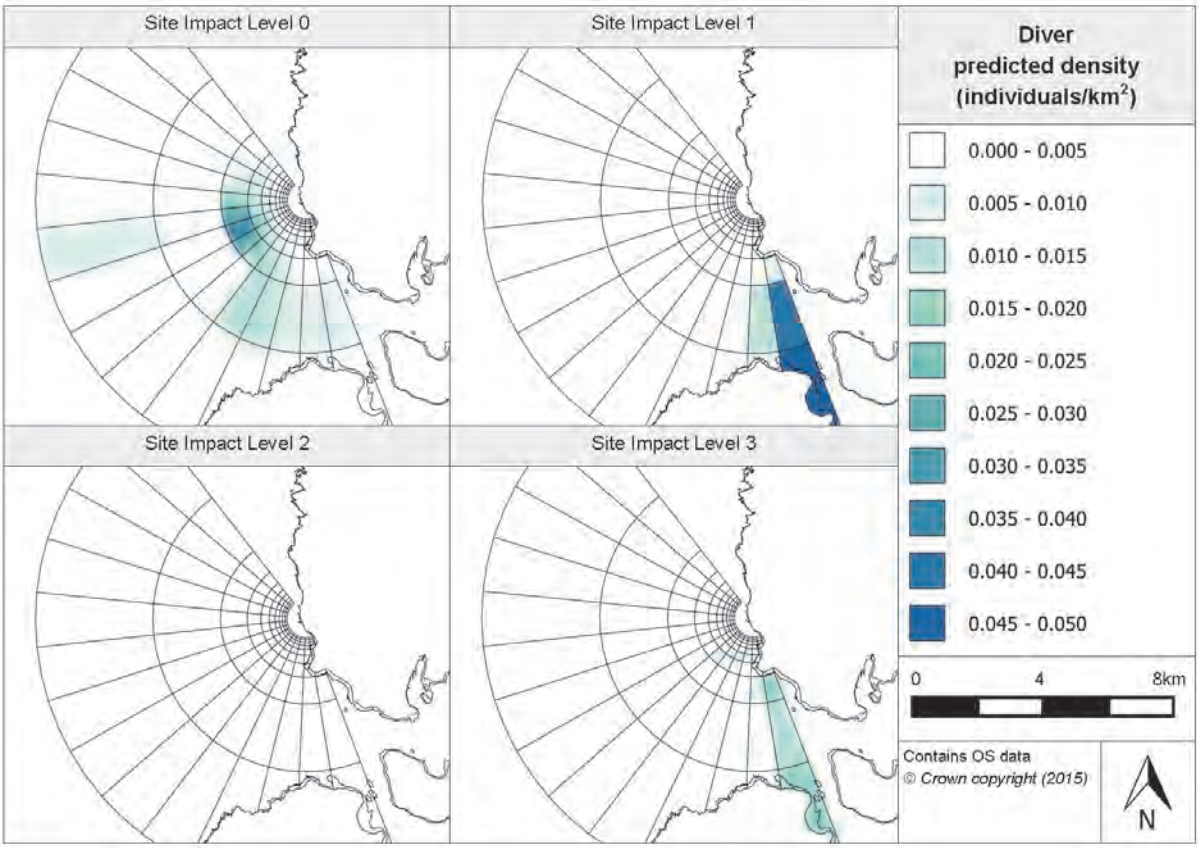

Figure 4.5.44. Prediction surfaces for divers density at Billia Croo

The prediction surface for SIL-0 shows a clear cluster of higher density predictions around grid cell C6 (Figure 4.5.44). There is also an area of grid cells at the mouth of Hoy Sound where estimated densities between 0.005 and 0.015 individuals/km^2 exist. The distinct cluster around grid cell C6 (where a density of 0.039 individuals/km^2 is anticipated) appears to reduce in density with increasing distance away from cell C6. This effect can be seen extending into grid bands D and E (Figure 4.5.45). Otherwise, the density across the area is not expected to be greater than 0.005 individuals/km^2 (except for cell A5 – 0.006 individuals/km^2).

Under SIL-1 conditions, the density prediction surfaces show highest values in Hoy Sound, reaching 0.047 individuals/km^2 in cell A13 and 0.042 individuals/km^2 in cell B13. Elevated densities extend into grid cells B12 and C13 with a density of between 0.005 and 0.015 individuals/km^2. Across the rest of the site, the density is expected to be lower than 0.005 individuals/km^2.

The prediction surface under SIL-2 conditions shows diver density is less than 0.005 individuals/km^2 across the entire surface.

The prediction surface for SIL-3 is similar to that for SIL-1 with a peak in Hoy Sound, SIL-1 with densities between 0.010-0.020 individuals/km^2 estimated in grid cells A13, B13 and C13. The rest of the area is expected to have densities less than 0.005 individuals/km^2 (Figure 4.5.44), except for a cluster of inner grid cells (Figure 4.5.45) in the vicinity of grid cells E7-9 where 19 cells have estimated densities of between 0.005 and 0.010 individuals/km^2. Additionally, grid cell F0 has a density prediction of 0.005-0.010 individuals/km^2.

In general, there are very low density predictions for divers across all the prediction surfaces. There appears to be a couple of areas of the observation grid where aggregations of observations are expected under certain conditions, but these clusters of higher density predictions most likely appear due to a lack of observations across the majority of the grid.

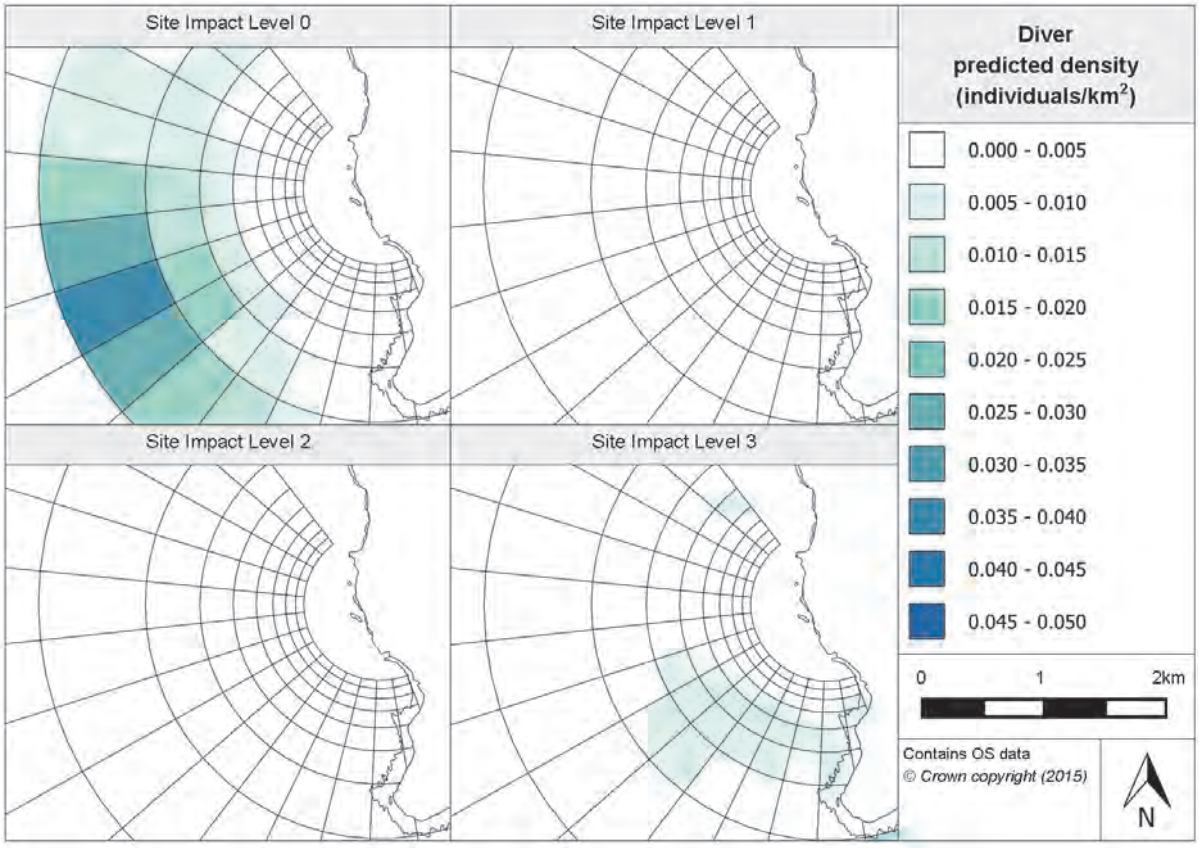

Figure 4.5.45. Inner prediction surfaces for divers density at Billia Croo

The lack of observations becomes clearer when considering the CV values associated with the predictions. As previously mentioned, the method of calculating CV values does not allow for very low predictions which results in unrealistic values. In these cases, the CV values have not been provided and are described as unavailable. From Figure 4.5.46 and Figure 4.5.47 below, it is clear that the very low predictions obtained for divers is affecting the number of grid cells in which realistic CV values can be obtained.

Under SIL-0 conditions, the majority of grid cells in the outer grid band do not have CV values available (Figure 4.5.46). In addition, the cells in the north of grid band B have high CV values which would imply that there is high variability in predictions for this area of the

site. The rest of the outer grid cells have CV values generally between 1.00-2.00, suggesting reasonable precision in the predictions. In addition, the majority of the inner grid bands have CV values between 1.00 and 2.00, again suggesting reasonable precision in the predictions (Figure 4.5.47). However, CV values are unavailable for the two innermost grid bands as well as grid cells H11-H13 and G12 at the southern edge of Billia Croo Bay.

Even more of the prediction surface under SIL-1 conditions has unavailable CV values and many of those cells with CV values appear to have values greater than 2 (Figure 4.5.46). This would suggest high uncertainty in the predictions for these cells. Even the two grid cells A13 and B13 with high density predictions have CV values between 3.00 and 4.00, which implies there is large variability in these predictions. In the inner grid bands, there is greater uncertainty in the results in the north as compared to the south, where the CV values generally range between 1.00 and 2.00 (Figure 4.5.47).

The very low density predictions for SIL-2 are evident in the number of grid cells where CV values are not available (Figure 4.5.46). Where values are available, there is fairly high precision with respect to the predictions in the south of the inner grid bands, with many of the cells having values between 0.00 and 1.00. These are surrounded by a few cells having CV values of 1.00 and 2.00 (Figure 4.5.47).

Again in SIL-3, the grid cells in the outer grid bands appear mostly to have unavailable CV values, with only the southern half of grid band C and cells A13 and B12-B13 in Hoy Sound having CV values available (Figure 4.5.46). The CV values for the inner grid bands suggest that there is high precision regarding the predictions in this area of the prediction surface, with almost all having CV values less than 1.00 (Figure 4.5.47). The higher precision seen in the inner grid band at SIL-3 may be due to a greater number of raw observations at this site impact level and, therefore, more evidence available upon which to base the model.

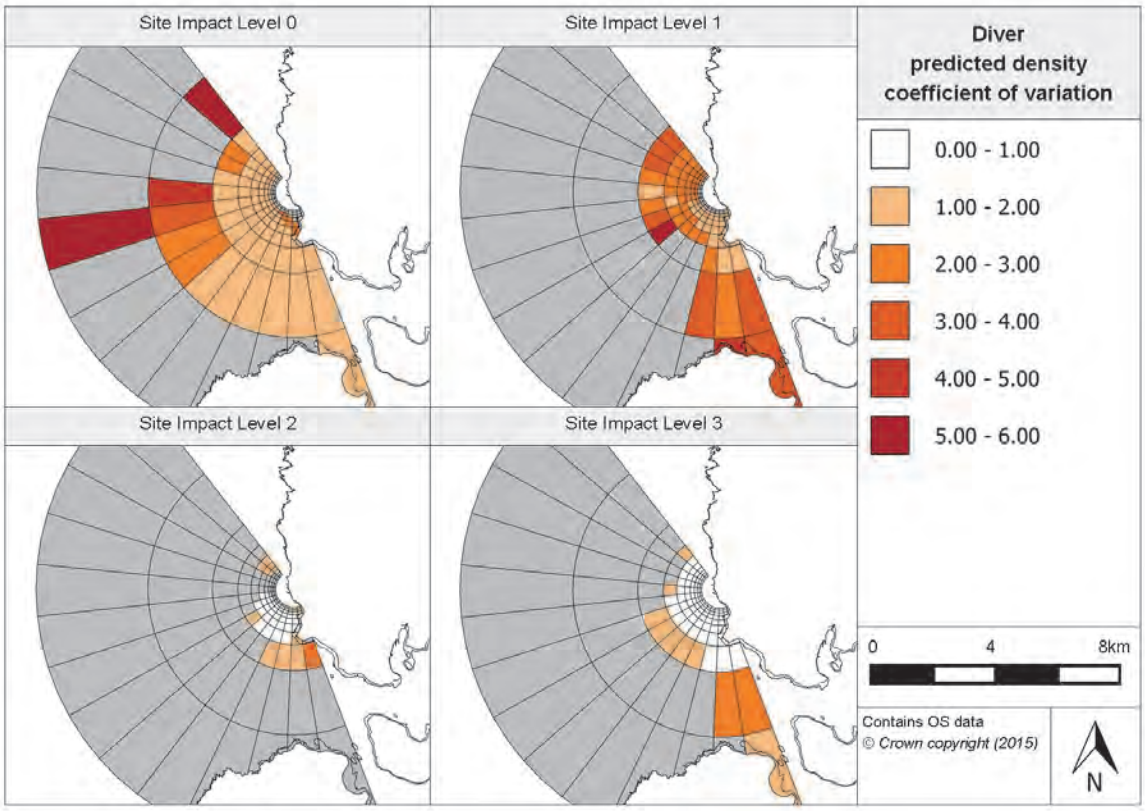

Figure 4.5.46. Associated coefficient of variation values for diver density prediction surfaces at Billia Croo

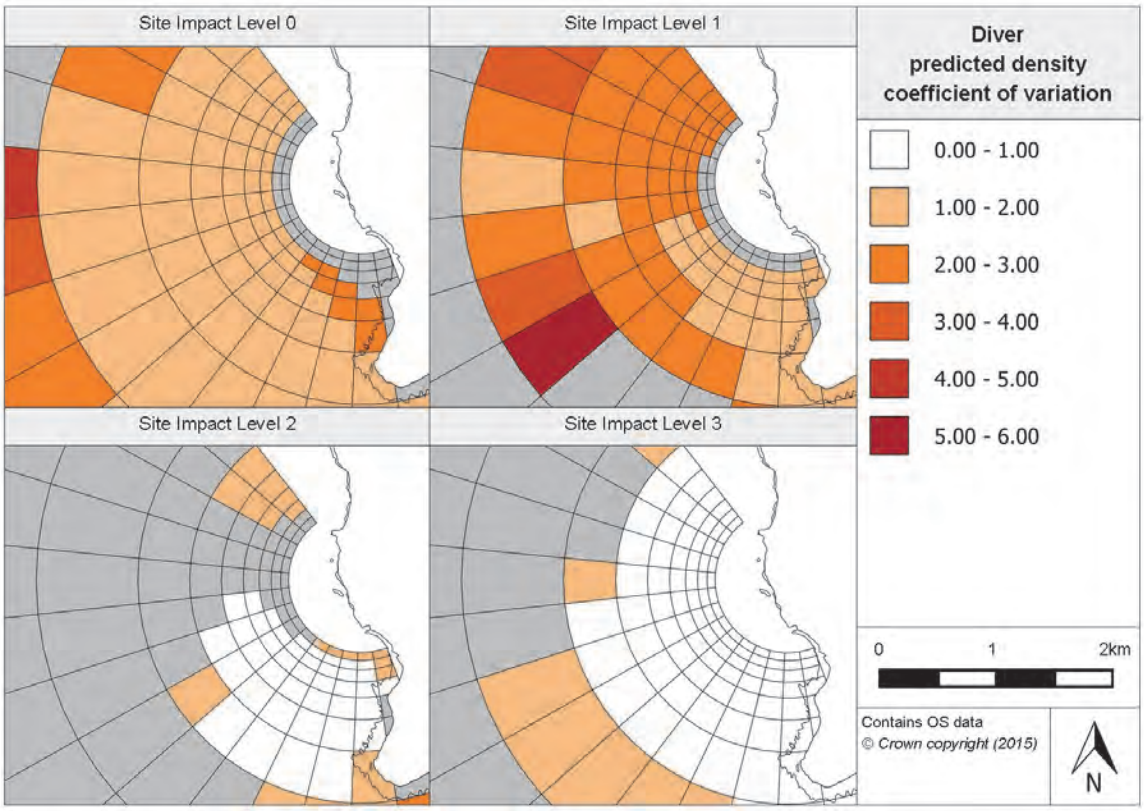

Figure 4.5.47. Associated coefficient of variation values for diver inner density prediction surfaces at Billia Croo

4.5.6.5 Relative abundance estimations

Relative abundance values can be produced for each survey month using the fitted diver model. These values are then combined to produce seasonal abundance estimates; these are given in Table 4.5.18 below. Such estimates are provided for each season within the programme's duration, using the same environmental covariates as discussed in Appendix 5.

Table 4.5.18. Relative abundance for divers during each season (associated confidence intervals are provided in brackets)

Year	Season			
	Winter (Dec, Jan, Feb)	Spring (Mar, Apr, May)	Summer (Jun, Jul, Aug)	Autumn (Sep, Oct, Nov)
2009	-	0.38 (0.17, 2.78)	0.19 (0.01, 2.02)	0.08 (0.01, 0.85)
2010	0.45 (0.12, 2.37)	0.15 (0.07, 0.45)	0.08 (0.02, 0.36)	0.16 (0.01, 0.61)
2011	0.95 (0.46, 1.79)	0.61 (0.31, 3.65)	0.36 (0.06, 3.66)	0.29 (0.04, 3.55)
2012	0.82 (0.23, 4.12)	0.50 (0.17, 2.73)	0.21 (0.03, 1.96)	0.11 (0.02, 0.46)
2013	1.03 (0.33, 3.04)	1.05 (0.60, 2.01)	0.55 (0.14, 1.44)	0.53 (0.07, 6.11)
2014	2.85 (0.97, 18.72)	1.23 (0.30, 11.52)	0.47 (0.06, 3.47)	0.27 (0.04, 1.47)
2015	1.12 (0.65, 2.63)	0.67 (0.35, 1.70)	-	-

The seasonality of the diver observations at Billia Croo is clearly represented by the model, with abundance estimates greater during winter. From Table 4.5.18, it appears that there is greatest diver abundances during winter, with slightly lower abundances in spring. In

general, lowest diver abundances are expected in autumn. This seasonality in the predictions is in line with diver behaviour as discussed in Section 4.3.4.1. When looking at the year on year variation, it appears that 2014 has considerably greater abundances predicted in comparison with other years. An interesting further study topic would be to look at what may have influenced this sudden increase in diver density. The relative abundance estimates against time for each site impact level are provided in Appendix 7.

Further to the prediction surfaces already created from the diver model, diver prediction surfaces have also been generated for typical surveying conditions in January and July. These surfaces and their associated CV values can be viewed in the Marine Scotland Information portal. The prediction surfaces for the two months are very similar, except that density predictions for January are approximately four times greater than those for July. Similar to that discussed above, these prediction surfaces suggest that more divers are expected during the winter months when compared to the summer months.

4.5.6.6 Spatially-explicit change

To understand the extent of any spatially-explicit changes in diver densities with changes to site operational status, the density difference between site impact levels was calculated. The 95% CIs can then be used to understand the significance of any changes. As 'year' was in the final fitted diver model, it was necessary to produce plots for both the least and most variable years (2010 and 2014, respectively). Figure 4.5.48 is the surface for the least variable year (2010) and the more detailed plot of the inner grid cells is provided in Figure 4.5.49, whereas the surfaces for the most variable year (2014) are given in Appendix 8.

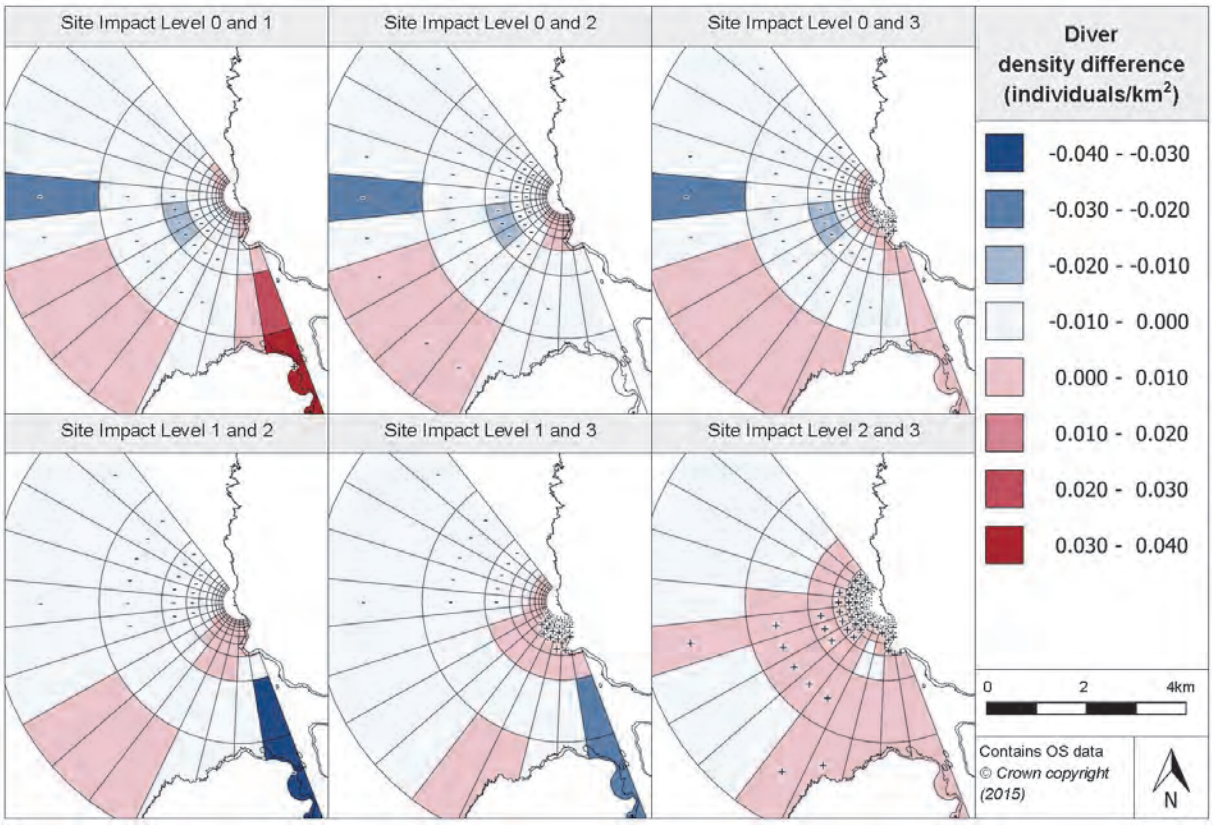

Figure 4.5.48. Estimated density difference between various site impact levels for divers during 2010 (year with least variation) at Billia Croo

Between SIL-0 and SIL-1, the majority of grid cells are expected to reduce in density with the introduction of device-associated infrastructure. Of the outer grid bands, there are five grid

cells at the mouth of Hoy Sound where an increase in density is expected (Figure 4.5.48). The positive change in density in grid cells A13 and B13 is expected to be between 0.020 and 0.040 individuals/km^2. In addition, an increase in density is also estimated between grid cells A6 and A9. There is a large decrease expected in cell A4, with a reduction of between 0.020 and 0.030 individuals/km^2 anticipated. Grid cells A4-A5, B4-B10 and C4-C10 all have significant decreases in density estimated. As seen in Figure 4.5.49, within the inner grid bands, the cells in the west tend to have a slight decrease expected whereas cells to the east have a slight increase in density. However, only three grid cells, D6-D8, have had their change in density marked as significant.

The changes in density between SIL-0 and SIL-2 appear to be very similar to those estimated for between SIL-0 and SIL-1, with the exception of an absence of any density increase at the mouth of Hoy Sound. Within the inner grid bands, see Figure 4.5.49, fewer grid cells are expected to show an increase in density and grid cells D0-D8 and E1-E6 have had their decrease in density deemed significant. Again, a similar distribution of density increases and decreases is anticipated between SIL-0 and SIL-3 (Figure 4.5.49). A slight increase in the grid cells located at the mouth of Hoy Sound has reappeared. Additionally, within the inner grid cells, the three innermost grid bands are expected to show an increase in density as well as further grid cells located around the peninsula south-east of Billia Croo. There appears to be no correlation between significant changes in density for SIL-0 andSIL-3 and the location of test berths, as some berths are located in grid cells that show a positive change and others in grid cells showing a negative change, but all changes are deemed statistically significant.

When the density difference between SIL-1 and SIL-2 is plotted spatially, the majority of grid cells are expected to decrease in density (Figure 4.5.48). The exceptions are a cluster of approximately 40 grid cells around cell E11 and grid cells A7-A9, where an increase of between 0.00 and 0.01 individuals/km^2 is estimated. However, none of these changes are marked as significant. It is grid cells in the north of grid bands B, C and D that have had their reduction in density deemed significant. There are large reductions in density (0.03-0.04 individuals/km^2) modelled for the grid cells located in the mouth of Hoy Sound (A13 and B13) but the change has not been deemed significant.

Between the SIL-1 and SIL-3 prediction surfaces, again the majority of grid cells in the outer grid bands are expected to reduce in density with the introduction of operational devices, see Figure 4.5.48. The decrease in the northern parts of grid bands B and C has been deemed significant as well as in grid cells A0 and A4. Similar to that between SIL-1 and SIL-2, the decrease in grid cells A13 and B13 has not been deemed significant but is expected to be up to 0.03 individuals/km^2. In terms of the grid cells where an increase in density is expected, the southern half of grid band C and cells A9-10 all have an increase of up to 0.01 individuals/km^2 estimated. As can be seen in Figure 4.5.49, for the internal grid cells, the majority show a slight increase (0.00-0.01 individual/km^2) except for the northern part of bands D and E, between SIL-1 and SIL-3. The cells in the south-east that adjoin the coastline at Billia Croo have all had their increase in density deemed significant.

In terms of the density difference between SIL-2 and SIL-3, the vast majority of cells show an increase of up to 0.01 individuals/km^2. The cells in the three innermost grid bands and the majority of grid band F have had all their grid cells deemed as significant. Further cells in grid bands A-E to the south-west have also been modelled to be significant. The only decreases are in grid cells A0-A4, A6-A8, B0-B3, C10-C11 and D10. These changes are less than 0.01 individual/km^2 and only the change in cell A8 is deemed significant.

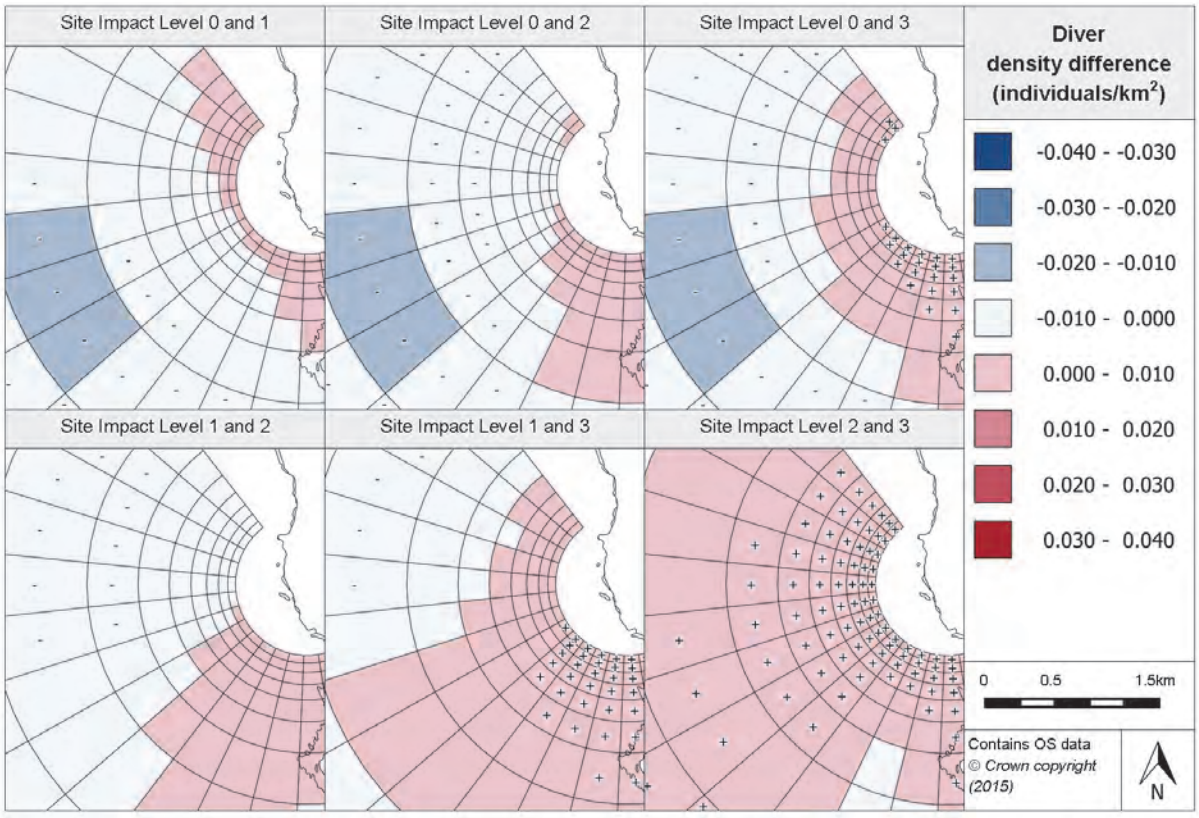

Figure 4.5.49. Density differences between divers site impact level inner prediction surfaces during 2010 (least variable year) at Billia Croo

4.5.6.7 Density change with distance from potential impact location

Due to large variability in the predictions for this species, it was not possible to produce a figure showing how the density difference between the predictions for each site impact level varied with increasing distance from a potential impact location.

4.5.6.8 Discussion

Two diver species (the great northern diver and the red-throated diver) have been observed at Billia Croo, albeit only as infrequent visitors. The model for their distribution includes six terms with five considered highly significant. These terms include distance from land and month and year. The model predicts an increase in numbers during the course of the observations.

Diver densities are generally low, less than 0.005 individuals/km^2, with only baseline conditions showing a wide distribution of cells with high densities. There seems to be no consistent pattern for changes in densities with regard to increasing site impact levels. The lack of observations has resulted, for many cells, in CV values not being available (that is, there is very high uncertainty in the predictions), principally in the outer grid for all site impact levels. In contrast, much of the inner grid has very high confidence values at SIL-3 (devices installed and operational).

Density differences show a reduction for most of the survey area corresponding with the installation of infrastructure. The extent of change is reduced when devices are installed and become operational. There appears to be no correlation between significant changes in density from baseline conditions to those pertaining when devices become operational and the location of test berths; some test berths are located in grid cells that show a positive

change and others in grid cells showing a negative change, but all changes are deemed statistically significant.

4.5.7 Gulls

4.5.7.1 Species overview

To aid the analysis, it was decided that the most appropriate method of assessing if there is any evidence for density changes that can be associated with site impact level in gull species was to consider the gull family (*Laridae*) in a single species group. This group was named *Gulls* and includes the following species, as well as any unidentified gull species*:*

- European herring gull (*Larus argentatus*)
- great black-backed gull (*Larus marinus*)
- common gull (*Larus canus*)
- black-legged kittiwake (*Rissa tridactyla*)
- Sabine's gull (*Xema sabini*)
- Iceland gull (*Larus glaucoides*)
- lesser black-backed gull (*Larus fuscus*)
- glaucous gull (*Larus hyperboreus*)

The following is a summary of the feeding and behavioural attributes for each of the species listed above.

Herring gulls tend to be a resident species in the British Isles, with regular observations in both summer and winter. This coastal species does not tend to have a clear preference in terms of breeding habitat, ranging from cliff and stacks to sandy beaches (BirdLife International, 2015). This well-known scavenging species is omnivorous with a full-ranging diet. Typical prey include fish, crabs, molluscs and even echinoderms (e.g. starfish) (Burger *et al*., 2013a).

The great black-backed gull is an opportunistic species, feeding on a large range of prey species including fish, birds, eggs, mammals and marine invertebrates (BirdLife International, 2015). The species is known to exhibit particularly aggressive feeding behaviour, especially in relation to chicks and eggs (Burger *et al*., 2013b). The range of this species is large and its migratory behaviour varies for the different regions within its range (BirdLife International, 2015). In the north of Scotland, it is unlikely that this bird performs any long migratory movements south during winter and instead is likely only to disperse short distances.

The common gull, otherwise known as the mew gull, tends to be a year-round resident of the British Isles (Burger *et al*., 2013c). The species typically breeds on coastal cliffs and islands and sometimes on beaches. Prey range from invertebrates and fish to the sporadic bird or mammal (BirdLife International, 2015).

The migratory, black-legged kittiwake tends to be found only in the coastal area around the breeding season and, after the breeding season, the species tends to disperse to the open ocean (Burger *et al*., 2013d). The breeding season is between May and June but the species regularly migrate back to the coastal areas a few months before May. Typical breeding habitat is high cliff with narrow ledges (Olsen and Larsson, 2004) (a regular feature around Orkney). The diet predominantly consists of fish and marine invertebrates but, during breeding season, the species can also be observed taking intertidal molluscs and crustaceans (BirdLife International, 2015).

The Arctic-dwelling Sabine's gull is highly pelagic during its winter migrations south and, therefore, is only very rarely observed at Billia Croo. The species' main prey includes

invertebrates and small fish but the eggs of conspecifics have also been recorded in their diet (BirdLife International, 2015). Typical feeding behaviour is a low-swoop over water, only taking prey from the surface; however, they have been observed swimming on some occasions (Burger *et al*., 2013e).

Similar to the Sabine's gull, the Iceland gull breeds in Arctic regions and winters further south, in locations such as Iceland, UK and Norway. During wintering, the species tends to inhabit rocky coastlines and steep clips and also shows an aversion to habitats in close proximity to freshwater (BirdLife International, 2015). Typical prey include small fish (e.g. salmon, sprat and herring) and marine invertebrates. The species have also been observed taking bird eggs and chicks as well as seeds and fruits (del Hoyo *et al*., 1996).

The lesser black-backed gull tends to breed around north-east Europe and disperses widely when not breeding, encompassing the North Sea region, the Mediterranean and the Black Sea (BirdLife International, 2015). Typical habitat is coastal and inland waters including estuaries; however, during breeding, the species tend to use sandy, rocky and grassy coastlines as well as rocky islands and sea cliffs (Burger *et al*., 2013f) (note that this is typical of the coastline at Billia Croo).

Similar to the Sabine's gull and Iceland gull, the glaucous gull is an Arctic-dwelling species which uses the UK shore whilst migrating south (Burger *et al*., 2014). Typical prey for the species include fish, molluscs, crustaceans and birds' eggs/chicks (particular species include ducks, auks and shorebirds) (BirdLife International, 2015). This species has only been observed once at Billia Croo throughout the duration of the observations programme.

4.5.7.2 Data summary

The most common gull species observed at Billia Croo are the great black-backed gull, the black-legged kittiwake and the European herring gull. Other species such as the Sabine's gull, Iceland gull and glaucous gull are only very rarely spotted at Billia Croo. The following table, Table 4.5.19, provides an overview of the raw data used in fitting the gull model. The data summary provides information for each site impact level including typical group sizes.

Table 4.5.19. Summary of gull raw data

	Total	Site Impact Level 0	Site Impact Level 1	Site Impact Level 2	Site Impact Level 3
Number of observations	2611	120	143	1206	1139
Minimum (group size)	1	1	1	1	1
Maximum (group size)	400	150	225	250	400
Mean (group size) (s.d)	6.78 (23.06)	11.02 (25.32)	21.29 (41.74)	3.77 (11.02)	7.72 (27.69)

4.5.7.3 Model overview

For the final fitted gull model, the GEE-based p-values have been produced for each of the remaining terms. There are five remaining terms in the fitted model, four of which are statistically highly significant and one statistically significant. A summary of these terms, and their associated p-values, are provided in Table 4.5.20.

Table 4.5.20. GEE-based p-values for the terms in the final gulls model for Billia Croo

Model term	p-value
Distance to land	<0.0001
Month	<0.0001
Site impact	0.007298
Spatial surface	<0.0001
Spatial surface / site impact	<0.0001

Within the final model, 'distance to land' as a term has been included. This is because the model has estimated that there is a clear relationship between gull abundance and distance to land. It predicts that, with increasing distance from land, there is a reduction in gull numbers. The model has also estimated clear seasonal trends in gull numbers which is unusual when modelling groups of species (due to each species' breeding and wintering seasons varying slightly). The model has estimated that there is a peak in gull density between April and July and then a clear low in abundance between August and October. Gull numbers are then expected to reach their highest during November, with another drop in numbers anticipated from December through to March. Figure 4.5.50 provides the model's partial plot for the term 'month' which shows the clear peaks and troughs in gull density.

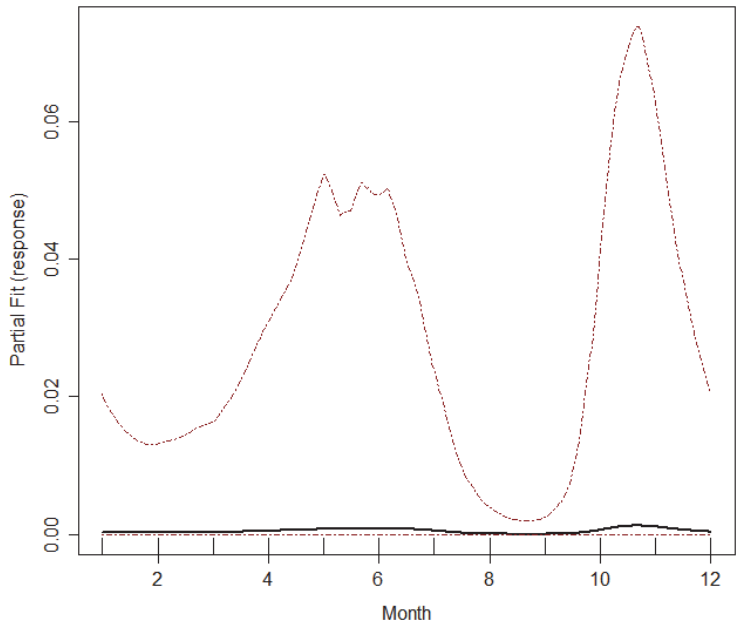

Figure 4.5.50. Estimated partial relationship of month against log(density) for gull at Billia Croo. The red lines represent 95% confidence intervals about the estimated relationship and the tick marks show where the data lie in the covariate range.

As with the model for the other species, the fitted gull model for Billia Croo has a spatial surface fitted. Four knots were used in fitting the surface. The interaction term (site impact/spatial surface) was also in the model, as found to be statistically highly significant.

4.5.7.4 Density predictions and uncertainty estimate

As the fitted gull model contains a spatial surface, it is possible to produce density estimates across the prediction surface at Billia Croo. A prediction surface for gull density has been

generated for each of the site impact levels, which is provided in Figure 4.5.51. A more focused view of the inner grid cells is given in Figure 4.5.52. As with previous species, to be able to make predictions, it is necessary to set the environment covariates; it was decided that the conditions in which the most number of gulls have been sighted should be set for the environmental covariates (see Appendix 5). In addition to the prediction surfaces, CV values have been produced for each prediction across the prediction surface, see Figure 4.5.53 and Figure 4.5.54.

Reference should be made to Figure 2.1.9 and Figure 2.1.10 for the grid cell labelling system.

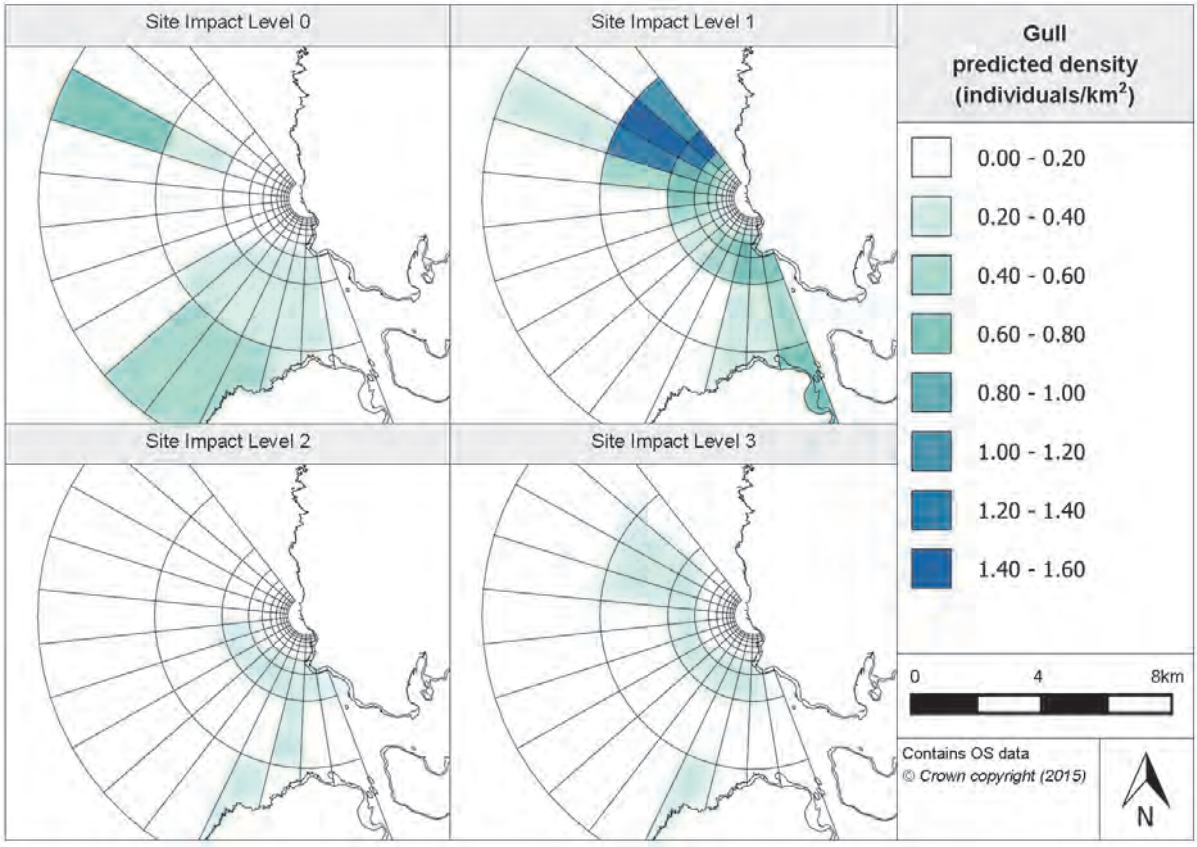

Figure 4.5.51. Estimated gull density at each site impact level across Billia Croo

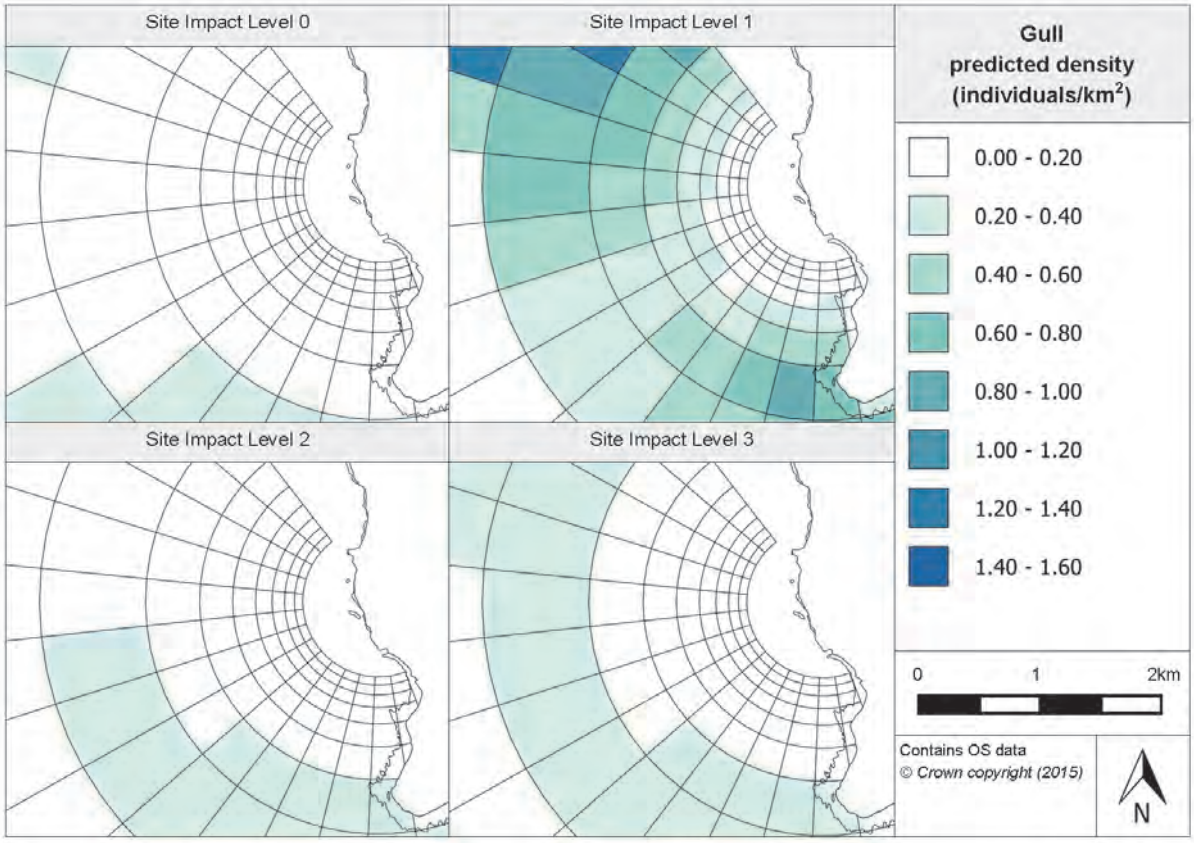

Figure 4.5.52. Inner prediction surfaces for gull density at Billia Croo

At SIL-0, baseline conditions, it is expected that there will generally be low abundance across the site, with the exception of the southern end of the site and grid cells A2 and B2 where there is a slight increase in abundance (Figure 4.5.51). In the south, there are 16 outer grid cells to the north of Hoy where there are heightened density predictions. In grid cells A8-A10, there are estimated densities of 0.40-0.60 individuals/km^2. There are also notable densities of 0.60-0.80 individuals/km^2 in grid cell A2. All of the grid cells within the inner grid bands (Figure 4.5.52) have density predictions between 0.00 and 0.20 individuals/km^2.

For the prediction surface for SIL-1, the highest predictions are in the grid cells B0-B2 and C0-C1. As can be seen in Figure 4.5.51, these are higher than any other density predictions across all four surfaces, and they range between 1.00 and 1.60 individuals/km^2. It is unclear what is causing these higher predictions in this area of the site at this impact level, as only a single test berth is contained within the grid cells marked as showing these higher predictions. If this effect is due to the presence of infrastructure at a test berth, it would likely be present at more than one berth. All of the cells in grid bands C, D, E and F (apart from cell F8) have been modelled to have densities of greater than 0.20 individuals/km^2 (Figure 4.5.52). In addition, there is an area of high density in grid cells in the south-eastern area of the site (A11-A13, B11-13), at the mouth of Hoy Sound.

At SIL-2, when devices are installed but not operational, very few grid cells have a estimated density greater than 0.20 individuals/km^2. There is a cluster of grid cells with an expected density between 0.20 and 0.40 individuals/km^2 at the southern end of grid bands C and D, near to the peninsula south of the observation vantage point (see Figure 4.5.51). In addition, grid cells A10 and B11 show a higher density than the other grid cells surrounding them. As seen in Figure 4.5.52, within the inner grid bands, all of the grid cells apart from D8-12, have estimated densities of lower than 0.20 individuals/km^2.

At SIL-3, grid cell A10 remains at a higher density than the surrounding grid cells; the number of grid cells with an estimated density greater than 0.20 individuals/km^2 is greater at SIL-3 compared to SIL-2. At SIL-3, the majority of grid cells in grid band C have densities of between 0.20 and 0.40 individuals/km^2 (Figure 4.5.51). In addition to these grid cells and those highlighted as having heightened density predictions in grid cell band D, three grid cells B1-3, have also been marked as having higher density predictions than the majority of the survey grid. Similar to the SIL-2 prediction surface, the density within the inner grid band is not expected to be greater than 0.20 individuals/km^2, with the exception of grid cells D8-D12.

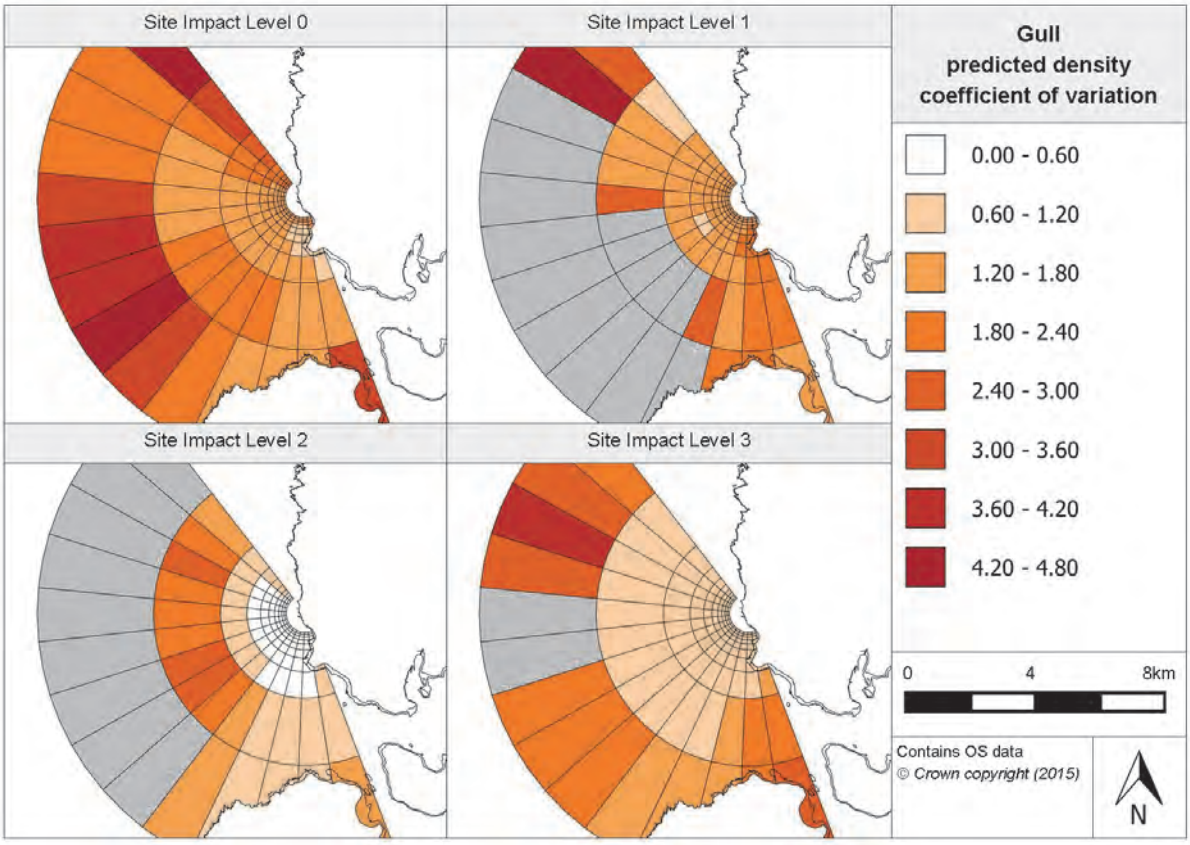

Figure 4.5.53. Associated coefficient of variation values for the density predictions for gulls at Billia Croo

Figure 4.5.53 provides the associated CV values for each of the prediction surfaces. The CV surface for SIL-0 suggests that there is fairly high uncertainty in predictions in the outermost grid band. There are also areas of low precision in the two/three northernmost cells of each grid band, as well as cells B6-B10. The rest of the surface appears to have CV values below 1.8, suggesting reasonable precision in the predictions in these areas whereas, for the SIL-1 CV surface, the majority of grid band A and part of grid band B does not have CV values available, reflecting perhaps few observations occurring in these areas of the grid. Otherwise, most of the cells across the surfaces, particularly the inner cells, have CV values below 1.80, suggesting reasonable precision in the predictions. It is worth noting that, as seen in Figure 4.5.54, the grid cells D11-D13, E11-E13, F12-F13 and G12-G13 all have CV values between 1.80 and 2.40 which suggests that there is greater variability behind the predictions made for these grid cells.

Overall, the CV surface for SIL-2 suggests that there is relatively low uncertainty in most of the predictions across the surface, particularly grid bands C-J. The CV values remain

unavailable for the northern part of the grid band A, and CV values range between 1.20 and 3.00 for the same region of grid band B. However, with the exception of these grid cells and A9, B9 and A13, all of the CV values are below 1.20 across the CV surface.

In terms of the CV surface for SIL-3, there are high CV values in the northern half of grid band A, as well as some grid cells having their CV values unavailable. In addition to this, as seen in Figure 4.5.53, the southern half of grid band A and grid cells B11-B13 and C13 have CV values ranging between 1.20 and 3.00, which would imply higher uncertainty in these predictions. However, the rest of the grid cells across the surface have CV values below 1.20 which suggests relatively high precision in the predictions across the majority of the surface.

Overall, for the CV surfaces, there appears to be generally low uncertainty in the gull density predictions as compared to the CV values obtained for the other Billia Croo bird species. This is probably due to there being many more raw observations of gulls than of other species (e.g. divers); therefore, the models are based on more evidence, which reduces variability in the predictions.

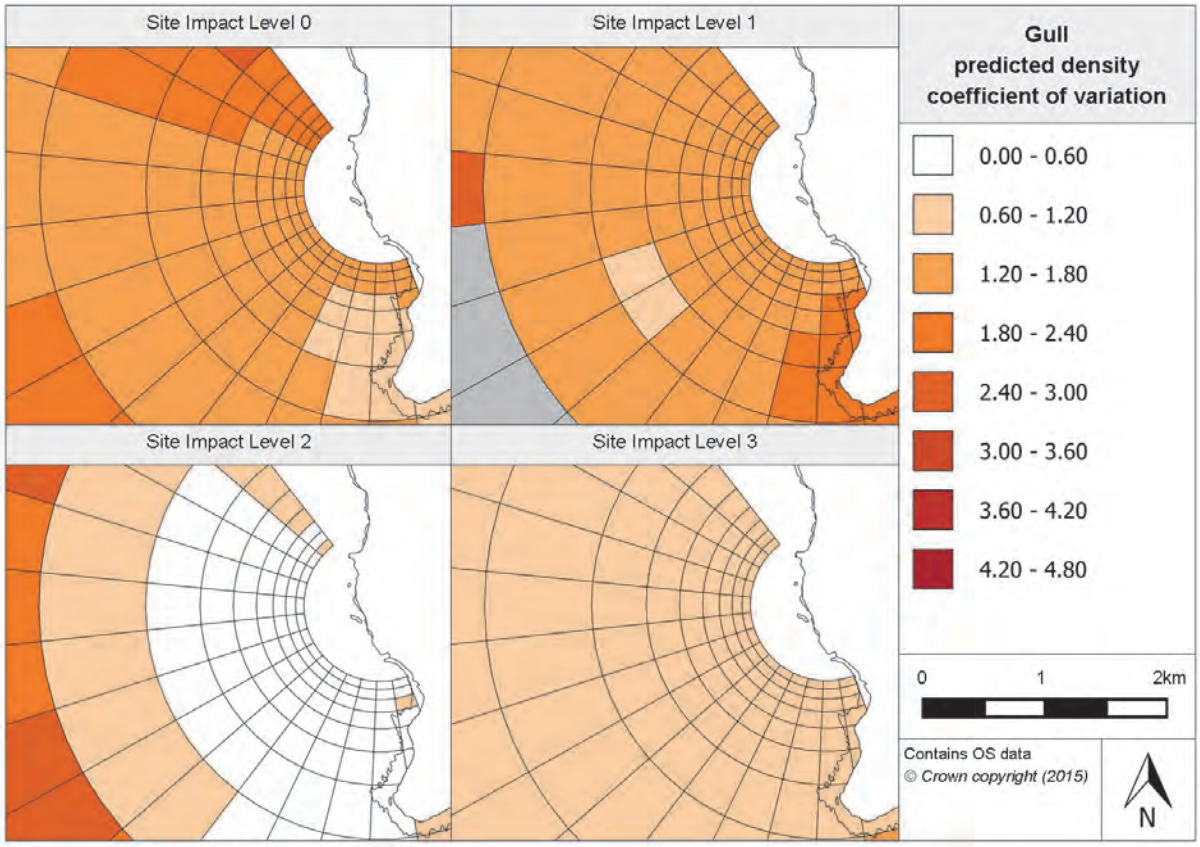

Figure 4.5.54. Associated coefficient of variation values for gull inner density prediction surfaces at Billia Croo

4.5.7.5 Relative abundance estimations

Relative abundance values for each survey month are able to be produced using the fitted gull model. By combining the model predictions, it is possible to produce seasonal abundance predictions which are provided in Table 4.5.21. The 95% CIs for each prediction are also provided.

Table 4.5.21. Relative abundance for gulls during each season (associated confidence intervals are provided in brackets)

Year	Season			
	Winter (Dec, Jan, Feb)	Spring (Mar, Apr, May)	Summer (Jun, Jul, Aug)	Autumn (Sep, Oct, Nov)
2009	-	19.70 (6.54, 61.95)	20.43 (6.26, 77.31)	89.59 (3.08, 439.67)
2010	49.21 (18.06, 154.34)	21.63 (8.56, 51.92)	19.45 (1.55, 61.80)	28.97 (0.85, 88.71)
2011	15.96 (8.41, 27.64)	22.56 (9.94, 61.95)	17.71 (1.36, 77.31)	22.69 (0.64, 104.21)
2012	49.21 (18.06, 154.34)	77.80 (22.66, 304.92)	47.96 (1.55, 318.57)	24.91 (0.85, 62.95)
2013	14.23 (8.41, 22.23)	25.24 (9.94, 56.38)	22.69 (1.88, 65.29)	22.69 (0.64, 104.21)
2014	12.46 (4.85, 35.00)	66.71 (6.54, 304.92)	69.95 (6.26, 318.57)	49.79 (3.08, 247.16)
2015	13.68 (7.26, 22.23)	21.63 (8.56, 51.92)	-	-

From Table 4.5.21 above, there is no clear evidence of seasonality as no abundance estimates for one season are particularly higher than another. This differs from the relationship modelled for 'month' discussed above (see Figure 4.5.50). It is likely that, although a relationship exists with 'month', there are other terms in the model that are having a greater influence on the gull abundance estimates (e.g. 'year'), outweighing the variations in seasonality that are caused by having 'month' in the fitted model.

However, there is evidence of great variability in abundance predictions between years. The winter, spring and summer of 2012 appear to have particularly high estimates, with often over twice the abundance estimated as compared to the same seasons in different years. Additionally, the autumn of 2009 and winter of 2010 appear to have greater abundance estimates as compared to equivalent seasons. The relative abundance estimates have also been plotted against time for each site impact level; this is provided in Appendix 7.

In addition to the gull prediction surface discussed above in Section 4.5.7.4, other gull prediction surfaces have been created for typical surveying conditions in January and July at Billia Croo. The produced surfaces and their associated CV values are provided in the Marine Scotland Information portal. As expected, due to the lack of seasonality modelled, the surfaces are very similar, with very slightly higher predictions in July compared to January.

4.5.7.6 Spatially-explicit change

To understand if there is any evidence of spatially-explicit change in gull abundance or distribution, the difference between gull surface predictions for each of the site impact levels has been produced. In addition to these density differences, the 95% CIs have also been generated to be able to calculate the significance of any changes. 'Year' was not in the final model so the prediction surface for each year was the same; thus, only one year's surface is provided, see Figure 4.5.55. For a detailed view of the inner grid cells of the spatially-explicit change surfaces, refer to Figure 4.5.56.

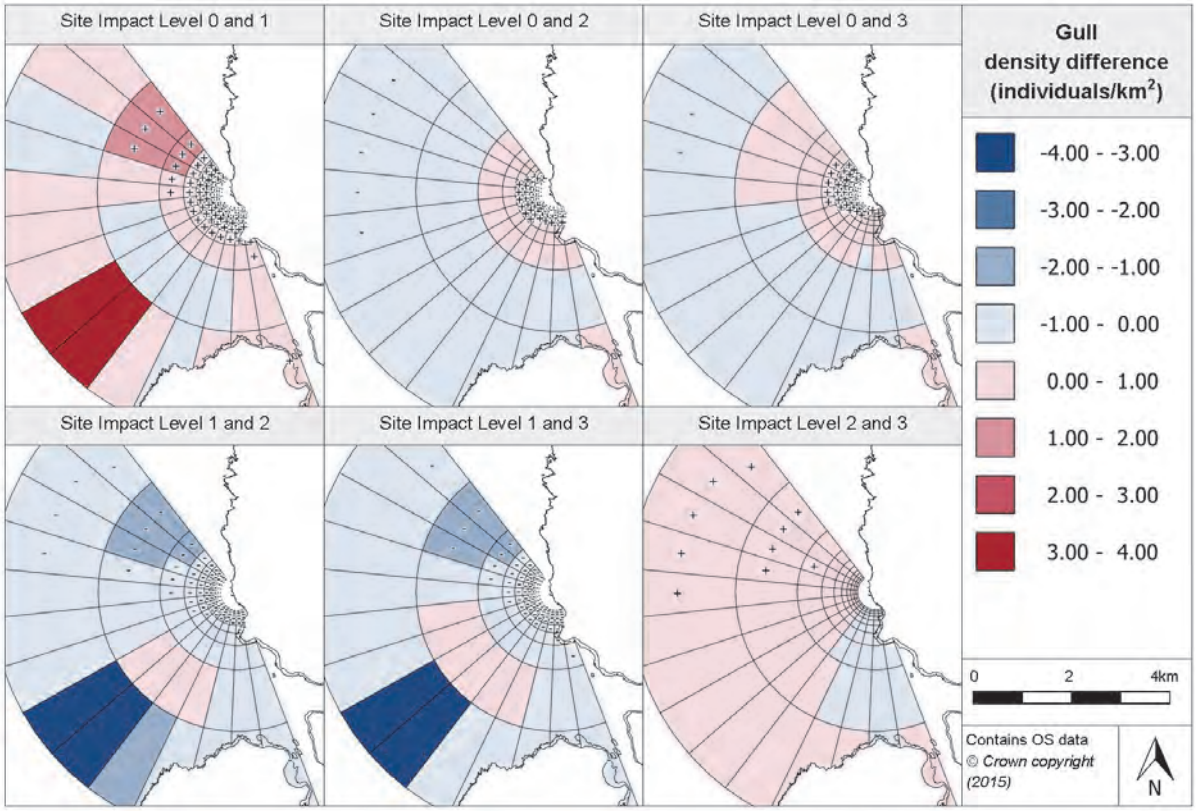

Figure 4.5.55. Estimated density difference between various site impact levels for gulls at Billia Croo

From Figure 4.5.55, it appears that the density difference surface between SIL-0 (baseline conditions) and SIL-1 (when infrastructure is installed) suggests that the majority of grid cells are expected to increase in density with the introduction of infrastructure. The only grid cells across the whole surface that are expected to reduce in density (up to 1.00 individual/km^2) are A2-A3, A10 and B5-B11. The majority of grid cells across the surface are only expected to rise in density by 1.00 individual/km^2 however, grid cells B0-B2 and C0-C2 are anticipated to increase in density between 1.00 and 2.00 individuals/km^2 and grid cells A7-A8 are expected to rise in density by 3.54 individuals/km^2 and 3.18 individuals/km^2, respectively. All of the grid cells in the inner grid bands, as well as grid cells B0-B2 and C0-C4, have had their positive change in density deemed as significant. This wide area includes all the test berths.

When considering the density change between SIL-0 and SIL-2 (when devices are installed but not operational), there is a clear reduction in density (up to 1.00 individual/km^2) in grid bands A and B (except for cell A13). The reduction has been deemed significant in grid cells A1-A5. However, an increase in density is expected in the inner grid calls, grid band C and cell A13 (Figure 4.5.55). The increase in density is only limited and expected not to be greater than 1.00 individual/km^2; however, most of the five innermost grid bands, as well as part of grid band E, have been marked as significant. This excludes most of the test berths.

Between SIL-0 and SIL-3 (when devices are installed and operational), again it appears that most of the outer two grid bands are expected to reduce in density. However, in addition to grid cell A13, grid cells B0-B4 also have a slight increase in density expected. All of the grid cells within the inner grid bands, as well as grid band C (with the exception of grid cell C11), have slight increases in density (up to 1.00 individual/km^2). The changes in cells in the north of the inner grid bands have been deemed significant. There is no apparent relationship between these cells showing significant change and the distribution of test berths.

The density difference between SIL-1 and SIL-2 is estimated to be negative across the entire prediction surface, except for cells B7-B10 which show an increase of less than 1.00 individual/km^2. Most of the decreases across the site are expected to be no more than 1.00 individual/km^2; however, grid cells A9, B0-B2 and C0-C1 are modelled to experience a reduction in density between 1.00 and 2.00 individuals/km^2 and grid cells A7-A8 are expected to show a decrease of between 3.00 and 4.00 individuals/km^2. These large density reductions should be questioned as these cells have very low density predictions (<0.2 individuals/km^2) (Figure 4.5.51) and CVs unavailable or very high CVs (Figure 4.5.53). Therefore, it would seem that the model is predicting a negative figure for birds and there is likely to be an insufficient number of observations in these cells.

As can be seen in Figure 4.5.56, the five innermost grid bands have their reductions in density deemed significant together with the northern half of grid bands D and E, as well as cells A0-A3, B0-B3 and C0-C4. The difference in density predictions between SIL-1 and SIL-3 is very similar to that between SIL-1 and SIL-2 (Figure 4.5.55). Similarly, a cluster of grid cells is expected to have an increase in density, with cells B5-B10 having an estimated increase of between 0.00 and 1.00 individuals/km^2. A decrease of between 3.00 and 4.00 individuals/km^2 continues to be predicted in grid cells A7-A8, and reductions in density of between 2.00 and 1.00 individuals/km^2 remain in grid cells B0-B2 and C0-C1. Similar to the changes in density between SIL-1 and SIL-2, changes in density in the six innermost grid bands have all been marked as significant as well as additional northern cells in grid bands A-D.

As seen in Figure 4.5.55, it appears that the majority of grid cells are estimated to increase in density with devices becoming operational (between SIL-2 and S1L-3). In terms of the outer grid bands, the only cells where a reduction in density is expected (up to 1.00 individual/km^2) are A12, B10-B13 and C9-C13. Otherwise, the rest of the grid cells in the outer grid bands have density increases estimated to be between 0.00 and 1.00 individuals/km^2. Additionally, the increases in density anticipated in grid cells A0-A4, B0-B3 and C2 have been deemed significant. There appears to be a north-south divide in terms of the density difference in the inner grid bands, with a slight increase in density in the northern part of the grid bands and a slight decrease in the southern half. None of these changes have been deemed significant.

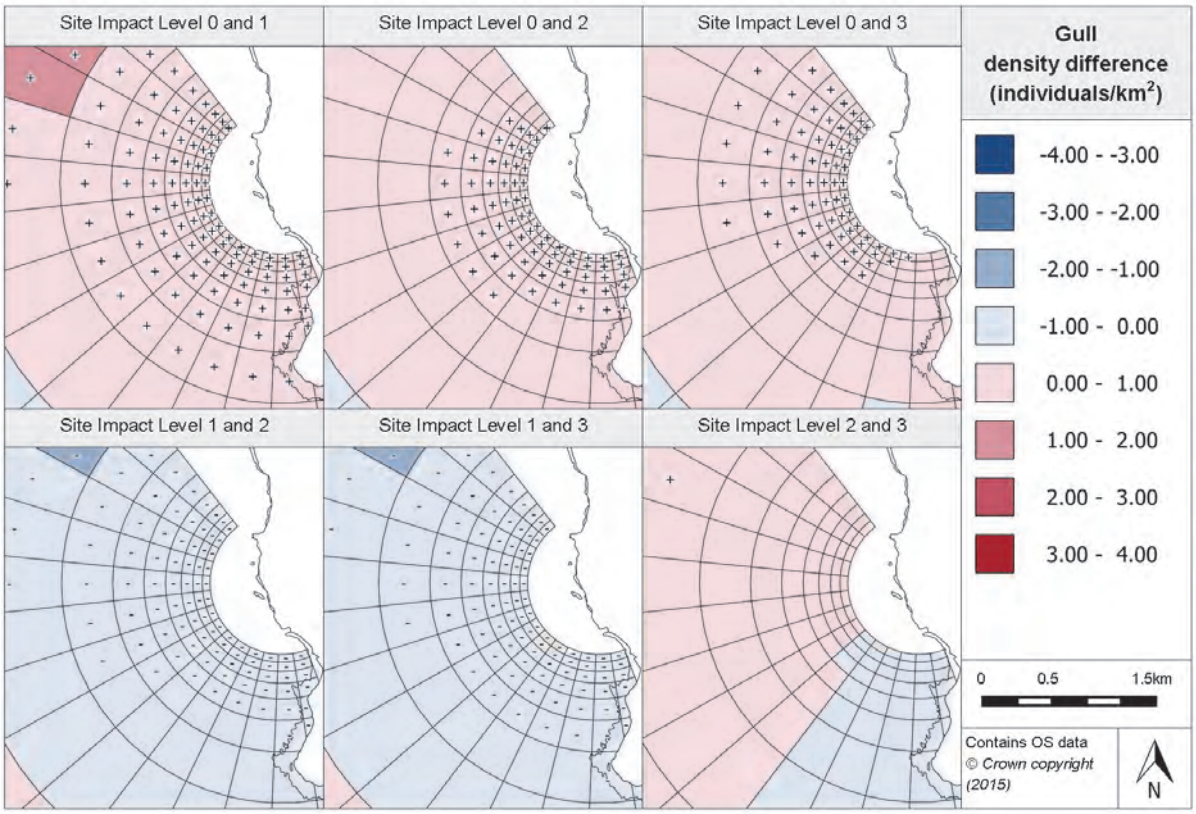

Figure 4.5.56. Density differences between gull site impact level inner prediction surfaces at Billia Croo

4.5.7.7 Density change with distance from potential impact location

By using the density difference projections discussed above, it has been possible to predict the density difference between prediction surface changes with increasing distance from a potential impact location (a single test berth). The changes for various site impact levels are shown in Figure 4.5.57.

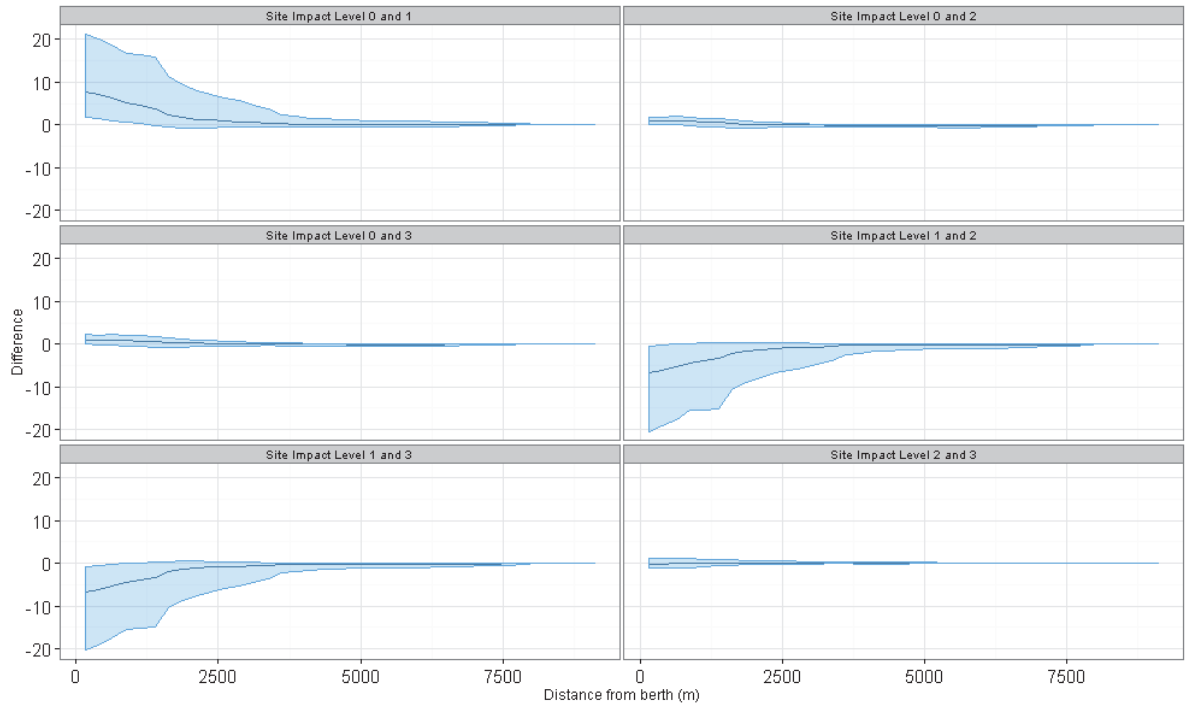

Figure 4.5.57. Density change between site impact levels with increasing distance from a potential impact location, with associated confidence intervals, for gulls at Billia Croo

Between baseline conditions and SIL-1, it appears that, at the location of the potential impact, there is an immediate increase in density which gradually returns to density experienced at baseline conditions beyond approximately 3.5km. As the lower CI is above zero for the first kilometre, it is likely that this increase is significant for up to 1km from the potential impact location. However, as can be seen in Figure 4.5.57, between baseline conditions and SIL-2 and SIL-3, there is little change expected between gull densities estimated under SIL-2 and SIL-3 conditions and those modelled for baseline conditions.

Conversely, the density difference between SIL-1 and SIL-2 suggests that there is an immediate decrease in density at the test berth location which gradually reduces in intensity, returning to SIL-1 conditions after approximately 3.5km. As the upper confidence limit sits around zero, it is reasonable to suggest that this density decrease may be significant. The density difference between SIL-1 and SIL-3 appears to follow a similar trend to that described between SIL-1 and SIL-2 (Figure 4.5.57). A large decrease in density is expected at the immediate location of the test berth which again slowly reduces in intensity with increasing distance away from the potential impact location. Again, it appears that the estimated density returns to SIL-1 levels at a distance of approximately 3.5km from the test berth. It is likely that, for at least the first kilometre if not further, the change in density modelled between these two impact levels is significant. As seen in Figure 4.5.57, there is very little density difference expected between SIL-2 and SIL-3. The large density changes at the impact site for SIL-0 to SIL-1, SIL-1 to SIL-2 and SIL-1 to SIL-3 all involve SIL-1 conditions. The other modelled density changes are much smaller. It maybe that the anomalous high densities estimated for SIL-1 for grid cells B0-B2 and C0-C1 are influencing these changes with distance from impact site, as one of the test berths is located in grid cell B2.

4.5.7.8 Discussion

Eight different species of gulls have been observed at Billia Croo. The most common species observed are the great black-backed gull, the black-legged kittiwake and the

European herring gull. The model for the gull family contains four terms which are statistically highly significant and one statistically significant. These include distance from land and month. The model's density surfaces show little consistency in the location of grid cells with higher estimated densities for the different site impact levels. The distribution of increases and decreases in density which coincident with the installation of infrastructure, are effectively reversed when devices are installed. Most cells show a density increase when the devices become operational; however, only a few of these changes are deemed significant. This suggests there is little consistency in the changes in gull density. Similarly, there is no apparent relationship between the distribution of test berths and either changes in density in cells, or whether such changes are statistically significant.

Examination of the changes in density at an impact site and with increasing distance from the site indicates that there is an increase in density with the installation of infrastructure compared to baseline conditions. Between baseline conditions and SIL-2 and SIL-3 there is virtually no change in density predicted. However, decreases in density are likely to occur with devices being installed onsite and devices becoming operational compared to SIL-1 conditions.

4.6 Billia Croo marine mammals

4.6.1 Seals

4.6.1.1 Species overview

Similar to the Fall of Warness and the rest of the UK, two species of seal have been observed at Billia Croo, the grey seal (*Halichoerus grypus*) and the harbour seal (also known as the common seal)(*Phoca vitulina*). The grey seal is much more common than the harbour seal at Billia Croo, with over ten times more observations of the former than the latter. As with the Fall of Warness, sometimes the observers at the site were unable to distinguish between the grey and harbour seal species and these observations are recorded as 'unidentified seal' i.e. unclassified seal. The following section provides a discussion of the outputs and predictions from a model based on a combined dataset of grey seal and harbour seal and unclassified seal observations.

For a summary on both the grey and harbour seal typical distribution and life history, refer back to Section 4.4.1.1.

4.6.1.2 Data summary

The following table, Table 4.6.1, provides a summary of the raw observation data used in the model selection process. Also included in the table is information regarding typical group size. The information has also been split across site impact levels, which provides an indication of the amount of observation data used in creating the prediction surfaces for each site impact level. As can be seen in Table 4.6.1, many fewer seal observations were recorded when site impact level conditions were 0 (baseline) or 1 (device-associated infrastructure installed), and therefore there may be less confidence behind these prediction surfaces when compared to the prediction surfaces for site impact levels 2 (devices installed) and 3 (devices operational).

Table 4.6.1. Summary of seal raw data

	Total	Site Impact Level 0	Site Impact Level 1	Site Impact Level 2	Site Impact Level 3
Number of observations	1323	45	74	579	625
Minimum (group size)	1	1	1	1	1
Maximum (group size)	31	2	2	31	30
Mean (group size)	1.56	1.04	1.08	1.21	1.98
(s.d)	(2.92)	(0.21)	(0.27)	(1.66)	(3.90)

4.6.1.3 Model overview

The final fitted seal model contains six terms. By considering their GEE-based p-values (as shown in Table 4.6.2), it was concluded that all six terms were statistically highly significant when predicting seal density.

Table 4.6.2. GEE-based p-values for the terms in the final seals model for Billia Croo

Model term	ρ-value
Distance to land	<0.0001
Month	<0.0001
Year	<0.0001
Site impact	<0.0001
Spatial surface	<0.0001
Spatial surface / site impact	<0.0001

The term ‘distance to land’ has been included in the final fitted model. This is due to the model predicting that seal density is affected by the distance from land, with seal abundance at its greatest closer to land. In terms of the seal density predictions and seasonality, ‘month’ is included as a term in the fitted model which would suggest the model predicts that seal abundance will vary throughout the year. These predictions are in line with the life history of grey seals (the most abundant species at the site). The clear peak and trough that would be seen if just grey seal observations were being recorded are damped by the differing seasonality of harbour seals in terms of breeding season, etc.. Within the final model, ‘year’ has also been included as a term. This is because the model has estimated there to be a clear relationship between seal abundance and survey year. It predicts that, over the observations programme’s duration, seal density is increasing. Figure 4.6.1 shows the modelled relationship between survey year and seal density. This is expected to rise at a nearly constant rate.

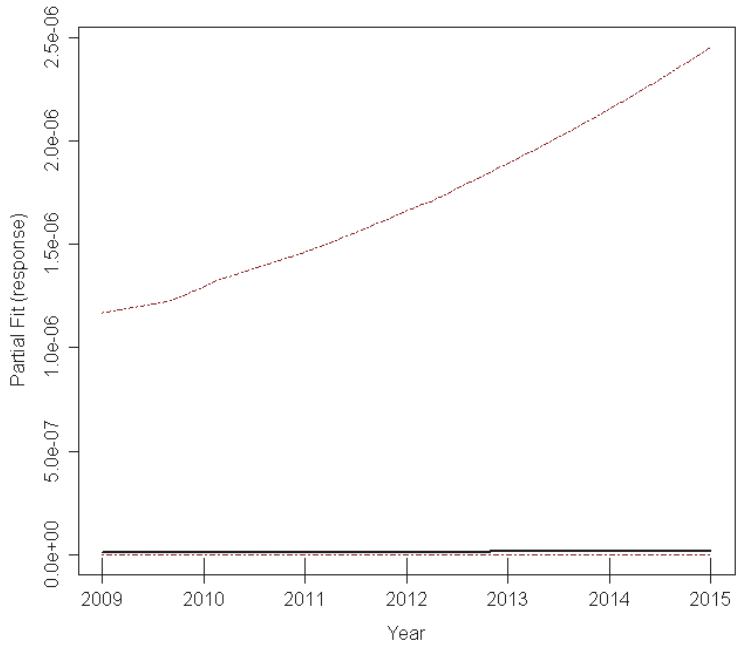

Figure 4.6.1. Estimated partial relationship of year against log(density) for seals at Billia Croo. The red lines represent 95% confidence intervals about the estimated relationship and the tick marks show where the data lie in the covariate range.

Similar to all the other fitted models, it has been possible to fit a spatial surface for the final fitted seal model. Four knots were required in the fitting of the surface. The interaction term (site impact/spatial surface) was also in the model, as it was found to be statistically highly significant.

4.6.1.4 Density predictions and uncertainty estimate

Using the final fitted seal model for Billia Croo, it was possible to produce density prediction surfaces as the model contained a spatial surface. Figure 4.6.2 illustrates the four density prediction surfaces created, one for each site impact level. There is also a more detailed view of the inner grid cells available in Figure 4.6.3. As it was necessary to select the environmental covariates that were to be contained in the model at a certain level, the optimum values for seal observations were chosen, as discussed further in Appendix 5. As with some of the other Billia Croo species, due to there being some anomalies in seal data, it was necessary to reduce the number of iterations in the bootstrap. In total, 860 iterations were implemented rather than the 1000 carried out for most other species/groups. In addition to the prediction surfaces, CV values have been produced for each prediction and are presented in Figure 4.6.4 and Figure 4.6.5.

Reference should be made to Figure 2.1.9 and Figure 2.1.10 for the grid cell labelling system.

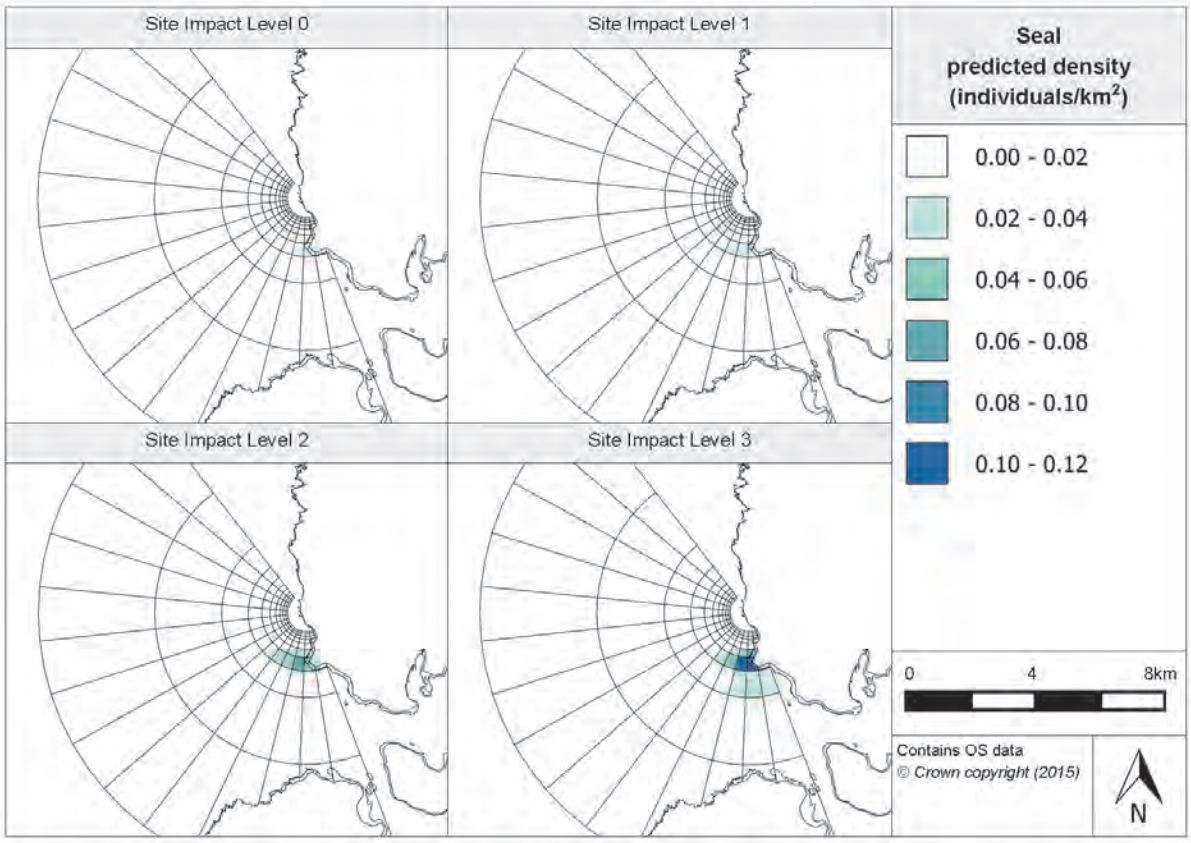

Figure 4.6.2. Estimated seal density at each site impact level across Billia Croo

As shown in Figure 4.6.2, very low seal density is estimated over the majority of the site. Under baseline conditions (SIL-0), it appears that there is a slight rise in density towards the Breck Ness headland in grid cells D10-D12. Across the rest of the prediction surface, seal density is less than 0.02 individuals/km^2. The density prediction surface for SIL-1 (when infrastructure is installed) is almost identical to that for SIL-0, as the only grid cells with a density greater than 0.02 individuals/km^2 are D10-D12, which are expected to have seal densities at SIL-1 of between 0.02 and 0.04 individuals/km^2.

The prediction surface for SIL-2 (when devices are installed but not operational) contains a greater number of grid cells with a density of more than 0.02 individuals/km^2, but the vast majority of cells are less than 0.02 individuals/km^2. However, as seen in Figure 4.6.3, there is a cluster of cells around the peninsula to the south of Billia Croo Bay which has estimated densities greater than 0.02 individuals/km^2. Grid cells D8-D9 and E10-E12 have densities of 0.02-0.04 individuals/km^2 and grid cells D10 and D12 have densities of between 0.04 and 0.06 individuals/km^2. At this site impact level (SIL-2), the cell with the highest estimated density is cell D11 with 0.07 individuals/km^2.

The same cluster of grid cells with density predictions greater than 0.02 individuals/km^2 includes further grid cells at SIL-3 (when devices become operational). As shown in Figure 4.6.3, the grid cells in the cluster are expected to have slightly higher densities. Grid cells C11-C13, D9, D10, D13, E10-E12 and F12 are expected to have varying densities between 0.02 and 0.08 individuals/km^2 whilst grid cells D11 and D12 have the highest seal density predictions of 0.11 individuals/km^2 and 0.12 individuals/km^2.

These results suggest that there is a small area of high abundance around the Breck Ness headland to the south of Billia Croo. It may be that these grid cells are close to a haul-out site used by the grey and harbour seals that visit the site.

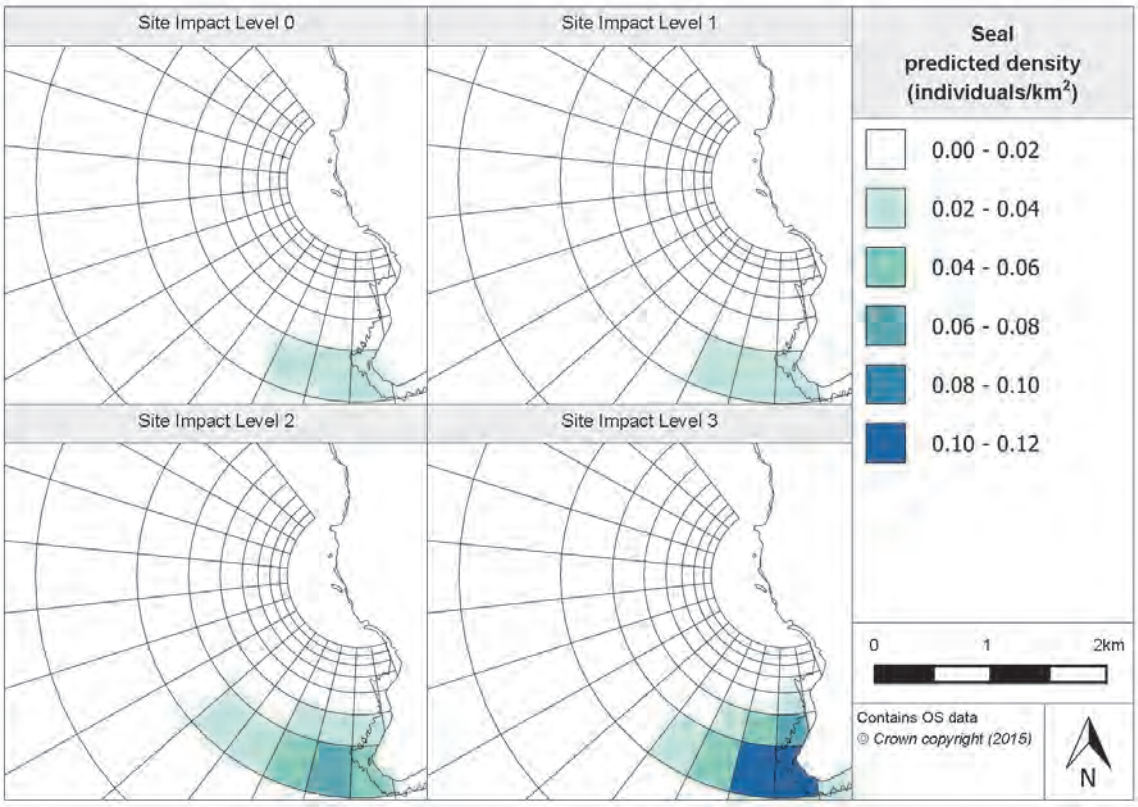

Figure 4.6.3. Inner prediction surfaces for seals density at Billia Croo

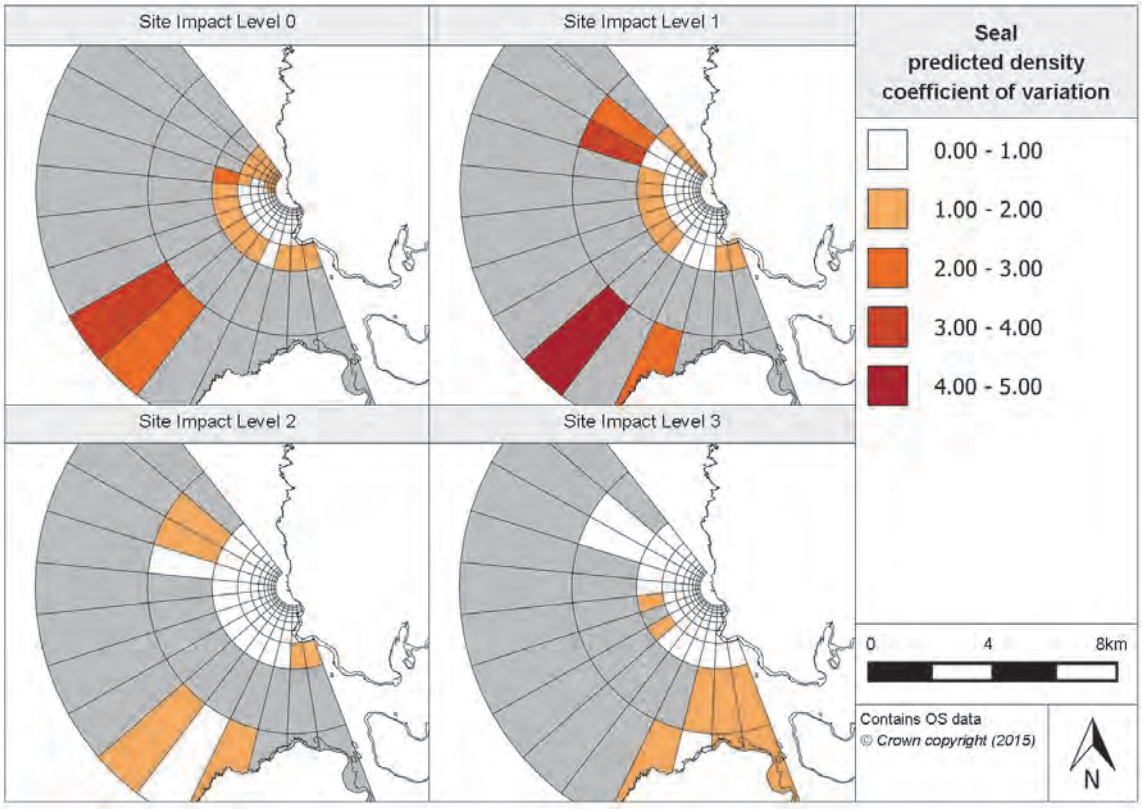

Figure 4.6.4. Associated coefficient of variation values for the density predictions for seals at Billia Croo

When looking at the CV value surfaces produced, for SIL-0 (baseline conditions), there is a lack of values available in most of the two outermost grid bands (Figure 4.6.4). Although CV values exist for grid cells A7-A8, they are both over 2, suggesting high uncertainty in the predictions in these grid cells. With the exception of grid cells C0-C3, the CV values for grid band C are below 2. As seen in Figure 4.6.5, the CV values within the inner grid cells are between 0.00 and 2.00, suggesting reasonable precision in the prediction results, with values below 1 for the southern two-thirds of the inner grid cells (Figure 4.6.5). A similar situation is seen at SIL-1 (when infrastructure is installed), with the two outermost grid bands having the majority of their CV values unavailable. This is likely to be due to a lack of raw observations of seals in these grid cells (and thus limited evidence upon which to base model predictions) and, also, to a very low density prediction. Grid band C and the inner grid bands have CV values below 2, with the vast majority less than 1, thus suggesting reasonable precision in the predictions. It is important to note that, in grid cells D10-D12 where density predictions are expected to be greater than 0.02 individuals/km^2, the CV values are expected to be 0.00-1.00 which suggests high precision in the peak in density for these grid cells.

Again, for the SIL-2 CV values (when devices are installed but not operational), the two outermost grid bands have their CV values unavailable in the majority of grid cells. Grid cells A8-A10 and B1-B3 have CV values between 0 and 2. This implies that there is limited variability behind the predictions for these grid cells but also suggests that the unavailable CV values for the remainder of the two outer grid bands is likely to be due to very low density predictions which produce unrealistic CV values. As can be seen in Figure 4.6.5, the grid cells located in grid band C and the inner grid bands all (with the exception of grid cells C12-C13) have CV values less than 1, suggesting low uncertainty in the predictions. The cluster of grid cells around D11 with density predictions greater than 0.02 individuals/km^2 have CV values below 1, again implying limited variability in the predictions and high precision in the result.

In terms of the CV value surface for SIL-3 (when devices become operational), more grid cells in the two outermost grid bands have CV values available, probably reflecting a greater number of observations made. As can be seen in Figure 4.6.4, there is an area of cells to the south (A10-A13 and B11-B13) which have CV values below 2. In addition, grid cells B1-B2 have CV values between 0 and 1. Other than grid cells C5-C7, all of the grid cells in grid bands C-J, see Figure 4.6.5, have CV values below 1. This suggests that there is low uncertainty in the seal density predictions for this entire area, including the grid cells offshore from Breck Ness where density predictions are greater than 0.02 individuals/km^2.

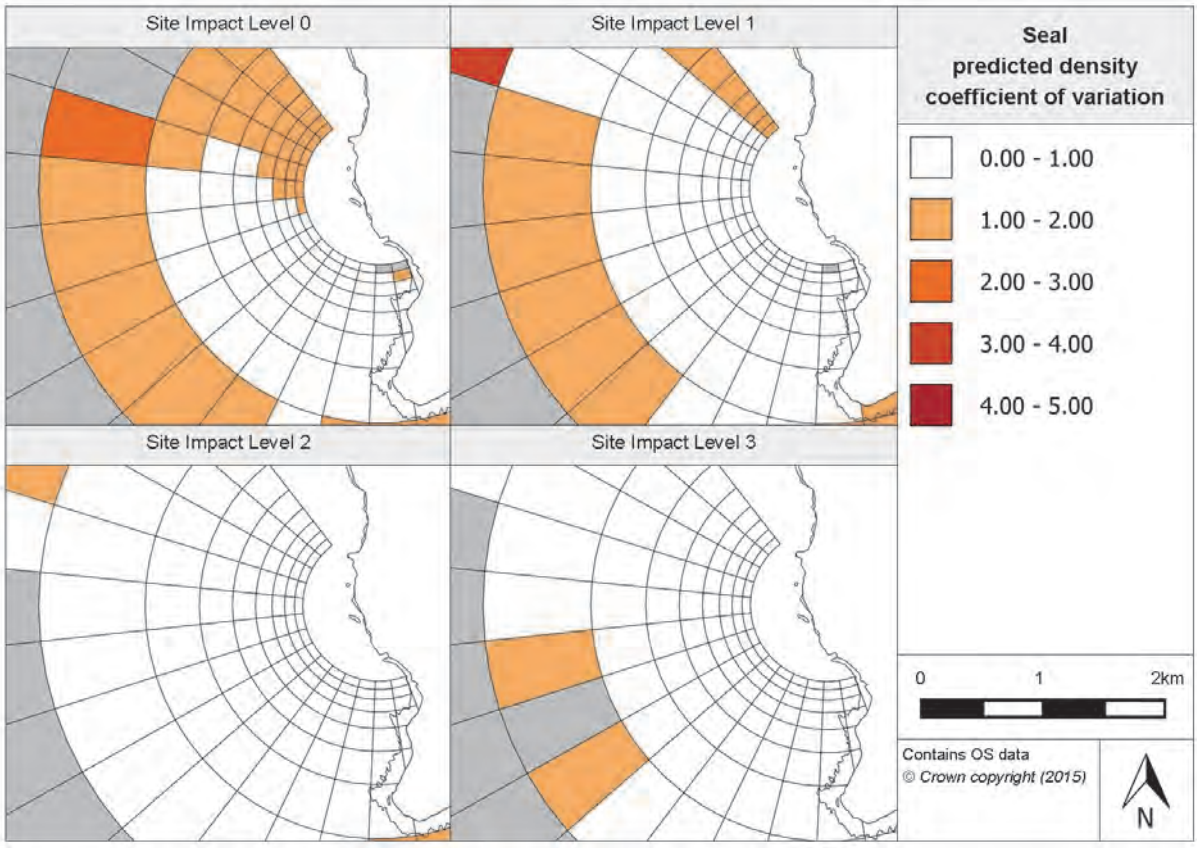

Figure 4.6.5. Associated coefficient of variation values for seals inner density prediction surfaces at Billia Croo

4.6.1.5 Relative abundance estimations

Using the fitted model, it was also possible to predict the relative abundance values for each survey month. These have been combined to provide seasonal (relative) abundance predictions, see Table 4.6.3. The 95% CIs for each prediction are also provided.

Table 4.6.3. Relative abundance for seals during each season (associated confidence intervals are provided in brackets)

Year	Season			
	Winter (Dec, Jan, Feb)	Spring (Mar, Apr, May)	Summer (Jun, Jul, Aug)	Autumn (Sep, Oct, Nov)
2009	0.51 (0.31, 1.07)	0.66 (0.31, 1.50)	1.58 (0.91, 2.73)	1.18 (0.56, 2.35)
2010	0.61 (0.38, 1.09)	2.13 (1.13, 4.06)	5.03 (2.87, 7.97)	3.40 (1.70, 6.65)
2011	1.68 (1.21, 2.43)	1.60 (0.80, 2.63)	2.07 (1.15, 4.16)	1.50 (0.67, 3.53)
2012	0.82 (0.50, 1.45)	1.07 (0.50, 2.24)	5.59 (1.39, 10.46)	4.87 (2.77, 8.62)
2013	2.45 (1.66, 3.53)	2.92 (1.58, 5.50)	6.89 (3.99, 10.31)	2.01 (0.87, 5.05)
2014	1.05 (0.61, 2.26)	1.42 (0.60, 3.28)	3.39 (1.71, 5.81)	3.38 (1.68, 5.74)
2015	3.40 (2.30, 5.06)	4.42 (2.15, 10.02)	9.24 (4.76, 14.91)	6.68 (3.51, 12.01)

Table 4.6.3 shows a lack of evidence of clear seasonality in seal numbers, with the exception that there are always greater numbers modelled in the summer months as compared to the other seasons. Although seals are highly seasonal species, with clear

breeding and moulting seasons when they spend a large majority of their time hauled out, as the two species' breeding/moulting periods are different, the distinction between such periods may not be as clear when modelling both species together. In addition, as there are no evident haul-out sites in Billia Croo, it is likely that both grey and harbour seals use the site for feeding and therefore their presence at the site will be less related to key life history periods. Considering the year-to-year variation in abundance predictions, higher predictions arise in 2013 as compared to the other years. This peak may actually stem from the previous year when particularly high densities of seals are estimated for the summer and autumn of 2012. In addition to summer 2012 and 2013, greater numbers were also anticipated during summer 2010 when compared to the summers of 2009, 2011 and 2014. In addition to the above table, the changing abundance of seals at Billia Croo over time is provided in Appendix 7. Separate plots have been created for each site impact level.

Further to the seal prediction surfaces provided in Figure 4.6.2, prediction surfaces for typical surveying conditions in January and July have been created. These surfaces and their associated CV values are available in the Marine Scotland Information portal. Although the distributions between the surfaces are very similar, approximately three times greater abundances are estimated in July as compared to January.

4.6.1.6 Spatially-explicit change

The density differences between site impact levels have been calculated in order to understand the extent of any spatially-explicit changes in seal densities. To find the significance of any change, the 95% CIs have been used. 'Year' was included in the final fitted seal model, which has meant that spatially-explicit change surfaces have been created for both the least and most variable year. For seals, the least variable year was 2010 and the most variable was 2014. The density differences between each site impact level for 2010 are presented in Figure 4.6.6. In addition to these plots, a detailed view of the inner grid bands of the plots is available in Figure 4.6.7. Both of these plots are also available for the most variable year, 2014, in Appendix 8.

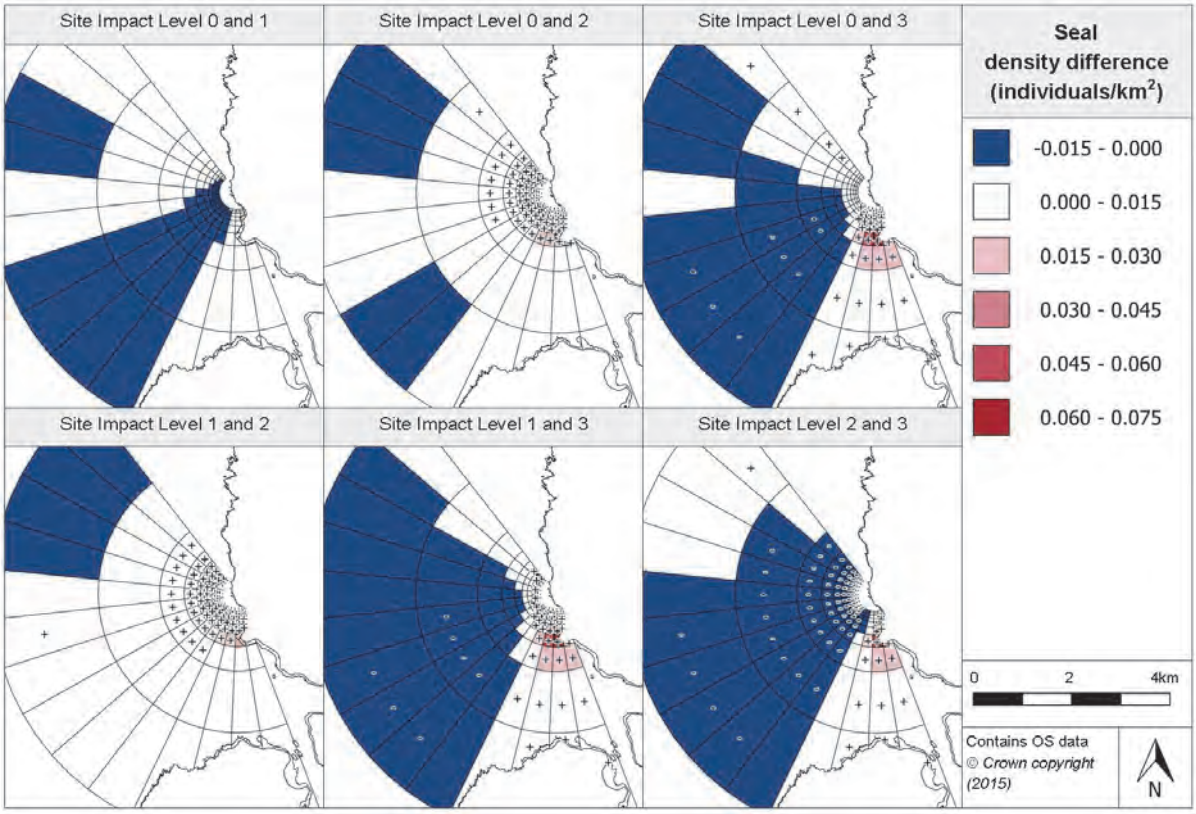

Figure 4.6.6. Estimated density difference between various site impact levels for seals during 2010 (year with least variation) at Billia Croo

Between SIL-0 (baseline conditions) and SIL-1 (infrastructure installed), all of the seal density changes are small scale between -0.015 and 0.015 individuals/km^2, reflecting the low density levels across the survey area in general. There appears to be a section of the grid where a reduction in density is estimated. This section is positioned between grid cells 6 to 9 in grid bands A-C. Within the inner grid bands, the section where a density decrease is expected, widens slightly and extends over more northern cells, see Figure 4.6.7. The reduction in density in these grid cells is only expected to be slight, between 0.000 and 0.015 individuals/km^2. With the exception of these cells and A2-A3, the remainder of the grid is expected to see an increase in density of up to 0.015 individuals/km^2. The cells where device-associated infrastructure is installed show no distinguishing change in density (SIL-0 to SIL-1) compared with the other grid cells within the survey area. None of the density change predictions between baseline conditions and device-associated infrastructure coming onsite, whether for grid cells with or without the infrastructure, are deemed to be statistically significant.

The density changes between baseline conditions and SIL-2 (devices installed but not operational) are different to those estimated between SIL-0 and SIL-1, most notably in that many grid cells show statistically significant changes in density, particularly for the inner grid bands. Changes are within a similar range to that noted for SIL-0 to SIL-1 (-0.015 to 0.015 individuals/km^2), except for increases in density of 0.015-0.030 individuals/km^2 in cells D10-D12 and E12. In the outer grid band, cells A1-A3 and A7-A8 have a reduction in density estimated of up to 0.015 individuals/km^2. Otherwise, an increase in density is expected across the rest of the grid. In Figure 4.6.6, grid cells B0 and C0-C6 show significant increases in density. For the inner grid bands, Figure 4.6.7, there is an increase in density of 0.015-0.030 individuals/km^2 in cells D10-D12 and E12, whereas, across the remaining inner

grid cells, the increase in density is expected to be lower than 0.015 individuals/km^2. All of the increases in these grid cells are deemed significant.

Density changes between baseline conditions and SIL-3 (devices installed and operational) indicate a reduction in the south-western section of the grid, as well as in the north in grid cells A1-A3 and B3. Eight of the decreases in density, which are not expected to be any greater than 0.015 individuals/km^2, are deemed significant. In terms of the outer grid bands, Figure 4.6.6, the most northern row of cells (A0-C0) and the four southernmost rows of cells (A10-A13, B10-B13 and C10-C13) have had their density increases deemed significant. All of the cells in the outer grid bands shows density increases, with the rise expected to be up to 0.015 individuals/km^2. However, in grid cells C11-C13 (the location of the peak in density in the SIL-3 prediction surface), the increase in density is expected to be between 0.015 and 0.030 individuals/km^2. Within the inner grid cells (Figure 4.6.7), large density increases are expected in the cells offshore of Breck Ness, with grid cell D12 having an increase of 0.07 individuals/km^2. In addition to this, many of the grid cells in the south of the inner grid bands have their density increase deemed to be significant, despite some increases being less than 0.015 individuals/km^2. Decreases in density are estimated in grid cells D4-D8 and E4-E7, although these have not been marked as significant. There appears to be no correlation between changes in density for SIL-0 and SIL-3 and the location of test berths, as some berths are located in grid cells that show a positive change and others in grid cells showing a negative change, and only some of the changes are deemed statistically significant. This suggests that changes in seal distribution are not influenced by the installation and operation of devices.

The majority of the grid is expected show an increase in seal density of less than 0.015 individuals/km^2 with the introduction of devices (SIL-2) as compared to only device-associated infrastructure being installed (SIL-1)(Figure 4.6.6). A reduction in density is only expected in four grid cells, these being A0-A3. In the outer grid bands, these increases have only been deemed significant in grid cells A5 and C0-C9. Apart from grid cells D10-D12 where increases in density of between 0.015 and 0.030 individuals/km^2 are estimated, the grid cells across the rest of the inner grid bands show increases of less than 0.015 individuals/km^2 anticipated (Figure 4.6.7). All of these density increases are statistically significant.

The majority of the grid cells in the outer grid bands are expected to have decreases in density between SIL-1 (baseline conditions) and SIL-3 (devices installed and operational) of up to 0.015 individuals/km^2. Seven of the grid cells have had their reduction in density deemed significant. In contrast, the grid cells in the northernmost rows (A0-C0, B1-C1) and in the four southernmost rows have had increases of up to 0.015 individuals/km^2 predicted. Grid cells C11-C13 have estimated density increases of 0.015-0.030 individuals/km^2. Eleven of these are deemed significant. Within the inner grid cells (Figure 4.6.7), except for grid cells D3-D7 and E4-E6, increases in density are estimated however, again a much greater increase is expected offshore of Breck Ness, with an increase of 0.07 individuals/km^2 in D12. This peak slowly reduces with increasing distance from D12. The cells in the southern part of the inner grid bands and those in the two innermost grid bands are all marked as having significant density increases.

However, between SIL-2 and SIL-3 (devices installed and operational), the majority of cells across the grid are expected to exhibit decreases in seal density. As can be seen in Figure 4.6.6, in the outer grid bands, the reduction is anticipated to be in grid cells A4-A9, B1-B9 and C0-C9 and all but three of the grid cells have had the decrease marked as significant. Otherwise, across the outer grid cells, in general, increases up to 0.015 individuals/km^2 are expected, with the change in nine cells deemed to be significant. Larger increases are anticipated in grid cells C12-C13, located close to Breck Ness headland. Nearly all the grid cells in the inner grid bands have reductions in density of up to 0.015 individuals/km^2

estimated, and the majority of the negative changes have been determined to be significant (Figure 4.6.7). Large increases in density remain around Breck Ness, cells D11-D12 and C12; these changes have been deemed significant as well as smaller increases in the cells adjoining the shore around Billia Croo.

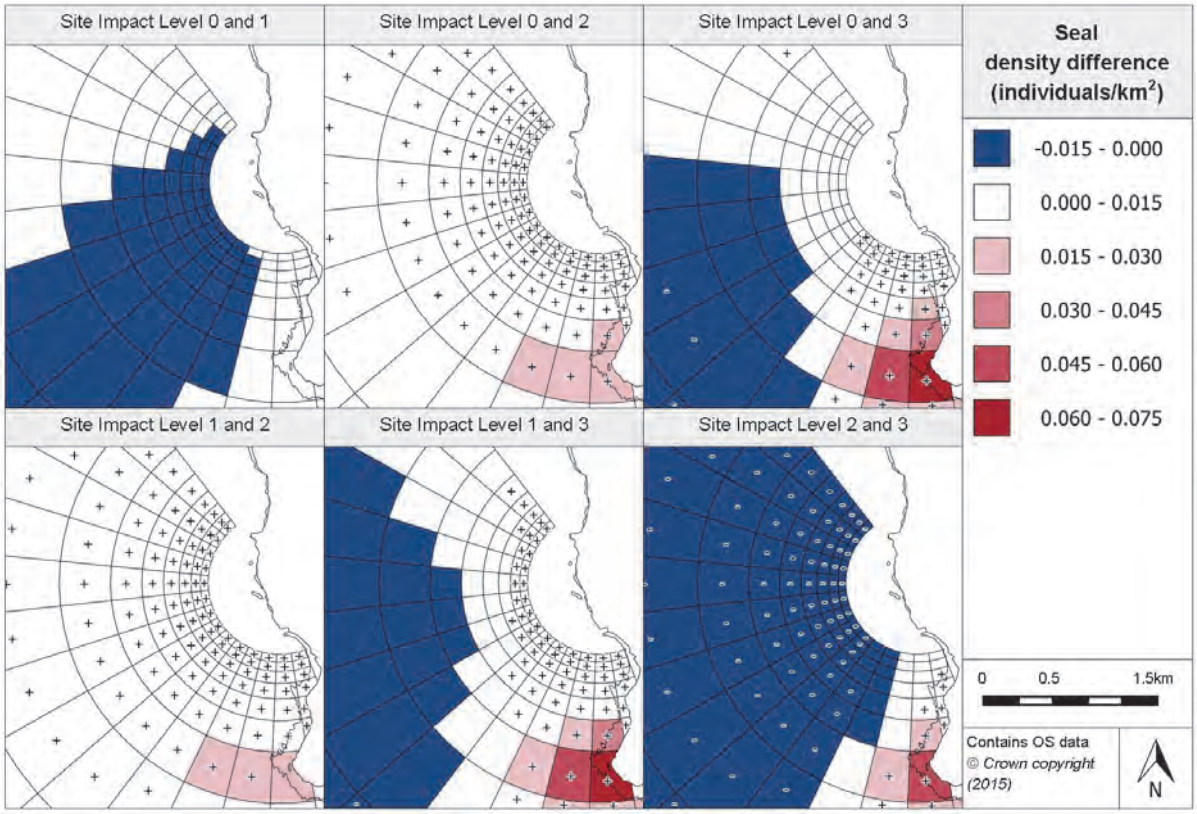

Figure 4.6.7. Density differences between seals site impact level inner prediction surfaces during 2010 (least variable year) at Billia Croo

4.6.1.7 Density change with distance from potential impact location

Using the estimated change in density discussed in Section 4.6.1.6 above, the following plot, Figure 4.6.8, has been created which displays how the extent of change varies with increasing distance from a potential impact location, i.e. a test berth. All plots show a return to baseline conditions within 2km of a potential impact location.

As noted above there appears that there is very little change in seal density between SIL-0 (baseline conditions) and SIL-1 (infrastructure installed), whereas, between baseline conditions and devices being installed onsite (SIL-2), an increase in density is expected at the test berth location which slowly decreases to the values seen at baseline conditions at about 2km from the test berth. It is likely that the increase is significant, as the lower CI is above zero for up to 1.3km away. Again, between baseline conditions and SIL-3 (devices installed and operational), an increase in density is modelled at the location of the potential impact. This gradually declines, reaching baseline conditions at approximately 1.8km from the test berth. The increase is only expected to be significant for the first 500m.

Between SIL-1 (infrastructure installed) and SIL-2 (devices installed but not operational), the increase in density is not expected to be as great. The rise in density slowly declines up to 0.4km from the test berth and then there is a peak in the CIs at 0.6km from the test berth. This is followed by a continued gradual density decrease with increasing distance from the test berth, reaching SIL-1 levels at approximately 1.4km.

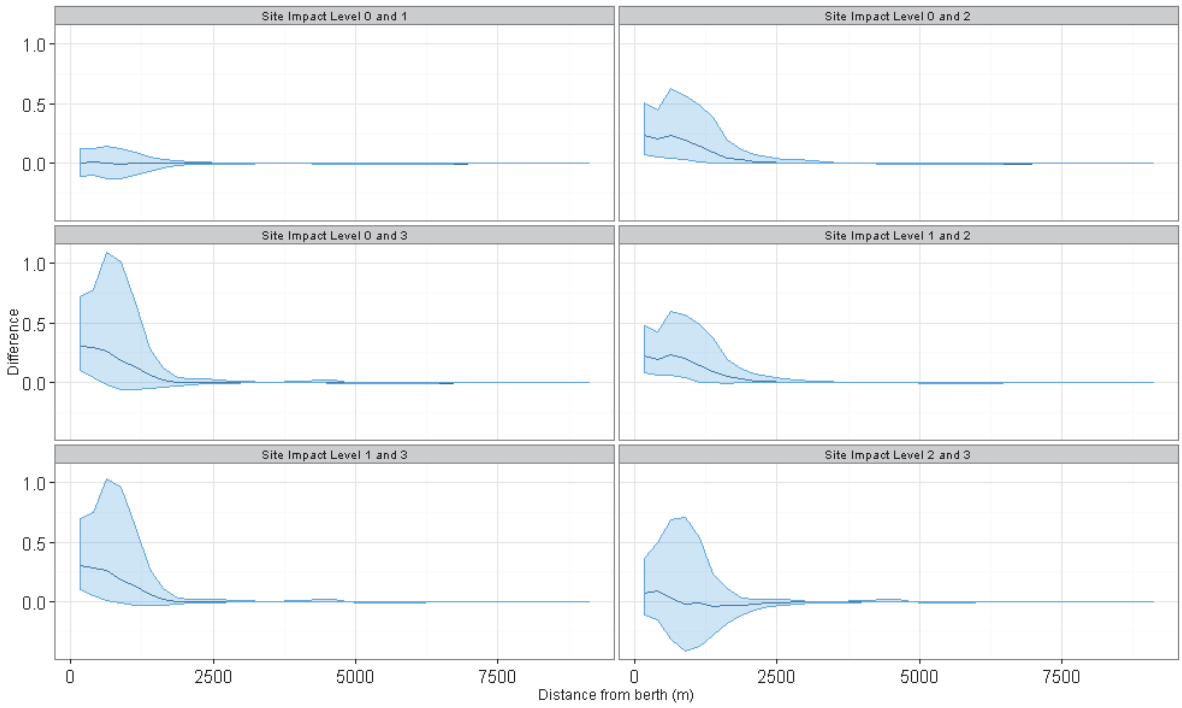

Figure 4.6.8. Density change between site impact levels with increasing distance from a potential impact location, with associated confidence intervals, for seals at Billia Croo

There is an increase in density at the test berth location between SIL-1 and SIL-3 (devices installed and operational) which gradually declines, returning to SIL-1 conditions at approximately 1.8km from the potential impact. This increase is likely to be significant for around 0.5km from the test berth.

There is only a slight increase in density expected between SIL-2 and SIL-3 which is anticipated to return to SIL-2 levels at approximately 0.8km. However, as there are large confidence limits on either side of this prediction, the variability behind the predictions suggests that there is negligible density difference between SIL-2 and SIL-3 and no clear relationship with increasing distance from a potential impact location.

It is worth noting that the results from only one grid cell containing a test berth are presented here. Under the seal prediction surface, the same relationship with estimated density difference is not observed for all of the other grid cells that contain test berths. The equivalent plots for the other grid cells are provided in the Marine Scotland Information portal.

4.6.1.8 Discussion

The model developed for all seals observed (both grey and harbour) indicates that their distribution incorporates six highly significant terms. These include distance from land, year and month and spatial terms that need to be considered when elucidating the impact of MECS. The analysis shows a clear peak in density extending westwards from Breck Ness. The estimated density within these grid cells increases with increasing site impact level.

There appears to be no correlation between changes in density and the location of test berths, as some berths are located in grid cells that show a positive change and others in grid cells showing a negative change, and only some of the changes are deemed statistically significant. When considering the change in seal density with increasing distance from a potential impact location, there is a clear increase in density with the presence and operation

of devices compared to baseline conditions and when infrastructure is installed; this increase tends to be significant up to the first kilometre away from the test berth location. Although a distinct increase in density in the immediate area of a grid cell containing a test berth was estimated, this was not the case for each grid cell containing a test berth. In addition, the densities for these cells are low and do not include the main areas where seals have been observed west of Breck Ness. This suggests that the changes in seal distribution are not influenced by the installation and operation of devices.

4.6.2 Harbour porpoise (Phocoena phocoena)

4.6.2.1 Species overview

The harbour porpoise is the most common cetacean species observed at Billia Croo where they are seen with much greater frequency than at the Fall of Warness. A brief summary of the distribution of harbour porpoises in UK waters and their life history is given in Section 4.4.3.1. The following section provides a discussion of the outputs and prediction surfaces from the fitted harbour porpoise model.

4.6.2.2 Data summary

A summary of the harbour porpoise raw observation data used in the model selection process is provided in Table 4.6.4. The information has been split across site impact levels to provide a representation of the data used in the model selection process. Information regarding the typical group size and maximum and minimum group sizes has also been provided.

Table 4.6.4. Summary of harbour porpoise raw data

	Total	Site Impact Level 0	Site Impact Level 1	Site Impact Level 2	Site Impact Level 3
Number of observations	495	37	37	207	214
Minimum (group size)	1	1	1	1	1
Maximum (group size)	8	8	5	8	5
Mean (group size)	1.70	2.41	2.11	1.51	1.69
(s.d)	(1.03)	(1.74)	(1.02)	(0.89)	(0.93)

4.6.2.3 Model overview

The final fitted harbour porpoise model contains five terms. Based on the GEE-based p-values, only one term is statistically highly significant and three significant. Table 4.6.5 provides the GEE-based p-value for each of the remaining terms in the model.

Table 4.6.5. GEE-based p-values for the terms in the final harbour porpoise model for Billia Croo

Model term	ρ-value
Distance to land	0.00154
Year	0.00213
Site impact	0.706
Spatial surface	<0.0001
Spatial surface / site impact	0.00348

The term ‘distance to land’ has been kept in the fitted harbour porpoise model. As seen in Figure 4.6.9, there is a clear relationship between harbour porpoise density and distance from land. Highest densities have been modelled closer to land, which tend to reduce with increasing distance[25]. A further remaining term in the fitted model is ‘year’, as survey year was found to be significant when predicting harbour porpoise numbers. The model shows a spike in harbour porpoise density in late 2009/early 2010 which slowly declines to a low in late 2012/early 2013. Density then rose to a higher peak in 2015. Figure 4.6.10 provides a visual representation of these modelled undulations in harbour porpoise density.

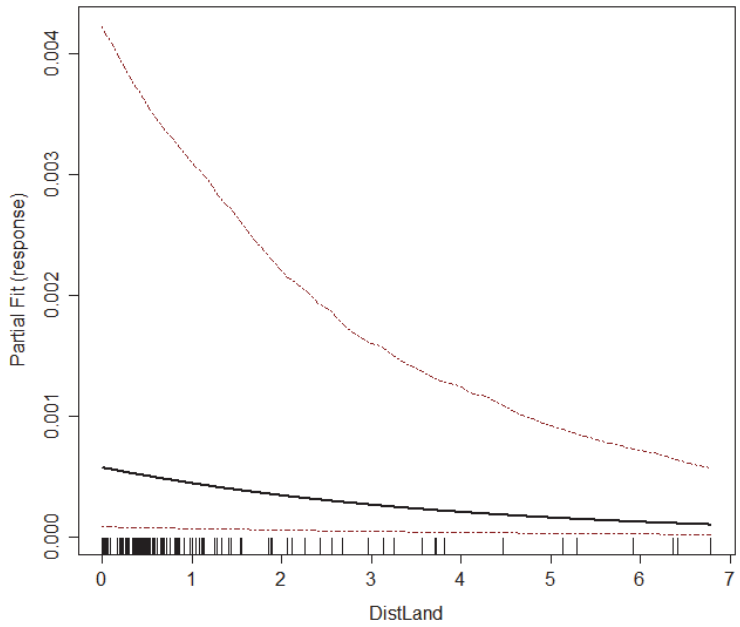

Figure 4.6.9. Estimated partial relationship of distance to land against log(density) for harbour porpoise at Billia Croo. The red lines represent 95% confidence intervals about the estimated relationship and the tick marks show where the data lie in the covariate range.

[25] As mentioned previously, this detected relationship may be explained as reducing detection rates with increasing distance from land.

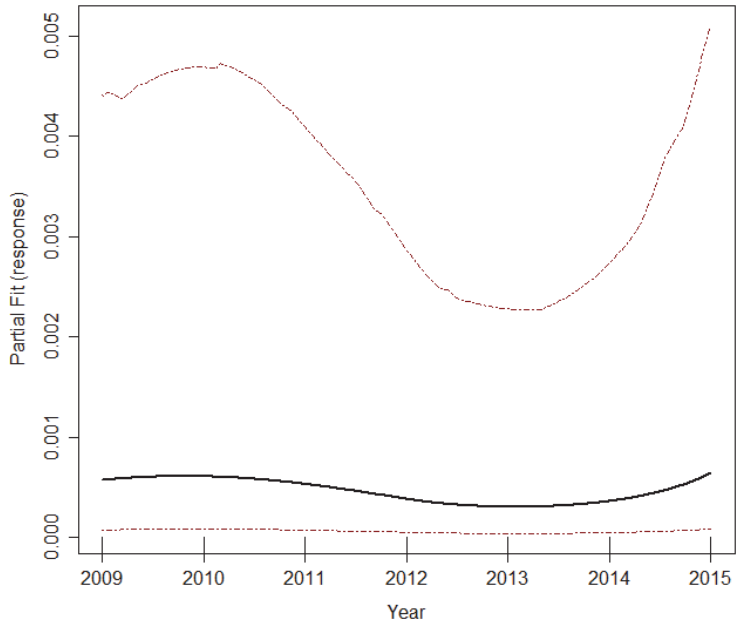

Figure 4.6.10. Estimated partial relationship of year against log(density) for harbour porpoise at Billia Croo. The red lines represent 95% confidence intervals about the estimated relationship and the tick marks show where the data lie in the covariate range.

As with the other fitted models, it has been possible to fit a spatial surface (using four knots) for the final fitted harbour porpoise model. Also included in the final fitted model was the interaction term (site impact/spatial surface), as it was found to be statistically significant.

4.6.2.4 Density predictions and uncertainty estimate

The final fitted harbour porpoise model contained a spatial surface; therefore, it was possible to produce density prediction surfaces, allowing the density to vary across the observation grid. Appendix 5 discusses the set values for the terms in the model. Figure 4.6.11 shows the plots generated for each site impact level. A more detailed view of the inner grid bands can be seen in Figure 4.6.12. In addition, the CV values for each of the predictions has also been plotted, see Figure 4.6.13 and Figure 4.6.14. These illustrate the confidence in the predictions.

Reference should be made to Figure 2.1.9 and Figure 2.1.10 for the grid cell labelling system.

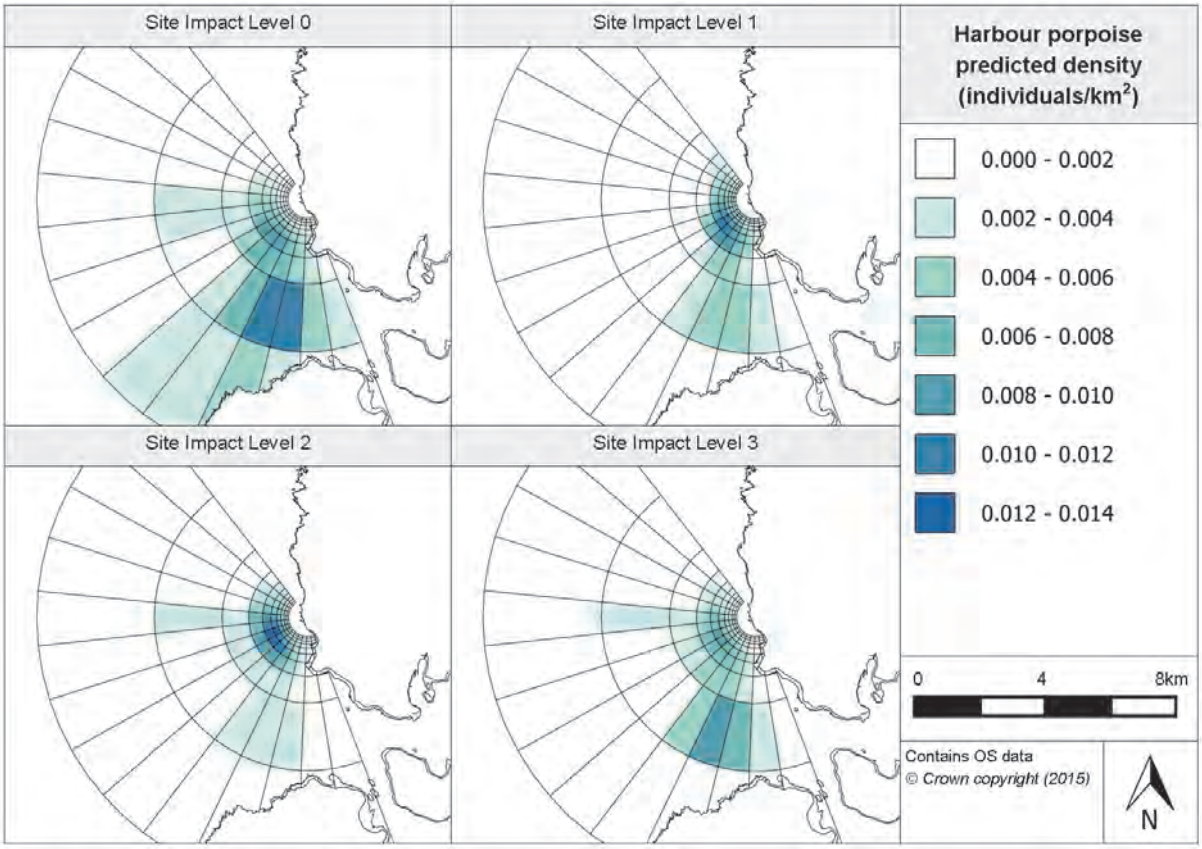

Figure 4.6.11. Estimated harbour porpoise density at each site impact level across Billia Croo

The prediction surface for baseline conditions shows a peak in harbour porpoise density in the south/south-west of the survey area as well as one towards the centre. For grid bands A and B, the majority of their northern halves have density predictions below 0.002 individuals/km^2, whereas towards the south, there is a cluster of cells with higher density predictions around B10-B11 at the entrance to Hoy Sound. The highest density in these two cells is 0.012 individuals/km^2 in grid cell B10. Within the inner grid bands, see Figure 4.6.12, there is again a large cluster of grid cells, around D7-D9 and E8, which have estimated densities of 0.008-0.010 individuals/km^2. The surrounding cells have density predictions which gradually decrease with increasing distance from these cells.

At SIL-1 (device-associated infrastructure installed), the outer grid cells of the prediction surface have typical density predictions between 0.000 and 0.002 individuals/km^2 (Figure 4.6.11). The cluster mentioned above in grid cells B10-B11 exists but to a lesser extent under SIL-1 conditions (between 0.004 and 0.006 individuals/km^2). Within the inner grid cells, see Figure 4.6.12, a cluster of cells is located which have been modelled to have high densities, this then continues into the centre of the survey area; however, the location of the grid cells with the highest densities is now E7-E8 and F7 (0.010-0.012 individuals/km^2). Again, the density predictions in the cells surrounding these gradually decrease with increasing distance. It is worth noting that low density predictions tend to be located in the cells adjacent to shore, which may reflect water depth.

The cluster of higher density predictions previously noted around grid cells B10-B11 is minimal under SIL-2 conditions (devices installed but not operational). As can be seen in Figure 4.6.11, all grid cells in the outer grid bands have density predictions between 0.000 and 0.004 individuals/km^2. In the inner grid bands, the peak estimated in grid cells E7-E8 and F7 under SIL-1 conditions is also present under SIL-2 conditions but to even higher

densities. Across these three grid cells, the highest density is 0.013 individuals/km^2 in grid cell E7 but all three have density predictions greater than 0.012 individuals/km^2. Again, density predictions slowly decline with increasing distance from these cells. The cells closest to land continue to have density predictions lower than 0.002 individuals/km^2.

Under SIL-3 conditions (devices installed and operational), the cluster previously seen slightly to the west of Hoy Sound emerges a little more clearly than under SIL-2 conditions. Cell B10 has an estimated density of between 0.008 and 0.010 individuals/km^2. As can be seen in Figure 4.6.11, adjacent cells to B10 also see heightened density predictions. In terms of the inner grid bands (Figure 4.6.12), high density predictions continue around grid cells E7-E8; where harbour porpoise densities of 0.008-0.010 individuals/km^2 are estimated. The expected density values for the grid cells located next to E7-E8 slowly reduce with increasing distance.

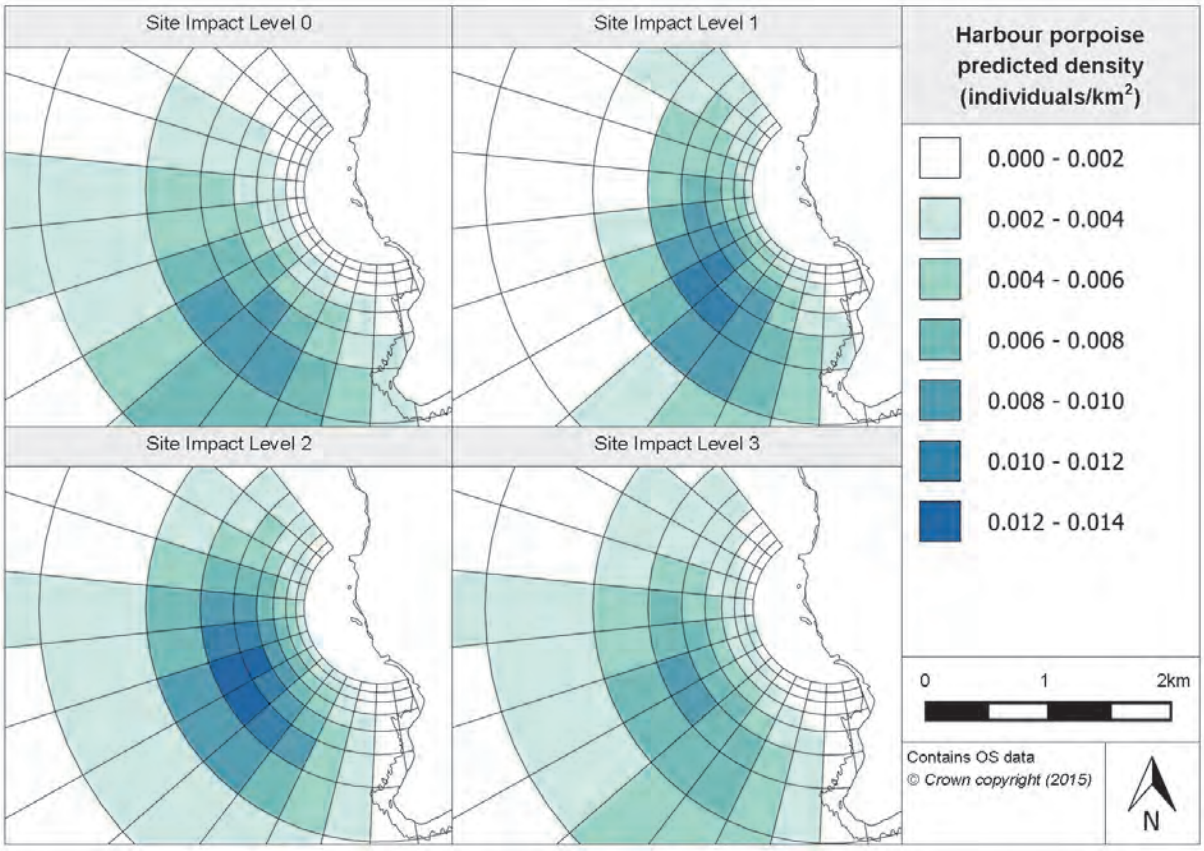

Figure 4.6.12. Inner prediction surfaces for harbour porpoise density at Billia Croo

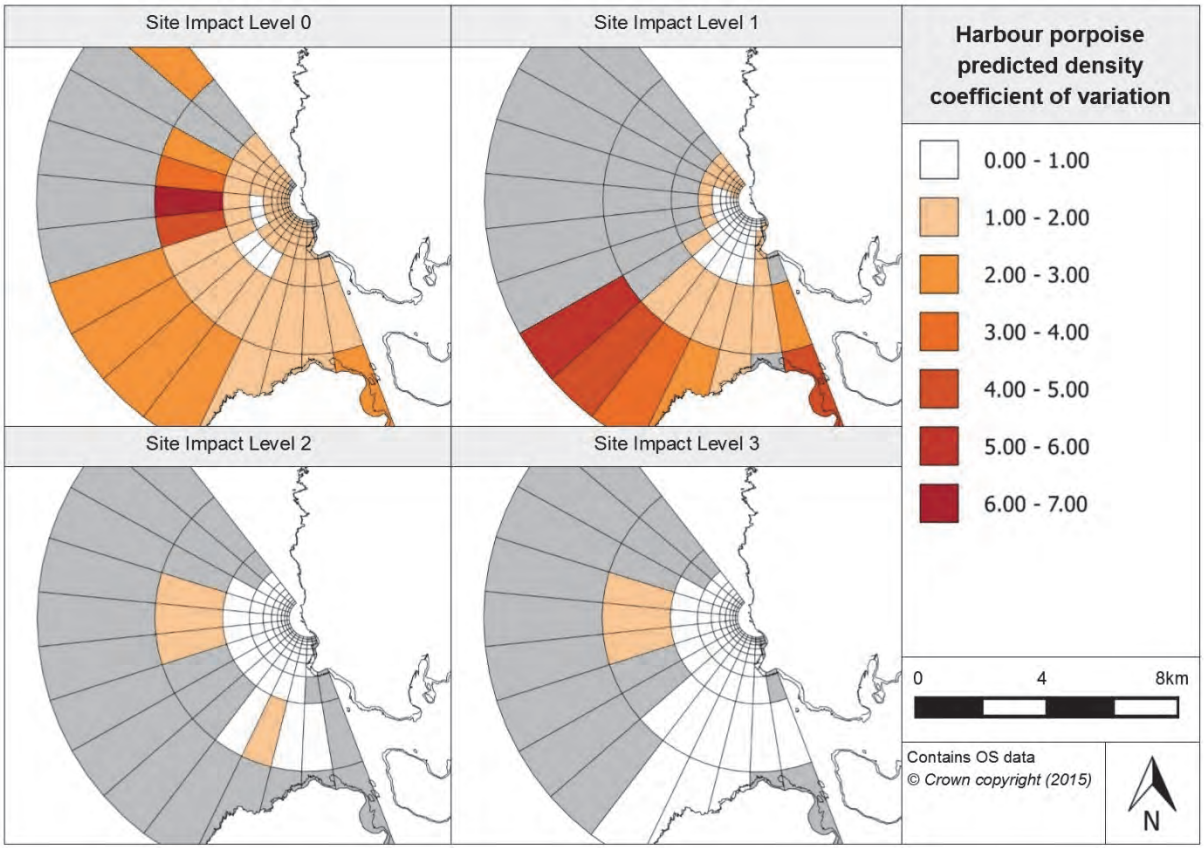

Figure 4.6.13. Associated coefficient of variation values for the density predictions for harbour porpoise at Billia Croo

When considering the CV values for the baseline prediction surface, the majority of grid cells in the outermost grid band, and in the northern half of grid band B, either have CV values greater than 2 or they are unavailable. This would suggest little precision in the predictions for these grid cells. Over the rest of the grid including the inner grid bands (Figure 4.6.14), the CV values are below 2, pointing to there being reasonable precision in the predictions for these grid bands which includes the cells where higher harbour porpoise densities are estimated. Interestingly, the cells alongside the shore at Billia Croo and to the south (excluding Breck Ness), and the cells below the observation point, have their CV values unavailable; this is likely due to a lack of observations of harbour porpoises in these cells and, therefore, very low density predictions.

CV values are unavailable for the northern parts of grid bands A-C, for SIL-1 density predictions. Additionally, high CV values occur in the rest of grid band A, suggesting that there is high uncertainty in these predictions. With the exception of cells B13 and C13, the grid cells in the rest of the outer grid bands, see Figure 4.6.13, all have CV values below 2, suggesting reasonable precision in these predictions. Within the inner grid bands, as shown in Figure 4.6.14, some of the cells adjacent to shore on the Billia Croo side of the shoreline have unavailable CV values, which again suggests very low density predictions for these cells. The rest of the inner grid cells have CV values between 0 and 2 with most less than 1, which implies high precision in the prediction results.

The CV values for the SIL-2 prediction surface show that the majority of the outer two grid bands have unavailable CV values (Figure 4.6.13). CV values are only available within grid band B in the vicinity of the few cells with higher density predictions than 0.002 individuals/km^2. As seen in Figure 4.6.13, grid band C also has four grid cells with CV values unavailable; however, the CV values for the rest of the grid band are below 1,

suggesting high reliability in the results. In terms of the inner grid bands, all of the grid cells, except for those with unavailable CV values that are located adjacent to the shore (as before), have CV values below 1, again suggesting high precision in the predictions.

The CV values for the final prediction surface (SIL-3), suggest that there is generally high precision in the results for the cells at the southern end of the two outermost grid bands, as compared to those in the north where CV values are unavailable. CVs are below 1 for cells C2-C12 but unavailable for the rest of grid band C. In the inner grid bands, see Figure 4.6.14, with the exception of the cells adjacent to the shoreline at Billia Croo (which do not have CV values available), the CV values across the inner grid cells are all below 1. This suggests high precision in the predictions for these grid cells.

As seen in the prediction surfaces for harbour porpoises (Figure 4.6.11), the density values are very low and therefore are likely to be based on very few observations. It is important to note that the great number of grid cells where CV values are unavailable is probably due to the lack of observations resulting in very low density predictions. The method of calculating the CV values means that unrealistic, very high CV values result from low density predictions.

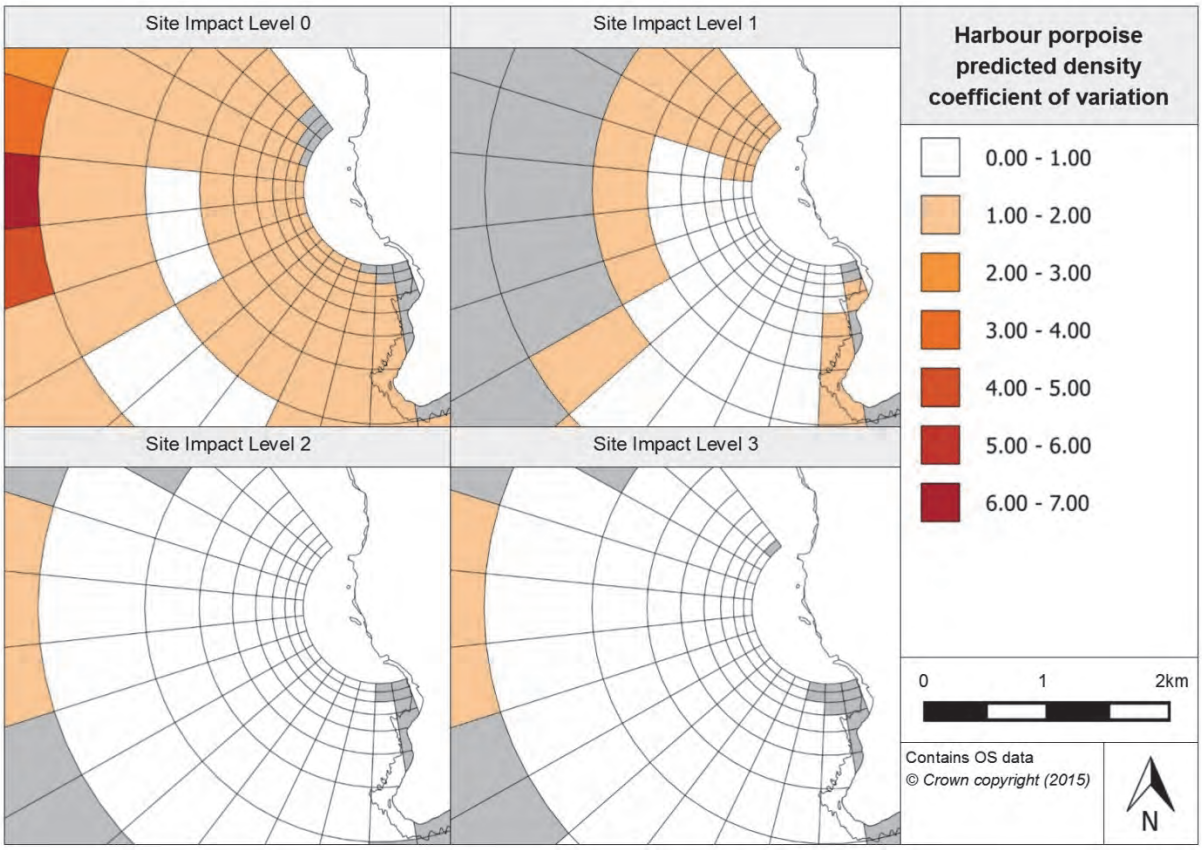

Figure 4.6.14. Associated coefficient of variation values for harbour porpoise inner density prediction surfaces at Billia Croo

4.6.2.5 Relative abundance estimations

In using the fitted model, it has been possible to calculate the relative abundance for harbour porpoises at Billia Croo for each month over the survey's duration. These figures have then been combined to give seasonal abundance estimates for each survey season from 2009 to 2015, as provided in Table 4.6.6. To understand the significance of these predictions, 95% CIs for each prediction are also provided.

Table 4.6.6. Relative abundance for harbour porpoise during each season (associated confidence intervals are provided in brackets)

Year	Season			
	Winter (Dec, Jan, Feb)	Spring (Mar, Apr, May)	Summer (Jun, Jul, Aug)	Autumn (Sep, Oct, Nov)
2009	1.89 (1.23, 3.43)	1.89 (1.23, 3.43)	2.00 (1.23, 3.65)	2.22 (1.53, 3.65)
2010	2.32 (1.53, 3.81)	2.58 (1.94, 3.45)	2.58 (1.94, 3.45)	2.14 (1.43, 3.45)
2011	1.75 (1.26, 2.68)	1.70 (0.99, 3.58)	1.75 (0.99, 3.58)	1.75 (0.99, 3.58)
2012	1.67 (1.01, 3.39)	1.48 (1.01, 2.49)	1.57 (1.01, 2.49)	1.62 (1.28, 2.07)
2013	1.29 (0.78, 2.07)	0.95 (0.78, 1.19)	0.95 (0.78, 1.19)	1.00 (0.55, 2.05)
2014	1.13 (0.55, 2.41)	1.33 (0.65, 2.44)	1.40 (0.91, 2.44)	1.44 (0.91, 2.44)
2015	2.33 (1.17, 3.65)	2.72 (2.07, 3.65)	2.02 (1.34, 3.04)	2.02 (1.34, 3.04)

Considering the predictions in Table 4.6.6, there appears to be no clear seasonality present in the predictions, nor much year-to-year variation. However, as 'year' has been included in the final fitted model, this suggests that the variation between years is significant. The relative abundance predictions for 2013 are slightly lower than for other years, particularly in spring, summer and autumn. It would be interesting to investigate if this drop in abundance estimated for this year is seen in other datasets that cover this period. Due to the large range of harbour porpoises, it would also be informative to investigate if similar reductions are occurring within the range, or if increases in numbers were seen, suggesting that wider redistribution is taking place.

In addition to the above table, the abundance estimates have also been plotted and split across site impact levels, (see Appendix 7). A 'blocking' effect, as illustrated in Appendix 7, emphasises the lack of variation in estimated abundance between seasons. However, the low abundance predictions in 2013 are highlighted in the plots for SIL-2 and SIL-3.

In addition to the prediction surfaces already discussed for harbour porpoise, prediction surfaces were also created for typical surveying conditions in January and July. Due to the lack of difference in abundance predictions across seasons, the prediction surfaces for January and July looked very similar in terms of the distribution of peaks and troughs in density but also with respect to the anticipated density level. The prediction surfaces, alongside their associated CV values, are provided in the Marine Scotland Information portal.

4.6.2.6 Spatially-explicit change

To understand the extent of spatially-explicit change in species abundance or distribution, the density differences between site impact levels have been calculated. The 95% CIs have been used to determine the significance of the change in density. As with other Billia Croo species, as 'year' is included in the final fitted harbour porpoise model, it was necessary to plot the extent of density change for both the least and most variable years. Figure 4.6.15 below presents the density change surfaces for the least variable year, 2013. A detailed view of the change expected in the inner grid cells is provided in Figure 4.6.16. Plots for the most variable year, 2010, are given in Appendix 8.

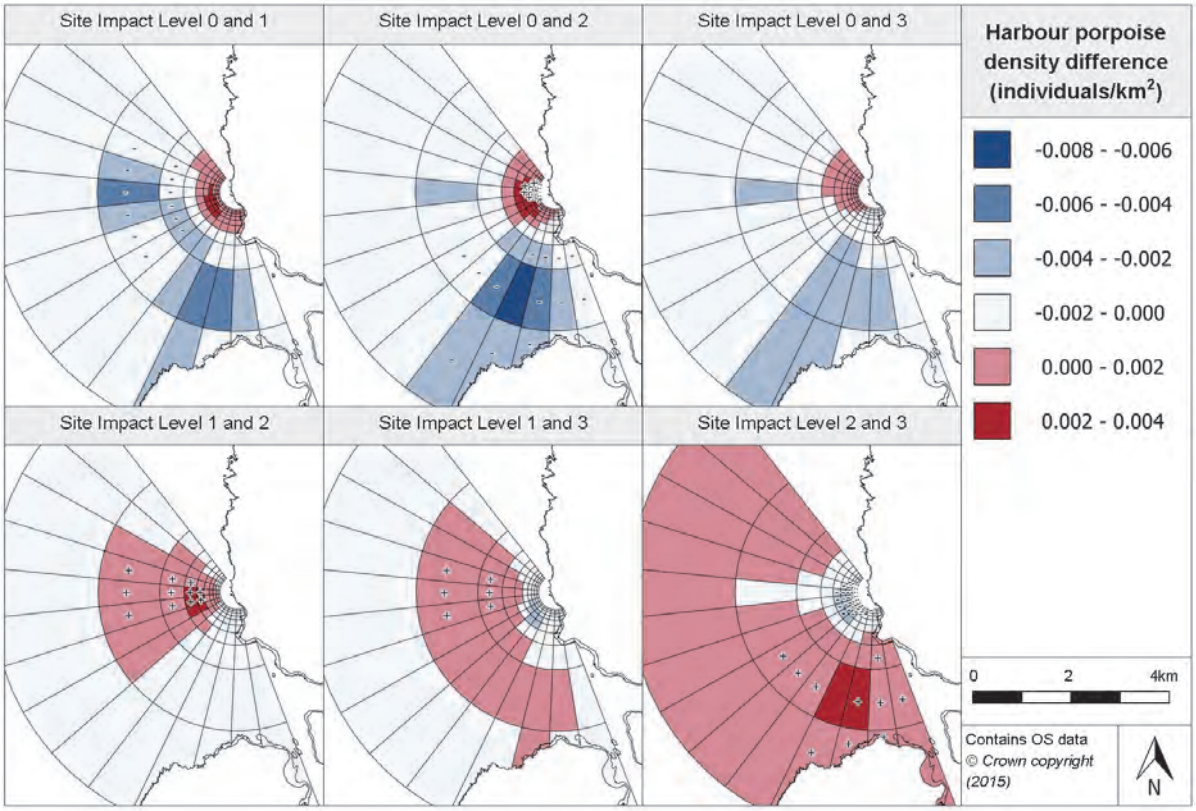

Figure 4.6.15. Estimated density difference between various site impact levels for harbour porpoises during 2013 (year with least variation) at Billia Croo

The density differences between baseline conditions (SIL-0) and SIL-1, SIL-2 and SIL-3 are all very similar. As seen in Figure 4.6.15, the three outermost grid bands experience reductions in density with a cluster of greater decreases in density around grid cells B10-B11, whereas density increases are generally restricted to the northern grid cells of the inner grid bands for all three site impact levels as compared with baseline conditions. There is no correlation between these increases and decreases and the disposition of grid cells with test berths.

Between SIL-0 (baseline conditions) and SIL-1 (when infrastructure is installed), there are two separate clusters of cells where greater density reductions are expected: cell B4 and, as already mentioned, cells B10-B11. All three of these grid cells have decreases in density estimated (as much as 0.004-0.006 individuals/km^2). The reduction in density modelled in the cells around B4 is deemed significant in 12 grid cells. In the inner grid bands, see Figure 4.6.16, density increases are expected in grid bands E-J. Although none of the positive changes in density are deemed significant, these vary in extent from 0.000 to 0.004 individuals/km^2. Reductions in density of up to 0.002 individuals/km^2 are expected in the majority of grid band D; however, cells D0-D1 have increases in density predicted.

When considering the density change between baseline conditions and SIL-2 (when devices are installed onsite but not operational) (Figure 4.6.15), the scale of the density decrease around grid cell B4 has reduced but the decrease around grid cells B9-B11 is greater. Grid cell D11 shows a decrease of 0.002 individuals/km^2 although this is not found to be significant. However, the density reductions in the surrounding grid cells (although maybe slightly lesser in scale) are found to be significant. The remainder of the outer grid cells continue to show a decrease in density ranging between 0.000 and 0.004 individuals/km^2.

Between SIL-0 and SIL-2, an increase in density is estimated in the northern and central regions of the inner grid bands, ranging between 0.000 and 0.004 individuals/km^2. A cluster of grid cells have their density increase marked as significant; these cells appear to be located around H3-H4. The cells adjacent to the shoreline at Billia Croo (where the substation is located), and around Breck Ness to the south of Billia Croo, have been modelled to experience a decrease in density. Further, the change in density between baseline conditions and SIL-3 (when devices become operational onsite) shows a slightly greater decrease in density in the region of grid cells B10-B11 and their surrounding cells as well as B4, where decreases of up to 0.004 individuals/km^2. None of the decreases in the outer grid cells have been deemed significant, as shown in Figure 4.6.15. In the inner grid cells, an increase in density of up to 0.002 individuals/km^2 is expected in the northern half of the grid bands, but none of the cells where increases are anticipated have been deemed significant. The reduction in density that is estimated adjacent to the shoreline at Billia Croo and the peninsula to the south, continues to exist but a reduction in density of up to 0.002 individuals/km^2 is seen in a greater number of cells in this area (Figure 4.6.16).

Figure 4.6.15 shows that, in 2013, the year with least variability, there was a reduction in porpoise density at the entrance to Hoy Sound, centred on cell B10 for all site impact levels 1, 2 and 3 when compared with baseline conditions (SIL-0). However, as this is an area without any test berths, it is difficult to consider that these factors are related. Similarly, there is a general increase in density in the north-east of the survey area for all site impact levels when compared with baseline conditions. This is closer to, but not coincident with, the location of the test berths. This too supports the concept that changes in porpoise density are not related to the installing of marine energy infrastructure, devices or their operation.

The distribution of the density differences varies between SIL-1 and SIL-2. There is a reduction in density expected across the majority of the site of up to 0.002 individuals/km^2. In none of the cells where a decrease in density is modelled, is the reduction deemed significant. However, as seen in Figure 4.6.15, there is a large cluster of grid cells spread across the inner and outer grid bands with an increase in density of up to 0.002 individuals/km^2. These appear to be centred around grid cells D3-D5 and E3-E5 where an increase of greater than 0.002 individuals/km^2 is estimated (Figure 4.6.16). Across these six cells, the highest increase in density is expected to be in grid cell D5 with a harbour porpoise density of 0.003 individuals/km^2. The density changes in 11 grid cells within this cluster are deemed to be significant.

In terms of the density difference between SIL-1 and SIL-3 (when devices are installed and operational), the cluster of cells showing an increase in density previously discussed between SIL-1 and SIL-2 appears to be larger in size, including in particular a greater number of cells in the outer grid bands (Figure 4.6.15); however, fewer of these cells show a statistically significant increase in density. In these bands, increases in density of up to 0.002 individuals/km^2 are expected in cells A11, B1-B12 and C1-C9. Six of these grid cells have been deemed significant. Within the inner grid bands, increases in density of between 0.000 and 0.002 individuals/km^2 have been anticipated in grid cells D2-D7 and E3-E5. Otherwise, the remaining grid cells have density reductions of up to 0.002 individuals/km^2, except for grid cells E8-E9, F7-F9 and G6-G8, where this is between 0.002 and 0.004 individuals/km^2.

When looking at the estimated density difference between SIL-2 and SIL-3 (devices becoming operational), see Figure 4.6.15, it appears that, across the outer grid bands, all but three grid cells (B4, C3-C5) have increases. These increases are less than 0.002 individuals/km^2, except for grid cells B10-B11 which have higher positive density changes of 0.002-0.004 individuals/km^2. Some of the grid cells where increases in density are expected have been marked as significant. As shown in Figure 4.6.16, the majority of the inner grid bands have density decreases estimated, with the exception of grid cells D11-D13 and E13

where slight density increases are projected. For the majority of cells within the inner grid bands, the decrease in density is expected to be no greater than 0.002 individuals/km$^{2;}$ however, grid cells E4-E8, F4-F8 and G4-G7 have decreases of 0.002-0.004 individuals/km^2 anticipated. Many of the grid cells in the centre of the inner grid bands have had their negative change in density marked as significant. The cluster of cells with the greatest decrease in density for SIL-2 to SIL-3 is comparable with the cluster of cells showing the greatest increase for SIL-0 to SIL-2, suggesting that any effect caused by device installation is mitigated through device operation. This is reflected in the low density changes for SIL-0 to SIL-3 and the absence of statistical significance for any of the cells.

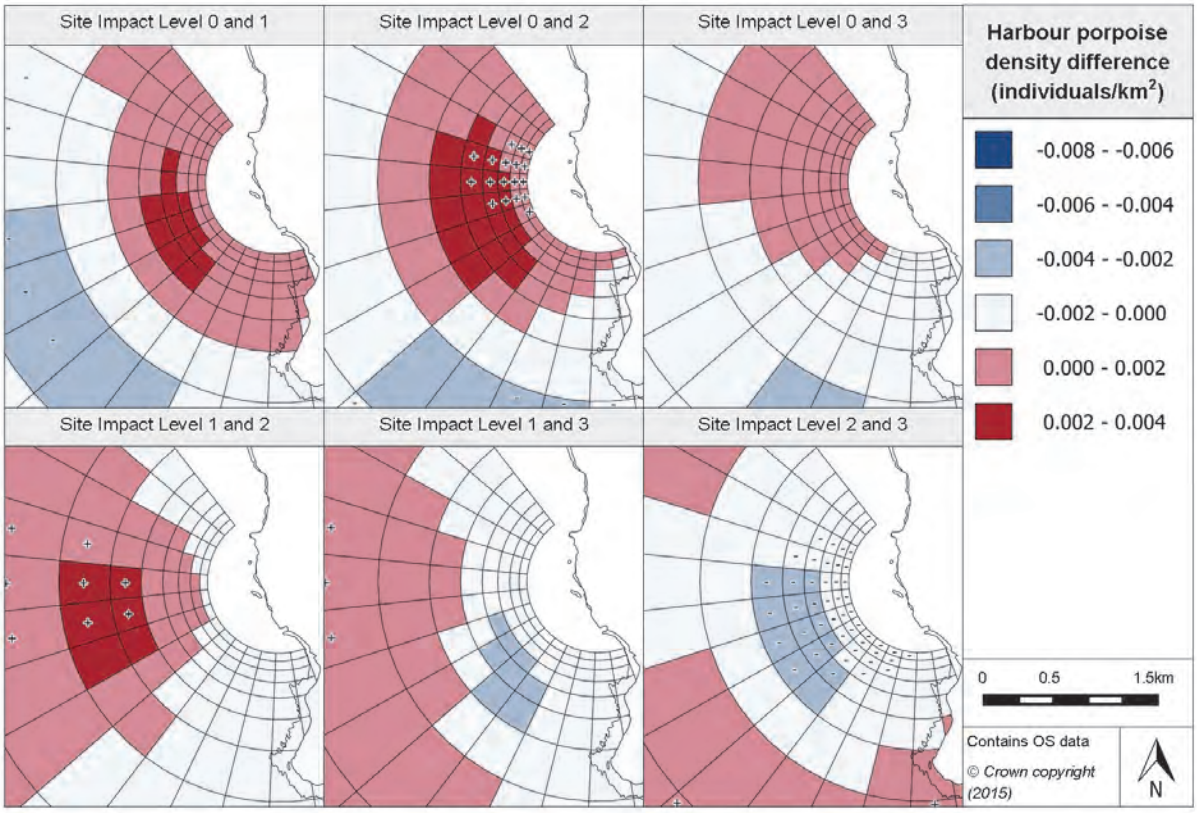

Figure 4.6.16. Density differences between harbour porpoises site impact level inner prediction surfaces during 2013 (least variable year) at Billia Croo

4.6.2.7 Density change with distance from potential impact location

Following the above discussion of the density differences between site impact levels, this section focuses on how the extent of density change between site impact levels varies with increasing distance from a potential impact. For the purposes of this project, a potential impact is seen as a test berth. Figure 4.6.17 below shows the extent of density difference with increasing distance from a single test berth.

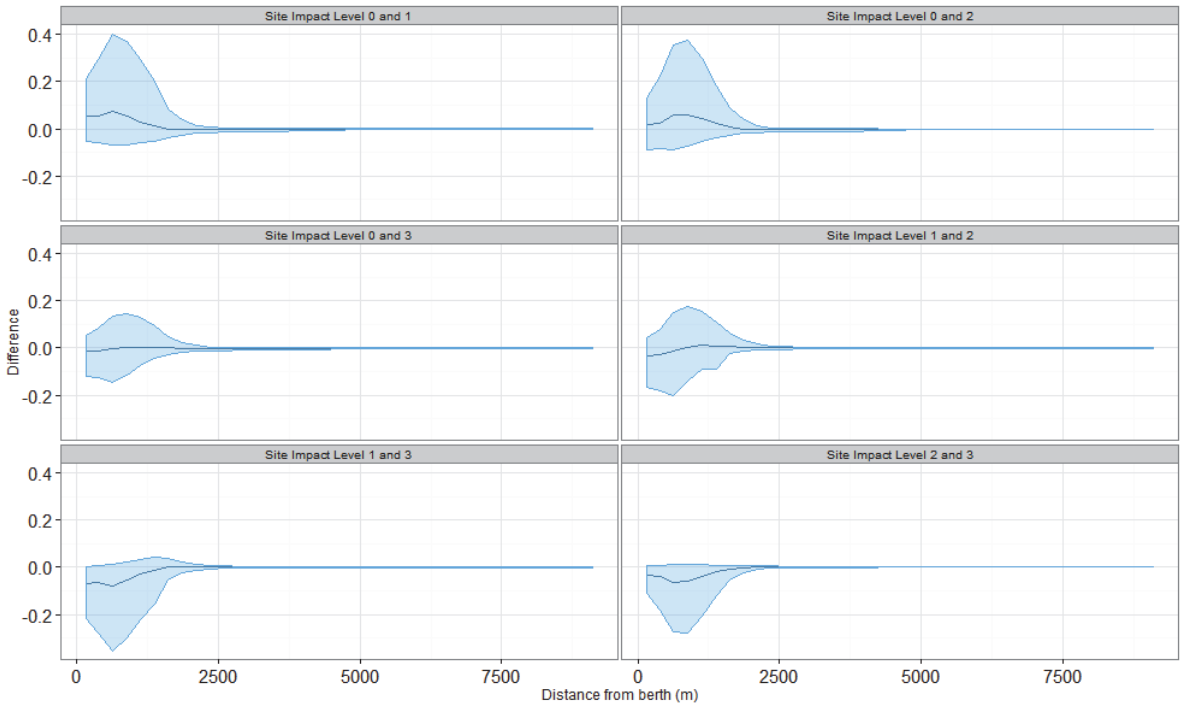

Figure 4.6.17. Density change between site impact levels with increasing distance from a potential impact location, with associated confidence intervals, for harbour porpoise at Billia Croo

There is an apparent increase in density at SIL-1 conditions as compared to baseline conditions at the immediate location of the potential impact. This increase between SIL-0 and SIL-1 rises slightly up to 0.7km from the test berth. As the lower CI is below zero, this change in density is not necessarily always going to be positive. A very similar trend in density difference is expected between SIL-0 and SIL-2; again, the changes between these two impact levels is unlikely to be significant, due to wide CIs.

The density changes between baseline conditions and SIL-3 are very low at the test berth site (with CIs on either side of zero) and remain such with increasing distance away from it.

Similarly, although a reduction in density is anticipated between SIL-1 and SIL-2 at the test berth location, which gradually reduces in extent returning to SIL-1 levels beyond 1.2km, the large confidence limits on either side of zero suggest there is very little significance in this prediction. However, between SIL-1 and SIL-3, the decrease at the test berth location is greater and the upper confidence limit is at or close to zero. The extent of density decrease gradually rises reaching SIL-1 levels at approximately 1.6km from the berth, with the exception of a small further dip at about 0.5km from the berth. As the upper confidence limit is closer to zero, this would suggest that there is less variation in the prediction and slightly more confidence in it; however, it remains unlikely that the prediction is significant.

Between SIL-2 and SIL-3, there is a reduction in density at the location of the test berth which increases in extent with distance up to 0.5km from the test berth. Beyond 0.5km, the level of density decrease gradually reduces reaching SIL-2 levels at approximately 1.8km from the test berth. Importantly, the upper confidence limit is at or very close to zero, suggesting that this change in density is likely to be significant.

As mentioned previously, it is worth considering that the above figure is from a single grid cell containing a test berth, is the modelled relationship between density difference and the

increasing distance from the grid cell. It appears as if the relationship varies dramatically between the various grid cells that contain a test berth. Reference should be made to the Marine Scotland Information portal for further plots from each grid cell containing a test berth.

4.6.2.8 Discussion

The harbour porpoise is the most common cetacean species observed at Billia Croo, where they are seen with much greater frequency than at the Fall of Warness. The model shows that the highest densities are estimated closer to land which reduce with increasing distance from the shoreline[26]. The model outputs suggest that there is a general consistency across the site impact levels as to the location of grid cells with higher densities (i.e. the grid cells where greater densities are predicted at SIL-0 tend to be the same grid cells at SIL-1, SIL-2 and SIL-3). These are found at the entrance to Hoy Sound and in a cluster 1km south-west of the cliffs at Black Craig.

The density differences between baseline conditions (SIL-0) and the other three site impact levels are all very similar. The three outermost grid bands experience reductions in density with a cluster of greater decreases in density at the entrance to Hoy Sound, whereas density increases are generally restricted to the northern grid cells of the inner grid bands for all three site impact levels, as compared with baseline conditions. There is no correlation between the estimated undulations in harbour porpoise density and the location of grid cells with test berths.

4.6.3 Cetaceans

4.6.3.1 Species overview

As already mentioned in Section 4.4.3.1, many different cetacean species can occur in the Orkney waters. The following is a list of all cetacean species that have been observed at Billia Croo since the commencement of the observations programme. There have also been a few sightings where the species has not been identified; these sightings are recorded as 'Cetacean spp.':

- Harbour porpoise (*Phocoena phocoena*)
- Minke whale (*Balaenoptera acutorostrata*)
- Risso's dolphin (*Grampus griseus*)
- White-sided dolphin (*Lagenorhynchus acutus*)
- Killer whale (*Orcinus orca*)
- Short-beaked common dolphin (*Delphinus delphis*)
- Long-finned pilot whale (*Globicephala melas*)
- Pilot whale (*Globicephala* spp.)
- White-beaked dolphin (*Lagenorhynchus albirostris*)
- Common dolphin (*Delphinus* spp.)
- Humpback whale (*Megaptera novaeangliae*)
- Bottlenose dolphin (*Tursiops truncatus*)
- Sperm whale (*Physeter macrocephalus*)

The frequency with which these animals are spotted at the site varies between species. A brief description of the distribution and life history of some of the most frequent visitors is provided in Section 4.4.3.1. Also included in this section is a brief description of the protection status afforded to cetaceans found in UK waters. In addition to the brief descriptions given in Section 4.4.3.1, further information on both the frequent and infrequent

[26] Note that a detection function was not applied to the raw observations, and therefore this prediction may be a result of the influence of declining detection with increasing distance from the observation point.

visiting cetacean species that have been observed within the Billia Croo test site can be found in Evans *et al*. (2011) and Reid *et al*. (2003).

4.6.3.2 Data summary

Table 4.6.7 below provides a summary of the cetacean raw observation data. The information provided includes minimum, maximum and mean group size. The summary has also been split across each site impact level to provide a representation of the data used in the model selection process.

Table 4.6.7. Summary of cetacean raw data

	Total	Site Impact Level 0	Site Impact Level 1	Site Impact Level 2	Site Impact Level 3
Number of observations	824	62	96	303	303
Minimum (group size)	1	1	1	1	1
Maximum (group size)	50	12	50	18	35
Mean (group size)	2.37	2.84	2.75	1.99	2.51
(s.d)	(3.12)	(2.38)	(5.15)	(1.98)	(3.26)

4.6.3.3 Model overview

Only four terms remained in the final fitted cetacean model. Each term's GEE-based p-values are provided in Table 4.6.8. Three of the remaining terms were concluded to be statistically highly significant.

Table 4.6.8. GEE-based p-values for the terms in the final cetacean model for Billia Croo

Model term	ρ-value
Sea state	<0.0001
Site impact	0.267
Spatial surface	<0.0001
Spatial surface / site impact	<0.0001

One of the remaining terms in the final fitted cetacean model was 'sea state' as it was concluded that sea state has affected the density of cetaceans. Figure 4.6.18 provides a visual representation of the relationship between sea state and cetacean density. From Figure 4.6.18, it is clear that highest densities are estimated when sea state is 1 (calm); the density predictions decrease with increasing sea state. Although the model is predicting lower density at the higher sea states, it is worth highlighting that, the higher the sea state, the more difficult it becomes to observe cetaceans. It is well known that cetaceans are easily spotted in smooth, calm seas. Therefore, the model is predicting a relative density of cetaceans and not an absolute density.

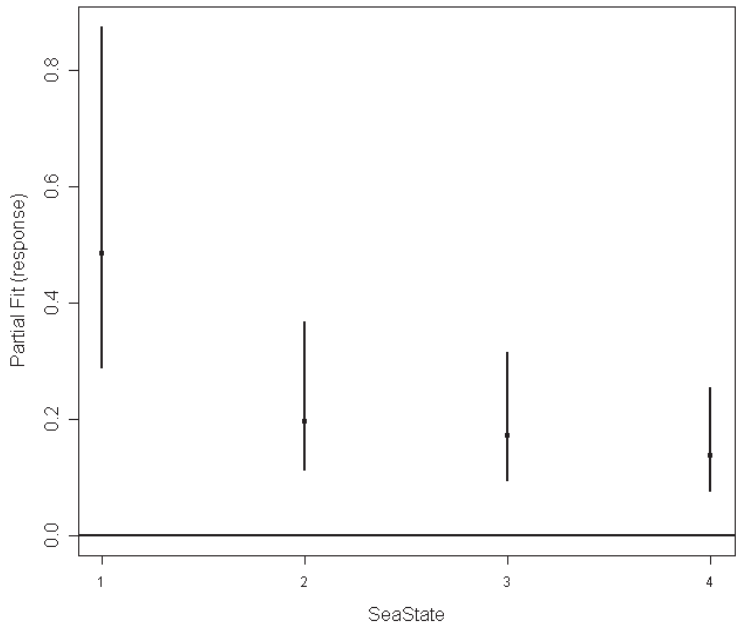

Figure 4.6.18. Estimated partial relationship of cetacean density (on the scale of the log link) with sea state at Billia Croo. The points are the parameters for the estimated change in log density from the baseline (seasate = 0) and the vertical lines represent 95% confidence intervals about the parameter estimates.

Similar to the other models fitted, a spatial surface was able to be fitted to the final cetacean model. It is important to note that six knots were required to be able to fit this surface, more than for any other Billia Croo species' spatial surface. Also included in the final fitted model was the interaction term (site impact/spatial surface), as it was found to be statistically highly significant.

4.6.3.4 Density predictions and uncertainty estimate

As a spatial surface is contained within the final fitted cetacean model, density prediction surfaces have been able to be produced for each site impact level. The environmental covariates in the model had to be set at certain values to be able to produce predictions, these are outlined in Appendix 5. As with other Billia Croo species, there were some anomalies in the cetacean data which meant it was necessary to reduce the number of iterations in the bootstrap. In total, 878 iterations were implemented rather than the 1000 carried out for most other species/groups. The following figure, Figure 4.6.19, provides the prediction surfaces for each impact; a detailed version of the inner grid cells in each prediction surface is available in Figure 4.6.20. CV values have also been produced for each of the prediction surfaces, and again a detailed view of the CV values for the inner grid bands in each surface can be seen in Figure 4.6.22.

Reference should be made to Figure 2.1.9 and Figure 2.1.10 for the grid cell labelling system.

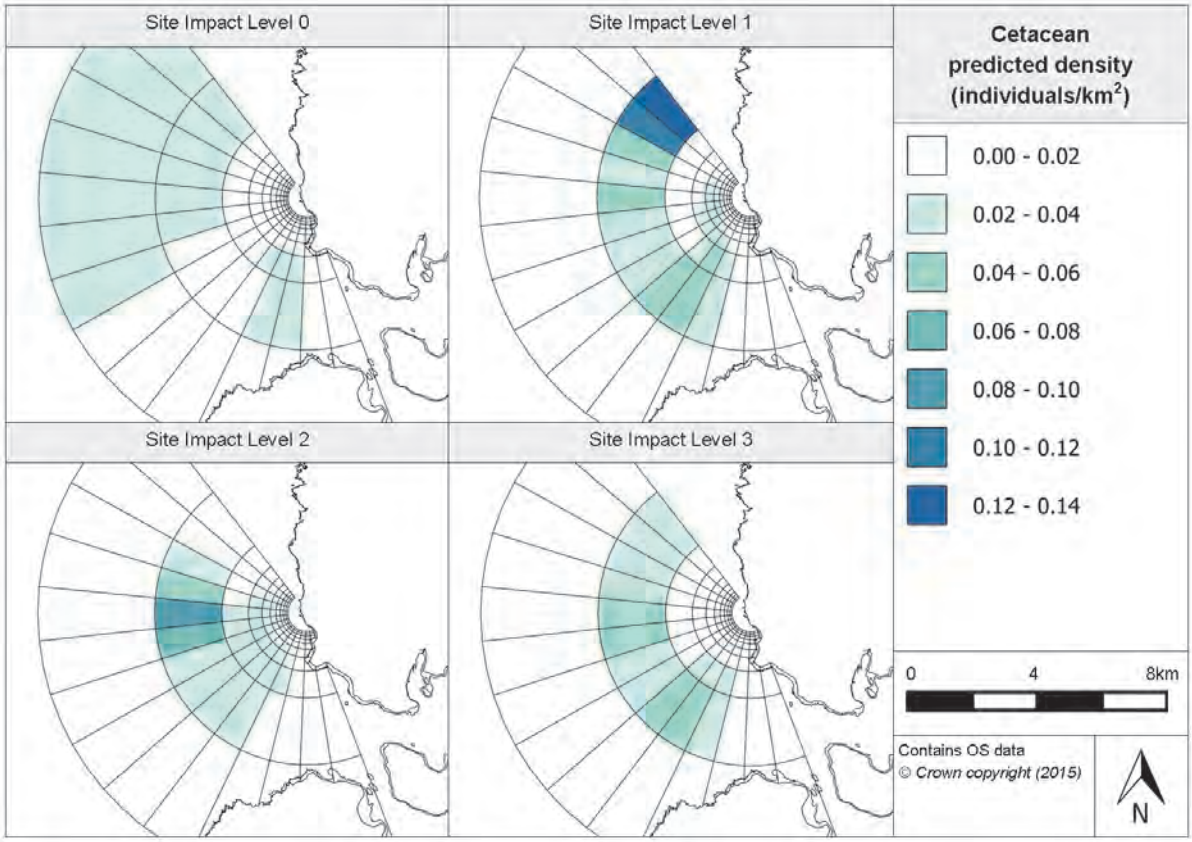

Figure 4.6.19. Estimated cetacean density at each site impact level across Billia Croo

The prediction surfaces show low densities for cetaceans at all site impact levels with only two grid cells with any values in grid band G above 0.02 individuals/km^2 and none at all within grid bands H-J.

The prediction surfaces for baseline conditions show grid cells A0-A6, B0-B5, B10-B11 and C9-C11 having density predictions of between 0.02 and 0.04 individuals/km^2. In contrast, the remaining grid cells in the outer grid bands and all cells in the inner grid bands, see Figure 4.6.19, have density predictions of below 0.02 individuals/km^2. This suggests that there are greater densities of cetacean estimated in the outer grid bands as compared to the inner grid bands, which would be expected in terms of the cetaceans' typical distribution with increasing water depth.

Under SIL-1 conditions, when device-associated infrastructure is installed onsite, an apparent cluster of high densities is estimated in the northern end of grid band B. In terms of grid cells B0-B1, both are expected to have densities greater than 0.10 individuals/km^2, with the density of B0 in particular being 0.14 individuals/km^2, see Figure 4.6.19. Cetacean density predictions of 0.02-0.06 individuals/km^2 are expected in grid cells B2-B10 and C8-C10. The remainder of the grid cells in the outer grid bands have density estimates of 0.00-0.02 individuals/km^2. Considering the inner grid cells, Figure 4.6.20, density predictions of greater than 0.02 individuals/km^2 have been modelled in grid cells D6-D9, E3-E8, F3-F7 and G4-G5. Otherwise, the remaining grid cells in these grid bands have density predictions below 0.02 individuals/km^2.

In terms of the density prediction surfaces for SIL-2, the highest density prediction exists in grid cell B4 where 0.08 individuals/km^2 are expected. Away from this cell, the density is expected to reduce gradually. Across the outer grid bands, densities above 0.02

individuals/km^2 are expected in grid cells B2-B9 and C4-C10, and in the rest of the grid cells in the outer grid bands (including grid band A), the cetacean density is expected to be 0.00-0.02 individuals/km^2. In terms of the inner grid bands, Figure 4.6.20, there appear to be no clusters of grid cells where high densities are estimated, with the exception of grid cells D3-D9, E2-E8 and F3-F7 showing densities between 0.02 and 0.04 individuals/km^2. The lack of densities greater than 0.02 individuals/km^2 for grid cells adjacent to shore, highlights the distance from the observation vantage point that the majority of raw cetacean observations occur.

When device/s are operational at the site (SIL-3), the density prediction surface anticipates there to be, in general, low densities across the site, with the majority of grid cells having densities between 0.00 and 0.02 individuals/km^2. As shown in Figure 4.6.19, the only grid cells across the entire grid with density predictions greater than 0.02 individuals/km^2 are B0-B10 and C8-C10; the density in these cells falls between 0.02 and 0.06 individuals/km^2. Within these cells, peaks in the modelled density are located in grid cells B4-B5 and B8-B9. It is worth noting, from Figure 4.6.20, that all cells in the inner grid bands have density predictions of less than 0.02 individuals/km^2.

The density predictions surfaces for SIL-0 and SIL-3 are the most similar with densities across all grid cells below 0.06 individuals/km^2, whereas higher densities are predicted for a few grid cells at both SIL-1 and SIL-2.

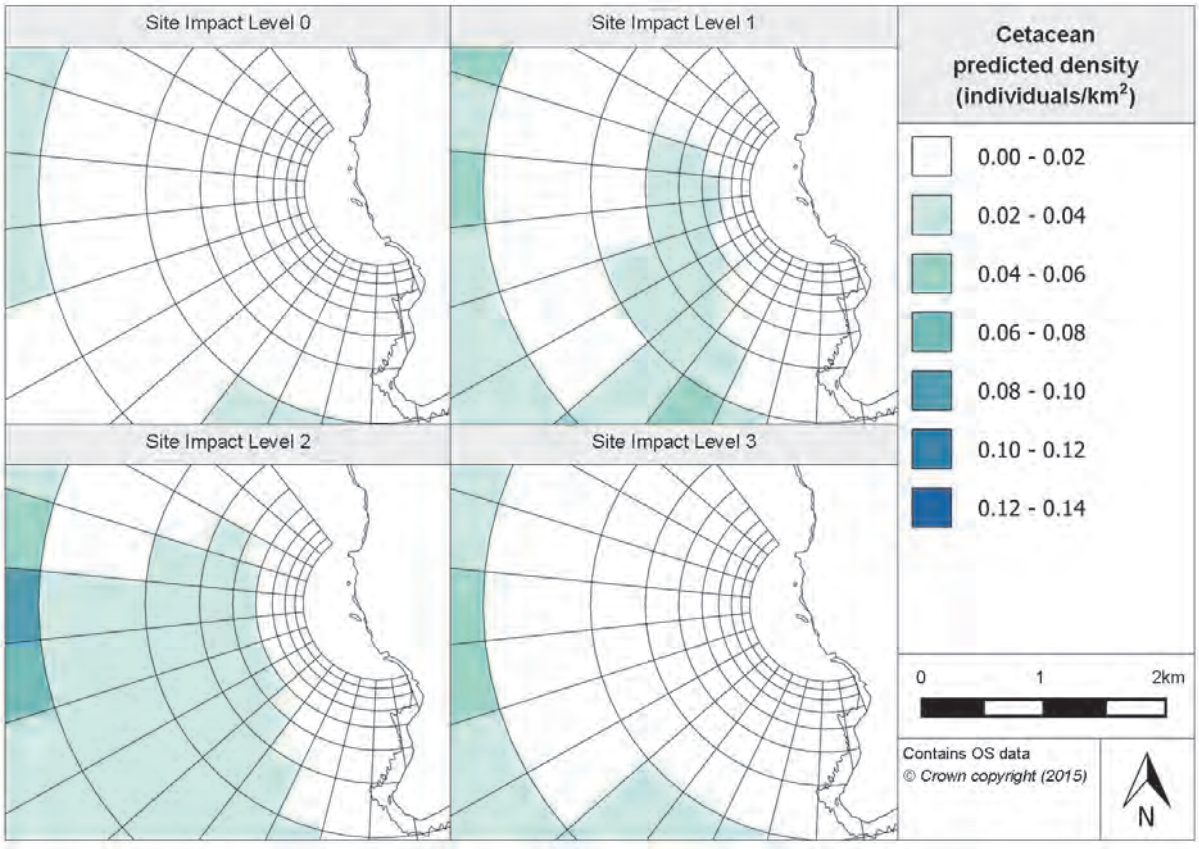

Figure 4.6.20. Inner prediction surfaces for cetacean density at Billia Croo

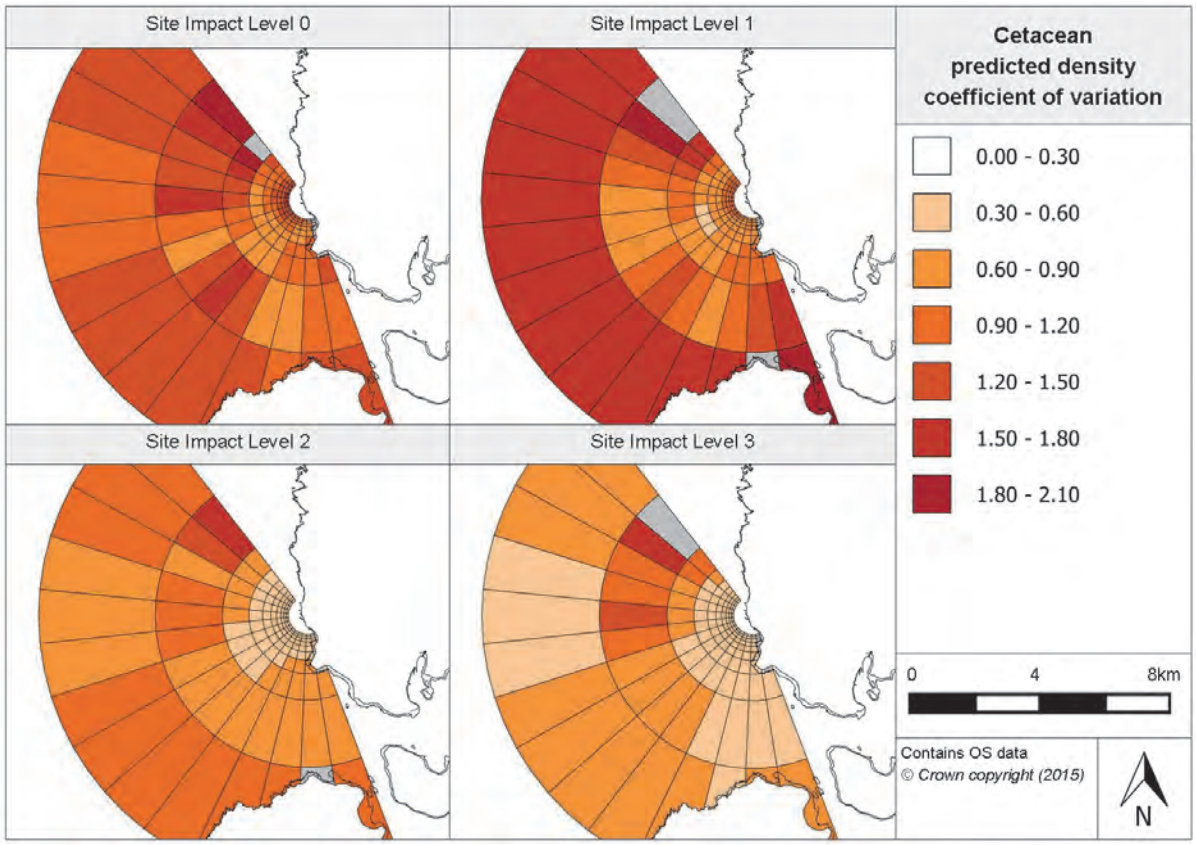

Figure 4.6.21. Associated coefficient of variation values for the density predictions for cetaceans at Billia Croo

Overall, the CV values obtained for the prediction surfaces are promising, as only a few cells across the surfaces have unavailable CV values and, in general, the CV values would support there being some precision in the results. The CV values for the baseline conditions' surface suggest that there is, in general, reasonable precision in the predictions. As can be seen in Figure 4.6.21, CV values are either greater than 1.8 or unavailable in grid cells B0 and C0-C1. The former is the grid cell with the highest estimated density at SIL-1. This small cluster of higher or unavailable CV values may suggest a particularly high variation in the predictions for these cells or else there is a lack of observations. In terms of the inner grid bands, Figure 4.6.22, the CV values generally appear to suggest reasonable precision in the predictions of very low densities (less than 0.02 individuals/km^2) for these cells, with the exception of unavailable CV values in the cells adjacent to the shoreline at Billia Croo and on either side of the Breck Ness headland. It is highly probable that CV values are unavailable in these grid cells due to a lack of observations recorded in this location.

The CV values across the SIL-1 prediction surface imply that, in grid band A, cells B0-B1, B13 and C0-C1, there is less reliability in the predictions due to CV values being greater than 1.5 or unavailable. The remaining grid cells in the outer grid bands have CV values less than 1.5 which provides reasonable precision with respect to the predictions for these cells. As can be seen in Figure 4.6.22, CV values for the inner grid cells vary from 0.3 to 1.2; these values suggest that, for the inner grid cells, there is less uncertainty surrounding the predictions. It is worth noting that cells located adjacent to land continue to have their CV values unavailable.

There is greater precision in the prediction surface for SIL-2 suggested by the CV values. In general, these values are lower for predictions at this surface as compared to SIL-0 and SIL-1. There continues to be heightened CV values in cells B0-B1. Apart from these two grid cells, Figure 4.6.21 shows that CV values range between 0.3 and 1.2, whereas, as seen in Figure 4.6.22, within the inner grid bands CV values are expected to lie between 0.30 and 0.60 for the majority of the grid cells, which suggests high precision in the density predictions for these cells. This suggests a distinction between the cells with low density predictions of below 0.02 individuals/km^2 and those marked as having density predictions of 0.02-0.04 individuals/km^2; the latter are more likely to be true relative densities. In addition, it is worth noting that grid cells D10-D12 have CV values between 0.6 and 0.9 and the cells adjacent to the shoreline continue to have unavailable CV values.

Finally, even lower CV values exist for the predictions for SIL-3, suggesting that there is less uncertainty in the predictions at this impact level than at any other impact level. The lower CV values obtained at SIL-2 and SIL-3 are probably due to the comparatively larger number of observations obtained at these site impact levels, as compared to SIL-0 and SIL-1, as can be seen in Table 4.6.7. With the exception of grid cells B0-B5 and C0-C1, all grid cells (including the inner grid bands) have CV values of 0.3-0.9, suggesting high precision in the results. It is worth noting the cluster of high CV values in grid cells B0-B5 and C0-C1 which align with an area of grid cells in the prediction surface where higher density predictions exist. This may be due to larger variation in the predictions due to the number of individuals fluctuating greatly between observations. It is also worth noting that CV values continue to be unavailable for the cells adjacent to the shoreline at Billia Croo probably reflecting that cetaceans do not come so close to shore.

The continuation of raised CV values in grid cells B0-B1 suggests large variability in the predictions for this grid cell. Taking the species into account, this is likely to be due to one or two large pods of cetaceans being sighted in these grid cells; the large variation in the observations means that the 95% CIs are affected.

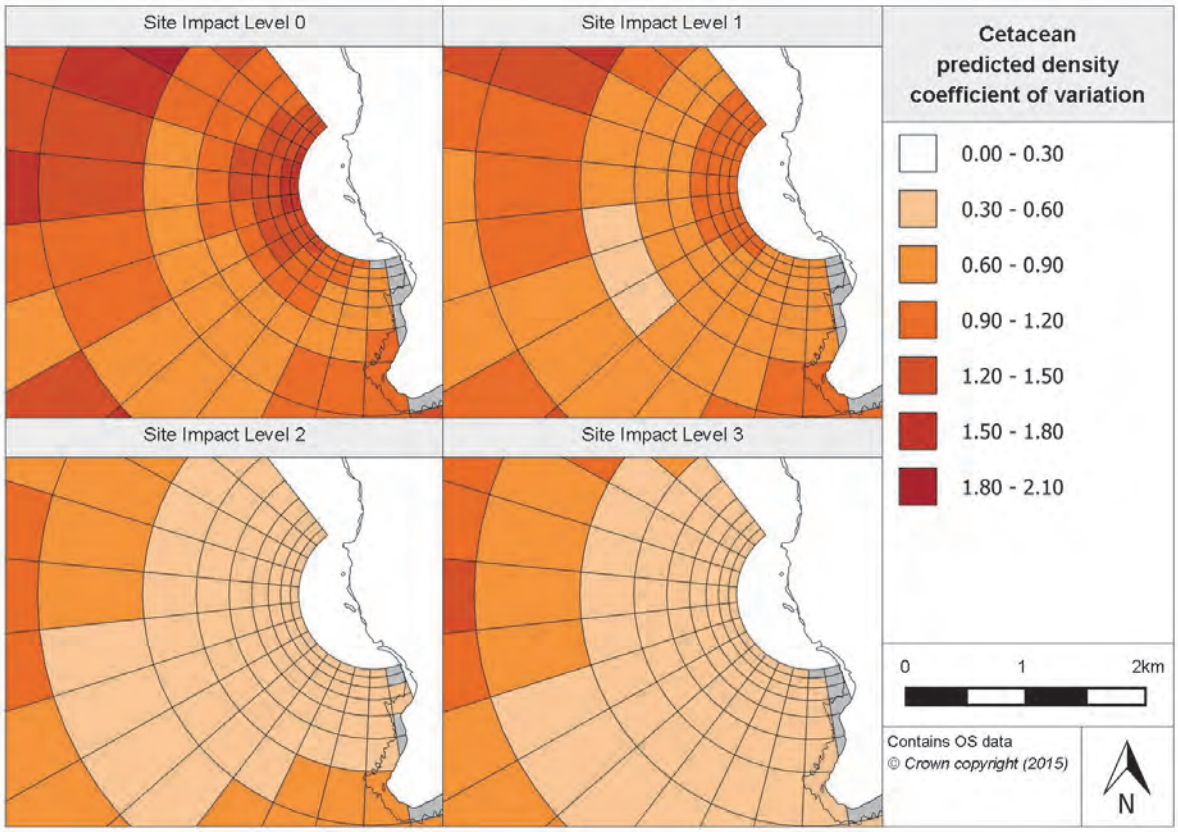

Figure 4.6.22. Associated coefficient of variation values for cetaceans inner density prediction surfaces at Billia Croo

4.6.3.5 Relative abundance estimations

Relative abundance estimates have been made for each survey month using the final fitted cetacean model for Billia Croo. By combining these values, seasonal abundance predictions have been produced and are available in Table 4.6.9. In the making of these estimates, the same environmental covariates as employed for the species' density prediction surfaces, were used. Further information on these covariates can be found in Appendix 5.

Table 4.6.9. Relative abundance for cetaceans during each season (associated confidence intervals are provided in brackets)

Year	Season			
	Winter (Dec, Jan, Feb)	Spring (Mar, Apr, May)	Summer (Jun, Jul, Aug)	Autumn (Sep, Oct, Nov)
2009	-	4.83 (3.36, 7.78)	5.80 (3.36, 11.82)	7.74 (5.34, 11.82)
2010	7.74 (5.34, 11.82)	7.39 (5.74, 9.60)	7.39 (5.74, 9.60)	6.15 (4.45, 9.60)
2011	5.53 (4.45, 6.99)	5.30 (3.36, 7.78)	4.83 (3.36, 7.78)	4.83 (3.36, 7.78)
2012	7.74 (5.34, 11.82)	7.74 (5.34, 11.82)	7.51 (5.34, 11.82)	7.39 (5.74, 9.60)
2013	6.77 (4.45, 9.60)	5.53 (4.45, 6.99)	5.53 (4.45, 6.99)	4.83 (3.36, 7.78)
2014	4.83 (3.36, 7.78)	6.77 (3.36, 11.82)	7.74 (5.34, 11.82)	7.63 (5.34, 11.82)
2015	7.39 (5.74, 9.60)	7.39 (5.74, 9.60)	-	-

There appears to be a lack of seasonality in the estimated abundances, with no season exhibiting clearly greater abundance predictions than others. This is to be expected due to

the number of different species included in the group, and the variety of species observations used when specifying and selecting the model. It is noticeable, from Table 4.6.9, that there is some interannual variation, with every second year generally having greater abundances when compared to the previous year. There is no explanation for this variation; however, it should be noted that, due the large range of cetaceans and the number of cetacean observations that were recorded at Billia Croo, it is unlikely that the model is very accurate in predicting trends.

The relative abundance estimates against time for each site impact level are presented in Appendix 7. The lack of variation expected between seasons is illustrated in the cetacean figure (see Appendix 7). However, the figure shows differences in predictions (and associated CIs) between site impact levels, although it should be noted that each site impact level's CIs do overlap. There are much larger CIs for predictions at SIL-1 as compared to SIL-3.

In addition to the prediction surfaces already created using the fitted cetacean model, surfaces have been generated for typical surveying conditions in January and July. The produced prediction surfaces and their corresponding CV values are available in the Marine Scotland Information portal. As already suggested, due to the limited difference in density predictions between seasons, there is minimal variation between the two predictions surfaces; however, the density predictions have been estimated to be up to 60% greater for July as compared to January.

4.6.3.6 Spatially-explicit change

In understanding the extent of any spatially-explicit changes in cetacean densities with change of site operational status, the density difference between site impact levels has been calculated. The 95% CIs have been used to understand the significance of any changes. As 'year' was not included as a term in the final fitted cetacean model, variability in predictions across years does not exist; this has resulted in a single year being presented below in Figure 4.6.23 and Figure 4.6.24. Grid cells where a significant change was found are marked with a corresponding '+' or '-'.

The changes in density predictions between baseline conditions (SIL-0) and SIL-1, SIL-2 and SIL-3 are all very similar with decreases in the outermost grid band and, generally, increases in the inner cells.

Between baseline conditions and SIL-1 (when infrastructure is installed), there are clearly defined areas of the grid where an increase in density is expected and other areas where decreases in density are anticipated. These include all the areas where the outer test berths are located. Within the outer grid band, Figure 4.6.23, a slight decrease in density is expected in grid cells A0-A13, B4, B11-B13 and C11-C13. Decreases of up to 0.04 individuals/km^2 are expected in these cells and seven cells have had their decreases marked as significant, whereas density increases are expected in grid cells B0-B10 (except B4) and C0-C10. The majority of cells are expected to increase in density by up to 0.04 individuals/km$^{2;}$ however, grid cell B8 has an estimated increase of 0.04-0.08 individuals/km^2. Grid cells B0 and B1 are expected to increase by up to 0.13 individuals/km^2 and 0.08 individuals/km^2. The increases in five grid cells have been deemed significant; these are located around grid cell B8. Considering the inner grid cells, Figure 4.6.24, the majority of cells show density increases up to 0.04 individuals/km^2. Only grid cells D5-D7 have been marked as significant. It is only the cells close to the shore at Billia Croo and Breck Ness headland that have density decreases expected with the introduction of device-associated infrastructure. These are up to 0.04 individuals/km^2.

The extent of the density increases between baseline conditions and SIL-2 (devices installed on site) is reduced in the outer grid bands compared with SIL-0 to SIL-1. Grid cells B3-B9 and C0-C9 have density increases between 0.00 and 0.04 individuals/km^2, with the exception of grid cell B4 where 0.04 individuals/km^2 are expected. The changes in grid cells C2-C8 and B6-B7 are all marked as significant. Reductions in density are anticipated between cells A0-A13, B0-B2, B10-B13 and C10-C13. The majority of cells in the outermost grid band have had their decrease in density marked as significant; however, the reduction in density in any of the outer grid cells is not expected to be greater than 0.04 individuals/km^2. As seen in Figure 4.6.24, in terms of the inner grid cells, an increase of up to 0.04 individuals/km^2 is expected in the majority of cells, with the exception of D11-D13 and C12-C13, located offshore of Breck Ness. Grid cells located in the north and west of the inner grid bands tend to have their increases in density deemed significant.

In terms of the outer grid cells, between SIL-0 and SIL-3 (when infrastructure is installed and operational), there is an increase in density of up to 0.04 individuals/km^2 estimated in grid cells B3-B10 and C0-C9 (Figure 4.6.23). The remainder of the cells have density reductions of up to 0.04 individuals/km^2. None of the changes in the outer grid bands have been deemed significant. When considering the inner grid bands, Figure 4.6.24, increases in density are expected in the northern half of each inner grid band and density reductions are anticipated in the southern half of the grid bands. The density increases and decreases are only expected to be up to 0.04 individuals/km^2. Grid cells D3-D5 have had their density increases marked as significant.

The density changes between SIL-1 and SIL-2 (devices being installed) are quite different to those expected between baseline conditions and SIL-1, SIL-2 and SIL-3. Increases in density are modelled in grid cells A2-A13, B3-B6 and C1-C8. The positive change in density is only expected to be up to 0.04 individuals/km^2, with the exception of grid cell B4 which shows an increase of 0.04-0.08 individuals/km^2. As can be seen in Figure 4.6.23, the remaining cells in the outer grid bands have decreases in density estimated. The majority of cells exhibit decreases of up to 0.04 individuals/km^2 but grid cells B0 and B1 have reductions of 0.16 individuals/km^2 and 0.11 individuals/km^2, respectively. Both of these cells have had their changes marked as significant. It should be noted that these were cells with particularly high densities for SIL-1 (Figure 4.6.23). With respect to the inner grid bands (Figure 4.6.24), slight increases in density are expected in cells at either end of the grid bands and limited reductions are estimated in the grid cells in the middle of the bands. Increases in density in cells D3-D6 are expected to be significant.

In terms of the density difference between SIL-1 and SIL-3 (devices installed and operational), an apparent increase in density is seen in grid cells A0-A13, B4-B7, B11-B13, C2-C6 and C13 in the outer grid bands. The increase, however, is only slight with changes of up to 0.04 individuals/km^2 expected. In terms of the remaining grid cells (Figure 4.6.23), a slight decrease of 0.00-0.04 individuals/km^2 is anticipated in the majority of grid cells, with the exception of B0 and B1. The decrease in density in these cells is anticipated to be 0.14 individuals/km^2 and 0.09 individuals/km^2; however, these decreases have not been deemed significant. As shown in Figure 4.6.24, in the inner grid bands, the majority of cells are modelled to experience decreases of between 0.00 and 0.04 individuals/km^2; the exception is D0 and grid row 13 (D-H) where increases in density of up to 0.04 individuals/km2 are expected.

Between SIL-2 and SIL-3, with devices becoming operational, the majority of grid cells in the outer grid bands are anticipated to experience a slight increase in density, with changes of up to 0.04 individuals/km^2 (Figure 4.6.23). The positive change in density has been marked significant in some grid cells. There are, however, several grid cells (B3-B6 and C0-C11) where density decreases are estimated. The decrease in these cells in not expected to be greater than 0.04 individuals/km^2; however, the changes in grid cells C3-C7 appear

significant. In Figure 4.6.24, it is clear that all cells in the inner grid bands have density decreases of between 0.00 and 0.04 individuals/km^2 expected. Many of the changes within these cells have been deemed significant.

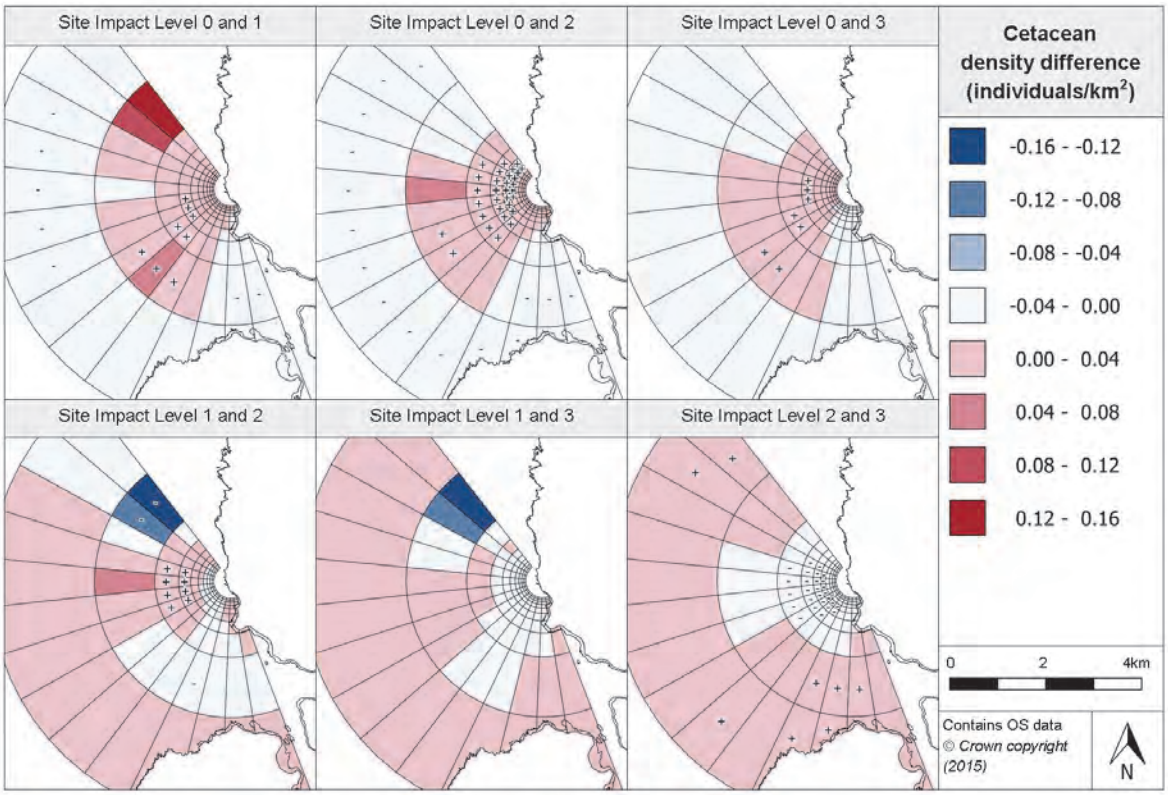

Figure 4.6.23. Estimated density difference between various site impact levels for cetaceans at Billia Croo

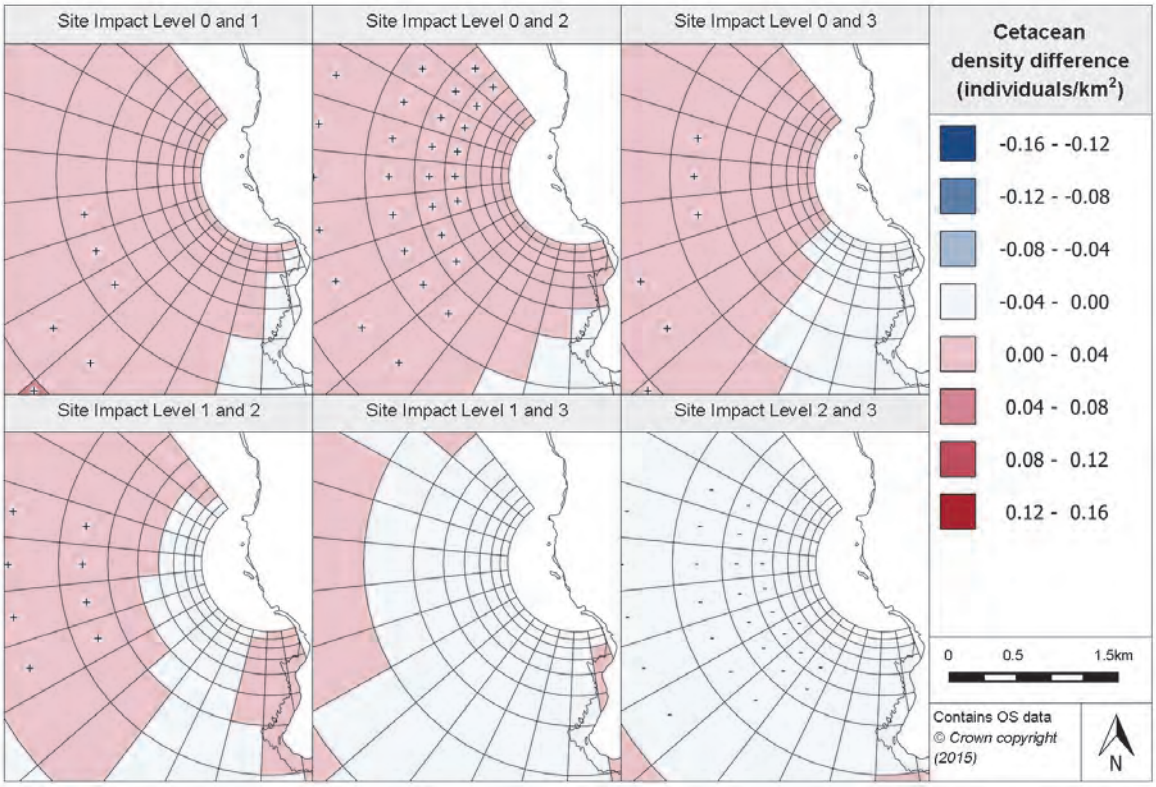

Figure 4.6.24. Density differences between cetaceans site impact level inner prediction surfaces at Billia Croo

4.6.3.7 Density change with distance from potential impact location

The following figure, Figure 4.6.25, illustrates how the density difference projections between site impact levels change with increasing distance from a potential impact location (a single test berth).

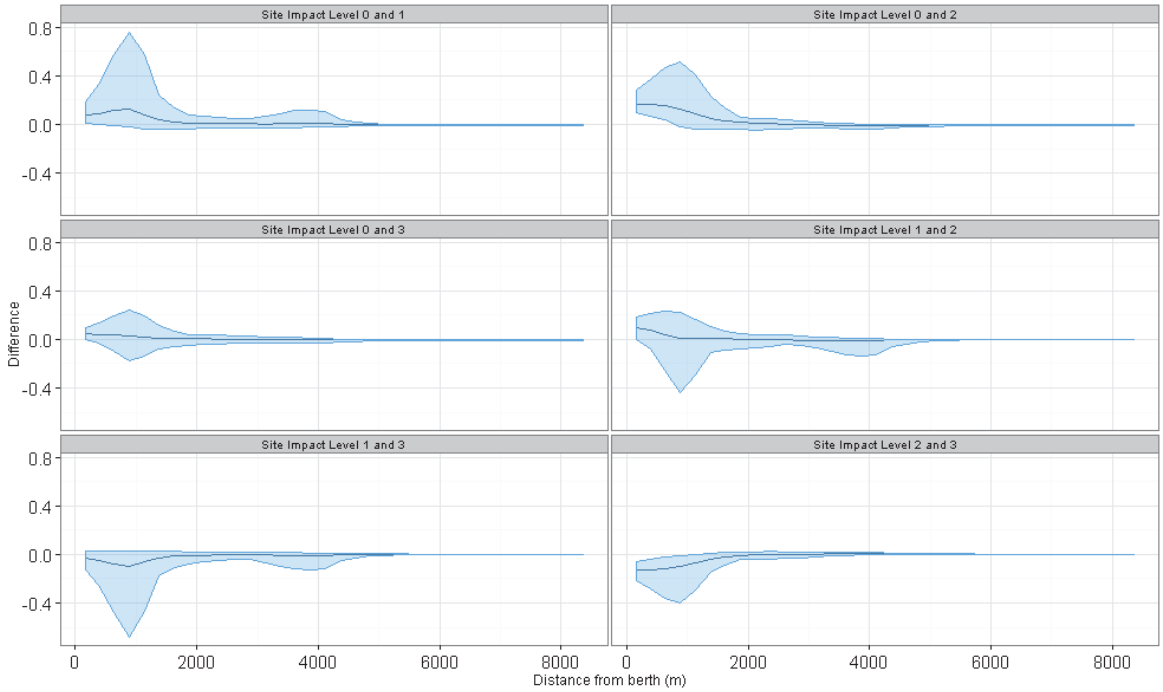

Figure 4.6.25. Density change between site impact levels with increasing distance from a potential impact location, with associated confidence intervals, for cetaceans at Billia Croo

From Figure 4.6.25, when considering the density difference between SIL-0 and SIL-1 with increasing distance, it is clear that there is an increase in density at the potential impact location which increases in value to 1km, beyond which it decreases in intensity, reaching SIL-0 levels at approximately 1.8km. Beyond 1.8km, there is little density difference between SIL-0 and SIL-1. However, the lower CI is below zero after the first 500m suggesting that this increase in density is unlikely to be significant. This increase in density at the test berth location is more evident between SIL-0 and SIL-2. There is likely to be a significant increase in density for at least 1km from the test berth when devices are installed as compared to baseline conditions. Beyond 1km, an increase in density is still evident but the lower CI is below zero, suggesting it is less likely that the increase is significant. Beyond 2km, there is very little difference in density between SIL-0 and SIL-2 (installation of devices).

There appears to be very limited density difference between SIL-0 and SIL-3 (devices installed and operational), which varies minimally with increasing distance.

However, for all these changes, the maximum CIs are very large (~±0.5 individuals/km^2) when compared with the predict density levels for cetaceans of around 0.03 individuals/km^2 (Figure 4.6.19 and Figure 4.6.20). It would seem that, for cetaceans as with other species at Billia Croo, the change in density at a single test berth and at distances away from it is less for SIL-0 to SIL-3 than for SIL-0 to SIL-1 and SIL-0 to SIL-2.

Between SIL-1 and SIL-2 (devices being installed), there is an increase in density estimated at the test berth location which gradually reduces to SIL-1 levels at around 1km from the test berth. As the lower CI appears to be below zero, it is unlikely that this change in density is significant. Beyond 1km, there is limited density difference between the two impact levels.

A decrease in cetacean density is expected between SIL-1 and SIL-3 (device installed and operational) at approximately 1km from the test berth, whereas, at the test berth's location, the extent of decrease appears to be limited. Beyond 1km, the density difference between

SIL-1 and SIL-3 slowly reduces, becoming minimal at around 1.7km. It is unlikely that the decrease modelled at around 1km from the test berth is significant, as the upper CI is above zero. However, between SIL-2 and SIL-3 (devices becoming operational), a density decrease is estimated at the test berth location. With increasing distance from the test berth, this decrease reduces in intensity, reaching SIL-2 levels at approximately 2km from the test berth. The decrease in density is likely to be significant for the first 1km but the upper CI behind the prediction is above zero, suggesting that it is not significant.

4.6.3.8 Discussion

Thirteen different species of cetaceans have been observed within the Billia Croo survey area. Modelling the distribution of this group of mammals is difficult as the observations will include occasional large groups (pods) passing through the area which can create anomalous local high densities. Overall estimated densities are low, typically less than 0.02 individuals/km^2, but cetaceans appear to frequent cells in grid band B the most. The spatial distribution that is evident may be associated with the distance from the coast in which cetaceans prefer to transit through this site at or be may linked to the location of tidal stream running through the site. Further investigation into cetacean behaviour would be required before either of these conclusions could be made.

Density changes have been modelled to be positive when infrastruce and devices are installated, but when the site impact level changes to operational conditions generally a slight reduction in density is estimated. However, these estimated changes are, on the whole, very small and few cells show significant changes.

It would seem that for cetaceans, as with several other species at Billia Croo, the change in density at a single test berth, and at distances away from it, is less for SIL-0 (baseline conditions) to SIL-3 (devices becoming operational) than between SIL-0 to SIL-1 (just infrastructure installed) and between SIL-0 to SIL-2 (devices installed but not operational). This may imply that the modelled density changes may be more related to vessel movement involved in the installation activities than to the presence/absence of a device in the water.

5. POWER ANALYSIS

Previous power analyses have been undertaken on the wildlife observation data collected at both sites during the early years of the programme (DMP Statistical Solutions UK Ltd, 2010; Waggitt *et al*., 2014). The results from these studies were promising as regards the power of the data to be able to detect changes in species abundance, although the power for some species appeared markedly higher than for others. A common comment in these early analyses was that the power of the dataset was expected to increase with time. On the basis that data collection at the Fall of Warness and Billia Croo had been running for ten and six years respectively, it was reasonable to believe that the power of the data collected during the Wildlife Observations Programme would have increased over this period. Although it would have been helpful to reassess the power of the data later on, or at the end of, the Wildlife Observations Programme[27], and in conjunction with the Wildlife Data Analysis Project, this did not prove possible due to time and budget restrictions.

5.1 Methodology

The initial scope developed for this project posed research questions that the project was to try to answer during its execution. One of the questions was: '*What power do the models possess in detecting change in species abundance and*/or *distribution due to an event?*' In order to answer this question, the effectiveness of the models in detecting species changes was assessed. This was achieved by carrying out a power analysis. It is important to understand whether a modelling result that showed no effect due to device infrastructure/presence/operation was the result of the effect present being unable to be detected by the modelling process. This could be due to a combination of several issues such as the magnitude of the specified effect size and the sufficiency of raw data for the context of the variability of the system, which may be extreme, particularly where there are no covariates to explain or describe this noise.

The power analysis was conducted using a simulations based approach and a range of scenarios were used to investigate the ability of each species model to detect various-sized reductions or redistribution in the underlying abundances of the relevant bird and marine mammal species. In addition, the power analysis allowed data for each species to be simulated (given the variability seen in the system) and sampled in a variety of ways (for example, for low survey effort or for current survey effort) to establish at what point changes in abundance could be detected.

The following three scenarios were developed for the power analysis:

- Scenario one: A site-wide decline in abundance of 50%. The decline would only happen when a device was present at the site (site impact levels 2 and 3 but with no additional reduction in abundance between level 2 and level 3).
- Scenario two: A redistribution in abundance defined as a 50% decline in grid cells with test berths[28], and an increase in grid cells without test berths. The increase in cells was proportional to the number observed, so the animals moved to areas already considered favourable. The redistribution only occurred when a device was present at the site (site impact levels 2 and 3, with no additional reduction between level 2 and 3).
- Scenario three: 50% site-wide decrease in abundance, but with an additional 50% reduction in survey effort (for example, if the survey was conducted every second fortnight rather than every fortnight).

[27] The Wildlife Observations Programme was discontinued at the end of December 2015.
[28] See Figure 2.1.3, Figure 2.1.9 and Figure 2.1.10 for an indication of which grid cells contain test berths.

If a distributional or site-wide change was detected in the original species' model, then a power analysis for these scenarios (1 and 2) was not necessary. It is known that the data have the power to detect such spatial changes, irrespective of whether those changes can be attributed to the installation/operation of devices. Therefore, for many species, only scenario three was considered, to determine if the site-wide decrease could have been detected with a 50% decline in survey effort.

In order to ensure that an efficient set of power analyses was conducted, scenario two power analyses were only performed on species models where the results (under the 'spatially-explicit change section' for each species) showed no evidence of a redistribution. By only conducting scenario two power analyses on these models, the assumption was made that the expected redistribution observed in the other models was being modelled correctly and was not a false result.

There are two key stages to be performed when carrying out a simulation based power analysis; 1) generation of simulated data; and 2) model fitting and assessment of detection of change. These are outlined below:

1) For each scenario, the fitted values from the final species model were used as a baseline. For scenarios one and three, a 50% decline between SIL-0/SIL-1 and SIL-2/SIL-3 was induced and for scenario two, the redistribution implemented. These new sets of values were considered 'truth'. A hundred sets of data were then simulated for each scenario by sampling from an overdispersed Poisson dataset, with the mean the 'true' values and using the estimated dispersion parameters from each species' model. Traditionally, if included at all, autocorrelation has been added to the data using a specific correlation structure. Here, the correlation seen in each block of the raw data is used to drive the correlation that is added to the simulated data. In this way, the simulated data closely respect the reality seen in the raw data. The correlation is added to the 500 sets of overdispersed Poisson data using a method not previously seen in ecology and developed by Iman & Conover (1982).

2) The second stage is the analysis phase; this is where the simulated data (which have had one of the scenarios imposed on them) are analysed using the original species model under investigation. The model is specified by keeping the covariates selected in the final model the same, but allowing the known locations to vary for any 1D or 2D smooth terms (the flexibility, known number, was fixed for efficiency). Regardless of the scenario being tested, three models, which kept all other covariates included but varied the implementation of the impact term, were tested to identify if the changes present in the data could be identified:

    1. A model with no impact term.
    2. A model with an impact term (allowed the detection of the 50% site-wide decline).
    3. A model with an interaction of the impact term with a spatial term (allowed the detection of the redistribution scenario).

    GEE-based p-values were used to assess which of the three models was preferred for each of the 100 sets of simulated data.

Some of the outputs of the power analyses vary depending on the scenario being tested. For all scenarios, the best model type (1, 2 or 3) was recorded. For scenarios one and three, if model type 2 was selected, the parameter estimate for the impact term was recorded along with its upper and lower 95% confidence interval. The true value of this parameter was known so it could be assessed if the truth was found within the 95% interval (which is expected 95% of the time). For scenario two (redistribution), if model type three is

chosen (which would be expected if the change can be detected), the parameter estimates are difficult to interpret so, instead, the spatially-explicit differences in each cell are recorded. A significant decrease in the berth cells, and an increase in the surrounding cells, is expected.

It is worth noting that, as the modelling work formed the basis of the power analyses, this allowed for any natural features of the system, such as nonlinearities, non-independence and the signal-to-noise levels in the data, to be reflected within the power analysis procedure.

For some of the Billia Croo power analyses, due to the size of the dataset, only 50 simulations of the data have been conducted. Where this is the case, it has been clearly stated.

5.2 Interpretation of power analyses results

The percentage of the correct models selected is provided for each scenario tested. The best models from scenarios one and three are expected to be model 2 and, from scenario two, model 3. However, it is unlikely that, in both cases, the correct model would be selected each and every time. Specifically, if model 3 is selected under scenarios one/three, there could still be a majority site-wide decline with only a few cells increasing.

5.2.1 Inference for the site-wide 50% decrease

For every species where a decrease in species density has been simulated across the grid (scenarios one and three), the percentage of models where the 95% confidence interval about the impact coefficient (when model two was selected) contains the true parameter, has been provided. In addition, a figure displaying the percentage of simulations, for each grid cell, that estimated a significant decrease (regardless of model type chosen), has also been provided. Each figure has three panels, showing the above, for the change between SIL-0 (baseline conditions) and each of the other site impact levels (SIL-1, SIL-2 and SIL-3). Figure 5.2.1 provides an example of the expected plotting outcomes from a well-performing model.

	SIL-0 – SIL-1	**SIL-0 – SIL-2**
	No Change All cells should be blue (no simulated decrease so no decreases should be identified)	100% change. All simulations should detect a significant decrease in all cells (red)
SIL-0 – SIL-3	100% change. All simulations should detect a significant decrease in all cells (red)	

Figure 5.2.1. The expected plotting outcomes for detecting a significant decrease from scenario one/three. The three descriptions in the table represent the plot shown as outcome.

A decrease of 50% was simulated across all grid cells at SIL-2 and SIL-3. In the figures, see example Figure 5.2.1, the first plot (SIL-0 – SIL-1) shows the percentage of simulations, for each grid cell, where there is a significant decrease in density between SIL-0 and SIL-1. As no decrease between SIL-0 and SIL-1 has been simulated during the power generation stage, any significant decrease identified by simulations between these site impact levels are likely to be due to variation in the prediction surface caused by the environmental and temporal terms in the fitted models rather than being associated with a change in site impact level.

However, as can be seen in Figure 5.2.1, between SIL-0 and SIL-2, a 50% decrease in density has been simulated and, therefore, it is expected that all simulations (100%) should pick up a significant decrease in density. As the same was simulated between SIL-0 and SIL-3, again if the model was performing very well, 100% of simulations are expected to detect a significant decrease in density in all of the grid cells across the site.

As mentioned previously, scenario three tests the effect of reducing survey effort. Survey effort has been reduced by 50% and the same 50% reduction in species density has been simulated. The reduction in survey effort has been carried out by removing every second sampling block; in other words, simulating that surveying only happens every other fortnight. This scenario tested whether, if sample size is cut by half, there are still sufficient data being collected to be able to continue to pick up the 50% decrease in density. If the models were performing extremely well, 100% of the simulations between SIL-0 and SIL-2, and SIL-0 and SIL-3 would detect a significant decrease in density. However, it is expected that the percentage of simulations that identify the 50% decrease in density will reduce from the percentages acquired under 100% survey effort, but the majority of simulations will continue to be able to detect the change.

5.2.2 Inference for the test berth-specific 50% redistribution

For every species where a redistribution has been simulated (scenario two), two sets of the figures have been produced. The first figure depicts the percentage of simulations, for each grid cell, where a significant decrease was estimated (regardless of the model type chosen). The second figure provides the percentage of the simulations, for each grid cell, where a significant increase in density has been predicted (again, regardless of the model type chosen).

Both of the figures (for the increase and decrease) are set up similarly to that for a site-wide 50% decrease. Each figure has three panels, showing the above, for the change between SIL-0 (baseline conditions) and each of the other site impact levels (SIL-1, SIL-2 and SIL-3). Figure 5.2.2 and Figure 5.2.3 provide examples of what should be the expected outcomes from a well-performing model.

	SIL-0 – SIL-1	SIL-0 – SIL-2
	No Change All cells should be blue (no simulated decrease so no decreases should be identified)	Decrease found in cells that contain test berths. All simulations should detect a significant decrease in these cells (red)
SIL-0 – SIL-3	Decrease found in cells that contain test berths. All simulations should detect a significant decrease in these cells (red)	

Figure 5.2.2. The expected plotting outcomes for detecting a significant decrease from scenario two. The three descriptions in the table represent the plots shown as outcome.

	SIL-0 – SIL-1	SIL-0 – SIL-2
	No Change All cells should be blue (no simulated decrease so no decreases should be identified)	Increase found in cells that do not contain test berths. All simulations should detect a significant increase in these cells (red)
SIL-0 – SIL-3	Increase found in cells that do not contain test berths. All simulations should detect a significant increase in these cells (red)	

Figure 5.2.3. The expected plotting outcomes for detecting a significant increase from scenario two. The three descriptions in the table represent the plots shown as outcome.

In the first figure for the redistribution power analysis, see Figure 5.2.2 as an example, the first plot shows the difference between SIL-0 and SIL-1 (infrastructure installed); this shows the percentage of simulations where a significant decrease in density was estimated for each cell. Between SIL-0 and SIL-1, as no change in density was simulated at the generation stage, 0% of simulations should detect a significant decrease in density. Any small changes in density between these impact levels are likely to be due to the variation caused by the environmental and temporal terms within the fitted model. In particular, no change is expected between grid cells containing test berths and those not containing test berths[29].

As summarised in Figure 5.2.2, between SIL-0 and SIL-2, and SIL-0 and SIL-3, 100% of simulations should pick up a significant decrease in grid cells that contain test berths. During the data generation stage, the data were simulated to shift 50% of animals out of these grid cells and into the cells where there are no tests berths (which tend to be located on the periphery of the site), under only SIL-2 (devices installed) and SIL-3 (devices installed

[29] See Figure 2.1.3, Figure 2.1.9 and Figure 2.1.10 for an indication of which grid cells contain test berths.

redistribution between SIL-0 and SIL-3, as for SIL-0 and SIL-2, very similar results are expected in this third panel, see Figure 5.2.3.

5.2.3 Remarks

In all three scenarios, if only low percentages of simulations were detecting the significant changes imposed on them, then the model was shown to be of low power and unlikely to be able to detect the changes in species abundance/distribution specified here. In addition, if a model struggled to detect a 50% change, it would be unlikely to be able to detect changes of lower extent (for example, a 30% decrease).

The poor power of a model could be due to several reasons. For example, there may be insufficient data or an extremely variable natural system for which there are no covariates to describe this variability.

The power analyses are very resource-intensive in terms of computational time due to their complexity, with the result that they have only been able to be conducted on selected species. For each test site, a bird species and a marine mammal species have been included in the power analyses.

5.3 Results - Fall of Warness bird species

5.3.1 Black guillemot

5.3.1.1 Site-wide 50% decrease (scenario one)

A site-wide decrease of 50% in black guillemot density was simulated during the power generation stage. Therefore, the model selected should have been model 2: where an impact term is included in the model but not an interaction of impact with a spatial term. It was found that 86% of the simulations (out of 100 simulations) selected the correct model (model 2). The remaining 14% of simulations estimated a species redistribution. This, however, does not imply that during these 14 simulations there were increases in density predicted. Instead, it could just imply that there is a negative distributional change and, therefore, there could be some spatial change between SIL-0 and SIL-2 or SIL-0 and SIL-3, making it necessary to include a spatial term. Within the 86 simulations where model 2 was selected, 95% of simulations had parameter estimate confidence intervals that contained the true decease parameter between SIL-0 and SIL-2 and, similarly, between SIL-0 and SIL-3, 95% of simulations had parameter estimate confidence intervals that contained the true decrease parameter.

Figure 5.3.1 below provides three plots showing the percentage of simulations (out of 100) where significant decreases in black guillemot density were estimated. See Figure 5.2.1 for information regarding what is expected in each panel of the plot.

Figure 5.3.1 below provides three plots showing the percentage of simulations (out of 100) where significant decreases in black guillemot density were estimated. See Figure 5.2.1 for information regarding what is expected in each panel of the plot.

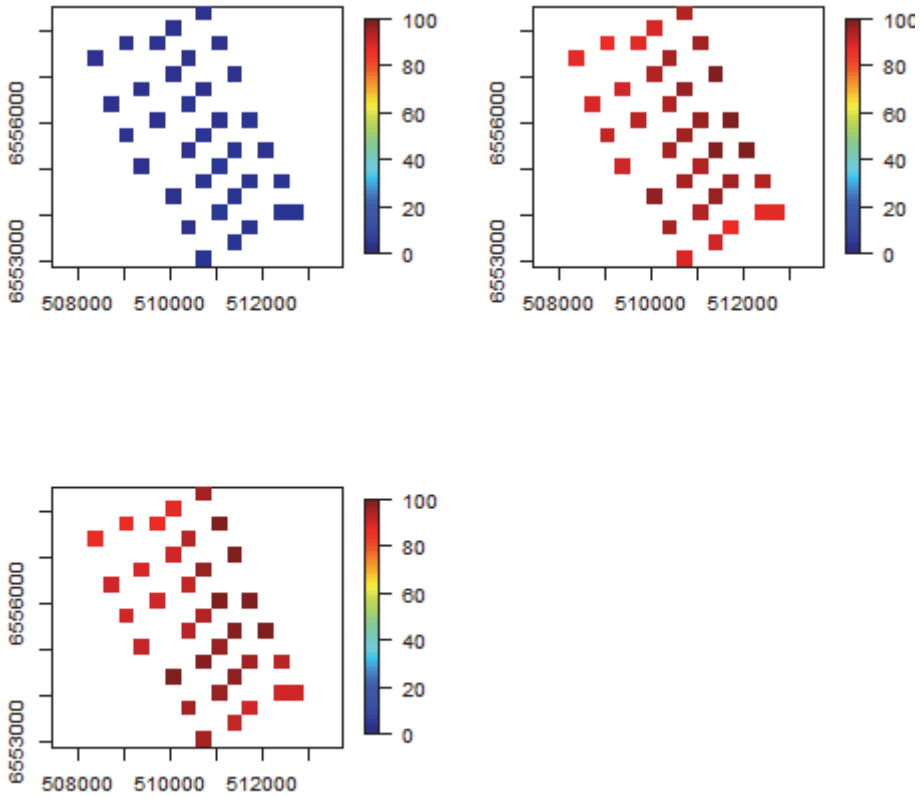

Figure 5.3.1. Percentage of power analysis simulations detecting a significant decrease in black guillemot density at site impact levels 1, 2 and 3, when applying a 50% site-wide decrease in density at SIL-2 and SIL-3 at full survey effort at the Fall of Warness

Between SIL-0 and SIL-1, there were very few simulations where significant decreases in density were estimated. As already mentioned, the 50% decrease in density was only simulated between SIL-0 and SIL-2 and between SIL-0 and SIL-3. However, between SIL-0 and SIL-2, Figure 5.3.1 shows that the majority of simulations (80-100%) have estimated significant decreases in density across each grid cell. The cells in the centre of the site and adjacent to the Eday shoreline are showing higher percentages of simulations predicting significant decreases. Similarly, between SIL-0 and SIL-3, there are high percentages of simulations predicting significant density decreases in all the cells across the grid. This is in line with the decrease simulated in the data during the power generation stage. Again, similar areas of the grid are showing higher percentages of the simulations estimating significant decreases.

The results indicate that the model shows good power to detect a 50% site-wide decline in black guillemot density. The higher percentage of simulations distinguished in the centre of the site, and close to the shore at Eday, suggests that these cells have the best power to detect such a change[30].

[30] This is likely to be because this area of the survey grid was where the majority of black guillemot observations were recorded, and hence it is easier to detect a change where the animals were in the first place. A decrease in a cell that is effectively already zero is difficult to identify.

5.3.2 Common guillemot

5.3.2.1 Site-wide 50% decrease (scenario one)

A site-wide 50% decrease in common guillemot density has been simulated during the power generation stage. It is therefore expected that model 2 would be selected the majority of the time. However, model 2 was selected for 48% of simulations and model 3 was selected 51% of the time. In addition, model 1 (where no interaction term is included in the fitted model) was selected for a single simulation. It is likely that some of the noise in the data has been identified as a distributional change, which caused model three to be selected slightly more frequently.

Of the 48 simulations that selected model 2, 96% had parameter estimate confidence intervals that contained the true decrease parameter for between SIL-0 and SIL-2 and, similarly, between SIL-0 and SIL-3, 96% of simulations had confidence intervals containing the true decrease parameter.

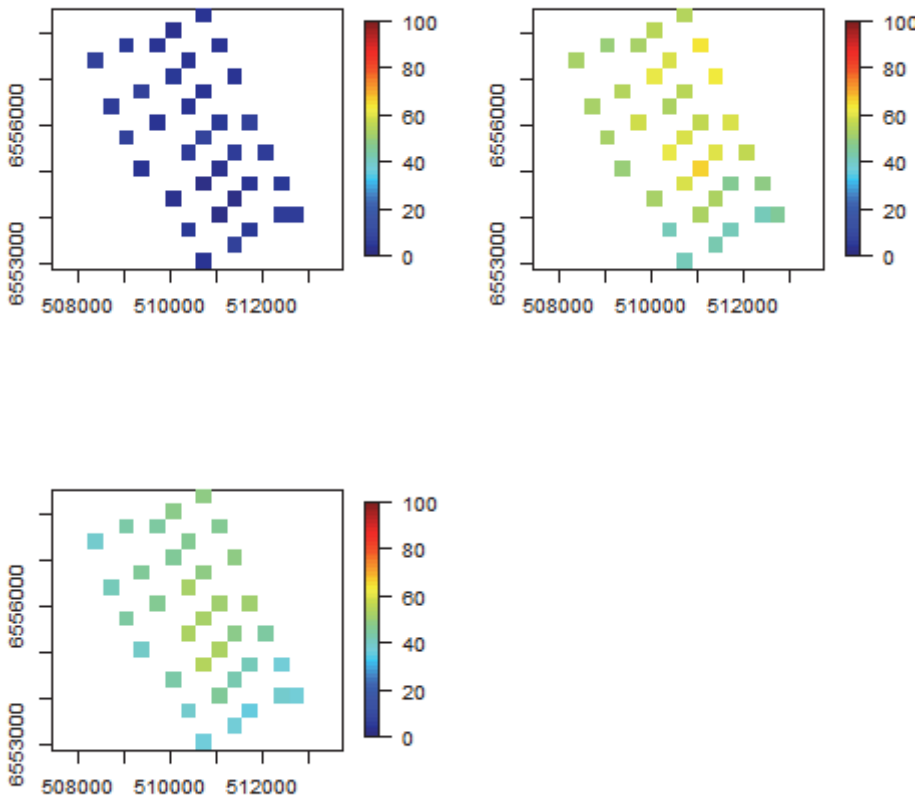

Figure 5.3.2. Percentage of power analysis simulations detecting a significant decrease in common guillemot density at site impact levels 1, 2 and 3, when applying a 50% site-wide decrease in density at SIL-2 and SIL-3 at full survey effort at the Fall of Warness

Very few simulations detected a significant decrease in density between SIL-0 and SIL-1 (Figure 5.3.2). However, in some cells approximately 70% of simulations detected a decrease in density between SIL-0 and SIL-2, whilst, in others, the decrease was only detected in 40% of simulations. Grid cells in the centre of the site and those adjacent to the shoreline at Eday tend to have higher percentages of simulations detecting a significant change in density compared to the grid cell in the south of the site. There are even fewer

simulations that have detected a significant decrease in density between SIL-0 and SIL-3. At best, approximately 55% of simulations detected a significant density change.

In summary, there is limited power across the whole site to detect the 50% site-wide decline in animal density imposed. Therefore, this suggests that, even if there was a 50% decrease in density, the model is only likely to detect the change around 50% of the time. The results also suggest that the model may perform slightly better in detecting density changes in the grid cells in the centre of the site and those adjacent to land at Eday[31].

5.3.3 Divers

5.3.3.1 Site-wide 50% decrease (scenario one)

During the power generation stage, a 50% decrease in diver density has been simulated across the site. As with the other species, the correct model to select in this case is model 2; this includes the interaction term. However, in terms of the diver power analysis, the correct model was only selected 19% of the time. Model 3 (which includes the interaction and spatial terms) was selected for 67% of simulations, and model 1 (includes neither an interaction term nor a spatial term) was selected 14% of the time. Model 3 may have been selected the majority of the time due to a distribution decrease in the estimated density and, therefore, a spatial term would be useful when making predictions. Where model 2 was selected (19 simulations), for between SIL-0 and SIL-2, 73% of simulations had parameter estimate confidence intervals that contained the true decrease parameter and, similarly, between SIL-0 and SIL-3, the same percentage of simulations had confidence intervals that contained the true decrease parameter.

Figure 5.3.3 shows the distribution of the percentage of simulations where a significant decrease in density was predicted. As no change in density between SIL-0 and SIL-1 was simulated, it is unsurprising that few simulations estimated a significant decrease in density in any of the grid cells between these site impact levels. It is possible that the cells in the south-west of the site had up to 15% of simulations detecting a significant decrease in density in these cells.

Between SIL-0 and SIL-2, the percentage of simulations where a significant decrease in density was predicted ranged between 14% and 24% across the grid. This suggests that the model does not perform well in detecting a 50% decrease in diver density. Similarly, between SIL-0 and SIL-3, between 11% and 22% of simulations detected a significant decrease in density' again suggesting that the model does not perform well in detecting such a change in density.

There is very low power in the data for this species to detect a 50% site-wide decrease in diver density.

[31] This may be due to an increased number of raw observations in this area of the survey grid. It is worth noting that, in general, the lower CV values occur in these areas, suggesting more precise density estimates.

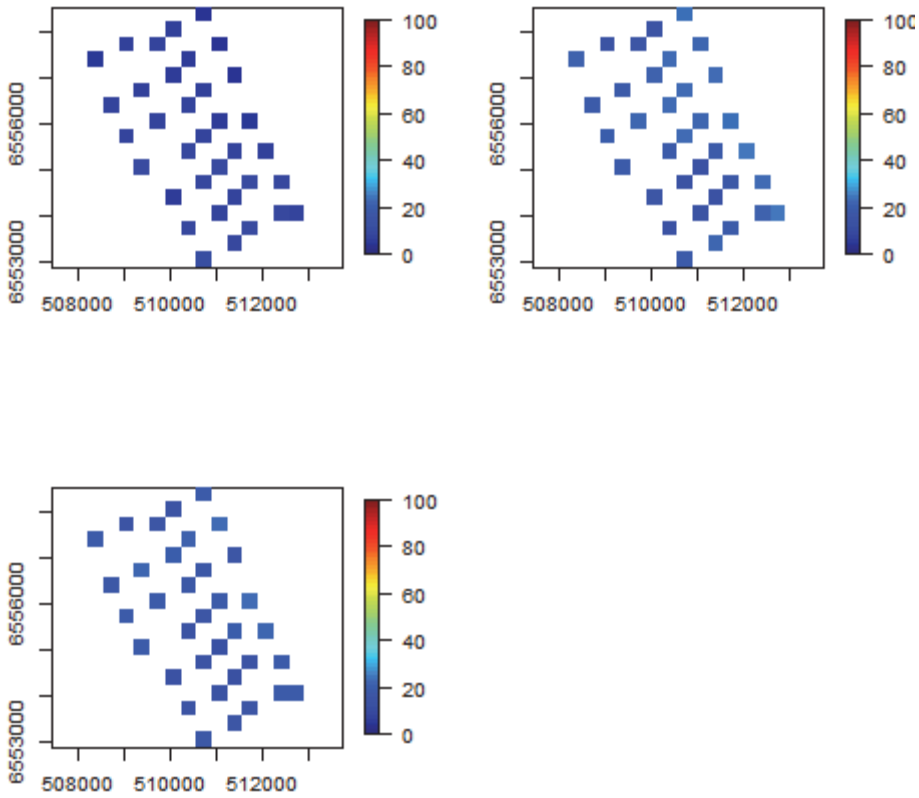

Figure 5.3.3. Percentage of power analysis simulations detecting a significant decrease in diver density at site impact levels 1, 2 and 3, when applying a 50% site-wide decrease in density at SIL-2 and SIL-3 at full survey effort at the Fall of Warness

5.3.3.2 Site-wide 50% decrease (scenario three)

When the same model is examined but with only half the survey effort performed, it is unsurprising that the model performs even more poorly than when full survey effort is applied. As can be seen in Figure 5.3.4, between SIL-0 and SIL-1, no change in diver density was simulated; however, grid cells in the south-eastern and north-western corners of the site possibly had up to 10% of simulations detecting significant decreases in density. But when a 50% decrease in density was simulated between SIL-0 and SIL-2, less than 20% of simulations were detecting such a change in density. As also observed in Figure 5.3.4, again only around 20% of simulations detect the significant density decrease that was simulated during the power generation stage.

This result and the findings in Section 4.3.4.4 suggest that the diver model does not perform well in detecting significant changes in diver density at the Fall of Warness and, therefore, little confidence can be placed in the model's density and spatially-explicit change predictions. It is expected that a greater occurrence of divers at the site is required to be able to form a model that has sufficient power to make accurate diver predictions. It is well-known that models that are based on very small density predictions have difficulty in detecting decreases in species density.

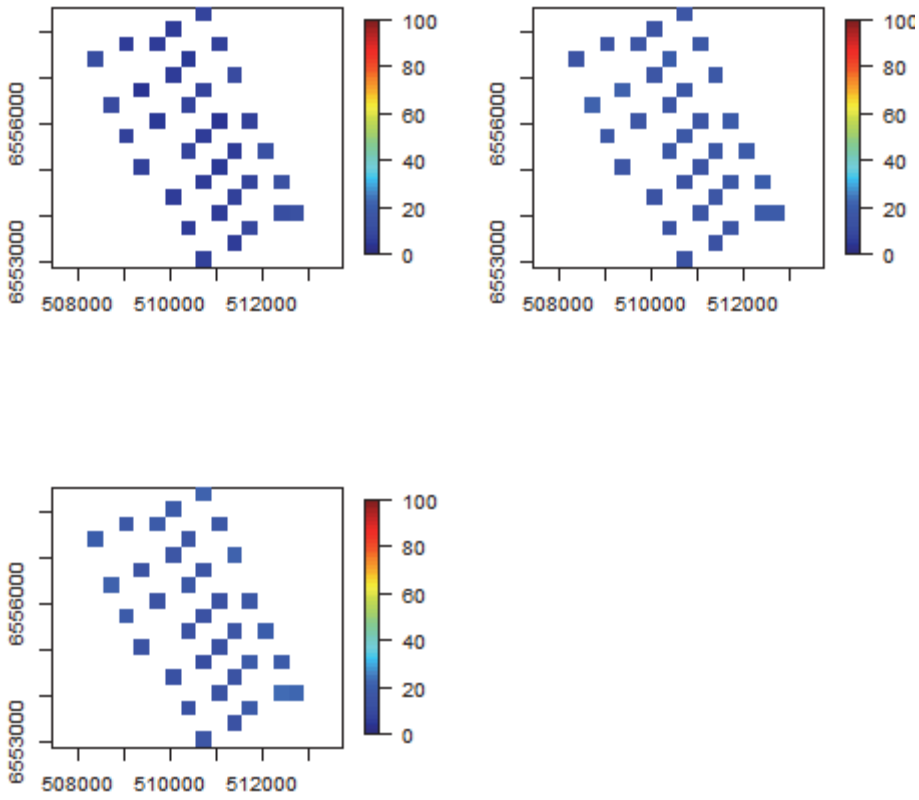

Figure 5.3.4. Percentage of power analysis simulations detecting a significant decrease in diver density at site impact levels 1, 2 and 3, when applying a 50% site-wide decrease in density at SIL-2 and SIL-3 at half survey effort at the Fall of Warness

5.3.4 Auks

5.3.4.1 Within-site redistribution (scenario two)

A redistribution of auks has been simulated based on scenario two. The correct model (model three) was selected 100% of the time, indicating that a redistribution in auk density was identified.

The following figures depict the percentage of simulations that have predicted a significant increase in density (Figure 5.3.5) and the percentage of simulations that have estimated a significant decrease in density (Figure 5.3.6) for grid cells across the site. Refer to Figure 5.2.2 and Figure 5.2.3 for information on interpreting the panels with these figures.

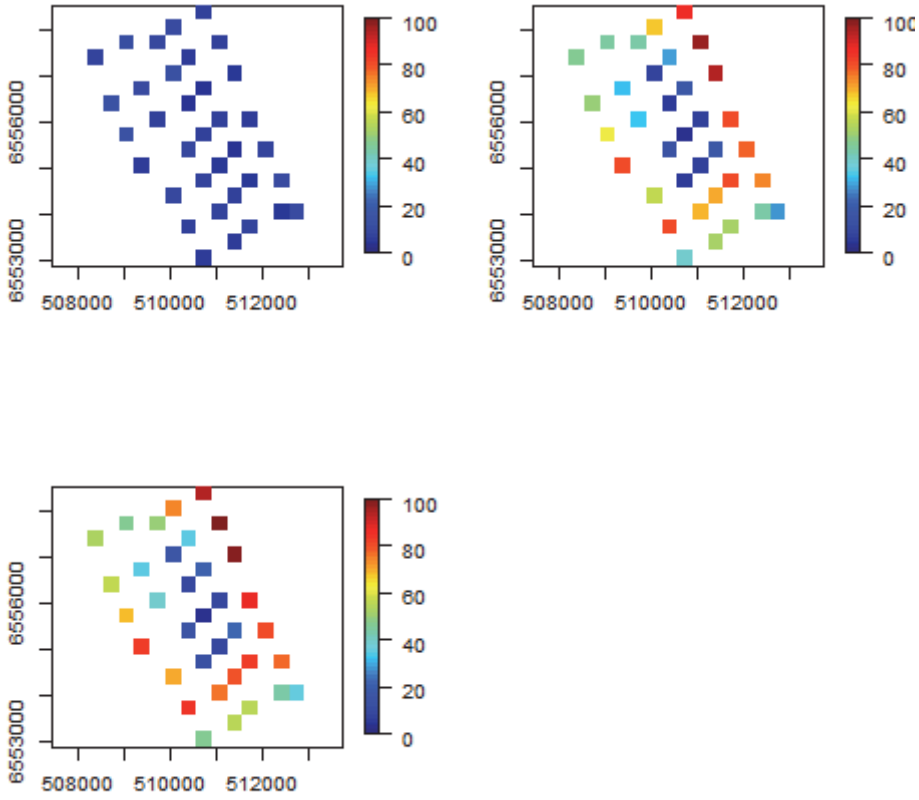

Figure 5.3.5. Percentage of power analysis simulations detecting a significant increase in auk density at site impact levels 1, 2 and 3, when applying a 50% redistribution in density between grid cells containing test berths and those not at SIL-2 and SIL-3 at the Fall of Warness

As was expected, very few simulations identify a significant increase in density for all grid cells between SIL-0 (baseline conditions) and SIL-1 (infrastructure installed) (Figure 5.3.5). However, between SIL-0 and SIL-2 (devices installed but not operational), there are a large percentage of simulations where significant increases in density are estimated in the peripheral cells, whereas the cells in the centre of the site (where the test berths are located) tend to have less than 20% of simulations showing significant increases in density predicted. Similar to the situation between SIL-0 and SIL-2, as shown in Figure 5.3.5, the majority of simulations are detecting significant increases in density in the peripheral cells between SIL-0 and SIL-3 (infrastructure installed and operational), and very few simulations are detecting significant increases in density in the grid cells in the centre of the site. This result shows that, on a large majority of occasions, the model had good power to detect the simulated increase in the peripheral grid cells caused by the redistribution.

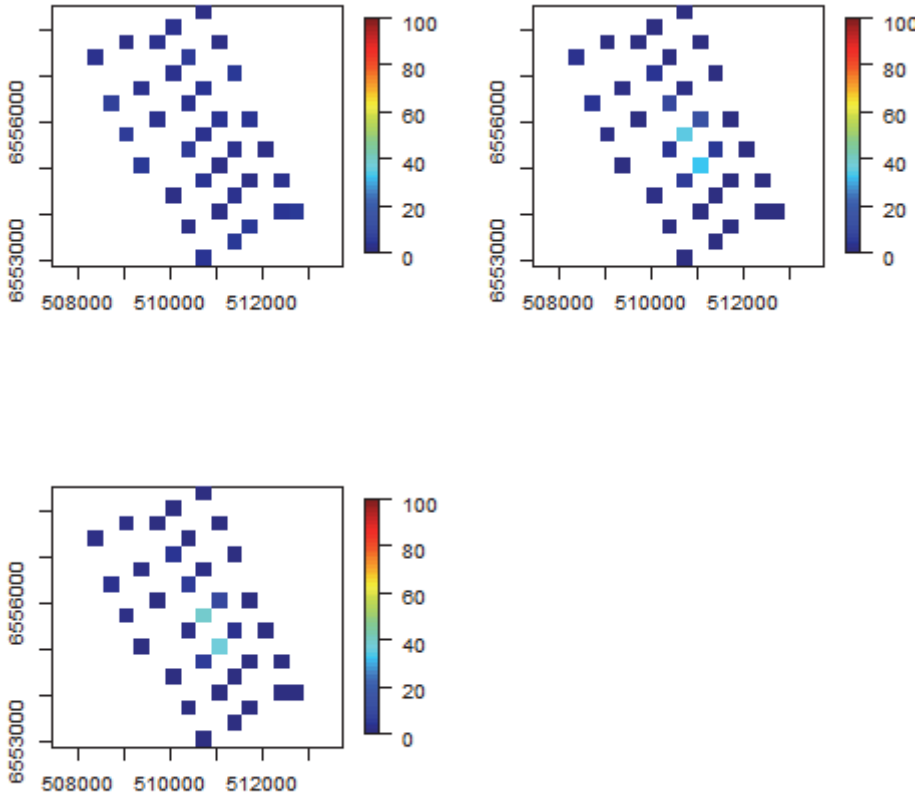

Figure 5.3.6. Percentage of power analysis simulations detecting a significant decrease in auk density at site impact levels 1, 2 and 3, when applying a 50% redistribution in density between grid cells containing test berths and those not at SIL-2 and SIL-3 at the Fall of Warness

Figure 5.3.6 shows the percentage of simulations where a significant decrease in density was estimated in each cell. As expected, between SIL-0 and SIL-1, there are few cells with more than 10% of simulations showing a decrease (Figure 5.3.6). However, between SIL-0 and SIL-2, there are two cells (C2 and C3, both of which contain test berths) that are highlighted as having 40% of simulations predicting a significant decrease in density. As can be seen in Figure 5.3.6, between SIL-0 and SIL-3, the same two cells show around 40% of simulations exhibiting a significant decrease. As a decrease has been simulated in all seven grid cells that contain test berths, and only two cells are showing over 20% of simulations predicting a significant decrease, this would suggest that the decrease in abundance simulated as part of the redistribution is not being detected well by the model.

In summary, for auks, it appears that the model has good power to detect an increase in density; however, the power to detect the 50% decline in density in the cells containing berths is very low (the decrease was only detected in two grid cells and less than 50% of the time)[32]

5.3.4.2 Site-wide 50% decrease (scenario one)

An additional power analysis for this species was conducted to further investigate the auk model's ability to detect a decrease in density. This time, during the power generation stage, a 50% decrease in diver density was simulated across the site. The correct model (model 2)

[32] The grid cells in the centre of the site tend to have the lowest density predictions for auks.

was only selected 47% of the time, whereas, model 3 was selected 53% of the time. When model 2 was selected (47 simulations), between SIL-0 and SIL-2, 76% of the parameter estimate confidence intervals contained the true decrease parameter, and similarly, between SIL-0 and SIL-3, the true decrease parameter was contained in 76% of the parameter estimate confidence intervals.

Figure 5.3.7, provides the percentage of simulations where a significant decrease in density was estimated across all of the grid cells between baseline conditions and each of the site impact levels. As no change in density between SIL-0 and SIL-1 was simulated, it is unsurprising that very few simulations predicted a significant decrease in density in any of the grid cells between these site impact levels. Between SIL-0 and SIL-2, the percentage of simulations where a significant decrease in density was predicted ranged between 60% and 70% in grids cells located in the south of the site and the north-western corner of the site. However, a much greater percentage of simulations (80-100%) had a significant decrease in density estimated in grid cells located in the centre of the site and towards Muckle Green Holm and the shoreline of Eday. Very similar percentages of simulations that are detecting a significant decrease in density, are obtained between SIL-0 and SIL-3.

These power analysis outputs suggest that the model is performing well in detecting such a change in density. This would indicate that there is good power in the data (particularly for grid cells in the centre of the site, and those neighbouring the land of Muckle Green Holm and Eday) for this species to detect a 50% site-wide decrease in auk density.

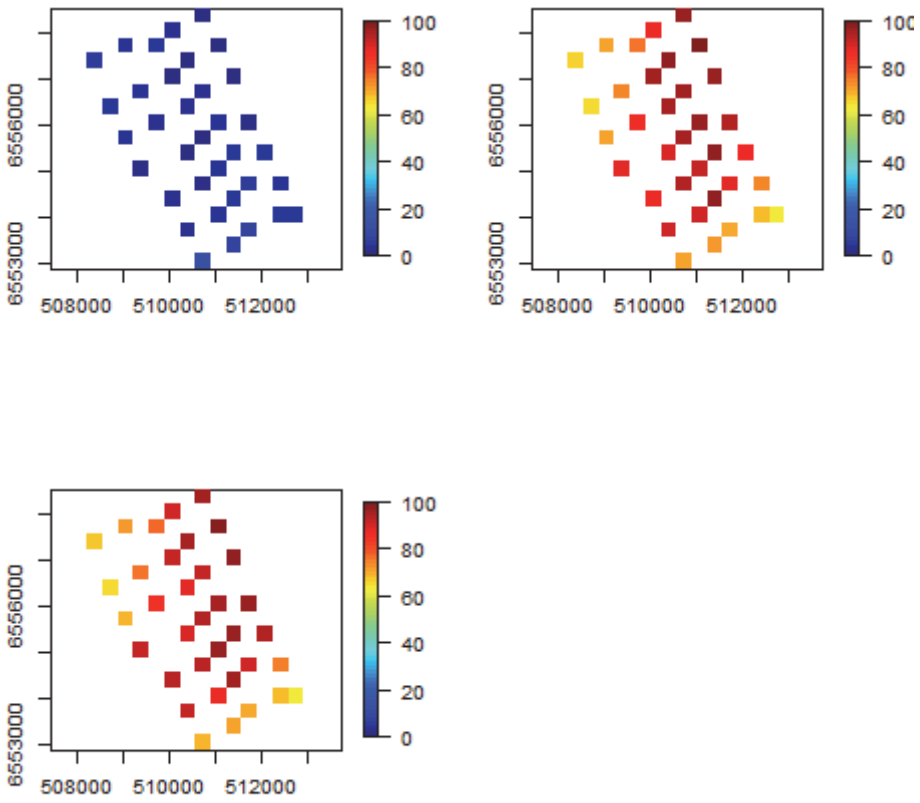

Figure 5.3.7. Percentage of power analysis simulations detecting a significant decrease in auk density at site impact levels 1, 2 and 3, when applying a 50% site-wide decrease in density at SIL-2 and SIL-3 at full survey effort at the Fall of Warness

5.3.5 Duck

5.3.5.1 Site-wide 50% decrease (scenario one)

As a 50% decrease in duck density was simulated across the site, it was expected that model 2 would be selected the majority of times. Model 2 was selected for 72 out of a total of 100 simulations (i.e. 72% of the time) as anticipated. Model 3 was selected the remaining 28% of the time. It is likely that there may be a slight distributional change in the density decrease simulated, resulting in 28 simulations fitting a spatial term to the model. Of the 72 simulations where model 2 was chosen, 95% of simulations had confidence intervals containing the true decrease parameter between SIL-0 (baseline conditions) and SIL-2 (devices installed). Similarly, between SIL-0 and SIL-3 (devices installed and operational), 92% of simulations had parameter estimate confidence intervals that contained the true decrease parameter.

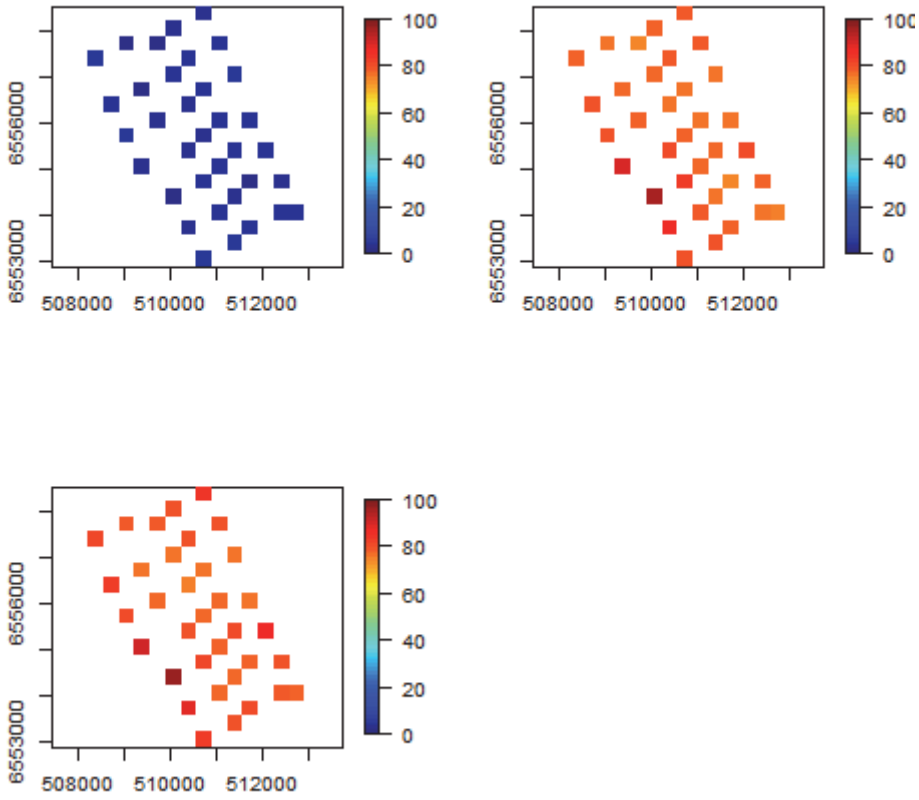

Figure 5.3.8. Percentage of power analysis simulations detecting a significant decrease in duck density at site impact levels 1, 2 and 3, when applying a 50% site-wide decrease in density at SIL-2 and SIL-3 at full survey effort at the Fall of Warness

As with the power analysis conducted on the other Fall of Warness species, no significant decrease in density was simulated between SIL-0 (baseline conditions) and SIL-1 (infrastructure installed) and, therefore, it was not anticipated that any simulations would detect such a change between these site impact levels. As can be seen in Figure 5.3.8, very few, if any, simulations detected such a change between SIL-0 and SIL-1.

However, a 50% decrease in duck density was simulated between SIL-0 and SIL-2 and between SIL-0 and SIL-3. As expected, the model performed well and detected a significant

decrease in duck numbers in 75-85% of simulations between SIL-0 and SIL-2. In Figure 5.3.8, grid cell A3 in the south-west can be identified as having the most number of simulations detecting this change, with approximately 95% picking up a significant decrease in density in this cell. Between SIL-0 and SIL-3, a similar percentage of simulations are detecting the simulated decrease in abundance. Again, grid cell A3 can be identified as having a higher percentage of simulations detecting the reduction in density. It is likely that there is greater confidence in predictions in this grid cell as there was a greater number of raw observations in the original dataset upon which to base the predictions, due to the cell's proximity to the shoreline at Muckle Green Holm.

5.3.5.2 Site-wide 50% decrease (scenario three)

Survey effort was then reduced by half in order to investigate if the model continues to detect the density change well. Every second block in the block structure was removed; this means that survey effort was altered, with surveying only performed every second fortnight. When survey effort was reduced, the number of simulations that returned the correct model reduced to 66 rather than 72. This level of reduction was unexpectedly small for the extent to which survey effort was reduced. Model 3 was selected for the remaining 34 simulations. Where model 2 was selected (66 simulations), 17% of simulations contained the true decrease parameter within their confidence intervals between SIL-0 and SIL-2; similarly, for SIL-0 and SIL-3, the same percentage of simulations had parameter confidence intervals containing the true decrease parameter.

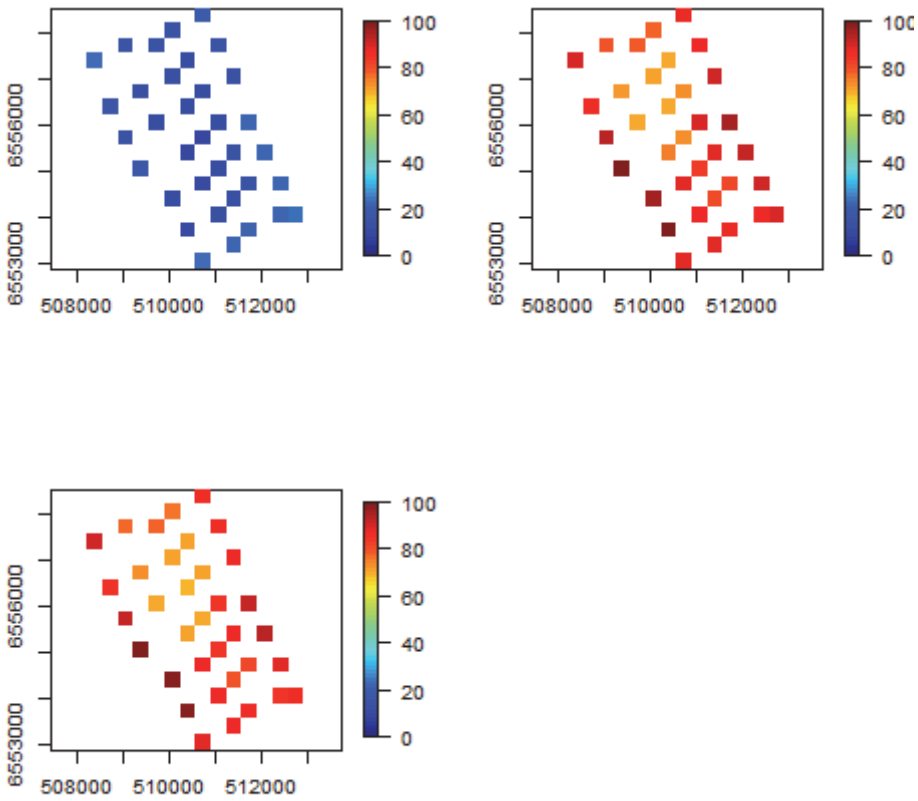

Figure 5.3.9. Percentage of power analysis simulations detecting a significant decrease in duck density at site impact levels 1, 2 and 3, when applying a 50% site-wide decrease in density at SIL-2 and SIL-3 at half survey effort at the Fall of Warness

Even though a density decrease was not simulated between SIL-0 and SIL-1, many simulations across the grid 'falsely' detected such a change (Figure 5.3.9).

In terms of the detection of the simulated decrease in density between SIL- 0 and SIL-2, there is again greater variability across the grid in how well the simulated change is being detected. Grid cells in the northern region of the central grid cells appear only to detect the significant decrease around 65% of the time, whereas cells close to Muckle Green Holm seem capable of detecting the shift in density 85-95% of the time (Figure 5.3.9). Finally, cells located in the south of the grid appear to detect the change the majority of the time, with approximately 80% of model 2 simulations detecting the change.

Again, a very similar distribution of simulations has detected the change in density between SIL-0 and SIL-3, to that noted between SIL-0 and SIL-2; there are similar areas of the site where the simulations are detecting the change nearly every time, whereas in other areas, such as around grid cells C0 and C1, the detection rate is not so good.

Therefore, in summary, it appears that, when the site is surveyed less, a decrease in density appears to be detected the majority of the time; however, there is greater variation across the site in how often such changes are detected.

5.4 Results - Fall of Warness marine mammals

In terms of the Fall of Warness marine mammals, a power analysis has only been conducted for the combined seals model. This is because, when the power analysis for the harbour seals individual model and for the cetacean model were attempted, anomalous results were produced. This was due to too few observations of harbour seals and cetaceans being recorded within the raw data, to enable generation and application of the power analysis tool.

5.4.1 Seals

5.4.1.1 Site-wide 50% decrease (scenario one)

Similar to ducks at the Fall of Warness, a 50% decrease in seal density was simulated across the data between SIL-0 (baseline conditions) and SIL-2 (devices installed) and between SIL-0 and SIL-3 (devices installed and operational). As before, model 2 was expected to be chosen the majority of the time. For seals, the correct model type (model 2) was selected 70% of the time. Out of the 70 simulations where model 2 was selected, 83% of simulations had the true decrease parameter within their confidence intervals for the density decrease between SIL-0 and SIL-2, whereas for the density decrease between SIL-0 and SIL-3, 89% of simulations contained the true decrease parameter within the parameter estimate confidence intervals. 30% of the simulations had a redistribution estimated, as a spatial term was found to be most appropriate for the model in these instances. Although the selection of model 3 is not expected for the density decrease that was simulated, there may still only be a negative distribution change. In addition, the fact that the same was noticed between SIL-0 and SIL-2 and between SIL-0 and SIL-3 means that there is the same spatial change between these site impact levels.

As anticipated, there are very few simulations that detect a change in density between SIL-0 and SIL-1, as this was not simulated between SIL-0 and SIL-1 (Figure 5.4.1). In terms of the detection of the simulated decrease in density between SIL-0 and SIL-2, it appears the simulations have detected the shift in density the majority of times, across all cells. However, as can be seen in Figure 5.4.1, there is some variation across the grid in the number of simulations detecting the change. It appears that grid cells in the north are only detecting the significant decrease 65-75% of the time, whereas, cells in the centre of the site and adjacent to both Muckle Green Holm and the shoreline of Eday seem to be capable of

detecting the significant decrease in density 85-95% of the time. Further, similar to the ducks at half survey effort, simulations for the grid cells in the far south of the site are able to detect changes in density around 80% of the time.

As shown in Figure 5.4.1, between SIL-0 and SIL-3, it appears that there is a very similar distribution of the number of simulations detecting density changes across the grid, with cells B-1, C-1 and D-1 performing the poorest, at around 65% of simulations detecting a change. However, it should be noted that this still represents the majority of simulations. Again, the cells in the centre of the site, stretching between Muckle Green Holm and the Eday shoreline, perform the best in terms of detecting the significant decrease.

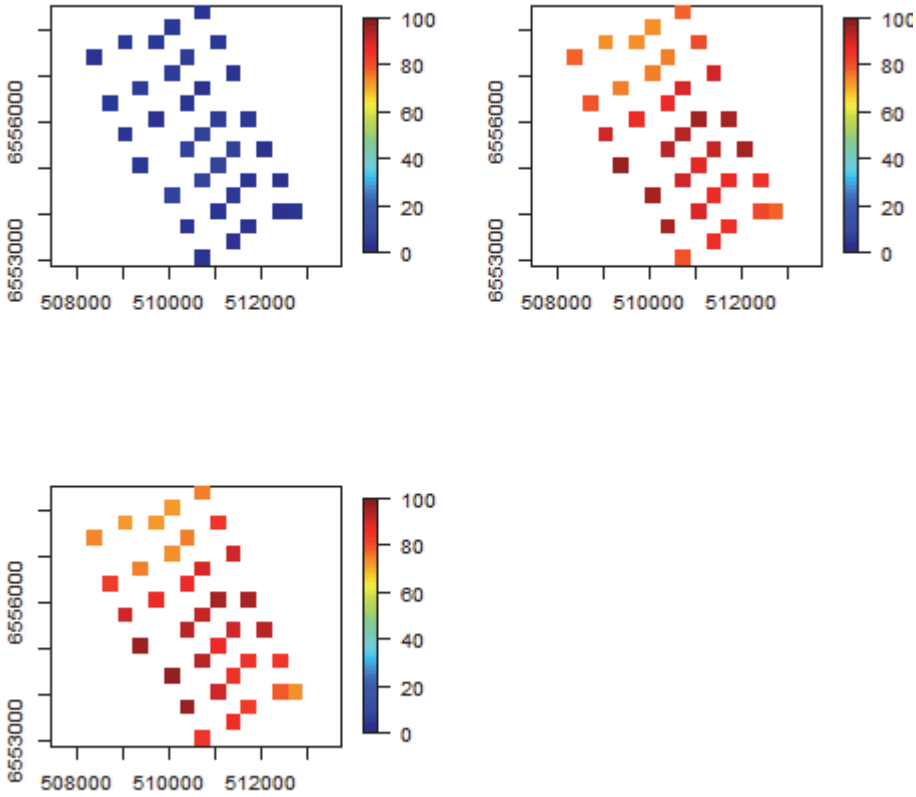

Figure 5.4.1. Percentage of power analysis simulations detecting a significant decrease in seal density at site impact levels 1, 2 and 3, when applying a 50% site-wide decrease in density at SIL-2 and SIL-3 at full survey effort at the Fall of Warness

In summary, it appears the seal model performs well in terms of detecting the simulated decrease in density. Grid cells in the centre of the site between Muckle Green Holm and the Eday shoreline apparently perform the best, maybe suggesting that there is highest confidence in the predictions in this area of the grid.

5.4.1.2 Site-wide 50% decrease (scenario three)

As the seal model performed well at full survey effort, it was worthwhile testing how well it performed when survey effort was halved. This meant taking every second block within the blocking structure, for instance, assuming the site was only surveyed every second fortnight.

The correct model (model 2) was chosen 69% of the time, whereas model 3 was selected 30% of the time. For the 69 simulations where model 2 was selected, 93% of simulations had the true decrease parameter within the confidence intervals between SIL-0 and SIL-2 and, similarly, 93% of simulations for between SIL-0 and SIL-3, had the true decrease parameter contained within the parameter estimate confidence intervals.

When considering the number of simulations detecting a change between SIL-0 and SIL-1, it appears that there is slight variability seen across the grid, with a few simulations predicting a density decrease between these site impact levels when it was not simulated during the power generation stage. As can be seen in Figure 5.4.2, between SIL-0 and SIL-2, there is quite a bit of variability across the grid in terms of how well the simulations are detecting the significant decrease in density. Grid cells in the north and northern centre of the grid appear to be detecting the change in around 65% of simulations, and cells in the far south of the grid appear to be detecting the change in density in 70-75% of simulations. Cells in the centre of the site stretching between Muckle Green Holm and the shoreline at Eday, from Figure 5.4.2, have their change in density detected around 80% of the time.

As indicated in Figure 5.4.2, it appears that, between SIL-0 and SIL-3, the grid cells where the density difference is detected the least are located in the far south, whereas in the north, there is a slight improvement in the detection rate, with around 70% of simulations identifying the significant change in density. Again, the cells just south of the centre of the site, located between Muckle Green Holm and the Eday shoreline, have the highest majority of simulations detecting the decrease in density, with around 80% of simulations identifying the shift.

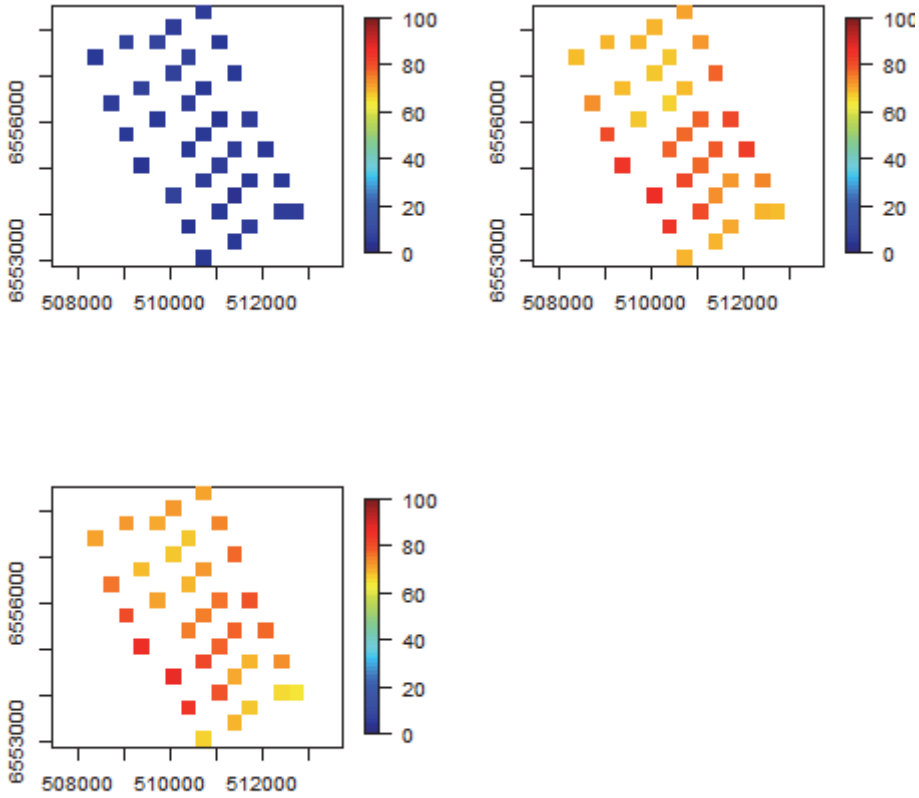

Figure 5.4.2. Percentage of power analysis simulations detecting a significant decrease in seal density at site impact levels 1, 2 and 3, when applying a 50% site-wide decrease in density at SIL-2 and SIL-3 at half survey effort at the Fall of Warness

In conclusion, it appears that there is a slight reduction in the ability of the model to detect a decrease in density when survey effort is halved. However, across each grid cell, the majority of simulations are detecting the change when it is simulated. The northernmost and southernmost cells of the observation grid appear to be most affected by a change in survey effort, which is probably due to the reduced survey effort that normally occurs in this area of the survey grid, and the resultant fewer raw observations in these areas, resulting in less confidence in these parts of the prediction surface.

5.5 Results - Billia Croo

In terms of the Billia Croo power analyses, due to the inclusion of the effort data required to account for all of the survey effort expended when no observations were made, the vast majority of the data are zeros. After conducting the first stage of the power analysis on the Billia Croo auk fitted data, this has resulted in the fitted data, used for simulation, to have means that are too small[33] to allow generation from an overdispersed Poisson distribution.

Due to the lack of resources available for further analysis, no alternatives were attempted. However, there are a few options that could be employed which may provide an adequate solution for future analysis, as follows:

[33] The mean for all grid cells is less than one, which generates, almost entirely, zeros from an overdispersed Poisson.

- As an intermediate step, the power analysis could use a different distribution for the data generation, but this is probably unwise as the model specified during the power analysis would be incorrect (if quassipoisson specified).
- A better solution would be to re-analyse the data from the beginning using a different distribution (e.g. Tweedie or Binomial – conversion to 0/1s), which may then allow generation at the power analysis stage.
- Alternatively, the inclusion of effort could be altered to create large grid cells, thus reducing the number of zero cells and increasing the counts per cell in general in the raw data; however, this would compromise the detail that currently exists in the data regarding the spatial location of recordings.

In general, many of the problems associated with the data from Billia Croo stem from the number of sightings made and the size of the site. Due to time constraints, it was necessary to use one common method for both the Fall of Warness and Billia Croo analyses, resulting in the original method (which was developed for the Fall of Warness) not necessarily being the most appropriate for the Billia Croo site. The data from these sites need to be analysed using tailored methods for each site to mirror the different data collection methods used for each of the sites.

To truly identify if the Billia Croo data are worthy of any further analysis, the data should be re-analysed for the most abundant species (or group) both with the existing grid (but using a more detailed consideration of the most appropriate distribution[34]) and with a coarser grid. By tailoring the analysis specifically for this site and for one species (or group), the analyst should have a clearer idea of what may be possible for other species.

[34] Perhaps trialling a Binary response may be useful in this case.

6. CONCLUSION

6.1 Project purpose

The main aim of this project was to assess the extent of any displacement of key wildlife species arising from the installation and operation of MECS (otherwise known as wave and tidal energy devices), at the EMEC wave and tidal test sites.

Firstly, considering the project's purpose and why it was initiated. An understanding of the environmental impacts that may arise from the siting and operation of developments is crucial to the future commercialisation of the wave and tidal industry. The unknowns surrounding a development will be project- or site-specific. The following is a summary of the key issues, as often cited, when placing objects in the sea, although it should be noted that there are many uncertainties beyond those listed here:

- collision – potential for physical interactions with marine mammals, diving birds and fish;
- displacement – potential for marine wildlife displacement from habitual waters;
- acoustic – noise emitted underwater during installation and operational phases;
- leisure and commercial activities – compatibility with other sea users, particularly fishing; and
- navigational safety – requirement for clear marking of devices and associated infrastructure.

To comply with the European Habitats Directive and other relevant legislation, a developer needs to demonstrate for purposes such as licensing that device installation and operation has no significant environmental effects, or any adverse effect upon the integrity of a qualifying European site or favourable conservation status of a European Protected Species (EPS). To help with this, this project has examined changes in species abundance and/or distribution during the deployment phases of test devices at both EMEC full scale test sites, in order to establish if, for these single devices, such changes are identifiable and, if so, to describe their extent and potential significance.

Although the project's scope was clearly defined at the outset, little was known at this early stage about species displacement or the quality of the data available to it (via the pre-existing land-based wildlife observation programmes running at both sites). The scope, therefore, has had to be sufficiently flexible over the project's duration to respond to emerging observation experience and constraints surrounding the use of commercially-sensitive data.

The key concerns at EMEC's test sites relate to the possible displacement of marine mammals and diving birds from sea areas that they habitually use, and therefore a particular set of species has been analysed in connection with each site. It is worth noting that, if feasible, the preference would have been to investigate more species but, due to time and data limitations, this did not prove possible. However, data permitting, the methods should be applicable with some adjustments necessary for rarer species.

The project aimed to comprehensively analyse all the data gathered during EMEC's Wildlife Observations Programme for the selected species and, ultimately, to identify any relationship between species abundance or distribution and changes in the operational status of devices.

The following are the research questions that have been developed over the project's duration:

- *Is there a relationship between changes in abundance and/or distribution of key species and the presence or operation of devices?*

- *How effectively can the models detect changes in species abundance and distribution due to an event (such as a change in device operational status)?*
- *Are any effects detected that can be associated with marine renewable devices?*
- *Are any such effects significant when considered against other factors that influence wider populations?*

6.2 Project summary

There are two key data sources that have been used in this project; the data collected during the EMEC Wildlife Observations Programme and the device operational data from developers deploying at EMEC's full-scale grid-connected test sites, Fall of Warness and Billia Croo.

The Wildlife Data Analysis Project was run over a period of three years in parallel with the latter stages of the EMEC Wildlife Observations Programme, funded by Marine Scotland and SNH. The data collected throughout the programme is extensive as the latter was operating over 11 years at the tidal energy test site, Fall of Warness, and six years at the wave energy test site, Billia Croo. At each site, approximately 20 hours of observation data were collected each week. This amounted to nearly 18,000 hours of observation data. The observations methodology varied considerably between the two sites, due to their differing sizes and topography. The methodologies for each site can be found in Annex 2 and Annex 3. In addition to species sightings, the observers collected data on the environmental conditions. The sheer size of these datasets means they are very valuable for the industry.

What sets this project apart from others is that it has used device operational data from developers testing at EMEC. Despite the project being facilitated by EMEC's close relationship with its industry clients and developers, the latter had to be convinced that the commercial sensitivity of the operational information needed to carry out this analysis effectively, would not be undermined. Once obtained, the commercial confidentiality of the device operational data was given priority throughout the project. To ensure confidentiality, an anonymization process was implemented, involving the use of site-wide impact levels. These capture the varying operational status of a device but only the highest operational status across the site is recorded. This anonymization process means that inferences cannot be drawn about developer- or device-specific impacts.

Ten species/species groups were analysed from each site. Sometimes, several species were grouped together to allow some of the less common species to be included in the analysis. The selection of which species would be included in the analysis was based upon those species highlighted as most sensitive in Furness *et al*. (2012) and the number of raw observations for those species at the two sites. This resulted in a different selection of species for each site, but with considerable overlap.

As already mentioned, the amount of data analysed during this project was extensive and, therefore, a data management system was required to enable the data to be cleansed to a state that would be useful for the analysis. Although Microsoft Excel and Microsoft Access were used during the data collection stages, an SQL database was created for the purposes of data integration, rationalisation and cleansing.

Using the expertise and training facilities available at the Centre for Research into Ecological and Environmental Modelling (CREEM) at the University of St Andrews, it was possible to produce models which estimated the distribution and abundance of species for the duration of the study and, therefore, also to investigate the effect (if any) of device presence and operation. As the observations programme only recorded species sightings, it was necessary to include the effort data. This process involved inserting zeros into the data to reflect the area surveyed rather than the areas identified as sightings. In addition, the

observation data were correlated, as many of the observations were close in both space and time. The covariates available did not alleviate this correlation resulting in correlation that was present in the model residuals. This violated a crucial assumption of Generalised Additive Models (GAMs), so the GAM models were run in a Generalised Estimating Equation (GEE) framework which explicitly permitted correlation in the model residuals.

There were two key stages to the model selection process: firstly, the one-dimensional variables were selected (for example, month, wind strength) and secondly, the two-dimensional spatial term was fitted (longitude and latitude) with an interaction with site impact level.

Importantly, the use of SALSA1D and 2D allowed for spatially-adaptive smooth terms rather than assuming uniform smoothness in the relationship between each covariate and the response.

Once models for each species/group were estimated, predictions for each species/group were made across all years (if year was a term in the final model) and at each site impact level. Density prediction surfaces (including the associated coefficient of variation values), abundance estimates, spatially-explicit change surfaces, and estimated density change with distance from a potential impact location, were produced, where possible. These predictions formed the basis of a discursive conclusion for each species, which has been summarised in the following section, 6.3. A power analysis was also run on some of the models to understand the power of the models to detect certain scenarios of change.

6.3 Summary of findings

For each species/group at each site, a detailed description of the models' outputs is provided in Section 4. A summary of the findings for each species/group (ten for the Fall of Warness and ten for Billia Croo) is provided below.

6.3.1 Fall of Warness

The black guillemot model at the Fall of Warness tidal energy test site suggests that they are most abundant close to the cliffs of Eday and on the eastern side of Muckle Green Holm; this distribution pattern is evident at all four site impact levels. Black guillemots were one of the most common species recorded at the Fall of Warness and, therefore, the density estimates gained from the fitted model for the species have greater certainty compared to other models. However, there is much less certainty in the estimates produced for the southernmost row of the prediction grid. The largest estimated density change from baseline conditions occurs with the emplacement of infrastructure; although density falls in the areas of highest occurrence, it returns to baseline conditions as devices are installed and become operational. When infrastructure is installed at test berths, areas where a low density of black guillemots is predicted at baseline conditions, are expected to experience a decrease in density; this effect is limited in distance from the impact location and shows recovery when the device becomes operational. This may reflect a reduction in site disturbance by vessels when devices are operating.

The common guillemot model shows that they are most abundant in the centre of the survey area and in deeper water areas in the west. Similar to the black guillemot model, due to the number of common guillemot observations throughout the observations programme, outputs from the fitted common guillemot model can be gleaned with a fairly high certainty. It is worth noting, however, that there is less certainty in predictions for the south-easternmost corner of the observation grid. There are changes in estimated abundance with varying site impact level; the biggest decrease from baseline conditions is modelled to occur with the emplacement of infrastructure. This is however limited to approximately 1.3km from the

impact location. The density reduction is greatest where the number of guillemots is highest but there is a recovery in density towards baseline conditions as devices are installed and become operational.

The razorbill model shows low densities across the survey area and for all site impact levels, with the exception of the south-western corner of the site under baseline conditions where a clear peak in density occurs. This appears to be the result of an anomalous peak in raw observations. The few razorbills sighted is probably the reason for there being very high uncertainty in the results for this species.

The diver model (great northern diver and red-throated diver) shows that, under the most favourable environmental conditions for sighting divers at the Fall of Warness, they are most abundant in close proximity to the coast of Eday and along the north-western edge of the survey area. This distribution pattern was evident at all four site impact levels, with the lowest densities occurring under baseline conditions. In general, there is fairly high certainty in the predictions gained from the grid. The biggest change in density from baseline conditions occurs with the emplacement of infrastructure, with a decrease in the centre of the survey area (including all test berths) and an increase along the eastern and north-western edges, where densities tend to be greatest. The extent of change decreases slightly with the progression through site impact levels (towards devices becoming operational).

The shag and cormorant model (European shag and great cormorant) shows that, under environmental conditions where most shag and cormorant observations were carried out, they are most abundant close to the coast of Eday and off the eastern coast of Muckle Green Holm for all site impact levels. Densities here tend to increase with increasing site impact levels. Generally, there is high certainty across the predication grid for each site impact level, with the exception of the north-western and south-western corners of the grid under baseline conditions where there is less certainty in the predictions gained. Changes in impact levels show redistribution from south to north within the central zone between Eday and Muckle Green Holm compared with baseline conditions, principally with the installation of infrastructure and device presence and operation. The reduction in density in the south of the site when devices are installed (from the density observed when only device-associated infrastructure is installed) are reversed when devices become operational. There is negligible change with distance from a potential impact location.

The auk model relates to the auk family comprising black guillemots, common guillemots, little auks, Atlantic puffin and razorbills. The model shows a large reduction in auk density from baseline conditions when infrastructure is installed. The estimated decrease in density is maintained until approximately 1.5km away from the potential impact location. A reduction, particularly in the central grid cells, exists between baseline conditions and when devices are installed and become operational. As many of the decreases are expected to be significant this would suggest that there is greater certainty behind the predictions. Numbers only recover slightly when devices are installed and become operational. The pattern of the change may suggest that it is vessel movements associated with the installation activities that impact on auk densities, rather than stationary objects. The change in auk density when infrastructure is installed is the strongest indicator of change amongst all the species and groups studied at the Fall of Warness.

The duck and geese model shows that the distribution of higher density areas is similar for all site impact levels, with greater numbers close to coastlines. As ducks and geese were a common sight at the Fall of Warness, there is a fair certainty in the predictions produced by the model. As with many other species/groups, the biggest density decrease occurs with the installation of infrastructure; there is a reduction over most of the survey area but with density increases along the eastern and northern edges. These changes are repeated with

the installation of devices but, when they become operational, there is an increase in numbers across virtually the entire survey area. This may imply that the emplacement of infrastructure or devices (or the vessel movements associated with installation activities) causes an impact on duck and geese density.

The seal model (both grey and harbour seals) shows a clear peak in density around Muckle Green Holm, a known haul-out site, at all site impact levels, together with smaller peaks adjacent to the War Ness headland and Seal Skerry. There is high certainty in estimates produced from the fitted seal model. Due to the fewer raw observations collected for baseline conditions, the certainty behind estimates under these conditions is significantly lower compared to the other site impact levels. Changes in seal density are apparent with each change in site impact levels. When infrastructure is installed, there is a density decrease between War Ness and Muckle Green Holm, and a corresponding increase to the north and south. These changes are repeated with the installation of devices but, when devices become operational, seal numbers return to previous levels. The greatest change from baseline conditions occurs with the installation of infrastructure, but the extent of this change is reduced with the installation of devices and their operation. As with other species, this again suggests that perhaps it is the movement of vessels that is influencing seal abundances rather than devices in the water. There also appears to be a decrease in density predicted immediately adjacent to a potential impact location (test berth) which is sustained to approximately 600m away.

The harbour seal model is similar to that for the seal group but shows a steady decline in densities over the survey's duration. Harbour seals exhibit a similar distribution to the wider seal group, except that they tend to be concentrated along the coastline of Eday. Abundance tends to increase adjacent to Eday and decline at Muckle Green Holm, as site impact levels increase. Due to the few seal observations being recorded as harbour seal, the fitted harbour seal model is based on significantly fewer raw observations compared to the seal model. Therefore, as would be expected, there is much less certainty behind the predictions produced for harbour seals. There is no obvious correlation between the location of test berths and estimated density change between baseline conditions and those occurring when devices are installed and operating. There is very little density variation with distance from a potential impact location, suggesting that harbour seal abundance is not influenced by the location of a test berth.

The cetacean model is subject to occasional localised high densities, due to cetacean pods passing through the area. There are fewer observations of cetaceans, particularly in comparison to other species, which means there is less confidence in the results. Higher estimated densities are restricted to the northern half of the survey area and there is little consistency in location between different site impact levels. Assessing density changes at and away from impact locations is inherently flawed, due to the effect of the anomalous observations. There would appear to be very little difference in cetacean behaviour between baseline conditions and when devices are installed and operational.

In summary, for most species in the Fall of Warness survey area the greatest change from baseline conditions occurs with the installation of infrastructure, but the extent of this change is reduced with the installation of devices and their operation. This suggests that perhaps it is the movement of vessels that is influencing abundances rather than, necessarily, devices in the water.

6.3.2 Billia Croo

The common guillemot model at the Billia Croo wave energy test site suggests that density predictions are similar for all site impact levels, with high levels of confidence in the predictions for the area 1-2km west/south-west of the Black Craig cliffs where the highest

densities are found. There is a high uncertainty in predictions for the outer grid cells across all four site impact levels, with much higher certainty for predictions in grid cells closer to the observation vantage point. Grid cells within this area show both increases and decreases in density in response to increases in site impact levels, with most showing an overall slight decrease in density from baseline conditions. No correlation is discernible between significant changes in density for the different site impact levels and the location of test berths. Although analyses suggest there is a decrease in density at a potential impact site when infrastructure is installed (compared to baseline conditions), this effect has disappeared within a distance of 500m.

The black guillemot model returns similar results to those seen for the common guillemot with two clusters of highest density; an area extending westwards from Breck Ness and an area 1-2km west of Black Craig. There is again a lack of certainty in the predictions for the outer grid cells and more certainty in predictions closer to the shoreline. The test berth locations show a density increase at all site impact levels compared to baseline conditions. When infrastructure is installed onsite, there is very little change in density predicted; however, when devices are installed, there are increases in density estimated in the north and south. When devices become operational, the modelled density reduces in some areas of the observation grid.

The Atlantic puffin model shows clusters of higher densities with varying increases and decreases in density between site impact levels 1, 2 and 3 but an apparent overall density reduction. As with the other Billia Croo species models, there is a lack of certainty in predictions in the outer grid cells. There is greater certainty in the inner grid cells; however, this varies across the site impact levels. Despite an observable relationship between estimated puffin density and varying site impact level and the location of a grid cell containing a test berth (Figure 4.5.25), this was not estimated for all the grid cells containing test berths and hence it is not possible to state that there is a clear correlation between changes in density for each of the site impact levels and the location of test berths.

The northern gannet model indicates that there is a general increase in northern gannet density with increasing site impact level over most of the survey area, with most results being considered statistically significant. There is generally a good degree of certainty across the prediction surface, particularly when compared to the other Billia Croo species models. Despite these site-wide estimated changes, there does not appear to be any direct correlation between changing density and the location of test berths within the site. Between baseline conditions and SIL-1, SIL-2 and SIL-3, there is a clear increase in density directly at the impact location which tends to extend to at least 1.8km away from the potential impact location. This suggests that the activity surrounding test berths may be causing an increase in northern gannet numbers.

The auk model points to highest densities under baseline conditions, with a density decrease over the survey area with the installation of infrastructure, these densities reducing further with increasing site impact levels. However, there is probably no correlation between test berths and estimated density changes. A density reduction is seen at the impact location (the biggest reduction in density coinciding with the installation of infrastructure), but density returns to baseline conditions at approximately 2.5km distance. Due to high uncertainty behind these predictions, it is unknown if this decrease in density is significant. However, when the change in density between baseline conditions and devices becoming operational is considered, it appears that there is a significant reduction in density predicted until about 1.2km away from the test berth.

Predicted diver densities are generally low, with highest densities during baseline conditions. There is very high uncertainty in the predictions produced from the fitted diver model which may be due to there being very few raw observations. There is no consistent pattern for

changes in densities with regard to increasing site impact level. However, there is a slight reduction in density expected that corresponds to the installation of infrastructure. The extent of change in density reduces with the installation and operation of devices.

Estimated gull densities vary between site impact levels, with highest densities expected when device-associated infrastructure is installed. As gulls are common at Billia Croo, there is greater certainty in the fitted prediction surface compared to other Billia Croo fitted models. However, the certainty tends to reduce with increasing distance from the observation vantage point. The gull model exhibits little consistency in the changes in gull density and no apparent relationship between density and the distribution of test berths. In terms of the density changes at a potential impact site and with increasing distance from it, there seems to be almost no change between baseline and operational conditions. Greater changes in density seem to occur at, and for 1km around, the potential impact location for the installation of infrastructure.

The seal model (pertaining to both grey and harbour seals) shows a peak in density extending westwards from Breck Ness which increases with the change from baseline conditions through the other site impact levels. There is high uncertainty in the seal density predictions in the outer grid cells across all the site impact levels. There is greater certainty in the predictions for the inner grid cells. There appears to be no correlation between changes in density and the location of test berths, with the densities here being low and excluding the main areas where seals are located in the model, west of Breck Ness. When considering the change in seal density with increasing distance from a potential impact location, there was a clear increase in density with the presence and operation of devices compared to baseline conditions and to when infrastructure is installed; this increase tended to be significant up to the first kilometre away from the test berth location. However, this change in density was not apparent at all test berths.

Generally, the harbour porpoise model shows that highest densities are located closer to land and reduce with increasing distance[35]. However, as a detection function was not applied to the raw observations this prediction may be a result of the influence of declining detection with increasing distance from observation point. In addition, clusters of high harbour porpoise densities are present which are consistent across the various site impact levels. The estimated density differences between baseline conditions and site impact levels 1, 2 and 3 are all very similar. There does not appear to be any correlation between density increases/decreases and the disposition of test berths.

The cetacean model is subject to occasional local high densities due to pods passing through the area. Despite the expectedly few cetacean raw observations, there is fairly high certainty in the density predictions produced by the fitted model, particularly for the prediction surfaces relating to when devices are installed and operational. Density increases are generally seen with the installation of infrastructure and devices but, when devices become operational, there is usually a slight density reduction. However, these changes are generally very small. As with several other species at Billia Croo, the density change for cetaceans at a test berth, and at distances from it, is less between baseline conditions and devices becoming operational, than when infrastructure or devices are installed (but not yet operational); the change may relate more to vessel movement arising from the installation activities than to the presence/absence of a device.

In summary, almost all the species analysed at the Billia Croo survey area show similar densities for all site impact levels and there appears to be a lack of correlation between changes in densities and the location of test berths. The predictions produced from the fitted

[35] Note that a detection function was not applied to the raw observations, and therefore this prediction may be a result of the influence of declining detection with increasing distance from observation point.

models tend to have a high uncertainty surrounding them, compared to the Fall of Warness models.

6.3.3 Concluding remarks

The Wildlife Data Analysis Project firstly considered the question of whether any evidence could be found to suggest that the presence and/or operation of marine renewable energy devices, or device-associated infrastructure, altered the abundance or distribution of the birds or mammals observed. In this respect, many of the analyses, particularly at the Fall of Warness, show that the biggest change in density, both within grid cells with test berths and beyond, occurs when infrastructure is installed. However, as the scale of this change is often reduced when the site impact level progresses to the device becoming operational, it is possible that it is not the physical presence of the infrastructure and the device that has altered the distribution or abundance of the relevant species. It is suggested that, for these test sites, vessel movements associated with installation activities may be instigating the changes in density observed, as it may be expected that vessel movements will be limited when devices are operating; at this latter stage, the scale of such activities may be closer to that occurring under baseline conditions.

Vessel movement information collected at the test sites by the wildlife observers has tended to be anecdotal and voluntary, with observers being requested to record information on vessels and their routes, rather than being set as a requirement. Therefore, further research is required to provide evidence of the importance of vessel movements to the relative abundance and distribution of birds and mammals.

In terms of addressing the second research question, to identify the nature and scale of such changes in density, if they exist, and whether it can be demonstrated that such changes are distinct from natural variation, the analyses concluded that, in many instances, the estimated density differences noted when infrastructure or devices are installed, are statistically significant, based upon temporal and spatial changes in abundance across developed areas, and upon modelling of the effects of other controlling factors. However, even though the impact term has been included in the final fitted models for all of the species, its inclusion in the models does not mean that links can necessarily be made between devices and their direct effect on species abundance. The impact term could be a proxy for something that was not measured, for instance, changes in the wider population. To overcome this issue, it was essential to plot the results spatially to see if the only place animal density significantly changes (increases or decreases) is in the grid cells containing test berths (or in close proximity to them). If it is the case that spatially-explicit changes are identified, (as opposed to general declines across the survey site or declines in areas of the site that do not contain test berths), then it can be suggested, with more confidence, that the declines are due to the infrastructure/device presence/operation. General changes everywhere, with no particular link to the grid cell that contain one or more test berths, would indicate natural variation in the population. It is, however, worth highlighting that, due to the limited period of baseline conditions compared to the total duration of the observations programme and the fact that baseline conditions only occurred in the first couple of years of the programme, the results obtained may to be undermined, resulting in false relationships observed between the baseline conditions and the other site impact levels. The impact of this issue on the models' outputs may have been limited by the inclusion of year as a term in the fitted models.

Throughout this analysis, all of the outputs that have been produced have accounted for natural variation through the covariates included in the model (e.g. the environmental and temporal terms). The variation that cannot be modelled remains in the residuals and, therefore, is reflected in the size of the confidence intervals pertaining to the predictions. It can therefore be concluded that the more residual variation that remains, the less certainty that can be placed on the parameter estimates for the model, consequently resulting in

larger standard errors and wider CIs relating to the predictions. As already mentioned, this has resulted in wider CIs around predictions under baseline conditions compared to predictions for the other site impact levels.

This has been demonstrated in the partial plots included in the Model Overview section for each of the fitted models (and additional plots provided in the Marine Scotland Information portal). Although the density predictions have been plotted at fixed levels (as specified in Appendix 5) from each of the environmental and temporal terms in the model, if these levels were changed the natural changes on the site would be apparent.

The third research question considered if any effects detected can be associated with the emplacement of marine renewable deivces or related infrastructure, or their subsequent operation. As noted above, many of the analyses show a change in density when infrastructure is installed, but the scale of these changes often reduces when the site impact level progresses to the device being operational. It is possible that the reduction in the scale of change is evidence of habituation, but a more plausible explanation is that it results from there being fewer vessel movements as MECS' deployment progresses through the site impact levels.

It is also useful to ask whether, if no changes associated with MECS are observed, it can be demonstrated conclusively that no such effects occur or the datasets are insufficient for this purpose; in other words, what is the power of the data? Initial power analyses were undertaken on the observations data from both test sites during the early years, producing promising results as regards the power of the data to be able to detect changes in species abundance under the scenarios trialled; it was expected that the power of the data would increase with time. However, although reassessment of the power of the data at the conclusion of the data collection would have been beneficial, time and budget restrictions meant that this was not possible.

The final key research question considered if any of the observed changes in species abundance and/or distribution associated with the deployment of MECS were significant when compared with changes in species abundance and/or distribution consequent upon other external factors (and therefore not attributable to device operational status levels). While the Wildlife Obaservations Programme did not include a control site to provide information to allow this question to be addressed more fully, the modelling of many of the species undertaken in the course of this project indicates seasonality and interannual changes in abundance. As an example of a temporal factor, the common guillemot at the Fall of Warness shows dramatic reductions in abundances for certain years (2010 and 2013) as well as strong seasonality, with abundances in autumn and winter only 1-2% of those seen in spring and summer. In terms of environmental factors that appear to be associated with changes in abundance, the modelling of seals indicates that sea state has a strong impact on the number of seal observations. Similarly, razorbill abundances seem to increase with increasing cloud cover, with highest abundances occurring when cloud cover is recorded as 7 or 8 oktas.

6.4 Model effectiveness

Power analyses have been conducted on the fitted models in order to address one of the key research questions, '*What power do the models possess in detecting changes in species abundance and/or distribution due to an event?*' It is important to be able to determine whether a modelling result that shows no change in species density actually reflects a true situation or is the result of the model being unable to detect such a change, possibly due to there being insufficient raw data for the model to perform effectively. It is well understood that models based on very small density predictions have difficulty in detecting decreases in species density.

6.4.1 Fall of Warness

The findings from the power analyses carried out on the Fall of Warness species models can be summarised as follows:

- The black guillemot model detected a redistribution in the raw data and, further, has the ability to detect a 50% site-wide decrease in density.
- The capability of the common guillemot model to detect a 50% change was determined to be low, suggesting the model is unlikely to detect a change to the extent of a 50% decline (or less), even when it is present.
- For both of the above species, the fitted models seem to perform slightly better in detecting density changes in the centre of the site and adjacent to the Eday shoreline compared with the peripheral areas of the survey site. This is in line with the general distribution of each species, with higher density predictions in these areas.
- The diver model appears to have lower power than the other models and struggles to detect a simulated density decrease of 50%; this is most likely due to there being too few diver observations in the raw data, producing a very low estimated density across the site and, consequently, high variability in the predictions.
- The auk model appears to be able to detect an increase in auk density well; however, it is less able to detect a density decrease associated with a redistribution. When simulating a 50% site-wide decrease in density across the site, the auk data tended to have a good ability to detect a reduction in density in the centre of the site and the areas adjacent to Eday and Muckle Green Holm, but poorer ability in detecting the decrease in density in the peripheral grid cells.
- The duck model performs well in detecting a significant decrease in duck numbers between baseline conditions and the installation of devices/when devices became operational. When survey effort is reduced (that is, when the site is surveyed less frequently), a decrease in density is detected most of the time but there is greater variation across the site in how often such changes are detected. Evenso, the model has a high power as it is able to detect change even when the survey effort is reduced.
- The capability of the seal model to detect a simulated density decrease is high, particularly for grid cells located in the centre of the site between Muckle Green Holm and the Eday shoreline, possibly indicating low uncertainty in the predictions in this area. However, there is a slight reduction in the ability of the model to detect a density decrease when survey effort is halved.

In summary, varying results have been gained from the models, with models for some species able to detect a 50% decline in density for certain species (even when the survey effort is halved) and others unable to do so. Where models have shown good power (80%+ detection) to detect change, there has tended to be variation across the site; the fitted models seem to perform slightly better in detecting density changes in the centre of the site and adjacent to the Eday shoreline compared with the peripheral areas of the survey site. It is possible that this is associated with areas of higher density predictions for some species or areas of low uncertainty.

6.4.2 Billia Croo

It has not proved possible to conduct a Billia Croo power analysis, due to the inclusion of the effort data required to account for all of the survey effort, resulting in the vast majority of the data being zeros. This has resulted in the fitted data, used for simulation, to have means that are too small to allow generation from an overdispersed Poisson distribution. In general, many of the problems associated with the data from Billia Croo stem from the number of sightings made and the size of the site. As one common method for analyses was used across both of the test sites, the method used was not necessarily the most appropriate for the Billia Croo site.

Due to the lack of resources available for analysis, no alternative methods were attempted for Billia Croo. However, various solutions for future analysis have been suggested in Section 5.5.

6.5 Limitations of the project

Certain aspects of the research project, primarily in relation to the data utilised for the analyses, compromised the ability to discern changes in species distribution and abundance that could be linked to development related activity. Foremost among these was the fact that the data analysed, although extensive (almost 18,000 observation hours), were not collected specifically for the purpose of this project but, rather, to aid site characterisation for the purposes of EIA and HRA. A bespoke survey programme, intended specifically to inform impact monitoring might therefore have adopted slightly different approaches, for example collecting more observations prior to any site activity and undertaking boat-based or aerial surveys to accompany the land-based observations, so as to allow a detection function to be derived. The project thus had to work with data already collected, rather than influencing or directing the survey design.

Analysing the wildlife observation data collected from the EMEC test sites was complicated by the fact that the operational status of a device generally varies throughout the testing phase. Therefore, it is believed that the impact that each operational status is having on the surrounding environmental may not have had sufficient time to become apparent before the operational status changed again. Also, the environmental impacts that may be identified may, in fact, be the result of the cumulative effects of different devices being tested in close proximity to each other. It is worth remembering that, although the highest operational status across the site was used, other devices may, at any one time, have been at an earlier development stage (i.e. at a lower operational status); the focus on the highest operational status may be masking a potential impact from the device(s) at the lower operational status or the latter may have an impact otherwise attributed to a higher site impact level.

As this was the first project of its kind, an additional limitation placed upon the Wildlife Data Analysis Project was the lack of any comparative study with such an extensive dataset from an area where MECS have not been deployed, that could be used to validate the long-term changes predicted by the models.

The raw observations made during baseline conditions at the two test sites were carried out over a relatively short period of time. This sometimes confounded the certainty surrounding some of the model predictions and, if a similar study were to be conducted, it would be advised to undertake observations over relatively equal proportions of operational statuses.

A further significant limitation was the need to anonymise the operational data as supplied by the developers. The anonymisation of these data, as required in response to the commercial sensitivities surrounding information of a site- or device-specific nature, does not allow for the potential cumulative environmental effects of devices (which may occur due to the proximity of test berths) to be tested.

Data anonymisation may also mean that any pattern emerging in the distribution of density change cannot be compared with the pattern in the distribution of active test berths (that is, with infrastructure or devices installed and/or operational).

Further research is required specifically in relation to the potential for arrays of devices to affect the abundance and/or distribution of key wildlife species, for example, by creating a barrier to free movement.

6.6 Constraints on the usefulness of the results

The power analysis undertaken on the fitted models in the current analysis has suggested that, for some species such as divers at the Fall of Warness tidal energy test site, the power to detect change in density is low (below 60% detection rate) and some models are not able to detect the significant decreases in abundance as simulated. The low density predictions (resulting from the low number of raw observations) at the site may offer a possible reason for this.

It is worth considering that the power analyses conducted on the models to determine their power in predicting change have served to highlight the limitations of data gathering for the purposes of environmental impact assessment, environmental monitoring, etc. when the species being observed occur in very low numbers. This point has emerged very clearly from the Wildlife Data Analysis Project, even with the amount of data (almost 18,000 observation hours) available in the very large datasets accumulated over extensive periods at both test sites.

Despite the extensive data cleansing exercise carried out on the database in order to ensure that the outputs are robust and reliable, there were certain errors in the datasets that remain as it was deemed to be not cost effective to address these in terms of the effort (time and cost) involved in relation to the improvements likely to be gained. These remaining errors are noted in Annex 1.

6.7 Recommendations for future data collection

Lessons have been learned with respect to the Wildlife Observations Programme that can inform any future resumption or new programme of wildlife observations. These can be summarised as follows:

- Introduce further restrictions on acceptable input values, guided by a handbook of acceptable values/terms for each environmental parameter, reinforced through extensive use by the observers of lookup tables and drop-down menus in the data entry process. Whilst this may increase the consistency of future datasets and reduce the scale of data cleansing needed (for example, removal of null or erroneous values), this has to be weighed against the fact that more observer effort would be required (at a cost) in order to make selections from the proscribed parameters.
- Incorporate an automated check of raw data soon after recording, with automated recording of some parameters also, for example, of declination and horizontal angles, and time.
- Consider the potential for repeated recording of declination and horizontal angles during a single observation in order to determine the direction of movement of birds or marine mammals.
- Examine the scope for reducing errors incurred through manual data recording and transcription through, for example, the development of a data logger initiated by the observer at the start and finish of each watch.
- Review whether there would be potential to introduce the automated insertion of data into a live database; however, the observers were resistant to the use of electronic recording as it was considered to be less time-efficient.
- Develop a more robust method for recording vessel presence and activity at the site, that allows statistical analysis to be conducted.

With reference to any future wildlife observation data gathering, best practice guidance should be used to assist with devising a suitable methodology tailored to the purpose of the study and local conditions. An example is SNH's report (SNH, 2011) which provides guidance on surveying and monitoring methodologies. For instance, the report advises that

the scan across the sea area should be as quick as possible, providing a 'snapshot' of the number and distribution of animals that are present at any one time. This should mean that there is insufficient time for animals to redistribute and potentially be recounted, although the chance of this happening within a defined period can be accounted for during modelling. However, the scan rate should be balanced so as to reduce the chance of overlooking an animal.

There is a particular issue that cetaceans, seals and basking sharks will frequently fail to be recorded during scanning due to the fact that they spend most of their time underwater. SNH (2011) recommends that observational data should be subject to a 'watch time' correction which represents the time period over which any one part of the sea surface is observed during a scan. Together with knowledge of surfacing patterns, watch time can be used to assist in estimating the proportion of these animals that go unrecorded because they are not on the surface when scanning takes place.

As highlighted in Band (2015), when carrying out surveys from fixed vantage points on land, it is necessary to make corrections for declining detectability of animals with distance. However, it should not be assumed that animal abundance is uniform with distance, as there is often an ecological gradient from coast to sea. Calculating a detection function for both test sites at EMEC is essential before any further analysis is conducted on the datasets obtained during the Wildlife Observations Programme.

6.8 Scope for further research

The Wildlife Data Analysis Project has modelled changes in species abundance and distribution across Orkney's tidal and wave energy test sites. However, it is recognised that there may be scope for alternative approaches to this modelling exercise. It is important to note that the raw data are still available in their original form for use in any future analysis. Recommendations have been made in relation to any further wildlife observations at these locations (which may also inform such data gathering at other locations). It may also be that device operational data may be released at some future date if the relevant developer/s deem them to be no longer commercially sensitive; the wildlife observations data could then be reassessed in light of this more device-specific information.

There remains a need to consider if any of the effects on species density detected through the current analysis which appear to be associated with the installation and/or operation of marine renewable devices, are in fact significant when considered against other factors that influence the wider populations of these species. This proved not possible to undertake within the realistic scope of this project. It should also be noted that the occurrence of some species is so low that the lack of statistically reliable observations data is likely to pose an ongoing challenge.

Managing risk and uncertainty is key to the process of environmental impact assessment and the Wildlife Data Analysis Project is an attempt to help to reduce uncertainty in the process by co-ordinating research on matters of common interest to multiple stakeholders; the potential displacement of wildlife species is one of the key uncertainties in the deployment of marine renewable energy devices, alongside collision risk and the impact of noise. A collaborative approach to data collection and analysis at test site level is a step in the right direction of co-ordinating research in assisting developers to progress towards commercial deployment.

The information requirements for consenting and licensing purposes can be onerous for individual developers to fulfil in terms of cost and time delays, to the extent that they can in some circumstances threaten the economic viability of a project. Data gathering may be expensive and time consuming, especially where tidal, seasonal or other cyclical data

(perhaps over several years to take account of natural variation) are required to be collected and analysed. Some data requirements are site-, or project-, or design-specific, whilst others are more generic and can be informed through an external research project with benefits across the industry and its regulators.

Defining what is regarded to be ‘significant’ in terms of environmental change is a complex issue. However, if it were possible to define what is considered to be a significant environmental change in terms of the species of interest found at a location, and taking account of the modelling that is to take place, then it may be possible to define the minimum observation effort needed to detect such a change. This is likely to make future data gathering more efficient in terms of time and resources required, and, if the available resources can be targeted towards the key areas of environmental concern, then environmental impact assessment will be more effective.

The publication of this report should assist in disseminating across the industry the findings of the Wildlife Data Analysis Project, and the very valuable wildlife observation database upon which they are based, as a contributor towards the environmental information requirements arising during the consenting and licensing process.

7. REFERENCES

Anderwald, P. and Evans, P.G.H. 2007. Minke whale populations in the North Atlantic: an overview with special reference to UK waters. In: Robinson, K.P, Stevick, P.T. and Macleod, C.D. (eds.) An integrated approach to nonlethal research on minke whales in European waters. Proceedings of the Workshop. European Cetacean Society Special Publication Series No. 47. 49pp.

Atkinson, A.C. 1980. A note on the generalized information criterion for choice of a model. Biometrika, 67, 413-418.

Anderwald, P., Evans, P.G.H., Hoelzel, A.R., & Papastavrou, V. 2008. Minke whale *Balaenoptera acutorostrata*. In: S. Harris, S. and Yalden, D.W. (eds.) Mammals of the British Isles: Handbook, 4th Edition. The Mammal Society, Southampton. 799pp.

Band, W. T. 2015. Assessing collision risk between tidal turbines and marine wildlife. Scottish Natural Heritage Guidance Note Series.

BirdLife International. 2015. Detailed regional assessment and species account from the European Red List of Birds [Online]. Available: http://www.birdlife.org

Buckland, S.T., Anderson, D.R., Burnham, K.P., Laake, J.L., Borchers, D.L. & Thomas, L. 2001. Introduction to Distance Sampling: Estimating abundance of biological populations, 1st ed., S. T. Buckland, Ed. Oxford, UK: Oxford University Press.

Burger, J., Gochfeld, M., Kirwan, G.M. & Christie, D.A. 2013a. European Herring Gull (*Larus argentatus*). In: del Hoyo, J., Elliott, A., Sargatal, J., Christie, D.A. & de Juana, E. (eds.) Handbook of the Birds of the World Alive. Barcelona: Lynx Edicions.

Burger, J., Gochfeld, M., Kirwan, G.M., Christie, D.A & Bonan, A. 2013b. Great black-backed Gull (*Larus marinus*). In: del Hoyo, J., Elliott, A., Sargatal, J., Christie, D.A. & de Juana, E. (eds.) Handbook of the Birds of the World Alive. Barcelona: Lynx Edicions.

Burger, J., Gochfeld, M., Kirwan, G.M. & Christie, D.A. 2013c. Mew Gull (*Larus canus*). In: del Hoyo, J., Elliott, A., Sargatal, J., Christie, D.A. & de Juana, E. (eds.) Handbook of the Birds of the World Alive. Barcelona: Lynx Edicions.

Burger, J., Gochfeld, M., Kirwan, G.M. & Christie, D.A. 2013d. Black-legged Kittiwake (*Rissa tridactyla*). In: del Hoyo, J., Elliott, A., Sargatal, J., Christie, D.A. & de Juana, E. (eds.) Handbook of the Birds of the World Alive. Barcelona: Lynx Edicions.

Burger, J., Gochfeld, M., Bonan, A. & de Juana, E. 2013e. Sabine's Gull (*Xema sabini*). In: del Hoyo, J., Elliott, A., Sargatal, J., Christie, D.A. & de Juana, E. (eds.) Handbook of the Birds of the World Alive. Barcelona: Lynx Edicions.

Burger, J., Gochfeld, M., Kirwan, G.M., Christie, D.A. & de Juana, E. 2013f. Lesser Blacked-backed gull (*Larus fuscus*). In: del Hoyo, J., Elliott, A., Sargatal, J., Christie, D.A. & de Juana, E. (eds.) Handbook of the Birds of the World Alive. Barcelona: Lynx Edicions.

Burger, J., Gochfeld, M. & de Juana, E. 2014. Glaucous Gull (*Larus hyperboreus*). In: del Hoyo, J., Elliott, A., Sargatal, J., Christie, D.A. & de Juana, E. (eds.) Handbook of the Birds of the World Alive. Barcelona: Lynx Edicions.

Bolt, H.E., Harvey, P.V., Mandleberg, L., & Foote, A.D. 2009. Occurrence of killer whales in Scottish inshore waters: temporal and spatial patterns relative to the distribution of declining

harbour seal populations. Aquatic Conservation: Marine and Freshwater Ecosystems, 19: 671-675.

Boran, J.R., Hoelzel, A.R., & Evans, P.G.H. 2008. Killer whale *Orcinus orca*. In: Harris, S. and Yalden, D.W. Mammals of the British Isles Handbook. 4th Edition. The Mammal Society, Southampton. 800pp.

Canning, S.J., Santos, M.B., Reid, R.J., Evans, P.G.H., Sabin, R.C., Bailey, N., & Pierce, G.J. 2008. Seasonal distribution of white-beaked dolphins (*Lagenorhynchus albirostris*) in UK waters with new information on diet and habitat use. Journal of Marine Biological Association U.K. 88(6): 1159-1166.

Carboneras, C., Christie, D.A. & Garcia, E.F.J. 2014a. Common Loon (*Gavia immer*). In: del Hoyo, J., Elliott, A., Sargatal, J., Christie, D.A. & de Juana, E. (eds.) Handbook of the Birds of the World Alive. Barcelona: Lynx Edicions.

Carboneras, C., Christie, D.A. & Garcia, E.F.J. 2014b. Red-throated Loon (*Gavia stellata*). In: del Hoyo, J., Elliott, A., Sargatal, J., Christie, D.A. & de Juana, E. (eds.) Handbook of the Birds of the World Alive. Barcelona: Lynx Edicions.

Carboneras, C., Christie, D.A. & Kirwan, G.M. 2014c. Common Eider (*Somateria mollissima*). In: del Hoyo, J., Elliott, A., Sargatal, J., Christie, D.A. & de Juana, E. (eds.) Handbook of the Birds of the World Alive. Barcelona: Lynx Edicions.

Carboneras, C., Christie, D.A. & Kirwan, G.M. 2014d. Common Goldeneye (*Bucephala clangula*). In: del Hoyo, J., Elliott, A., Sargatal, J., Christie, D.A. & de Juana, E. (eds.) Handbook of the Birds of the World Alive. Barcelona: Lynx Edicions.

Carboneras, C., Christie, D.A. Jutglar, F. & Garcia, E.F.J., 2014e. Northern Gannet (*Morus bassanus*). In: del Hoyo, J., Elliott, A., Sargatal, J., Christie, D.A. & de Juana, E. (eds.) Handbook of the Birds of the World Alive. Barcelona: Lynx Edicions.

Carboneras, C. & Kirwan, G.M. 2014a. Long-tailed Duck (*Clangula hyemalis*). In: del Hoyo, J., Elliott, A., Sargatal, J., Christie, D.A. & de Juana, E. (eds.) Handbook of the Birds of the World Alive. Barcelona: Lynx Edicions.

Carboneras, C. & Kirwan, G.M. 2014b. Red-breasted Merganser (*Mergus serrator*). In: del Hoyo, J., Elliott, A., Sargatal, J., Christie, D.A. & de Juana, E. (eds.) Handbook of the Birds of the World Alive. Barcelona: Lynx Edicions.

Carboneras, C. & Kirwan, G.M. 2014c. Goosander (*Mergus merganser*). In: del Hoyo, J., Elliott, A., Sargatal, J., Christie, D.A. & de Juana, E. (eds.) Handbook of the Birds of the World Alive. Barcelona: Lynx Edicions.

DMP Statistical Solutions UK Ltd. 2010. Power analyses for the visual monitoring scheme at the Billia Croo site. Report prepared for SMRU Limited.

Duck, C. and Morris, C. 2011. Surveys of harbour (common) seals in Orkney in August 2010. Scottish Natural Heritage Commissioned Report No. 439.

Duck, C.D. and Morris, C.D. 2014. Surveys of harbour and grey seals on the east, north and north-west coast of Scotland and in Orkney, including the Moray Firth and the Firth of Tay, in August 2013. Scottish Natural Heritage Commissioned Report No. 759.

Evans, P.G.H., Anderwald, P., & Baines, M.E. 2003. UK Cetacean Status Review. Final Report to English Nature & Countryside Council for Wales. Sea Watch Foundation, Oxford, UK. 150pp.

Evans, P.G.H., Lockyer, C.H., Smeenk, C., Addink, M., & Read, A.J. 2008. Harbour Porpoise *Phocoena phocoena*. In: Harris, S and Yalden, D.W. Mammals of the British Isles Handbook. 4th Edition. The Mammal Society, Southampton. 800pp.

Evans, P.G.H., Baines, M.E., Coppock, J. 2011. Abundance and behaviour of cetaceans and basking sharks in the Pentland Firth and Orkney Waters. Report by Hebog Environmental Ltd & Sea Watch Foundation. Scottish Natural Heritage Commissioned Report No. 419.

Foote, A.D., Newton, J., Piertney, S.B., Willerslev, E., & Gilbert, M.T. 2009. Ecological morphological and genetic divergence of sympatric North Atlantic killer whale populations. Molecular Ecology, 18 (24): 5207-5217

Foote, A.D., Similä, T., Vikingsson, G.A., & Stevick, P.T. 2010. Movement, site fidelity and connectivity in a top marine predator, the killer whale. Evolutionary Ecology, 24(4): 803-814.

Furness, R.W., Wade, H.M., Robbins, A.M.C. & Masden, E.A. 2012. Assessing the sensitivity of seabird populations to adverse effects from tidal stream turbines and wave energy devices. ICES Journal of Marine Science, 69(8), 1466-1479.

Hammond P.S. 2008. Small cetaceans in the European Atlantic and North Sea (SCANS II). Final report to the European Commission under contract LIFE04NAT/GB/000245.

Hardin, J. & Hilbe, J. 2002. Generalized Estimating Equations, 1st ed., Boca Raton, Ed. FL, USA: Chapman & Hall/CRC Press.

Harrison, P. J., Buckland, S. T., Thomas L., Harris, R., Pomeroy, P. & Harwood, J. 2006. Incorporating movement into models of grey seal population dynamics. Journal of Animal Ecology, 75, 634-645.

Hastie, T.J. & Tibshirani, R.J. 1990. Generalized Additive Models, 1st ed., FL, USA: Chapman & Hall/CRC Press.

Hastie, T., Tibshirani, R. & Friedman, J. 2009. The Elements of Statistical Learning: Data Mining, Inference and Prediction. 2nd ed., ser. Springer Series in Statistics. Berlin, Germany: Springer.

Del Hoyo, J., Elliott, A., Sargatal, J. 1996. Handbook of the Birds of the World, vol. 3: Hoatzin to Auks. Barcelona: Lynx Edicions.

Højsgaard, S., Halekoh, U. & Yan, J. 2006. The R Package geepack for Generalized Estimating Equations. Journal of Statistical Software, 15(2), 1-11.

Iman, R. & Conover, W. 1982. A distribution-free approach to inducing rank correlation among input variables. Communication in Statistics – Simulation and Computation, 11(3), 311-334.

Langton, R., Davies, I.M. & Scott, B.E. 2011. Seabird conservation and tidal stream and wave power generation: information needs to predicting and managing potential impacts. Marine Policy, 35(5), 623-630.

Lavers, J. L. & Jones, I. L. 2007. Impacts of intraspecific kleptoparasitism and diet shifts on Razorbill productivity at the Gannet Islands, Labrador. Marine Ornithology, 35, 1-7.

Luque, P.L., Davis, C.G., Reid, D.G., Wang, J., & Pierce, G.J. 2006. Opportunistic sightings of killer whales from Scottish pelagic trawlers fishing for mackerel and herring off North Scotland (UK) between 2000 and 2006. Aquatic Living Resources, 19: 403-410.

Mackenzie, M.L., Scott-Hayward, L.A.S., Oedekoven, C.S., Skov, H., Humphreys, E. & Rexstad, E. 2013. Statistical Modelling of Seabird and Cetacean Data: Guidance Document. University of St. Andrews contract for Marine Scotland, SB9 (CR/2012/05).

Marine Scotland. 2014. Seal Haul-Out Sites. Crown Copyright. Topic Sheet No. 132 V1.

Mendenhall, W. & Reinmuth, J.E. 1982. Statistics for Management and Economics, 4th ed., Boston, USA: Duxbury Press.

Mitchell, P.I., Newton, S.F., Ratcliffe, N. & Dunn, T.E. 2004. Seabird Populations of Britain and Ireland. T. & A.D Poyser, London.

Murray, S., Harris, M.P. & Wanless, S. 2015. The status of the Gannet in Scotland in 2013-14. Scottish Birds, 35(1), 3-18.

Nettleship, D.N. & Garcia, E.F.J. 2015. Little Auk (*Alle alle*). In: del Hoyo, J., Elliott, A., Sargatal, J., Christie, D.A. & de Juana, E. (eds.) Handbook of the Birds of the World Alive. Barcelona: Lynx Edicions.

Nettleship, D.N. Kirwan, G.M., Christie, D.A. & de Juana, E. 2014. Atlantic Puffin (*Fratercula arctica*). In: del Hoyo, J., Elliott, A., Sargatal, J., Christie, D.A. & de Juana, E. (eds.) Handbook of the Birds of the World Alive. Barcelona: Lynx Edicions.

Olsen, K.M. and Larsson, H. 2004. Gulls of Europe, Asia and North America. Christopher Helm, London.

Orta, J., Garcia, E.F.J., Jutglar, F., Kirwan, G.M. and Boesman, P. 2014a. European Shag (*Phalacrocorax aristotelis*). In: del Hoyo, J., Elliott, A., Sargatal, J., Christie, D.A. & de Juana, E. (eds.) Handbook of the Birds of the World Alive. Barcelona: Lynx Edicions.

Orta, J., Garcia, E.F.J., Jutglar, F., Kirwan, G.M. and Boesman, P. 2014b. Great Cormorant (*Phalacrocorax carbo*). In: del Hoyo, J., Elliott, A., Sargatal, J., Christie, D.A. and de Juana, E. (eds.) Handbook of the Birds of the World Alive. Barcelona: Lynx Edicions.

Pan, W. 2001. Akaike's Information Criterion in Generalised Estimating Equations. Biometrics, 57(1), 120-125.

Pesante, G., Evans, P.G.H., Baines, M.E., & McMath, M. 2008. Abundance and Life History Parameters of Bottlenose Dolphin in Cardigan Bay: Monitoring 2005-2007. CCW Marine Monitoring Report No. 61: 1-75.

Piatt, J.F. & Nettleship, D.N. 1985. Diving depths of four *alcids*. The Auk, 102(2), 293-297.

Pierce, G.J, Santos. M.B, Reid. R.J, Patterson. I.A.P., & Ross. H.M. 2004. Diet of minke whales Balaenoptera acutorostrata in Scottish (UK) waters with notes on strandings of this species in Scotland 1992–2002. Journal of the Marine Biological Association of the UK, 84: 1241–1244.

R Core Team. 2015. R: A language and environment for statistical computing. R Foundation for Statistical Computing. [Online]. Available: http://www.R-project.org/

Reid, J.B., Evans, P.G.H., & Northridge, S.P. 2003. Atlas of Cetacean Distribution in North-west European Waters. Joint Nature Conservation Committee, Peterborough. 76pp.

Robbins, A. 2012. Analysis of Bird and Marine Mammal Data for Billia Croo Wave Test Site, Orkney. Scottish Natural Heritage Commissioned Report No. 592.

Robbins, A. 2011. Summary of Bird and Marine Mammal Data for the Fall of Warness and Billia Croo, Orkney and Review of Observation Methodologies.

Santos, M.B, Pierce. G.J, Ross. H.M, Reid. R.J., & Wilson. B. 1994. Diets of small cetaceans from the Scottish coast. ICES Marine Mammal Committee, C.M. 1994 / No. 11, 1- 16.

Santos, M.B., Pierce, G.J., Reid, R.J., Patterson, I.A.P., Ross, H.M., & Mente, E. 2001. Stomach contents of bottlenose dolphins (*Tursiops truncatus*) in Scottish waters. Journal of the Marine Biological Association U.K., 81: 873-878.

Santos, M.B., Pierce, G.J., Learmonth, J.A., Reid, R.J., Ross, H.M., Patterson, I.A.P., Reid, G.D., Beare, D. 2004. Variability in the diet of harbour porpoises (*Phocoena phocoena*) in Scottish Waters (1992-2003). Marine Mammal Science, 20(1): 1-27.

SCOS. 2011. Scientific Advice on Matters Related to the Management of Seal Populations: 2011. SCOS Main Advice 2011.

SCOS. 2012. Scientific Advice on Matters Related to the Management of Seal Populations: 2012. SCOS Main Advice 2012.

Scottish Government. 2014. Haul-Out sites. [Online]. Available: http://www.gov.scot/Topics/marine/marine-environment/species/19887/20814/haulouts

Scottish Natural Heritage (SNH). 2011. Guidance on Survey and Monitoring in relation to Marine Renewable Deployments in Scotland. Prepared for Scottish Natural Heritage by Royal Haskoning. In draft.

Scottish Natural Heritage (SNH). 2012. Seabirds in Scotland. Scottish Natural Heritage, Trend Note Number 021.

Scott-Hayward, L.A.S., Oedekoven, C.S., Mackenzie, M.L., Walker, C.G. & Rexstad, E. 2013a. MRSea package (version 0.2.0): Statistical Modelling of bird and cetacean distribution in offshore renewables development area. [Online]. Available: http://creem2.st-and.ac.uk/software.aspx

Scott-Hayward, L., Oedekoven, C.S., Mackenzie, M.L., Walker, C.G. & Rexstad, E. 2013b. User Guide for the MRSea Package: Statistical Modelling of bird and cetacean distributions in offshore renewables development area. University of St. Andrews contract for Marine Scotland, SB9 (CR/2012/05).

Scott-Hayward, L.A.S., Mackenzie, M.L. & Oedekoven, C.S. 2014a. Modelling impact assessment in renewables development areas using the new R package, MRSea v0.1.1," in Proc. EIMR, 2014, paper 2014-596.

Scott-Hayward, L., Mackenzie, M.L., Donovan, C.R., Walker, C.G. & Ashe, E. 2014b. Complex region spatial smoother (CReSS), Journal of Computational and Graphical Statistics, 23(2), 340-360.

SMRU Ltd. 2010. Estimating locations from 'Big-Eyes' angle data at Billia Croo. SMRU Limited, MMM.0908.EME.

SMRU Ltd. 2011. Utilisation of space by grey and harbour seals in the Pentland Firth and Orkney waters. Scottish Natural Heritage Commissioned Report No. 441.

SMRU. 2013. Identifying Seals. Sea Mammal Research Unit, University of St Andrews. SMRU Fact Sheets.

Swann, R. 2013. Marine Protected Area and Marine Renewable – related black guillemot surveys. Scottish Natural Heritage Commissioned Report No. 612.

Thompson, P.M., Cheney, B., Ingram, S., Stevick, P., Wilson, B., & Hammond, P.S. (Eds.) 2009. Distribution, abundance and population structure of bottlenose dolphins in Scottish waters. Scottish Natural Heritage Commissioned Report. 99pp.

Waggitt, J.J., Bell, P.S. & Scott, B.E. 2014. An evaluation of the use of shore-based surveys for estimating spatial overlap between deep-diving seabirds and tidal stream turbines. International Journal of Marine Energy, 8, 36-49.

Walker, C.G., Mackenzie, M.L., Donovan, C.R., Kidney, D., Quick, N.J. & Hastie, G.D. 2011. SALSA: A Spatially Adaptive Local Smoothing Algorithm. Journal of Statistical Computation and Simulation, 81(2), 179-191.

Wilson, B. 2008. Bottlenose dolphin, Tursiops truncatus. Pp. 709-715. In: Mammals of the British Isles. (Eds. S. Harris & D.W. Yalden). Handbook. 4th Edition. The Mammal Society, Southampton. 800pp

APPENDIX 1: OBSERVER-SPECIFIC OBSERVATION PATTERNS

Introduction

Information has been obtained from the observers at the Fall of Warness and Billia Croo regarding the general pattern followed when carrying out observations. This observer-specific information has been applied alongside grid cell area information to provide an effort function within the model. Any sightings made in grid cells where the observer has stated that the grid cell is not included in the general observation pattern has been excluded from the analysis. It is recognised that this is a generalised assumption that may lead to a few sightings being lost from the analysis; however, it is believed to be necessary due to the number of 'zeros' that would be required to be added for the inclusion of survey effort in order to enable the analysis to be conducted.

EMEC and the Centre for Research into Ecological and Environmental Modelling (CREEM) worked jointly on finding the most appropriate method for accounting for observer effort within each of the datasets.

Fall of Warness

In an attempt to accurately account for survey effort, information was obtained from the observers at the Fall of Warness regarding the general observation pattern followed. This information, alongside metadata pertaining to the site, allowed an effort function to be included in the model. An effort value was assigned to each grid cell which took account of the area of the grid cell and the number of times it was generally observed by each observer. This led to the assigned effort values being observer-specific. In using these values to denote effort, a few assumptions were applied, which are summarised below.

- The observers followed the same observation pattern during every watch. This assumes that the observer never made any sightings in grid squares that were not within 'his' observation pattern. This is a generalised assumption, as it was clear from the data that the observers did not keep strictly to their observation patterns; species observations were recorded within grid cells that, according to their observation pattern, were never observed. This also assumes that the observation patterns matched those supplied by the observers, either verbally or in writing.
- The extent of the grid and the placement of grid lines were fixed. Although it is likely that these were fairly consistent between watches by the same observer, it is probable that there was some variation between observers in the position of the superimposed grid.
- An equal amount of time was spent observing each grid square even between sweeps within a watch. This principle is important as the observers tended to spend less time on the third and fourth sweeps but observed considerably fewer grid squares.
- A full hour was used each time to complete a watch; this assumes that an observation period was only abandoned once an hour-long watch came to an end. This assumption does not take account of instances when observation periods were abandoned mid-watch; however, the observer tended to resume from the same point when a watch restarted.

Each of the observers at the Fall of Warness carried out observations in a certain pattern. The observers tended to implement four sweeps of the site within an hour (equating to a single scan). A watch typically lasted for a four-hour period and there was generally only one watch per day. The pattern followed during each sweep was individual to the observer, even though observer calibration exercises were followed when new observers commenced observations. There were four observers consistently at the site with Observer 5 carrying out the majority of watches in the early years and Observers 3 and 4 sharing watches more recently. Observer 6 carried out watches in an ad-hoc manner. Individual observation

patterns were gathered from the observers verbally whilst undertaking a watch. Appendix 1. Figure 7.1 shows the observation patterns obtained from each of the observers.

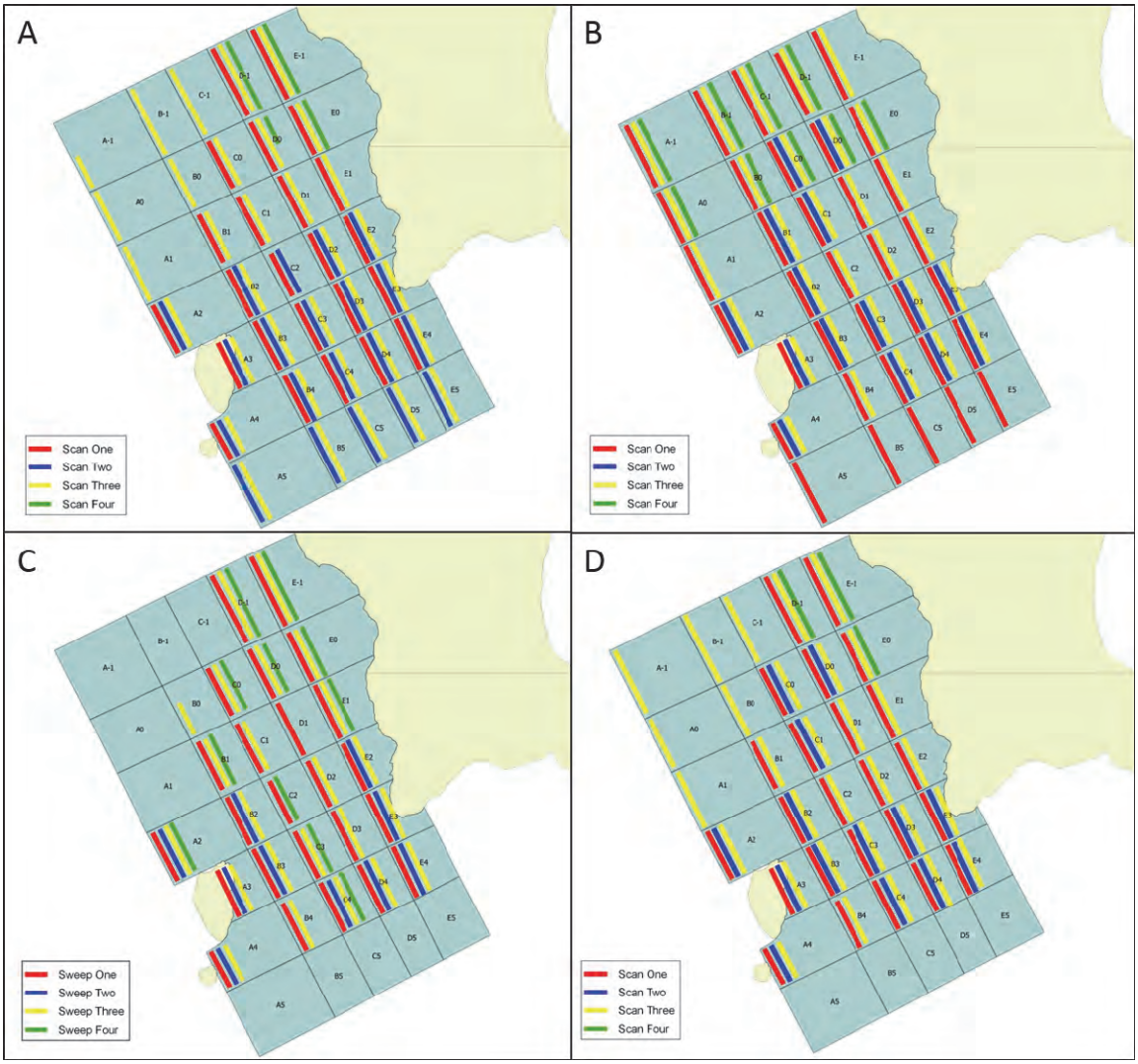

Appendix 1. Figure 7.1. Observer-specific scan patterns for a single scan of the observation grid at the Fall of Warness. A: Observer 3; B: Observer 6; C: Observer 5; and D: Observer 4

Billia Croo

Observations at Billia Croo were recorded a little differently from those at the Fall of Warness, with a watch being split into a variable number of sweeps which alter in duration rather than a watch being split into four separate hours. It was decided that the best method of applying an effort value to an observation was through determining the duration of the sweep and the extent of the area covered in that sweep. Sweep duration varied due to differences in the size of the area covered in a sweep e.g. the area covered by the inner sweep was considerably less than that covered in the outer sweep. Additionally, the area covered within a sweep was observer-specific as the observers' radial distance from the vantage point to the inner and outer boundary of a sweep differed. All observations at Billia Croo were conducted by two observers who were consistent throughout the programme's duration. Appendix 1. Figure 7.2 provides a sample of the sighting locations over a brief period at the site for the two observers (extent of sweeps marked by red, green and yellow points). The figure demonstrates the varying extent in the sweep extents between the two observers.

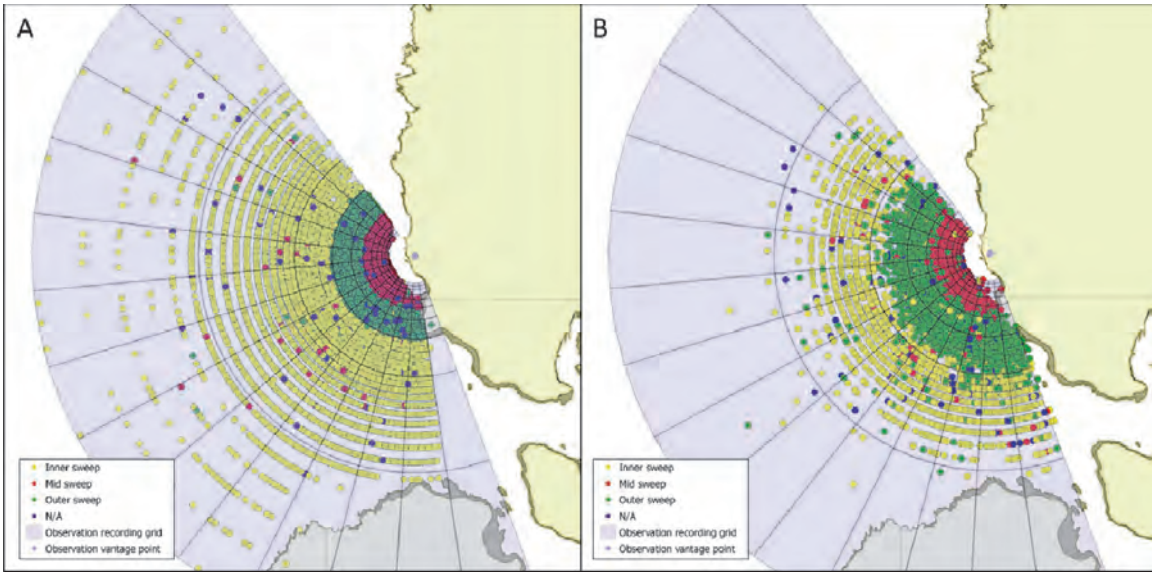

Appendix 1. Figure 7.2. Sample observation recordings from both observers at Billia Croo. A: Observer 1; B: Observer 2

Within the observation protocol, it states that the observers should note down the environmental conditions when a change in conditions is experienced. This led to the observers tending to record the environmental conditions at the start and end of a sweep. These records have allowed the duration of each sweep to be calculated. Information on the duration of a sweep, whether the sweep was inner, mid or outer and the observer conducting observations can all be used to assign an effort function for each sweep. In coming to this conclusion, various assumptions were made as summarised below.

- The observer surveyed the area equally in each sweep and a sweep only finished once the whole sweep area had been surveyed.
- Any observations that had not had a sweep number assigned to them, were assigned such a number by identifying which sweep area the observation lay within when considering their horizontal and declination angles.
- When a start and end time for a sweep was unavailable, the timing of observations and their locations were used to determine the duration of a sweep.
- Any observations made outwith the prescribed grid were either not in a viewable area or were on land and, therefore, not assigned an effort value and not included in the analysis.

To help assign an observer effort function that could be included in the analysis for Billia Croo, a radial grid was constructed using software packages R and QGIS. The radial grid was superimposed on the site and was not used in any form by observers who always recorded observations by supplying horizontal and declination angles. The extent of the grid was limited to the conceivable viewing area, in terms of the angle through which the 'Big Eyes' were able to move. The radial gridlines match the extent of the maximum parameters of the observation viewing area, whereas the non-radial gridlines, which stretch across the site, are positioned at exponentially increasing radial distances from the vantage point and approximate to the radial extents (maximum and minimum) of the sweeps for the different observers.

Appendix 1. Figure 7.3 and Appendix 1. Figure 7.4 show the radial grid superimposed on the site and mark the extents on the inner, mid and outer sweeps (sweep 1, 2 and 3, respectively).

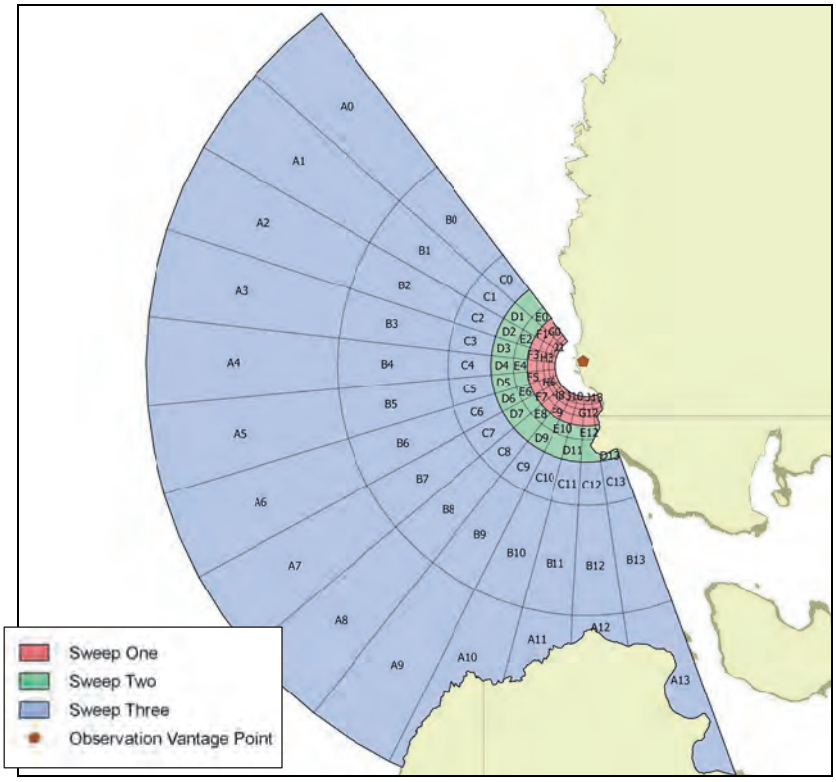

Appendix 1. Figure 7.3. Radial grid superimposed onto the wildlife observation area at Billia Croo

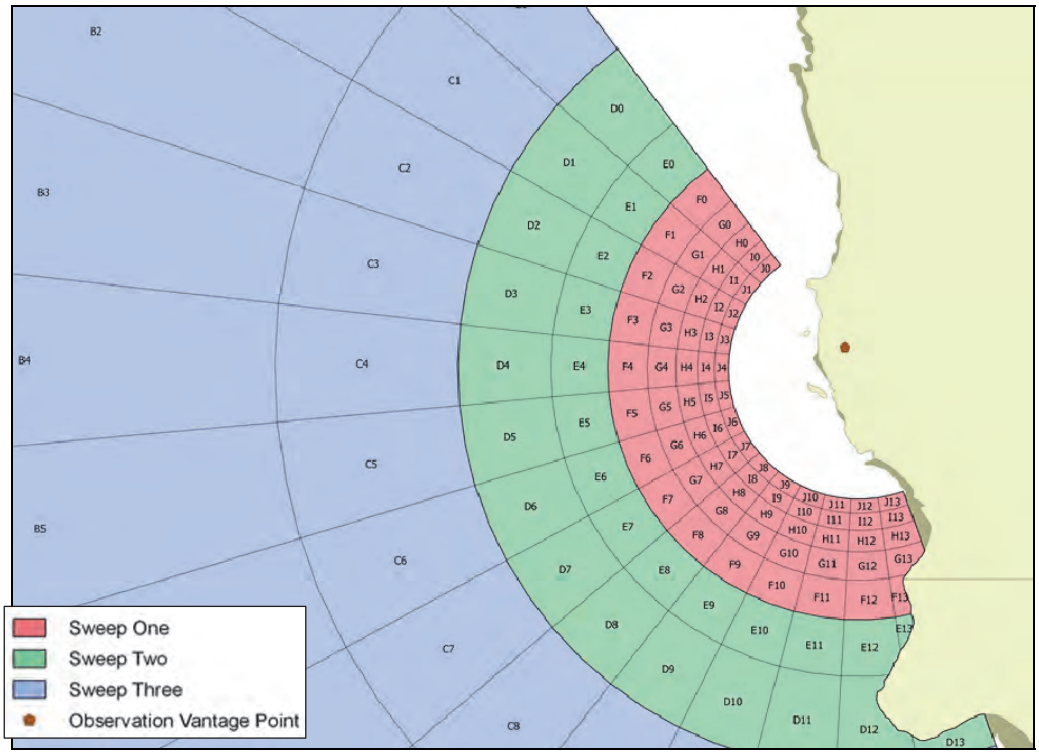

Appendix 1. Figure 7.4. Inner section of radial grid superimposed onto the wildlife observation area at Billia Croo

APPENDIX 2: ACCOMPANYING DATASETS AVAILABLE FROM MARINE SCOTLAND INFORMATION (MSI) PORTAL

The following is a contents list of all data and plots available for this project on the Marine Scotland Information (MSI) portal: http://marine.gov.scot/ . The data are presented in separate folders for each of the survey sites: 'Fall of Warness' and 'Billia Croo'.

Within each site folder is a folder containing the cleansed data, 'Cleansed data'. The cleansed data has been split into 'Radial_Point_Data' and either 'FoW_CompleteData' or 'BC_CompleteData'.

The 'Radial_Point_Data' contains the depth and location coordinates for radial circles around each of the centre points of grid cells that contain test berths. In terms of the data contained with the 'FoW_CompleteData' and 'BC_CompleteData' folders, an explanation of each excel spreadsheet is provided in each site's complete data folder. It is worth noting that the data relating to device operational status has not been included on MSI due to commercial sensitivity.

In addition to the cleansed data folder, for each site, there are folders for each of the species/group that have undergone analysis. The following provides the species/groups analysed for each site and the associated species codes:

Fall of Warness

- Auks (AUK)
- Black guillemot (TYSTI)
- Cetacean (CETA)
- Common guillemot (GUILL)
- Divers (DIVER)
- Ducks and geese (DUCK)
- Harbour seal (HARBSL)
- Razorbill (RAZOR)
- Seals (SEAL)
- Shags and cormorants (PHASP)

Billia Croo

- Atlantic puffin (PUFFI)
- Auks (AUK)
- Black guillemot (TYSTI)
- Cetaceans (CETA)
- Common guillemot (GUILL)
- Divers (DIVER)
- Gulls (GULL)
- Harbour porpoise (HARBPO)
- Northern gannet (GANNE)
- Seals (SEAL)

A breakdown of the contents of all the species folders is provided below:

- o Abundance
  - Abundance_SPECIES.csv
  - SPECIESAbundance.png
- o Diagnostics
  - SPECIES_MeanVar.png
  - SPECIES_MeanVar_log.png
  - SPECIES_ObsFit.png

        - SPECIES_Rsq.png
        - SPECIES_Rsq_cuts.png
- Difference data
    - DifferenceData_SPECIES.csv
    - SPECIES_dif10.png
    - SPECIES_dif20.png
    - SPECIES_dif21.png
    - SPECIES_dif30.png
    - SPECIES_dif31.png
    - SPECIES_dif32.png
    - SPECIES_sigdif10.png
    - SPECIES_sigdif20.png
    - SPECIES_sigdif21.png
    - SPECIES_sigdif30.png
    - SPECIES_sigdif31.png
    - SPECIES_sigdif32.png
- Distance from test berths
    - DistanceData_GRIDCELL_SPECIES.csv
    - SPECIESdisrfromberth_GRIDCELL.png
- Exploratory data analysis
    - Raw_SI_summary_SPECIES.csv
    - Raw_summary_SPECIES.csv
    - RawObs.jpeg
    - SPECIESRawObs_SI0.png
    - SPECIESRawObs_SI1.png
    - SPECIESRawObs_SI2.png
    - SPECIESRawObs_SI3.png
- Fitted data
    - FittedData_SPECIES.csv
- Partial plots
    - PartialFits_TERM.png
- Power analysis (if applicable)
    - Scenario 1 (if applicable)
        - Modelselected.csv
        - SPECIES_power_decrease.csv
        - SPECIES_power_decrease.png
        - SPECIESpower_beta_model.csv
        - SPECIESpower_decrease_plottingdata.csv
    - Scenario 2 (if applicable)
        - SPECIES_power_redist.csv
        - SPECIES_power_redist_dec.png
        - SPECIES_power_redist_inc.png
        - SPECIESpower_beta_model.csv
        - SPECIESpower_redist_plottingdata.csv
        - Modelselected.csv
    - Scenario 3 (if applicable)
        - Modelselected.csv
        - SPECIES_power_decrease.csv
        - SPECIES_power_decrease.png
        - SPECIESpower_beta_model.csv
        - SPECIESpower_decrease_plottingdata.csv
- Prediction data (all years)
    - PredictionOutput_allyrs_SPECIES.csv
    - SPECIES_SIL_allyrs.png

- Prediction data (each year)
  - PredictionData_SPECIES.csv
  - SPECIES_SI0.png
  - SPECIES_SI0_CV.png
  - SPECIES_SI1.png
  - SPECIES_SI1_CV.png
  - SPECIES_SI2.png
  - SPECIES_SI2_CV.png
  - SPECIES_SI3.png
  - SPECIES_SI3_CV.png
- Seasonal prediction surfaces
  - PredictionData_JANSPECIES.csv
  - PredictionData_JULSPECIES.csv
  - PredictionOutput_allyrs_SPECIES_JAN.csv
  - PredictionOutput_allyrs_SPECIES_JUL.csv
  - SPECIES_SI_allyrs_JAN.png
  - SPECIES_SI_allyrs_JUL.png
  - SPECIES_SI_CV_allyrs_JAN.png
  - SPECIES_SI_CV_allyrs_JUL.png
  - SPECIES_SI0_CV_JAN.png
  - SPECIES_SI0_CV_JUL.png
  - SPECIES_SI0_JAN.png
  - SPECIES_SI0_JUL.png
  - SPECIES_SI1_CV_JAN.png
  - SPECIES_SI1_CV_JUL.png
  - SPECIES_SI1_JAN.png
  - SPECIES_SI1_JUL.png
  - SPECIES_SI2_CV_JAN.png
  - SPECIES_SI2_CV_JUL.png
  - SPECIES_SI2_JAN.png
  - SPECIES_SI2_JUL.png
  - SPECIES_SI3_CV_JAN.png
  - SPECIES_SI3_CV_JUL.png
  - SPECIES_SI3_JAN.png
  - SPECIES_SI3_JUL.png

APPENDIX 3: ANALYTICAL ASSUMPTIONS

A summary of the analytical assumptions applied throughout the project is provided below.

Device operational data

- Where devices were continually changing operational state (e.g. constantly switching between device presence and operation), the times considered during the analysis were limited to only operational durations greater than one minute and resulting in prolonged durations of greater than one minute of operational status.
- SIL-1 excludes developer owned cables (that are not directly involved in the installation works) and EMEC owned cables.
- Device-specific assumptions were implemented for one developer due to the format of the device operational data supplied. Further information regarding these assumptions cannot be supplied due to commercial confidentiality.
- It is assumed that the test berth location is at the cable end which is not necessarily the exact location of the test berth. The centre point of the grid cell containing the test berth (cable end) was used at the impact location.
- It should be noted that at the Fall of Warness two test berths are located in one grid cell.

Fall of Warness Observation Data

- As bathymetry data was only available for half of grid cell A5, the depth used for this grid cell is an average of the data available.
- All observations where the zone was recorded as ‘not known’ or ‘NK’ were removed from the analyses.
- Glare was not taken account during the analyses.
- All observations that were recorded in a grid cell which, according to the observation patterns, was not surveyed were removed from the analyses.
- It was assumed that the same survey effort (i.e. observer-specific observed patterns) was maintained for all watches.

Billia Croo Observation Data

- The analysis grid developed only begins a certain distance away from the vantage point as it was not possible to make accurate recording of species due to viewable angles. Therefore, all observations in this area have not been included in the analyses.
- All observations that were not within the sweep that the observer recorded as being conducted were excluded from the analyses. This equated to around 5% of observations being removed from the analyses.
- Recorded observations with unrealistic horizontal and declination angles were removed from the analyses. This included observations that were recorded as behind the observer.
- Duplicate records were removed from the analysis. There were 101 instances where the ID number, species, date, time, number of individuals in group and observer were identical.
- Observations out with the viewable area were remove from the analysis; there were 167 such observations removed.
- Although observers at Billia Croo recorded the area of the survey area that was obscured by glare, glare was not included in the analyses.
- The method that survey effort has been accounted for has assumed that the observer completes the sweep, no matter the duration of the sweep i.e. it does not account for an observer stopping observations half way through a sweep. This assumption is incorrect as the observer tends to stop mid sweep and start from the same position.
- Survey effort at Billia Croo has had to be assigned to sweep and cannot be differentiated to individual grid cells.

APPENDIX 4: MODELS' GEE-BASED P-VALUES SUMMARY

Summary of GEE-based p-values obtained from each fitted model

Appendix 4. Table 0.1 is a summary of the GEE-based p-values for the final fitted models for the study species/species groups for both the Fall of Warness and Billia Croo test sites.

Appendix 4. Table 0.1. GEE-based p-values obtained from final fitted models for both the Fall of Warness and Billia Croo species/groups

	Covariates												
	Year	Month	Depth	Wind strength	Wind direction	Sea state	Precip-itation	Cloud cover	Distance to land	Tide state	Site impact	Spatial term	Interaction term
Fall of Warness birds													
Black guillemot	---	<0.0001	<0.0001	<0.0001	<0.0001	<0.0001	<0.0001	<0.0001	---	<0.0001	<0.0001	<0.0001	<0.0001
Common guillemot	<0.0001	<0.0001	<0.0001	<0.0001	---	<0.0001	<0.0001	0.0010	---	<0.0001	<0.0001	0.0195	<0.0001
Razorbill	<0.0001	<0.0001	<0.0001	---	<0.0001	<0.0001	---	0.0217	---	---	0.0090	<0.0001	<0.0001
Divers	<0.0001	<0.0001	<0.0001	0.0002	---	<0.0001	---	<0.0001	---	0.0003	0.0055	<0.0001	<0.0001
Shags and cormorants	0.0211	<0.0001	<0.0001		<0.0001	---	0.0029	<0.0001	---	<0.0001	<0.0001	<0.0001	<0.0001
Auks	<0.0001	<0.0001	<0.0001	<0.0001	---	<0.0001	<0.0001	<0.0001	---	<0.0001	<0.0001	<0.0001	<0.0001
Ducks and geese	0.0041	<0.0001	<0.0001	<0.0001	---	---	---	0.0005	---	<0.0001	0.0003	<0.0001	<0.0001
Fall of Warness marine mammals													
Seals	<0.0001	<0.0001	<0.0001	<0.0001	---	0.0043	0.0029	<0.0001	---	---	0.0268	<0.0001	<0.0001
Harbour seal	<0.0001	<0.0001	<0.0001	---	<0.0001	<0.0001	0.0004	---	---	---	0.0324	<0.0001	<0.0001
Cetaceans	---	<0.0001	0.0112	<0.0001	---	0.0009	---	0.0017	---	---	<0.0001	<0.0001	0.0579
Billia Croo birds													
Common guillemot	---	<0.0001	---	---	---	---	---	---	<0.0001	---	0.1070	<0.0001	<0.0001
Black guillemot	---	<0.0001	---	---	---	---	---	<0.0001	<0.0001	---	<0.0001	<0.0001	<0.0001
Atlantic puffin	<0.0001	<0.0001	---	---	---	---	---	---	<0.0001	---	0.0002	<0.0001	<0.0001
Northern gannet	<0.0001	<0.0001	---	---	---	0.0203	---	---	---	---	<0.0001	<0.0001	<0.0001
Auks	0.0002	<0.0001	---	---	---	---	---	---	<0.0001	---	<0.0001	<0.0001	<0.0001
Divers	<0.0001	<0.0001	---	---	---	---	---	---	<0.0001	---	0.0001	<0.0001	<0.0001
Gulls	---	<0.0001	---	---	---	---	---	---	<0.0001	---	0.0073	<0.0001	<0.0001
Billia Croo marine mammals													
Seals	<0.0001	<0.0001	---	---	---	---	---	---	<0.0001	---	<0.0001	<0.0001	<0.0001
Harbour porpoises	0.0021	---	---	---	---	---	---	---	0.0015	---	0.7060	<0.0001	0.0035
Cetaceans	---	---	---	---	---	<0.0001	---	---	---	---	0.2668	<0.0001	<0.0001

APPENDIX 5: SPECIES' ENVIRONMENTAL AND TEMPORAL TERMS

Selected values for the environmnetal and temporal terms for each fitted model

Appendix 5. Table 0.1 provides an overview of the values set for the environmental and temporal covariates that were included in the fitted models. It was necessary to fix these values for the model to be able to make predictions. Environmental and temporal covariates were allocated at a set level during modelling to ensure that, when assessing the effect of changing site impact level, only this effect was being considered and not the impact of changing other covariates that are contained in the final fitted model.

The levels set for the covariates are those where the greatest numbers of observations of the species/group were made during the observations programme run at each of the sites. Therefore, it is important to note that these are not necessarily the best conditions for being able to observe a species, but the conditions when observations of such a species were most prevalent during the observations programme's duration. It is likely that the latter reflect, at least in part, the prevailing conditions at each of the sites. It is worth noting that the prediction surfaces (where not otherwise specified) are based upon the survey month with the greatest number of sightings. Some environmental covariates were excluded from being set at certain values; these were the grid-specific covariates (e.g. depth, distance to land).

Appendix 5. Table 0.1. Set conditions of environmental and temporal terms included in fitted models for both the Fall of Warness and Billia Croo species/groups

	Month	Wind strength	Wind direction	Tide state	Sea state	Swell height (metres)	Weather	Precipitation	Cloud cover (oktas)	Glare extent
Fall of Warness birds										
Black guillemot	July	Light breeze (2)	E-SSE	Flood	Calm (1)	N/A	N/A	None	8	N/A
Common guillemot	June	Light air (1)	E-SSE	Ebb	Calm (1)	N/A	N/A	None	8	N/A
Razorbill	June	Light breeze (2)	E-SSE	Flood	Calm (1)	N/A	N/A	None	8	N/A
Divers	November	Light breeze (2)	S-WSW	Ebb	Smooth (2)	N/A	N/A	None	8	N/A
Shags and cormorants	March	Light breeze (2)	S-WSW	Ebb	Smooth (2)	N/A	N/A	None	8	N/A
Auks	June	Light breeze (2)	E-SSE	Flood	Calm (1)	N/A	N/A	None	8	N/A
Ducks and geese	March	Light breeze (2)	S-WSW	Ebb	Smooth (2)	N/A	N/A	None	8	N/A
Fall of Warness marine mammals										
Seals	October	Light breeze (2)	S-WSW	Flood	Calm (1)	N/A	N/A	None	8	N/A

Harbour seal	July	Light air (1)	E-SSE	Flood	Calm (1)	N/A	N/A	None	6	N/A
Cetaceans	August	Light air (1)	W-NNW	Flood	Calm (1)	N/A	N/A	None	8	N/A
Billia Croo birds										
Common guillemot	June	Moderate breeze and above (4+)	N/A	Flood	Calm (1)	1	Fair	N/A	8	No glare
Black guillemot	March	Moderate breeze and above (4+)	N/A	Flood	Calm (1)	1	Fair	N/A	8	No glare
Atlantic puffin	July	Moderate breeze and above (4+)	N/A	Ebb	Calm (1)	1	Fair	N/A	8	No glare
Northern gannet	August	Moderate breeze and above (4+)	N/A	Ebb	Calm (1)	2	Fair	N/A	8	No glare
Auks	June	Moderate breeze and above (4+)	N/A	Flood	Calm (1)	1	Fair	N/A	8	No glare
Divers	January	Moderate breeze and above (4+)	N/A	Ebb	Calm (1)	1	Fair	N/A	8	No glare
Gulls	November	Moderate breeze and above (4+)	N/A	Flood	Calm (1)	2	Fair	N/A	8	No glare
Billia Croo marine mammals										
Seals	October	Moderate breeze and above (4+)	N/A	Flood	Calm (1)	1	Fair	N/A	8	No glare
Harbour porpoises	August	Moderate breeze and above (4+)	N/A	Slack	Calm (1)	1	Fair	N/A	8	No glare
Cetaceans	August	Moderate breeze and above (4+)	N/A	Flood	Calm (1)	1	Fair	N/A	8	No glare

APPENDIX 6: TOPOGRAPHY OF LAND SURROUNDING TEST SITES

Topography of land surrounding the Fall of Warness test site

Appendix 6. Figure 0.1 provides a visualisation of the land surrounding the tidal test site, the Fall of Warness off the island of Eday. The relative steepness of the land is illustrated by the spacing of the contour lines with Ward Hill, where the observation vantage point is located, being the highest on Eday with some of the steeper slopes. The vantage point is positioned at approximately 50m in height on the slopes of this hill.

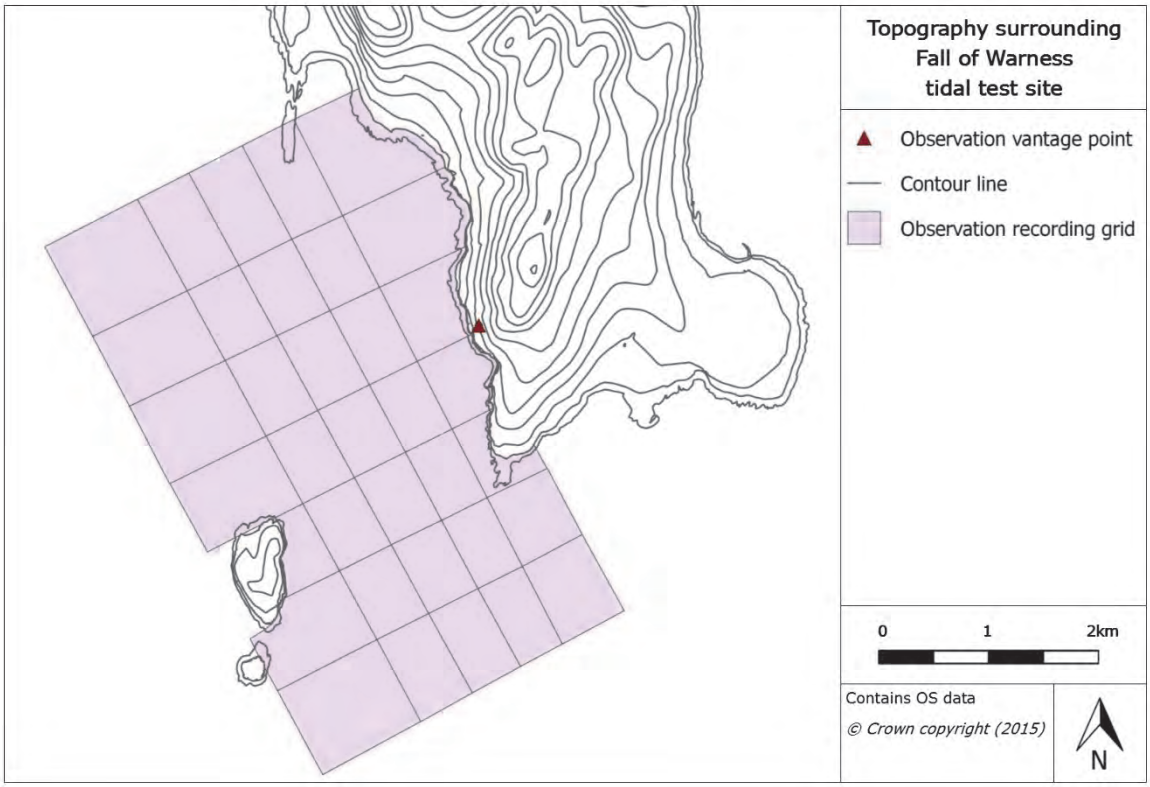

Appendix 6. Figure 0.1. Topography of the land surrounding the Fall of Warness tidal test site (contour interval: 10metres)

TopograpHy of land surrounding the Billia Croo test site

Appendix 6. Figure 0.2 below provides an illustration of the topography of the land surrounding the wave test site, Billia Croo. It should be noted that the scale of this map differs from the one shown in Figure 1.1 above due to the extent of the observation grid at Billia Croo. The observation vantage point is positioned at Black Craig overlooking Hoy Sound, at a height of 90m. The very close spacing of the contour lines on the island of Hoy demonstrates the particular steepness of Ward Hill and the Cuilags.

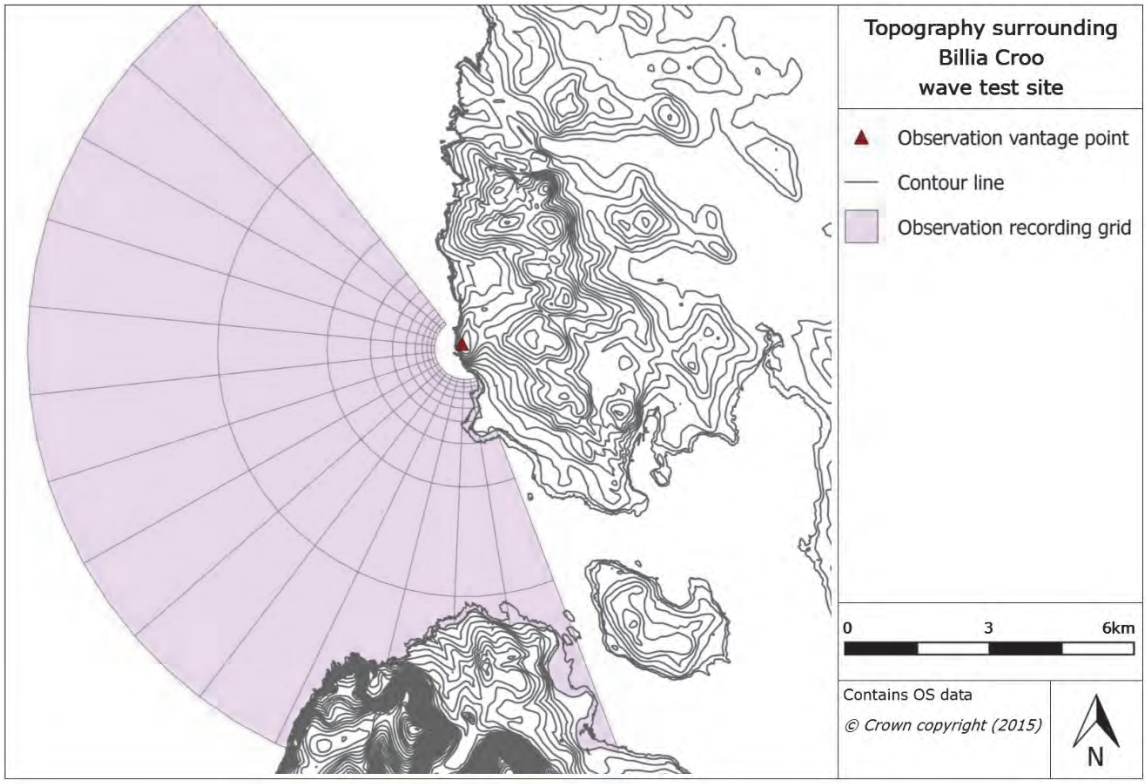

Appendix 6. Figure 0.2. Topography of the land surrounding Billia Croo wave test site (contour interval: 10 metres)

APPENDIX 7: ESTIMATING ABUNDANCE PLOTS

Introduction

Using the prediction surfaces produced from each fitted model, it was possible to generate relative abundance estimates for each month throughout the observations programme's duration. By combining month estimates, seasonal abundance estimates for each survey year were produced. As bootstrapping was conducted during the prediction surface creation, it was possible to generate 95% confidence intervals (CIs) for each abundance estimate. The following provides plots of the changing seasonal abundance estimates (and associated CIs) across the programme's duration split across site impact levels.

Fall of Warness Birds

Black guillemot

Appendix 7. Figure 6.8.1 below provides the predicted abundance values for black guillemots across site impact levels, taking into consideration the site impact status for each month. It shows that there tends to be a seasonal peak in spring with numbers lower during the late autumn months for all SILs.

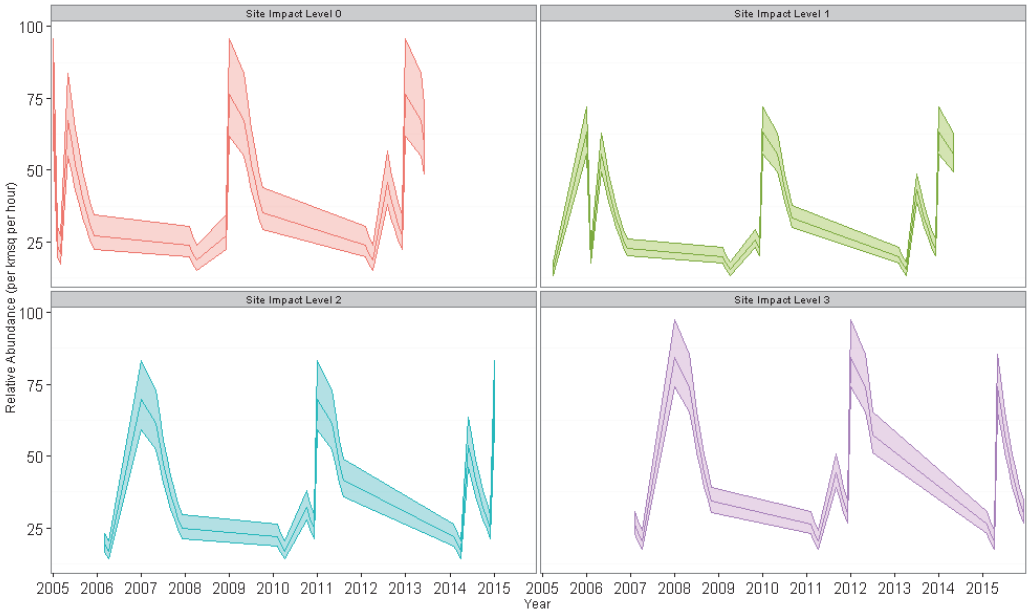

Appendix 7. Figure 6.8.1. Relative abundance, with associated confidence intervals, for black guillemots for each site impact level

Common guillemot

Common guillemot predicted abundance values are split into each of the site impact levels and shown in Appendix 7. Figure 6.8.2 alongside their associated CIs. All site impact levels show a seasonal peak which tends to emerge in spring and extend into summer with numbers lower during winter.

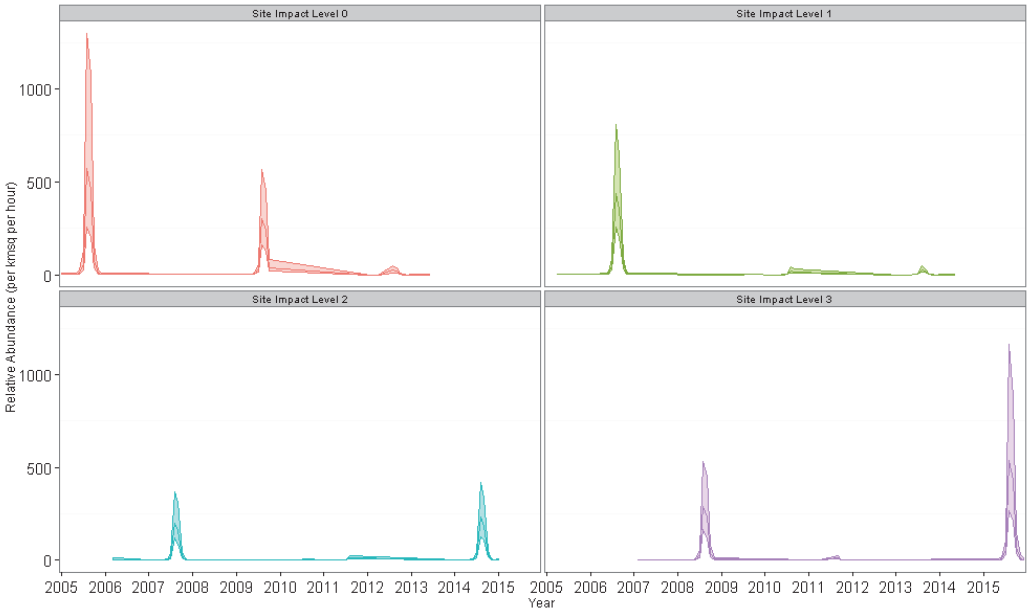

Appendix 7. Figure 6.8.2. Relative abundance, with associated confidence intervals, for common guillemots for each site impact level

Razorbill

The following Appendix 7. Figure 6.8.3 provides the predicted relative abundance values (alongside their associated CIs) for razorbills, split into each of the site impact levels.

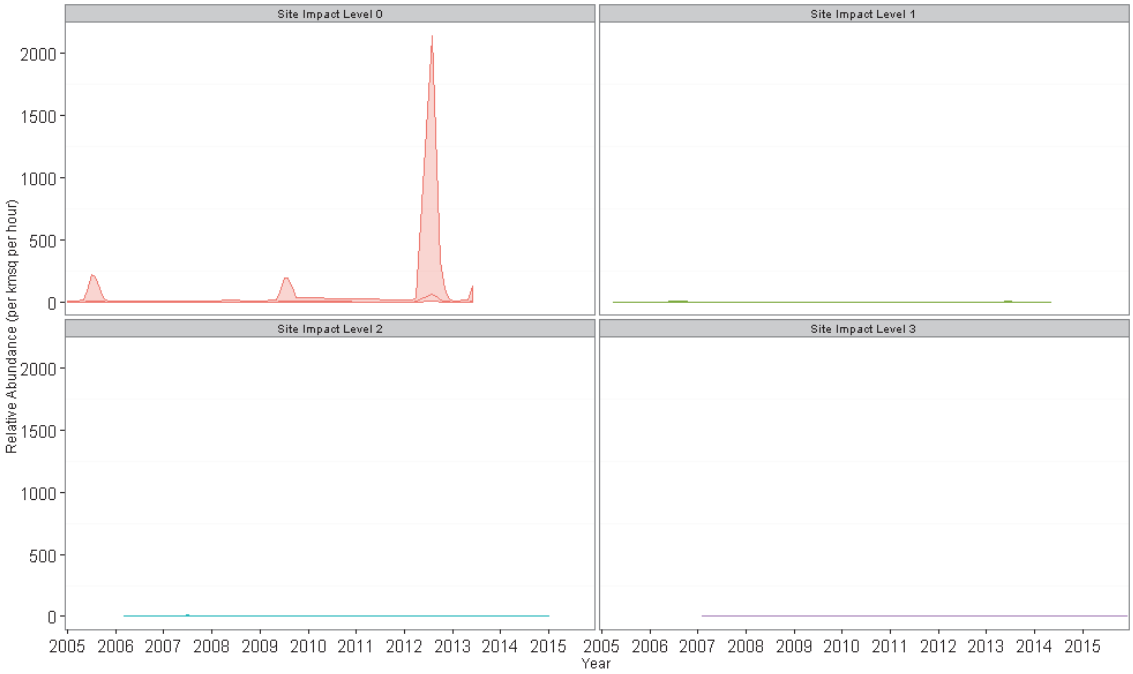

Appendix 7. Figure 6.8.3. Relative abundance, with associated confidence intervals, for razorbills for each site impact level

Divers

The predicted abundance for divers at Fall of Warness has been provided across site impact levels with their associated CIs (Appendix 7. Figure 6.8.4). This highlights the degree of precision underlying each predicted abundance and the high degree of inter-annual variability.

Appendix 7. Figure 6.8.4. Relative abundance, with associated confidence intervals, for divers for each site impact level

Shags and cormorants

The estimated abundance predictions for shags and cormorants have been split across site impact levels to produce a visual representation of the changing relative abundance values across the survey years (Appendix 7. Figure 6.8.5).

Appendix 7. Figure 6.8.5 shows a well-defined seasonal peak in abundance during autumn and winter months, with lowest numbers observed during summer months. In addition, shag and cormorant numbers are shown to have varied quite substantially over the years, particularly during the winter months. This may suggest that external environmental factors are having a marked effect on numbers. This may warrant further research to understand if the dramatic changes in abundance are associated with particularly harsh winters.

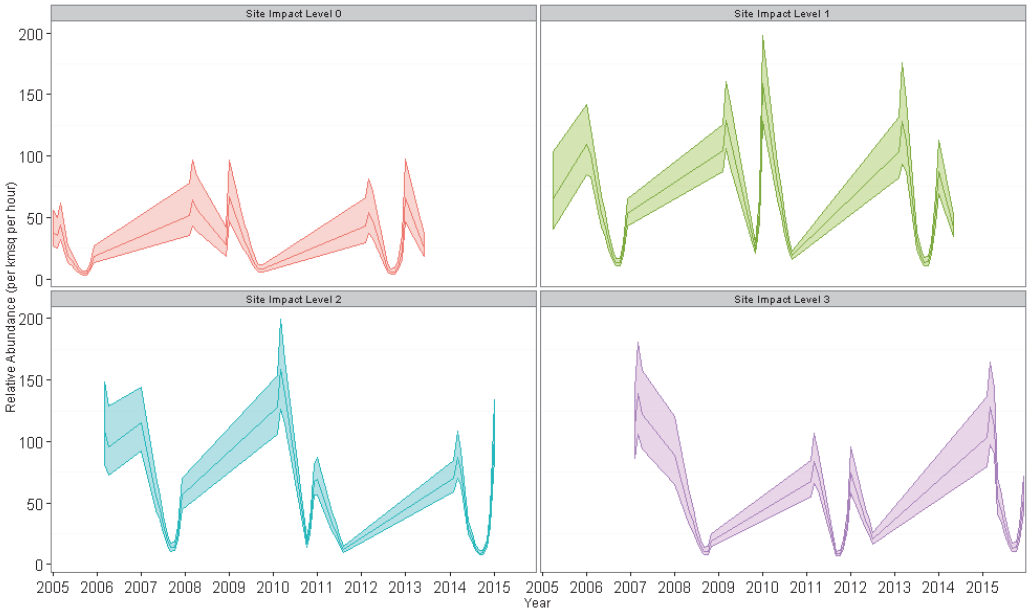

Appendix 7. Figure 6.8.5. Relative abundance, with associated confidence intervals, for shags and cormorants for each site impact level

Auks

The predicted abundance values for auks have been split into each of the site impact levels and are provided in Appendix 7. Figure 6.8.6. The associated CIs for each density prediction are also shown. The 2009 peak in abundance is clear under SIL-0 (as baseline conditions were the site operational conditions during this period) as well as an additional smaller peak in abundance in 2012.

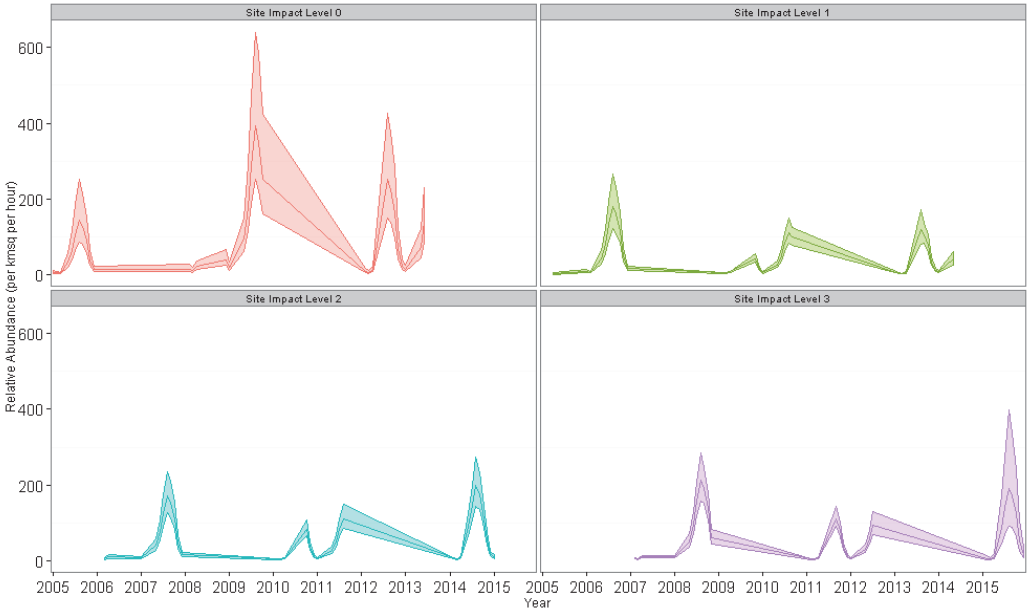

Appendix 7. Figure 6.8.6. Relative abundance, with associated confidence intervals, for auks at each site impact level

Ducks and geese

The predicted abundance values for ducks and geese have been used to produce Appendix 7. Figure 6.8.7, which presents the predicted relative abundance throughout the survey programme but divided across the appropriate site impact levels for each prediction. The associated CIs are included to show the variability behind the relative abundance estimates. This plot shows the clear peaks observed in spring of each year and how the extent of the peak has reduced over the programme's duration.

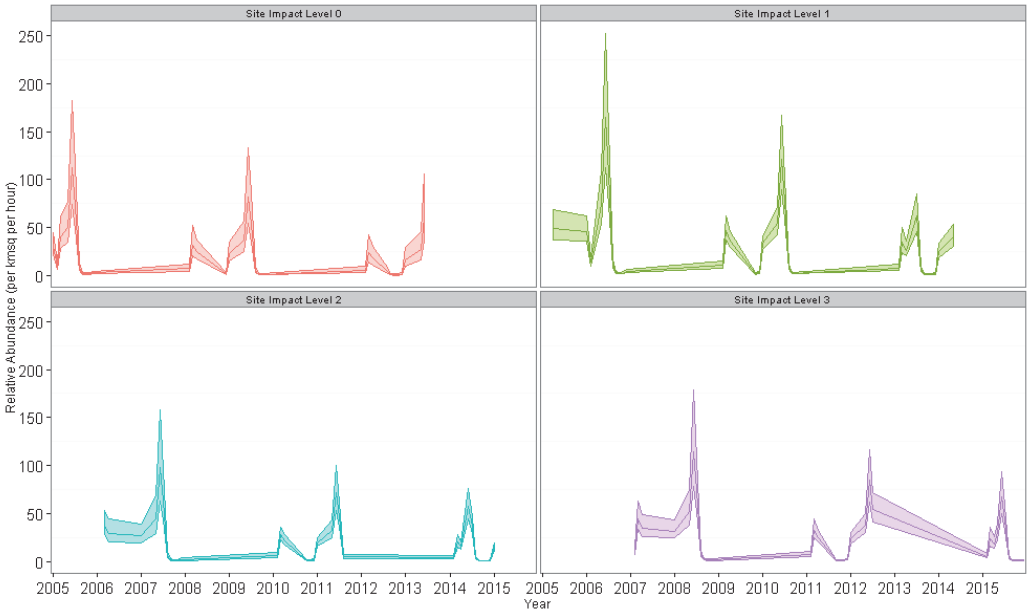

Appendix 7. Figure 6.8.7. Relative abundance, with associated confidence intervals, for ducks and geese for each site impact level

Fall of Warness Marine Mammals

Seals

The abundance predictions for seals at the Fall of Warness have been divided into each of the site impact levels in Appendix 7. Figure 6.8.8. Their associated CIs are also provided to give an indication of the reliability of the estimate. The seasonal peak in abundance during autumn can be observed in each year.

Appendix 7. Figure 6.8.8. Relative abundance, with associated confidence intervals, for seals for each site impact level

Harbour seals

Figure 3.2.1 provides the predicted abundance values for harbour seals split into each of the site impact levels, together with the predictions' associated CIs. It is very clear from the figure that highest predicted abundances occurred in 2006 when the operational status of the site was SIL-1 (infrastructure installed). It is unclear whether this spike in abundance in 2006 is due to an anomaly.

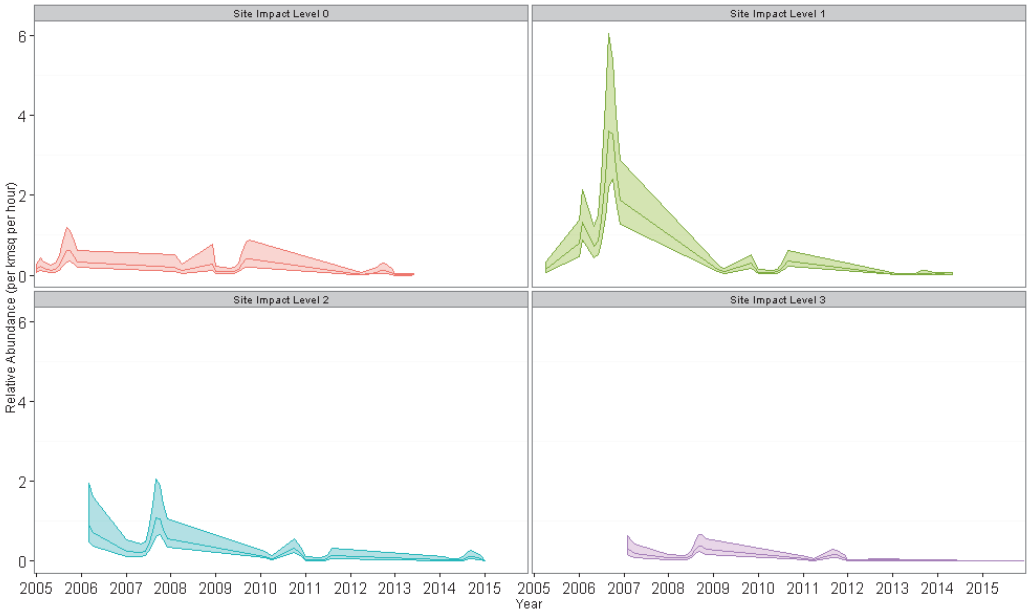

Appendix 7. Figure 6.8.9. Relative abundance, with associated confidence intervals, for harbour seals for each site impact level

Cetaceans

Appendix 7. Figure 6.8.10 provides relative abundance estimates for cetaceans across the years for each of the site impact levels. To illustrate the extent of uncertainty behind some of the predictions, the associated upper and lower CIs for the predictions are also provided.

Appendix 7. Figure 6.8.10. Relative abundance, with associated confidence intervals, for cetaceans for each site impact level

Billia Croo Birds

Common guillemot

The predicted abundance estimates for common guillemots at Billia Croo are presented in Appendix 7. Figure 6.8.11, split across site impact levels. To illustrate the extent of uncertainty behind some of the predictions, the associated upper and lower CIs for the predictions are also provided. Due to the disparity in abundance predictions between seasons, the only clear peaks in abundance occur during the summer. The high abundance prediction in the summer of 2010 is particularly notable.

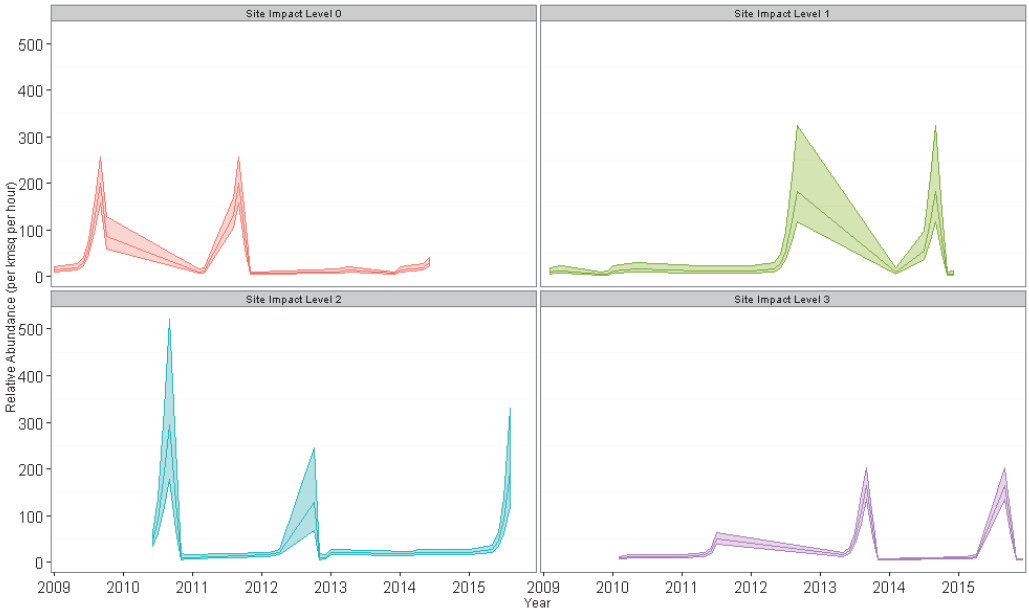

Appendix 7. Figure 6.8.11. Relative abundance, with associated confidence intervals, for common guillemots for each site impact level

Black guillemot

The relative abundance predictions for black guillemots are presented in Appendix 7. Figure 6.8.12, together with their associated CIs. These have been split across site impact levels to illustrate any relationships between site operational status and predicted abundance. The peaks in abundance during spring can be observed at each site impact level.

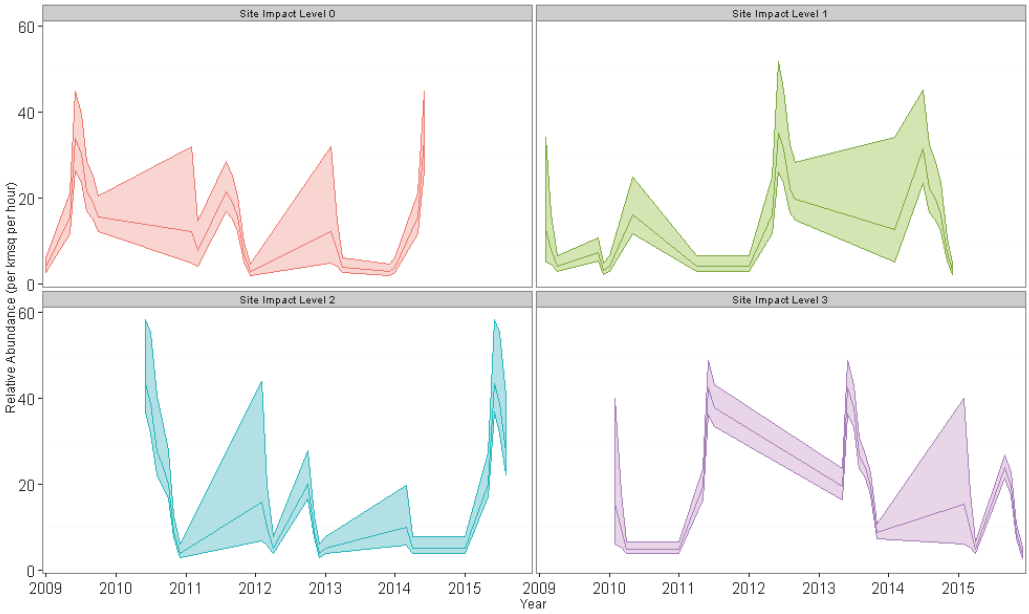

Appendix 7. Figure 6.8.12. Relative abundance, with associated confidence intervals, for black guillemots for each site impact level at Billia Croo

Atlantic puffin

The relative abundance predictions for Atlantic puffin are given for each site impact level in Appendix 7. Figure 6.8.13, which highlight any relationships between site operational status and relative abundance predictions. The seasonal peaks in abundance during spring and summer of each year are depicted clearly. The CIs associated with the predictions are also provided, in order to illustrate the extent of uncertainty inherent in them.

Appendix 7. Figure 6.8.13. Relative abundance, with associated confidence intervals, for Atlantic puffins for each site impact level

Northern gannet

Appendix 7. Figure 6.8.14 provides the abundance estimates for northern gannet at Billia Croo alongside their associated CIs. The estimates have been split across site impact levels. The seasonal drop in northern gannet abundance during the winter period is clearly visible from Appendix 7. Figure 6.8.14 as well as the interannual variability.

Appendix 7. Figure 6.8.14. Relative abundance, with associated confidence intervals, for northern gannets for each site impact level

Auks

The relative abundance estimates for auks at Billia Croo have been plotted against time for each site impact level (Appendix 7. Figure 6.8.15), together with their associated CIs. The spring and summer peaks are evident in this plot as well as the particularly high peak in summer 2011 (under SIL-0 baseline conditions).

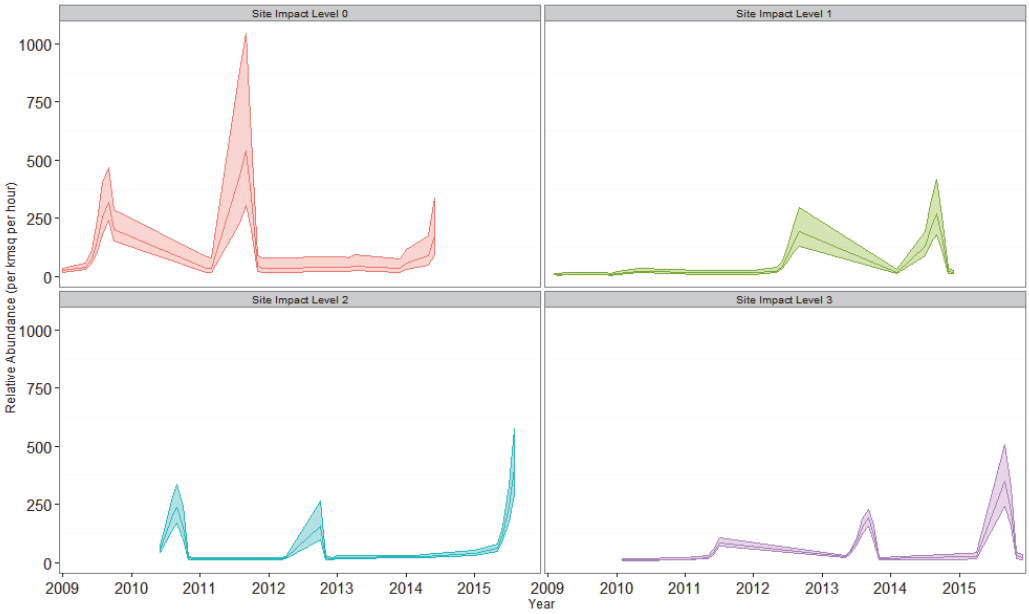

Appendix 7. Figure 6.8.15. Relative abundance for auks, with associated confidence intervals, for each site impact level at Billia Croo

Divers

The predicted abundance values for divers at Billia Croo have been used to produce Appendix 7. Figure 6.8.16, which presents the predicted relative abundance throughout the survey programme but divided across the appropriate site impact levels for each prediction. The associated CIs are included to show the variability behind the relative abundance estimates. This illustrates the lower variability in the predictions associated with SIL-2 (devices installed but not operating) and SIL-3 (devices operating) but also the exceptionally high variability under SIL-0 conditions.

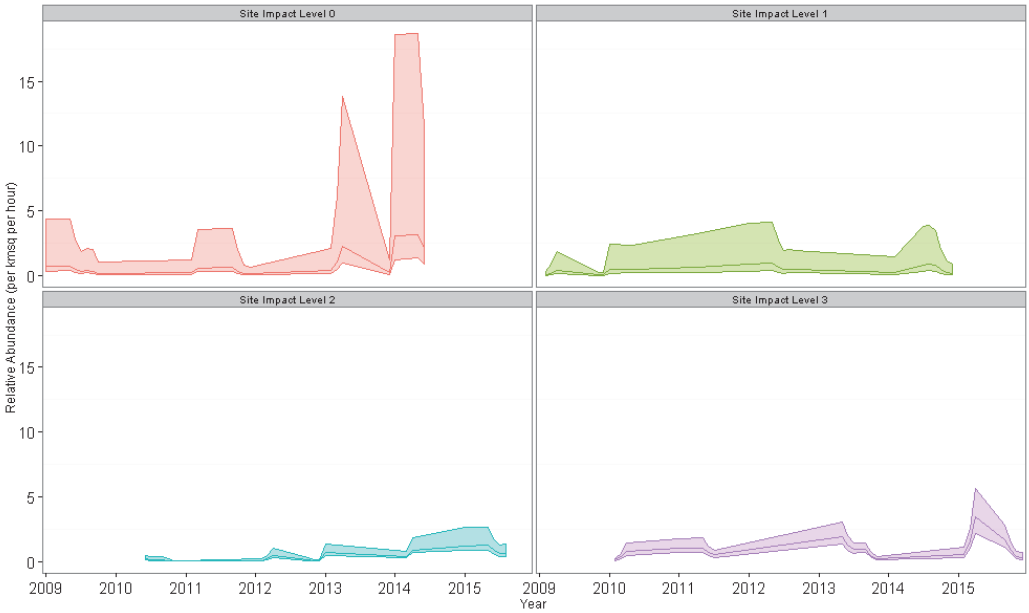

Appendix 7. Figure 6.8.16. Relative abundance, with associated confidence intervals, for divers for each site impact level at Billia Croo

Gulls

Gull predicted abundance values are split into each of the site impact levels and shown in Appendix 7. Figure 6.8.17, alongside their associated CIs. Appendix 7. Figure 6.8.17 This demonstrates greater variability in the predictions (shown by the associated wide CIs) relating to SIL-1 (infrastructure installed), and to a lesser extent to SIL-0 (baseline conditions), as compared to SIL-2 (devices installed) and SIL-3 (devices operating).

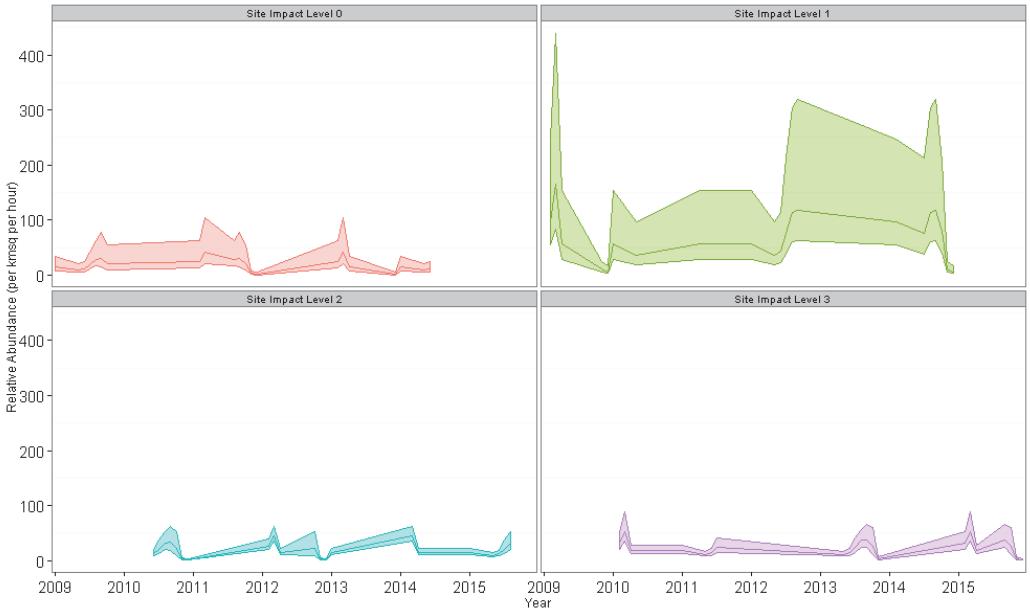

Appendix 7. Figure 6.8.17. Relative abundance, with associated confidence intervals, for gulls for each site impact level at Billia Croo

Billia Croo Marine Mammals

Seals

The changing predicted abundance of seals at Billia Croo over time is illustrated in Appendix 7. Figure 6.8.18, together with their associated CIs. Separate plots have been created for each site impact level. Appendix 7. Figure 6.8.18 appears to indicate a large increase in predicted seal abundance at Billia Croo in the later years of the observations programme.

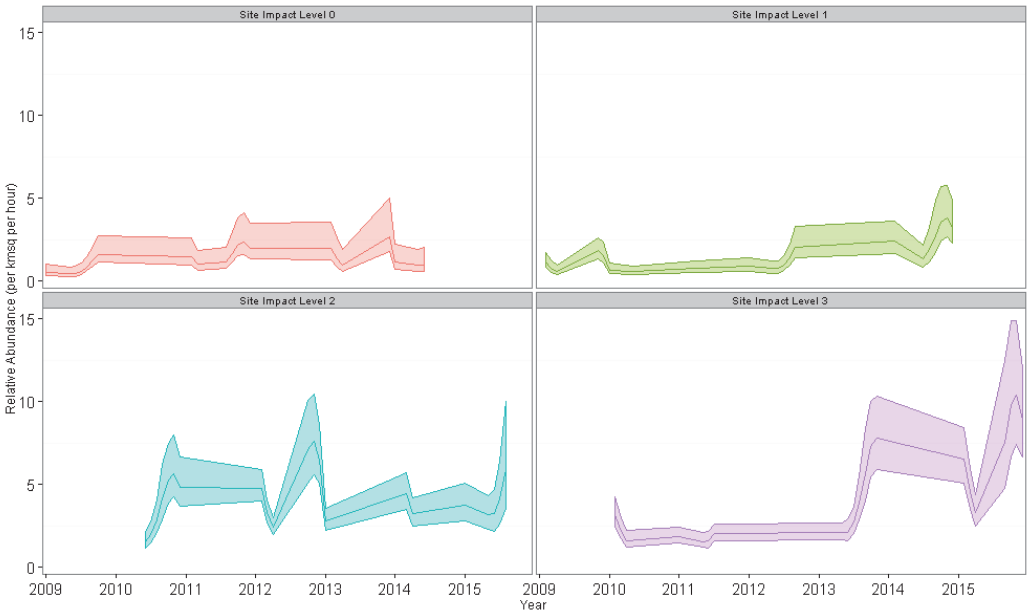

Appendix 7. Figure 6.8.18. Relative abundance, with associated confidence intervals, for seals for each site impact level at Billia Croo

Harbour porpoise

The abundance estimates for harbour porpoises have been plotted and split across site impact levels, and are shown in Appendix 7. Figure 6.8.19 together with their associated CIs. A 'blocking' effect, as illustrated in Appendix 7. Figure 6.8.19, emphasises the lack of variation in predicted abundance between seasons. However, the low abundance predictions in 2013 are highlighted in the plots for SIL-2 (devices installed but not operating) and SIL-3 (devices operating).

Appendix 7. Figure 6.8.19. Relative abundance, with associated confidence intervals, for harbour porpoises for each site impact level at Billia Croo

Cetaceans

Appendix 7. Figure 6.8.20 provides the relative abundance estimates for cetaceans at Billia Croo against time for each site impact level. The figure highlights the lack of variation predicted between seasons. However, it shows differences in predictions (and the associated CIs) between site impact levels, although it should be noted that each site impact level's CIs do overlap. There are much larger CIs for predictions at SIL-1 (infrastructure installed) as compared to SIL-3 (devices installed and operating).

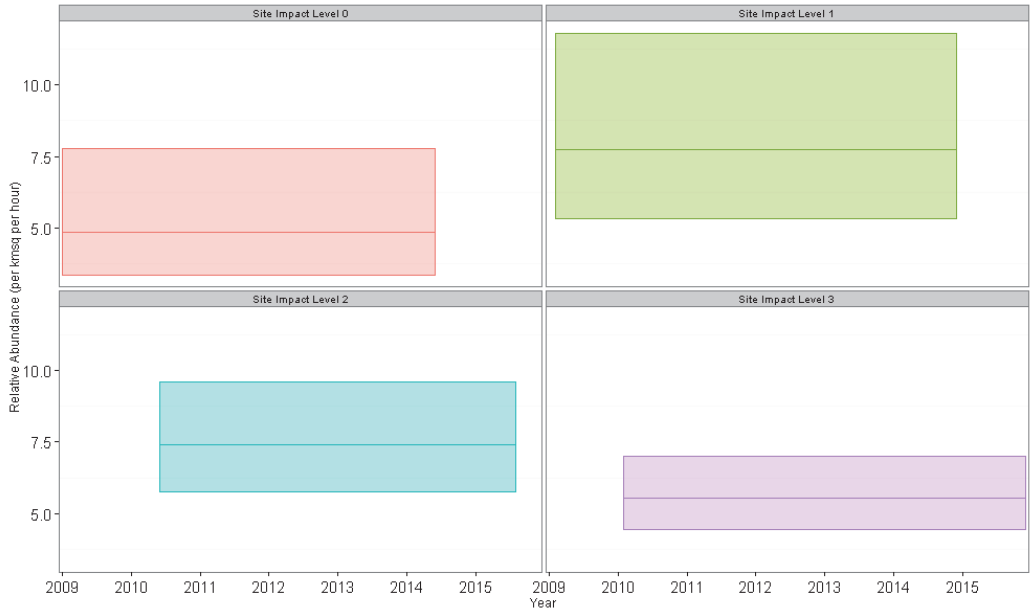

Appendix 7. Figure 6.8.20. Relative abundance, with associated confidence intervals, for cetaceans for each site impact level at Billia Croo

APPENDIX 8: BILLIA CROO SPATIALLY-EXPLICIT CHANGE SURFACES FOR MOST VARIABLE YEAR

Introduction

Using the prediction surfaces for each site impact level, the predicted change in density and distribution of densities between site impact levels for each study species/group has been calculated. For models where 'year' has been included as the covariate, density difference surfaces for the most and least variable year have been generated. As it is necessary to present outputs from the outer and inner grid bands for each species at Billia Croo, the outputs from the most variable year have been presented in the following appendix.

As with the least variable surfaces, the surfaces display the predicted change in density between the various site impact levels as well as positive ('+') and negative ('-') symbols to indicate where the difference has been deemed statistically significant. When interpreting whether these results show any evidence of spatially-explicit change it is important to recognise that when generating the models' outputs the highest device operational status from across the site was assumed when forming the site impact level and therefore, any effect from lower device operational statuses where not considered.

Billia Croo

Atlantic puffin

Appendix 8. Figure 6.8.1 presents the prediction surface for the Atlantic puffin model for the outer grid cells and Appendix 8. Figure 6.8.2 provides a more detailed view of the inner grid cells.

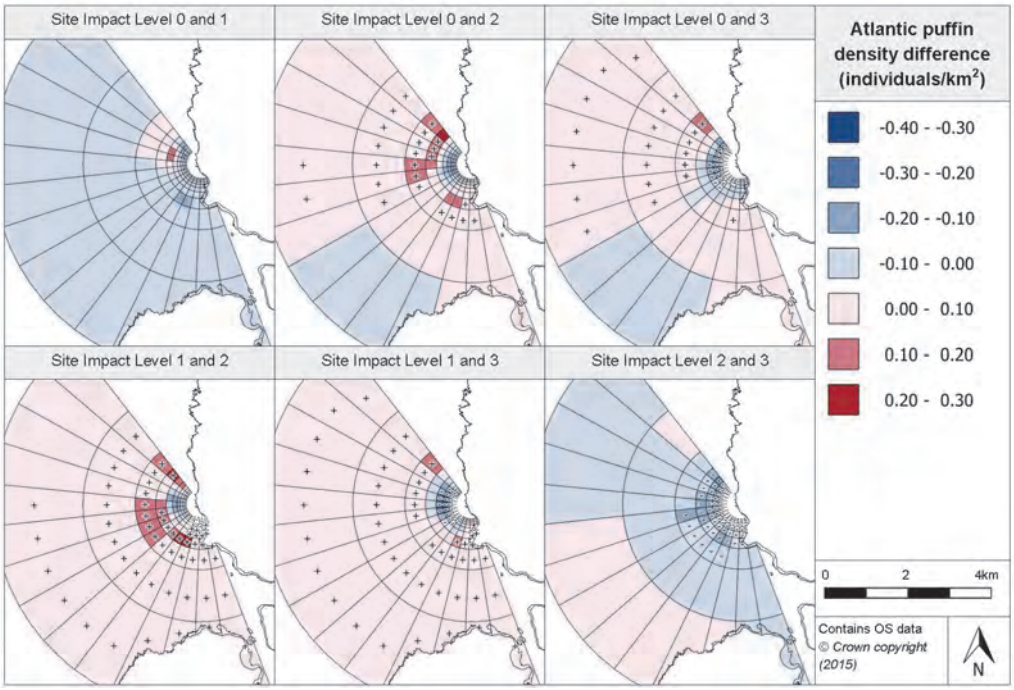

Appendix 8. Figure 6.8.1. Predicted density difference between various site impact levels for Atlantic puffin during 2014 (year with most variation) at Billia Croo

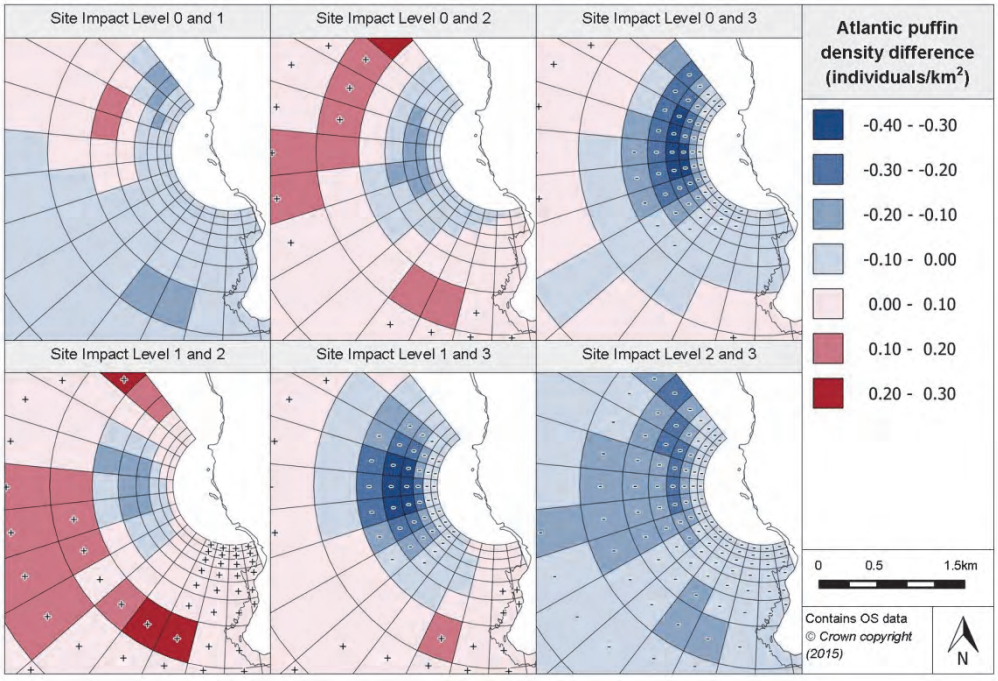

Appendix 8. Figure 6.8.2. Density differences between Atlantic puffin site impact level inner prediction surfaces during 2014 (most variable year) at Billia Croo

Northern gannet

The prediction surface for northern gannet for the outer grid cells is presented in Appendix 8. Figure 6.8.3 and for the inner grid cells in presented in Appendix 8. Figure 6.8.4.

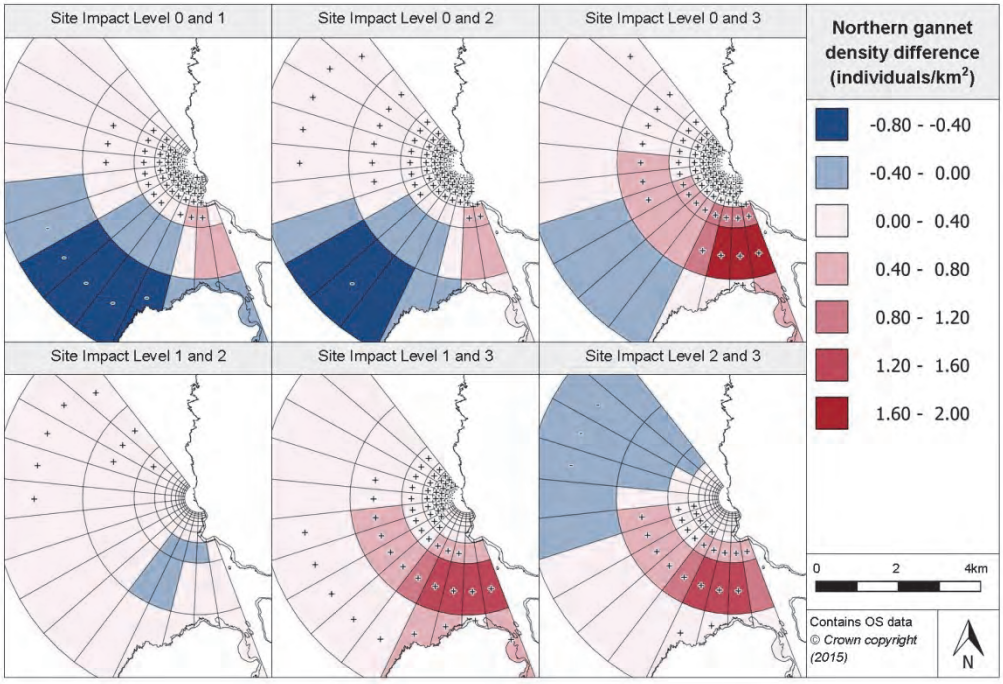

Appendix 8. Figure 6.8.3. Predicted density difference between various site impact levels for Northern gannet during 2010 (year with most variation) at Billia Croo

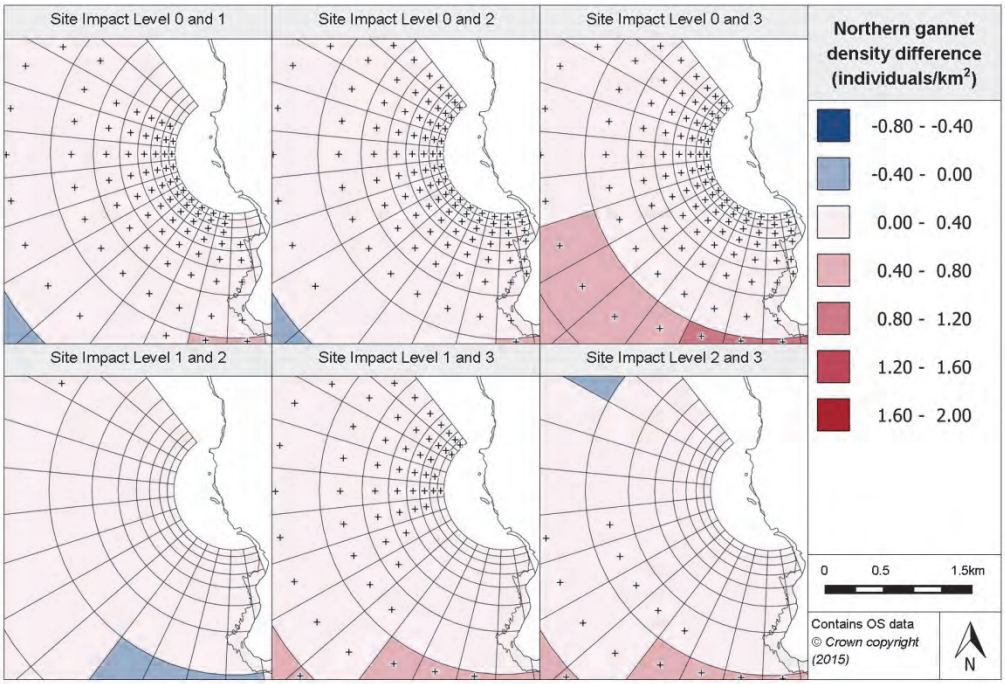

Appendix 8. Figure 6.8.4. Predicted density difference between various site impact levels for Northern gannet during 2010 (year with most variation) at Billia Croo

Auks

Appendix 8. Figure 6.8.5 provides the prediction surface for auks outer grid cells. Further detail regarding the predicted density difference in provided in Appendix 8. Figure 6.8.6.

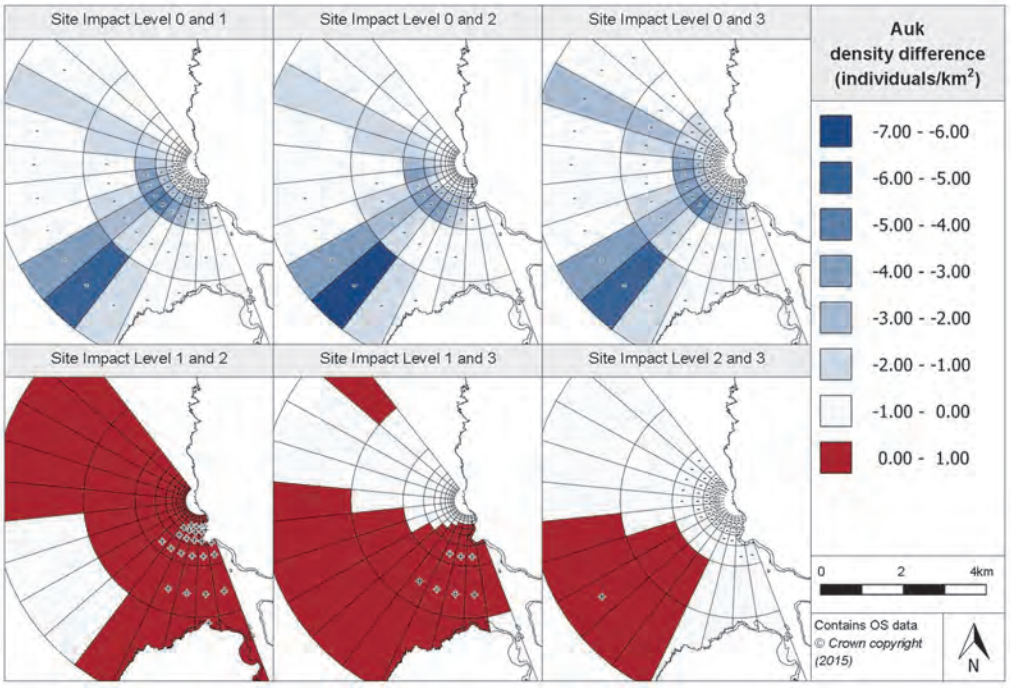

Appendix 8. Figure 6.8.5. Predicted density difference between various site impact levels for auks during 2014 (year with most variation) at Billia Croo

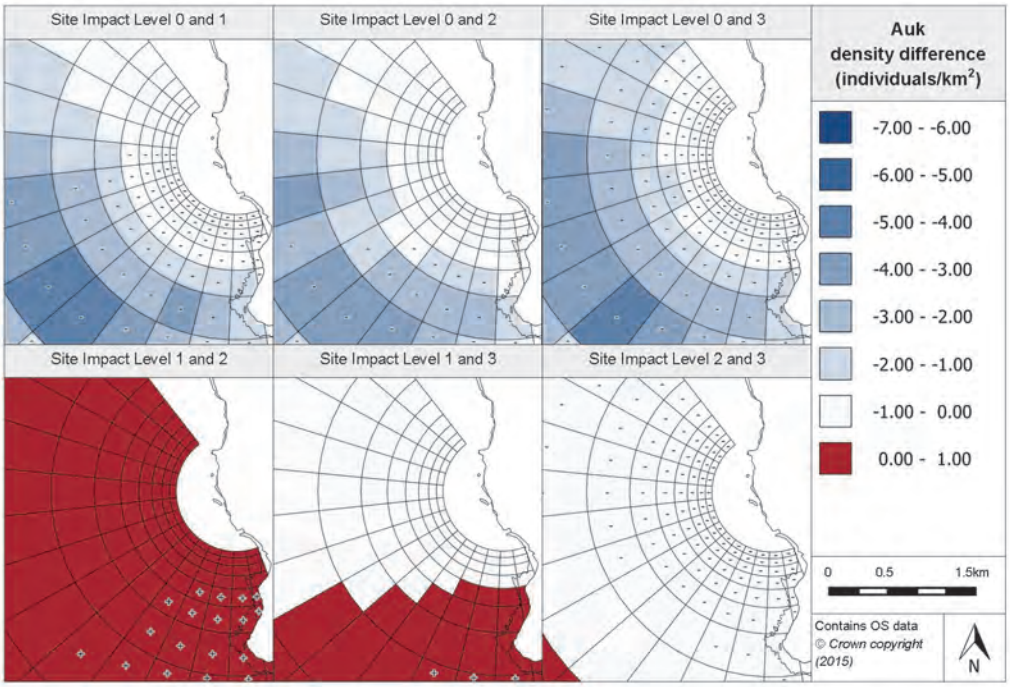

Appendix 8. Figure 6.8.6. Density differences between auks site impact level inner prediction surfaces during 2014 (most variable year) at Billia Croo

Divers

The density difference prediction surfaces for divers are provided in Appendix 8. Figure 6.8.7 for the outer grid bands and Appendix 8. Figure 6.8.8 for the inner grid bands.

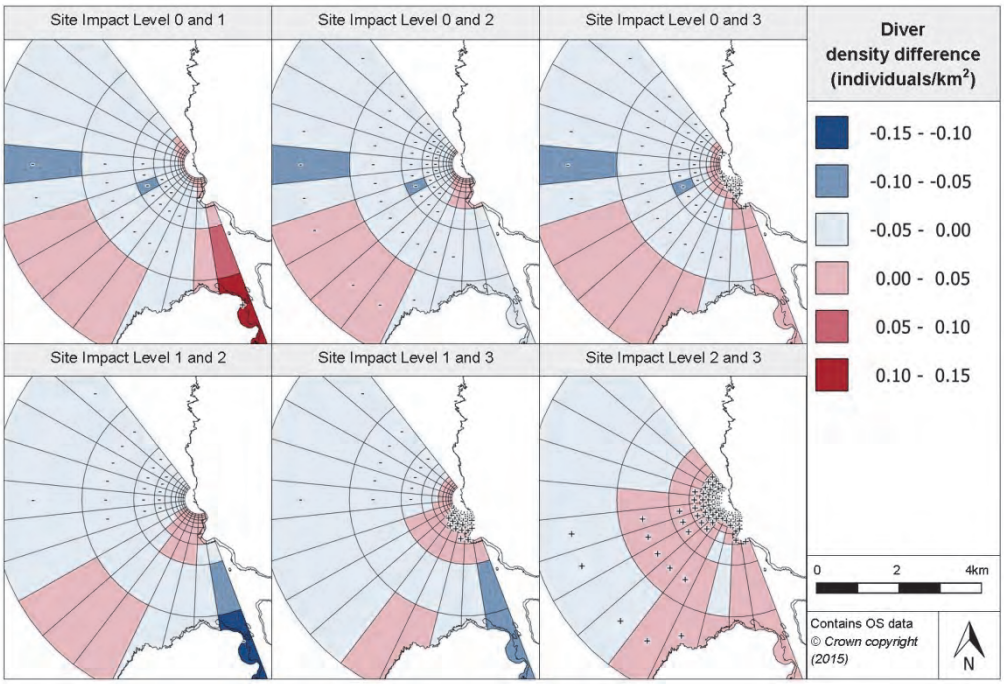

Appendix 8. Figure 6.8.7. Predicted density difference between various site impact levels for divers during 2014 (year with most variation) at Billia Croo

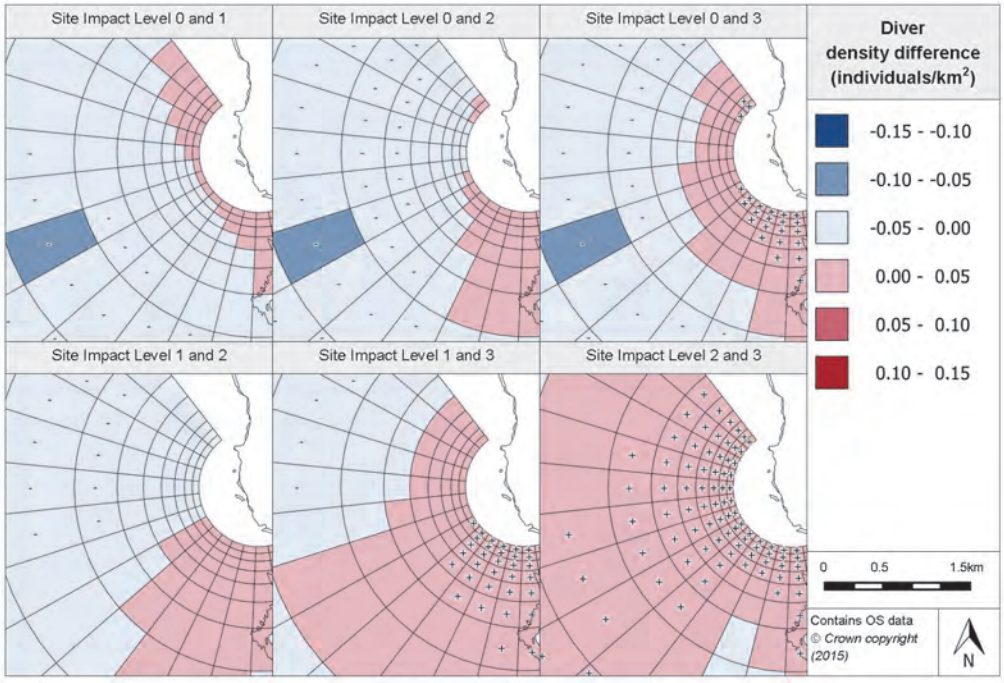

Appendix 8. Figure 6.8.8. Density differences between divers site impact level inner prediction surfaces during 2014 (most variable year) at Billia Croo

Seals

Appendix 8. Figure 6.8.9 below provides the prediction surface for the most variable year for seals. The inner grid bands surface is provided in more detail in Appendix 8. Figure 6.8.10.

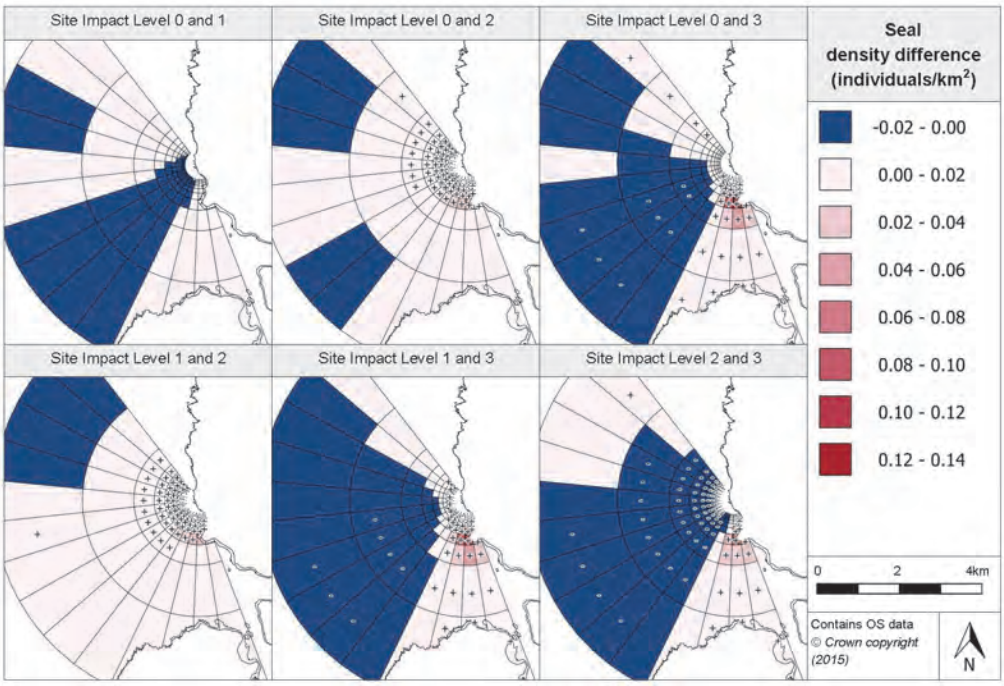

Appendix 8. Figure 6.8.9. Predicted density difference between various site impact levels for seals during 2014 (year with most variation) at Billia Croo

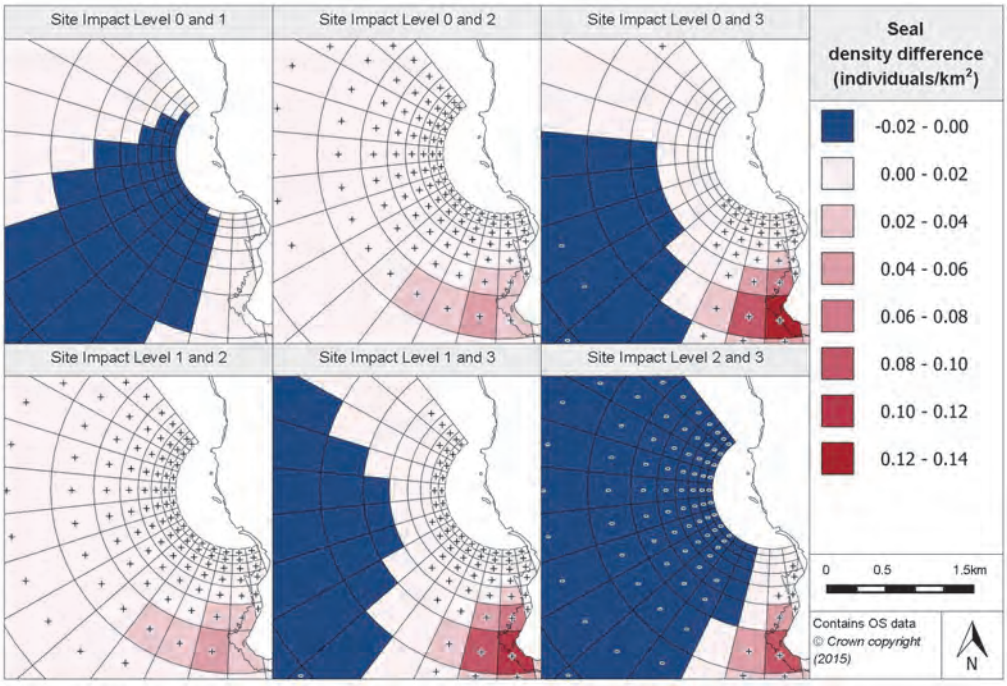

Appendix 8. Figure 6.8.10. Density differences between seals site impact level inner prediction surfaces during 2014 (most variable year) at Billia Croo

Harbour porpoises

The prediction surfaces generated using the harbour porpoise fitted model are provided in Appendix 8. Figure 6.8.11 for the outer grid bands and Appendix 8. Figure 6.8.12 for the inner grid bands.

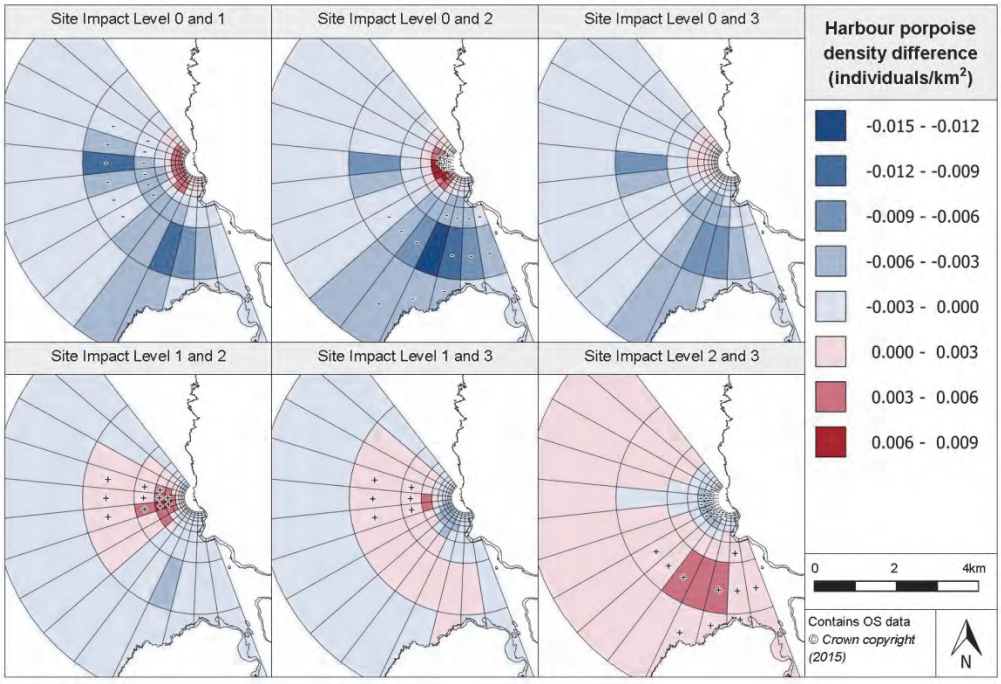

Appendix 8. Figure 6.8.11. Predicted density difference between various site impact levels for harbour porpoises during 2010 (year with most variation) at Billia Croo

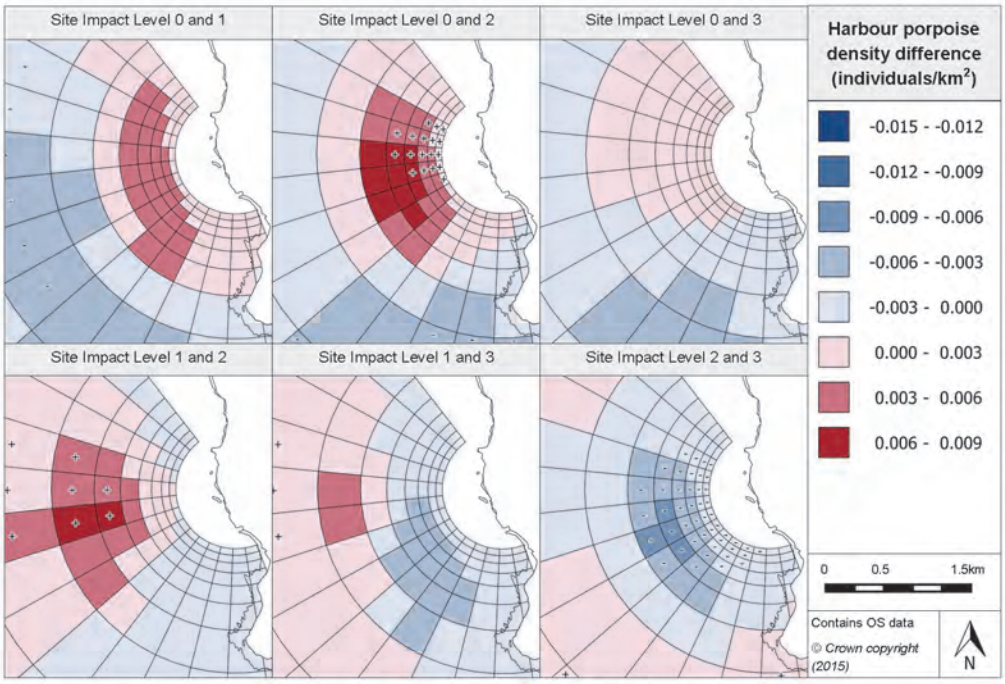

Appendix 8. Figure 6.8.12. Density differences between harbour porpoises site impact level inner prediction surfaces during 2010 (most variable year) at Billia Croo

Annex 1 - EMEC Wildlife Data Analysis Project: Data Cleansing Guidelines and Assumptions

Annex 2 - Fall of Warness Observation Methodology

Annex 3 - Billia Croo Observation Methodology

For brevity, Annexes 1-3 are not included within this report but are available, on request, from:

Caitlin Long
Project and Consents Officer
The European Marine Energy Centre (EMEC) Limited
Old Academy Business Centre
Back Road
Stromness
Orkney
KW16 3AW

Email: caitlin.long@emec.org.uk

www.snh.gov.uk

ISBN: 978-1-78391-420-3

Policy and Advice Directorate, Great Glen House,
Leachkin Road, Inverness IV3 8NW
T: 01463 725000

You can download a copy of this publication from the SNH website.

recycle

Scottish Natural Heritage
Dualchas Nàdair na h-Alba
All of nature for all of Scotland
Nàdar air fad airson Alba air fad